NOAA Technical Memorandum NMFS-AFSC-

Model-based Essential Fish Habitat Definitions for Eastern Bering Sea Groundfish Species

by
Laman, EA, Rooper, CN, Rooney, S, Turner, K, Cooper, D, and Zimmermann, M

U.S. DEPARTMENT OF COMMERCE
National Oceanic and Atmospheric Administration National Marine Fisheries Service Alaska Fisheries Science Center
December 2015

NOAA Technical Memorandum NMFS

The National Marine Fisheries Service's Alaska Fisheries Science Center uses the NOAA Technical Memorandum series to issue informal scientific and technical publications when complete formal review and editorial processing are not appropriate or feasible. Documents within this series reflect sound professional work and may be referenced in the formal scientific and technical literature.

The NMFS-AFSC Technical Memorandum series of the Alaska Fisheries Science Center continues the NMFS-F/NWC series established in 1970 by the Northwest Fisheries Center. The NMFS-NWFSC series is currently used by the Northwest Fisheries Science Center.

This document should be cited as follows:

> Laman, EA, Rooper, CN, Rooney, S, Turner, K, Cooper, D, Zimmermann, M. 2015. Model-based Essential Fish Habitat Definitions for Eastern Bering Sea Groundfish Species. U.S. Dep. Commer., NOAA Tech. Memo. NMFS-AFSC-XXX, XXX p.

Reference in this document to trade names does not imply endorsement by the National Marine Fisheries Service, NOAA.

Model-based Essential Fish Habitat Definitions for Eastern Bering Sea Groundfish Species

by
Laman, EA, Rooper, CN, Rooney, S, Turner, K, Cooper, D, and Zimmermann, M

Alaska Fisheries Science Center
7600 Sand Point Way N.E.
Seattle, WA 98115
www.afsc.noaa.gov

U.S. DEPARTMENT OF COMMERCE
Penny Pritzker, Secretary
National Oceanic and Atmospheric Administration
Kathryn Sullivan, Under Secretary and Administrator
National Marine Fisheries Service
Eileen Sobeck, Administrator for Fisheries
December 2015

This document is available to the public through:

National Technical Information Service
U.S. Department of Commerce 5285 Port Royal Road Springfield, VA 22161

www.ntis.gov

ABSTRACT

Defining essential habitats for federally managed fishes and invertebrates is an important step in managing groundfish in Alaska. Species distribution models have been widely used in conservation biology and terrestrial systems to define the potential habitat for organisms of interest. The models themselves can take a number of forms, from relatively simple frameworks such as generalized linear or additive models to complex modeling frameworks such as boosted regression trees, maximum entropy models, two-stage models, or other formulations. We employed a variety of modeling methods and data sets from scientific surveys and commercial fisheries to define the habitats for over 30 federally managed species in the Eastern Bering Sea. Adult, juvenile, larval, and egg stages were modeled in four seasons where data were available. Geographic location and bottom depth were dominant habitat covariates in models describing the distribution of most crabs and adult fishes. Sea surface temperature was consistently an important predictor of ichthyoplankton distribution. Species distribution modeling was used to produce maps identifying essential habitat for each species and life stage. These maps will be used for marine spatial planning and assessing impacts of anthropogenic activities in Alaska's marine environment.

CONTENTS

INTRODUCTION

The 1996 reauthorization of the Magnuson-Stevens Fishery Conservation and Management Act (MSFCMA) mandates that the National Marine Fisheries Service (NMFS) identify habitats essential for managed species and conserve habitats from adverse effects of fishing and other anthropogenic activities. Essential Fish Habitat (EFH) is defined under this act as 'those waters and substrates necessary to fish for spawning, breeding, feeding or growth to maturity.' As part of this mandate, EFH descriptions for all species listed under a Fisheries Management Plan (FMP) in Alaskan waters are needed. In addition, these descriptions must be revisited on a five-year cycle that reviews and updates EFH information (including species descriptions) with new data and research.

Essential fish habitat descriptions consist of maps of EFH and text descriptions. In Alaska, most EFH descriptions for groundfish have been limited to qualitative statements on the distribution of adult life stages. These are useful, but could be relatively easily refined both in terms of spatial extent and life history stage using species distribution models and available data from a variety of sources. Distribution models have been widely used in conservation biology and terrestrial systems to define the potential habitat for organisms of interest (e.g. DeLong and Collie 2004[1], Lozier et al. 2009, Elith et al. 2011, Sagarese et al. 2014). Recently species distribution models have been developed for coral and sponge species in the eastern Bering Sea, Gulf of Alaska, and Aleutian Islands (Rooper et al. 2014, Sigler et al. 2015, Rooper et al. in review).

Species distribution models themselves can take a number of forms, from relatively simple frameworks such as generalized linear or additive models to complex modeling frameworks such as boosted regression trees, maximum entropy models, two-stage models or other formulations. The models can be used to predict potential habitat, probability of presence or even abundance, but they all have some features in common; 1) the underlying data consists of some type of independent variables (predictors)

[1] DeLong, A.K., and J.S. Collie. 2004. Defining Essential Fish Habitat: A Model-Based Approach. Rhode Island Sea Grant, Narragansett, R.I. 4pp.

and a dependent response variable (presence, presence/absence or abundance), 2) raster maps of independent variables are used to predict a response map, 3) confidence bounds on the predictions and partitioning of the data can produce test statistics useful for evaluating the model. The outputs of species distribution models are designed to be raster maps that can show the predicted abundance of a species at each of the raster cells. This type of product is useful for EFH descriptions, as it lends itself to producing maps of areas of high abundance or hotspots of distribution and the models themselves can be used to generate the required text descriptions.

The goal of the study generating this Data Report was to produce species distribution models of EFH for all major species of groundfish and invertebrates in the eastern Bering Sea. Accompanying Data Reports will be generated for Aleutian Islands and Gulf of Alaska fishes and invertebrates. We attempted to generate models and text descriptions of EFH for each species in the eastern Bering Sea where data exists for egg, larval, juvenile and adult life history stages in four seasons. From these we generated complementary distribution maps that showed the location of EFH. It is anticipated that this research could form a basis for future updates and integration of new data and studies.

METHODS

Area

The eastern Bering Sea continental shelf and upper continental slope represent a diverse mosaic of benthic habitats that extend northward from the Aleutian Islands to the United States-Russia border at 180°W. The eastern Bering Sea has a broad highly productive continental shelf that extends > 200 km from shore (Figure 1). The shelf is very shallow and flat, with the majority of the seafloor at depths > 100 m. The seafloor of the eastern Bering Sea shelf is comprised mostly of soft unconsolidated sediments. The upper continental shelf (~200 m – 1000 m) is steep and inundated by 5 major canyon regions. The seafloor is more diverse, with some areas of rocky substrate occurring especially in Pribilof Canyon. However, much of the continental slope area is dominated by soft unconsolidated sediments.

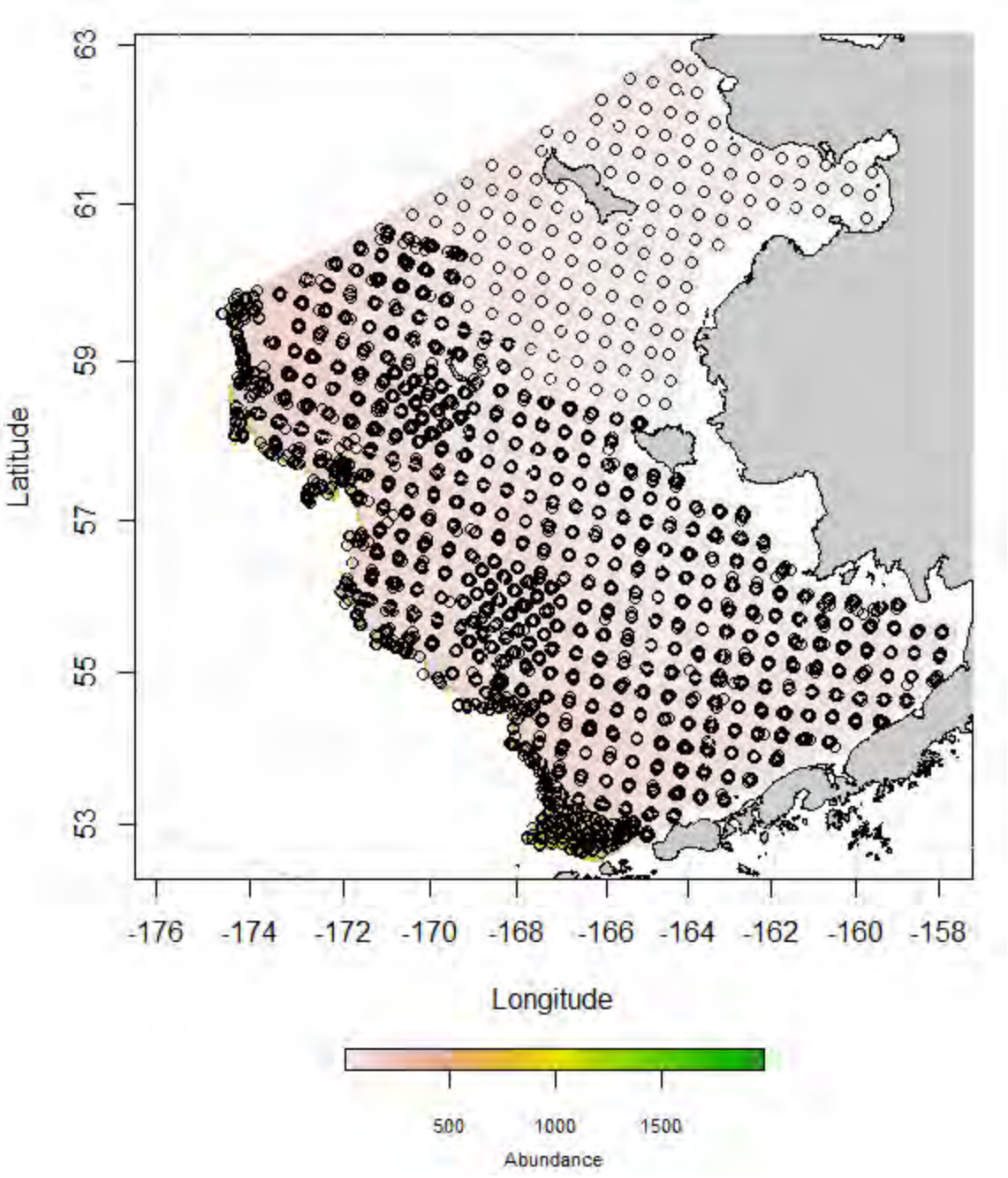

202

Figure 1 – Eastern Bering Sea from the Northern Bering Sea to the Alaska Peninsula where this modeling study was carried out. Circles indicate the locations of bottom trawl hauls from the eastern Bering Sea shelf annual bottom trawl survey (1982-2014) and eastern Bering Sea slope biennial bottom trawl survey (2002-2012).

The species and life stages of fishes and invertebrates examined for this study are included in Table 1.

The data available for early life history stages (egg, larval and early juvenile) came from the Ecosystems and Fisheries Oceanography Coordinated Investigations (EcoFOCI) ECODAAT database. The summer

distributions of juvenile and adult life history stages were modeled using the RACE eastern Bering Sea bottom trawl survey database (RACEBASE). The seasonal adult distributions were modeled using commercial catch data from the fishery observer program Catch in Areas database (CIA). All of the data were divided into four seasons for analyses: fall (October-November), winter (December-February), spring (March-May), and summer (June-September).

Table 1. Species and life history stages modeled for the eastern Bering Sea slope and shelf.

Species	Eggs	Larvae	Early juveniles	Late juveniles	Adults
Pollock					
Pacific cod					
Sablefish					
Yellowfin sole					
Greenland turbot					
Arrowtooth flounder	*Atheresthes* spp. as group				
Kamchatka flounder					
Southern rock sole					
Northern rock sole					
Alaska plaice					
Rex sole					
Dover sole					
Flathead sole					
Pacific ocean perch	*Sebastes* spp. as group				
Northern rockfish					
Shortraker rockfish					
Blackspotted/rougheye rockfish					
Dusky rockfish					
Thornyhead rockfish					
Atka mackerel					
Great sculpin					
Yellow Irish lord					
Bigmouth sculpin					
Alaska skate					
Bering skate					
Aleutian skate					
Mud skate					
Pacific giant octopus					
Red king crab					
Blue king crab					
Tanner crab					
Snow crab					

	no data available or NA
	Presence or presence absence models
	Density (CPUE) models

Species distribution data – Recruitment processes data

EcoFOCI's ECODAAT database contains historical ichthyoplankton catches from across the entire eastern Bering Sea (Figure 2). The data considered includes catches from 1991 to 2013. These catches have been collected during a number of different types of surveys with different survey objectives. As such, many different gear types have been used, including bongo and Methot nets. Because of this, samples were collected from a variety of depths in the water column. Samples have been collected across all months and seasons of the year, although not all month-year combinations occurred in the database. For this reason, the data were combined across years for analysis. The spatial coverage of the ECODAAT data was uneven, with most samples coming from the region in the southwestern part of the Bering Sea shelf, reflecting the focus on pollock recruitment mechanisms that have been an important line of research for EcoFOCI.

Each species in the ECODAAT data was classified as either egg, larval, or juvenile (we considered all of these juveniles to be "early" juvenile stages, as they were found in the water column rather than settled to the benthos). We used these data for presence-only models where the number of presence observations in a species-life stage combination exceeded 50. The numbers of catches for each species, season, and life stage are shown in Table 2.

An important caveat to the species distribution models developed using the ECODAAT database is that these data were not collected over the entire area of the eastern Bering Sea. Typically, these data were collected from a smaller regional survey grid, rather than conducted over a regular grid. The distribution of sampling effort should be considered when drawing conclusions from maps produced from these data.

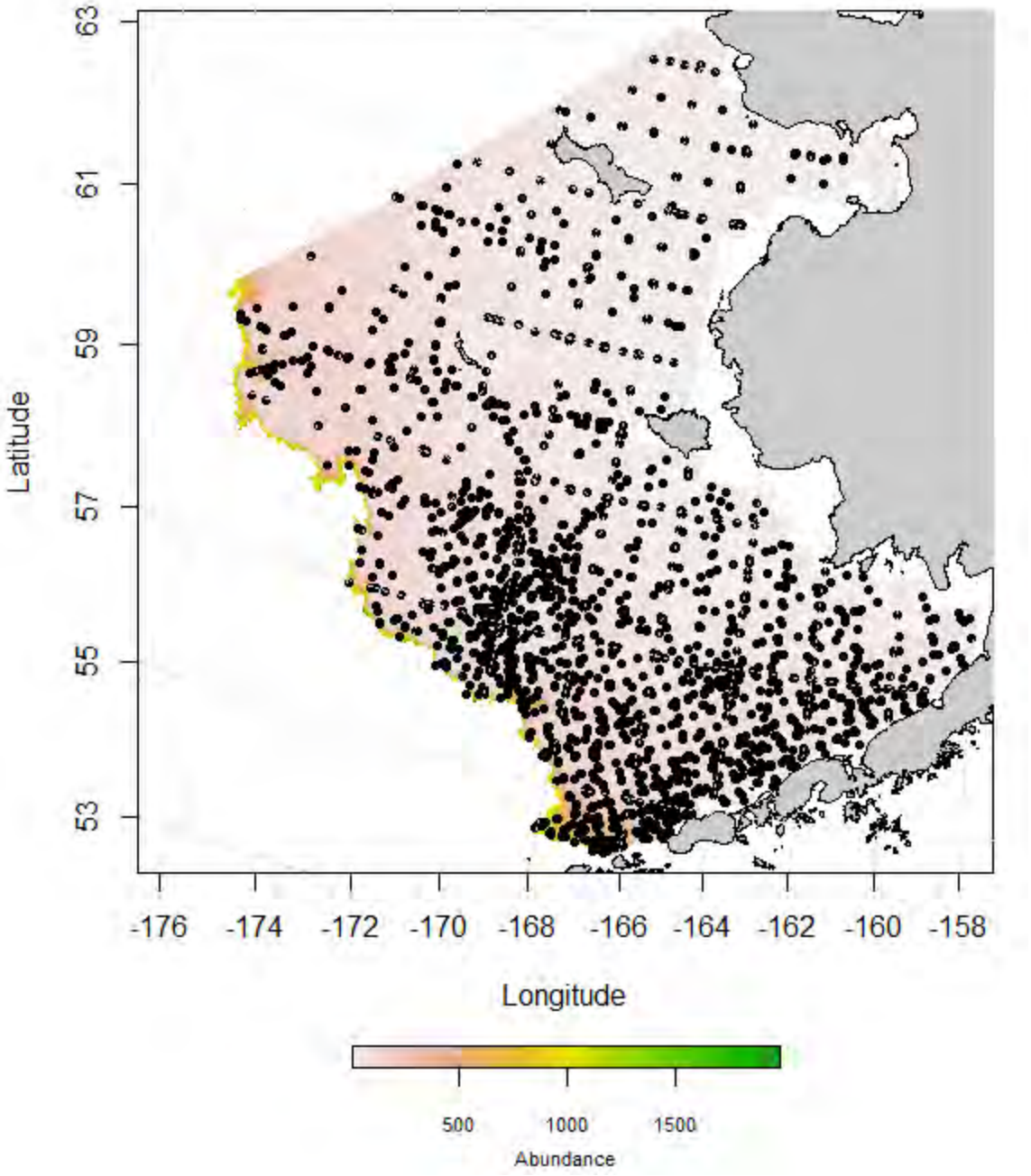

Figure 2. -- Locations (n = 24,505) of sampling for ichthyoplankton in the Eastern Bering Sea (1991-2012) from the EcoFOCI ECODAAT database.

Table 2. Numbers of presence records for species and life history stages of ichthyoplankton recorded in ECODAAT database from the eastern Bering Sea. Some species were grouped by genus where the species were not individually identifiable. Maximum entropy modeling was conducted for species, season, and life history stages where the number of presence observations exceeded 50.

		Fall			Spring			Summer			Winter	
Species	Eggs	Larvae	Early juveniles	Eggs	Larvae	Early juveniles	Eggs	Larvae	Early juveniles	Eggs	Larvae	Early juveniles
Alaska plaice (*Pleuronectes quadrituberculatus*)	--	--	--	948	206	--	159	75	--	1	--	--
Atheresthes sp.	--	--	--	5	636	--	--	230	13	50	50	--
Atka mackerel (*Pleurogrammus monopterygius*)	--	--	--	--	190	--	--	1	--	--	39	--
Bering flounder (*Hippoglossoides robustus)*	--	--	--	30	--	--	--	5	--	--	--	--
Dover sole (*Microstomus pacificus*)	--	--	--	17	--	--	18	5	--	--	--	--
Greenland turbot (*Reinhardtius hippoglossoides*)	--	--	--	12	326	--	--	91	3	41	21	--
Cottidae sp.	--	--	--	--	193	29	--	105	3	--	1	--
Flathead sole (*Hippoglossoides elassodon*)	--	1	--	1396	270	--	108	457	10	--	--	--
Yellowfin sole (*Limanda aspera*)	1	17	--	132	--	--	687	482	2	--	--	--
Pacific cod (*Gadus macrocephalus*)	--	1	--	27	311	--	5	86	124	--	1	--
Pollock (*Gadus chalcogramma*)	23	--	3	2378	1815	4	529	741	541	7	1	--
Rex sole (*Glyptocephalus zachirus*)	--	1	--	296	--	--	138	36	--	1	--	--
Southern rock sole (*Lepidopsetta bilineata*)	--	--	--	--	48	--	--	63	1	--	--	--
Northern rock sole (*Lepidopsetta polyxystra*)	--	1	--	--	815	--	--	235	3	--	--	--
Sablefish (*Anoplopoma fimbria*)	--	--	--	7	54	--	--	4	7	18	4	--
Rockfish *(Sebastes* sp.)	--	--	--	--	556	--	--	425	31	--	2	--
Thornyhead *(Sebastolobus* sp.)	--	--	--	2	--	--	5	2	--	1	--	--

Species distribution data – Groundfish bottom trawl surveys

The modeling analyses also included data collected during bottom-trawl surveys of the eastern Bering Sea ecosystem. These data were the most comprehensive and useful of the three types of data analyzed, as they are all from the summer season and are conducted with a rigorous statistical design. The National Marine Fisheries Service (NMFS), Alaska Fisheries Science Center (AFSC), has conducted standard bottom-trawl surveys in these ecosystems since 1982 (Lauth and Conner 2014). The eastern Bering Sea shelf survey is conducted on a regular 25 nautical mile (nm) grid, that has been extended to include the northern Bering Sea and Norton sound in recent years. The eastern Bering Sea slope survey is conducted on the upper continental shelf at depths from 200 to 1200 m (Hoff and Britt 2011). This survey employs a methodology that randomly samples existing stations within depth and area strata, with the addition of new stations each year. For our analyses, AFSC bottom trawl data were combined across years for the eastern Bering Sea slope and shelf.

The eastern Bering Sea shelf survey utilizes an 83-112 flatfish trawl with cookie cutter gear along the footrope (Stauffer 2004). The eastern Bering Sea slope bottom trawl survey utilizes a poly Nor'Eastern high-opening bottom trawl with 24.2 m roller gear constructed with 36 cm rubber bobbins separated by 10 cm rubber disks with mud sweeps (Stauffer 2004). Trawl tows were conducted at a target speed of 5.6 km h^{-1} (3 knots) for 30 min. Bottom contact and net dimensions were recorded throughout each trawl using net mensuration equipment. For these analyses, records were only used if trawl performance was satisfactory and if the distance fished, geographic position, average depth, and water temperature were recorded. Tows were deemed satisfactory if the net opening was within a predetermined normal range, the footrope maintained contact with the seafloor, and the net suffered little or no damage during the tow. Data from a total of 12,702 bottom-trawl tows were used for this analysis.

All fishes and invertebrates captured during a survey tow were sorted either by species or into larger taxonomic groups and the total weight in the catch was determined. Catch per unit effort (CPUE, no.·ha^{-1}) for each taxonomic group was calculated using the area swept which was computed from the net width

for each tow multiplied by the distance towed recorded with the vessel's GPS. For some species both juvenile and adult sizes were captured during the bottom trawl survey. In these cases, an approximate length at first maturity was used to partition the catches into juvenile and adult stages (Table 3). For some species only a subset of years was used in the modeling due to taxonomic changes that have occurred throughout the time series. For example, dusky and dark rockfishes were considered one species prior to the 1996 survey, so only data from surveys beginning in this year were used to model these two species.

Table 3. Species modeled using bottom trawl survey data including years in each of the modeling efforts, the percentage of positive catches (frequency of occurrence) in the bottom trawl hauls for juvenile and adult life history stages, and the length at first maturity considered the maximum juvenile size.

Species	Years modeled	Percent positive catches - Juveniles	Percent positive catches - adults	Maximum juvenile length (cm)
Alaska plaice (*Pleuronectes quadrituberculatus*)	All	34.37	55.24	28
Alaska skate (*Bathyraja parmifera*)	1990-	37.03	27.7	92
Aleutian skate (*Bathyraja aleutica*)	1990-	6.69	1.2	132
Arrowtooth flounder (*Atheresthes stomias*)	1993-	34.08	40.63	35
Atka mackerel (*Pleurogrammus monopterygius*)	All	--	0.46	25
Bering skate (*Bathyraja interrupta*)	1990-	7.5	8.07	69
Bigmouth sculpin (*Hemitripterus bolini*)	All	4.82	8.51	51
Snow crab (*Chionoecetes opilio*)	All	--	68.76	
Blackspotted rockfish (*Sebastes melanostictus*)	2007-	0.36	0.43	43
Tanner crab (*Chionoecetes bairdi*)	All	--	59.17	
Red king crab (*Paralithodes camtschaticus*)	1996-	--	21.19	
Blue king crab (*Paralithodes platypus*)	All	--	11.06	
Dover sole (*Microstomus pacificus*)	All	0.86	0.88	38
Dusky rockfish (*Sebastes variabilis*)	1996-	--	0.23	29
Flathead sole (*Hippoglossoides elassodon*)	All	49.99	65.8	25
Great sculpin (*Myoxocephalus polyacanthocephalus*)	All	15.48	10.34	51
Greenland turbot (*Reinhardtius hippoglossoides*)	All	18.57	11.6	65
Kamchatka flounder (*Atheresthes evermanni*)	1993-	30.25	13.93	52
Longspine thornyhead (*Sebastolobus altivelis*)	All	--	0.03	
Mud skate (*Bathyraja taranetzi*)	1990-	1.3	0.75	62
Northern rock sole (*Lepidopsetta polyxystra*)	2001-	32.75	46.47	24
Northern rockfish (*Sebastes polyspinis*)	All	--	0.51	25
Octopus sp. (*Octopus dofleini*)	All	--	3.89	
Pacific cod (*Gadus macrocephalus*)	All	72.72	80.28	46
Pacific ocean perch (*Sebastes alutus*)	All	0.95	3.64	25
Pollock (*Gadus chalcogramma*)	All	68.35	84.72	25
Rex sole (*Glyptocephalus zachirus*)	All	5.39	15.07	24
Rougheye rockfish (*Sebastes aleutianus*)	2007-	0.48	0.19	43
Sablefish (*Anoplopoma fimbria*)	All	0.26	4.81	40
Shortraker rockfish (*Sebastes borealis*)	All	0.65	1.15	44
Shortspine thornyhead (*Sebastolobus alascanus*)	All	1.81	4.94	21
Southern rock sole (*Lepidopsetta bilineata*)	2001-	0.14	0.22	24
Yellow Irish lord (*Hemilepidotus jordani*)	All	1.08	5.31	22
Yellowfin sole (*Limanda aspera*)	All	54.08	61.37	25

Standard GAM model
Hurdle GAM model
Maximum entropy model

Species distribution data – Commercial catch (observer) data

Data from CIA observer database was used to model fishes caught in commercial catches during the non-summer seasons (Table 4). The CIA data were provided by John V. Olson and Steve Lewis (AKRO). The data from observed catches, regardless of the type of fishing gear, were combined across years for analyses. We used the presence of species in catches for MaxEnt (presence-only) models where the number of presence observations for a species exceeded 50. The numbers of catches for each species and season are shown in Table 4. All of these fish and invertebrates were assumed to be adult life history stages. Only the fall, winter, and spring seasons were considered, as the summer distributions were modeled using bottom trawl survey data.

An important caveat to the distribution models developed using the CIA database is that for most species, the distribution of catches was dependent on the distribution of fishing activity. So, instead of being a regular survey conducted over a regular grid, these observations are typically clustered around areas of high catches for target species. As such, they should be viewed with some caution compared to the fishery-independent data informing the bottom trawl survey distribution maps.

Table 4. Numbers of presence records by species available from the CIA database in the Eastern Bering Sea. Maximum entropy modeling was conducted for species and season where the number of presence observations exceeded 50.

Species	Fall	Winter	Spring
Alaska plaice (*Pleuronectes quadrituberculatus*)	1236	10440	5388
Alaska skate (*Bathyraja parmifera*)	9427	11410	18391
Aleutian skate (*Bathyraja aleutica*)	1741	567	1776
Arrowtooth flounder (*Atheresthes stomias*)	12572	10630	23700
Atka mackerel (*Pleurogrammus monopterygius*)	519	1027	1490
Bigmouth sculpin (*Hemitripterus bolini*)	3469	2170	4479
Blackspotted, rougheye rockfish (*Sebastes aleutianus, S. melanostictus*)	164	148	230
Blue king crab (*Paralithodes platypus*)	225	91	86
Dover sole (*Microstomus pacificus*)	51	77	75
Dusky rockfish (*Sebastes variabilis*)	446	238	467
Flathead sole (*Hippoglossoides elassodon*)	12920	20231	34782
Great sculpin (*Myoxocephalus polyacanthocephalus*)	738	1722	2437
Greenland turbot (*Reinhardtius hippoglossoides*)	2253	1599	1279
Kamchatka flounder (*Atheresthes evermanni*)	4123	3260	4182
Mud skate (*Bathyraja taranetzi*)	144	169	230
Northern rock sole (*Lepidopsetta polyxystra*)	3549	20079	20004
Northern rockfish (*Sebastes polyspinis*)	557	359	429
Octopus sp. (*Octopus dofleini*)	823	626	1939
Pacific cod (*Gadus macrocephalus*)	14187	23888	38312
Pacific ocean perch (*Sebastes alutus*)	778	915	1966
Pollock (*Gadus chalcogramma*)	15838	27189	44786
Red king crab (*Paralithodes camtschaticus*)	311	508	1669
Rex sole (*Glyptocephalus zachirus*)	1659	4002	9469
Sablefish (*Anoplopoma fimbria*)	693	545	770
Shortraker rockfish (*Sebastes borealis*)	171	474	738
Shortspine thornyhead (*Sebastolobus alascanus*)	174	811	1632
Snow crab (*Chionoecetes opilio*)	4132	6390	6320
Southern rock sole (*Lepidopsetta bilineata*)	267	3712	4899
Tanner crab (*Chionoecetes tanneri*)	1867	5601	6406
Yellow Irish lord (*Hemilepidotus jordani*)	266	1412	1406
Yellowfin sole (*Limanda aspera*)	4411	14134	15491

Habitat-related variables

Independent variables for modeling included the standard suite of habitat variables typically collected on the bottom trawl survey as well as a few derived and modeled variables (Table 5). These variables were chosen for their availability and for their potential influence on the distribution of fishes as found from historical studies

The early life history stages of each of the fishes were generally sampled in pelagic waters. Therefore, surface water temperature, surface current speed and surface current direction were chosen as potential variables to explain early life history distributions. In addition surface current direction variability was used as well, as an indication of potential eddy vorticity or other current variability processes that might be present. These variables were derived from ROMS model runs from 1969-2005 provided by A. Hermann (in Danielson et al. 2011). The data monthly were monthly values originally on a 10 km by 10 km grid. These values were interpolated via inverse distance weighting to a 1 km by 1 km grid for modeling and summarized by season (Figure 3).

Additional variables used for modeling the early life history stages of fish species included the depth, slope, color and tidal current (Figure 4). A bathymetry raster for the eastern Bering Sea was also produced for this analysis using data from Steve Lewis (AKRO) and Zimmermann (unpublished data). Zimmermann derived bathymetric point data from available soundings on available NOS smooth sheets that were digitized and compiled according to the methods in Zimmermann and Benson (2013). These point data were linearly interpolated from a triangular irregular network (TIN) layer to a 100 m by 100 m raster grid and empty spaces were filled using data from the AKRO. This interpolation was conducted using the Spatial Analyst package in ArcGIS software (ESRI 2009). Slope was derived from the 100 m by 100 m bathymetry raster. Slope for each raster grid cell was computed as the maximum difference between the depth at a cell and its surrounding cells. Slope was computed using the *raster* package[2] in R

[2] R v3.0.1; Hijams, R.J., J. van Etten, M. Mattiuzzi, M. Sumner, J.A. Greenberg, O.P., Lamigueiro, A. Bevan, E.B. Racine, and A. Shortridge. 2015. Geographic data analysis and modeling: package 'raster' version 2.3-24. 232 pages.

(R Core Development Team 2013). For the analysis of early life history data, these two layers were averaged to a 1 km by 1 km grid.

To reflect average ocean productivity ($g \cdot C \cdot m^{-2} \cdot day^{-1}$) at each of the ichthyoplankton survey sites, we used MODIS ocean color data for five spring-summer months (May-September) that encompass the spring and summer phytoplankton blooms over eight years (2003-2011) for the eastern Bering Sea region (Behrenfeld and Falkowski 2007). These data were downloaded from the Oregon State University Ocean Productivity website and were averaged by cell and by month and then averaged again by cell and by year (to account for differences in the number of samples within each cell). The averages were then interpolated to a 1 km by 1 km raster grid using inverse distance weighting.

Haul position and depth were collected during each bottom trawl haul. A start and end position for the vessel during the on-bottom portion of the trawl were collected using the vessel-mounted GPS receiver. Vessel position was corrected for the position of the bottom trawl itself by triangulating how far the net was behind the vessel (based on the seafloor depth and the wire out) and subtracting this distance from the vessel position in the direction of the bottom trawl haul. We assumed that the bottom trawl was directly behind the vessel during the tow and that all bottom trawl tows were conducted in a straight line from the beginning point to the end point. The mid-point of the start and end positions of the net was used as the location variable in the modeling. The longitude and latitude data for each tow (and all other geographical data including the raster layers described below) were projected into Alaska Albers Equal Area Conic projection (center latitude = 50° N and center longitude = 154° W) and degrees of latitude and longitude were transformed into 100 m by 100 m square grids of eastings and northings for modeling. The location variable was used to capture any significant spatial trends across the eastern Bering Sea region in bottom trawl survey catches.

The depth for each tow was estimated from a SeaBird SBE-39 microbathythermograph attached to the headrope of the net and the measured net height. Mean depth during the tow was calculated for inclusion as an explanatory variable in the modeling. The bathymetry raster described above was used for

prediction, but not for parameterizing the models. The slope estimate derived from the bathymetry raster at each bottom trawl survey tow location was used as a habitat variable in the model, and the slope raster was used for prediction.

The average summer temperature at each site was estimated from data collected during Gulf of Alaska bottom trawl surveys from 1996-2013. Bottom temperatures are collected during each bottom trawl tow using the SBE-39 attached to the headrope of the net. Mean bottom temperatures for each haul were interpolated to the 100 m by 100 m grid for the entire eastern Bering Sea region. These data were interpolated using ordinary kriging (Venables and Ripley 2002) with an exponential semi-variogram model. This resulted in a single temperature raster layer that reflects the average temperature conditions in surveys from 1996-2013. The temperature data used in our models reflect long-term averages that could be compared spatially to the distribution of bottom trawl survey catches. Mean bottom temperature underneath each bottom trawl tow path was used as a habitat variable in the modeling. The 100 m by 100 m raster layers of average temperature were used for prediction.

Two measures of water movement and its potential interaction with the seafloor were used as habitat variables in modeling and prediction. The first variable was the maximum tidal speed at the site of each bottom trawl haul. Tidal speeds were estimated for 368 consecutive days (January 1st, 2009 to January 3rd, 2010) using a tidal inversion program parameterized for the eastern Bering Sea on a 1 km by 1 km grid (Egbert and Erofeeva 2002). This tidal prediction model was used to produce a series of one lunar year of tidal currents for spring and neap cycles at each bottom trawl survey location. The maximum of the series of predicted tidal current was then extracted for the position of each bottom trawl survey haul. This maximum value was used as a habitat variable in the modeling. Maximum tidal current at each bottom trawl survey site were also interpolated to the entire eastern Bering Sea using ordinary kriging and an exponential semi-variogram. The kriging model was then used to interpolate a raster of maximum current values on a 1 km by 1 km cell size that was used for predictions.

The second water movement variable was the predicted bottom water layer current speed from ROM's model runs from 1969-2005 (Danielson et al. 2011). This long-term current speed and direction were available as points on a 10 km by 10 km grid. The ROM's model was based on a three-dimensional grid with 60 depth tiers for each grid cell. For example, a point at 60 m water depth would have 60 depth bins at 1 m intervals, while a point at 120 m depth would have 60 depth bins at 2 m depth intervals, etc.). The current speed and direction for the deepest depth bin at each point (closest to the seafloor) was used in this analysis. These regularly spaced data were interpolated to a 100 m by 100 m cell size raster covering the entire Gulf of Alaska using inverse distance weighting (Figure 4). Then the values from this raster at each of the bottom trawl survey haul locations were extracted and the mean value computed for the path of each bottom trawl survey tow. The raster was also used for prediction.

To reflect average ocean productivity ($g \cdot C \cdot m^{-2} \cdot day^{-1}$) at each of the bottom trawl survey sites, we used MODIS ocean color data for five spring-summer months (May-September) that encompass the spring and summer phytoplankton blooms over eight years (2003-2011) for the eastern Bering Sea region (Behrenfeld and Falkowski 2007). These data were downloaded from the Oregon State University Ocean Productivity website. These data were averaged by cell and by month and then averaged again by cell and by year (to account for differences in the number of samples within each cell). The averages were then interpolated to 100 m by 100 m raster grids using inverse distance weighting (Figure 4). The mean value in this grid underlying each bottom trawl survey tow was extracted from this raster. The raster was used for prediction.

Sediment grain size was also used as a variable to predict bottom trawl survey catches (Eastern Bering Sea Sediment Database (EBSSED; Smith and McConnaughey 1999); National Geophysical Data Center Seafloor Sediment Grain Size database[3]. Mean grain size (mm) is expressed as "phi" which is negative $\log_2$-transform of grain size (e.g., a large "phi" indicates fine grains). The sampling tools for this sediment information are bottom grabs and corers, which do not distinguish boulder or bedrock habitat, and as a

[3] ngdc.noaa.gov/geosamples/metadata.jsp?g=G00127

result, these habitat types are implicitly excluded from our analysis. The grain size and sorting values from the sediment data (n = 803) were kriged using an exponential model (Venables and Ripley 2002), which was the best fit to the semi-variogram of both grain size and sorting values.

The final variables included in the modeling of bottom trawl survey data were the catches of structure forming invertebrates (corals, sponges, and pennatulaceans). The presence of each of these categories of invertebrates was a binomial (presence or absence) term in the model. The prediction was accomplished by using the prediction surfaces from distribution models for each of these species (Rooper et al. in review).

The same variables were used for commercial catch data (observer data) as were employed in the bottom trawl survey models (with the exception of the structure forming invertebrate layers; Table 5).

There was some collinearity in the habitat variables included in the model (Table 6). The largest correlations were between latitude and longitude ($r = 0.60$) and slope and depth ($r = 0.53$). The remaining pairwise correlations among variables were < 0.5. Variance inflation factors were calculated using the method of Zuur et al. (2009) for each of the variables to be included in the modeling, resulting in values ranging from 1.0 to 4.2. These values were all acceptable (below 5.0). Thus, all of the selected habitat variables were included in the models of habitat suitability, presence or absence, and fish or invertebrate abundance in the eastern Bering Sea.

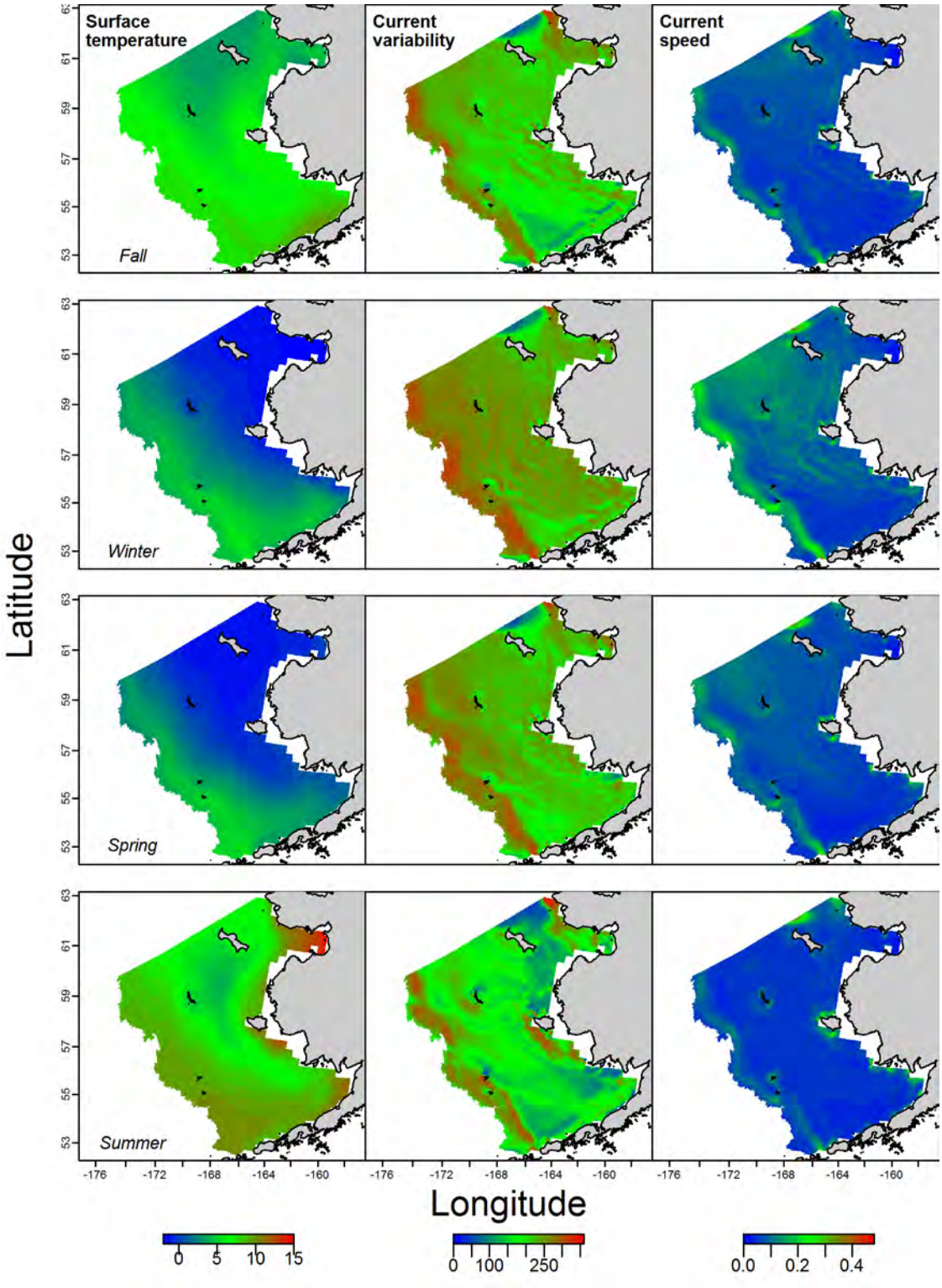

Figure 3. Seasonal habitat covariate rasters from FOCI ichthyoplankton surveys of early life history stages of fishes in the eastern Bering Sea.

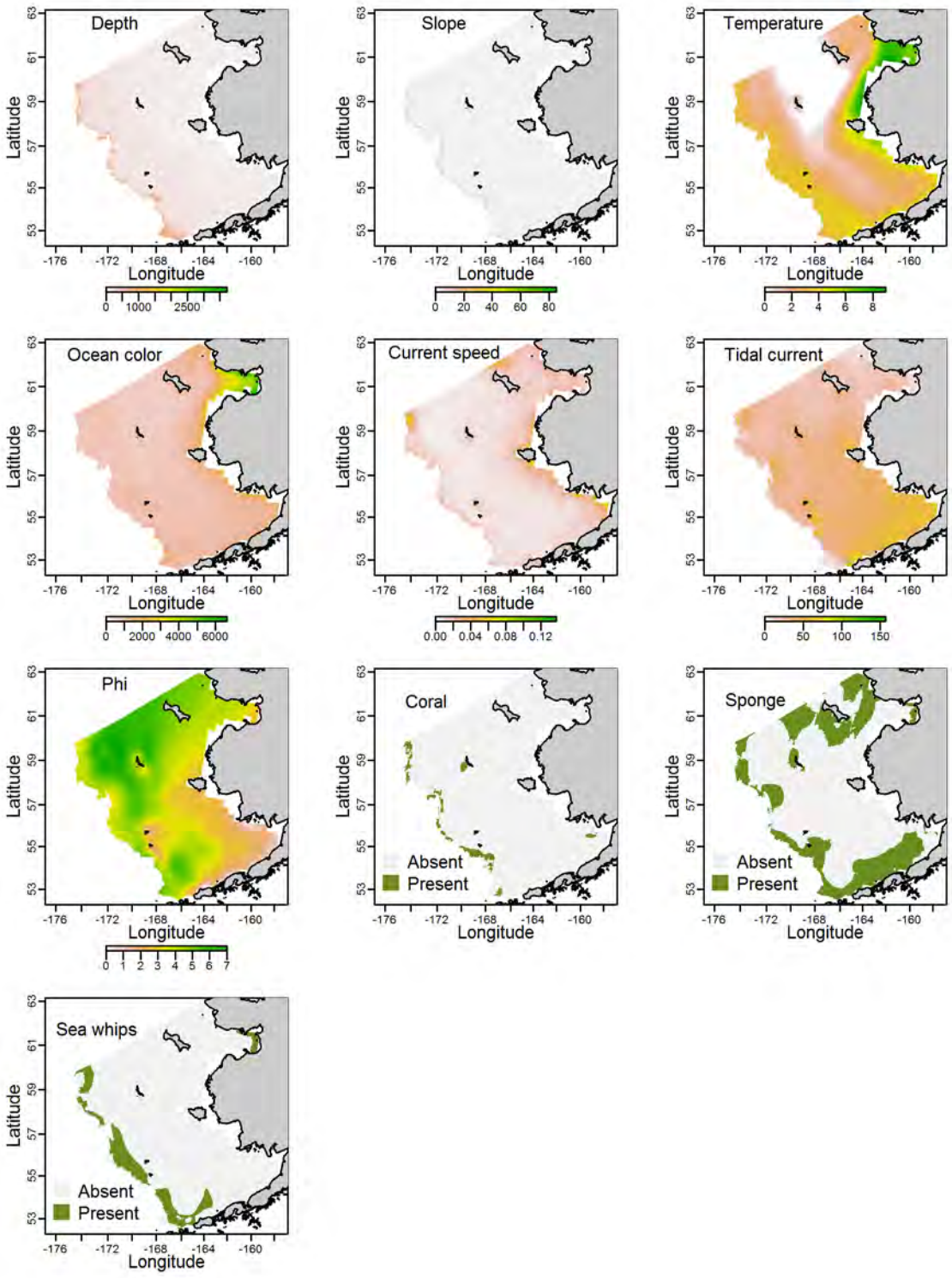

Figure 4. -- Habitat covariate rasters used to parameterize species distribution models in the eastern Bering Sea.

Table 5. Variables used in modeling the distributions of fishes and invertebrates in the eastern Bering Sea.

Variable	Unit	Definition	Interpolation method	Source	
Position	eastings, northings	Latitude and longitude of bottom trawl hauls in Alaska Albers projection corrected for the position of the trawl net relative to the vessel	--	DGPS collected at bottom trawl hauls	
Depth	m	Bathymetry of the seafloor based on digitized and position corrected NOS charts	Linear interpolation	Mean depth of bottom trawl hauls (modeling), Zimmermann, M, unpublished data (prediction)	
Slope	percent	Maximum difference between a depth measurement and its adjoining cells	--	Zimmermann, M, unpublished data	
Bottom temperature	°C	Mean summer bottom temperature for the region measured during bottom trawl surveys from 1996-2010	Ordinary kriging	Temperature data collected at bottom trawl hauls	
Surface temperature	°C	Ocean current speed predicted from the ROMS model during the years 1970-2004 and averaged on a 10 km by 10 km grid	Inverse distance weighting	Danielson et al. 2011	1
Ocean color	$Carbon*m^{-2}*day^{-1}$	Net primary production in surface waters in May to September averaged by 1080 by 2160 grid cells then averaged across years (2002-2011)	Inverse distance weighting	Behrenfeld and Falkowski 1997	
Mean bottom ocean current	$m*sec^{-1}$	Seafloor ocean current speed predicted from the ROMS model during the years 1970-2004 and averaged on a 10 km by 10 km grid	Inverse distance weighting	Danielson et al. 2011	
Maximum tidal current	$cm*sec^{-1}$	Maximum of the predicted tidal current at each bottom trawl location over a 1-year cycle	Ordinary kriging	Egbert and Erofeeva 2000	
Mean surface ocean current speed	$m*sec^{-1}$	Surface ocean current speed predicted from the ROMS model during the years 1970-2004 and averaged on a 10 km by 10 km grid	Inverse distance weighting	Danielson et al. 2011	1
Mean surface ocean current direction	angle	Surface ocean current direction predicted from the ROMS model during the years 1970-2004 and averaged on a 10 km by 10 km grid	Inverse distance weighting	Danielson et al. 2011	1
Surface ocean current direction variability	--	Variability in surface ocean current direction predicted from the ROMS model during the years 1970-2004 and averaged on a 10 km by 10 km grid	Inverse distance weighting	Danielson et al. 2011	1
Sediment grain size (phi)	--	Sediment grain size derived from historical bottom sampling in the eastern Bering Sea compiled in the EBSSED database	Ordinary kriging	Smith and McConnaughey 2000	
Coral presence or absence	--	Coral presence or absence in bottom trawl catch and raster of predicted presence or absence of coral	--	Catch data from bottom trawl hauls (modeling), Rooper et al. (in review) (prediction)	2
Sponge presence or absence	--	Sponge presence or absence in bottom trawl catch and raster of predicted presence or absence of Sponge	--	Catch data from bottom trawl hauls (modeling), Rooper et al. (in review) (prediction)	2
Pennatulacean presence or absence	--	Pennatulacean presence or absence in bottom trawl catch and raster of predicted presence or absence of Pennatulacean	--	Catch data from bottom trawl hauls (modeling), Rooper et al. (in review) (prediction)	2
[1] Used to model egg, larval and early juvenile stages only					
[2] Used to model bottom trawl survey data only					

Table 6. Cross-correlations among explanatory variables and variance inflation factors for eastern Bering Sea data.

Variable	Variance Inflation Factor (Trawl survey data)	Variance Inflation Factor (CIA data)	Fall Variance Inflation Factor (FOCI data)	Winter Variance Inflation Factor (FOCI data)	Spring Variance Inflation Factor (FOCI data)	Summer Variance Inflation Factor (FOCI data)
Depth	2.98	2.80	3.02	2.95	2.98	2.85
Slope	2.16	2.14	1.95	1.97	1.95	1.93
Temperature	1.61	1.60				
Ocean color	1.75	1.75	1.29	1.24	1.23	1.53
Current speed	1.60	1.58				
Tidal current	3.49	3.45	2.53	2.08	2.06	2.02
Phi	3.13	3.05				
Coral	1.11					
Sponge	1.16					
Sea whips	1.05					
Surface temperature			1.70	1.27	1.34	1.64
Surface current speed			1.85	2.19	1.86	1.35
Surface current variability			2.08	2.06	2.14	1.61

Modeling Methods – Recruitment processes data

The maximum entropy (MaxEnt) modeling method was used for estimating species distribution for early life history stages in the ECODAAT database (Phillips et al. 2006, Elith et al. 2011). It was implemented in R software using the *dismo* package[4]. MaxEnt models use only presence observations and are based on raster grids of explanatory variables (habitat variables) and point observations of presence. The MaxEnt model predicts the probability of suitable habitat based on habitat related variables (i.e. given the depth, temperature, slope, and current speed at each grid cell – what is the probability that this is suitable for a yellowfin sole?) and not probability of presence. Note that geographic location is implicit in the results from MaxEnt models.

Modeling Methods – Bottom trawl survey data

Three types of distribution modeling were used for the bottom trawl survey data based on the prevalence of each species in the overall catch. For species that occurred in > 30% of bottom trawl hauls, such as arrowtooth flounder (Table 3), a standard Generalized Additive Modeling (GAM) method was used to produce maps of predicted density. Generalized additive models (Hastie and Tibshirani 1990) applied with the *mgcv* package[5] were used to predict the dependent variables from the suite of untransformed habitat variables. In each case, the basis degrees of freedom used in the smoothing function were limited to ≤ 4 for univariate variables and ≤ 30 for the bivariate term (geographic location). Insignificant terms were sequentially removed. In this case model, terms were removed until the Akiake Information Criterion (AIC) was minimized (Wood 2006). For each species, the model with the lowest AIC score was deemed the best fitting model and used for further prediction and model validation. For the standard GAM's, the CPUE was fourth-root transformed prior to analyses. For species where frequency of occurrence was between 10% and 30%, a hurdle model (hGAM) was used (Cragg 1971, Potts and Elith

[4] R, v3.0.1; Hijams, R.J., S. Phillips, J. Leathwick, and J. Elith. 2014. Species distribution modeling: package 'dismo' version 1.0-5. 65 pages.
[5] R, v3.0.1; Wood, S. 2014. Mixed GAM computation vehicle with GCV/AIC/REML smoothness estimation: package 'mgcv' version 1.8-4. 243 pages.

2006) to predict spatial distribution of fishes and crabs (Table 3). Hurdle models predict the spatial distribution of abundance in three stages: 1) probability of presence is predicted from presence-absence data using a GAM and binomial distribution for each species; 2) a threshold presence probability is determined that defines presence or absence of the species; and 3) a conditional GAM is constructed that predicts a species' abundance by modeling the fourth-root transformed CPUE data from the bottom trawl survey at locations where the probability of presence was predicted to meet or exceed the threshold established in step 2 above. As was done for the standard GAM's above, the number of inflection points were limited and insignificant terms were sequentially removed to determine the best-fitting model. For species with < 10% frequency of occurrence, but > 50 presence observations, or where data were treated as presence only (i.e., ichthyoplankton survey and commercial catch observer data), the MaxEnt methodology was used to develop suitable habitat models.

For all species distribution models, separate training (80%) and testing (20%) data sets were randomly selected from the data. The training and testing data sets were selected before modeling began and remained the same for species analysis of each data class. The larger (80%) segment of data was used to train the model of choice while the remaining 20% was used to test and validate the model fit.

Modeling Methods – Commercial catch (observer) data

The maximum entropy (MaxEnt) modeling method was used for estimating species distribution for commercial catch data in the CIA database (Phillips et al. 2006, Elith et al. 2011). It was implemented in R software (R Core Development Team, 2013) using the *dismo* package. MaxEnt models use only presence observations and are based on raster grids of explanatory variables (habitat variables) and point observations of presence. As with the other models, separate training (80%) and testing (20%) data were randomly selected for MaxEnt model developed in order to assess model performance.

Modeling Methods – Model validation

To test the performance of the best-fitting models, the predictions were compared to the observations. For presence and presence-absence models the area under the curve (AUC) was computed to judge model performance. The AUC calculates the probability that a randomly chosen presence observation would have a higher probability of presence than a randomly chosen absence observation using rank data. We used the scale of Hosmer and Lemeshow (2005)**,** where AUC value > 0.5 is estimated to be better than chance, a value > 0.7 is considered acceptable, and values > 0.8 and 0.9 are excellent and outstanding. Confidence intervals for the AUC (95%) were calculated according to the methodology of DeLong et al. (1988). For abundance models the performance was directly tested by correlating the predictions with the observations. Model testing was also performed on the 20% of the data withheld at random, using the same metrics. Because of space limitations, figures showing the model validation results are generally not shown. Where appropriate, deviations from model assumptions or models with very poor predictive ability relative to the testing data are highlighted. Where these occur, the results of the modeling may not be robust.

Modeling Methods – Essential Fish Habitat Maps

Maps of essential fish habitat based on model predictions were developed for each species and life history stage. These maps were produced as population quantiles from predictions of the distribution of suitable habitat (for species where maximum entropy modeling was used) or predictions of the distribution of abundance (for species where CPUE was modeled using either a GAM or hGAM). For each map of model predictions 300,000 points were randomly sampled from the raster surface. These values were then ordered by cumulative distribution and zero

abundance values were removed. Four population quantiles were selected from these cumulative distributions (5%, 25%, 50% and 75%). These quantiles were then used as break points to translate the model predictions (maps of suitable habitat or abundance) to map the distribution of categories of the amount of the species abundance or suitable habitat. For example, if the 5% quantile of species A was 0.024 individuals/ha, this meant that 95% of the population occurred at values higher than 0.024. Similarly, a 75% quantile of species A at 2.1 individuals/ha meant that values above 2.1 represented the top 25% of the population proportion, or the predicted highest abundance areas. The four categories for each species, life history stage, and season were mapped to show the distribution of the areas containing 95%, 75%, 50% and 25% of the population. It is important to note that these values were chosen somewhat arbitrarily (except 95% which is the current definition of EFH in Alaska), and other values could be equally appropriate.

RESULTS

Flatfishes

Atheresthes spp.

Arrowtooth flounder (*Atheresthes stomias*) eggs, larvae, and early juveniles cannot be distinguished from those of the other species in the genus, Kamchatka flounder (*A. evermanni*). Consequently, models and results for early life history stages of the genus *Atheresthes* are presented in composite.

Seasonal distribution of *Atheresthes* spp. early life history stages from EcoFOCI ichthyoplankton surveys of the Eastern Bering Sea -- There were 50 occurrences of *Atheresthes* spp. eggs reported from EcoFOCI ichthyoplankton surveys of the Eastern Bering Sea (Figure 5); 45 in the winter and 5 in the spring. All observations, except one, were reported from near the Bering Canyon.

Atheresthes spp. larvae were collected on EcoFOCI ichthyoplankton surveys in winter, spring, and summer months (Figure 6). They occurred in the Northern Bering Sea, across the middle and outer shelf, and along the Alaska Peninsula. There were insufficient records of *Atheresthes* spp. larvae from the winter surveys to model their distribution in this season.

Maximum entropy model predictions of suitable larval *Atheresthes* spp. habitat differed between spring and summer (Figure 7). In the spring, suitable habitat extended from the Bering Canyon northward to around Pribilof Canyon and eastward onto the middle shelf. It extended further onto the shelf and further north during summer months. The most important variable for modeling larval *Atheresthes* spp. suitable habitat distribution was sea surface temperature (relative importance = 67.7% in spring and 54.9% in summer). Additionally bottom depth was important in spring (20.6%) and ocean productivity was important in summer (18.7%). For both the spring and summer models, the model fits were outstanding to the training data (AUC $\geq$ 0.95) and excellent to the testing data (AUC $\geq$ 0.80) validating the model. The

percent of cases correctly classified was high in both seasons (≥ 86% for the training data and ≥ 80% for the test data).

Early juvenile stages of *Atheresthes* spp. were observed at only 13 EcoFOCI ichthyoplankton survey stations (Figure 8). All of these occurrences were during summer months and most were near the Pribilof Islands. There were not enough incidences of early juvenile *Atheresthes* spp. to parameterize a distribution model for this life stage.

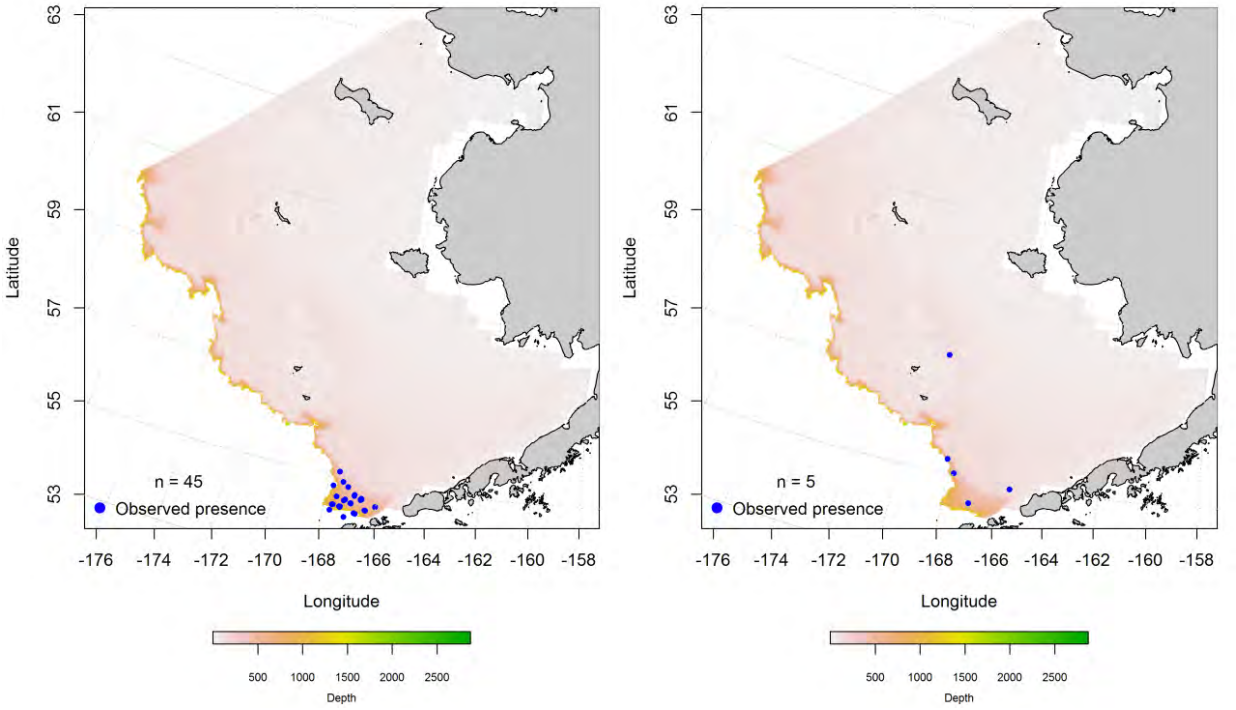

Figure 5. -- Winter and spring observations (left and right panel) of *Atheresthes* spp. eggs from EcoFOCI ichthyoplankton surveys of the Eastern Bering Sea.

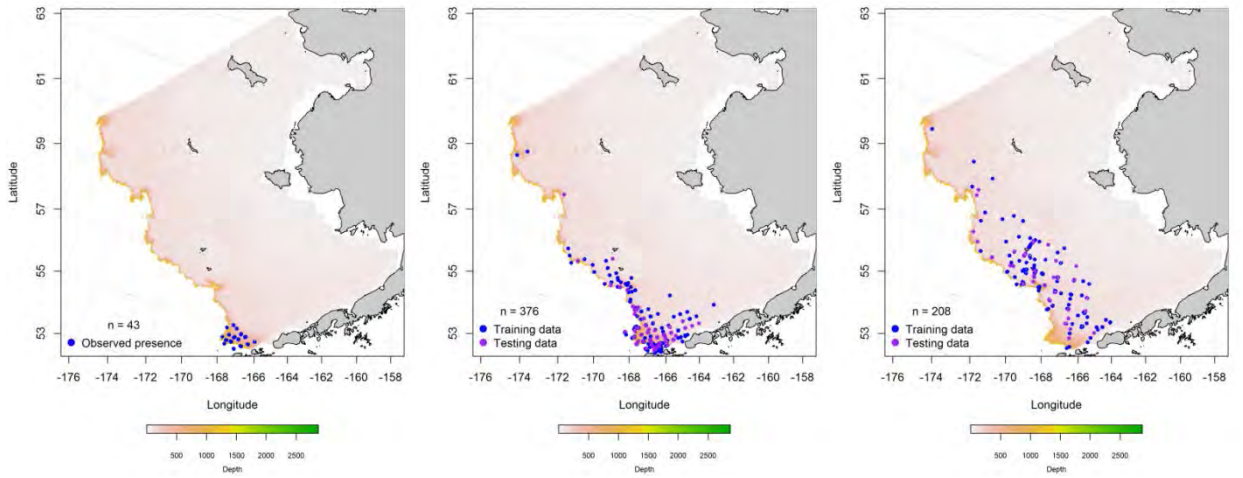

Figure 6. -- Winter, spring, and summer observations (left, middle, and right panel, respectively) of larval *Atheresthes* spp. from EcoFOCI ichthyoplankton surveys of the Eastern Bering Sea.

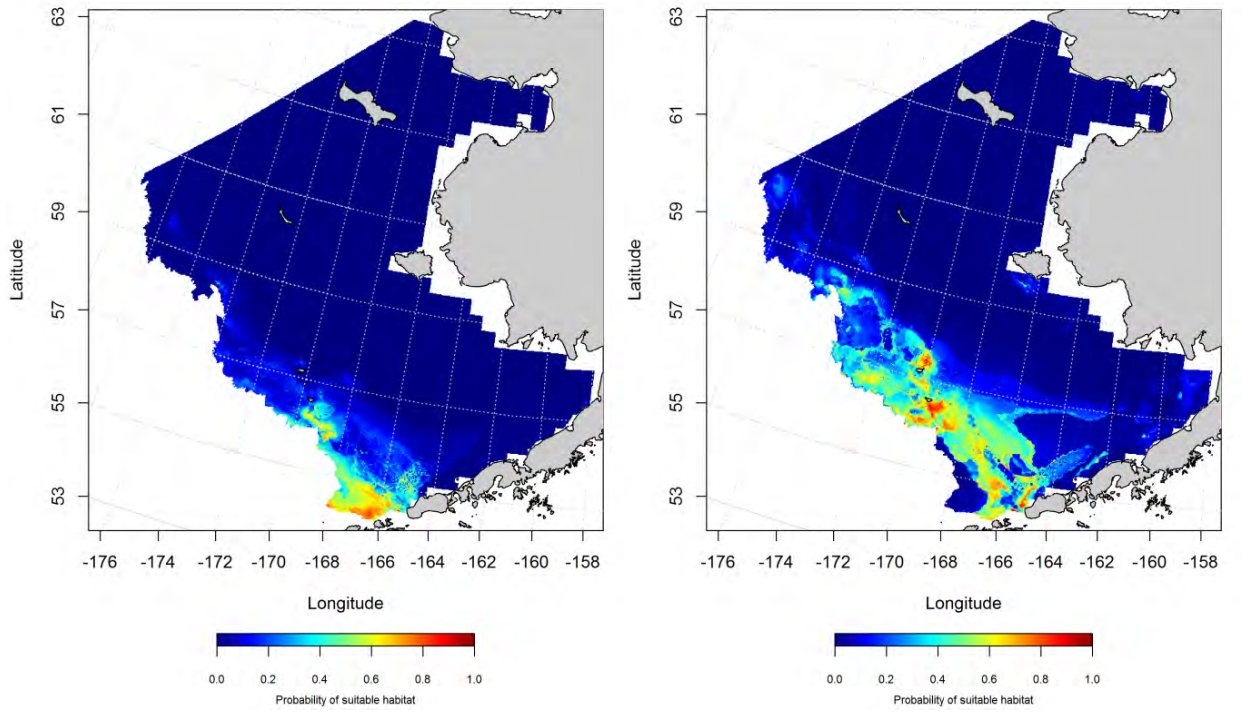

Figure 7. -- Probability of suitable larval *Atheresthes* spp. spring and summer habitat (left and right panel) predicted from MaxEnt modeling of presence in EcoFOCI ichthyoplankton surveys of the Eastern Bering Sea.

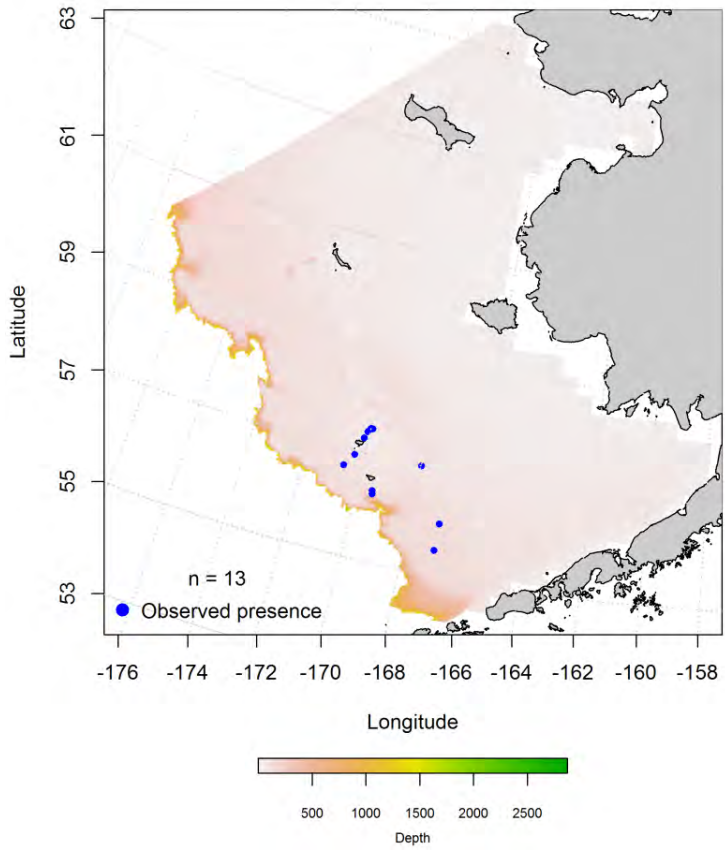

Figure 8. -- Summer catches of early juvenile *Atheresthes* spp. from EcoFOCI ichthyoplankton surveys of the Eastern Bering Sea.

Essential early life history habitat maps and conclusions for Eastern Bering Sea

***Atheresthes* spp. --** Essential larval *Atheresthes* spp. habitat differed between spring and summer months (Figure 9). The habitat in spring crosses the central and southern domains of the Eastern Bering Sea shelf and slope. In summer, the essential habitat extends farther northward along the outer shelf and slope and eastward along the Alaska Peninsula onto the inner shelf. There were not enough incidences of *Atheresthes* spp. eggs or early juveniles from the Eastern Bering Sea to model essential habitat for these life stages.

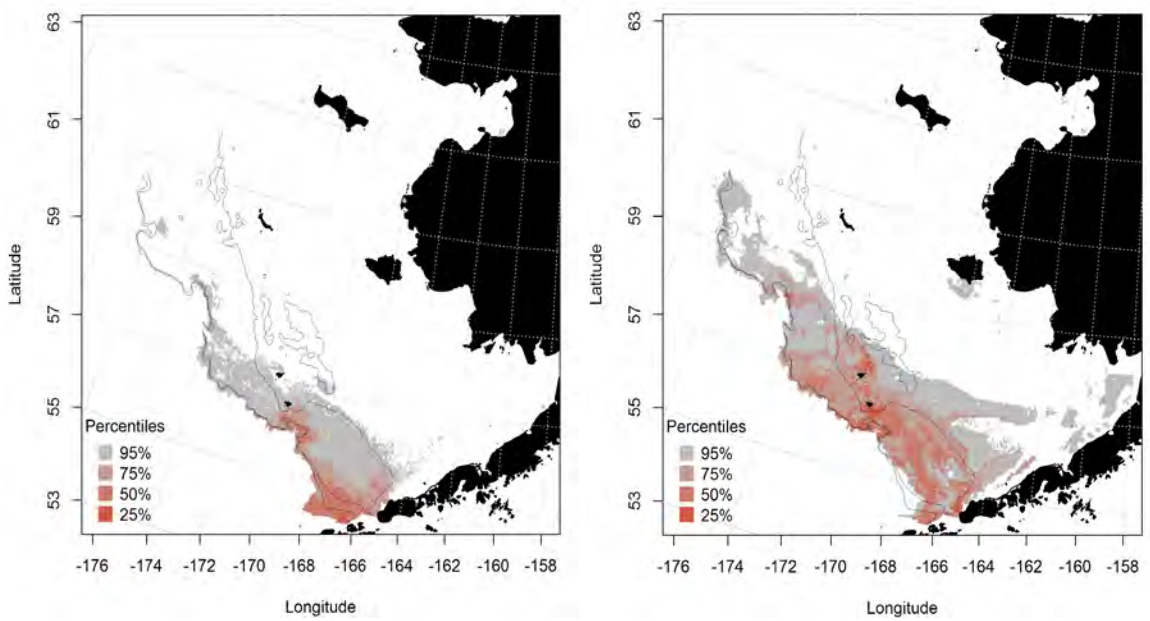

Figure 9. -- Spring and summer essential larval *Atheresthes* spp. habitat (right and left panel) predicted from EcoFOCI ichthyoplankton surveys of the Eastern Bering Sea.

arrowtooth flounder (*Atheresthes stomias*)

Arrowtooth flounder are widely distributed throughout Alaska. They are the flatfish species with the highest biomass in AFSC RACE bottom trawl surveys of the Eastern Bering Sea shelf and slope (Hoff 2012, Lauth and Conner 2014).

Summertime distribution of late juvenile and adult *Atheresthes stomias* from RACE bottom trawl surveys of the Eastern Bering Sea -- Arrowtooth flounder are broadly distributed across the RACE Eastern Bering Sea bottom trawl survey area (Figure 10). They are not common in waters shallower than 50 m. Late juvenile and adult life stages co-occur throughout their range.

Generalized additive models predicting the abundance of late juvenile arrowtooth flounder explained 68.1% of the deviance in the bottom trawl CPUE data. Geographical location, bottom depth, and bottom temperature were the most significant variables explaining their distribution. Model effects were highest

in the southern domain of the Eastern Bering Sea, increased with increasing bottom temperature, and decreased with increasing bottom depth. The correlation coefficient of the model for both the training and test data sets ($r^2 = 0.68$) indicates an acceptable fit and moderately successful model validation. The areas predicted to have the highest late juvenile arrowtooth flounder abundance were along the outer shelf edge from near Unimak Pass along the Alaska Peninsula to well north of the Pribilof Islands (Figure 11).

Adult arrowtooth flounder abundance was greatest over the outer shelf of the Eastern Bering Sea extending from the Bering Canyon in the southern domain to the northern extent of the survey area (Figure 12). The best-fitting GAM explained 73.1% of the deviance in bottom trawl CPUE estimates and showed that geographical location, bottom depth, and bottom temperature were the most important habitat covariates influencing adult arrowtooth abundance. The model fit to the training and test data was good ($r^2 = 0.73$).

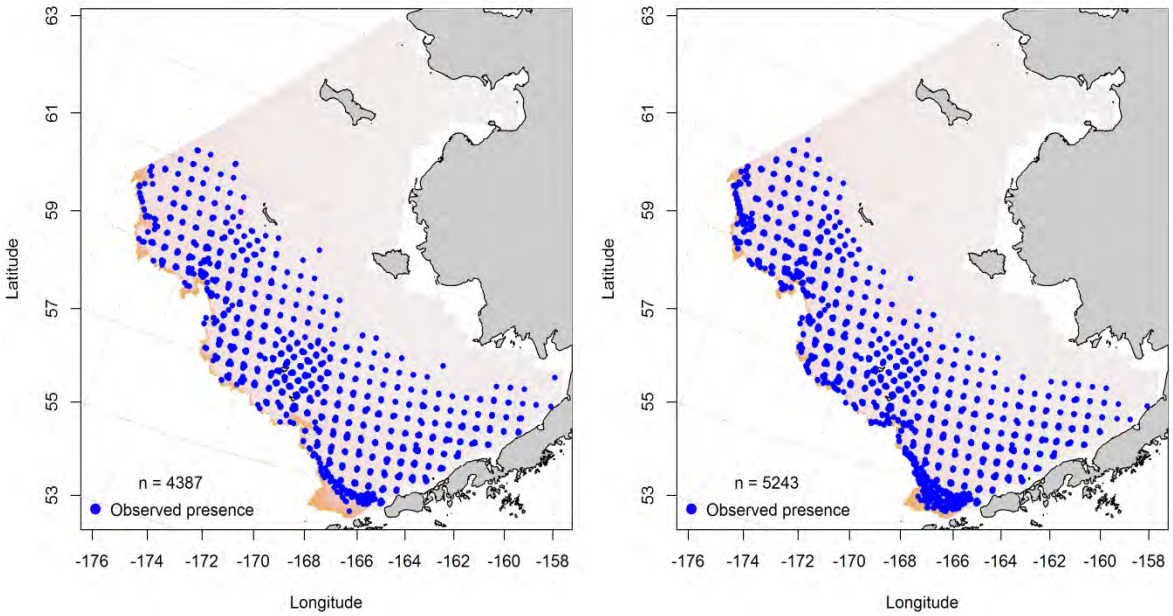

Figure 10. -- Distribution of late juvenile and adult arrowtooth flounder catches (left and right panels) in RACE summer bottom trawl surveys of the Eastern Bering Sea.

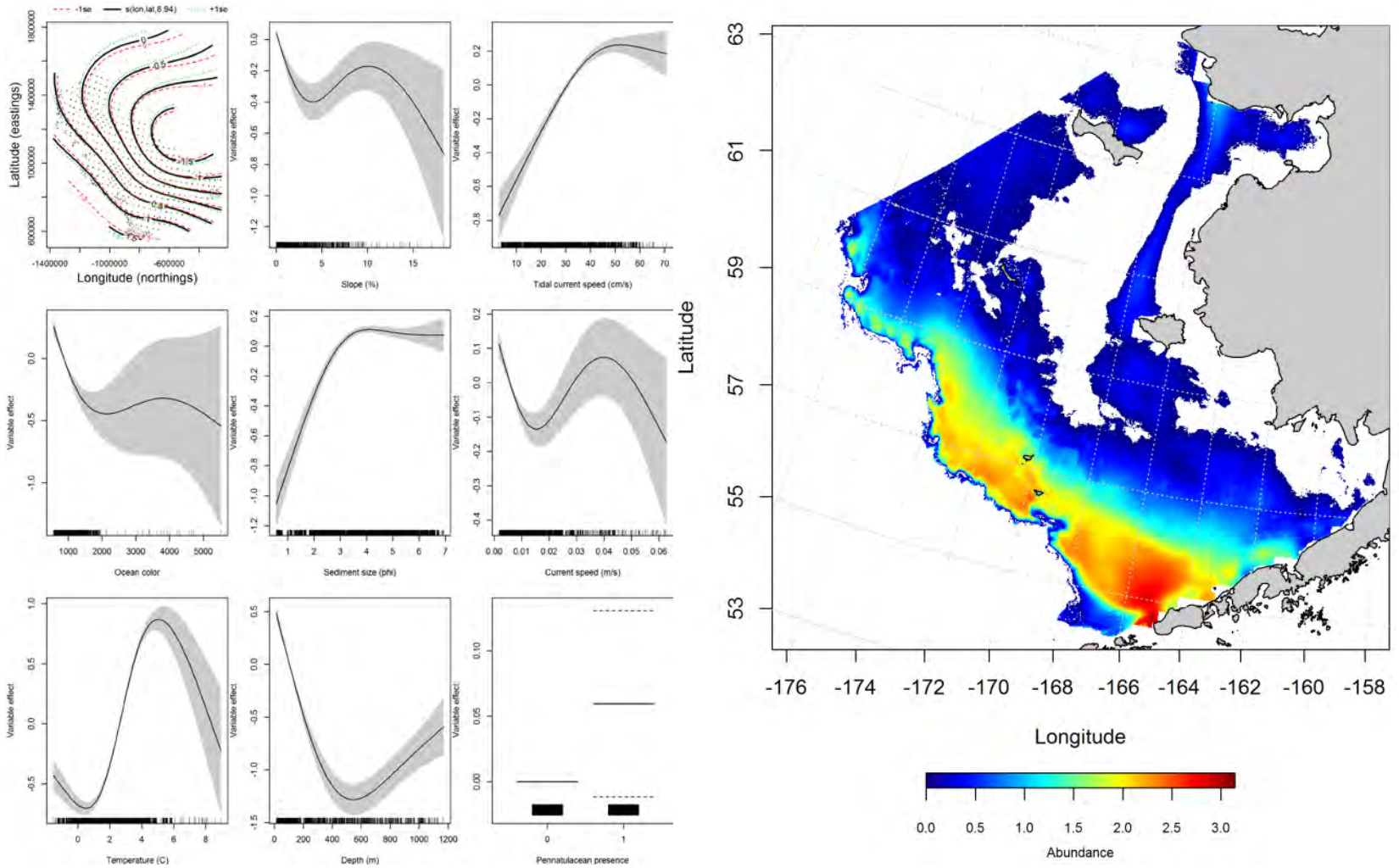

Figure 11. -- Effects of retained habitat covariates on the best-fitting generalized additive model (GAM; left panel) of late juvenile arrowtooth flounder abundance in RACE summer bottom trawl surveys of the Eastern Bering Sea Shelf, Slope, and Northern Bering Sea alongside their predicted abundance (right panel).

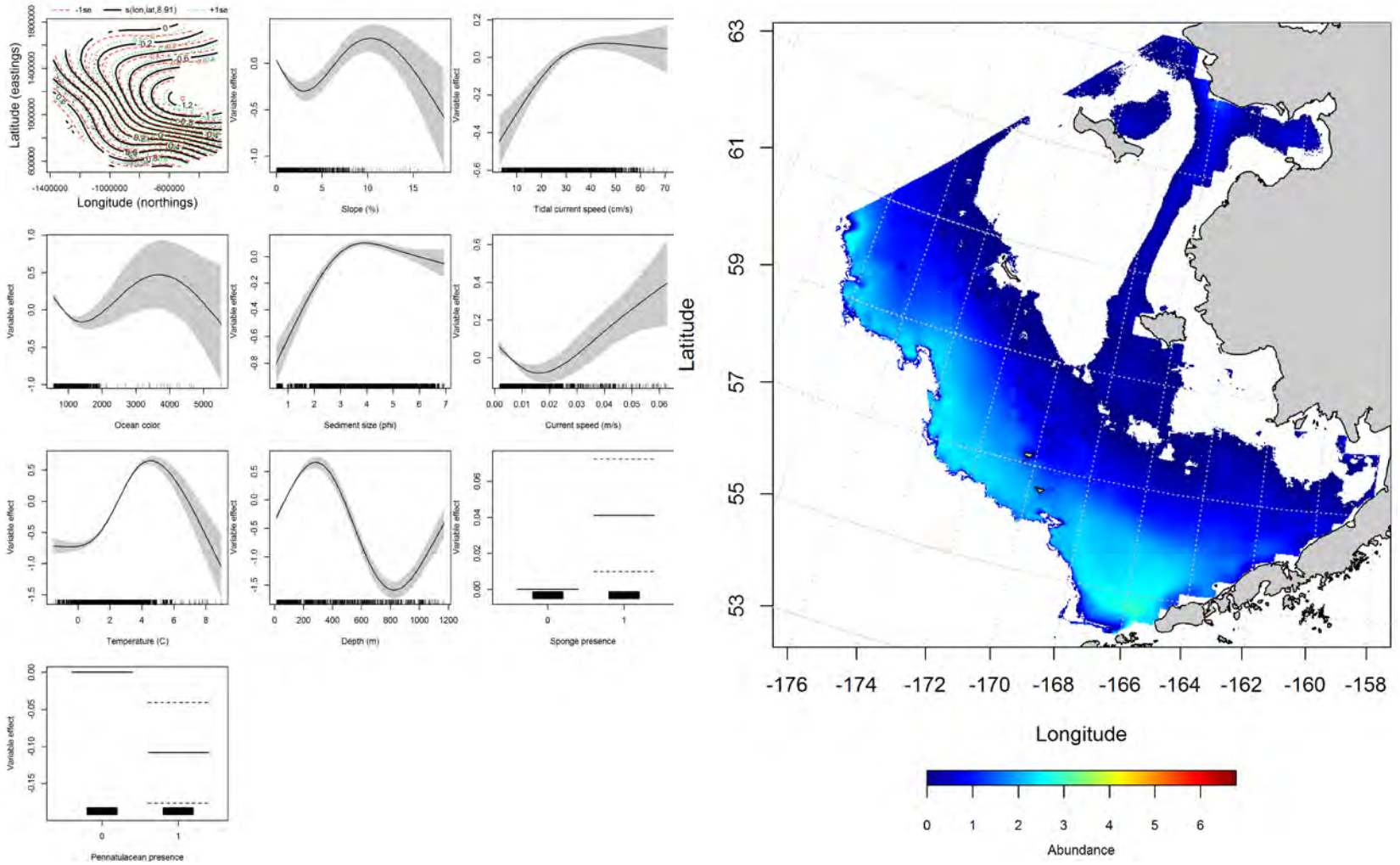

Figure 12. -- Effects of retained habitat covariates on the best-fitting generalized additive model (GAM; left panel) of adult arrowtooth flounder abundance in RACE summer bottom trawl surveys of the Eastern Bering Sea Shelf, Slope, and Northern Bering Sea alongside their predicted abundance (right panel).

Seasonal distribution of arrowtooth flounder in commercial fishery catches from the Eastern Bering Sea -- Arrowtooth flounder were not routinely distinguished in commercial catches from Kamchatka flounder until 2007 (Spies et al. 2014). Depth and bottom temperature were the dominant habitat covariates in the MaxEnt models predicting suitable arrowtooth flounder habitat from seasonal commercial fishery catches throughout the Eastern Bering Sea.

In fall, the distribution of suitable arrowtooth flounder habitat predicted from commercial catches extended over the outer and middle shelf of the Eastern Bering Sea from the Bering Canyon in the southern domain to the northern extent of the survey area (Figure 13). Depth and bottom temperature comprised 91.4% of the leverage of all habitat covariates in the model. The model fits to the training and test data were excellent (AUC = 0.88) and acceptable (AUC = 0.79); 79% of cases in both data sets were correctly classified by the model.

From winter commercial catches, the predicted distribution of suitable arrowtooth flounder habitat was similar to that in fall (i.e., over the outer shelf from Bering Canyon to the northern extent of the survey area) with an eastward extension of habitat into the southern half of Bristol Bay (Figure 14). Depth and bottom temperature provided 94.5% of the leverage of all habitat covariates in the model. The model fits to the training and test data were outstanding (AUC = 0.92) and excellent (AUC = 0.84); 84% of the cases in both data sets were correctly classified by the model.

Spring distribution of suitable arrowtooth flounder habitat predicted from commercial catches extended over the outer shelf and the middle shelf from the Bering Canyon in the southern domain of the Eastern Bering Sea to the northern extent of the survey area (Figure 15). Depth and bottom temperature comprised 85.9% of the leverage from habitat covariates in the model. The model fits to the training and test data were outstanding (AUC = 0.92) and excellent (AUC = 0.85). The model correctly classified 85% of predicted cases from both training and test data.

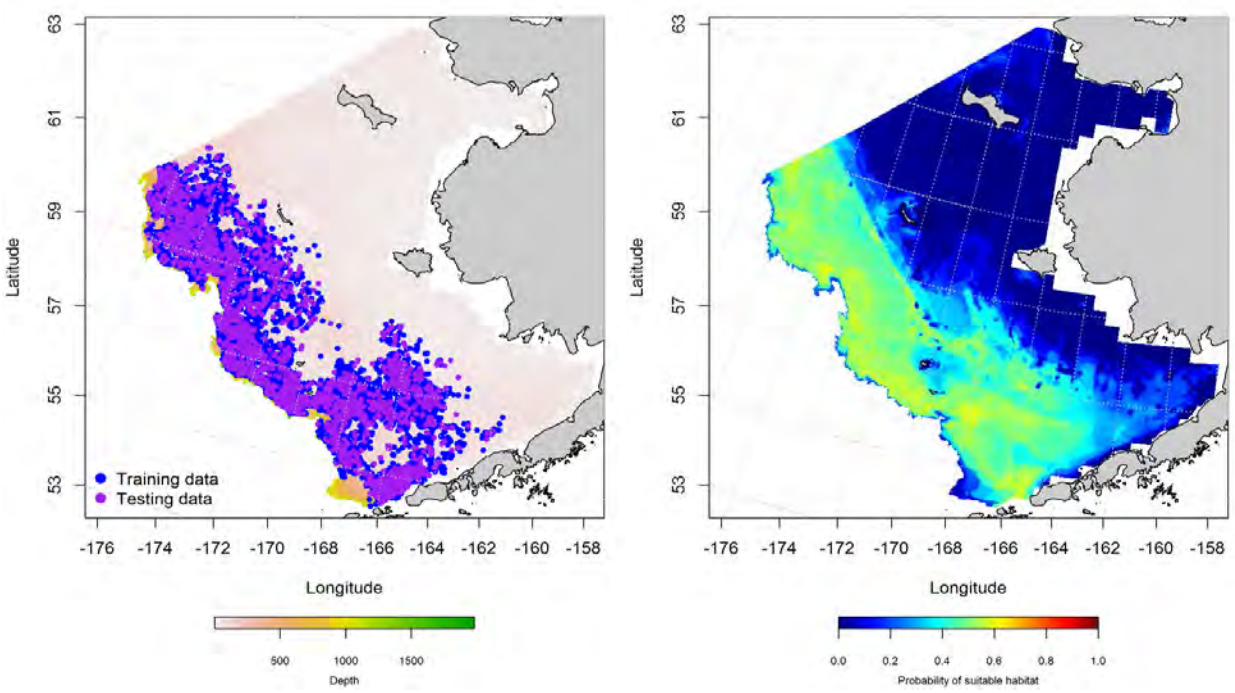

Figure 13. -- Locations of fall (October-November) catches of arrowtooth flounder in commercial fisheries of the Eastern Bering Sea (left panel). Blue points were used to train the MaxEnt model predicting the probability of suitable habitat (right panel) and the purple points were used to validate the model.

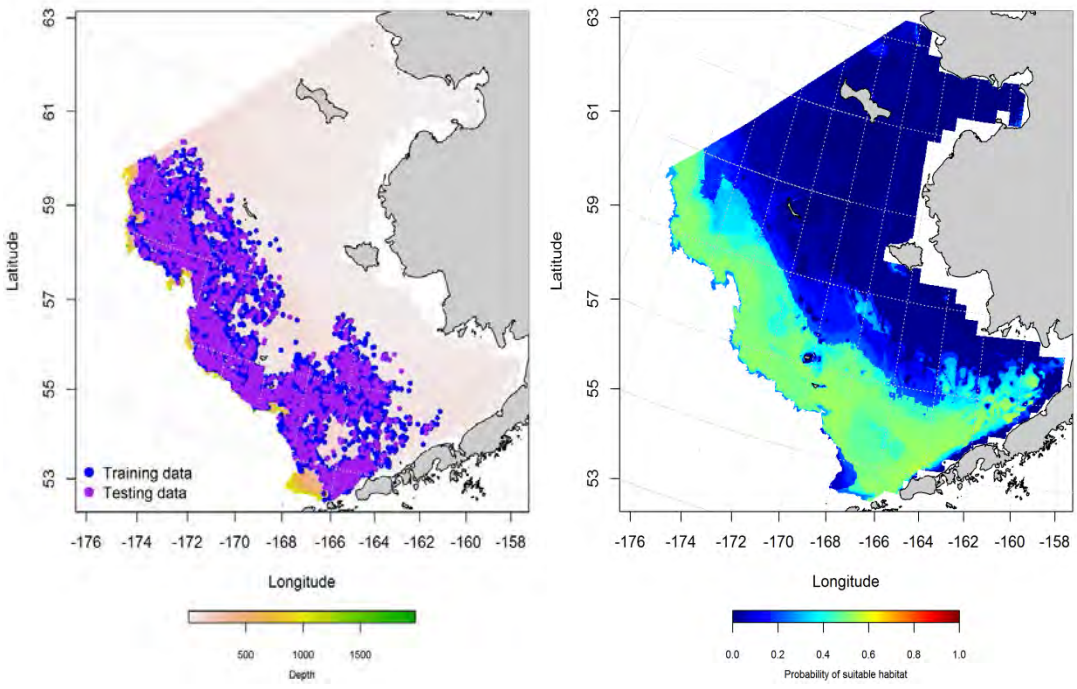

Figure 14. -- Locations of winter (December-February) catches of arrowtooth flounder in commercial fisheries of the Eastern Bering Sea (left panel). Blue points were used to train the MaxEnt model predicting the probability of suitable habitat (right panel) and the purple points were used to validate the model.

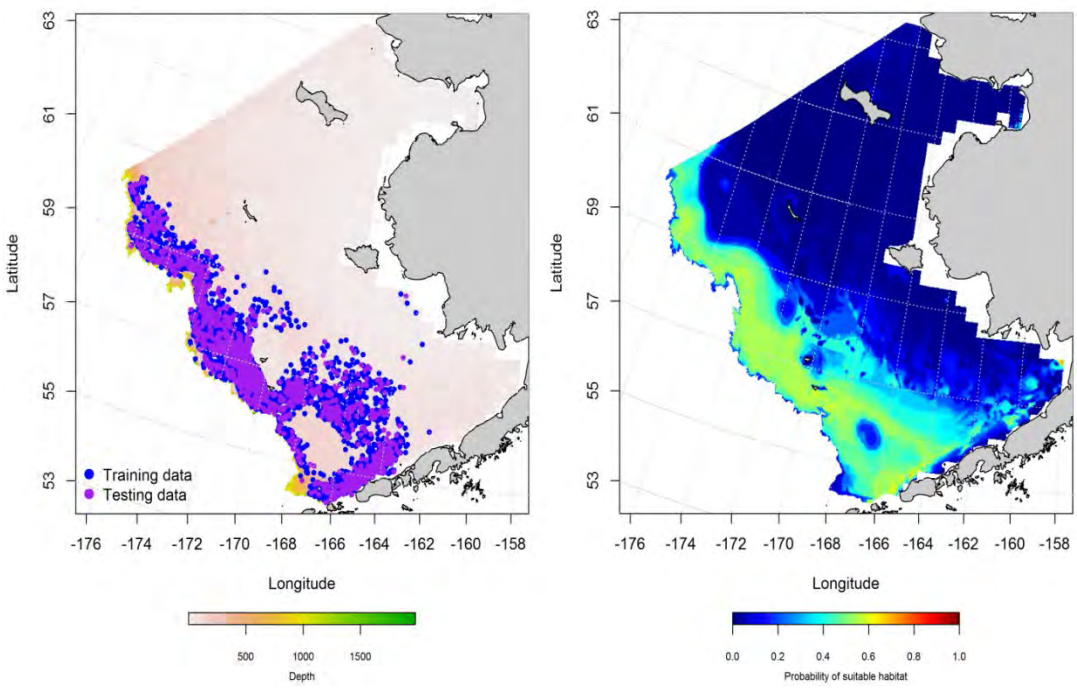

Figure 15. -- Locations of spring (March-May) catches of arrowtooth flounder in commercial fisheries of the Eastern Bering Sea (left panel). Blue points were used to train the MaxEnt model predicting the probability of suitable habitat (right panel) and the purple points were used to validate the model.

Eastern Bering Sea arrowtooth flounder (*Atheresthes stomias*) essential fish habitat maps and conclusions – Late juvenile and adult arrowtooth flounder EFH predicted from RACE summer bottom trawl surveys are very similar (Figure 16). The highest abundances of both life stages are predicted over the middle and outer shelf from Bristol Bay and the Bering Canyon in the southern domain to the northern extent of the survey area. The top 95% of abundance estimates for both life stages cover the majority of the RACE summer bottom trawl survey area.

Arrowtooth flounder EFH predicted from commercial fishery catches changed seasonally and, presumably, with fishing activity in the Eastern Bering Sea (Figure 17). The highest probabilities of suitable habitat showed the most seasonal variation. In fall and winter, more of these areas were found along the outer shelf. In winter, however, some of this high probability habitat extended into Bristol Bay. Overall, the shape of the distribution containing the top 95% of the most probable habitat predicted from commercial catches changed little between seasons.

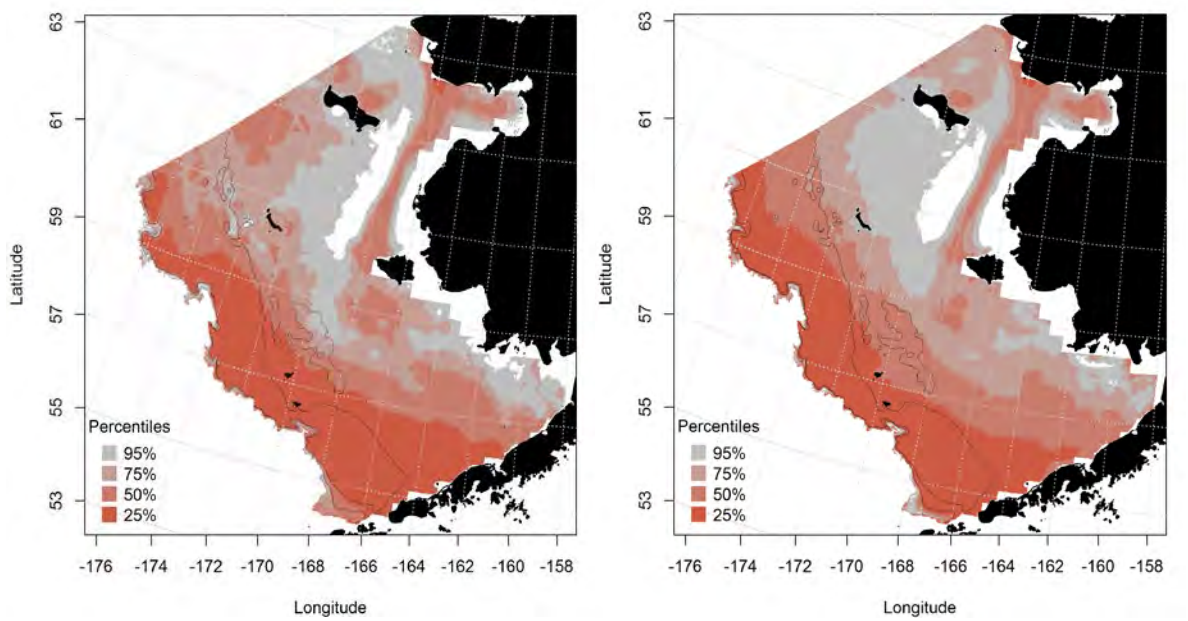

Figure 16. -- Essential arrowtooth flounder habitat predicted for late juveniles and adults (left and right panel) from RACE summertime bottom trawl surveys.

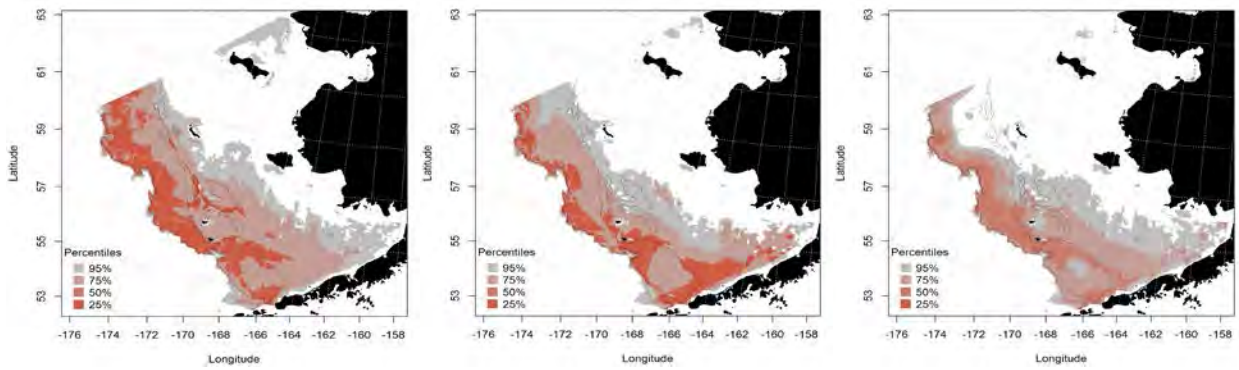

Figure 17. -- Essential arrowtooth flounder habitat predicted during fall (left panel), winter (middle panel), and spring (right panel) from commercial fishery catches.

Kamchatka flounder (*Atheresthes evermanni*)

Kamchatka and arrowtooth flounder are very similar in appearance. The two species were not consistently separated in survey trawl catches from the Eastern Bering Sea until around 1992. They were not routinely distinguished in commercial catches until 2007. Kamchatka flounder were managed as part of a complex with arrowtooth until 2010 when a directed fishery developed for them in the BSAI management area.

Summertime distribution of late juvenile and adult Kamchatka flounder from RACE bottom trawl surveys of the Eastern Bering Sea -- Catches of Kamchatka flounder in RACE summer bottom trawl surveys show that this species is distributed from the middle shelf on to the continental slope in all three domains of the Eastern Bering Sea (Figure 18). Catches of late juveniles were more widely distributed than adults during the summer with catches coming from well east into Bristol Bay.

The area with the highest predicted abundance of late juvenile Kamchatka flounder was near Unimak Pass in the southern domain of the Eastern Bering Sea (Figure 19). The best-fitting generalized additive model explained 60.9% of the deviance in late juvenile Kamchatka flounder CPUE from the bottom trawl survey. Depth, geographic location, and bottom temperature were the most important covariates predicting their abundance. Sea pens were also an important covariate in the model and higher juvenile abundance was predicted when they were present. Model effects increased in the southwest portion of the survey area and with increasing temperature and depth. The model fit to the training and test data was acceptable ($r^2 = 0.61$ for both data sets).

A hurdle GAM was used to describe the distribution and abundance of adult Kamchatka flounder in RACE summer bottom trawl survey catches. Adult Kamchatka flounder were predicted to occur with the highest probability during the summertime over benthypelagic waters (200 - 1000 m) off the Eastern Bering Sea shelf (Figure 20). The six habitat covariates retained in the model explained 46.4% of the deviance in the adult Kamchatka flounder distribution. The most important covariates leveraging the model were bottom depth, geographic location, and bottom temperature. Probability of encountering adult Kamchatka flounder increased with increasing bottom temperature and depth in the western portion of the Eastern Bering Sea survey area. This model was an outstanding fit to the training data (AUC = 0.92) and correctly classified 84% of presence-absence cases. Using the test data, the best-fitting model was validated with an outstanding fit (AUC = 0.92) and 83% of cases correctly classified.

Summertime adult Kamchatka flounder abundance was predicted from locations where the presence probability threshold established in the presence-absence GAM above (0.23) was exceeded. This

conditional abundance GAM explained 43.4% of the deviance in the CPUE data (Figure 21). Highest predicted abundances were in benthypelagic waters and over submarine canyons on the Eastern Bering Sea Slope. The most important of the 8 habitat covariates retained in the model were bottom depth, geographical location, and coral presence. This GAM fit to the training data ($r^2 = 0.43$) and test data ($r^2 = 0.41$) was poor.

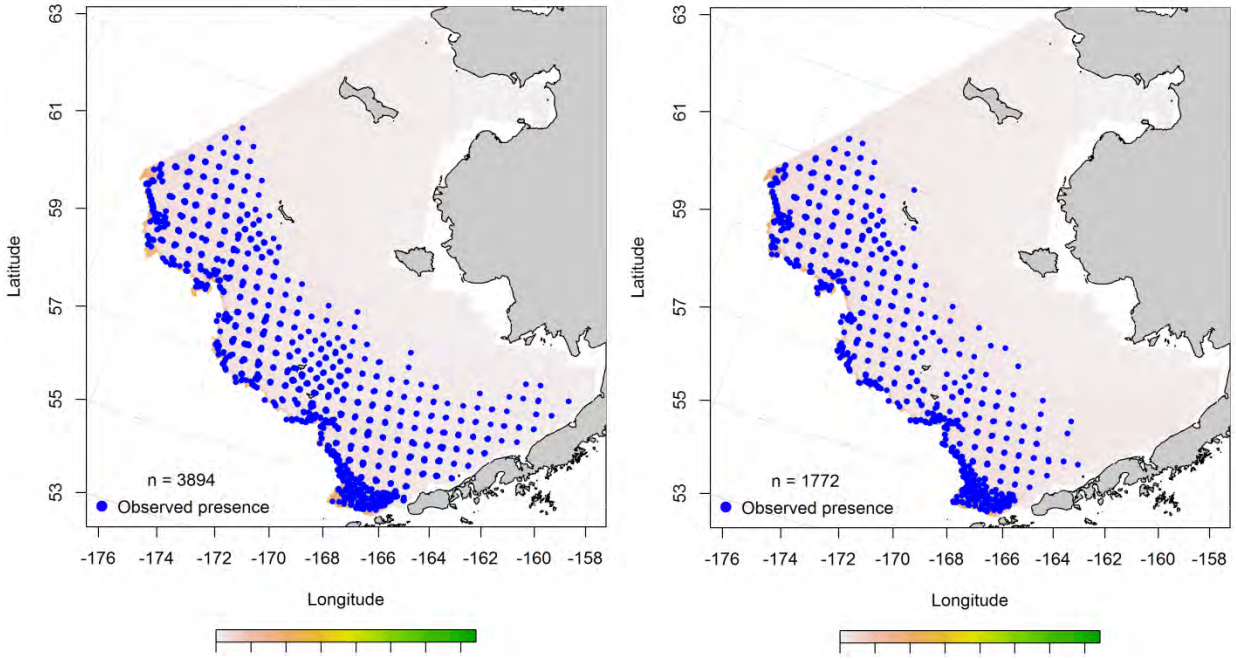

Figure 18. -- Distribution of late juvenile and adult Kamchatka flounder catches (left and right panels) in RACE summer bottom trawl surveys of the Eastern Bering Sea.

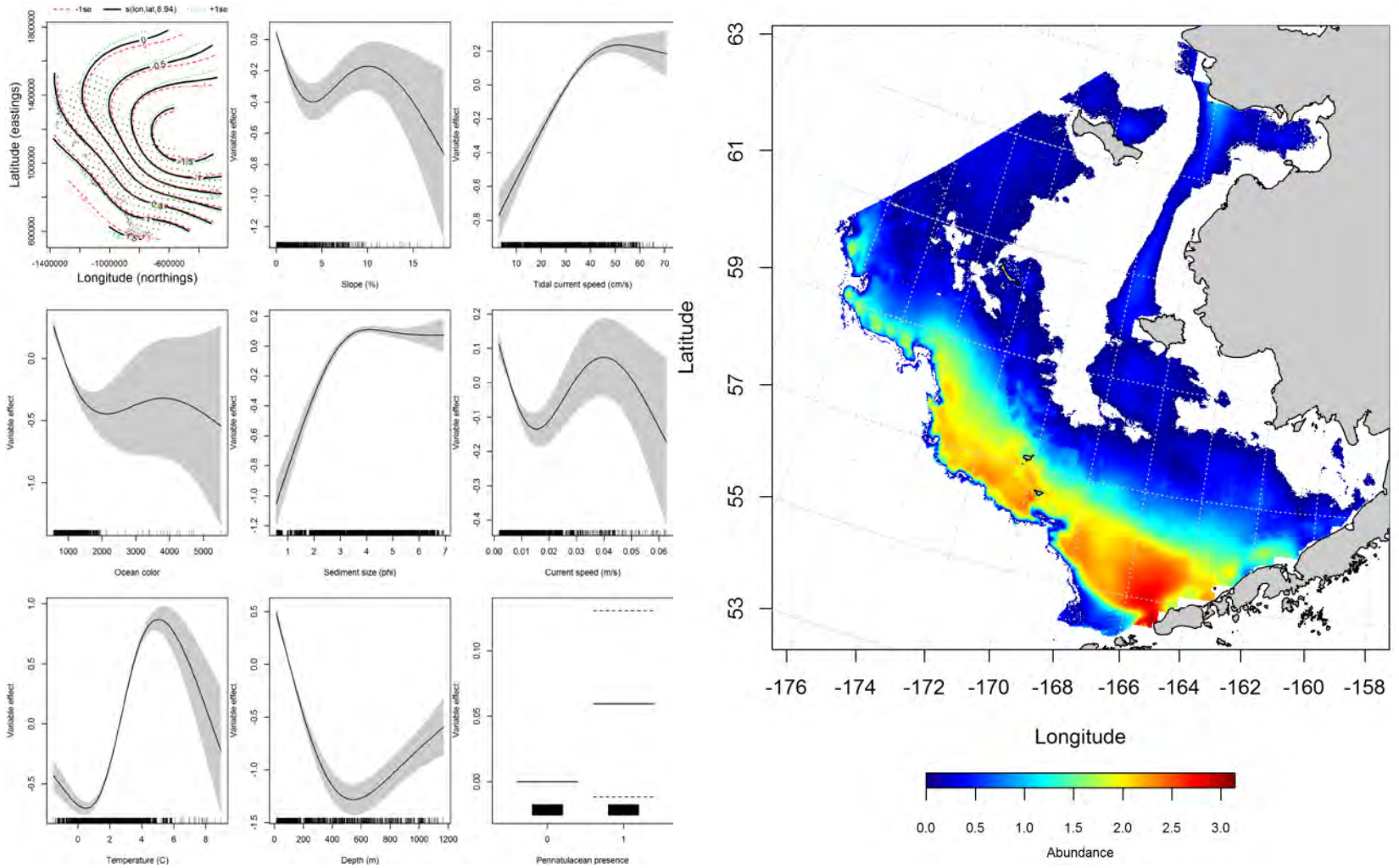

Figure 19. -- Effects of retained habitat covariates on the best-fitting generalized additive model (GAM; left panel) of late juvenile Kamchatka flounder abundance from RACE summer bottom trawl surveys of the Eastern Bering Sea Shelf, Slope, and Northern Bering Sea alongside their predicted abundance (right panel).

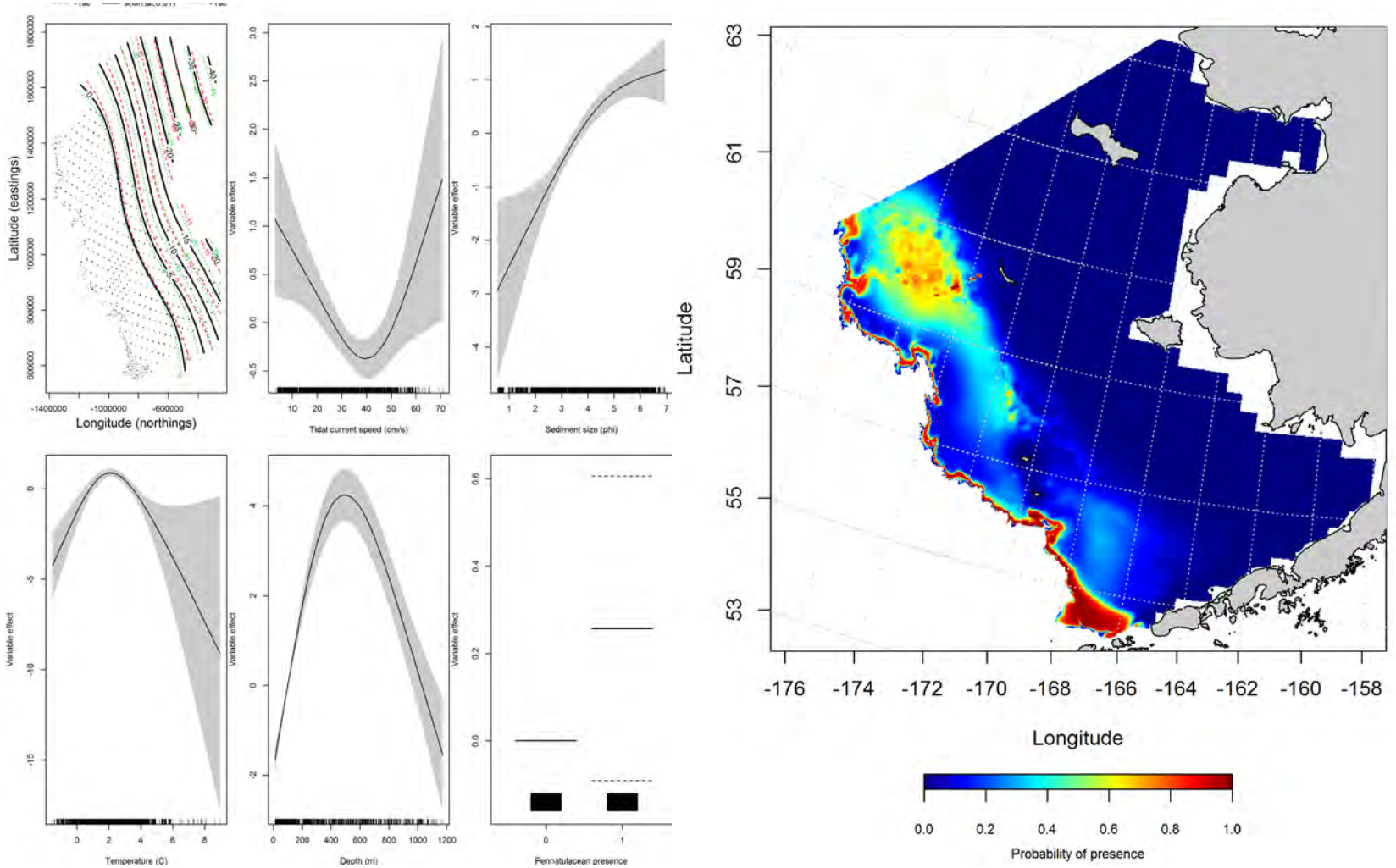

Figure 20. -- Effects of retained habitat covariates on the best-fitting generalized additive presence-absence model (GAM) of adult Kamchatka flounder from RACE summer bottom trawl surveys of the Eastern Bering Sea Shelf, Slope, and Northern Bering Sea alongside their predicted presence (right panel).

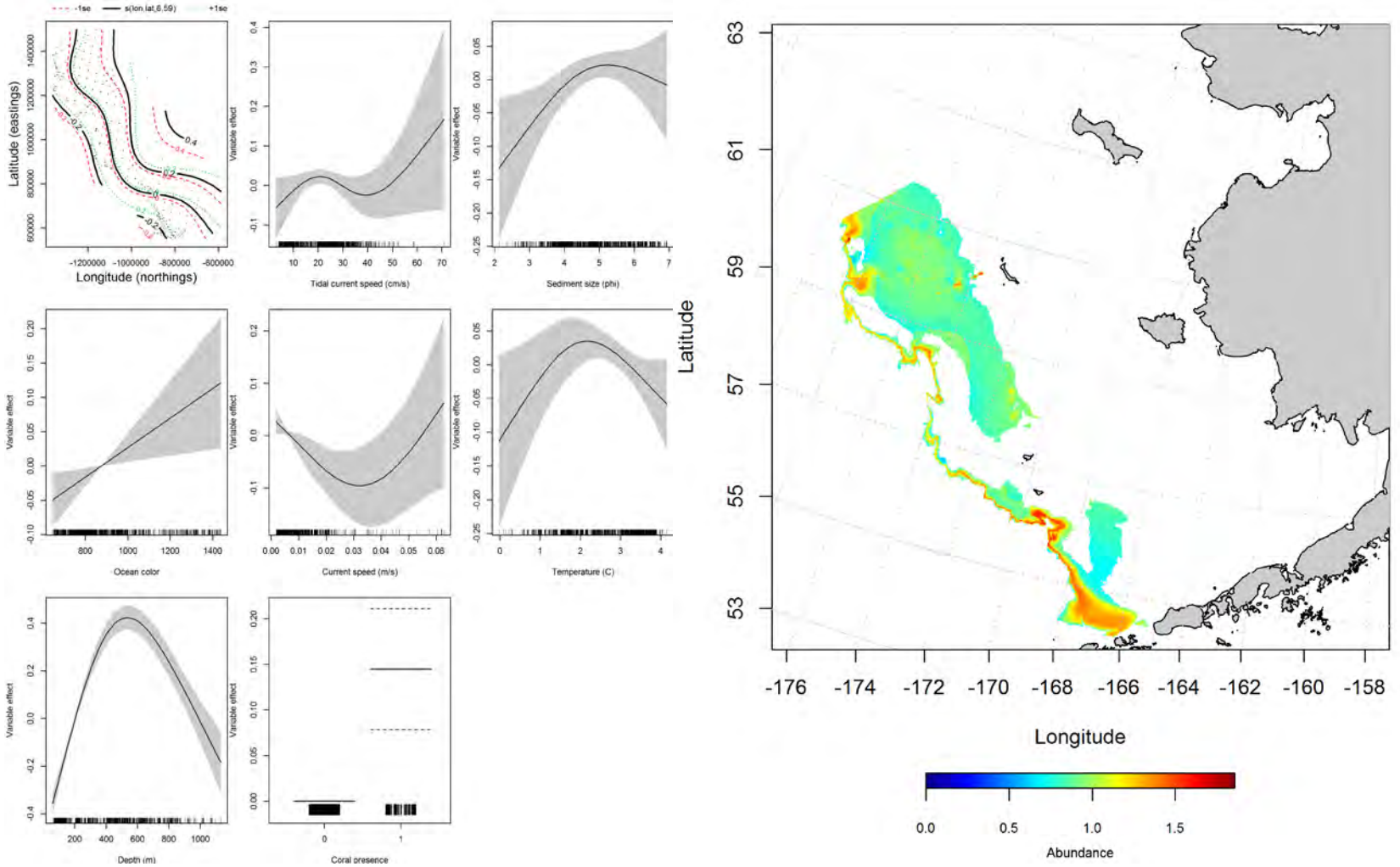

Figure 21. -- Effects of retained habitat covariates on the best-fitting generalized additive model (GAM; left panel) of adult Kamchatka flounder abundance in RACE summer bottom trawl surveys of the Eastern Bering Sea Shelf, Slope, and Northern Bering Sea alongside their predicted conditional abundance (right panel).

Seasonal distribution of Kamchatka flounder in commercial fishery catches from the Eastern Bering Sea -- Most of the commercial catches of Kamchatka flounder appeared to come from the outer shelf in fall (Figure 22). The bottom depth and bottom temperature covariates in the MaxEnt model provided 85.2% of the leverage of all habitat covariates predicting distribution of Kamchatka flounder in the Eastern Bering Sea. This model was an outstanding fit to the training data (AUC = 0.90) and correctly predicted 83% of cases. Model validation with the test data did not fit as well but was still excellent (AUC = 0.82) with 82% of cases correctly classified.

In winter, depth and bottom temperature comprised 91.0% of the relative importance of all covariates in the MaxEnt model predicting distribution of Kamchatka flounder in the Eastern Bering Sea (Figure 23). Similar to fall, most of the commercial catches came from the outer shelf and upper slope. The model was an outstanding fit to the training data (AUC = 0.94) with 86% of cases correctly predicted. Model validation with the test data did not fit as well but was still excellent (AUC = 0.86) with 86% of cases correctly classified.

In the spring, depth and bottom temperature comprised 92.0% of the relative importance of all covariates in the model predicting distribution of Kamchatka flounder in the Eastern Bering Sea (Figure 24). Similar to winter and fall, most of the commercial catches came from the outer shelf and upper slope. The model fit to the training data was outstanding (AUC = 0.95) with 87% of cases correctly predicted. Model validation with the test data did not fit as well but was still excellent (AUC = 0.88) with 88% of cases correctly classified.

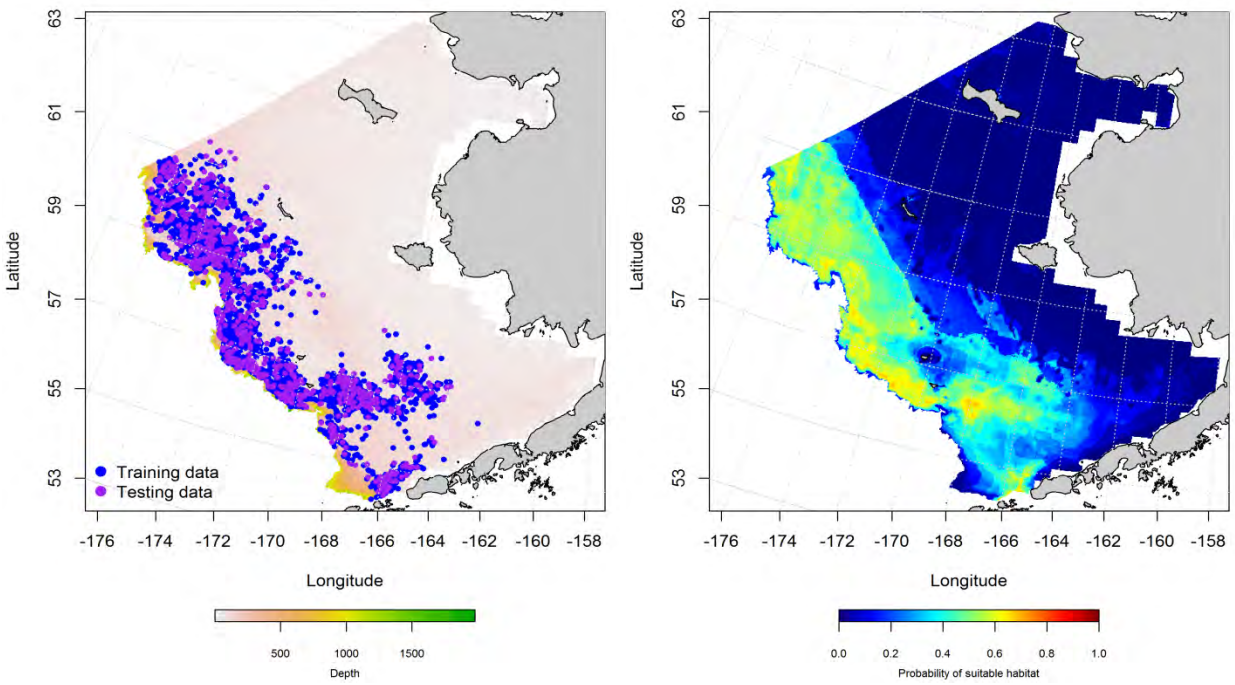

Figure 22. -- Locations of fall (October-November) catches of Kamchatka flounder in commercial fisheries of the Eastern Bering Sea (left panel). Blue points were used to train the MaxEnt model predicting the probability of suitable habitat (right panel) and the purple points were used to validate the model.

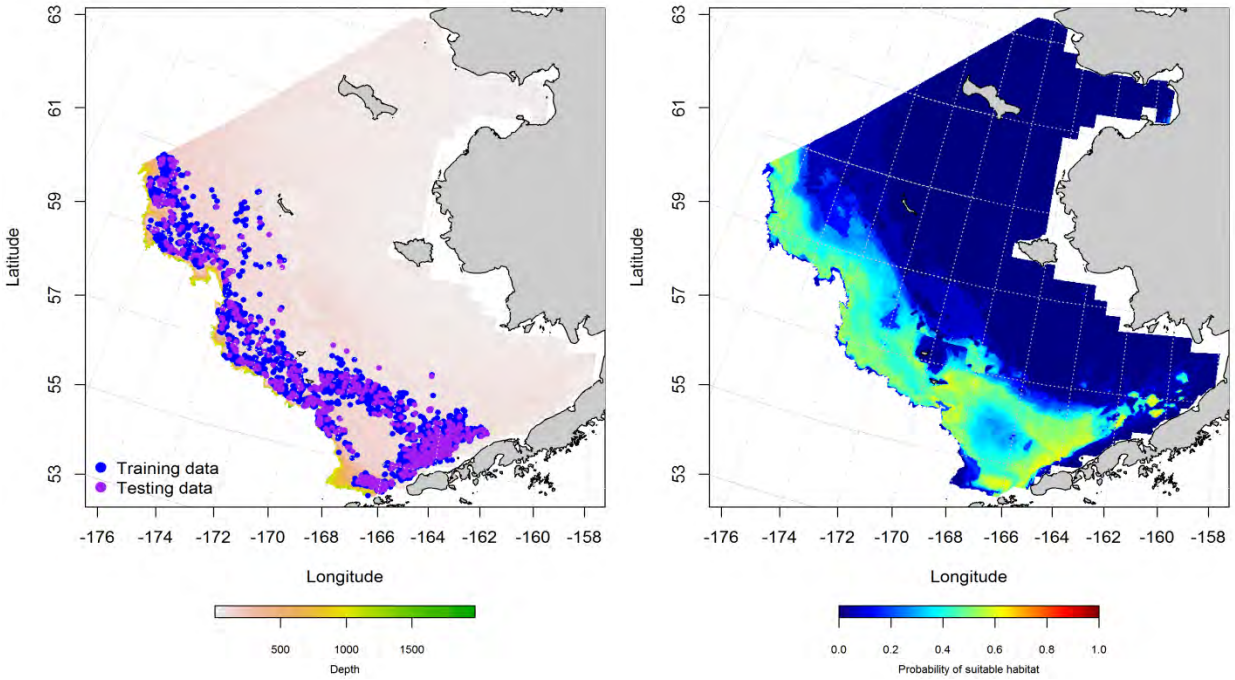

Figure 23. -- Locations of winter (December-February) catches of Kamchatka flounder in commercial fisheries of the Eastern Bering Sea (left panel). Blue points were used to train the MaxEnt model

predicting the probability of suitable habitat (right panel) and the purple points were used to validate the model.

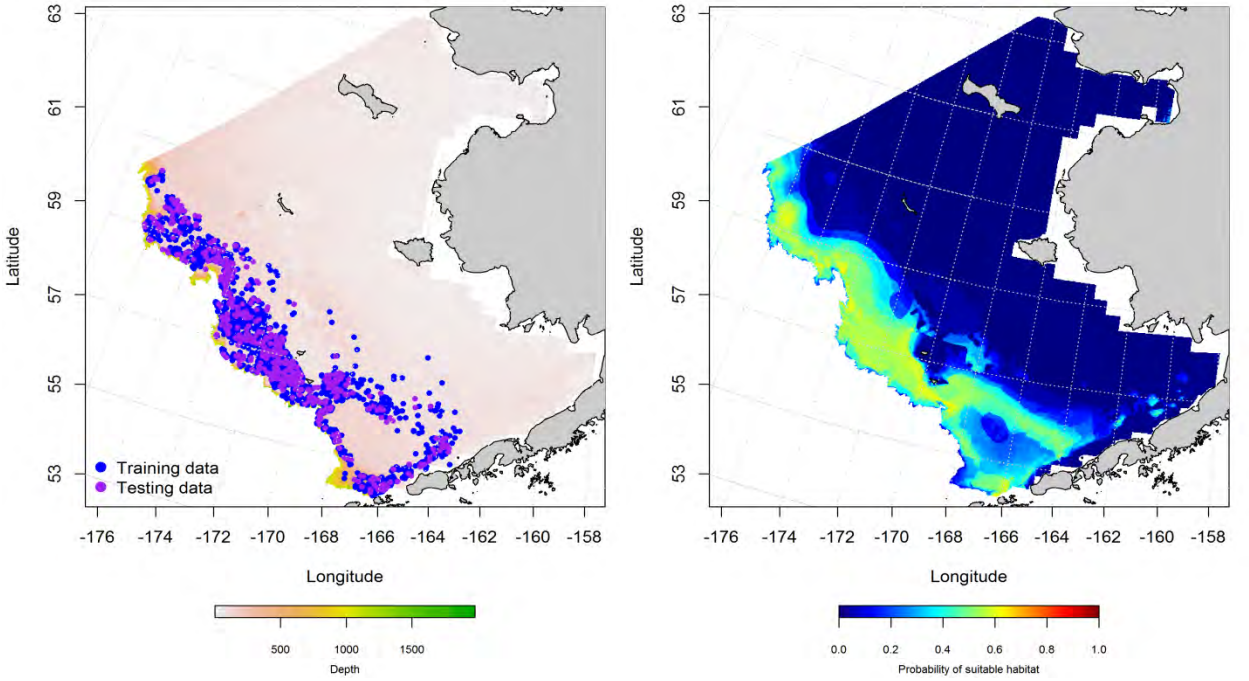

Figure 24. -- Locations of spring (March-May) catches of Kamchatka flounder in commercial fisheries of the Eastern Bering Sea (left panel). Blue points were used to train the MaxEnt model predicting the probability of suitable habitat (right panel) and the purple points were used to validate the model.

Eastern Bering Sea Kamchatka flounder (*Atheresthes evermanni*) essential fish habitat maps and conclusions – Summertime EFH of late juvenile and adult Kamchatka flounder was centered over the outer shelf and slope (Figure 25). Juveniles were most abundant over the outer shelf and upper slope. Where adult Kamchatka flounder presence was predicted, they were abundant over shelf edge and in patches over the middle and outer shelf in the central and northern domains of the Eastern Bering Sea.

There were some seasonal differences in Kamchatka flounder EFH predicted from commercial fishery catches (Figure 26). In fall and spring, the highest probability EFH was predicted from near the head of Pribilof Canyon northward along the outer shelf and slope. During winter, the distribution of EFH shifted further to the south.

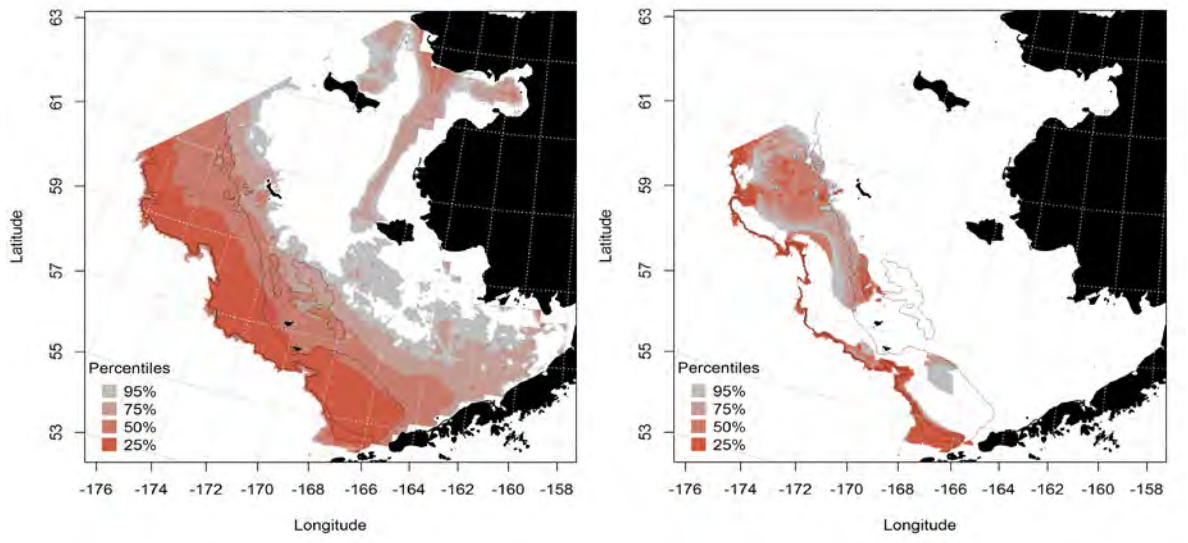

Figure 25. -- Essential Kamchatka flounder habitat predicted for late juveniles and adults (left and right panel) from RACE summertime bottom trawl surveys.

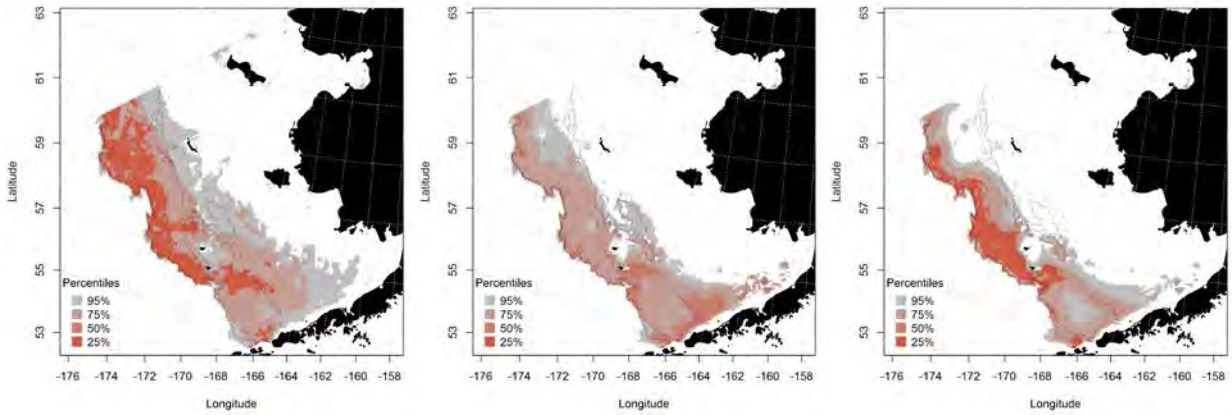

Figure 26. -- Essential Kamchatka flounder habitat predicted during fall (left panel), winter (middle panel), and spring (right panel) from commercial fishery catches.

rex sole (*Glyptocephalus zachirus*)

Rex sole inhabit waters of the continental shelf and slope in the North Pacific Ocean and range from Mexico to the Bering Sea.

Seasonal distribution of rex sole early life history stages in EcoFOCI ichthyoplankton surveys of the Eastern Bering Sea – Rex sole eggs were observed in EcoFOCI ichthyoplankton surveys of the Eastern Bering Sea in winter, spring, and summer (Figure 27); early juvenile stages of rex sole were not reported. The egg stage was more prevalent in spring and summer samples than in winter. The occurrence of eggs was concentrated over deeper waters of the outer shelf and slope (> 100 m) in the southwestern portion of the Eastern Bering Sea.

Maximum entropy modeling of rex sole egg presence in EcoFOCI ichthyoplankton samples predicted that suitable egg habitat varies seasonally (Figure 28). In springtime, the high probability habitat is found over benthypelagic waters of the Bering Canyon. In summer, the habitat is more widely dispersed and extends north and east from these deeper Bering Canyon waters. Surface temperature (relative importance of 66.8% in spring and 51.6% in summer) and ocean productivity (10.2% and 9.6% by season) were important covariates common to both seasons. Also important were the covariates bottom slope in spring (8.5%) and bottom depth in summer (28%). Model fits to the training data were outstanding in both seasons (AUC = 0.96 in spring and 0.9 in summer) with the two models correctly classifying 89 and 87% of predicted cases. Model validation returned outstanding to excellent fits to the test data (AUC = 0.92 for spring and 0.85 for summer). Models based on the test data correctly classified 92 and 85% of cases in spring and summer.

Rex sole larvae were reported from summer EcoFOCI ichthyoplankton surveys (Figure 29). The larvae were collected over the outer shelf (100 to 200 m) from near the head of the Bering Canyon in the southern domain of the Eastern Bering Sea northward to around Zhemchug Canyon in the central domain. There were not enough records of rex sole larvae to model their distribution.

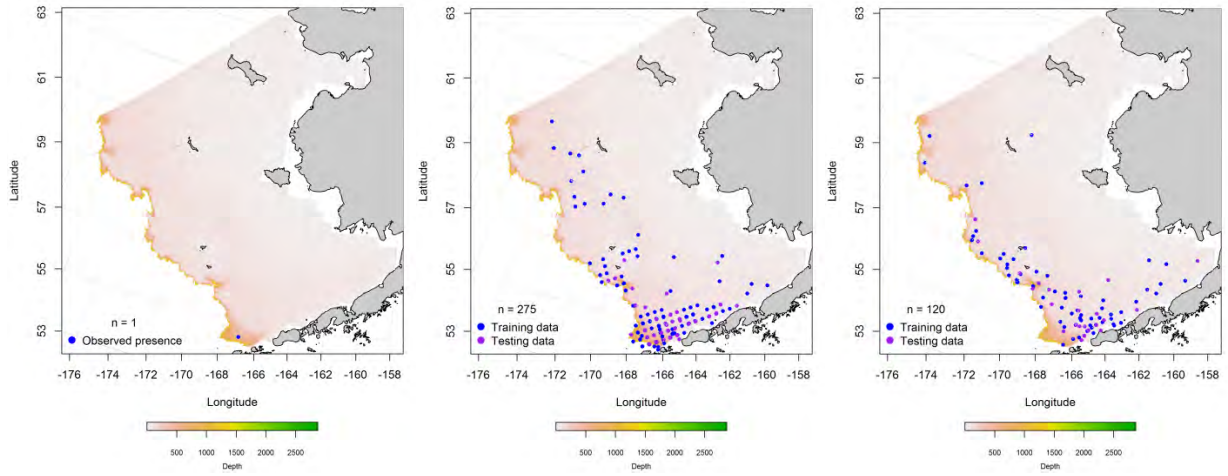

Figure 27. -- Winter, spring, and summer observations of rex sole eggs (left, middle, and right panels, respectively) from EcoFOCI ichthyoplankton surveys of the Eastern Bering Sea.

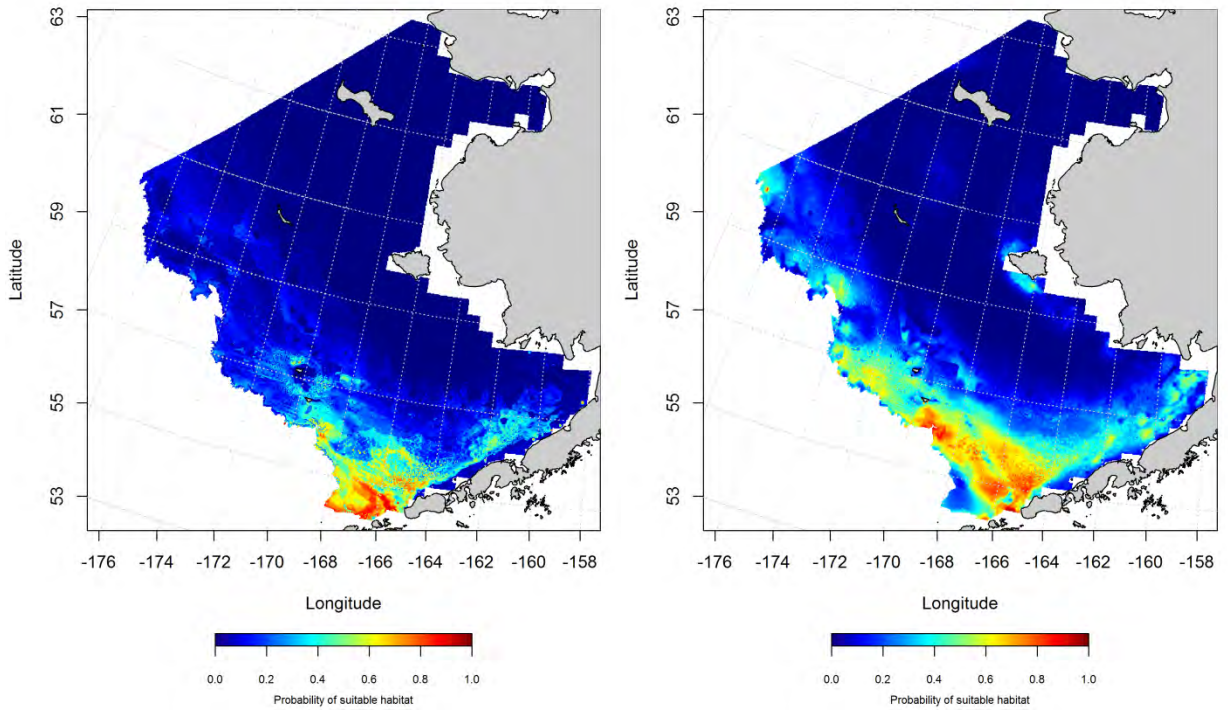

Figure 28. -- Probability of suitable rex sole egg habitat during spring and summer (left and right panels) predicted from MaxEnt modeling of presence in EcoFOCI ichthyoplankton surveys of the Eastern Bering Sea.

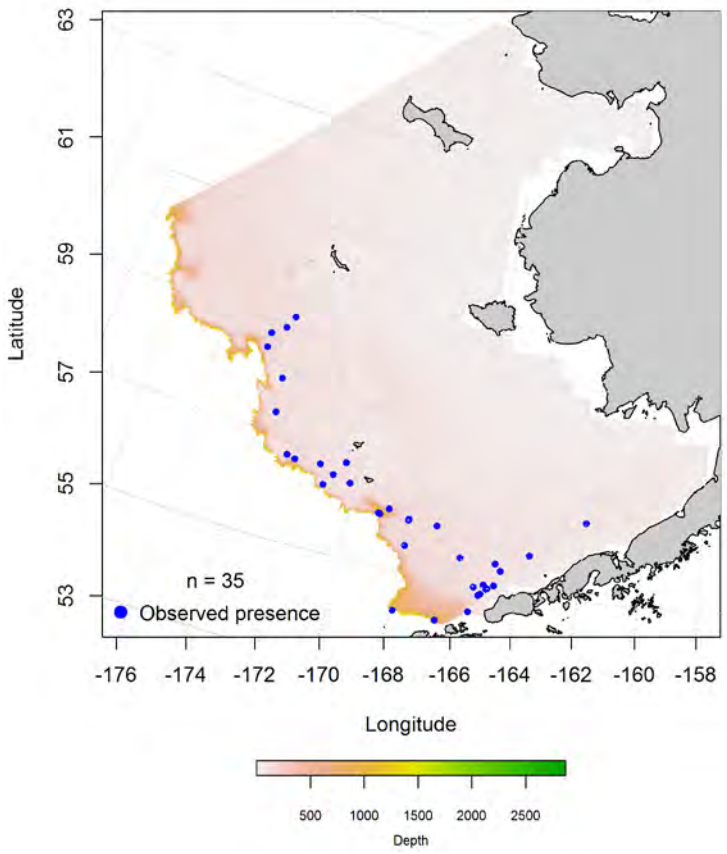

Figure 29. -- Summer observations of larval rex sole from the EcoFOCI ichthyoplankton surveys of the Eastern Bering Sea.

Essential early life history habitat maps and conclusions for Eastern Bering Sea rex sole (*Glyptocephalus zachirus*) – Essential habitat of rex sole eggs was modeled from spring and summer EcoFOCI ichthyoplankton surveys of the Eastern Bering Sea (Figure 30). Essential egg habitat is predicted to extend from the southern to the northern domain of the Eastern Bering Sea from the inner shelf in Bristol Bay over the middle and outer shelf northward to the northern extent of the survey area. There were some areas of suitable habitat predicted in summer around Nunivak Island and near Kuskokwim Bay that were not predicted in spring.

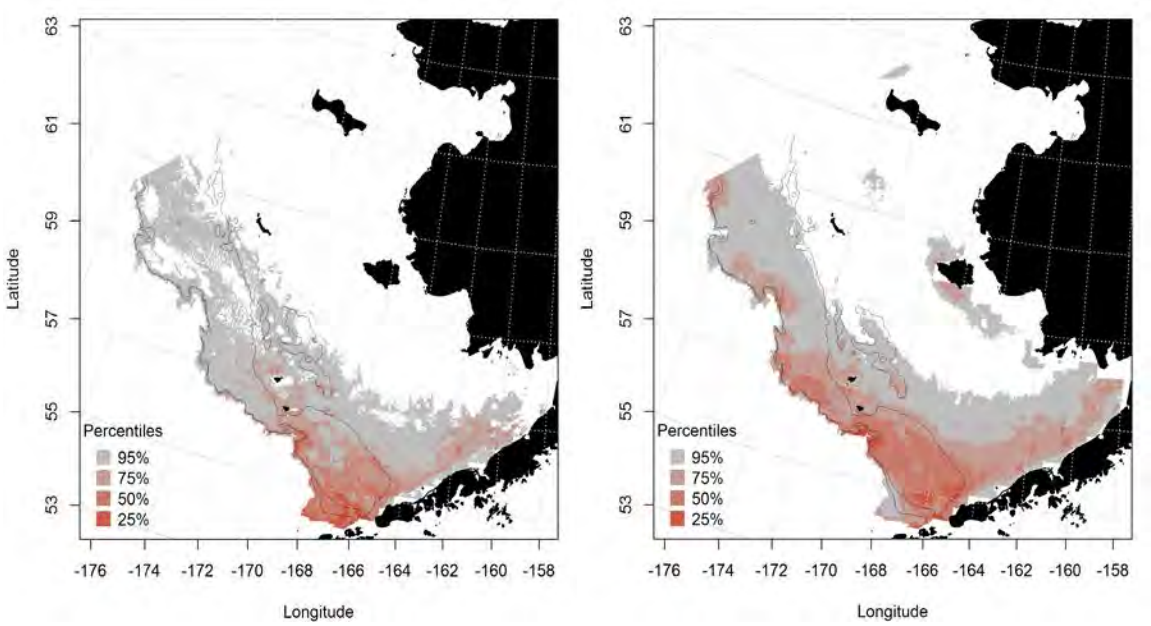

Figure 30. -- Essential habitat of rex sole eggs predicted from spring and summer (left and right panels) EcoFOCI ichthyoplankton surveys of the Eastern Bering Sea.

Summertime distribution of late juvenile and adult rex sole from RACE bottom trawl surveys of the Eastern Bering Sea – Late juvenile and adult rex sole were distributed from the inner shelf in Bristol Bay across the middle and outer shelf northward to the northern extent of the survey area in summertime (Figure 31). Rex sole also occurred in deeper benthypelagic waters over the Bering Slope.

A hurdle GAM was used to describe late juvenile rex sole distribution and abundance based on habitat covariates. The best-fitting presence-absence GAM describing late juvenile rex sole distribution in the Eastern Bering Sea indicates that the highest probability locations for juvenile rex to occur are along the continental shelf edge and slope (Figure 32). This model explained 44.1% of the deviance in their distribution and geographical location, bottom temperature, and the presence of sea pens were among the most important habitat covariates retained in the model. Model effects decreased from southwest to northeast, suggested an optimum bottom temperature around 4°C, and increased in the presence of sea pens. Both the training and test data models correctly classified 88% of predicted cases. The model fit to the training data and to test data in the model validation step was outstanding (AUC = 0.94).

Late juvenile rex sole abundance predicted by the best-fitting GAM where their presence was predicted returned a distribution of abundance largely constrained to the outer shelf of the Eastern Bering Sea (Figure 33). This model explained just 12.5% of the deviance in the CPUE data and retained geographic location and bottom slope as the most significant predictors. Model fits to the training and test data sets were minimal (r^2 = 0.13 and 0.06).

A hurdle GAM was also used to describe adult rex sole distribution and abundance from RACE summer bottom trawl surveys of the Eastern Bering Sea. The GAM describing presence-absence of rex sole adults explained 56.9% of the deviance in their distribution (Figure 34). The most important predictors in this model were geographical location, bottom depth, and bottom temperature. Model effects increased from north to south over the survey area and increased with increasing depth and bottom temperature up to an apparent optimum (around 4°C and 300 m). The highest probability of adult rex sole presence occurred in waters > 200 m out to the shelf edge. The model was an oustanding fit to the training data and to the test data in model validation (AUC = 0.96 for both data sets) and correctly classified 89 and 88% of predicted cases.

The best-fitting GAM for adult rex sole abundance where present predicted the highest conditional abundances over the Bering Canyon near Unimak Pass and along the shelf edge just north of Zhemchug Canyon (Figure 35). The model explained 44.3% of the deviance in the conditional CPUE data and geographical location, bottom depth, and current speed were the most significant covariates retained. Model fits to the training and test data were poor (r^2 = 0.44 and 0.36).

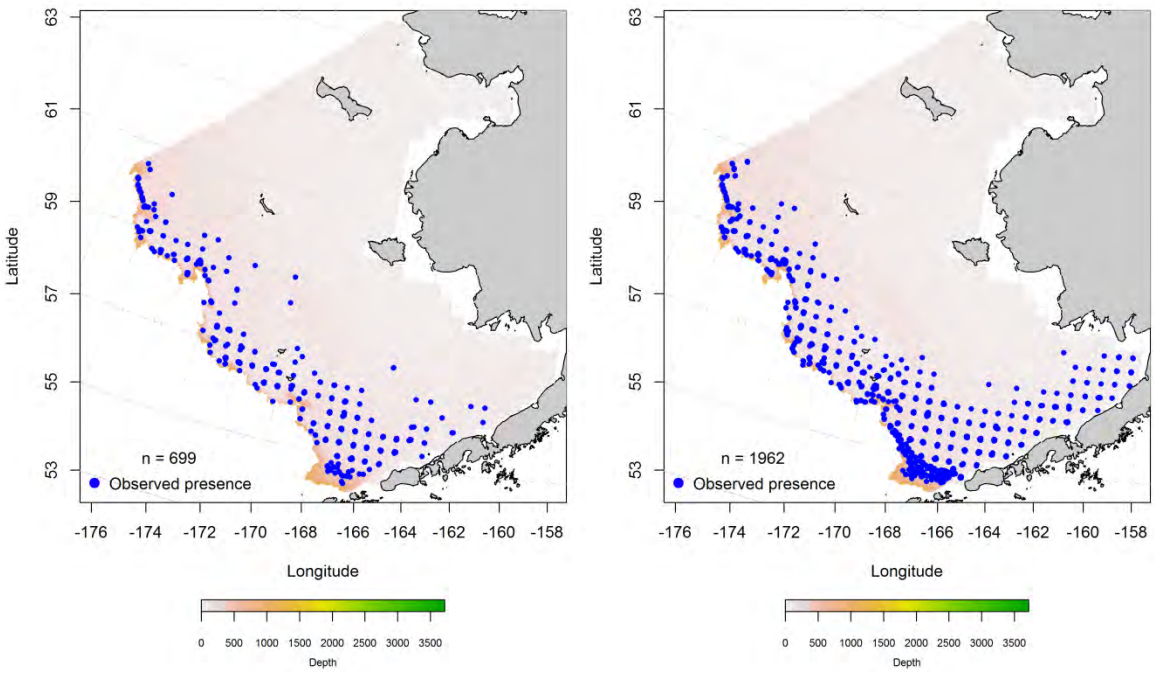

Figure 31. – Distribution of late juvenile and adult rex sole catches (left and right panels) in RACE summer bottom trawl surveys of the Eastern Bering Sea.

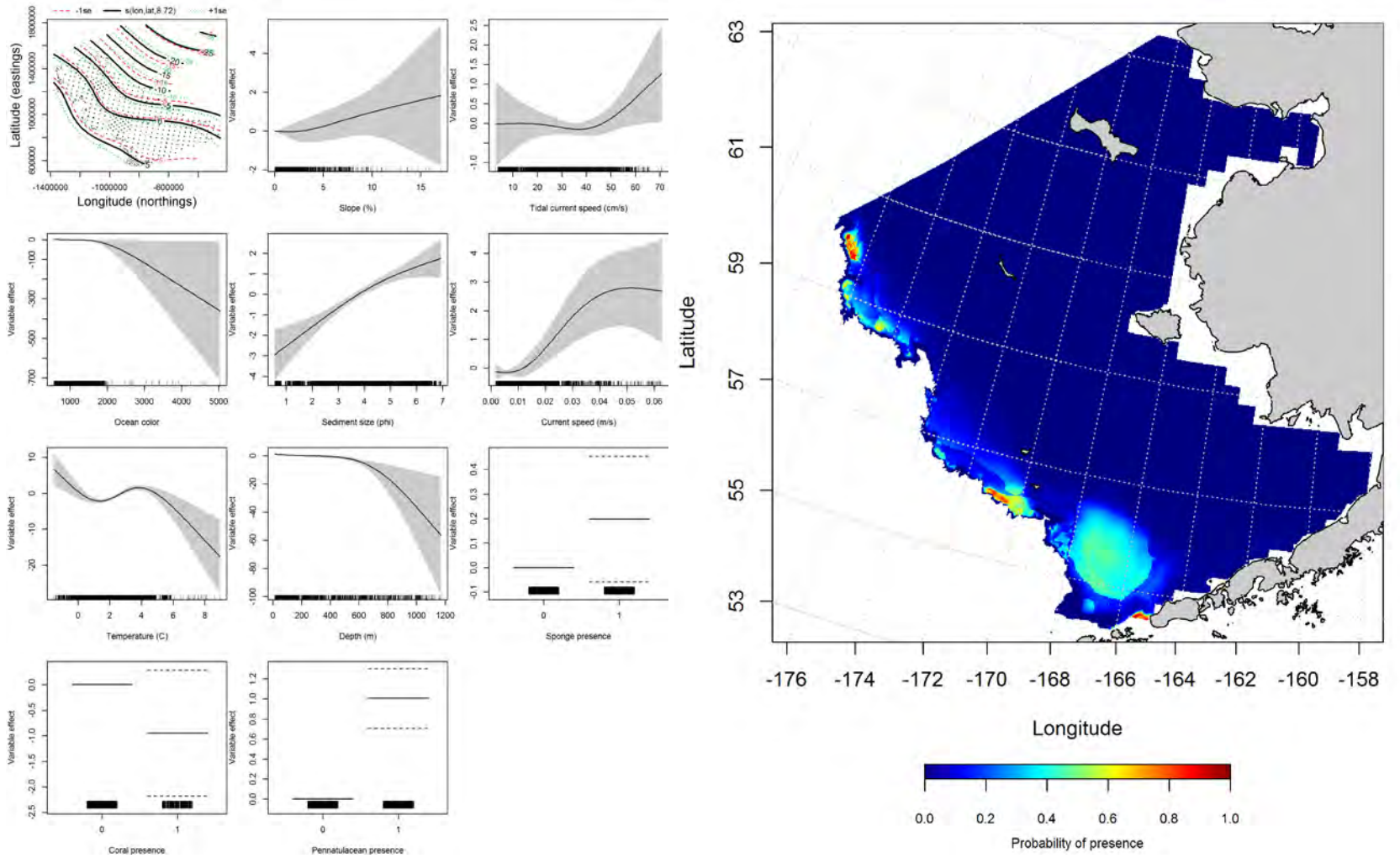

Figure 32. -- Effects of retained habitat covariates on the best-fitting generalized additive presence-absence model (GAM) of late juvenile rex sole from RACE summer bottom trawl surveys of the Eastern Bering Sea Shelf, Slope, and Northern Bering Sea alongside their predicted presence (right panel).

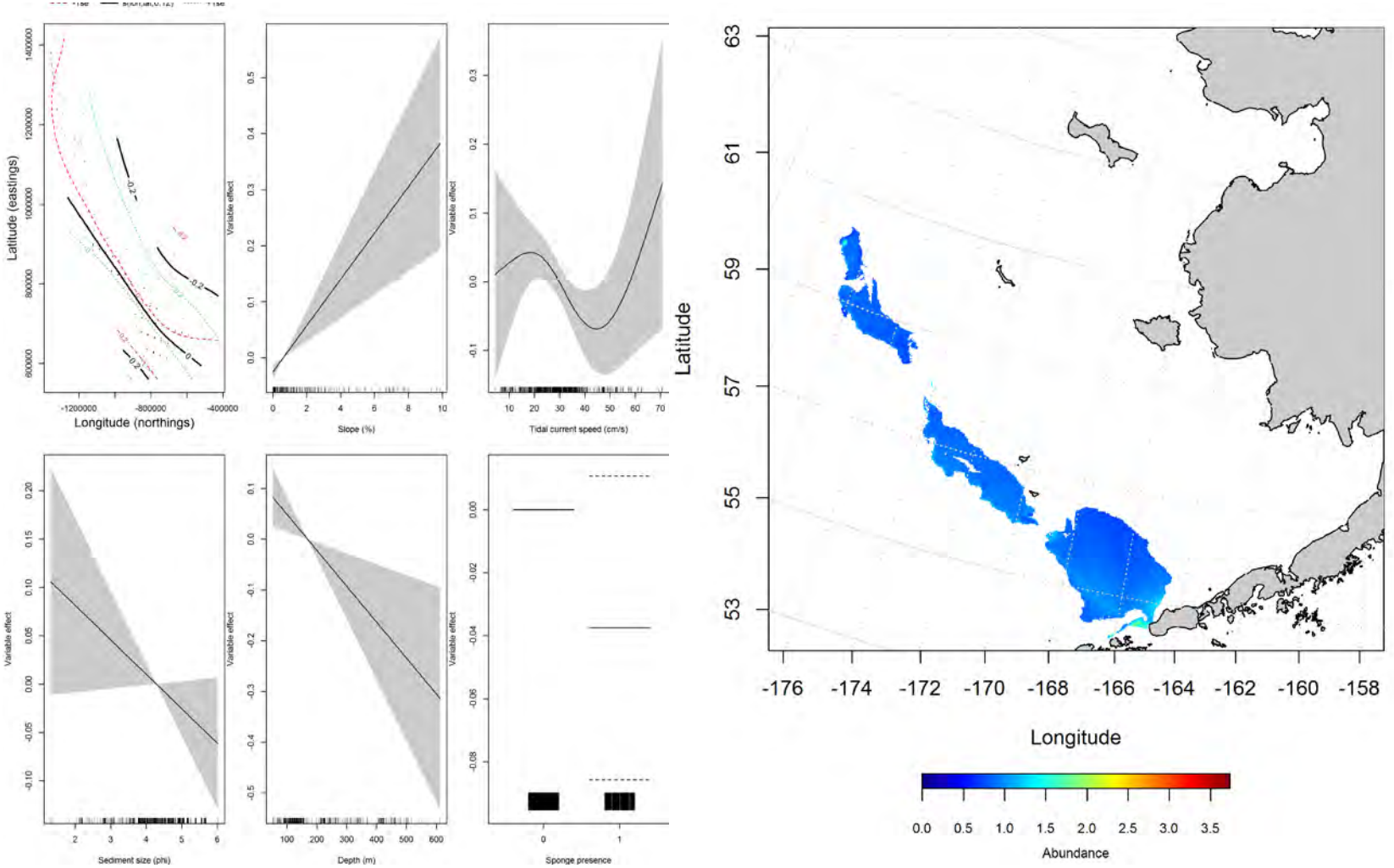

Figure 33. -- Effects of retained habitat covariates on the best-fitting generalized additive model (GAM; left panel) of late juvenile rex sole abundance from RACE summer bottom trawl surveys of the Eastern Bering Sea Shelf, Slope, and Northern Bering Sea alongside their predicted conditional abundance (right panel).

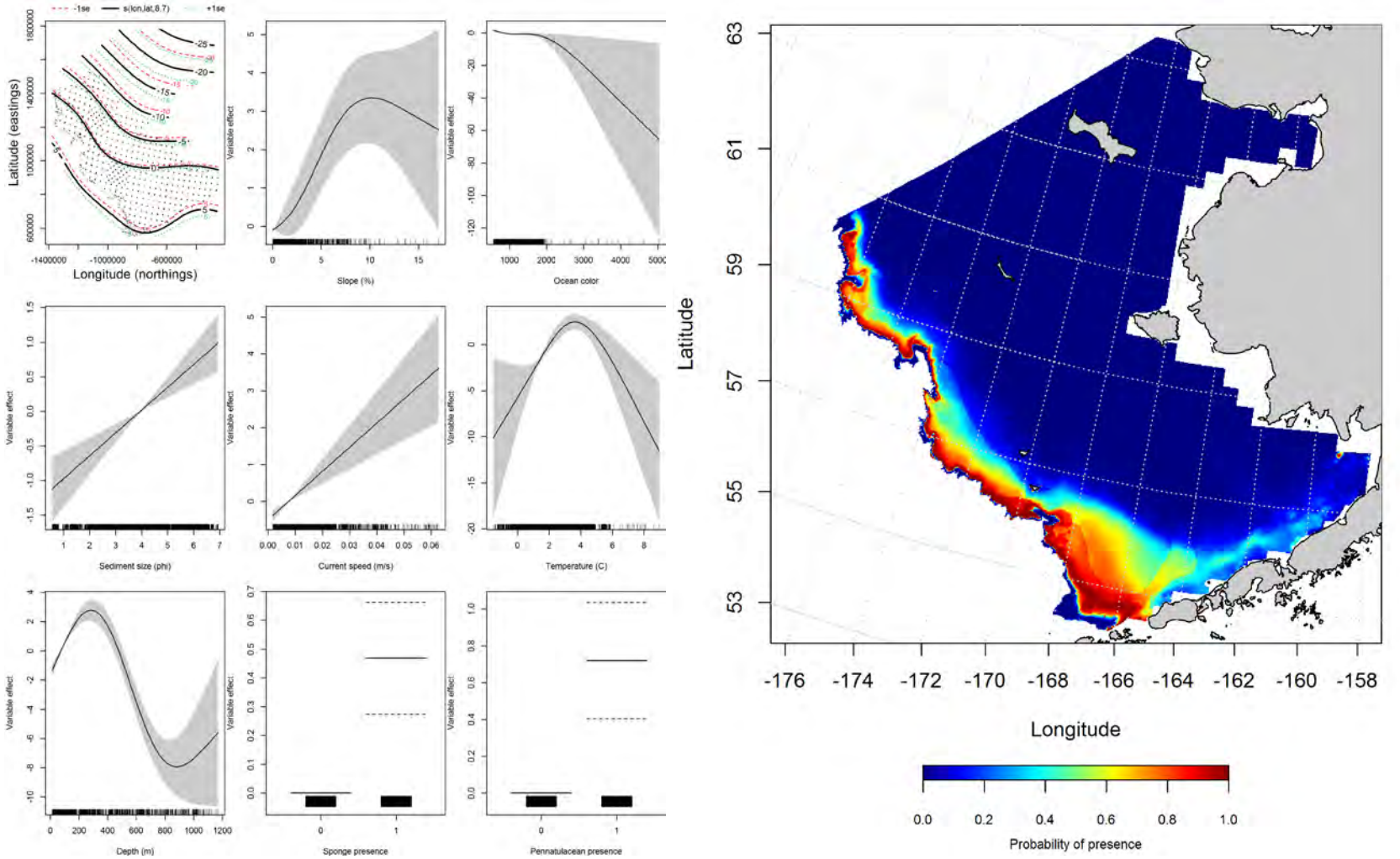

Figure 34. -- Effects of retained habitat covariates on the best-fitting generalized additive presence-absence model (GAM) of adult rex sole from RACE summer bottom trawl surveys of the Eastern Bering Sea Shelf, Slope, and Northern Bering Sea alongside their predicted presence (right panel).

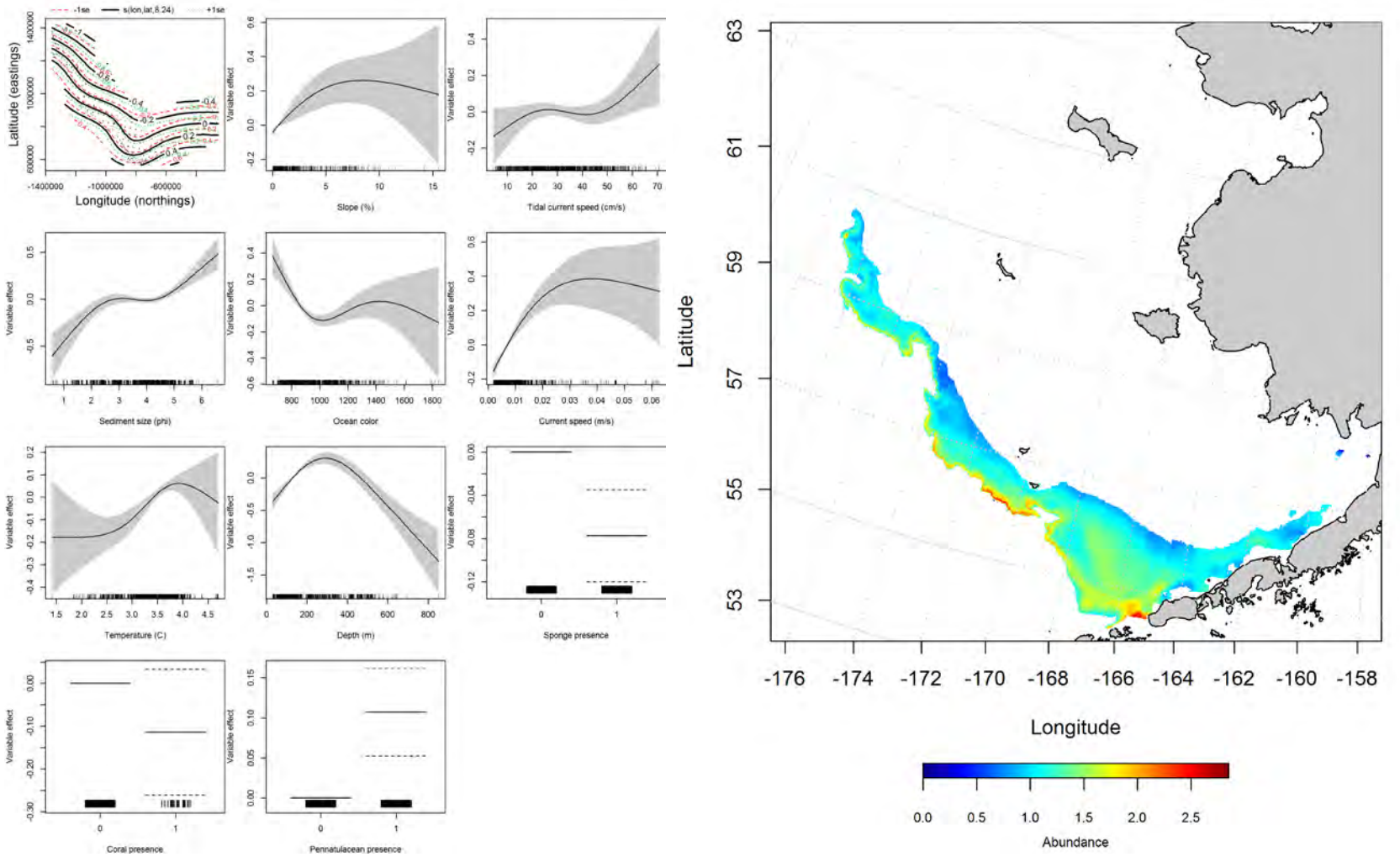

Figure 35. -- Effects of retained habitat covariates on the best-fitting generalized additive model (GAM; left panel) of late juvenile rex sole abundance from RACE summer bottom trawl surveys of the Eastern Bering Sea Shelf, Slope, and Northern Bering Sea alongside their predicted conditional abundance (right panel).

Seasonal distribution of rex sole in commercial fishery catches from the Eastern Bering Sea -- Seasonal differences in the occurrence of rex sole in commercial catches from the Eastern Bering Sea were apparent. It is unclear whether these differences result from changes in the distribution of rex sole across the region or changes in fishing activities during those seasons. In general, rex sole were distributed over the outer shelf and upper slope edge from the Bering Canyon northward to the northern extent of the survey area.

In fall, the highest probability habitats were in the southern domain of the Eastern Bering Sea over the Bering Canyon and near the head of Pribilof Canyon (Figure 36). The most important covariates predicting probability of suitable rex sole habitat from the MaxEnt model were bottom depth and bottom temperature (combined relative importance of 91.3%). The model fit to the training data was outstanding (AUC = 0.96); it correctly classified 90% of predicted cases. Model validation with the test data was successful and the fit was excellent (AUC = 0.88), correctly classifying 88% of cases.

During wintertime, rex sole catches primarily occurred from the Bering Canyon eastward into Bristol Bay (Figure 37). The most important covariates predicting probability of suitable rex sole habitat from the MaxEnt model were bottom depth, ocean productivity, and bottom temperature (combined relative importance of 92.8%). The model fit to the training data was outstanding (AUC = 0.98); it correctly classified 93% of predicted cases. Model validation with the test data set was successful (AUC = 0.93), correctly classifying 93% of cases.

In the spring, the pattern of suitable habitat resembled that during the fall months with high probability areas predicted over Bering Canyon near the Alaska Peninsula and around the head of Pribilof Canyon (Figure 38). The most important covariates predicting probability of suitable rex sole habitat from the MaxEnt model were bottom temperature and bottom depth (combined relative importance of 91.9%). The model fit to the training data was outstanding (AUC = 0.96); it correctly classified 90% of predicted

cases. Model validation with the test data set was successful and the fit was excellent (AUC = 0.88), correctly classifying 88% of cases.

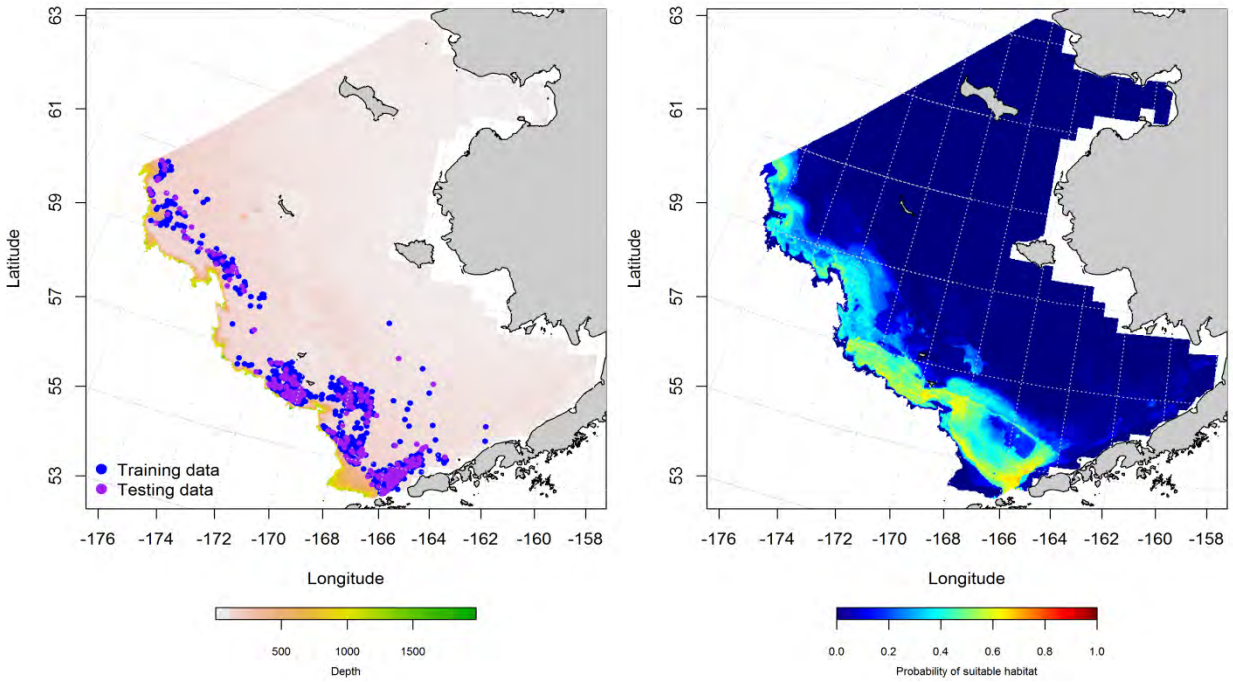

Figure 36. -- Locations of fall (October-November) catches of rex sole in commercial fisheries of the Eastern Bering Sea (left panel). Blue points were used to train the maximum entropy model predicting the probability of suitable habitat (right panel) and the purple points were used to validate the model.

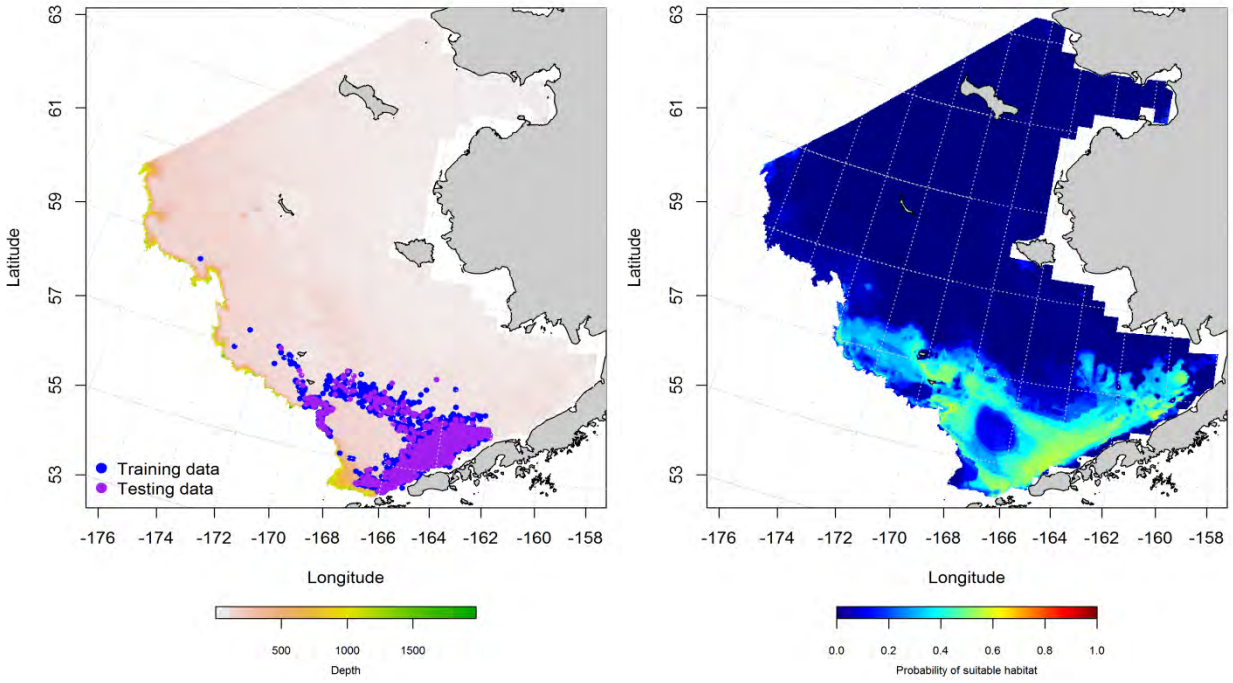

Figure 37. -- Locations of winter (December-February) catches of rex sole in commercial fisheries of the Eastern Bering Sea (left panel). Blue points were used to train the maximum entropy model predicting the probability of suitable habitat (right panel) and the purple points were used to validate the model.

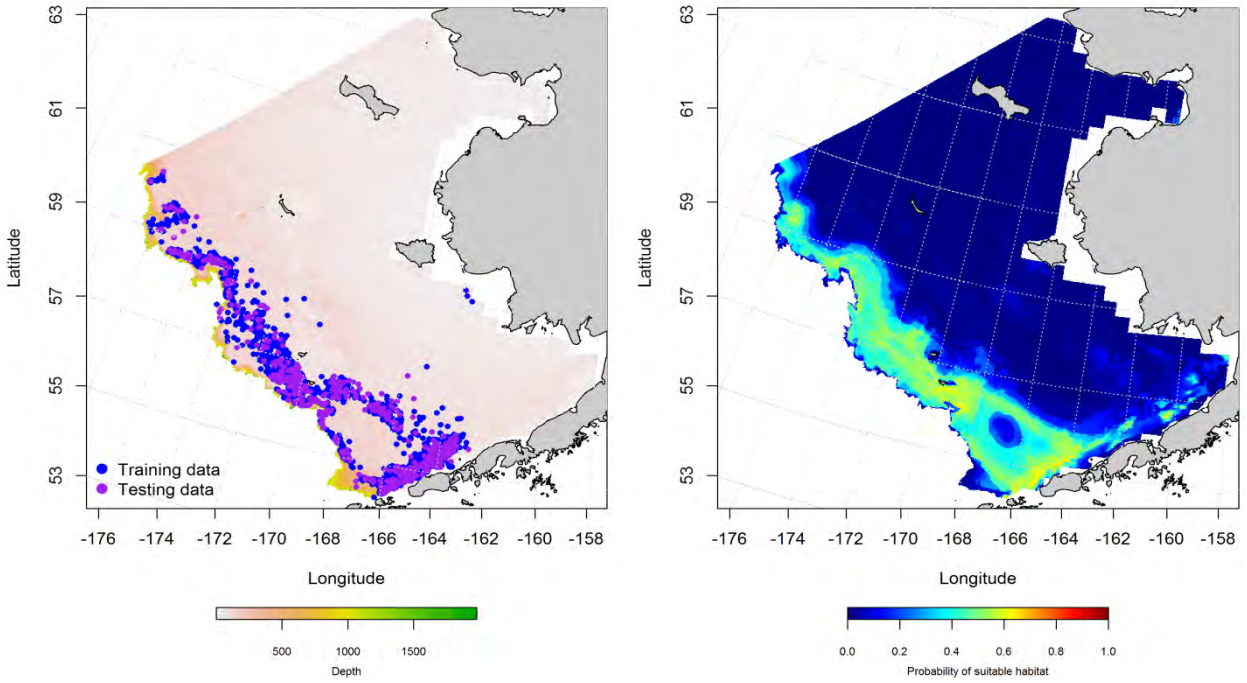

Figure 38. -- Locations of spring (March-May) catches of rex sole in commercial fisheries of the Eastern Bering Sea (left panel). Blue points were used to train the maximum entropy model predicting the probability of suitable habitat (right panel) and the purple points were used to validate the model.

Eastern Bering Sea rex sole (*Glyptocephalus zachirus*) essential fish habitat maps and conclusions – Summertime EFH for rex sole differed between late juvenile and adult life stages, but was primarily distributed over the outer shelf of the Eastern Bering Sea (Figure 39). The late juveniles occurred exclusively in waters > 100 m. Adults could be found in shallower waters along the Alaska Peninsula on the southern margin of Bristol Bay.

Rex sole EFH determined from commercial fishery activity showed a more widespread distribution than that seen from the RACE summer bottom trawl surveys (Figure 40). While the pattern of suitable habitat along the outer shelf and shelf edge was apparent, there was more habitat predicted for the middle shelf and in Bristol Bay from the commercial catches. Distribution of EFH predicted from commercial fishing

activity may have more to do with the focus of the fishery than with actual changes in distribution of rex sole on the fishing grounds.

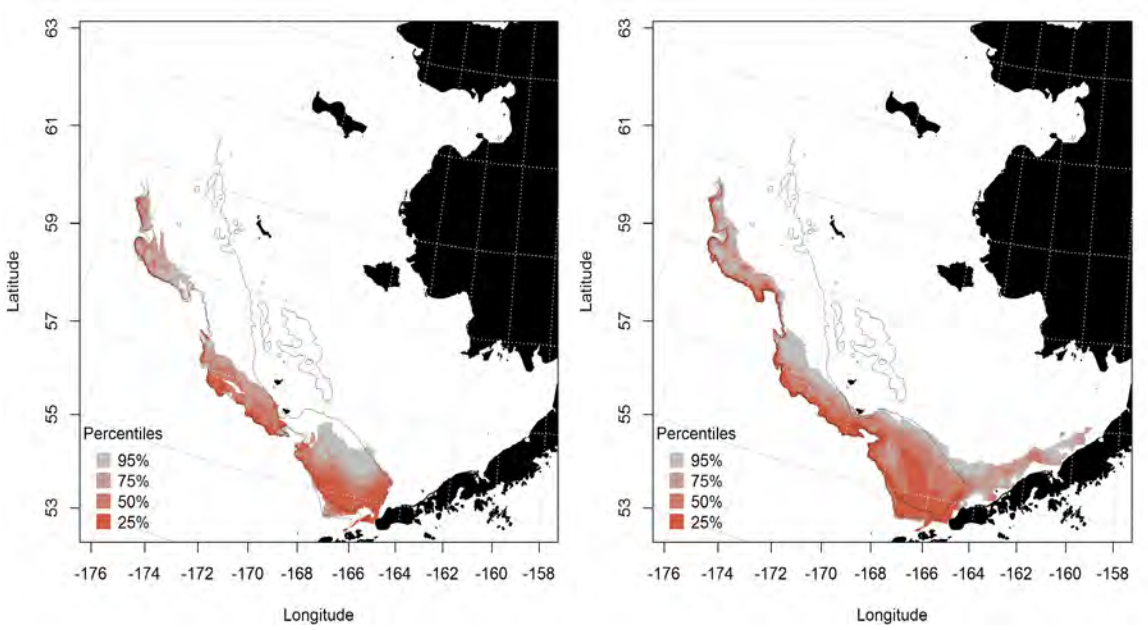

Figure 39. -- Essential habitat of late juvenile and adult rex sole (left and right panels) predicted from RACE summertime bottom trawl surveys of the Eastern Bering Sea.

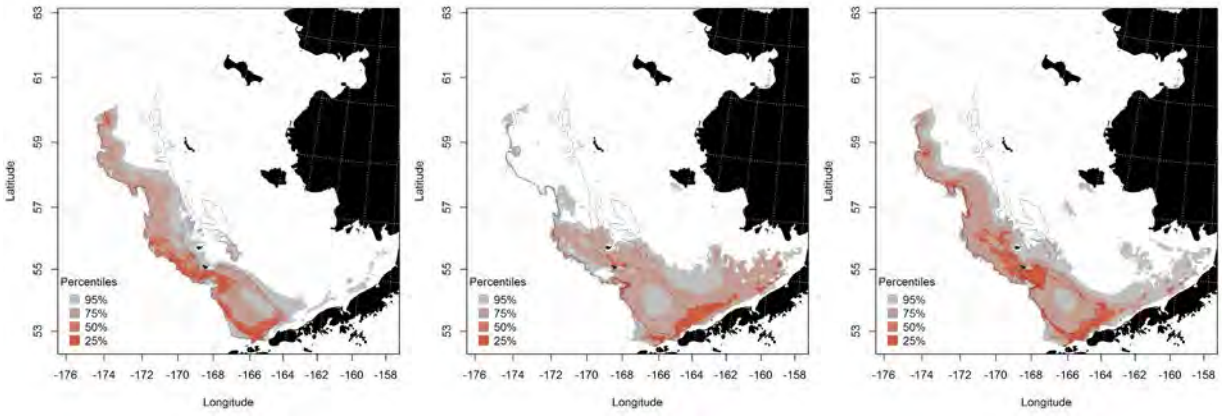

Figure 40. -- Essential rex sole habitat predicted from commercial fishery catches in the Eastern Bering Sea during fall (left panel), winter (middle panel), and spring (right panel).

Dover sole (*Microstomus pacificus*)

Dover sole inhabit waters of the continental shelf and slope in the North Pacific Ocean and range from the Northern Bering Sea out to Stalemate Bank and south to Baja California, Mexico. During non-spawning season, adults tend to be distributed from the inner shelf to the outer slope, but move in to deeper waters to spawn. Eggs have been found in surface waters near spawning areas and, while Dover sole larvae do not actively migrate toward coastal nursery grounds, they do appear to settle to their juvenile habitat in winter (Abookire and Bailey 2007).

Seasonal distribution of the early life stages of Dover sole in EcoFOCI ichthyoplankton surveys of the Eastern Bering Sea – A few Dover sole eggs were observed in spring and summer EcoFOCI ichthyoplankton surveys of the Eastern Bering Sea (Figure 41). There were not enough of these observations to parameterize a distribution model for Dover sole eggs. In springtime, Dover sole eggs were reported from the inner shelf in Bristol Bay, across the middle and outer shelf, and from benthypelagic waters (200 to 1,000 m) over the Bering Sea slope and shelf edge. During summer EcoFOCI surveys, observations of Dover sole eggs were concentrated on the outer shelf and over the benthypelagic waters of the Bering Canyon in the southern domain of the Eastern Bering Sea.

Dover sole larvae were rarely observed in EcoFOCI ichthyoplankton surveys of the Eastern Bering Sea (Figure 42). The few observations were from summer months over the outer shelf and benthypelagic waters of the Bering Canyon in the southern domain of the EBS. There were not enough larval Dover sole observations to parameterize a habitat model for this early life stage.

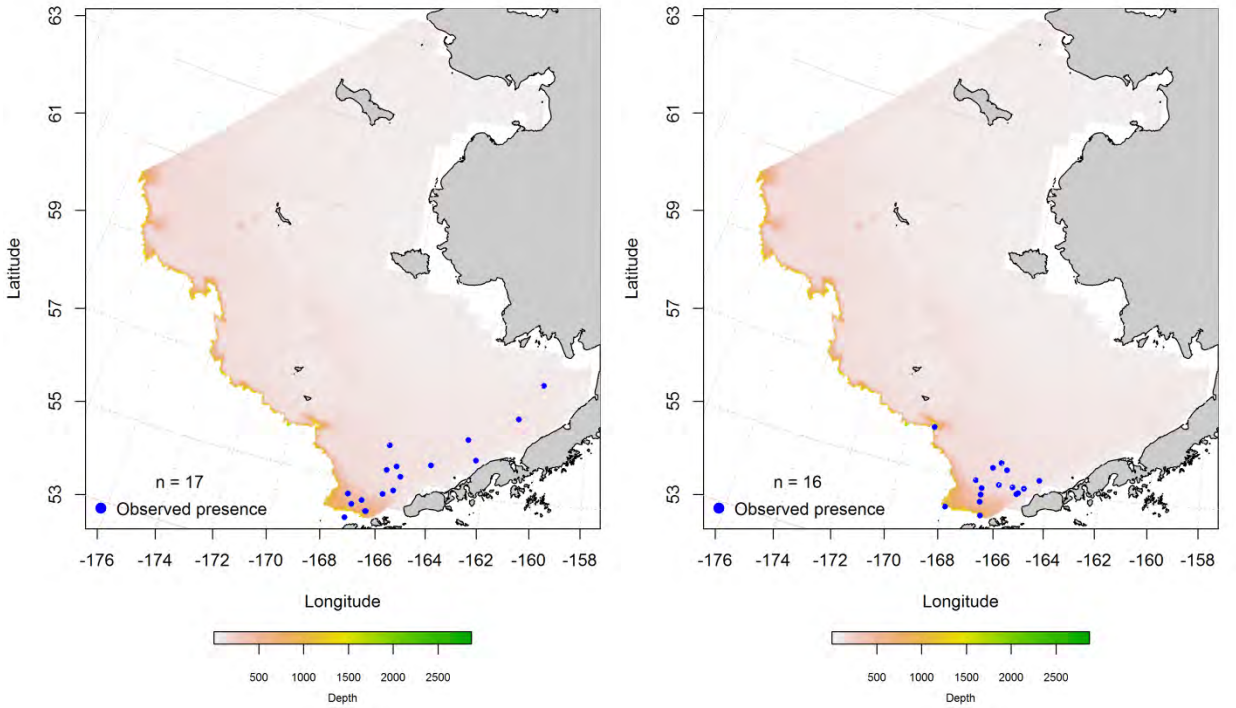

Figure 41. -- Spring and summer observations of Dover sole eggs (left and right panels) from EcoFOCI ichthyoplankton surveys of the Eastern Bering Sea.

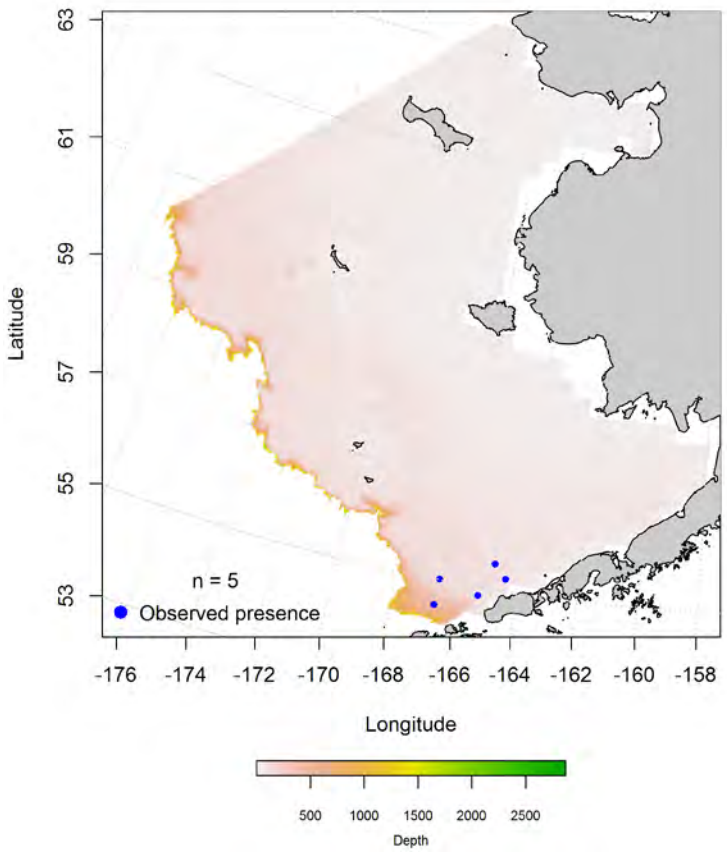

Figure 42. -- Summer observations of larval Dover sole from EcoFOCI ichthyoplankton surveys of the Eastern Bering Sea.

Summertime distribution of late juvenile and adult Dover sole from RACE bottom trawl surveys of the Eastern Bering Sea – Late juvenile and adult Dover sole were collected on RACE summer bottom trawl surveys of the Eastern Bering Sea (Figure 43). Both life stages were distributed over the shelf edge and slope of the Bering Canyon in the southern domain of the EBS but also occurred near the northern limit of the survey area. Late juvenile Dover sole were somewhat more prevalent over the middle shelf than were adults.

A MaxEnt model was used to describe late juvenile Dover sole distribution. The region predicted to have the most suitable habitat for late juvenile Dover sole was in the southern domain of the Eastern Bering Sea along the 200 m isobath and deeper waters over the Bering Canyon (Figure 44). The most important habitat covariates for predicting late juvenile Dover sole habitat were, in order of importance, bottom

depth, ocean productivity, and bottom temperature. Combined, these three terms accounted for 89.3% of the leverage provided by all covariates in the model. The model fit to the training data was outstanding (AUC = 0.94), correctly classifying 86% of predicted presence-absence cases. Model validation using the test data was excellent (AUC = 0.82) and correctly classified 82% of the predicted cases.

A MaxEnt model was also used to describe adult Dover sole distribution and to predict suitable habitat. The region predicted to have the most suitable habitat for late juvenile Dover sole was in the southern domain of the Eastern Bering Sea in waters > 200 m over the Bering Canyon (Figure 45). The most important habitat covariates for predicting adult Dover sole habitat were, in order of importance, bottom depth, bottom temperature, and ocean productivity. Combined, these three terms accounted for 97.1% of the leverage provided by all covariates in the model. The model fit to the training data was outstanding (AUC = 0.99), correctly classifying 97% of predicted cases. Model validation using the test data also outstanding (AUC = 0.98) and correctly classified 98% of the predicted cases.

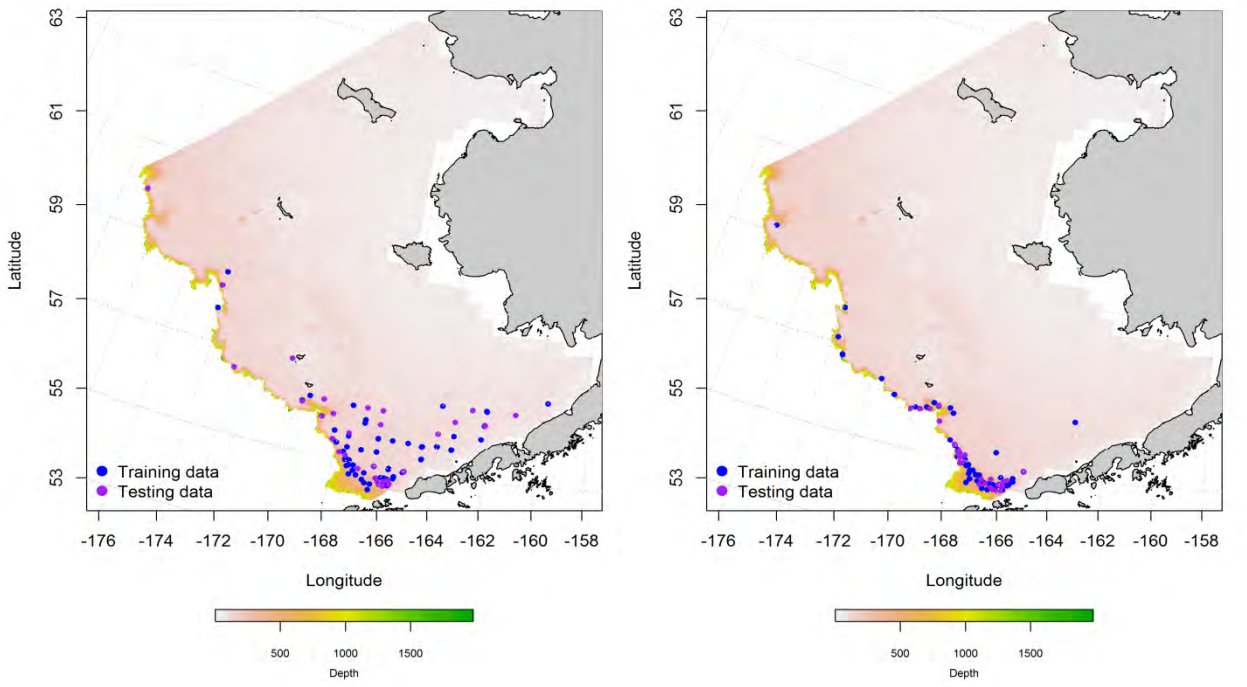

Figure 43. -- Dover sole late juveniles (left panel) and adults (right panel) from RACE summer bottom trawl survey catches in the Eastern Bering Sea. Blue points were used to train the maximum entropy

(MaxEnt) model predicting the probability of suitable habitat and the purple points were used to validate the model.

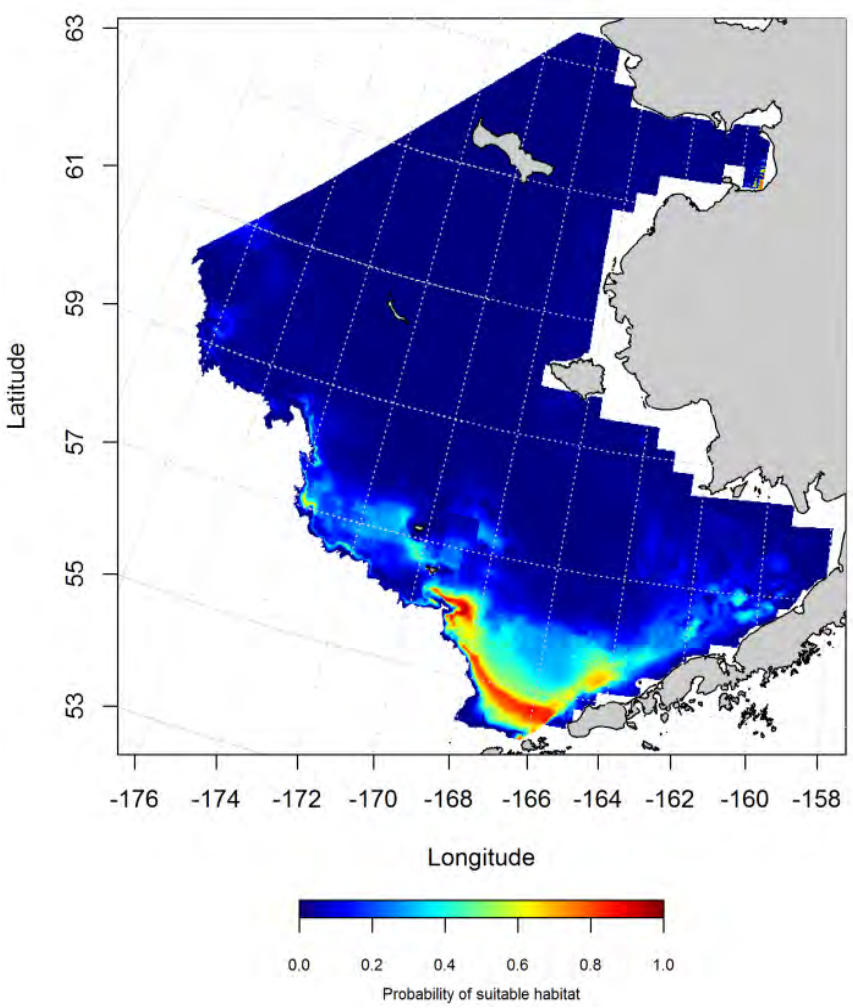

Figure 44. -- Maximum entropy (MaxEnt) model predictions of the probability of suitable habitat for late juvenile Dover sole from RACE summer bottom trawl surveys of the Eastern Bering Sea Shelf, Slope, and Northern Bering Sea.

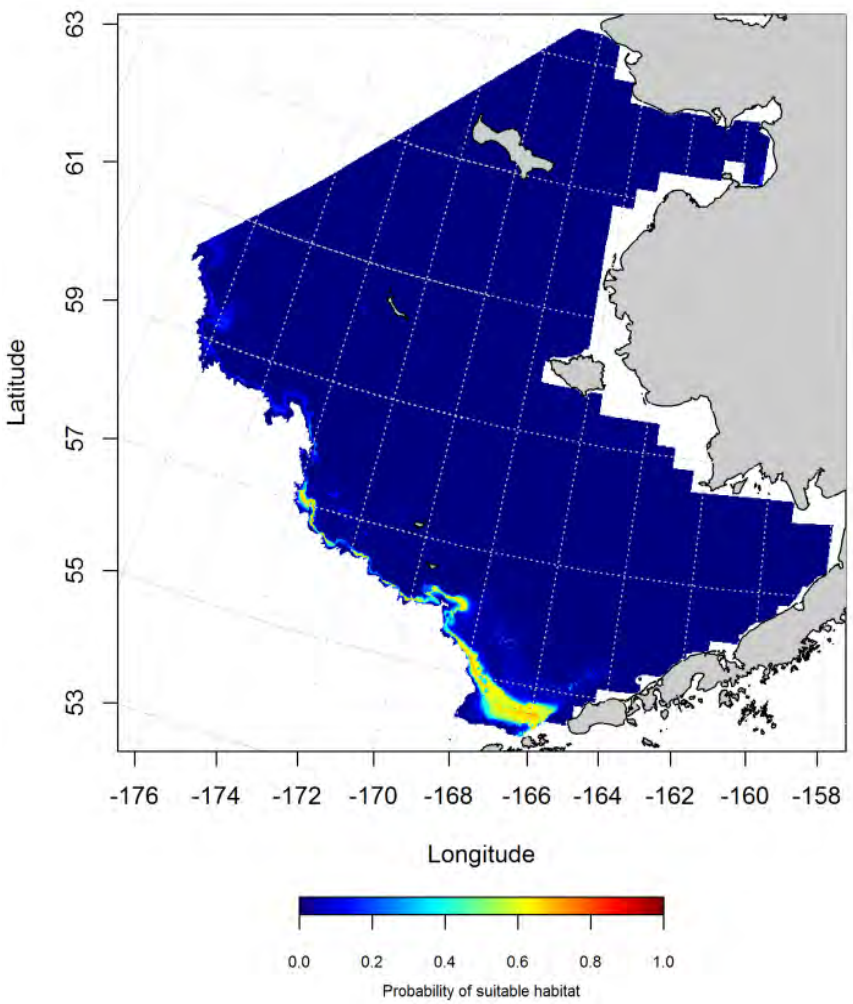

Figure 45. -- Maximum entropy (MaxEnt) model predictions of the probability of suitable habitat for adult Dover sole from RACE summer bottom trawl surveys of the Eastern Bering Sea Shelf, Slope, and Northern Bering Sea.

Seasonal distribution of Dover sole in commercial fishery catches from the Eastern Bering Sea -- In fall, the highest probability Dover sole habitats predicted by the MaxEnt model were in the southern domain of the Eastern Bering Sea over the Bering Canyon and near the head of Pribilof Canyon (Figure 46). The most important covariates predicting suitable habitat were, in order of importance, bottom depth, bottom slope, and ocean productivity with a combined relative importance of 87.7%. The model fit to the training data was outstanding (AUC = 0.99); it correctly classified 92% of predicted cases. Model validation with the test data set was excellent (AUC = 0.89), correctly classifying 89% of cases.

During wintertime, high probability Dover sole habitat extended eastward from the Bering Canyon into Bristol Bay (Figure 47). The most important covariates predicting suitable habitat from the MaxEnt model were, in order of importance, bottom temperature, sediment grain size, and bottom depth (combined relative importance of 67%). The model fit to the training data was outstanding (AUC = 1.0); it correctly classified 100% of predicted cases. Model validation with the test data set was also outstanding (AUC = 0.96), correctly classifying 96% of cases.

In the spring, the pattern of suitable habitat resembled that seen in fall with high probability areas predicted over Bering Canyon and near the head of Pribilof Canyon (Figure 48). The most important covariates predicting probability of suitable Dover sole habitat from the MaxEnt model were, in order of importance, bottom slope, bottom depth, and ocean productivity (combined relative importance of 85.3%). The model fit to the training data was outstanding (AUC = 0.99); it correctly classified 93% of predicted cases. Model validation with the test data set was excellent (AUC = 0.87), correctly classifying 87% of cases.

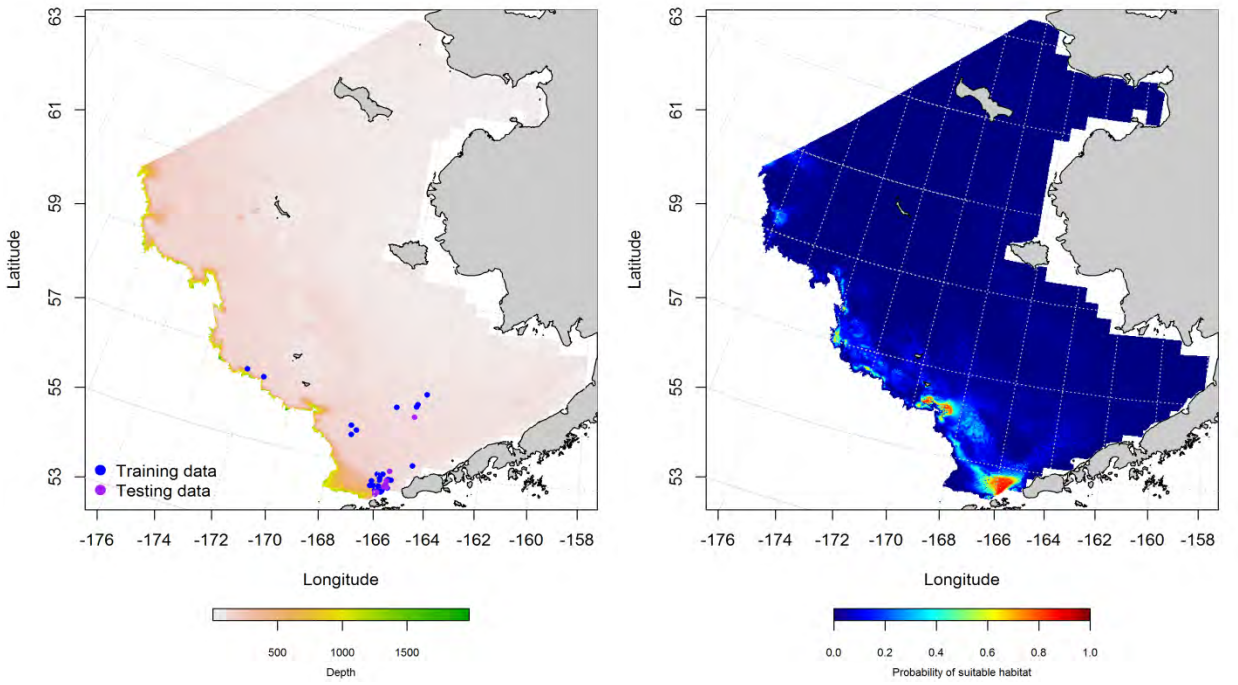

Figure 46. -- Locations of fall (October-November) catches of Dover sole in commercial fisheries of the Eastern Bering Sea (left panel). Blue points were used to train the maximum entropy (MaxEnt) model predicting the probability of suitable habitat (right panel) and the purple points were used to validate the model.

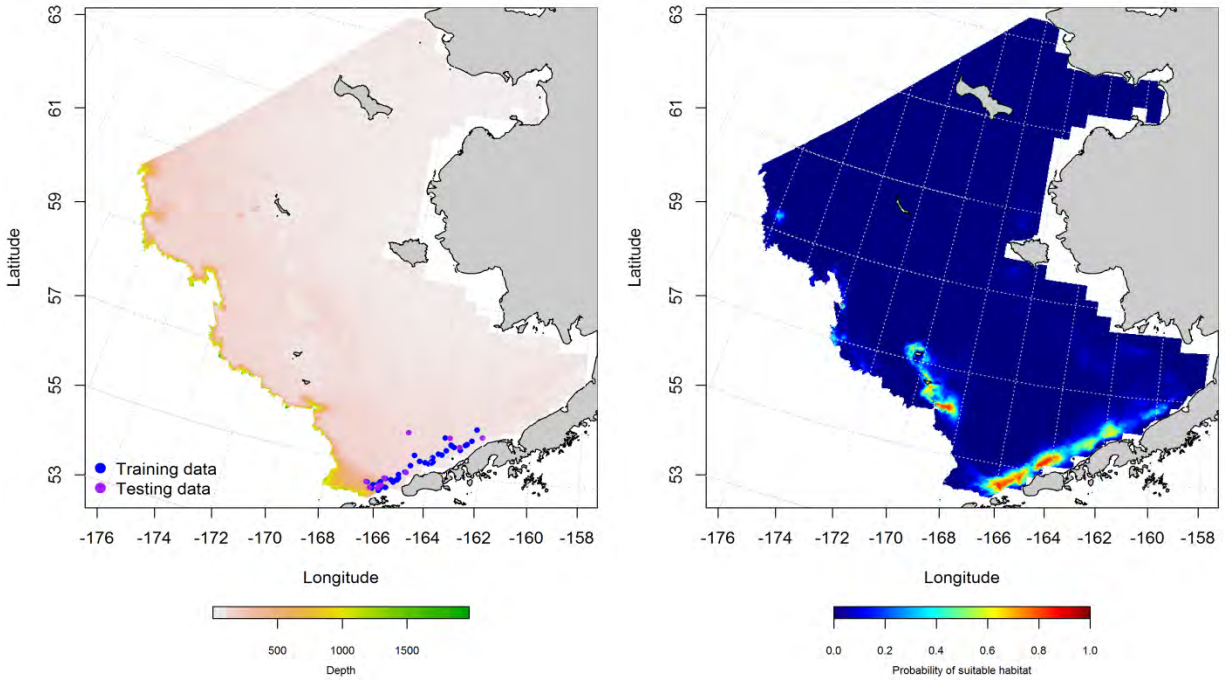

Figure 47. -- Locations of winter (December-February) catches of Dover sole in commercial fisheries of the Eastern Bering Sea (left panel). Blue points were used to train the maximum entropy (MaxEnt) model predicting the probability of suitable habitat (right panel) and the purple points were used to validate the model.

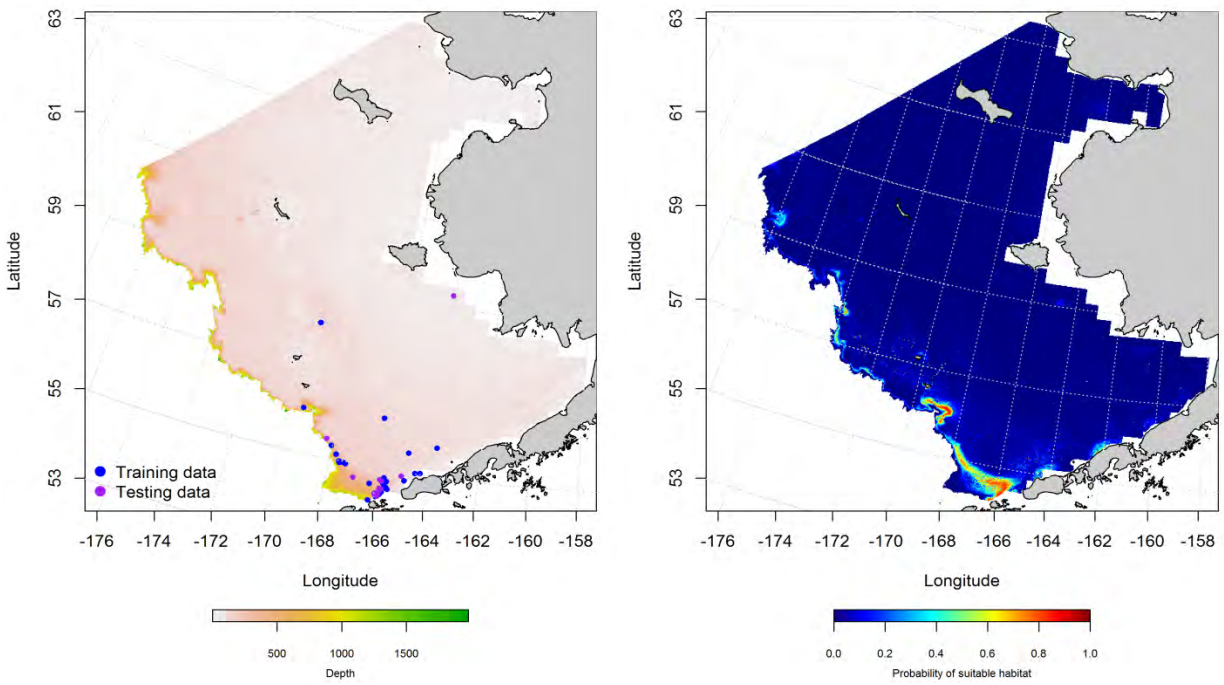

Figure 48. -- Locations of spring (March-May) catches of Dover sole in commercial fisheries of the Eastern Bering Sea (left panel). Blue points were used to train the maximum entropy (MaxEnt) model predicting the probability of suitable habitat (right panel) and the purple points were used to validate the model.

Eastern Bering Sea Dover sole (*Microstomus pacificus*) essential fish habitat maps and conclusions – Summertime EFH of late juvenile Dover sole differed from the adults (Figure 49). Late juvenile EFH was widely spread across the southern domain of the Eastern Bering Sea. Both life history stages shared the areas with the highest likelihood of providing suitable habitat. These were along the shelf edge in waters ≥ 200 m in the southern domain.

There were marked seasonal differences in the spatial distribution of Dover sole EFH determined from commercial fishery catches (Figure 50). In general, the highest probability areas were over deeper waters of the outer shelf and slope edge like what was seen from the RACE summer bottom trawl survey. Persistent areas of high probability habitat were over the Bering Canyon and near the head of Pribilof Canyon. Seasonal differences in the spatial distribution of Dover sole EFH predicted from commercial

fishery catches may be more dependent upon the locations of fishing activity than actual distribution of the species.

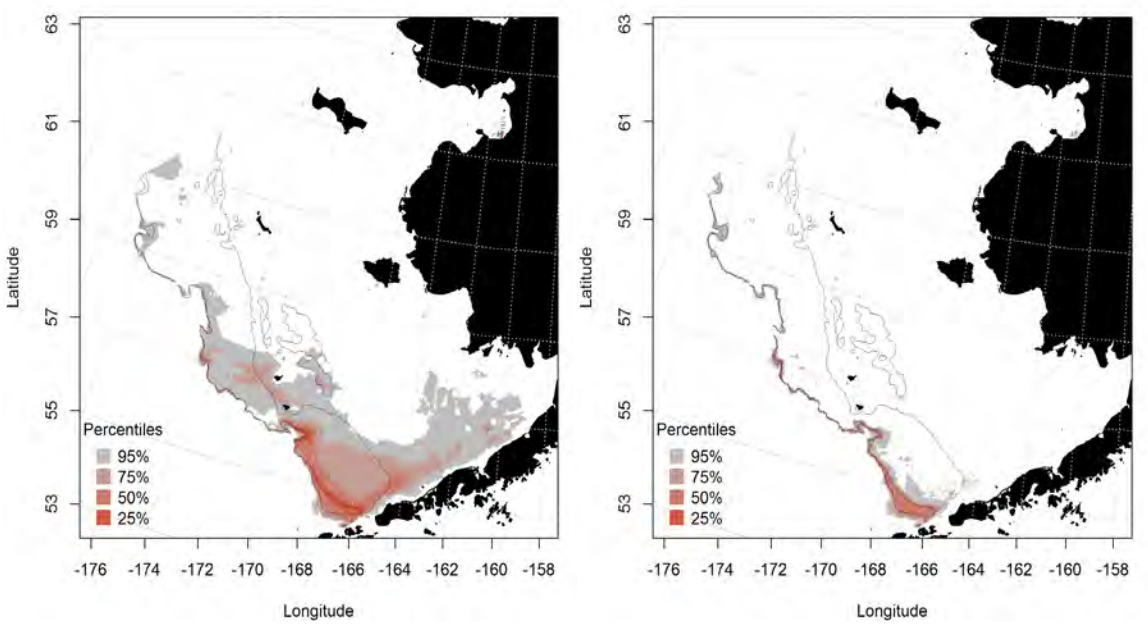

Figure 49. -- Essential habitat for late juvenile and adult Dover sole collected in RACE summertime bottom trawl surveys of the Eastern Bering Sea.

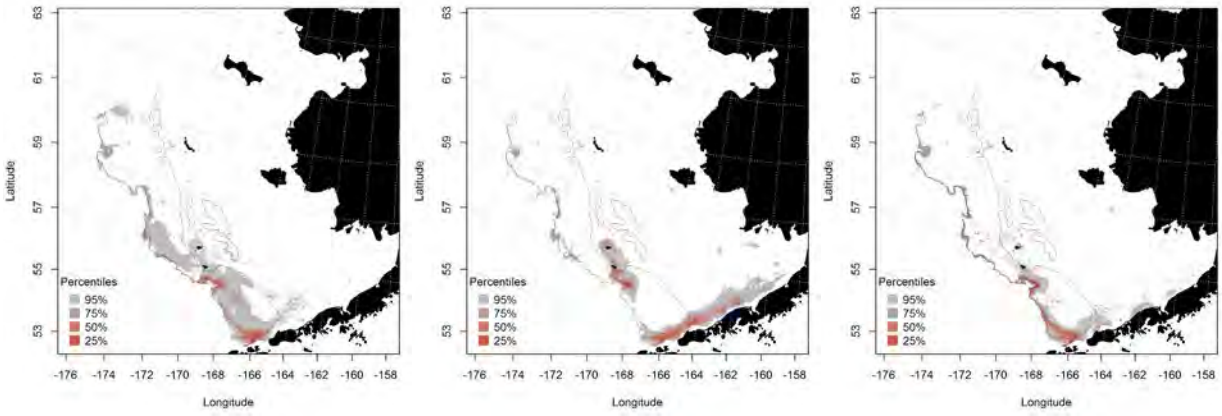

Figure 50. -- Essential fish habitat predicted for Dover sole from commercial fishery catches during fall (left panel), winter (middle panel), and spring (right panel).

flathead sole (*Hippoglossoides elassodon*)

Flathead sole are among the "other" commercially harvested flatfish species in the Eastern Bering Sea which includes yellowfin and the rock soles. Flathead sole and Bering flounder are from the same genus and are difficult to separate on appearance alone. There is low confidence in their identification in commercial catches and, consequently, the two species are combined into a single stock assessment by the NPFMC (Stockhausen and Nichol 2011).

Seasonal distribution of the early life history stages of flathead sole from EcoFOCI ichthyoplankton surveys of the Eastern Bering Sea -- Flathead sole eggs, larvae, and early juveniles can be distinguished from the other flatfish species in EcoFOCI ichthyoplankton samples. These early life stages are generally observed in the southern domain of the Eastern Bering Sea but distribution of these life stages varies seasonally.

Flathead sole eggs were widely reported from EcoFOCI ichthyoplankton samples during springtime in the Eastern Bering Sea (Figure 51). Most of the observations were made in the southern and southwestern portions of the region extending from the inner shelf (< 50 m) to benthypelagic waters off the shelf edge (200 to 3,000 m). There were also a few clusters of flathead sole egg observations from the Northern Bering Sea around St. Matthew's Island and Pervenets Canyon.

The most suitable habitat for flathead sole eggs was predicted with a MaxEnt model from EcoFOCI ichthyoplankton samples and was located along the northern side of Unimak Pass near the Bering Canyon (Figure 52). The most influential habitat covariates in this model were surface temperature (relative importance of 76.7%) and ocean productivity (11.5%). The fit to the training data was excellent (AUC = 0.94) and the model correctly classified 86% of predicted cases. Model validation with the test data was successful (AUC = 0.85) and correctly classified 85% of cases.

Flathead sole larvae were not observed in winter EcoFOCI ichthyoplankton surveys (Figure 53). There was only one record of a larval flathead sole reported during fall and that was near St. Matthew's Island in the Northern Bering Sea. Larvae observed in springtime were largely constrained to the southern domain

of the Eastern Bering Sea from the Bering Canyon to the inner shelf in Bristol Bay. Summertime distribution of flathead sole larvae in EcoFOCI samples was widely dispersed and occurred from Bristol Bay westward off the shelf edge and north to around St. Lawrence Island.

Distribution modelling for larval flathead sole was undertaken for the spring and summer months with a MaxEnt model (Figure 54). In spring, the highest probability areas of suitable habitat were near the head of the Bering Canyon. During summertime, the model predicted high probability habitats arrayed south to north between Unimak and St. George Islands with a small patch of suitable habitat out in Bristol Bay. Surface temperature and ocean productivity were the two dominant habitat covariates exerting leverage on the models in both of these seasons. Their combined influence summed to 61.4% of relative importance in spring and 70.4% in summer. The third most important predictor of suitable larval flathead sole habitat was bottom depth in spring (relative important of 7.8%) and surface current speed in summer (10.4%). The MaxEnt models were outstanding fits to the training data in both seasons (AUC = 0.98 and 0.91 in spring and summer) and correctly classified 83 and 94% of predicted cases. Model validation using the test data demonstrated excellent model fits (AUC = 0.83 and 0.84 in spring and summer) correctly classifying 83 and 84% of cases.

Early juvenile stage flathead sole were not common in EcoFOCI ichthyoplankton samples in the Eastern Bering Sea (Figure 55). The 10 occurrences reported were spread from the Alaska Peninsula to the Pribilof Islands. These did not provide sufficient data for distribution modeling.

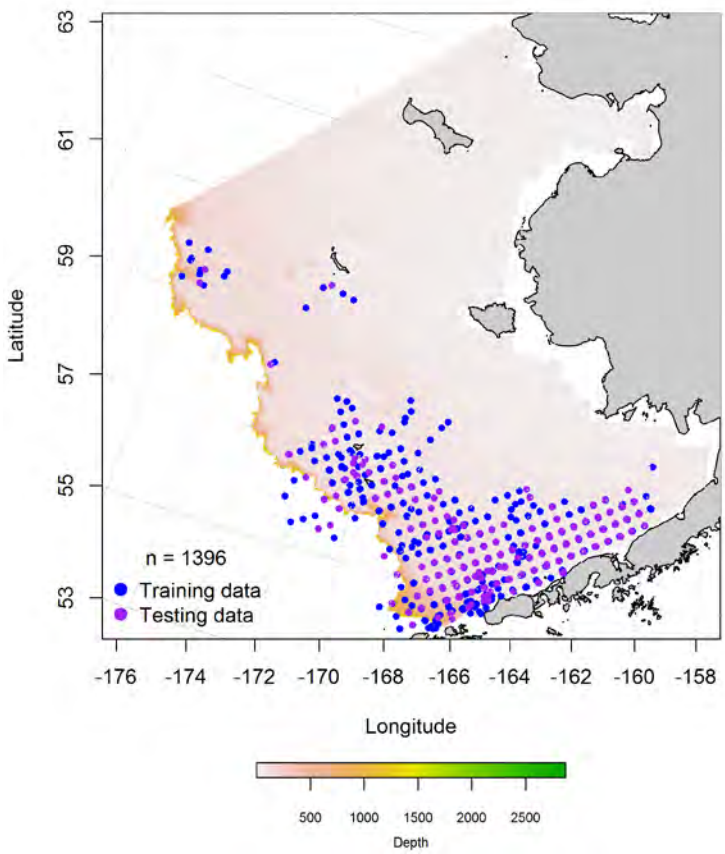

Figure 51. -- Springtime observations of flathead sole eggs from EcoFOCI ichthyoplankton surveys of the Eastern Bering Sea. Blue points were used to train the maximum entropy (MaxEnt) model predicting the probability of suitable habitat (right panel) and the purple points were used to validate the model.

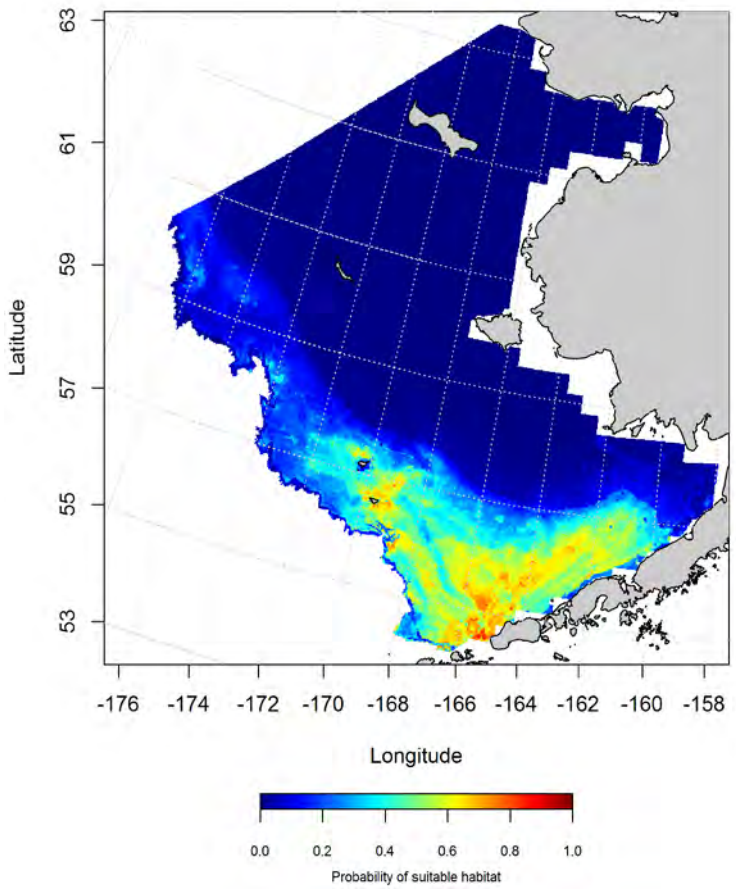

Figure 52. -- Maximum entropy (MaxEnt) model predictions of the probability of suitable habitat for flathead sole eggs from EcoFOCI ichthyoplankton surveys of the Eastern Bering Sea.

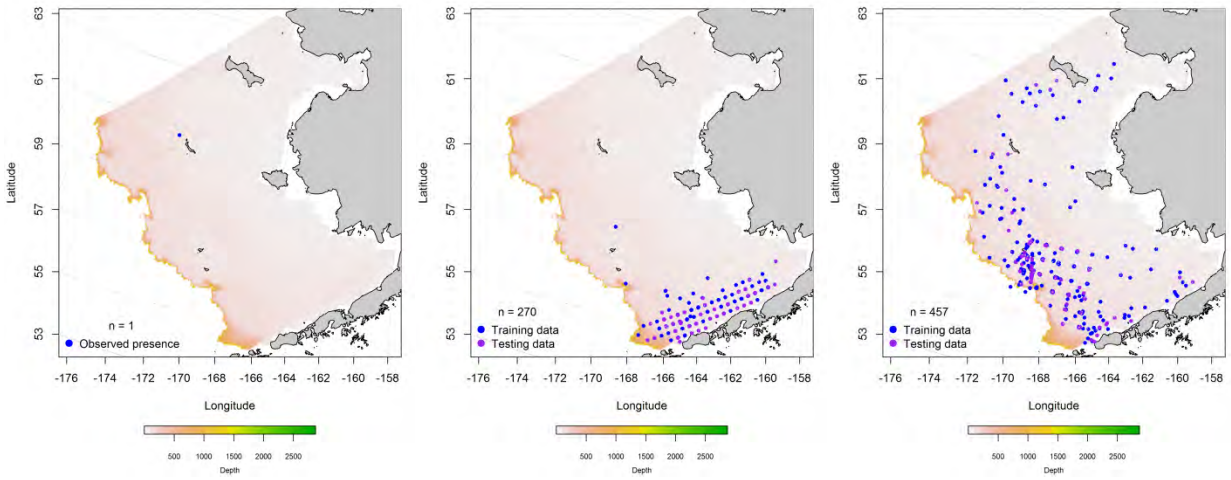

Figure 53. -- Fall, spring, and summer observations (left, middle, and right panel, respectively) of larval flathead sole from EcoFOCI ichthyoplankton surveys of the Eastern Bering Sea. Blue points were used to train the maximum entropy (MaxEnt) model predicting the probability of suitable habitat (right panel) and the purple points were used to validate the model.

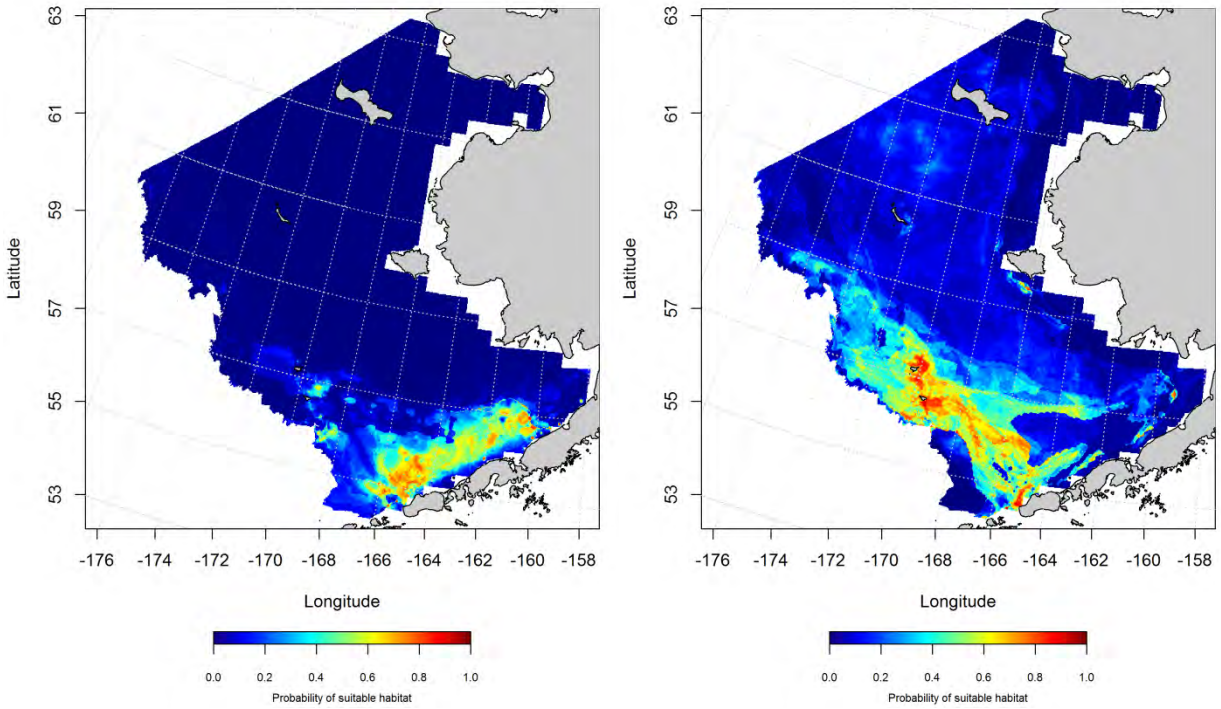

Figure 54. -- Maximum entropy (MaxEnt) model predictions of the probability of suitable spring and summer (left and right panels) habitat of larval flathead sole from EcoFOCI ichthyoplankton surveys of the Eastern Bering Sea.

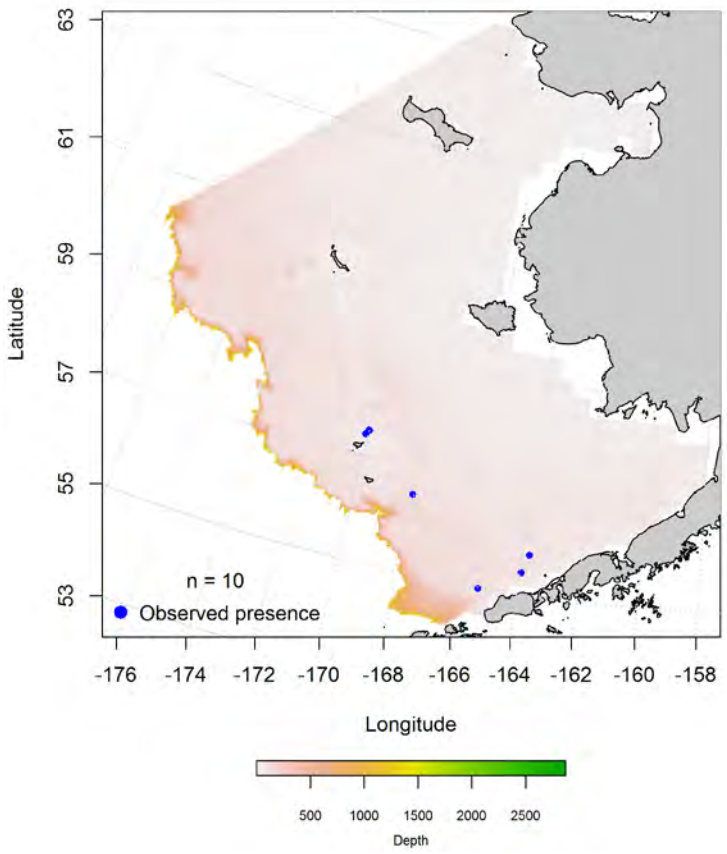

Figure 55. -- Summertime observation of early juvenile flathead sole from EcoFOCI ichthyoplankton surveys of the Eastern Bering Sea.

Essential fish habitat maps and conclusions for early life history stages of flathead sole from the Eastern Bering Sea – Essential habitat of flathead sole eggs was modeled from springtime EcoFOCI ichthyoplankton surveys of the Eastern Bering Sea (Figure 56). Essential egg habitat for this species extended from the outer shelf in the northern domain over the middle shelf of the central domain and into Bristol Bay in southern domain. Areas with the highest probability of holding suitable flathead sole egg habitat were found between St. George Island in the Pribilof Islands and Bristol Bay.

The distribution of essential larval flathead sole habitat predicted from EcoFOCI ichthyoplankton surveys of the Eastern Bering Sea differed between spring and summer (Figure 57). In spring, larval EFH was predicted to run east to west over the outer and middle shelf parallel to the Alaska Peninsula. In summer

months, high probability EFH extended from Unimak Pass and Bristol Bay northward across the outer and middle shelf to the Pribilof Islands.

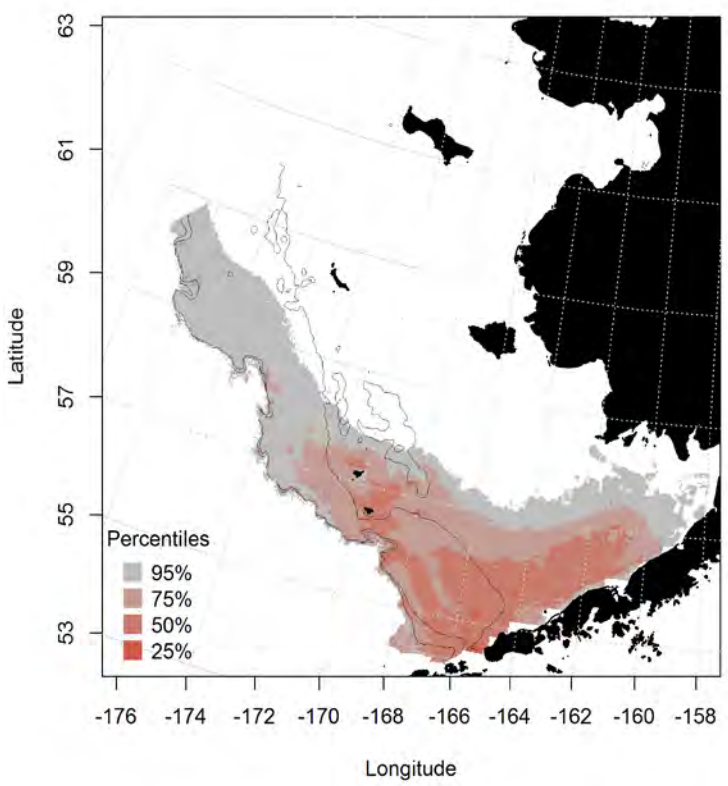

Figure 56. -- Essential habitat of flathead sole eggs in springtime predicted from EcoFOCI ichthyoplankton surveys of the Eastern Bering Sea.

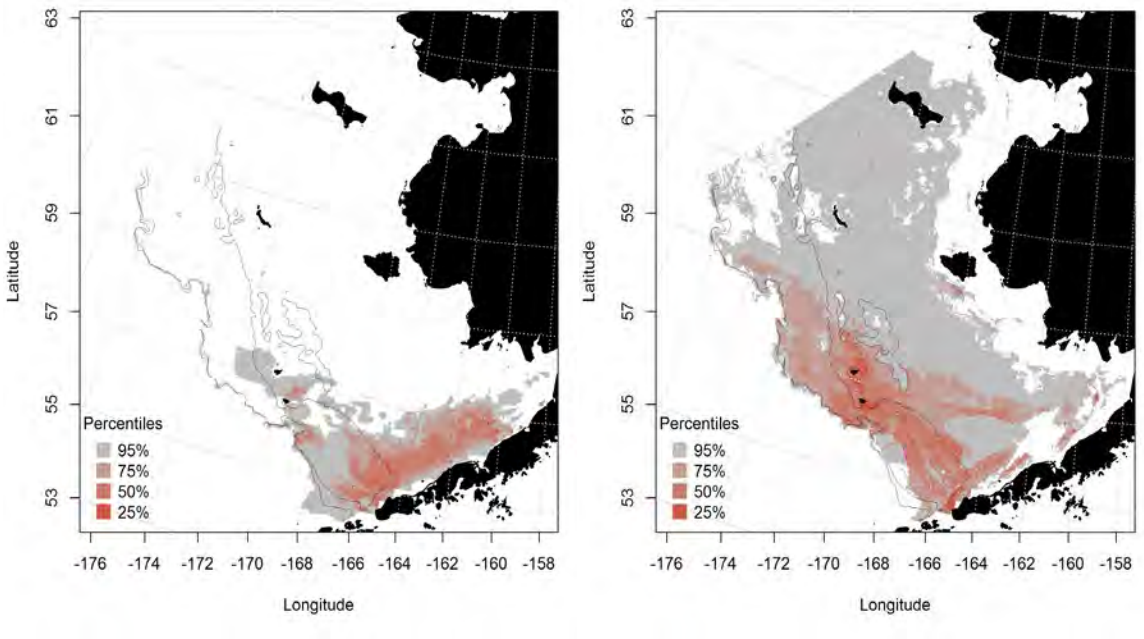

Figure 57. -- Spring and summer (left and right panels) essential larval flathead sole habitat predicted from EcoFOCI ichthyoplankton surveys of the Eastern Bering Sea.

Summertime distribution of late-juvenile and adult flathead sole from RACE bottom trawl surveys of the Eastern Bering Sea – Late juvenile and adult flathead sole catches in RACE summer bottom trawl surveys of the Eastern Bering Sea were spread from the northern to southern extent of the survey area from the inner to the outer shelf (Figure 58). Historically, high flathead sole CPUEs have been recorded on the middle shelf around the Pribilof Islands (Lauth and Conner 2014).

The best-fitting GAM for late juvenile flathead sole abundance in the Eastern Bering Sea explained 57.9% of the deviance in the CPUE data (Figure 59). Geographical location, sediment grain size, bottom depth, and temperature were the most important predictors amongst the 10 habitat covariates retained in the GAM. Juvenile flathead sole abundance decreased from southwest to northeast across the survey area and bottom depth and increased with increasing bottom temperature and decreasing sediment grain size. The fit of this model was fair ($r^2 = 0.58$). The fit to the test data in the model validation step was nearly the same ($r^2 = 0.58$).

The best-fitting GAM describing adult flathead abundance explained 58.7% of the deviance in the CPUE data from the Eastern Bering Sea (Figure 60). Geographical location, bottom depth, sediment grain size, and bottom temperature were the most influential habitat covariates retained in the model. Model effects on abundance were highest in the southeast portion of the survey area and decreased to the north and northeast. Modeled abundance increased over finer sediments and warmer temperatures and decreased with increasing bottom depth. The GAM fit to the training data was fair ($r^2 = 0.59$). The fit to the test data in the model validation step was slightly higher ($r^2 = 0.61$).

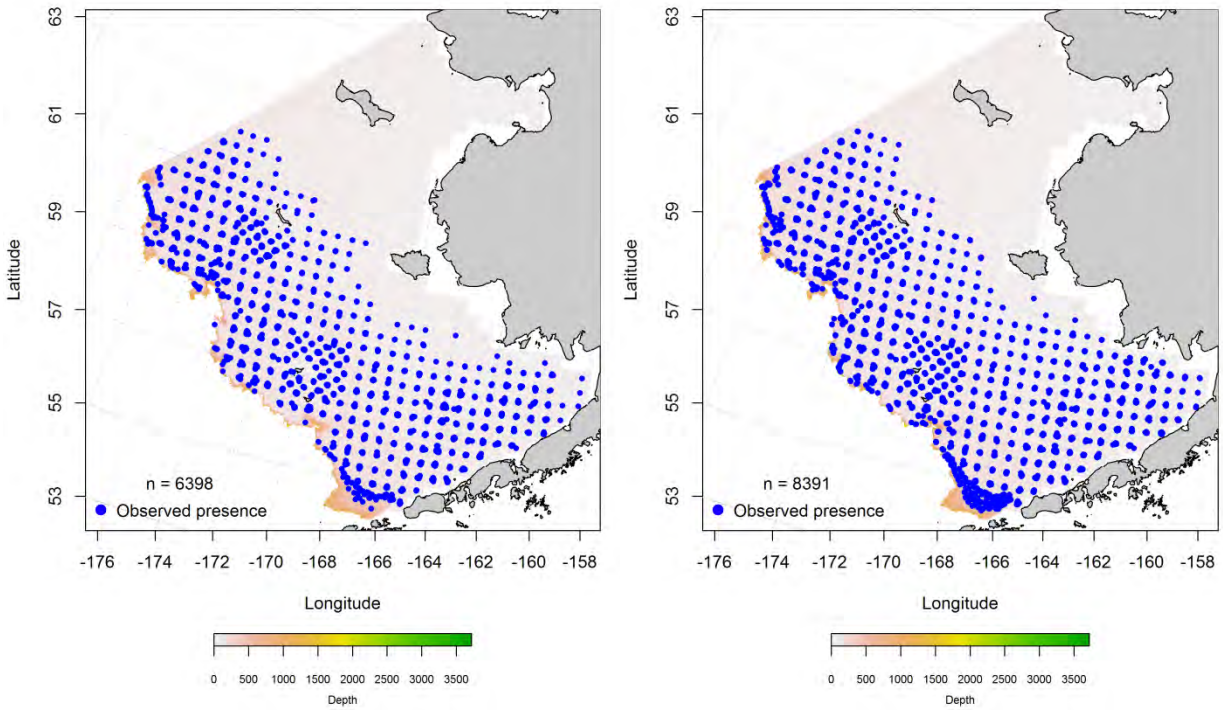

Figure 58. -- Distribution of late-juvenile (left) and adult (right) flathead sole catches from RACE summer bottom trawl surveys of the Eastern Bering Sea.

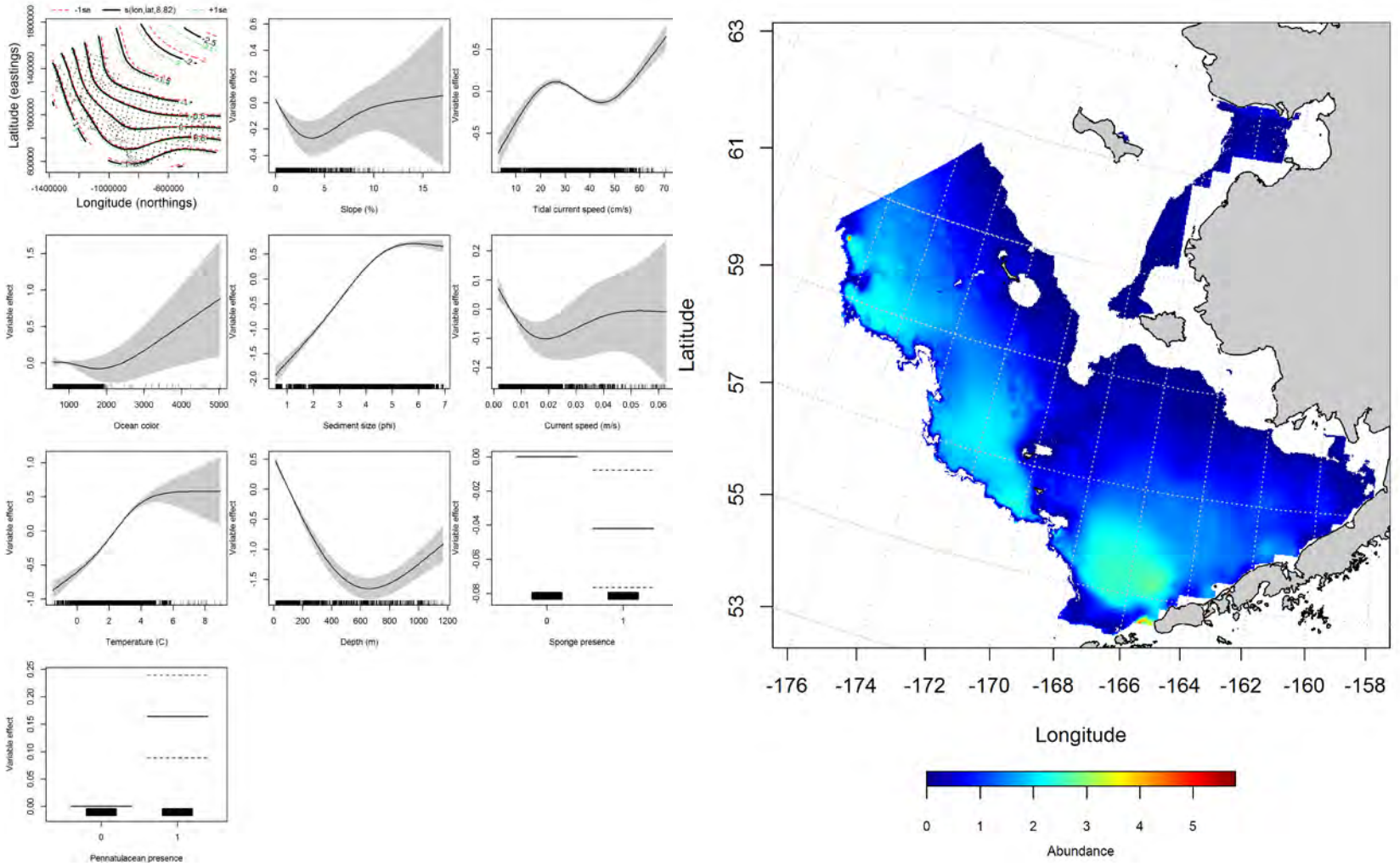

Figure 59. -- Effects of retained habitat covariates on the best-fitting generalized additive model (GAM; left panel) of late juvenile flathead sole abundance in RACE summer bottom trawl surveys of the Eastern Bering Sea Shelf, Slope, and Northern Bering Sea alongside their predicted abundance (right panel).

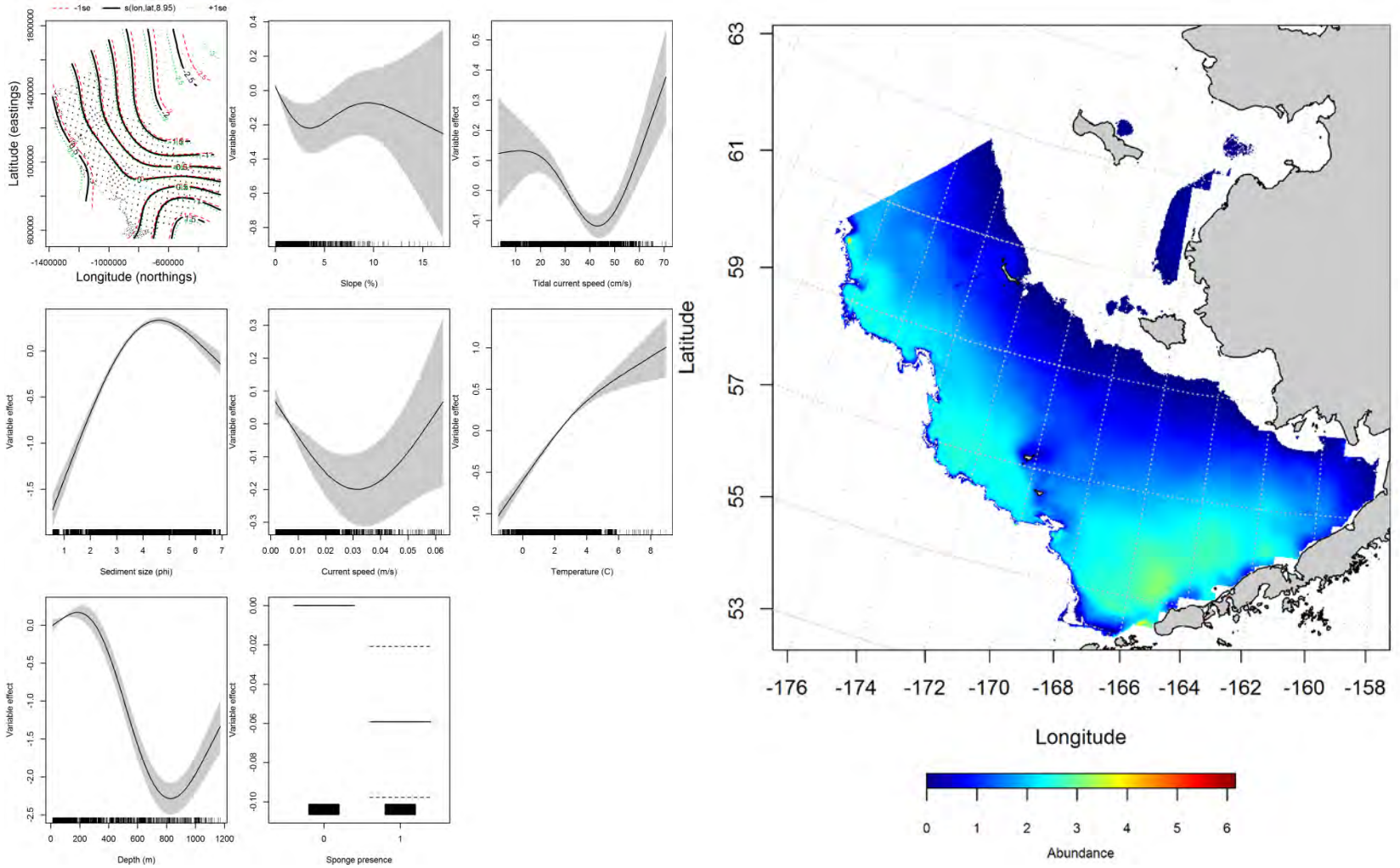

Figure 60. -- Effects of retained habitat covariates on the best-fitting generalized additive model (GAM; left panel) of adult flathead sole abundance in RACE summer bottom trawl surveys of the Eastern Bering Sea Shelf, Slope, and Northern Bering Sea alongside their predicted abundance (right panel).

Seasonal distribution of flathead sole in commercial fishery catches from the Eastern Bering Sea – In the fall, depth and bottom temperature were the most important variables determining the distribution of flathead sole in commercial catches (relative importance = 73.3 and 18.4%). The probability of encountering flathead sole decreased with increasing bottom depth and increased with increasing bottom temperature. Their distribution in commercial catches extended over the middle and outer shelf across the north-south extent of the Eastern Bering Sea survey area (Figure 61). The MaxEnt model for fall observations of flathead sole was an excellent fit to the training data (AUC = 0.87) correctly classifying 79% of predicted cases. The fit to the test data in the model validation step was acceptable (AUC = 0.79) and correctly classified 79% of cases.

In the winter, depth and bottom temperature were the most important variables determining the distribution of flathead sole (relative importance = 60.0 and 30.6%). Flathead sole in wintertime commercial catches were primarily encountered over the outer shelf in the northwest portion of the Eastern Bering Sea and extended from the outer shelf into Bristol Bay in the southern domain (Figure 62). The MaxEnt model for flathead sole presence in winter was an outstanding fit to the training data (AUC = 0.92) and correctly classified 84% of predicted cases. Validation using the test data was excellent (AUC = 0.84) and the best-fitting model correctly classified 84% of cases predicted.

In the spring, depth and bottom temperature were once again the most important variables determining the distribution of flathead sole in commercial catches from the Eastern Bering Sea (relative importance = 58.8 and 23.3%). Flathead sole in spring commercial catches extended from the outer shelf into Bristol Bay in the southern domain, but were primarily encountered over the outer shelf in the northwest portion of the Eastern Bering Sea and (Figure 63). The MaxEnt model for flathead sole presence in springtime was an outstanding fit to the training data (AUC = 0.90) and correctly classified 82% of predicted cases. Validation using the test data was excellent (AUC = 0.82) and the best-fitting model correctly classified 82% of cases predicted.

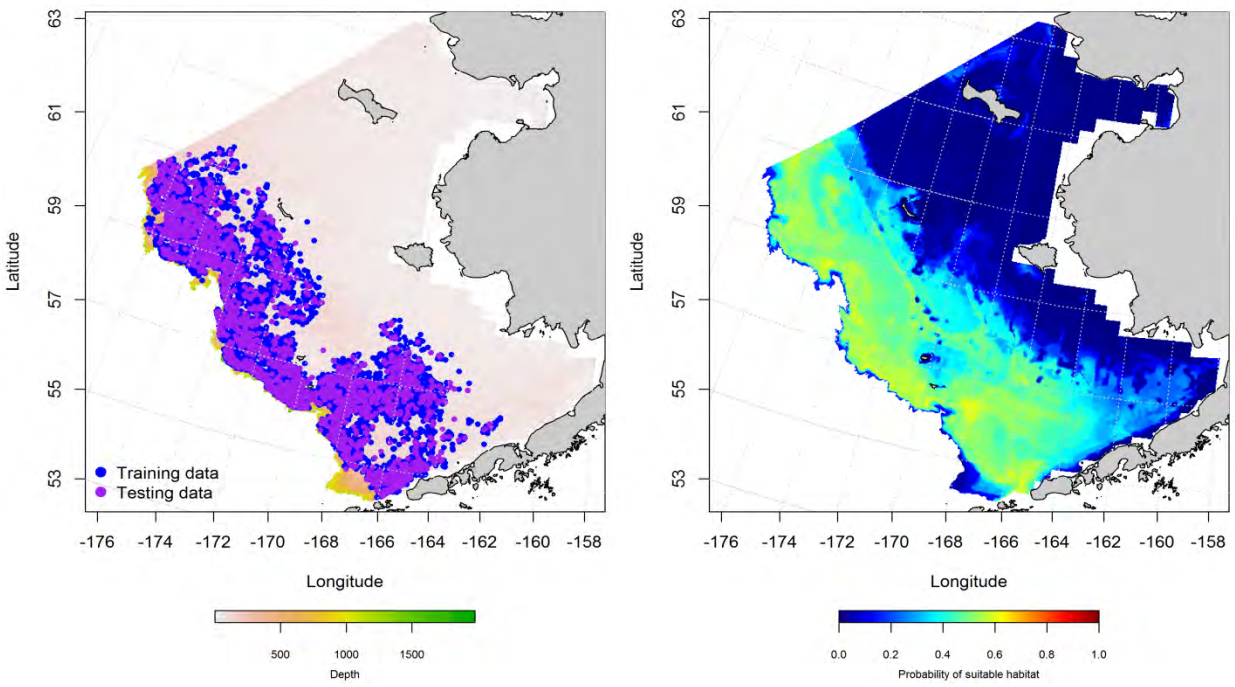

Figure 61. -- Locations of fall (October-November) catches of flathead sole in commercial fisheries of the Eastern Bering Sea (left panel). Blue points were used to train the maximum entropy model predicting the probability of suitable habitat (right panel) and the purple points were used to validate the model.

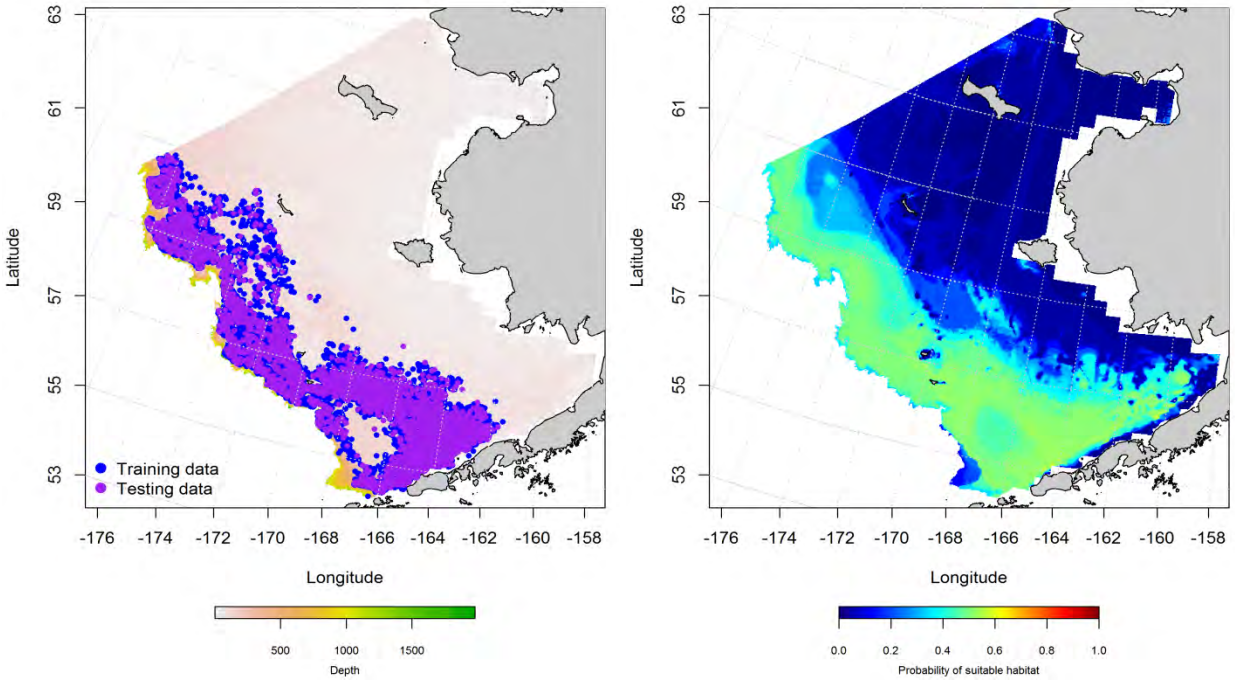

Figure 62. -- Locations of winter (December-February) catches of flathead sole in commercial fisheries of the Eastern Bering Sea (left panel). Blue points were used to train the maximum entropy model predicting the probability of suitable habitat (right panel) and the purple points were used to validate the model.

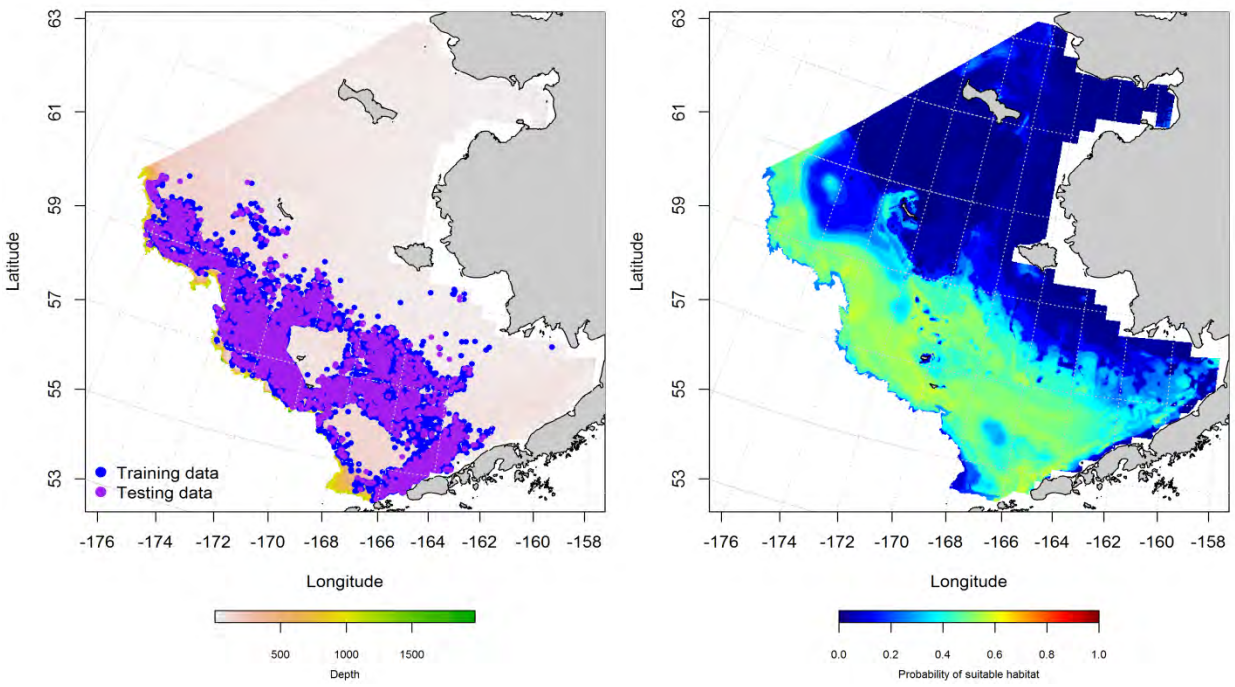

Figure 63. -- Locations of spring (March-May) catches of flathead sole in commercial fisheries of the Eastern Bering Sea (left panel). Blue points were used to train the maximum entropy model predicting the probability of suitable habitat (right panel) and the purple points were used to validate the model.

Eastern Bering Sea flathead sole (*Hippoglossoides elassodon*) essential fish habitat maps and conclusions -- Summertime EFH of late-juvenile and adult flathead sole was spread across the outer and middle shelf from the southern domain of the Eastern Bering Sea to the northwest portion of the survey area (Figure 64). In general, EFH of both life stages were similarly distributed although there were more late-juveniles in Norton Sound. Areas of highest predicted abundance persisted over the outer and middle shelf of the southern domain as well as along the outer shelf in the central and northern domains of the Eastern Bering Sea.

Overall, distribution of flathead sole EFH determined from commercial fishery activity showed very little seasonal difference and was spread over the outer shelf in the northwest portion of the Eastern Bering Sea, extending from the outer shelf to Bristol Bay in the southern domain (Figure 65). Areas of highest probability were consistently located over the outer shelf in the central domain of the Eastern Bering Sea.

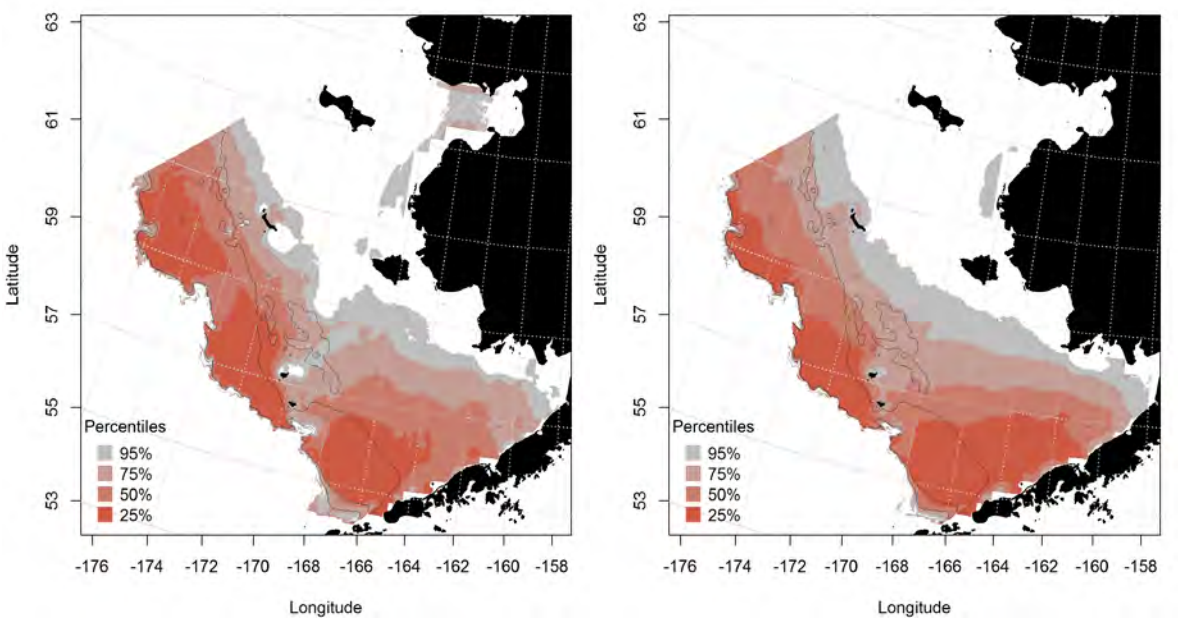

Figure 64. -- Summertime essential fish habitat predicted for flathead sole late juveniles and adults (left and right panel) from RACE bottom trawl surveys.

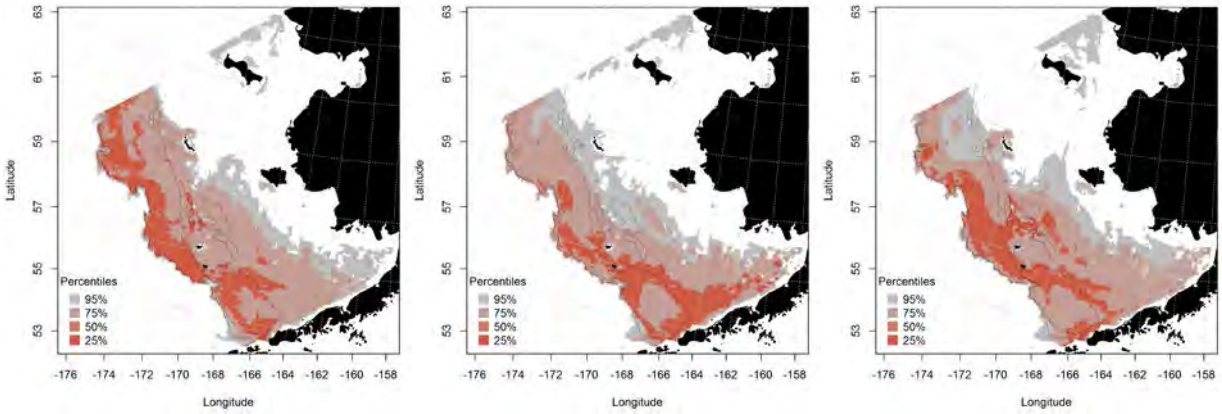

Figure 65. -- Essential fish habitat predicted for flathead sole from commercial fishery catches during fall (left panel), winter (middle panel), and spring (right panel).

yellowfin sole (*Limanda aspera*)

Yellowfin sole support an important commercial fishery in the Eastern Bering Sea. They are one of the most abundant flatfish in the region. Yellowfin are found primarily in waters shallower than 100 m over the continental shelf.

Seasonal distribution of early life history stages of yellowfin sole from EcoFOCI ichthyoplankton surveys of the Eastern Bering Sea –Yellowfin sole eggs were collected during fall, spring, and summer EcoFOCI ichthyoplankton surveys of the Eastern Bering Sea (Figure 66). Eggs appeared to be most common in the summer surveys. Presence of yellowfin sole eggs in spring and summer EcoFOCI surveys was sufficient to support MaxEnt modeling of yellowfin sole egg distribution.

Spring and summer predictions of suitable yellowfin sole egg habitat were produced using MaxEnt modeling (Figure 67). During spring months, the areas with the highest likelihood to provide suitable habitat for yellowfin sole eggs were along the Alaska Peninsula and southern margin of Bristol Bay. The most important habitat covariates in the model were surface temperature (relative importance = 32.8%) and ocean productivity (relative importance = 30%). The habitat covariates with the greatest influence on the summer model were bottom depth (relative importance = 24.8%) and ocean productivity (relative importance = 14%). Both the spring and summer models were outstanding fits to the egg presence data (AUC = 0.98 and 0.89). These MaxEnt models correctly classified 96% of the predicted cases in spring and 81% in summer. Model validation runs fit the test data well in both seasons (AUC = 0.90 was outstanding in spring and acceptable (0.76) in summer) with 90% and 76% of predicted cases correctly classified.

Larval yellowfin sole were observed in EcoFOCI ichthyoplankton surveys during the fall and summer seasons (Figure 68). Occurrences of this life stage in both seasons were observed over the middle shelf of the Eastern Bering Sea in waters shallower than 100 m. Observations of larval yellowfin sole in survey samples were more common in summer and provided sufficient data to parameterize a MaxEnt model to describe larval yellowfin sole habitat.

Suitable summer habitat for larval yellowfin sole in the Eastern Bering Sea was predicted to occur primarily over the middle and outer shelf in < 100 m of water (Figure 69). The most influential habitat covariates in the summer MaxEnt model were bottom depth and ocean productivity (relative importance

= 47.8% and 24.7%). The model fit to summer yellowfin sole larval presence data was excellent (AUC = 0.88) and correctly classified 80% of the cases it predicted. Model validation produced an acceptable fit of the model to the test data (AUC = 0.74) with 74% of predicted cases correctly classified.

Two records of early juvenile yellowfin sole were observed in summer EcoFOCI surveys (Figure 70). Both observations were recorded in shallow water at the mouth of Kuskokwim Bay off the west coast of continental Alaska. These two records of presence did not provide sufficient data to model early juvenile yellowfin sole habitat.

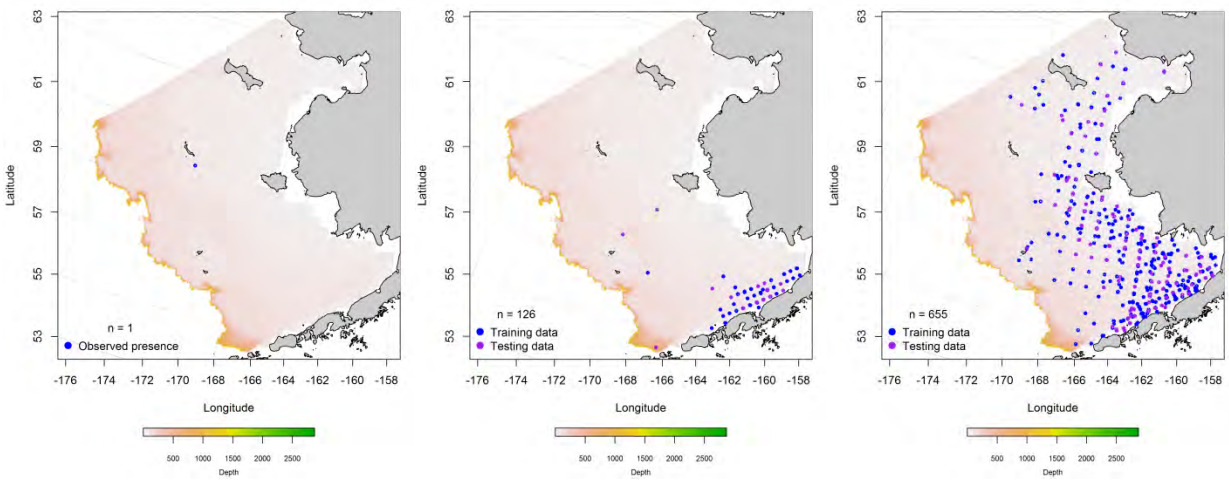

Figure 66. -- Fall (left panel), spring (middle panel), and summer (right panel) observations of yellowfin sole eggs from EcoFOCI ichthyoplankton surveys of the Eastern Bering Sea.

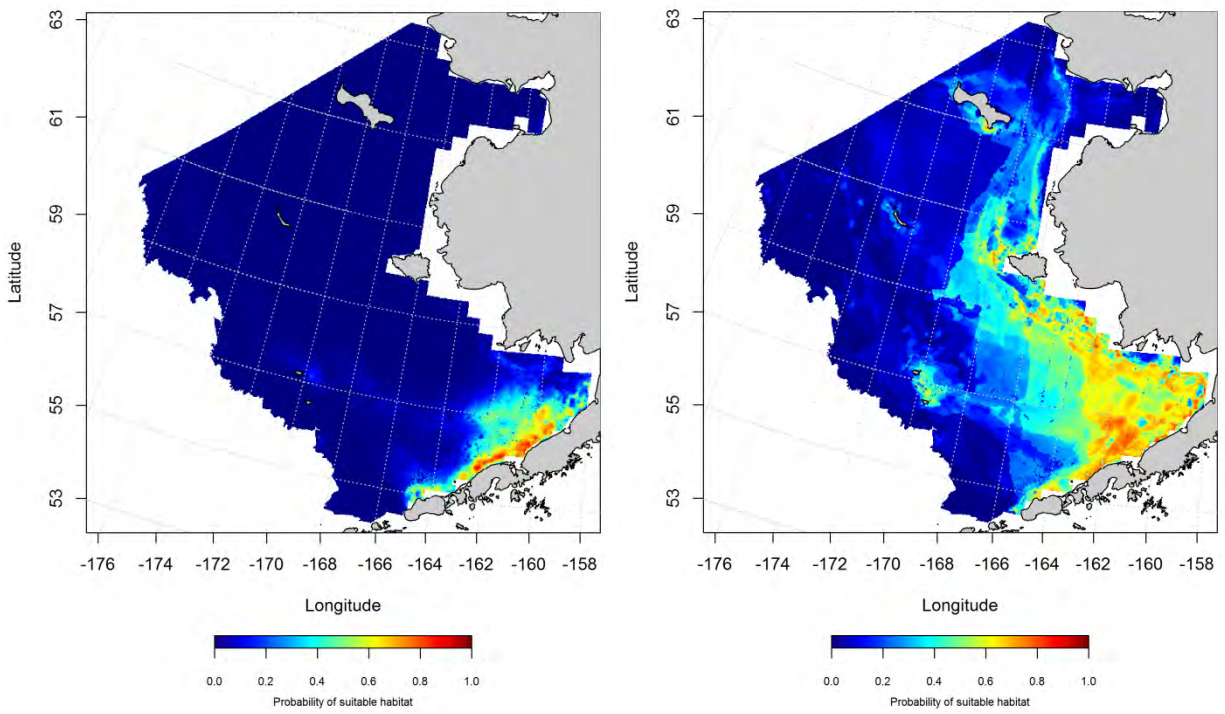

Figure 67. -- Maximum entropy (MaxEnt) model predictions of the probability of suitable spring and summer (left and right panels) yellowfin sole egg habitat from EcoFOCI ichthyoplankton surveys of the Eastern Bering Sea.

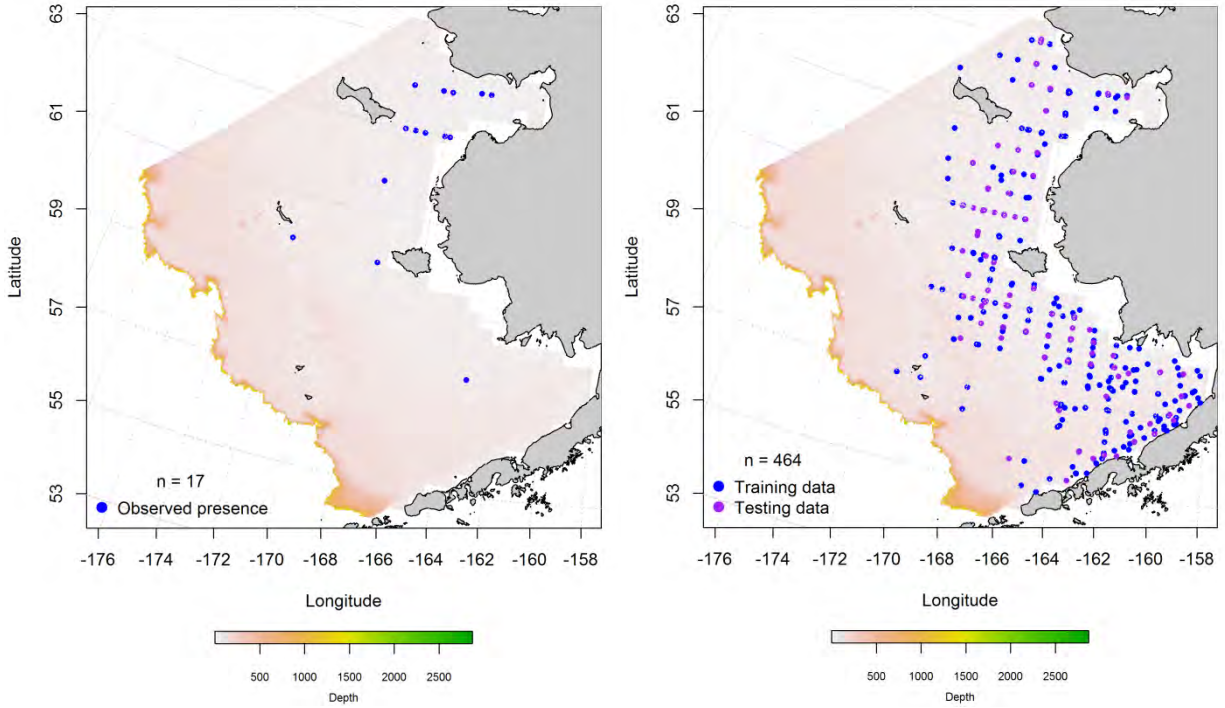

Figure 68. -- Fall (left panel) and summer (right panel) observations of larval yellowfin sole from EcoFOCI ichthyoplankton surveys of the Eastern Bering Sea; blue points were used to train the maximum

entropy model predicting the probability of suitable habitat and the purple points were used to validate the model.

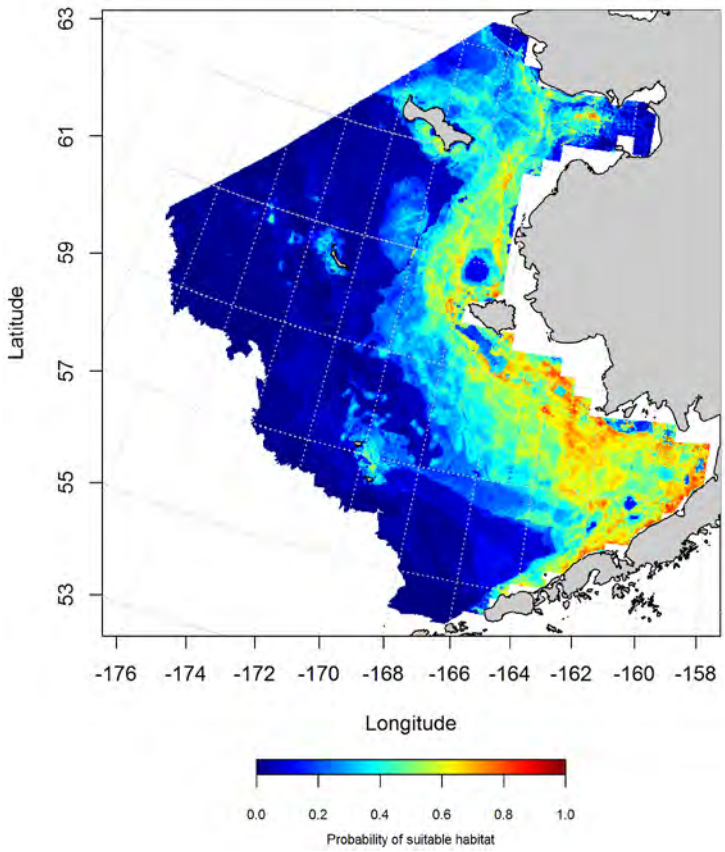

Figure 69. -- Maximum entropy (MaxEnt) model predictions of the probability of suitable summer larval yellowfin sole habitat from EcoFOCI ichthyoplankton surveys of the Eastern Bering Sea.

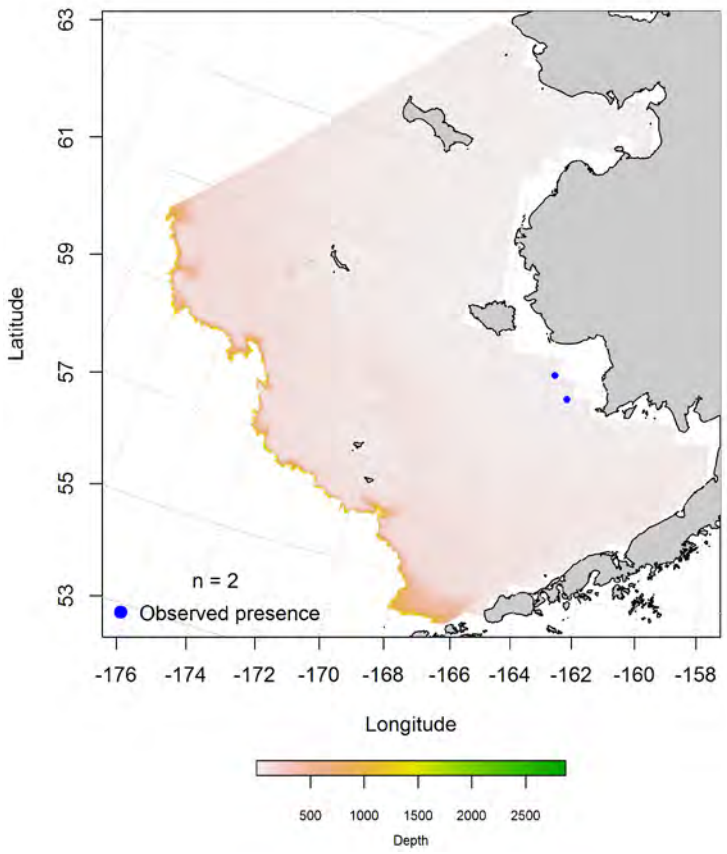

Figure 70. – Summer observations of early juvenile yellowfin sole from EcoFOCI ichthyoplankton surveys of the Eastern Bering Sea.

Essential fish habitat maps and conclusions for early life history stages of yellowfin sole (*Limanda aspera*) from the Eastern Bering Sea -- Essential habitat for yellowfin sole eggs differed between spring and summer (Figure 71). Spring predictions of high probability EFH were largely constrained to Bristol Bay. During the summer months, essential egg habitat was more widely dispersed from Bristol Bay north and westward. In both seasons, essential yellowfin sole egg habitat was generally limited to waters inshore of the 100 m isobath.

Summer distribution of EFH predicted for larval yellowfin sole overlapped the distribution of summer egg habitat (Figure 72). The areas of greatest likelihood to hold larval yellowfin sole habitat were along the inner shelf of the Eastern Bering Sea (< 50 m depths) from Bristol Bay northward into Norton Sound.

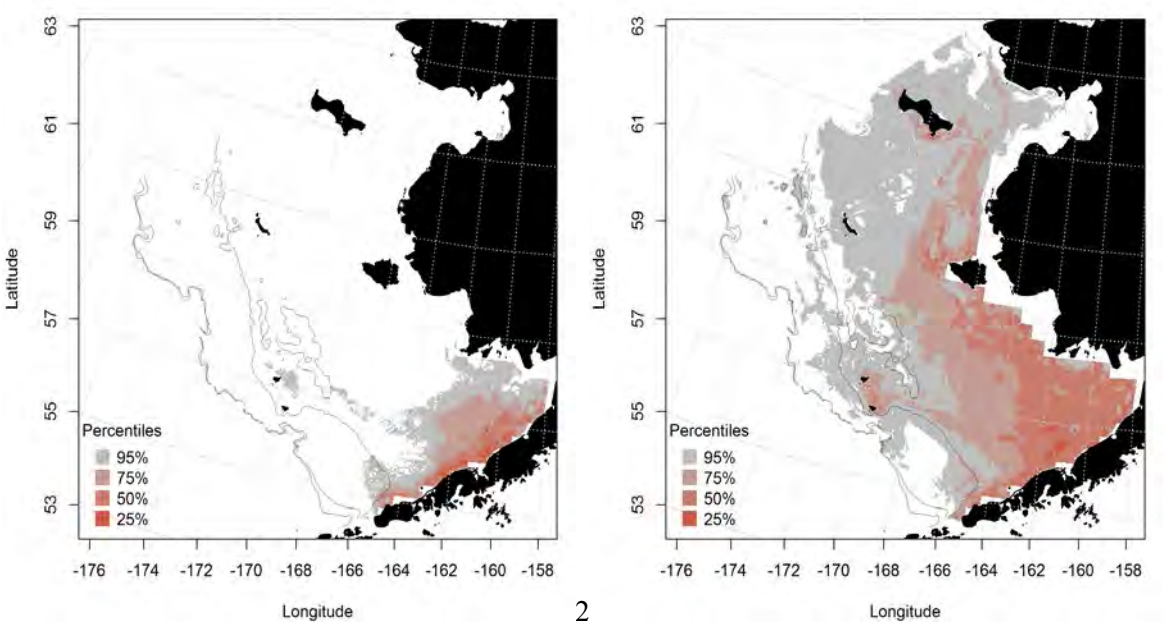

2

Figure 71. -- Spring (left panel) and summer (right panel) essential egg habitat predicted for yellowfin sole from EcoFOCI ichthyoplankton surveys of the Eastern Bering Sea.

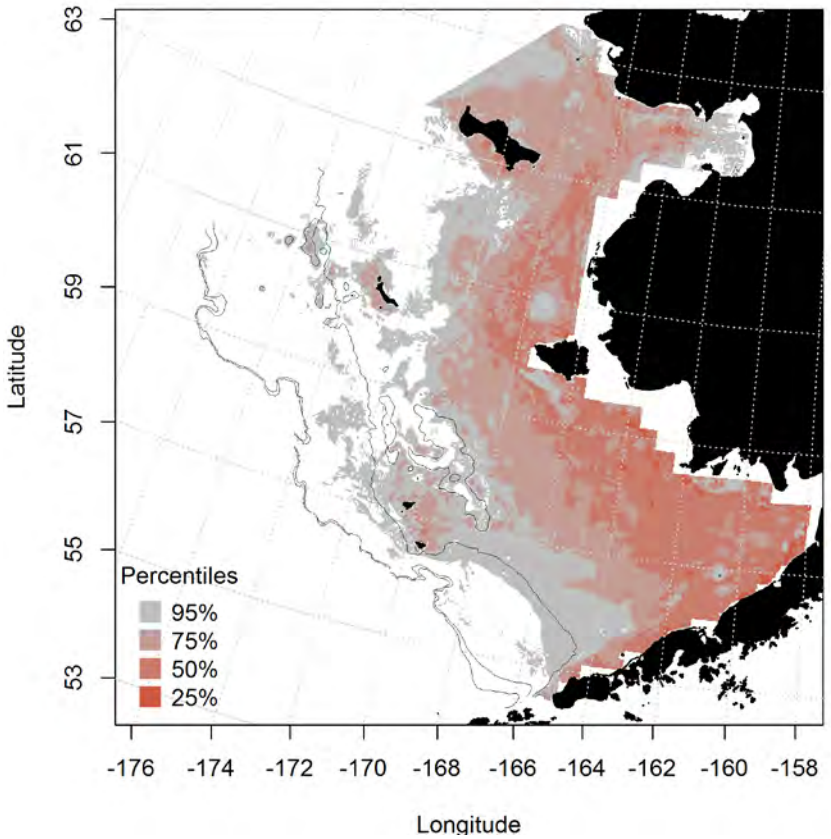

Figure 72. -- Summer essential fish habitat predicted for larval yellowfin sole from EcoFOCI surveys of the Eastern Bering Sea.

Summertime distribution of late-juvenile and adult yellowfin sole from RACE bottom trawl surveys of the Eastern Bering Sea -- Late juvenile and adult yellowfin sole collected in RACE summer bottom trawl surveys of the Eastern Bering Sea are broadly distributed across the survey area (Figure 73). The offshore extent of yellowfin sole appears to be constrained by the 100 m isobaths. Late juveniles were collected in bottom trawl catches in Norton Sound but adults were not.

The best-fitting GAM predicting late juvenile yellowfin sole abundance from RACE summer bottom trawl surveys was highest from Nunivak Island south into Bristol Bay (Figure 74). The GAM explained 80.6% of the deviance in juvenile yellowfin sole CPUE. The most important habitat covariates retained in the model were geographical location and sediment size. The fit to the training data was good ($r^2 = 0.81$) and model validation using the test data set had a similar fit ($r^2 = 0.80$).

The best-fitting GAM predicting adult yellowfin sole abundance from RACE summer bottom trawl surveys predicted the highest abundances from Bristol Bay to north of Nunivak Island and inshore of the 100 m isobath over the middle and inner shelf of the Eastern Bering Sea (Figure 75). Of the 10 habitat covariates retained in the model, the most influential predictors were geographical location, bottom temperature, and sediment size. The model explained 83.1% of the variability in the adult yellowfin sole CPUE data and was a good fit to both the training and test data ($r^2 = 0.83$ for both).

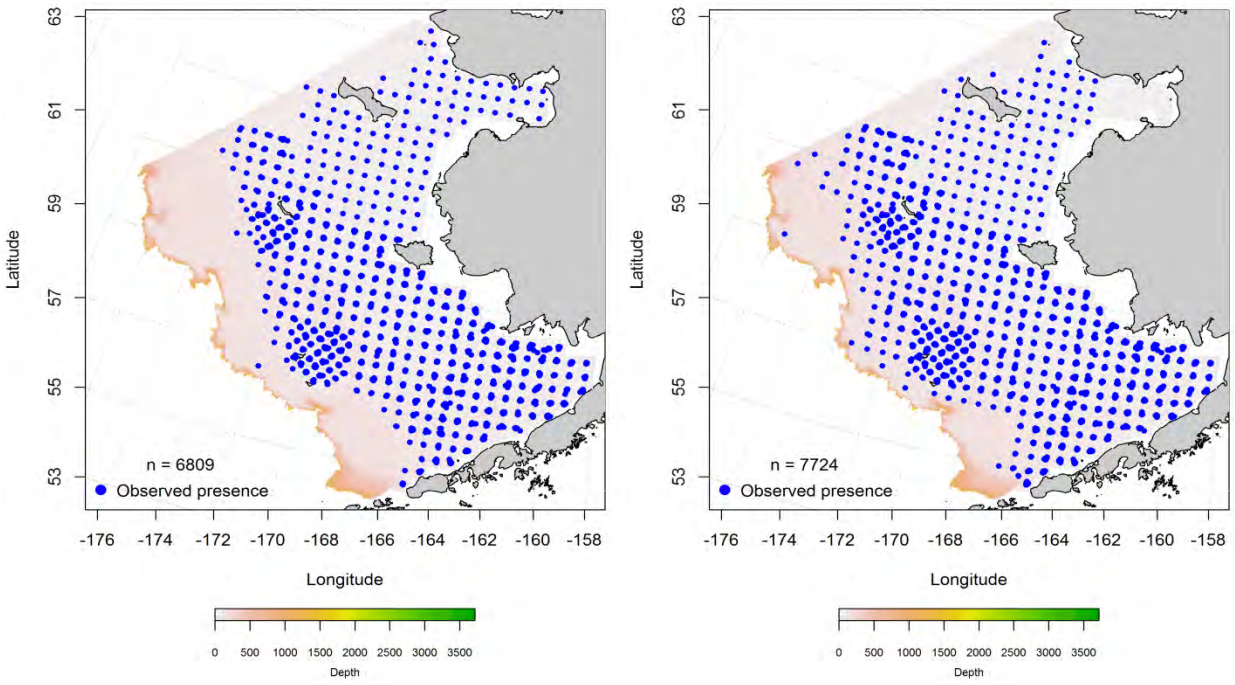

Figure 73. -- Distribution of late-juvenile (left) and adult (right) yellowfin sole catches from RACE summer bottom trawl surveys of the Eastern Bering Sea.

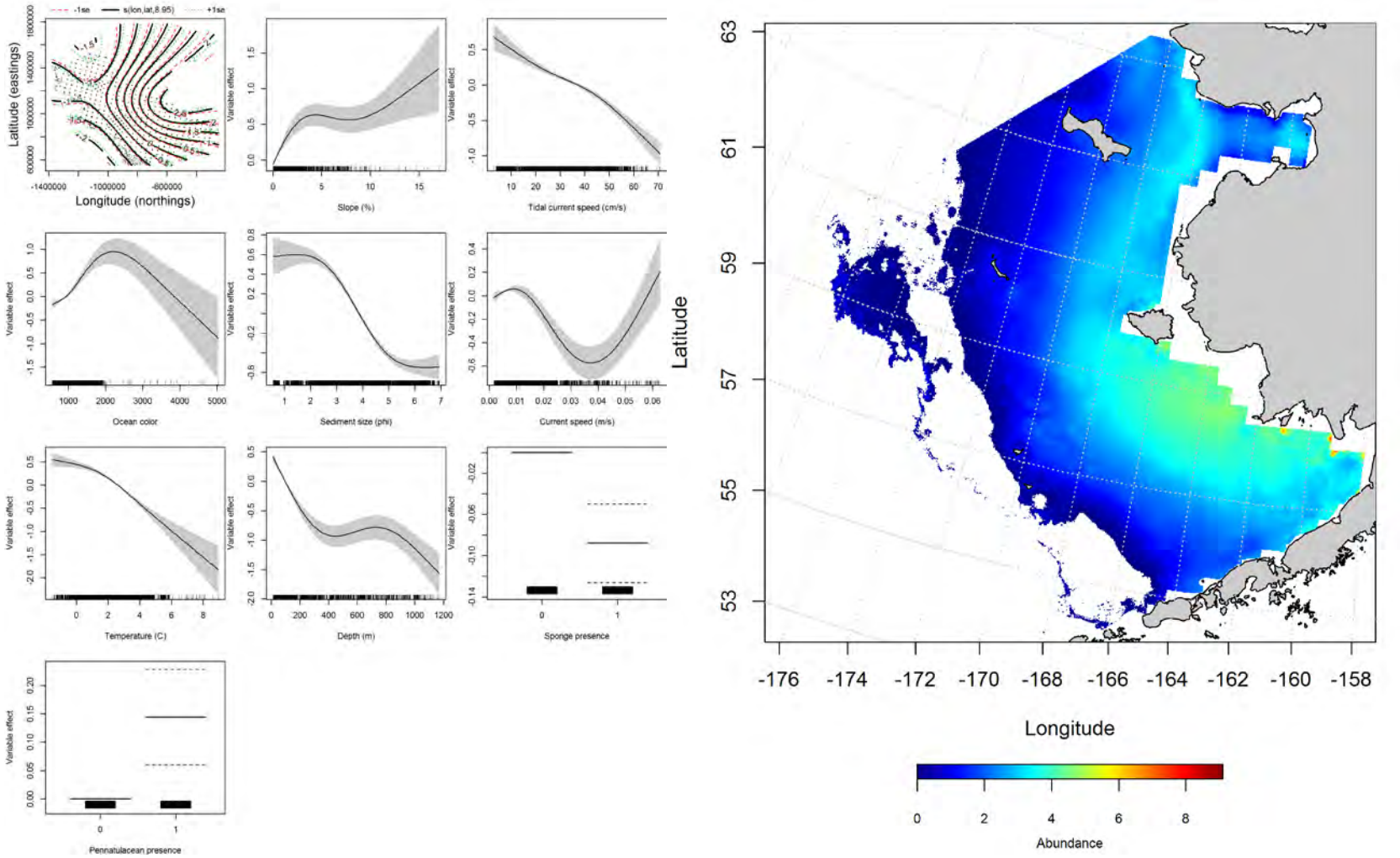

Figure 74. -- Effects of retained habitat covariates on the best-fitting generalized additive model (GAM; left panel) of late juvenile yellowfin sole abundance in RACE summer bottom trawl surveys of the Eastern Bering Sea Shelf, Slope, and Northern Bering Sea alongside their predicted abundance (right panel).

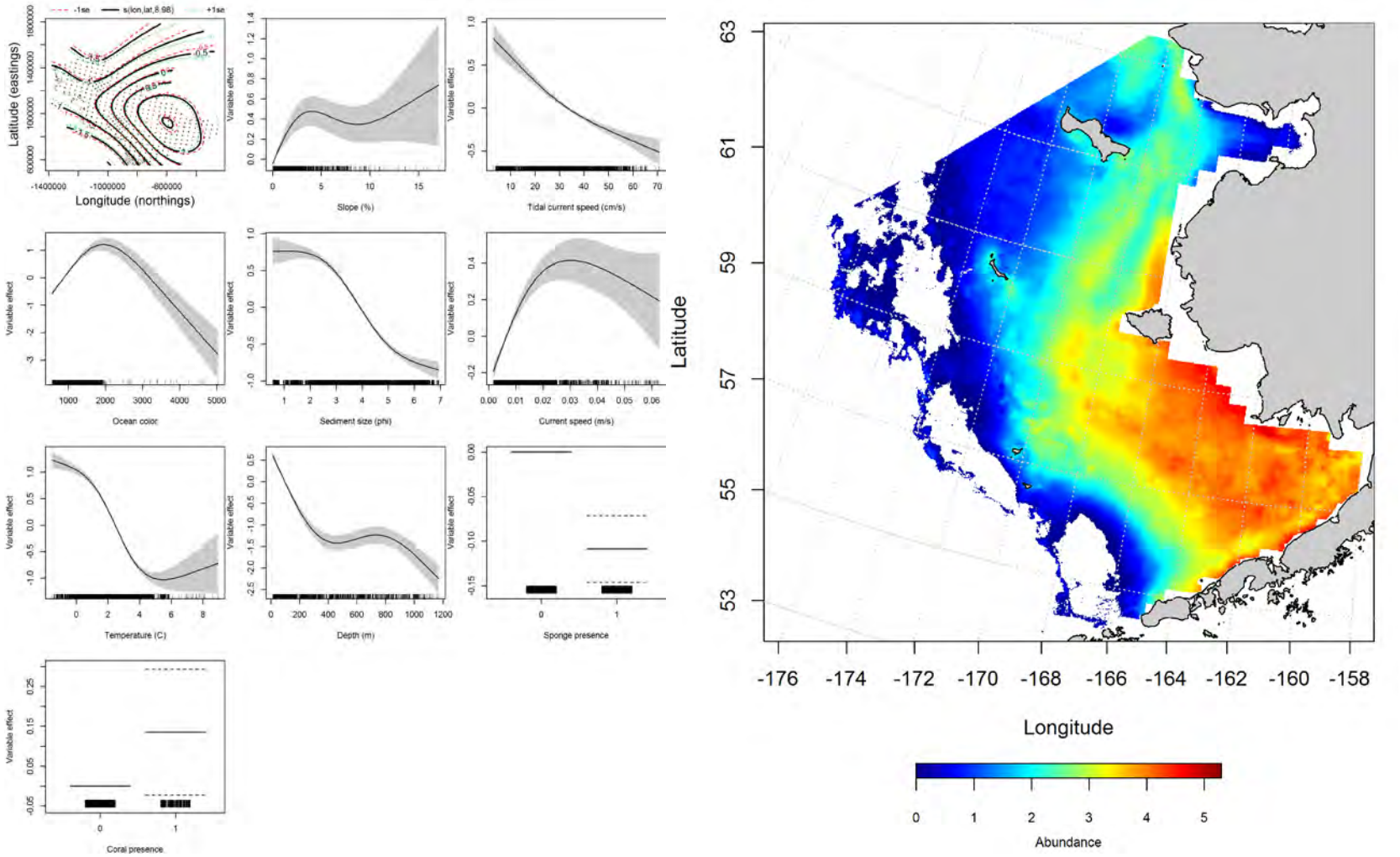

Figure 75. -- Effects of retained habitat covariates on the best-fitting generalized additive model (GAM; left panel) of adult yellowfin sole abundance in RACE summer bottom trawl surveys of the Eastern Bering Sea Shelf, Slope, and Northern Bering Sea alongside their predicted abundance (right panel).

Seasonal distribution of yellowfin sole in commercial fishery catches from the Eastern Bering Sea -- Yellowfin sole commercial fishery catches during fall in the Eastern Bering Sea were spread across the middle shelf between 50 and 100 m of water (Figure 76). Maximum entropy modeling predicts that suitable habitat for adult yellowfin sole caught in the commercial fishery was most likely to occur on the middle shelf in the southern domain of the Eastern Bering Sea and around St. Lawrence Island to the north. Bottom depth and tidal current were the most influential habitat covariates in the model (relative importance = 41.7 and 26.9%). The AUC of the fall model for the training data was outstanding (0.92) and 85% of cases were correctly predicted. Model validation produced an excellent fit to the test data (AUC = 0.84) with 84% of cases correctly classified.

Similar to fall, the distribution of yellowfin sole commercial catches in winter was primarily over the middle shelf (Figure 77). Nearly all of the influence on the MaxEnt model predictions by habitat covariates was attributable to bottom depth (relative importance = 51.4%), ocean productivity (relative importance = 19.6%), and tidal current (relative importance = 19.3%). The model was an outstanding fit to the training data (AUC = 0.95) with 90% of cases correctly classified. Model validation also produced an outstanding fit to the test data (AUC = 0.90) and 90% of cases were correctly classified.

In spring, the distribution of commercial catches of yellowfin sole extended further inshore onto the inner shelf of the Eastern Bering Sea near the mouth of Kuskokwim Bay (Figure 78). The most influential habitat covariates in the MaxEnt model were tidal current, bottom temperature, and bottom depth. Their combined relative importance was high at 80%. The model predicted 82% of cases correctly and was an outstanding fit to the training data (AUC = 0.90). Model validation also produced an excellent fit (AUC = 0.83) with 83% of cases correctly classified using the test data.

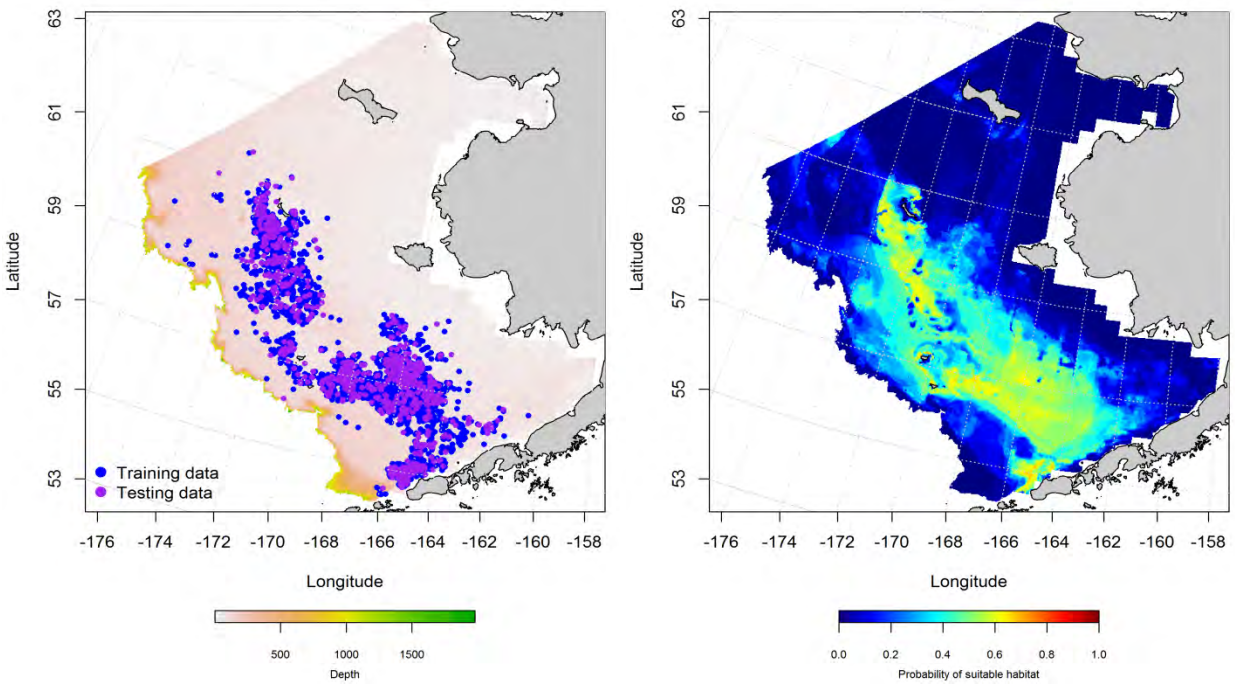

Figure 76. -- Locations of fall (October-November) catches of yellowfin sole from commercial fisheries of the Eastern Bering Sea (left panel). Blue points were used to train the maximum entropy (MaxEnt) model predicting the probability of suitable habitat (right panel) and the purple points were used to validate the model.

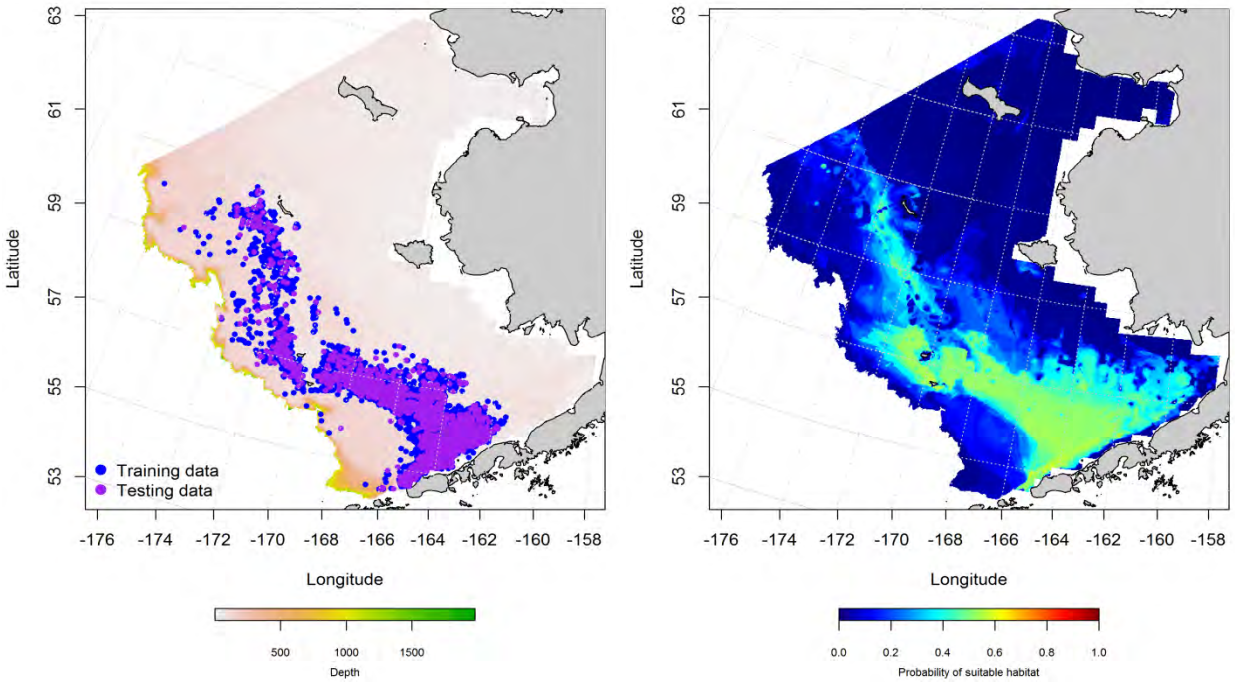

Figure 77. -- Locations of winter (December-February) catches of yellowfin sole from commercial fisheries of the Eastern Bering Sea (left panel). Blue points were used to train the maximum entropy

(MaxEnt) model predicting the probability of suitable habitat (right panel) and the purple points were used to validate the model.

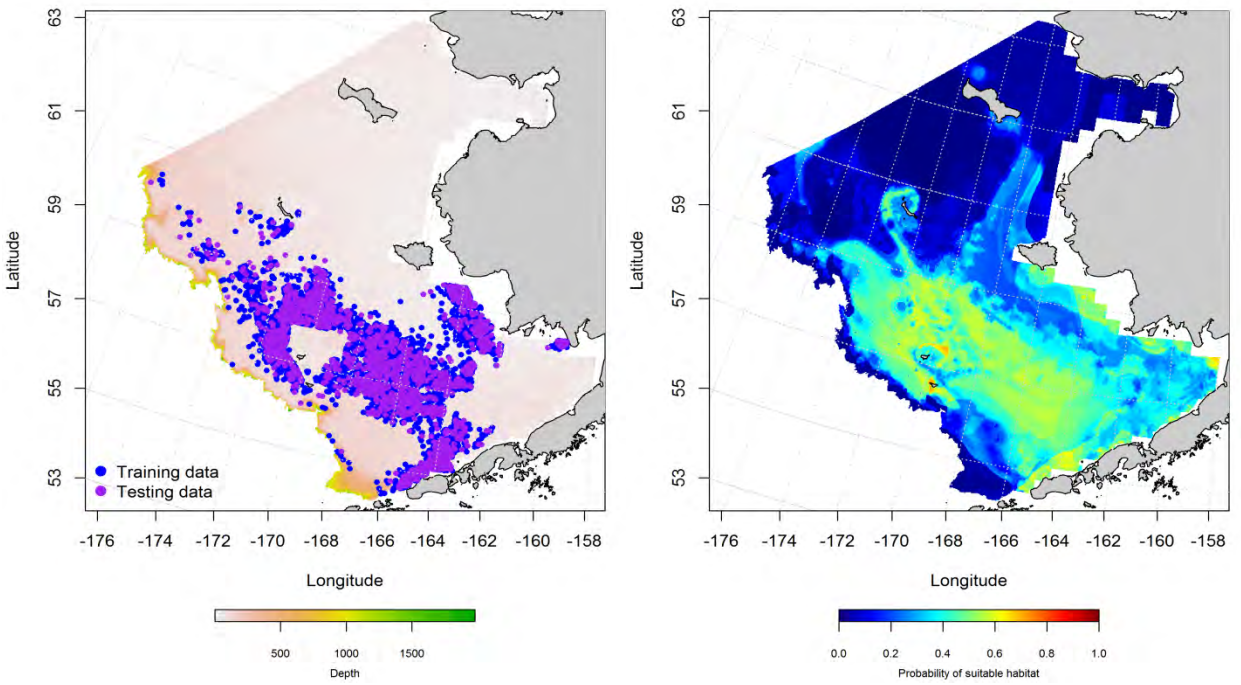

Figure 78. -- Locations of spring (March-May) catches of yellowfin sole from commercial fisheries of the Eastern Bering Sea (left panel). Blue points were used to train the maximum entropy (MaxEnt) model predicting the probability of suitable habitat (right panel) and the purple points were used to validate the model.

Essential fish habitat maps and conclusions for late juvenile and adult yellowfin sole (*Limanda aspera*) in the Eastern Bering Sea – Species distribution modelling of late juvenile and adult yellowfin sole from RACE summertime bottom trawl surveys of the Eastern Bering Sea predicts that EFH for this species encompasses most of the Eastern Bering Sea. The EFH for these two yellowfin sole life stages extends from the inner shelf across the middle shelf to some isolated patches of habitat on the shelf edge and Bering Sea Slope (Figure 79). There are some differences in EFH distribution with some late juvenile habitat north of Nunivak Island near Norton Sound that is not duplicated on the adult EFH map. For the most part though, EFH for both life stages overlaps from Bristol Bay north to Nunivak Island.

The predictions of suitable yellowfin sole habitat from commercial fishery catches in the Eastern Bering Sea extend farther offshore than what was predicted from summertime bottom trawl models (Figure 80).

Seasonal differences among EFH maps from these commercial catch data were minimal. Notably, the spring EFH map extends further on to the inner shelf than do the fall and winter maps.

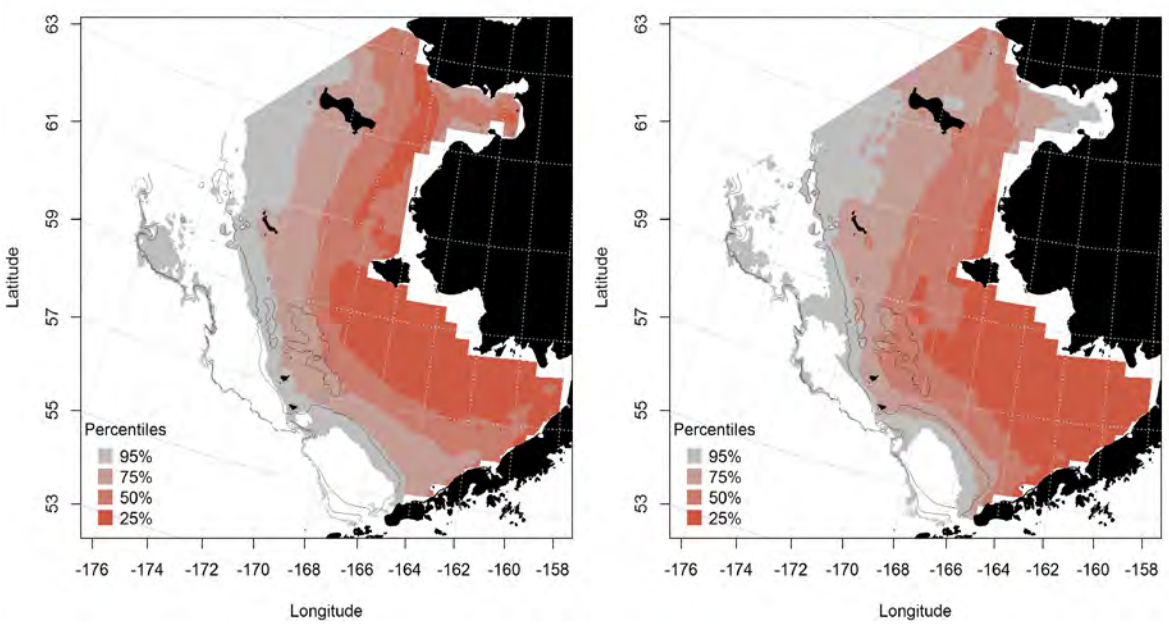

Figure 79. -- Essential fish habitat for yellowfin sole late juveniles and adults (left and right panel) from summertime bottom trawl surveys.

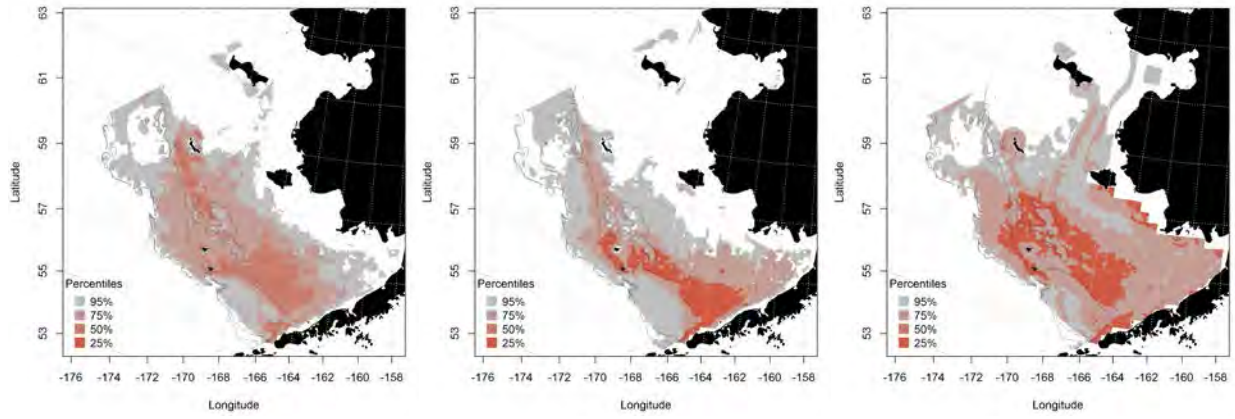

Figure 80. -- Essential fish habitat predicted for yellowfin sole during fall (left panel), winter (middle panel) and spring (right panel) from commercial fishery catches.

rock sole (*Lepidopsetta* spp.)

Rock sole are difficult to separate by species and are treated as a complex in commercial catches. The eggs of southern rock sole (*Lepidopsetta bilineata*) cannot be distinguished from those of northern rock sole (*L. polyxystra*), the other species in the genus, but their larvae and juveniles can be separately identified. There were no *Lepidopsetta* spp. eggs and too few early juveniles of either species reported from EcoFOCI ichthyoplankton samples to conduct distribution modeling so modeling EFH for early life stages of *Lepidopsetta* spp. consists of only models for larval stages of northern and southern rock sole. Before addressing the individual rock sole species, however, we will treat the rock sole complex managed as a commercial fishery in the BSAI.

Seasonal distribution of rock sole (*Lepidopsetta* spp.) in commercial fishery catches from the Eastern Bering Sea – Due to the high likelihood that southern rock sole from commercial catches north of 56°N latitude are misidentified (D. Stevenson pers. comm.), modifications were made to the reporting protocols for Eastern Bering Sea observers in 2006 that have subsequently severely curtailed reported occurrences of southern rock sole north of that line. The combination of inconsistent identification of this species over time, the spatially restricted distribution of southern rock sole in the EBS, and the relative rarity of this species in summer bottom trawl surveys, we combined the two species when analyzing their presence data from Eastern Bering Sea commercial catches.

Once heavily fished by foreign fleets in the 1960s, rock sole population levels are annually assessed by NMFS in the Eastern Bering Sea. Rock sole roe is highly valued in Japan. To supply this market, roe is mainly harvested in February and March, when females are bearing eggs. The Alaska rock sole fisheries, along with yellowfin sole, are the largest flatfish fisheries in the United States. Most of this catch is shipped to Asia.

Fall commercial catches of rock sole were spread from the southeast middle shelf to the northwest outer shelf of the Eastern Bering Sea (Figure 81). In the southern domain of the Eastern Bering Sea catches were concentrated along the Alaska Peninsula north and west of Unimak Island. In the central domain,

fishing activity appeared to be concentrated on the middle shelf around the Pribilof Islands. In the northern domain of the Eastern Bering Sea, catches were concentrated along the shelf edge near Zemchug Canyon, and on the middle shelf. Three predictors in the MaxEnt model accounted for the majority (> 85% of the relative importance amongst terms) of the model's ability to describe the distribution of rock sole catches in fall. The three terms were bottom depth, ocean color, and bottom temperature (relative importance = 32.4%, 30.3%, and 22.9%, respectively). The model predicted that the most favorable habitats for encountering rock sole in fall commercial catches were near the heads of the Zemchug, Pribilof, and Bering Canyons. The AUCs of 0.90 for the training data and 0.81 for the test data indicate outstanding and excellent model fits. A total of 82% of cases were correctly predicted from the training data set and 81% from the test data.

In the wintertime, catches were more concentrated from the Pribilof Islands south and southeastward (Figure 82). Three of the seven predictors in the MaxEnt model accounted for the majority (> 93% of the relative importance amongst terms) of the model's power to describe the distribution of rock sole catches in winter. The three terms were bottom depth, tidal maxima, and ocean color (relative importance = 38.3%, 30.8%, and 24.1%, respectively). The model predicted that the most favorable habitats for encountering rock sole in winter commercial catches were spread from the Pribilof Islands southeastward across the middle and inner shelf and along the Bering Canyon axis. The AUCs of 0.96 for the training data and 0.89 for the test data indicate outstanding and excellent model fits. A total of 89% of cases were correctly predicted from both data sets.

During the spring months, commercial catches were more widely dispersed across the southern half of the Bering Sea (Figure 83). The top three most influential predictor terms in the MaxEnt model accounted for > 80% of the relative importance of terms parametrizing the model. They were bottom temperature, tidal maxima, and bottom depth (relative importance = 35.5%, 28.5%, and 17.0%, respectively). The model predicted that the most favorable habitats for encountering rock sole in spring commercial catches were

between the Pribilof Islands and the head of Pribilof Canyon. The AUCs of 0.87 for the training data and 0.79 for the test data indicate excellent and acceptable model fits. A total of 79% of cases were correctly predicted from both data sets.

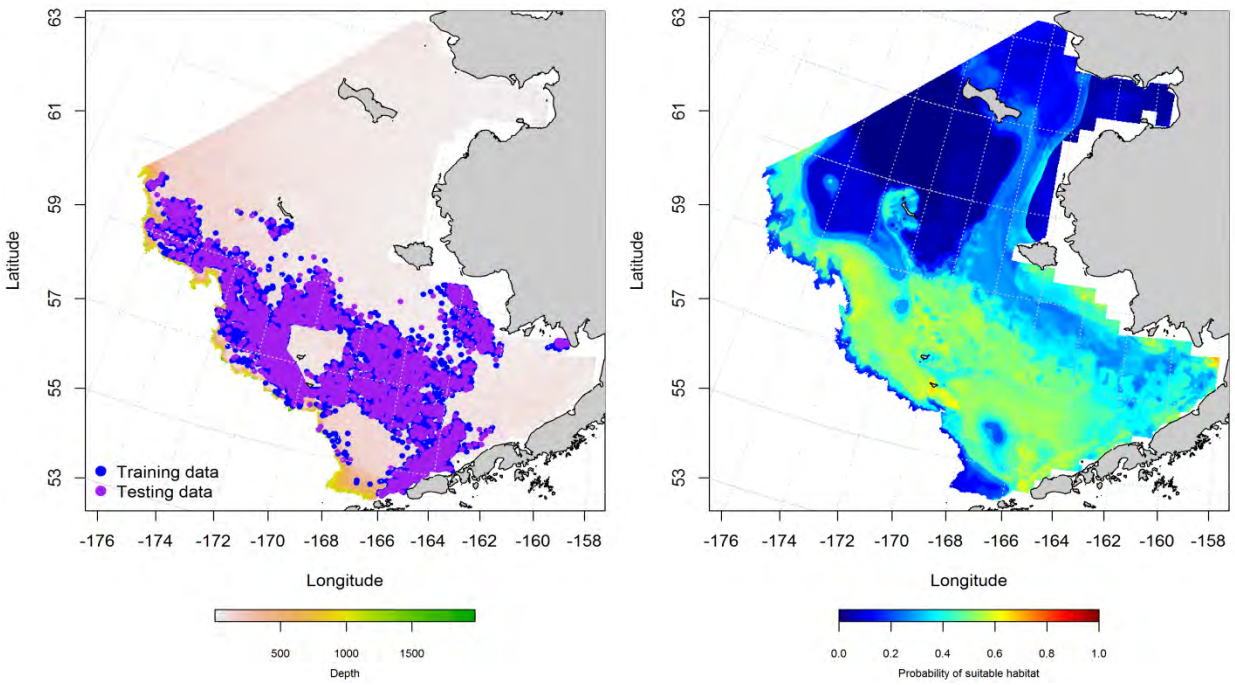

Figure 81. -- Locations of rock sole catches from fall (October-November) commercial fisheries of the Eastern Bering Sea (left panel). Blue points were used to train the maximum entropy (MaxEnt) model predicting the probability of suitable habitat (right panel) and the purple points were used to validate the model.

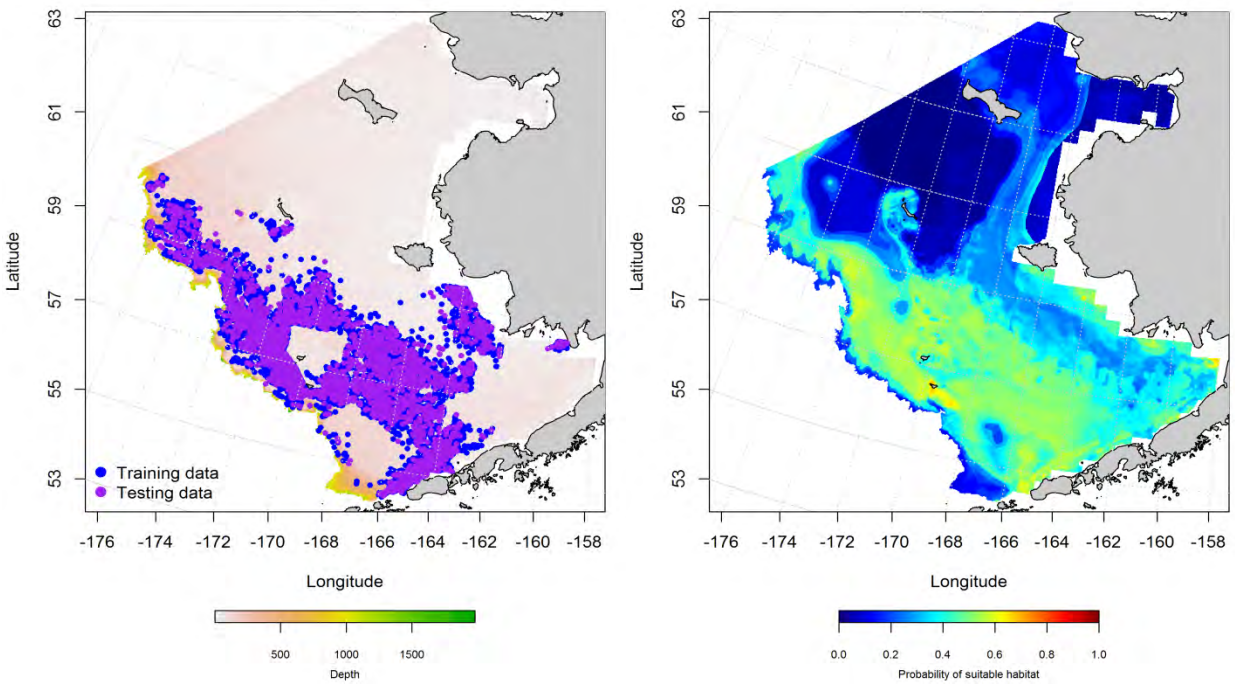

Figure 82. -- Locations of rock sole catches from winter (December-February) commercial fisheries of the Eastern Bering Sea (left panel). Blue points were used to train the maximum entropy (MaxEnt) model predicting the probability of suitable habitat (right panel) and the purple points were used to validate the model.

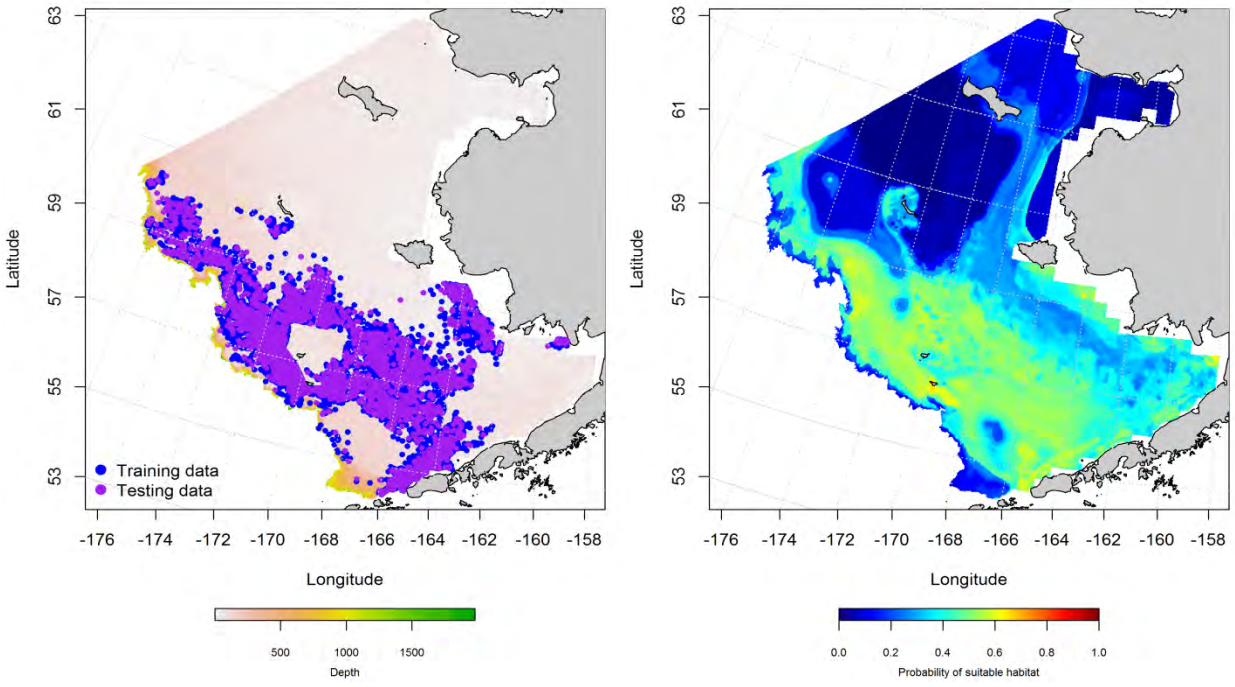

Figure 83. -- Locations of rock sole catches from spring (March-May) commercial fisheries of the Eastern Bering Sea (left panel). Blue points were used to train the maximum entropy (MaxEnt) model predicting the probability of suitable habitat (right panel) and the purple points were used to validate the model.

Eastern Bering Sea rock sole (*Lepidopsetta* spp.) essential fish habitat maps and conclusions from commercial catches -- The distribution of rock sole EFH predicted from commercial catches varied little across seasons (Figure 84). In general, regions of higher catch predicted from EFH were found on the middle shelf, outer shelf, and slope of the central and southern Eastern Bering Sea.

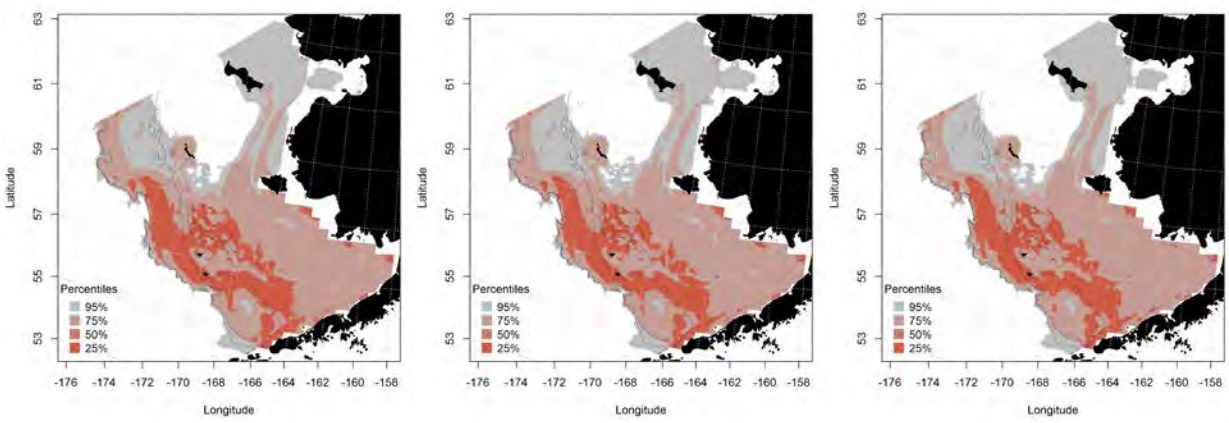

Figure 84. -- Essential fish habitat predicted for rock sole during fall (left panel), winter (middle panel) and spring (right panel) from commercial catches in the Eastern Bering Sea.

southern rock sole (*Lepidopsetta bilineata*)

Southern rock sole were recognized as a species distinct from northern rock sole (*L. polyxystra*) in 1996. Rock sole larvae (*Lepidopsetta* spp.) collected from EcoFOCI surveys prior to 1996 were re-examined after the two species were recognized and were separated into southern and northern rock soles. Therefore, EFH for the early life history stages of these two species are described separately.

Southern rock sole are distributed along the west coast of the United States and are caught from Alaska to California with most of those catches coming from Alaska. They are uncommon in catches from RACE summer bottom trawl surveys of the Eastern Bering Sea; occurring in <1% of the stations sampled on average. Where there were sufficient data we described EFH for late-juvenile and adult southern rock sole.

Seasonal distribution of early life history stages of southern rock sole from EcoFOCI ichthyoplankton surveys of the Eastern Bering Sea – Southern rock sole larvae were caught on EcoFOCI ichthyoplankton surveys during spring and summer months and their distribution differed between seasons (Figure 85). During spring (March – May), larval southern rock sole primarily occurred along the southern margin of the Eastern Bering Sea and Bristol Bay. In summer (June – August), these larvae were present over a broader spatial area that extended from the southern portions of the Eastern Bering Sea observed in spring northward to west of St. Matthew Island.

There were sufficient data to model EFH for summer southern rock sole larvae. The MaxEnt model predicts that suitable habitat for larval southern rock sole is found in < 100 m depths around Pribilof Islands and northeast of Unimak Pass (Figure 86). The most important variables predicting larval southern rock sole summer habitat were sea surface temperature (relative importance = 28.0%) followed by bottom depth (relative importance = 20.1%). The AUC for the training data was 0.91 with 79% of cases correctly classified; AUC for the test data set was 0.74 and 74% of cases were correctly classified.

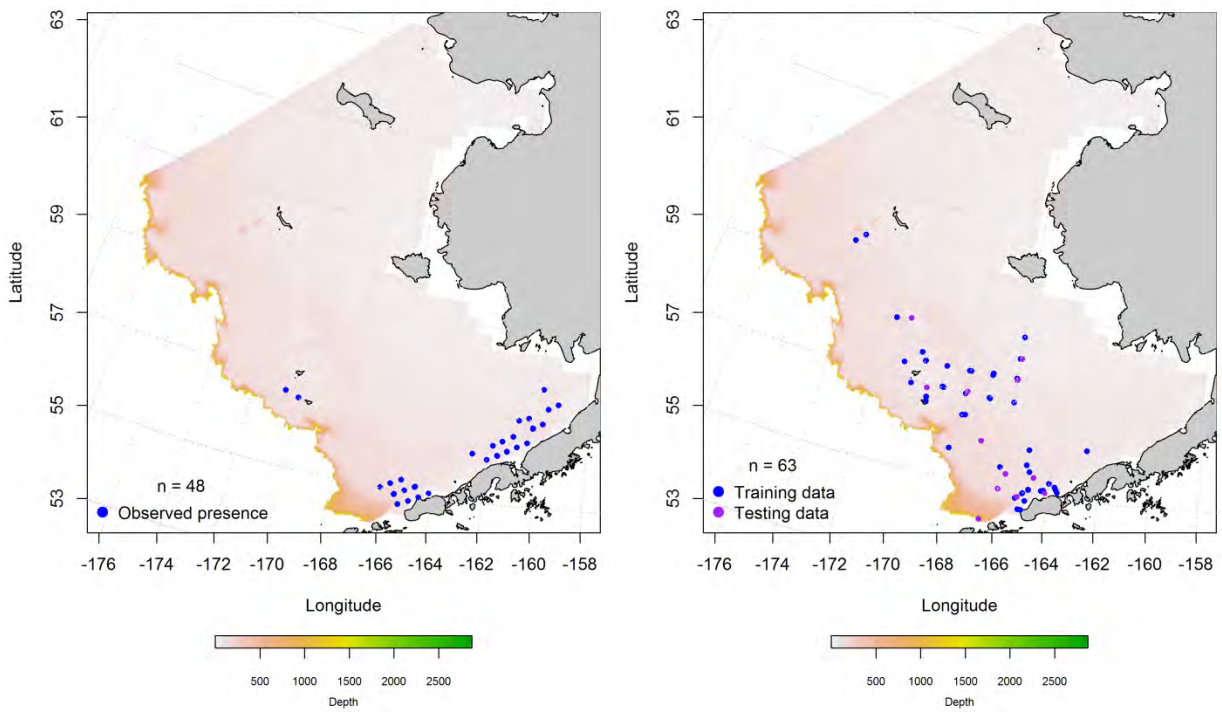

Figure 85. -- Spring and summer observations (left and right panel) of larval southern rock sole from EcoFOCI ichthyoplankton surveys of the Eastern Bering Sea. Blue points were used to train the maximum entropy (MaxEnt) model predicting the probability of suitable habitat and the purple points were used to validate the model.

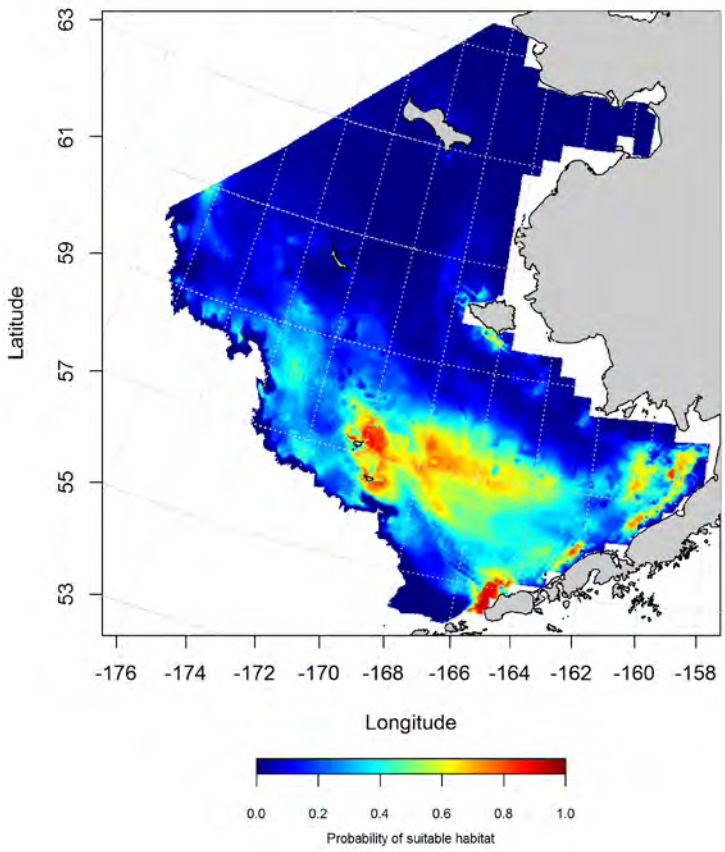

Figure 86. -- Maximum entropy (MaxEnt) model predictions of the probability of suitable summer larval southern rock sole habitat from EcoFOCI ichthyoplankton surveys of the Eastern Bering Sea.

There was just one occurrence of an early juvenile southern rock sole on a EcoFOCI ichthyoplankton survey (Figure 87). This observation was collected on a summer survey near Unimak Pass. The single record did not provide sufficient data to undertake distribution modeling for the early juvenile life stage of southern rock sole.

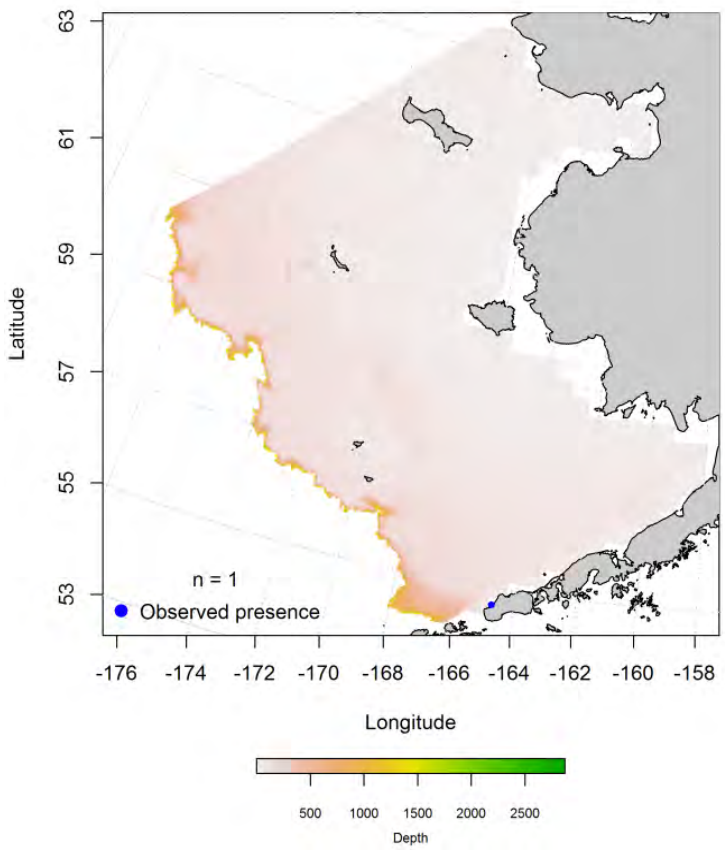

Figure 87. -- Summertime observation of early juvenile southern rock sole from EcoFOCI ichthyoplankton surveys of the Eastern Bering Sea.

Essential fish habitat maps and conclusions for larval southern rock sole in the Eastern Bering Sea -- Essential habitat predicted for larval southern rock sole collected during summer in the Eastern Bering Sea is centered near St. Paul Island in the Pribilofs and above Unimak Pass to the south (Figure 88). Both of these areas of EFH share a common depth < 100 m. In general, the areas of EFH supporting greater abundances of larval southern rock sole are shallower than 100 m and extend east from the areas of higher concentration into the southern portion of the Eastern Bering Sea and Bristol Bay.

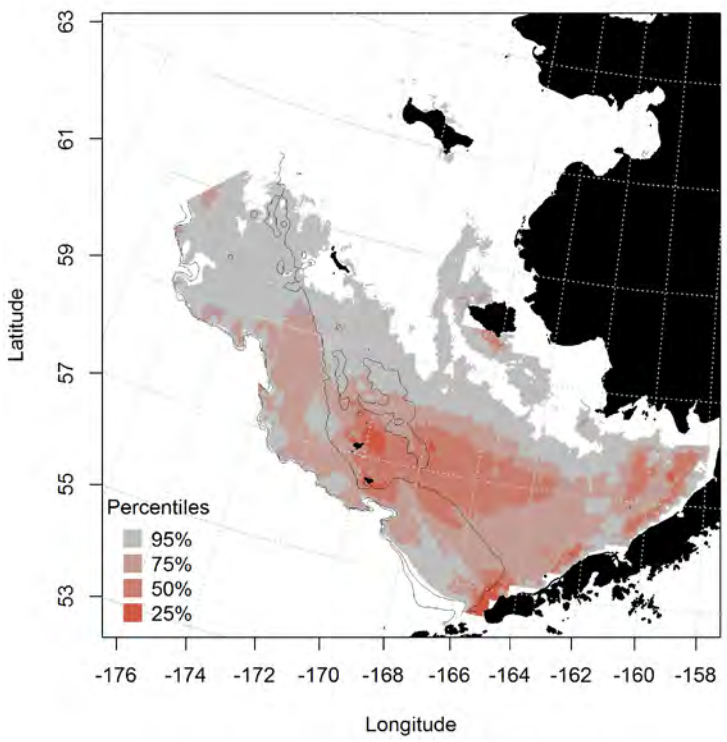

Figure 88. -- Summer essential fish habitat predicted for larval southern rock sole in the Eastern Bering Sea.

Summertime distribution of late-juvenile and adult southern rock sole from RACE bottom trawl surveys of the Eastern Bering Sea -- Southern rock sole juveniles and adults have been distinguished from northern rock sole in Bering Sea bottom trawl catches since 1996. Previously both species were jointly identified under single rock sole category (*Lepidopsetta* spp.). Southern rock sole are not common in bottom trawls from the Eastern Bering Sea trawl survey area occurring at < 1% of stations considered here. When encountered, juveniles and adults occur primarily in the southern portion of the survey area close to the Alaska Peninsula (Figure 89). There were too few collections of southern rock sole juveniles or adults from summer bottom trawl surveys of the Eastern Bering Sea to undertake species distribution modeling with this data set.

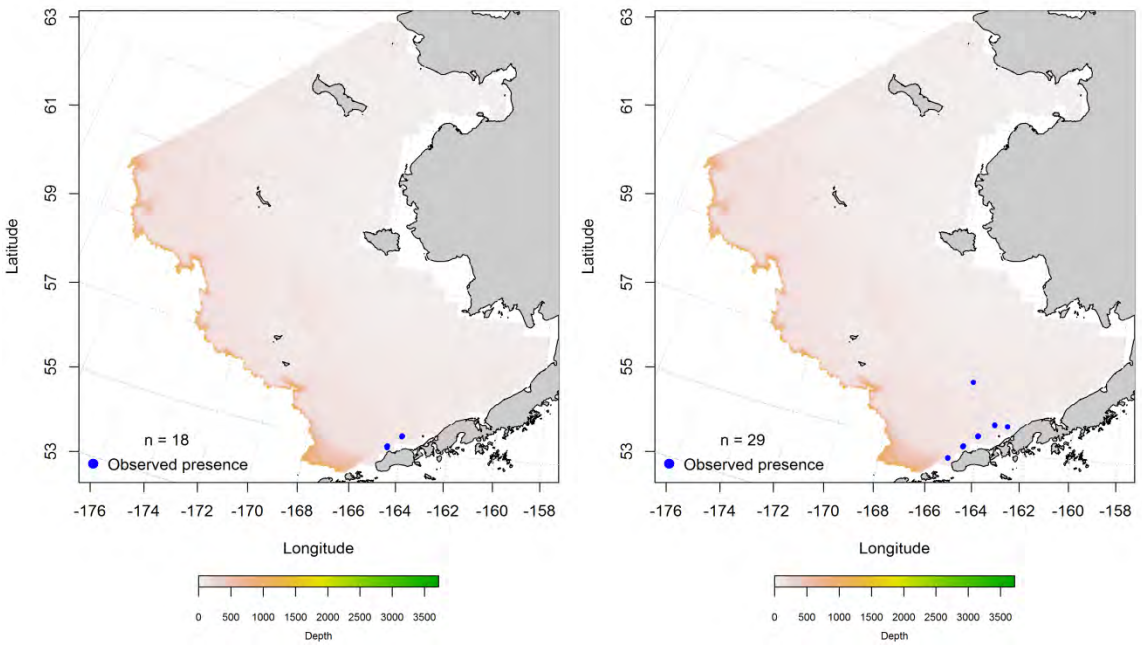

Figure 89. -- Distribution of late-juvenile (left) and adult (right) southern rock sole catches from RACE summer bottom trawl surveys of the Eastern Bering Sea.

northern rock sole (*Lepidopsetta polyxystra*)

Northern rock sole have been identified to species in Bering Sea bottom trawl surveys since 1996 and from EcoFOCI ichthyoplankton surveys since 1991. They are among the more abundant adult and late-juvenile fishes (based on catch-per-unit-effort) collected in this region (Lauth and Conner 2014). According to Nichol and Somerton (2009), northern rock sole may use tidal stream transport to migrate from shallow summer feeding grounds to deeper winter and spring spawning grounds.

Seasonal distribution of early life history stages of northern rock sole from EcoFOCI ichthyoplankton surveys of the Eastern Bering Sea – Northern rock sole larvae were collected on EcoFOCI ichthyoplankton surveys during fall, spring, and summer months (Figure 90); there was only one record from the fall. During spring (March – May), larval northern rock sole were widely distributed across the southern and central domains of the Eastern Bering Sea from the inner shelf (0 to 50 m) to the

outer shelf and slope (> 200 m) with a few records in the northern Bering Sea as well. In summer (June – August), these larvae appear to be somewhat more sparsely distributed over the same general areas although changing sampling design could account for this apparent difference.

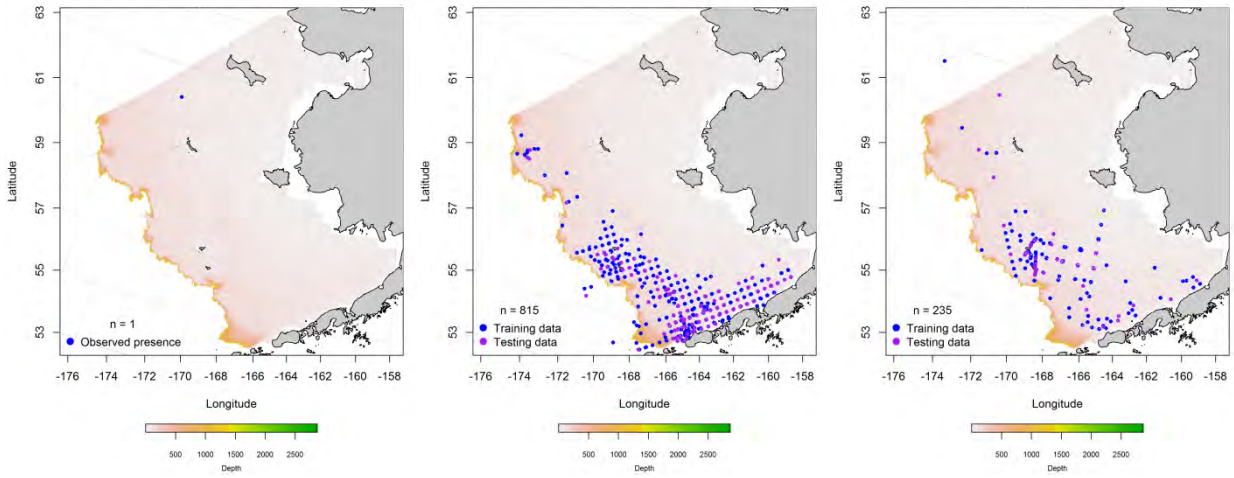

Figure 90. -- Fall, spring, and summer observations (left, middle, and right panel, respectively) of larval northern rock sole from EcoFOCI ichthyoplankton surveys of the Eastern Bering Sea. Blue points were used to train the maximum entropy (MaxEnt) model predicting the probability of suitable habitat and the purple points were used to validate the model.

Habitat covariates were fit to the larval northern rock sole presence data using MaxEnt modeling for the spring and summer months (Figure 91); there were not sufficient data to fit a model for fall. The models predicted that larval northern rock sole habitat differed between spring and summer with the distribution of suitable habitat shifting northward from around the Alaska Peninsula in spring to around the Pribilof Islands in summer. The three most important predictors of larval northern rock sole habitat were shared between spring and summer. They were surface temperature, ocean productivity, and bottom depth. The relative importance of these predictors in the two seasons differed. In spring, surface temperature alone accounted for 73.6% of the leverage in the MaxEnt model while all three of the shared terms combined accounted for 68.4% of the leverage in the summer model (i.e., surface temperature (32%), ocean productivity (6.4%), and bottom depth (3.1%)). The model fits in spring and summer to the training data set were outstanding (AUC = 0.95 and 0.94) with 88 and 87% of cases correctly classified. The model

was validated using the test data where 87 and 83% of cases were correctly classified in spring and summer and the AUCs indicate excellent model fits (0.87 and 0.83).

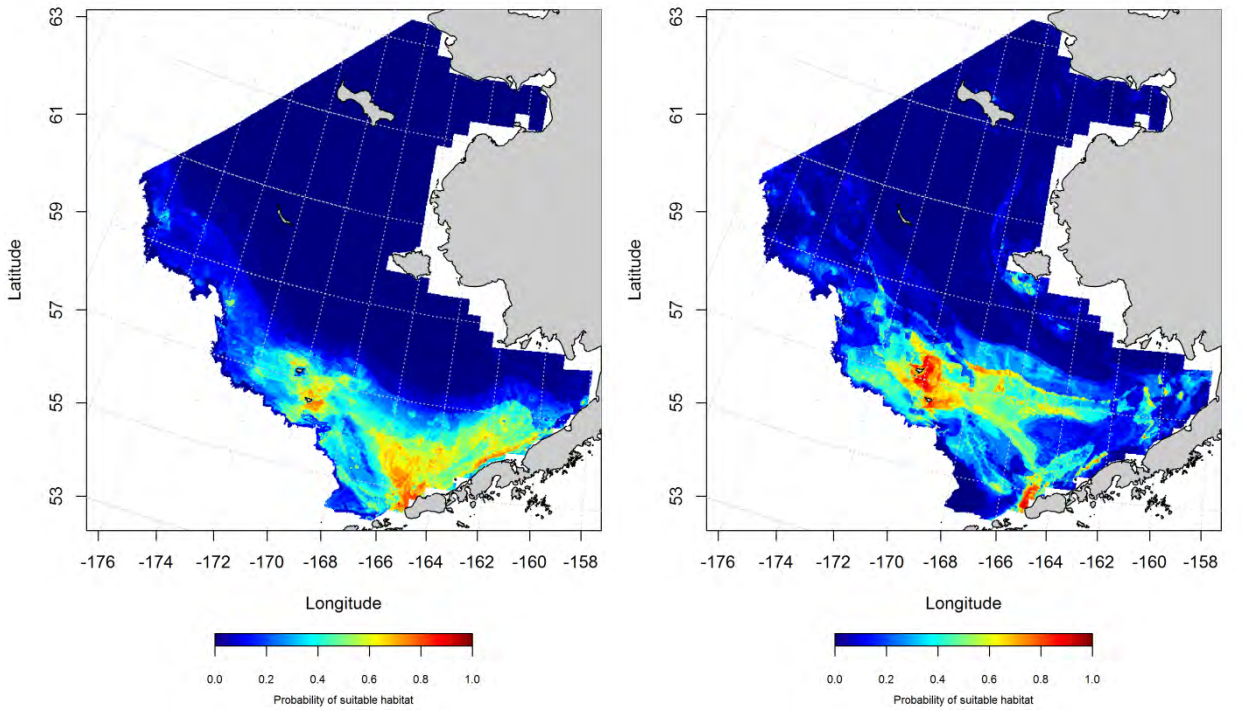

Figure 91. -- Maximum entropy (MaxEnt) model predictions of the probability of suitable spring and summer (left and right panels) larval northern rock sole habitat from EcoFOCI ichthyoplankton surveys of the Eastern Bering Sea.

There were three occurrences of early juvenile northern rock sole in EcoFOCI ichthyoplankton samples from the Eastern Bering Sea (Figure 92). They were collected in summer near Unimak Pass, over the inner shelf in Bristol Bay, and near the Pribilof Islands. These did not provide sufficient data to parameterize a distribution model for the early juvenile life stage of northern rock sole.

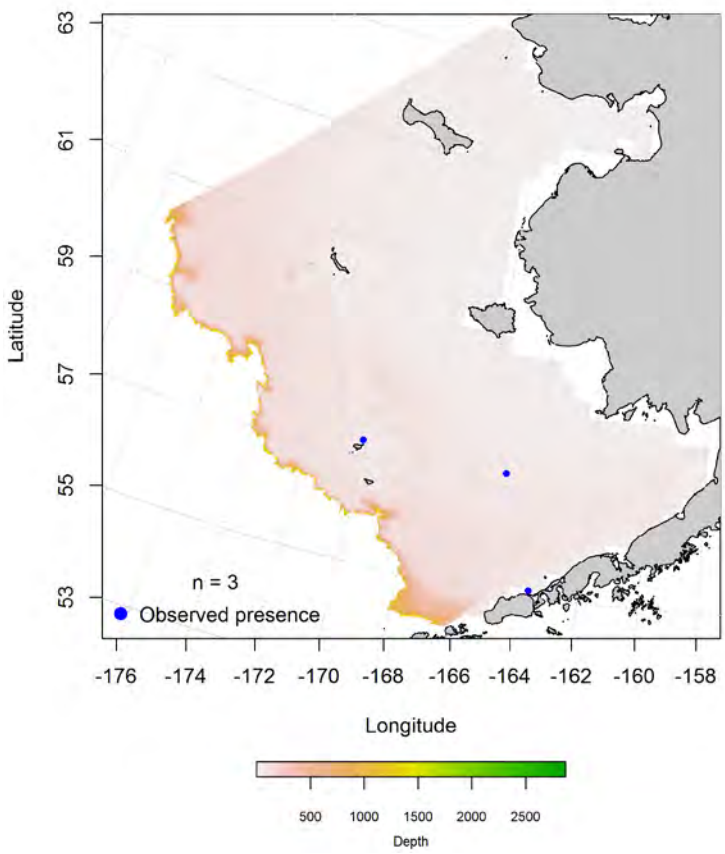

Figure 92. -- Summertime catch of early juvenile northern rock sole from EcoFOCI ichthyoplankton surveys of the Eastern Bering Sea.

Summertime distribution of late juvenile and adult northern rock sole from RACE bottom trawl surveys of the Eastern Bering Sea – Late juvenile and adult northern rock sole are common and widely distributed throughout the Eastern Bering Sea summer bottom trawl survey area (Figure 93). Since 1996, juvenile or adult northern rock sole have occurred in 78% of Bering Sea summer bottom trawl stations on average annually. The western extent of the juvenile distribution appears to be constrained by the 100 m isobath while the adult distribution extends over the deeper waters of the outer shelf and slope.

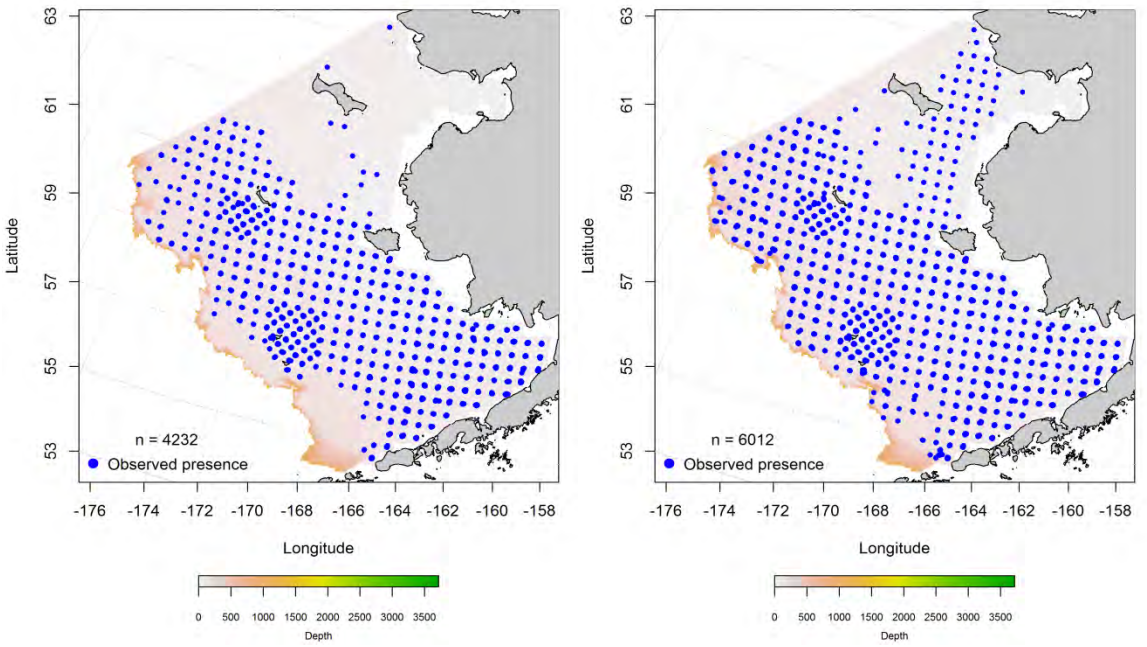

Figure 93. -- Distribution of late juvenile (left) and adult (right) northern rock sole catches in RACE summer bottom trawl surveys of the Eastern Bering Sea.

Generalized additive models predicting the abundance of juvenile northern rock sole explained 68.2% of the deviance in the CPUE data from the bottom trawl survey ($r^2 = 0.68$). The independent variables retained as significant predictors of juvenile northern rock sole CPUE in the best-fitting GAM were, in order of significance, geographic location, sediment grain size, and current speed (tide corrected). When applied to the test data, this GAM explained 69.3% of the deviance in the test data CPUE ($r^2 = 0.69$). From the training data, the model predicts that the highest juvenile northern rock sole abundance in summertime bottom trawl surveys should occur in the eastern portion of Bristol Bay and inshore of the 100 m isobaths (Figure 94). In both cases, the r^2-values indicate a moderately good fit of the model to the data.

The best-fitting GAM for adult northern rock sole predicts that their distribution roughly corresponds to that of the late juveniles, but that they should be slightly more abundant throughout their range (Figure 95). The independent variables retained as significant predictors of adult northern rock sole CPUE in the best-fitting GAM were sediment grain size, bottom depth, geographic location, and bottom temperature.

This model accounted for 72.1% of the deviance in adult northern rock sole abundance estimated from the Eastern Bering Sea summer bottom trawl surveys ($r^2 = 0.72$). When applied to the test data, it explained 73.4% of the deviance in the abundance ($r^2 = 0.73$). In both cases, the r^2-values indicate a moderately good fit of the model to the data.

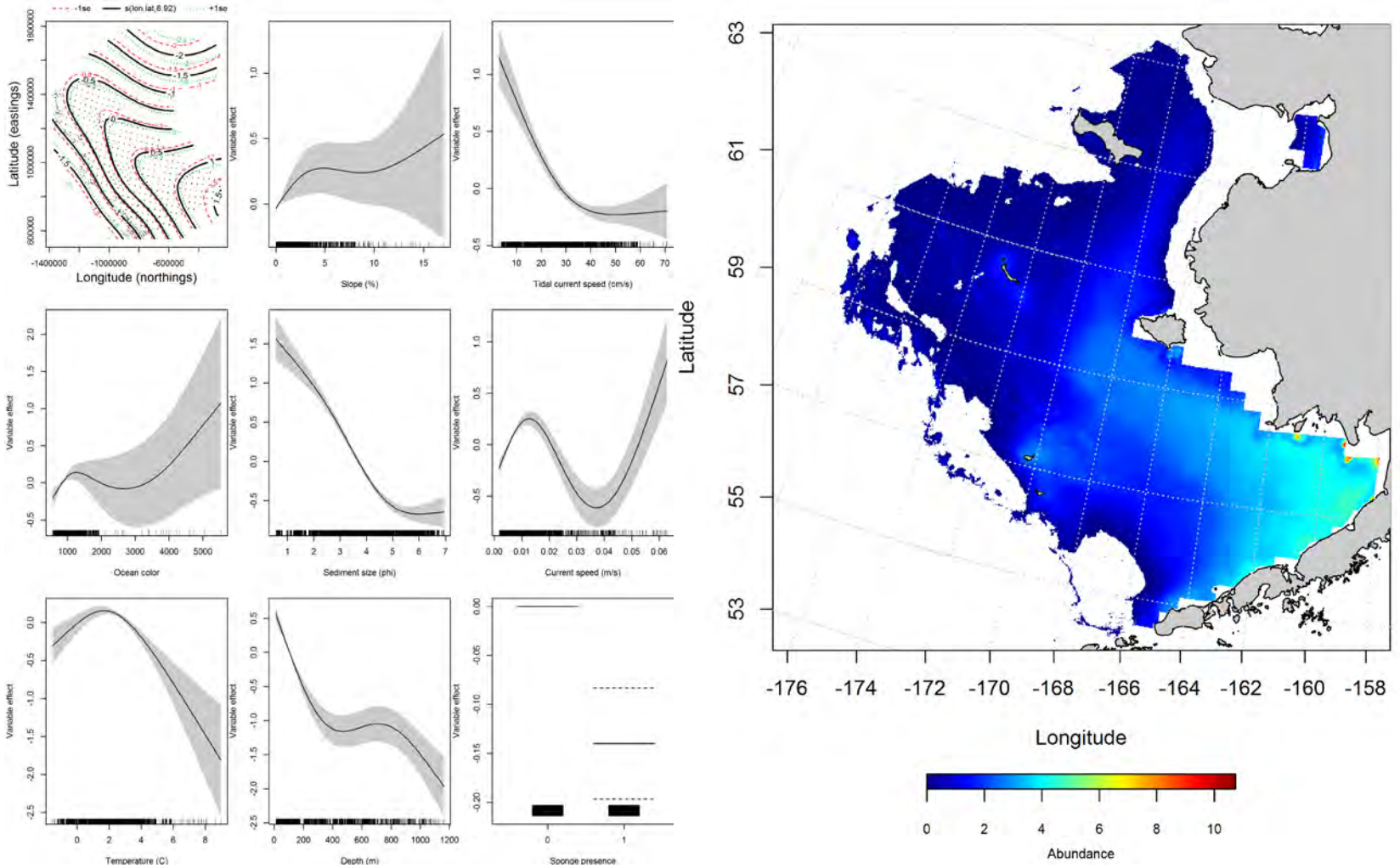

Figure 94. -- Effects of retained habitat covariates on the best-fitting generalized additive model (GAM; left panel) of late juvenile northern rock sole abundance in RACE summer bottom trawl surveys of the Eastern Bering Sea Shelf, Slope, and Northern Bering Sea alongside their predicted conditional abundance (right panel).

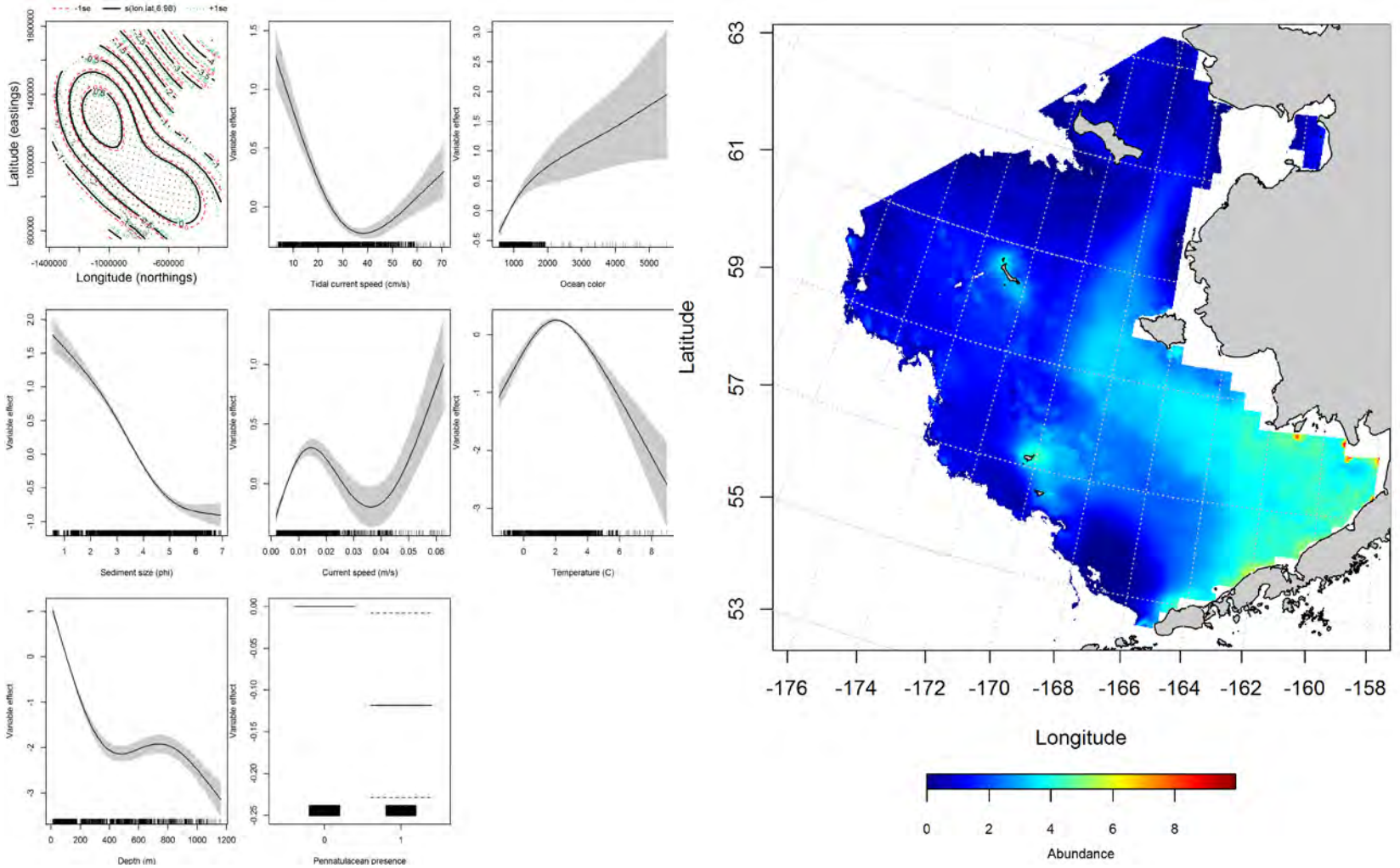

Figure 95. -- Effects of retained habitat covariates on the best-fitting generalized additive model (GAM; left panel) of adult northern rock sole abundance in RACE summer bottom trawl surveys of the Eastern Bering Sea Shelf, Slope, and Northern Bering Sea alongside their predicted conditional abundance (right panel).

Essential fish habitat maps and conclusions for northern rock sole from RACE summer bottom trawl surveys of the Eastern Bering Sea — Summertime EFH of northern rock sole juveniles and adults was primarily distributed across the middle and inner shelves of the central and southern domains of the Eastern Bering Sea (Figure 96). The offshore extent of the habitat where juveniles and adults were most abundant appears to be the 50 m isobath. Overall, northern rock sole EFH covers the majority of the survey area.

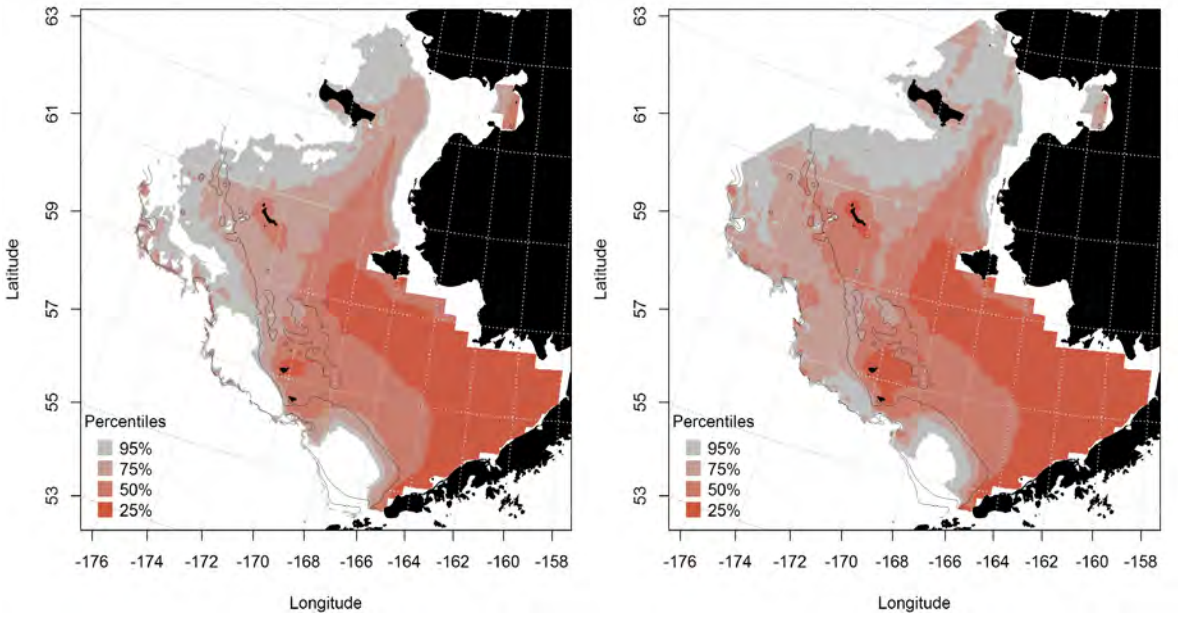

Figure 96. -- Predicted summer essential fish habitat for northern rock sole juveniles and adults (left and right panel) from summertime bottom trawl surveys.

Alaska plaice (*Pleuronectes quadrituberculatus*)

Alaska plaice inhabit waters of the continental shelf in the North Pacific Ocean and range from the Gulf of Alaska to the Bering and Chukchi Seas (Pertseva-Ostroumova 1961, Quast and Hall 1972).

Seasonal distribution of early life history stages of Alaska plaice in EcoFOCI ichthyoplankton surveys of the Eastern Bering Sea – Alaska plaice eggs and larvae can be separated

from other species in EcoFOCI ichthyoplankton samples from the Eastern Bering Sea. These life stages were generally found across the entire survey area, but there were seasonal differences in distributions.

Alaska plaice eggs were collected in EcoFOCI ichthyoplankton samples from the Eastern Bering Sea in spring and summer, but were not common in winter surveys (Figure 97). They occurred across the shelf in < 200 m of water from Bristol Bay to north of St. Lawrence Island.

Maximum entropy modeling of Alaska plaice egg presence from EcoFOCI ichthyoplankton samples predicted that the likeliest egg habitats vary seasonally (Figure 98). In springtime, the high probability habitat is in southern domain of the Eastern Bering Sea along the Alaska Peninsula. In summer, the habitat is more widely dispersed with areas of high probability inshore and farther north than seen in spring. The most important habitat covariates in both seasons were surface temperature (relative importance of 60.4% in spring and 10% in summer) and bottom depth (13% and 23.1% in spring and summer). Model fits to the training data were outstanding and excellent (AUC = 0.91 in spring and 0.83 in summer) and both correctly classified >70% of predicted cases. Model validation demonstrated excellent to acceptable fits to the test data (AUC = 0.80 for spring and 0.65 for summer) and correctly classified 80 and 65% of cases, respectively.

Alaska plaice larvae were reported from spring and summer EcoFOCI ichthyoplankton surveys (Figure 99). In springtime, Alaska plaice larvae were found in the southern domain of the Eastern Bering Sea along the Alaska Peninsula. During summer months, larvae were collected across all domains from the inner (< 50 m) and middle (50 to 100 m) shelf.

Maximum entropy modeling of larval Alaska plaice presence from EcoFOCI ichthyoplankton surveys of the Eastern Bering Sea predicted that the areas with the highest probability of suitable habitat differed between spring and summer (Figure 100). In spring, the highest probability areas were in the southern domain of the EBS roughly tracking the east-west axis of the Bering Canyon along the Alaska Peninsula. The most important habitat covariates determining the relationship between larval Alaska plaice presence

and habitat in springtime were surface temperature (relative importance = 25.1%) and ocean productivity (24.2%). During summer months, the areas of suitable habitat were more widely distributed across all domains of the Eastern Bering Sea and the most important habitat covariates for describing the spatial relationships were bottom depth (relative importance = 31.3%), bottom slope (7.7%), surface temperature (7.1%), and variability of currents (6.6%). The springtime model was an outstanding fit to the training data (AUC = 0.98) correctly classifying 95% of cases predicted. Model validation using the test data also produced an outstanding fit (AUC = 0.94) and correctly classified 94% of cases. Model fit and validation demonstrated excellent fits to the training and test data sets in summer (AUC = 0.80 and 0.82) while the training data model correctly classified fewer cases (73%) than did the test data validation run (82%).

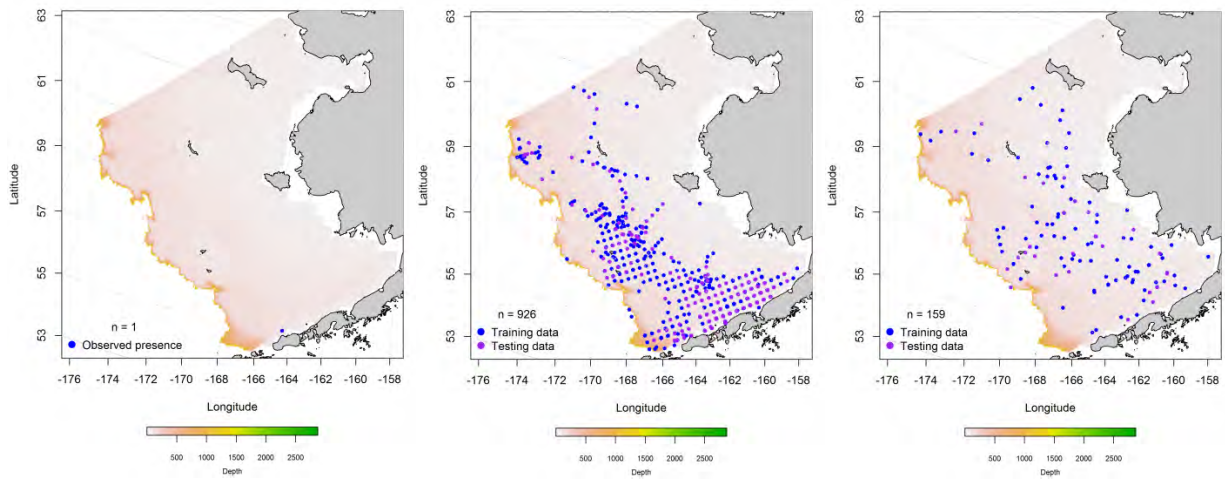

Figure 97. – Winter, spring, and summer observations (left, middle, and right panel, respectively) of Alaska plaice eggs from EcoFOCI ichthyoplankton surveys of the Eastern Bering Sea.

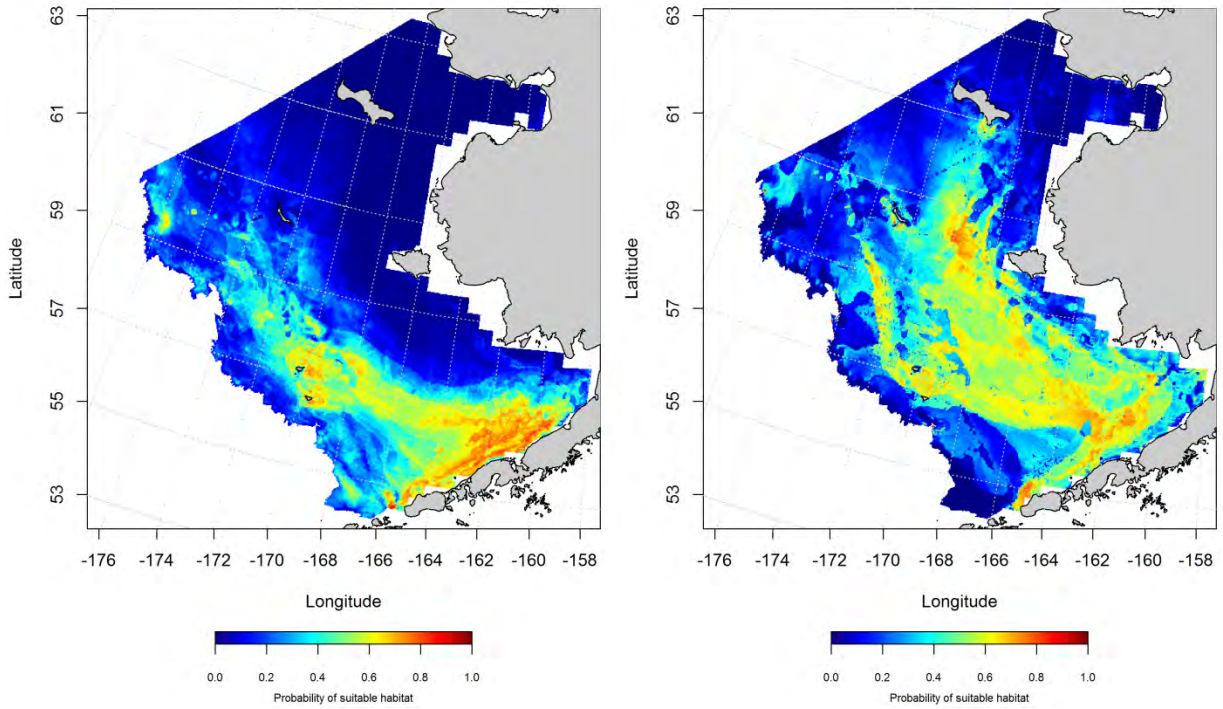

Figure 98. -- Maximum entropy (MaxEnt) model predictions of the probability of suitable spring and summer (left and right panels) Alaska plaice egg habitat from EcoFOCI ichthyoplankton surveys of the Eastern Bering Sea.

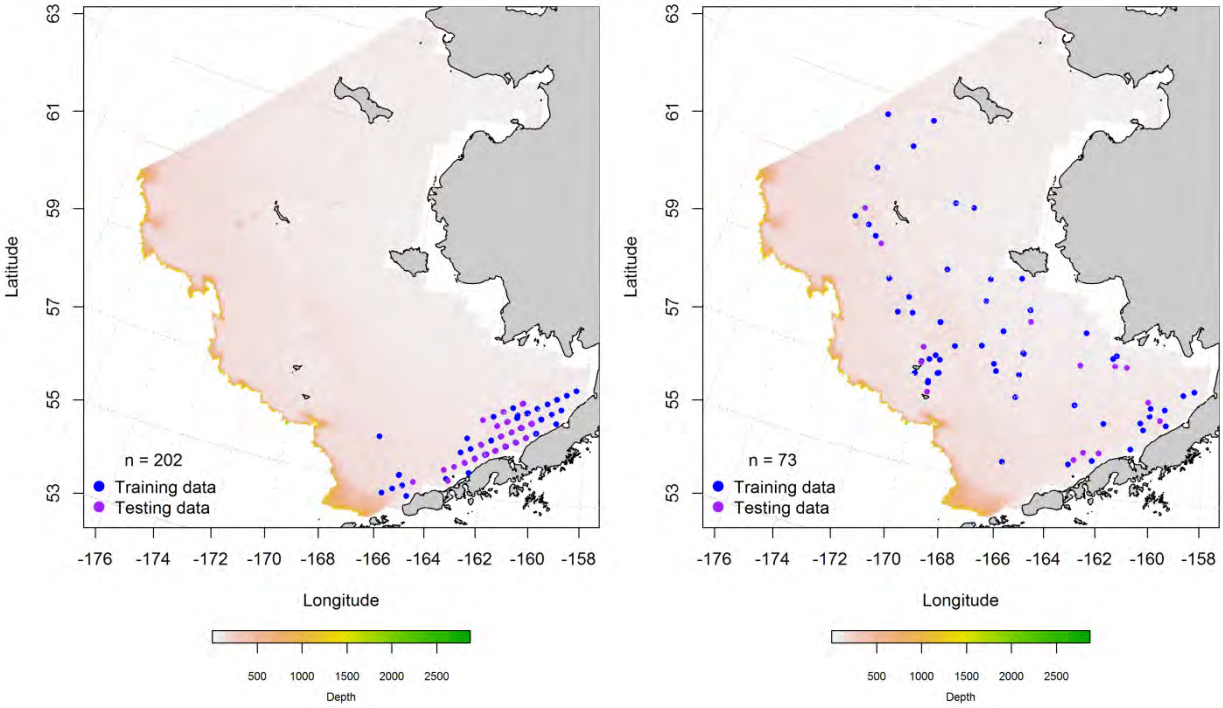

Figure 99. – Spring (left panel) and summer (right panel) observations of larval Alaska plaice from the Eastern Bering Sea.

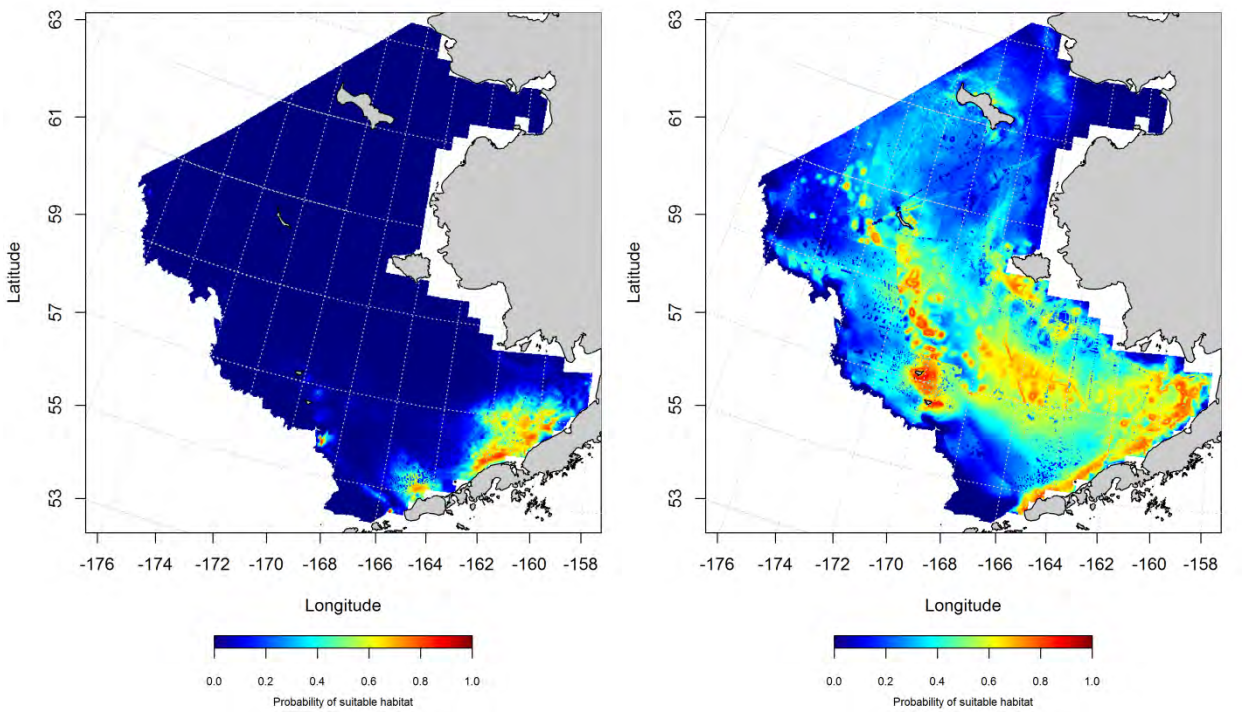

Figure 100. -- Maximum entropy (MaxEnt) model predictions of the probability of suitable spring and summer (left and right panels) larval Alaska plaice habitat from EcoFOCI ichthyoplankton surveys of the Eastern Bering Sea.

Essential fish habitat maps and conclusions for early life history stages of Alaska plaice from the Eastern Bering Sea – Essential habitat of Alaska plaice eggs was modeled from spring and summer EcoFOCI ichthyoplankton surveys of the Eastern Bering Sea (Figure 101). The predicted habitat extends from the southern to the northern domain of the Eastern Bering Sea over the middle and outer shelf in springtime. In summer, the pattern was similar to spring, but with Alaska plaice egg habitat extending on to the inner shelf across the southern, central, and northern domains of the Eastern Bering Sea.

Larval Alaska plaice essential habitat predicted from EcoFOCI ichthyoplankton surveys was more spatially constrained in springtime compared to summer (Figure 102). In spring, larval EFH was predicted primarily from east to west along the Alaska Peninsula. In summer months, larval Alaska plaice EFH extended from there northward from the inner to outer shelf across the southern, central, and northern domains of the Eastern Bering Sea.

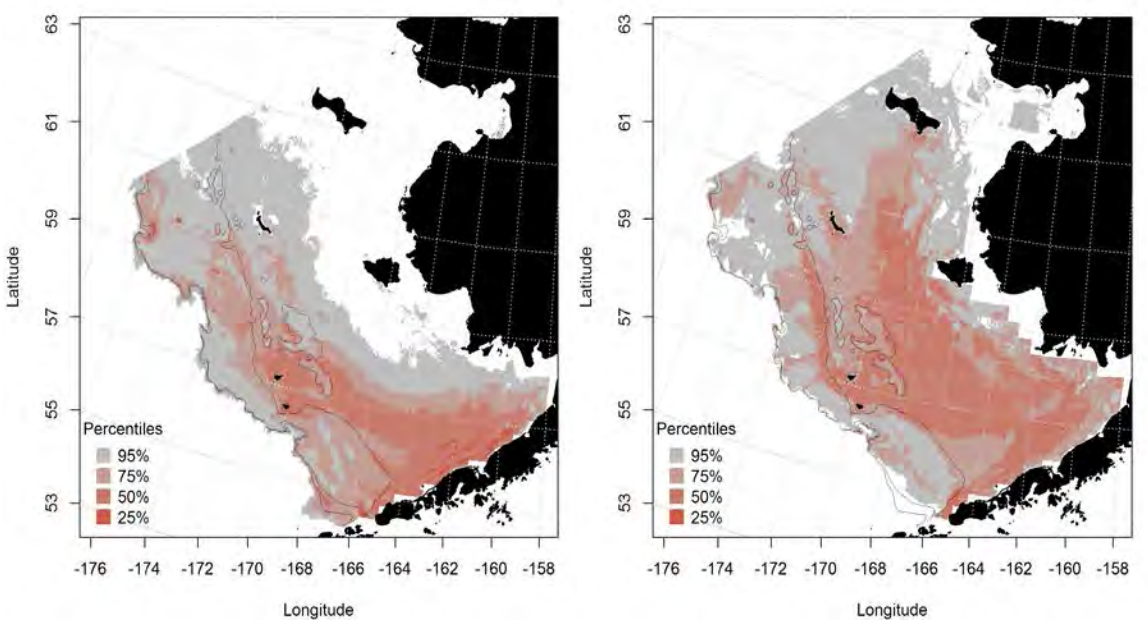

Figure 101. -- Essential habitat of Alaska plaice eggs predicted from spring (left panel) and summer (right panel) EcoFOCI ichthyoplankton surveys of the Eastern Bering Sea.

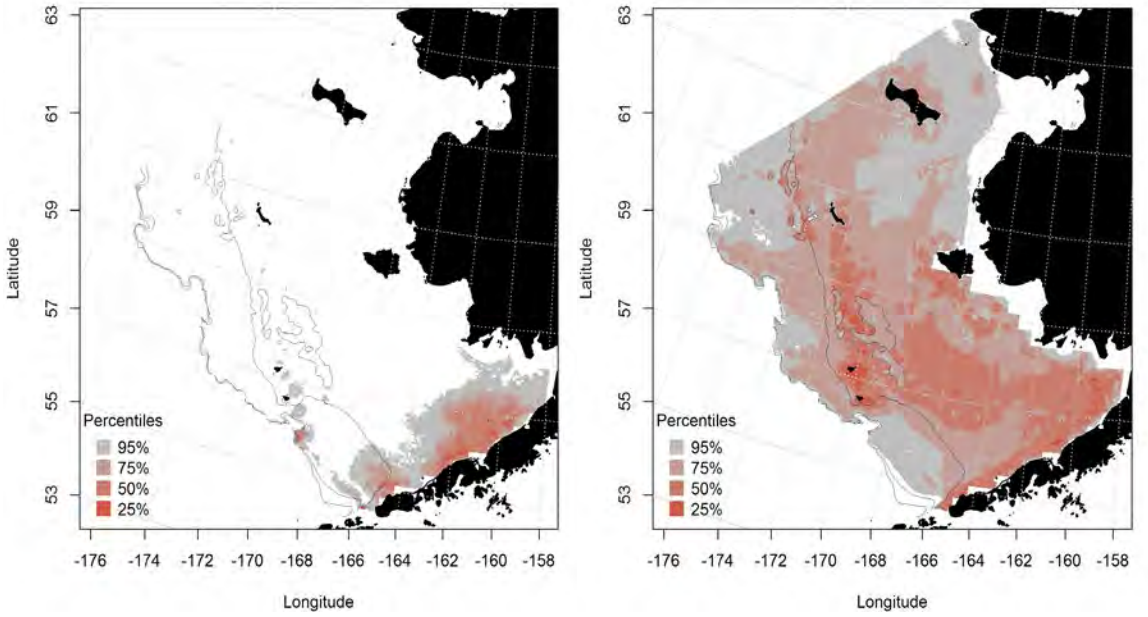

Figure 102. -- Spring (left panel) and summer (right panel) essential larval Alaska plaice habitat predicted from EcoFOCI ichthyoplankton surveys of the Eastern Bering Sea.

Summertime distribution of adult Alaska plaice from RACE bottom trawl surveys of the Eastern Bering Sea – Adult Alaska plaice were distributed across the inner and middle shelf from Bristol Bay to the northern extent of the survey area; juvenile Alaska plaice were not reported from the RACE

summertime bottom trawl surveys. The distribution of Alaska plaice in the Eastern Bering Sea appears to be dependent upon the geographic extent of the Bering Sea cold pool (Lauth and Conner 2014). Alaska plaice are well-adapted to cold water temperatures and carry an antifreeze glycoprotein in their blood to prevent ice crystal formation (Knight et al. 1991).

The best-fitting GAM describing adult Alaska plaice abundance explained 63% of the deviance in the CPUE data from the Eastern Bering Sea (Figure 103). Geographical location, bottom depth, and sediment grain size were the habitat covariates with the greatest leverage in the model. Model effects predict highest Alaska plaice abundance in the central domain of the Eastern Bering Sea over the middle shelf close to the 50 m isobath. Their predicted abundance increased in shallower depths over finer sediments. The GAM fit to the training data was fair ($r^2 = 0.63$). The fit to the test data in the model validation step was slightly higher ($r^2 = 0.65$).

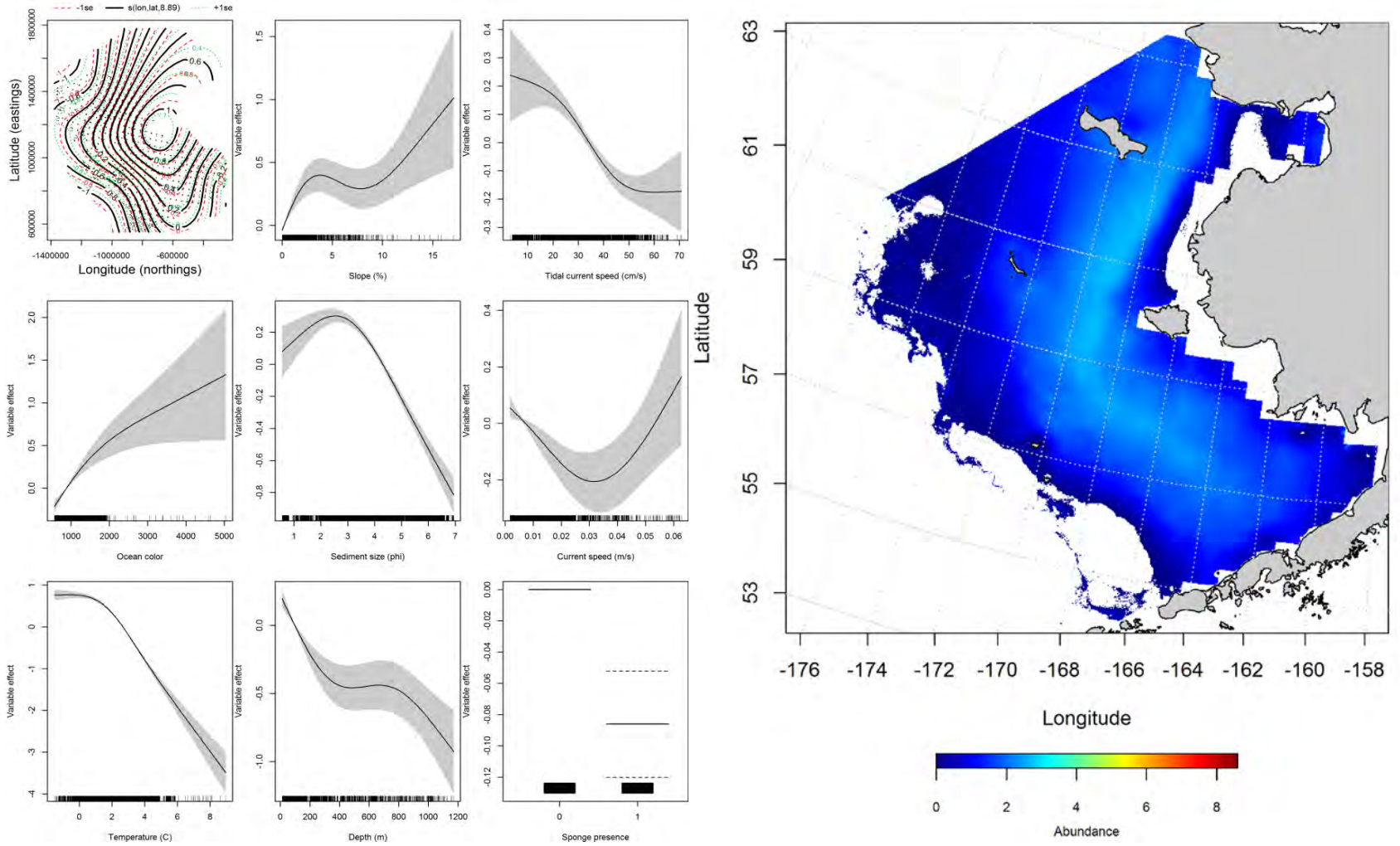

Figure 103. -- Effects of retained habitat covariates on the best-fitting generalized additive model (GAM; left panel) for adult Alaska plaice abundance in RACE summer bottom trawl surveys of the Eastern Bering Sea Shelf, Slope, and Northern Bering Sea alongside their predicted abundance (right panel).

Seasonal distribution of Alaska plaice in commercial fishery catches from the Eastern Bering Sea – In the fall, current measures and bottom temperature were the most important variables describing the presence of Alaska plaice in commercial catches: tidal maximum (relative importance = 35.7%), tide-corrected current speeds (25%), and bottom temperature (21.2%). The greatest number of observations from commercial catches came from the middle shelf near the 50 m isobath on the border between the central and southern domains of the Eastern Bering Sea (Figure 104). The fall MaxEnt model was an outstanding fit to the training data (AUC = 0.98) and correctly classified 93% of predicted cases. The fit to the test data in the model validation step was also outstanding (AUC = 0.92) and correctly classified 92% of cases.

In winter, depth, tidal maximum, and ocean productivity were the most important variables determining the distribution of Alaska plaice (relative importance = 40.5, 28.9, and 24.5%, respectively). Alaska plaice in wintertime commercial catches were primarily encountered over the middle shelf in the southern domain of the Eastern Bering Sea between St. George Island and the Bering Canyon (Figure 105). The MaxEnt model for Alaska plaice presence in winter was an outstanding fit to the training data (AUC = 0.97) and correctly classified 92% of predicted cases. Validation using the test data was also an outstanding fit (AUC = 0.91) and correctly classified 91% of the cases predicted.

In the spring, tidal maximum, bottom depth, and current speed were the most important habitat covariates describing the presence of Alaska plaice in commercial catches (relative importance = 43.2, 20.3, and 17.7%, respectively). Alaska plaice in spring commercial catches were much more widely distributed across the middle shelf of the southern and central domains of the Eastern Bering Sea than in the other two seasons (Figure 106). The occurrence of Alaska plaice on the inner shelf of the central and southern domains was unique to springtime catches. The MaxEnt model for Alaska plaice presence in springtime was an outstanding fit to the training data (AUC = 0.90) and correctly classified 84% of predicted cases.

Validation using the test data was an excellent fit (AUC = 0.83) and correctly classified 83% of cases predicted.

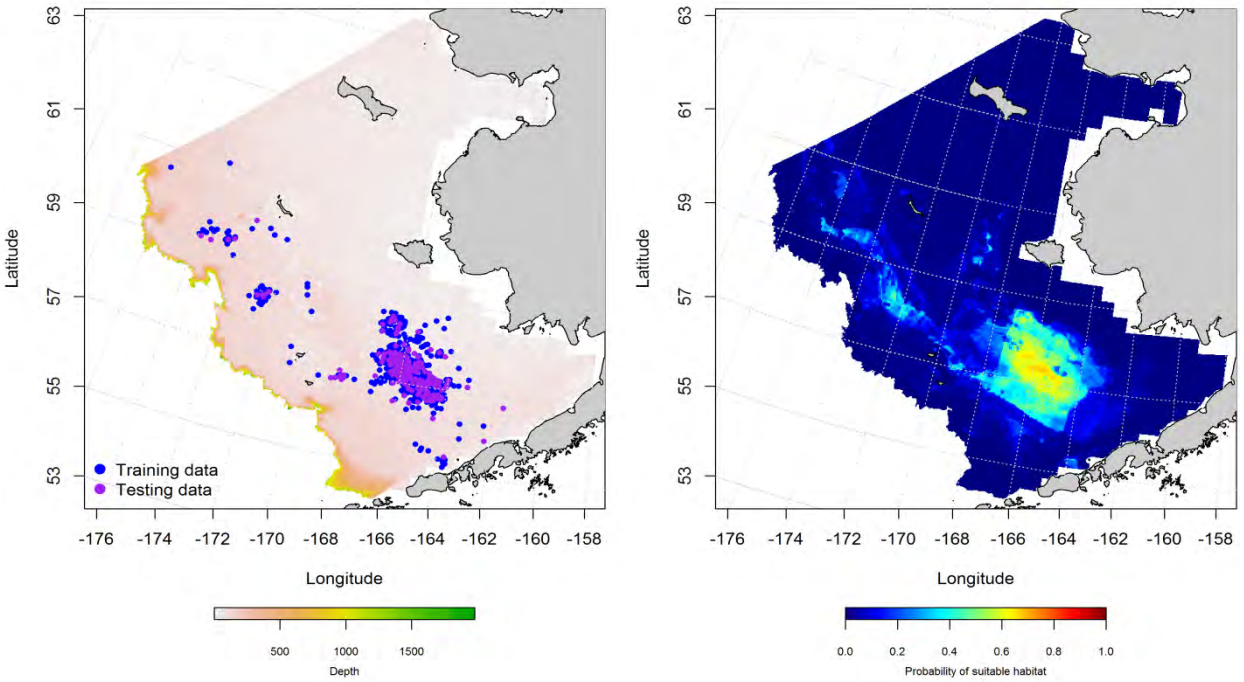

Figure 104. -- Locations of fall (October-November) catches of Alaska plaice in commercial fisheries of the Eastern Bering Sea (left panel). Blue points were used to train the maximum entropy model predicting the probability of suitable habitat (right panel) and the purple points were used to validate the model.

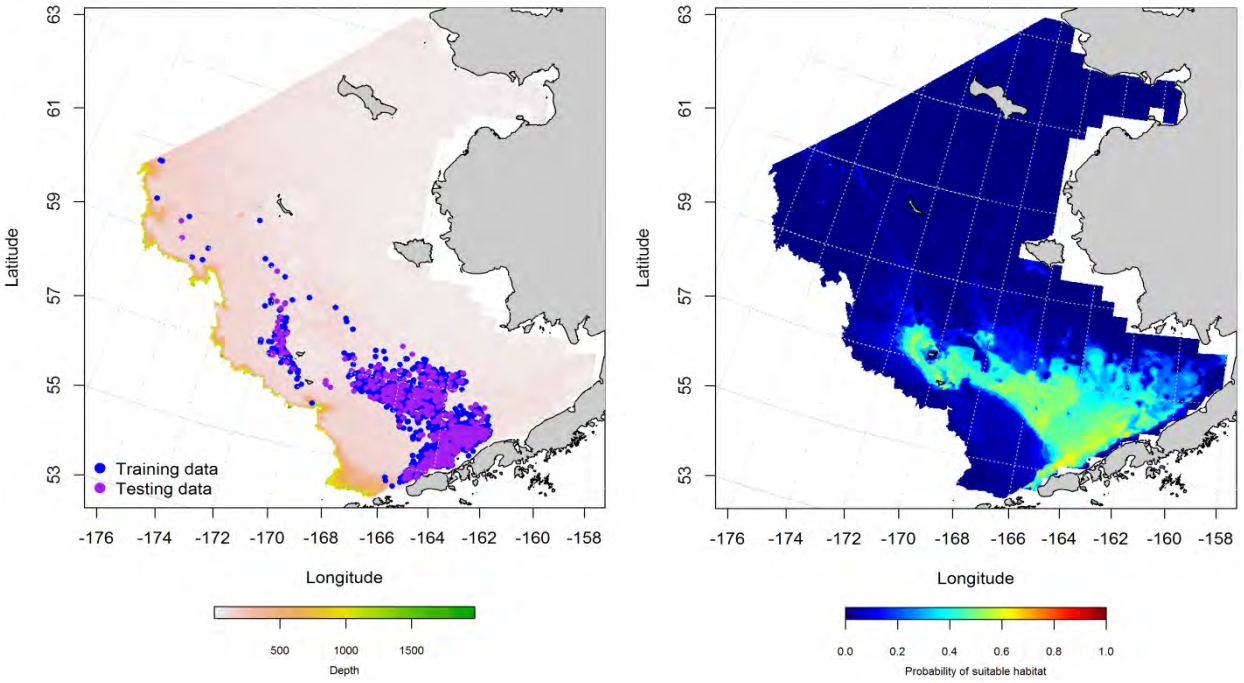

Figure 105. -- Locations of winter (December-February) catches of Alaska plaice in commercial fisheries of the Eastern Bering Sea (left panel). Blue points were used to train the maximum entropy model predicting the probability of suitable habitat (right panel) and the purple points were used to validate the model.

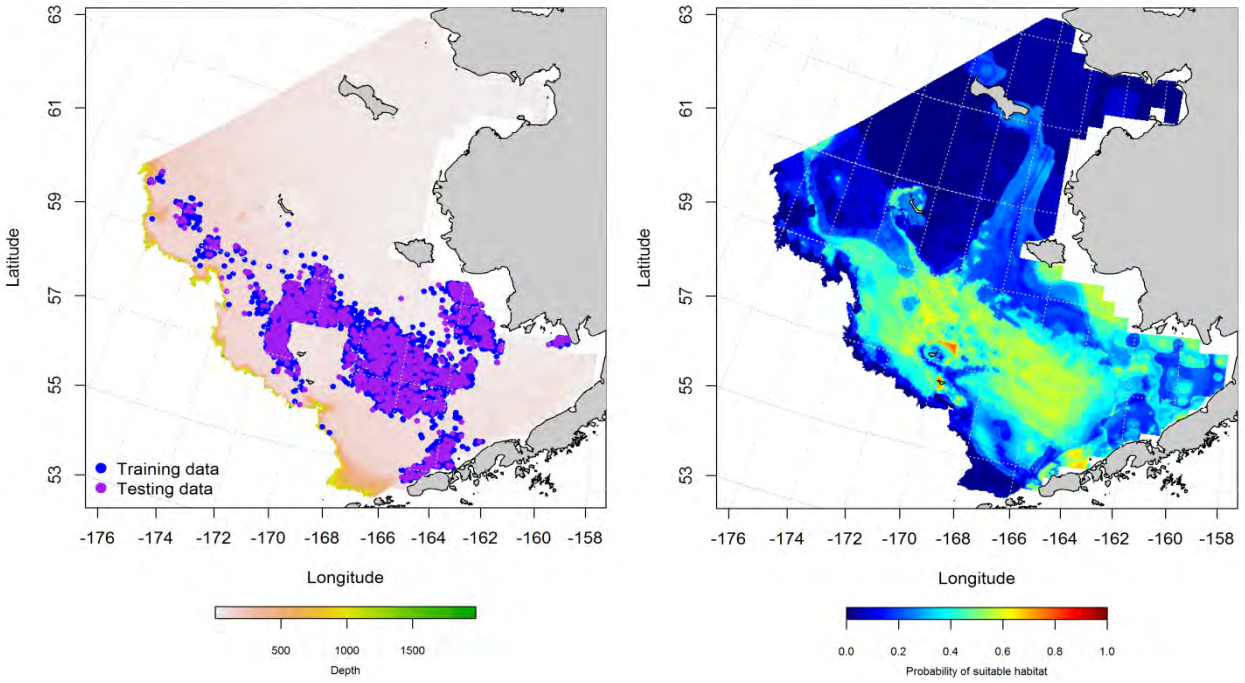

Figure 106. -- Locations of spring (March-May) catches of Alaska plaice in commercial fisheries of the Eastern Bering Sea (left panel). Blue points were used to train the maximum entropy model predicting the probability of suitable habitat (right panel) and the purple points were used to validate the model.

Eastern Bering Sea Alaska plaice (*Pleuronectes quadrituberculatus*) essential fish habitat maps and conclusions – Summertime EFH for adult Alaska plaice covered the southern, central, and northern domains of the Eastern Bering Sea from Bristol Bay to the northern extent of the survey area across the middle and outer shelf (Figure 107). The portion of the habitat with the highest Alaska plaice abundance generally tracked the 50 m isobath from south to north across the survey area.

Alaska plaice EFH determined from commercial fishery activity showed a strong seasonal component with fall EFH more spatially constrained than spring (Figure 108). While fall habitat was centered in the southern domain of the Eastern Bering Sea over the middle shelf the springtime habitat extended across all three domains from the inner to the outer shelf. In all seasons, the areas of most likely suitable habitat were found along the 50 m isobath of the Eastern Bering Sea.

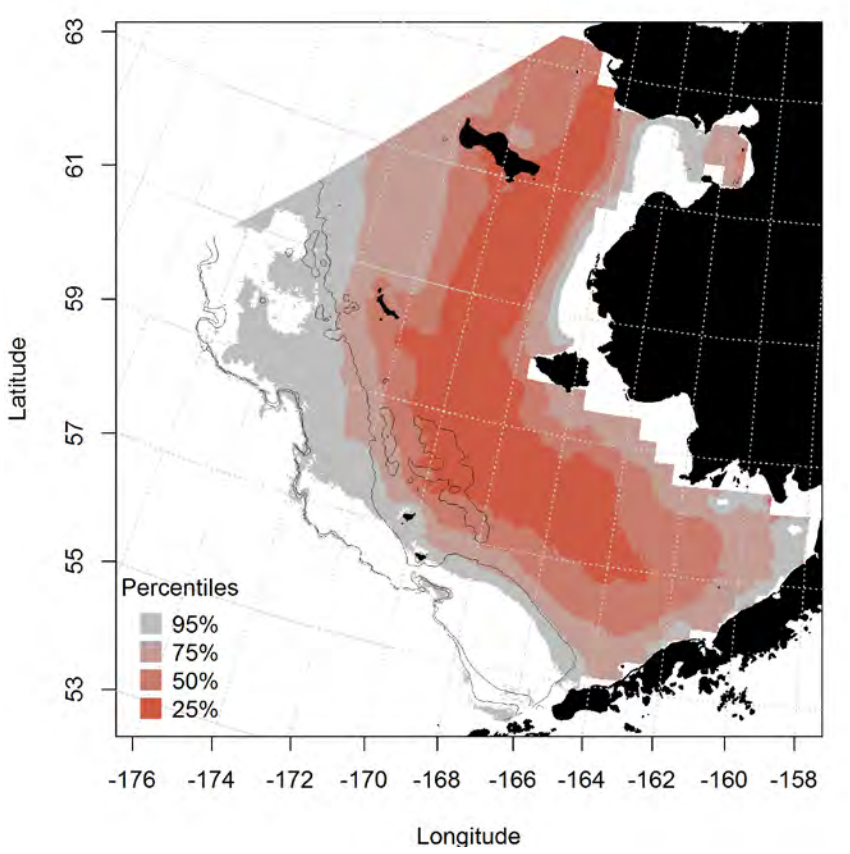

Figure 107. -- Essential habitat for adult Alaska plaice collected in RACE summertime bottom trawl surveys of the Eastern Bering Sea.

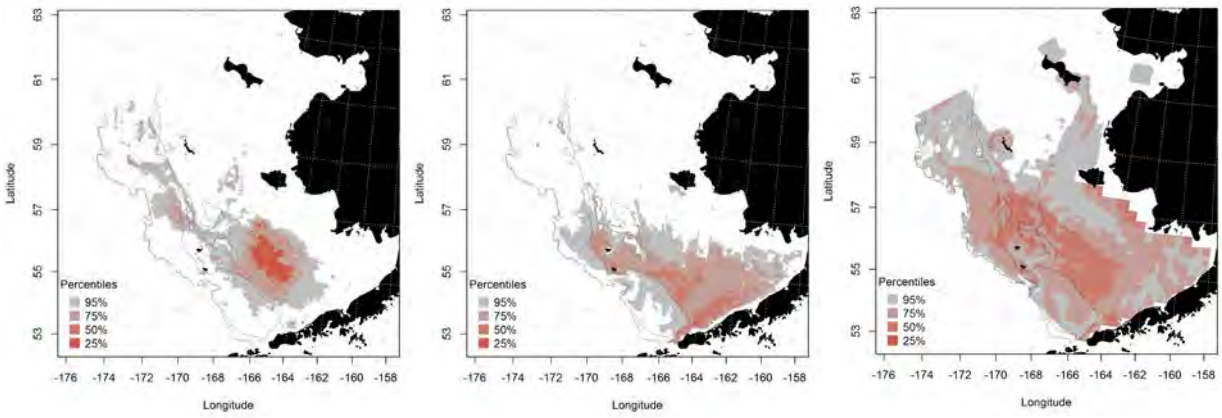

Figure 108. -- Essential fish habitat predicted for Alaska plaice from commercial fishery catches during fall (left panel), winter (middle panel), and spring (right panel).

Greenland turbot (*Reinhardtius hippoglossoides*)

Greenland turbot has a circumpolar distribution but have not been recorded from the intervening Arctic Ocean. On the Pacific side, they are most abundant on the Bering Sea continental shelf and upper slope (Allen and Smith 1988). They inhabit relatively shallow waters when immature (< 200 m) before joining the adult population in deeper water (200 to 1000 m; Templeman 1973). Adults appear to undergo seasonal shifts in depth distribution moving deeper in winter and shallower in summer (Chumakov 1970, Shuntov 1965).

Greenland turbot eggs, larvae, and early juveniles can be distinguished from the other flatfish species in EcoFOCI ichthyoplankton samples. These early life stages are generally distributed in the western and central portions of the southern Bering Sea but vary seasonally. Late-juveniles and adults of this species occur across the region in summer bottom trawl survey catches with higher CPUEs in the northwestern portion of the Eastern Bering Sea. Greenland turbot are also a valuable commercially harvested species in the Eastern Bering Sea.

Seasonal distribution of early life history stages of Greenland turbot from EcoFOCI ichthyoplankton surveys of the Eastern Bering Sea – There were < 50 occurrences of Greenland turbot eggs recorded in EcoFOCI ichthyoplankton samples in the southwestern portion of the Eastern Bering Sea (Figure 109); 37 in the winter and 11 in the spring. Eggs were observed over the outer shelf (100 to 200 m) and slope (200 to 3,000 m) of the Eastern Bering Sea and along the eastern end of the Aleutian Islands chain; there were also two records of Greenland turbot eggs recorded over Pribilof Canyon in spring. These data were insufficient to parameterize a distribution model for Greenland turbot eggs.

Greenland turbot larvae were encountered throughout the year in EcoFOCI ichthyoplankton samples (Figure 110). They primarily occurred over the outer shelf (100 to 200 m) and slope (200 to 3,000 m) of the Eastern Bering Sea. The distribution of Greenland turbot larvae appears to vary by season, but since survey effort also varied seasonally these differences may be sampling artifacts.

The areas of suitable habitat predicted from MaxEnt modeling of larval Greenland turbot presence also vary seasonally in the Eastern Bering Sea (Figure 111). In spring, the area with the highest probability of providing suitable habitat is in the southwest portion of the Eastern Bering Sea in benthypelagic waters over the Bering Canyon (200 to 3,000 m). During summer, the predicted habitat shifted northward to the Pribilof Islands and inshore over the outer (100 to 200 m) and middle (50 to 100 m) portions of the central and southern domains of the Eastern Bering Sea. Maximum entropy models utilizing the training data were excellent fits in spring (AUC = 0.98) and summer (AUC = 0.92). The percent of cases correctly predicted by the model was highest in spring (94%) and lowest in summer (80%). The most important habitat variables predicting larval Greenland turbot distribution were surface temperature and bottom depth in both seasons. These two terms were more than twice as influential in the spring than summer with a combined relative importance of 93% in spring compared with 44% in the summer. Ocean productivity comprised an additional 26% of the leverage in the summer model while accounting for < 1% of the leverage in the springtime model. The MaxEnt model also fit the test data well during model validation. In spring, AUC = 0.92 and 92% of cases were correctly predicted; in summer the values were slightly lower but still indicated an excellent fit (AUC = 0.85 with 85% of cases correctly classified).

Early juveniles of Greenland turbot were uncommon in EcoFOCI ichthyoplankton samples in the Eastern Bering Sea (Figure 112). Reported occurrences were near the Pribilof Islands and did not provide sufficient data for habitat modeling.

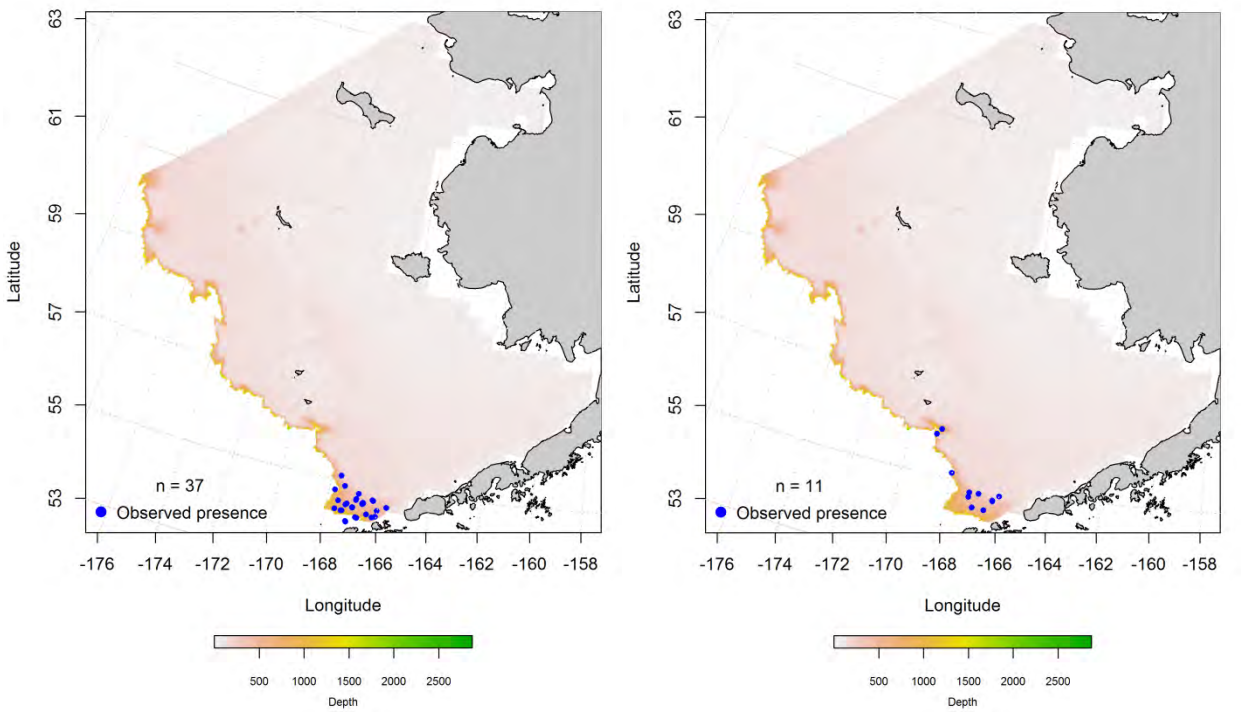

Figure 109. -- Winter and spring observations (left and right panel) of Greenland turbot eggs from EcoFOCI ichthyoplankton surveys of the Eastern Bering Sea.

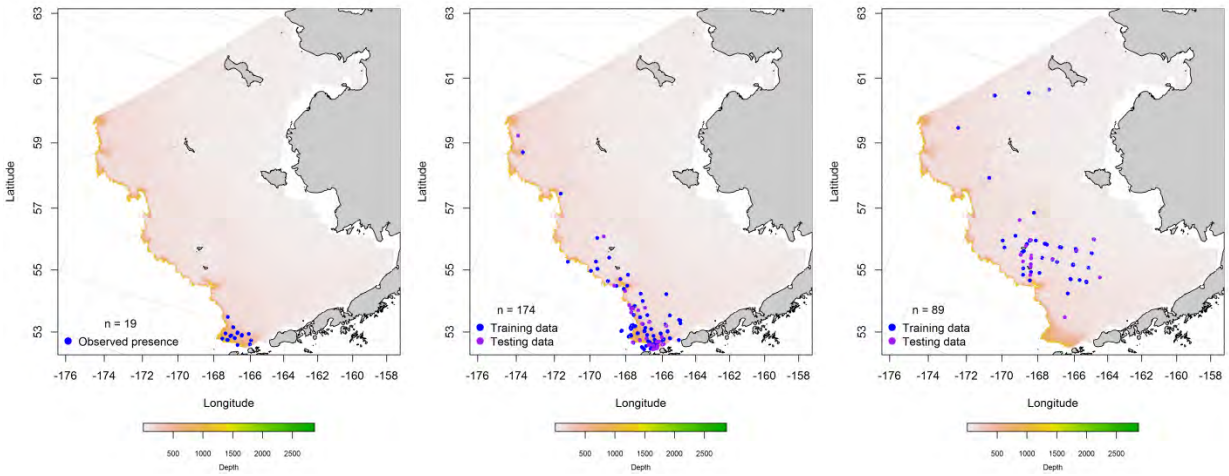

Figure 110. -- Winter, spring, and summer observations (left, middle, and right panel, respectively) of larval Greenland turbot from EcoFOCI ichthyoplankton surveys of the Eastern Bering Sea.

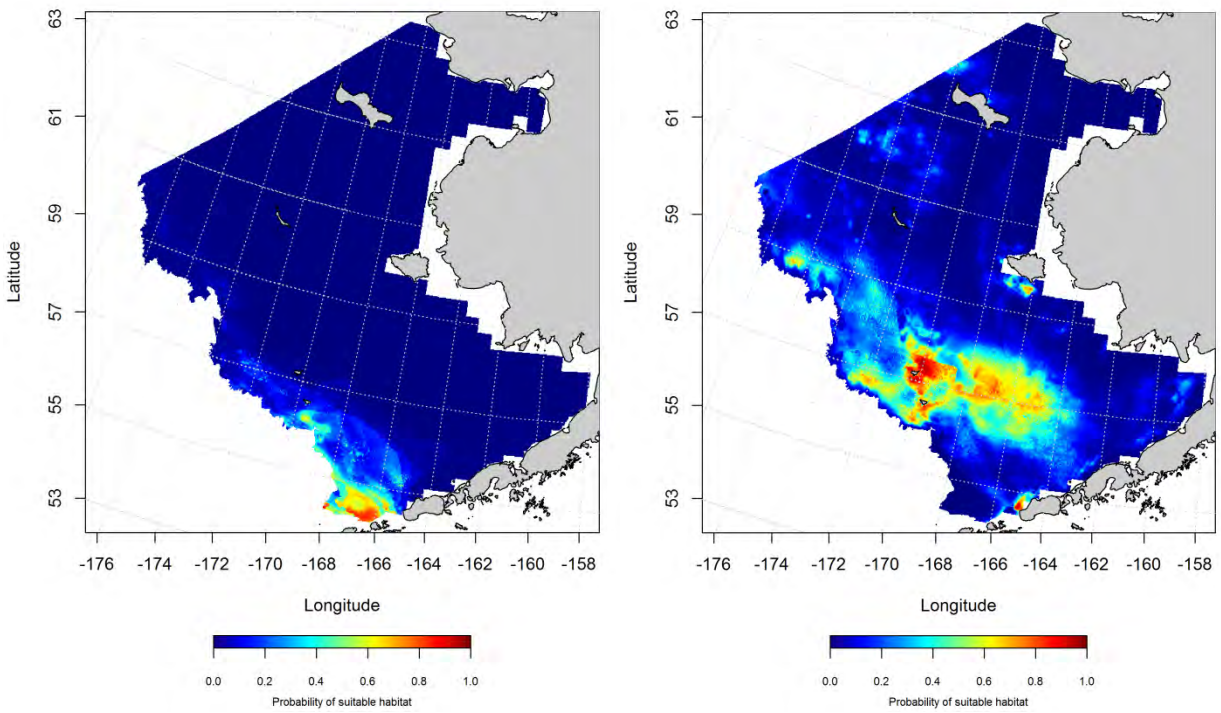

Figure 111. -- Maximum entropy (MaxEnt) model predictions of the probability of suitable spring and summer (left and right panels) larval Greenland turbot habitat from EcoFOCI ichthyoplankton surveys of the Eastern Bering Sea.

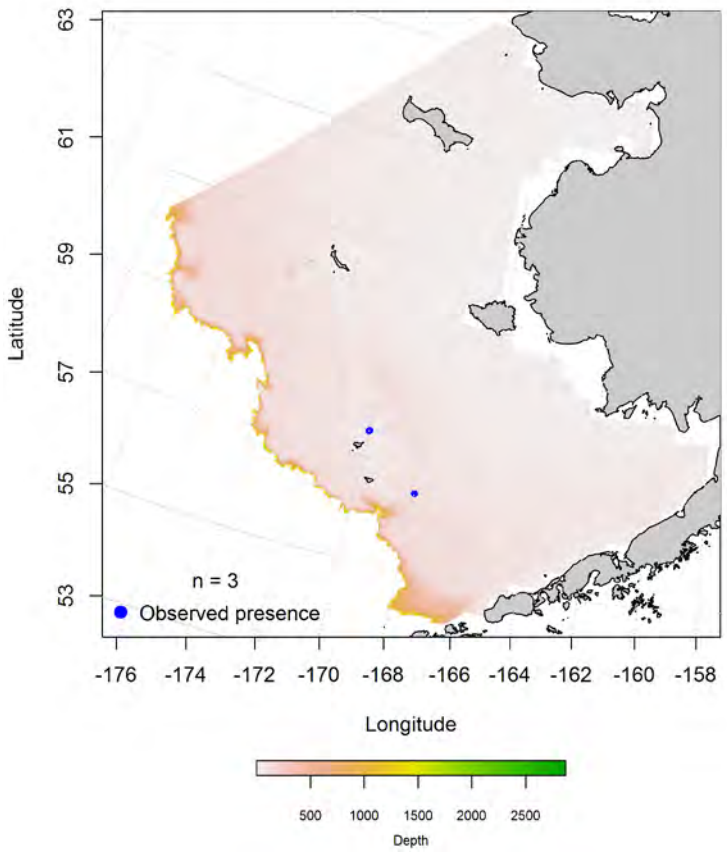

Figure 112. -- Summertime observation of early juvenile Greenland turbot from EcoFOCI ichthyoplankton surveys of the Eastern Bering Sea.

Essential fish habitat maps and conclusions for early life history stages of Greenland turbot from the Eastern Bering Sea -- Essential habitat for larval Greenland turbot varied seasonally (Figure 113). In spring, larval EFH was predicted to be in the southwestern portion of the EBS sampling area along the outer shelf and slope. In summer months, EFH for these larvae was much broader. Occurrences of egg and early juvenile stages of Greenland turbot in EcoFOCI ichthyoplankton samples were insufficient to predict EFH for these life stages.

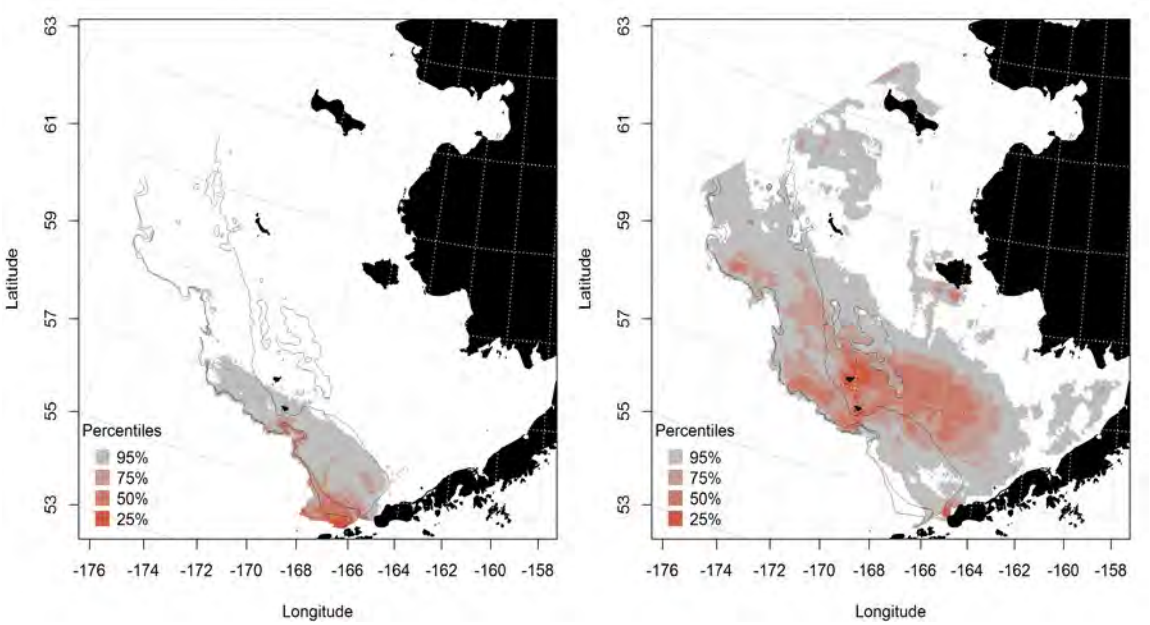

Figure 113. -- Spring (left panel) and summer (right panel) essential habitat predicted for larval Greenland turbot in the Eastern Bering Sea.

Summertime distribution of late juvenile and adult Greenland turbot from RACE bottom trawl surveys of the Eastern Bering Sea – Late juvenile and adult Greenland turbot collected in RACE summer bottom trawl surveys of the Eastern Bering Sea occur primarily over the middle and outer shelf (50 to 200 m) and continental slope (100 to 1000 m; Figure 114). Juveniles were also caught on RACE summer bottom trawl surveys in the Northern Bering Sea and occur in shallower depths than adults over their shared range.

A hurdle GAM was used to describe late juvenile Greenland turbot distribution and abundance in the Eastern Bering Sea. In the first stage of the hurdle model, the best-fitting presence-absence GAM explained 45.4% of the variability in their distribution across the Northern and Eastern Bering Sea sampling areas (Figure 115). Bottom depth, bottom temperature, and sediment grain size were the most important predictors amongst the 8 habitat covariates retained in the presence-absence GAM. The fit of this model was outstanding (AUC = 0.92) with 85% of cases of presence-absence correctly predicted. The AUC using the test data for model validation also indicated an outstanding fit of the presence-absence GAM to these data (0.94) with 86% of cases correctly classified. The presence GAM informed the

conditional abundance GAM in the second stage of the hurdle. The conditional abundance GAM accounted for 23.6% of the variability in CPUE over habitats where presence was predicted (Figure 116). The most important habitat predictors of abundance where present were geographical location, current speed, and temperature. The greatest conditional abundance of juvenile Greenland turbot was predicted in the northwestern portion of the Eastern Bering Sea Shelf in waters deeper than 100 m.

The best-fitting presence-absence GAM for adult Greenland turbot explained around 55% of the variability in their distribution across the Eastern and Northern Bering sea sampling areas (Figure 117). Sediment grain size, bottom temperature, bottom depth, and geographic location were the most important variables explaining their distribution. The GAM predicting adult Greenland turbot presence was an outstanding fit indicated by an AUC of 0.95 with 89% of cases (predicting presence-absence) correctly classified. The AUC for the test data (0.95) indicated an outstanding fit of the GAM to these data as well.

The best-fitting conditional abundance GAM informed by the presence-absence GAM above accounted for around 35% of the variability in CPUE over habitat where they were predicted to be present (Figure 118). The most important habitat predictors of abundance where present were geographic location, bottom depth, ocean productivity, and local slope. The areas of greatest conditional abundance of adult Greenland turbot were predicted in the southwestern portion of the Bering Sea Slope.

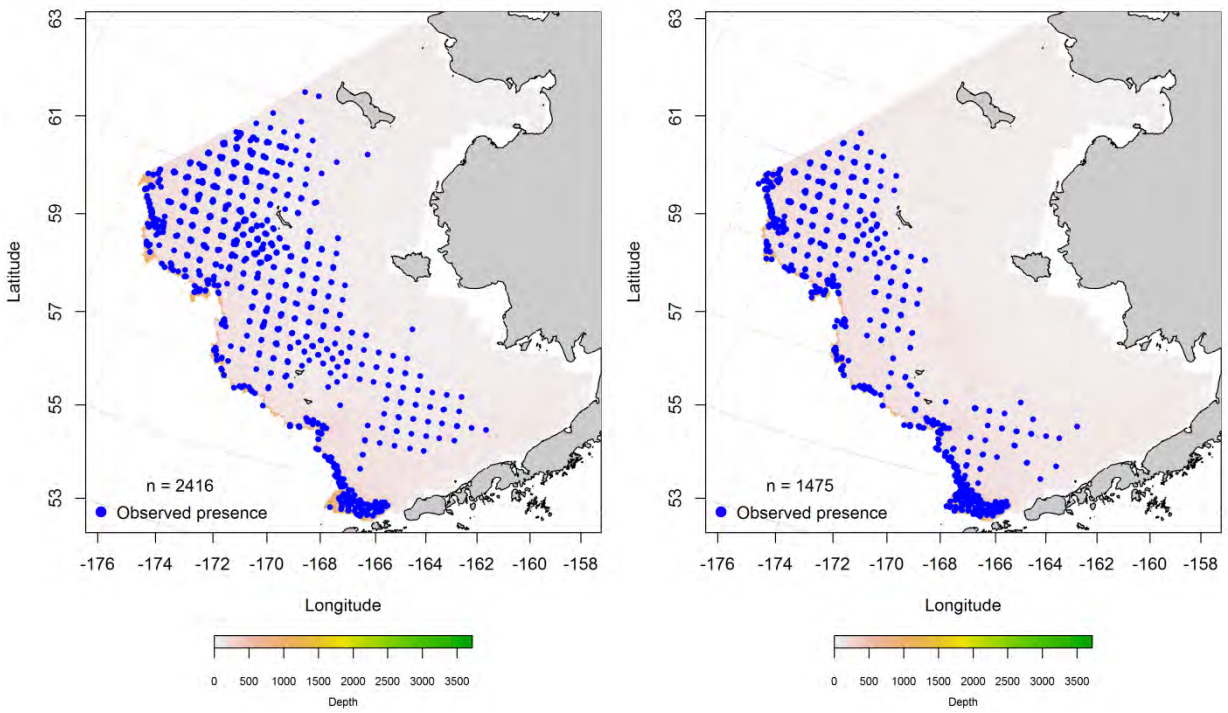

Figure 114. -- Distribution of late-juvenile (left) and adult (right) Greenland turbot catches from RACE summer bottom trawl surveys of the Eastern Bering Sea.

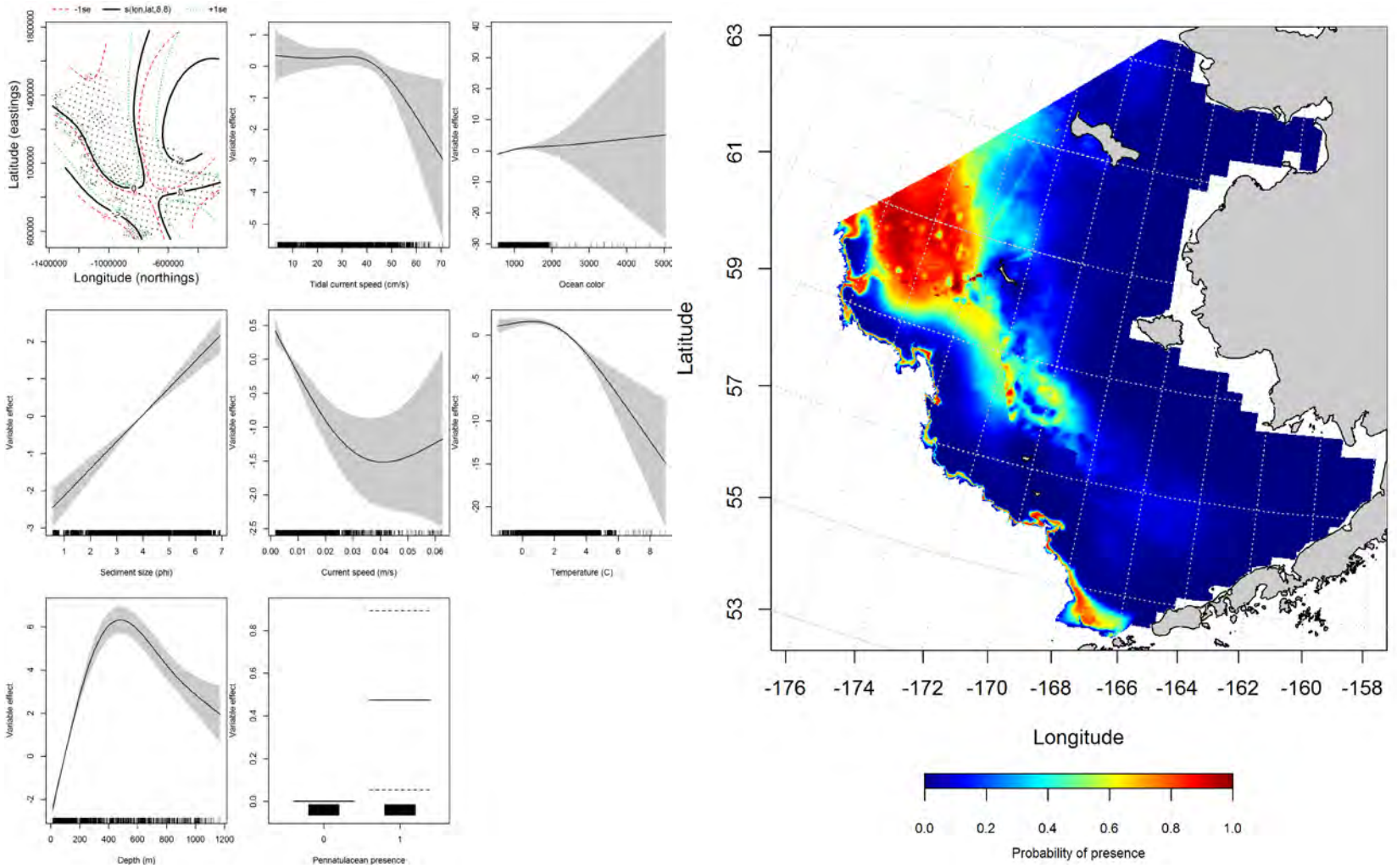

Figure 115. -- Effects of retained habitat covariates on the best-fitting generalized additive presence-absence model (GAM) of late juvenile Greenland turbot from RACE summer bottom trawl surveys of the Eastern Bering Sea Shelf, Slope, and Northern Bering Sea alongside their predicted presence (right panel).

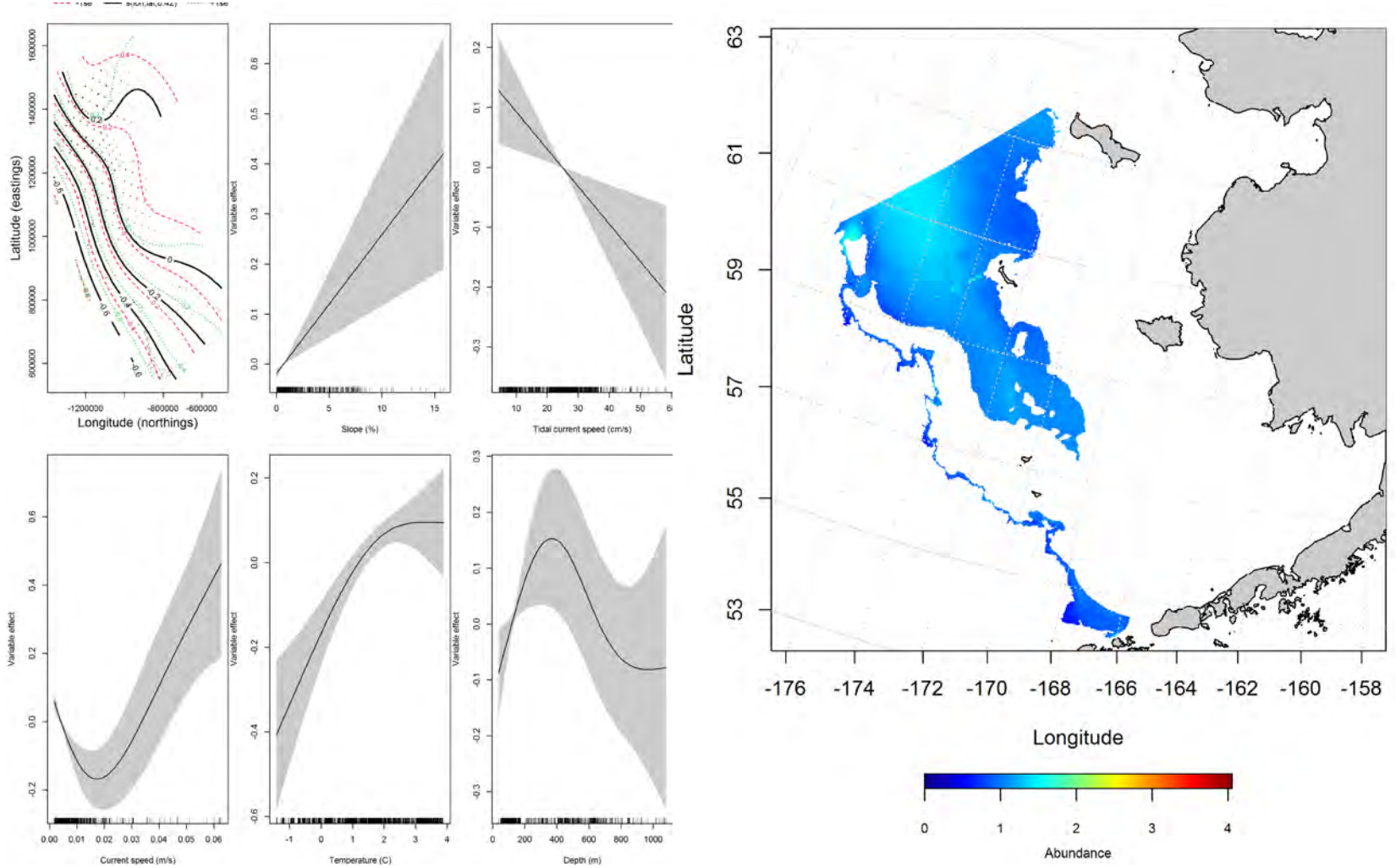

Figure 116. -- Effects of retained habitat covariates on the best-fitting generalized additive model (GAM; left panel) of late juvenile Greenland turbot abundance in RACE summer bottom trawl surveys of the Eastern Bering Sea Shelf, Slope, and Northern Bering Sea alongside their predicted conditional abundance (right panel).

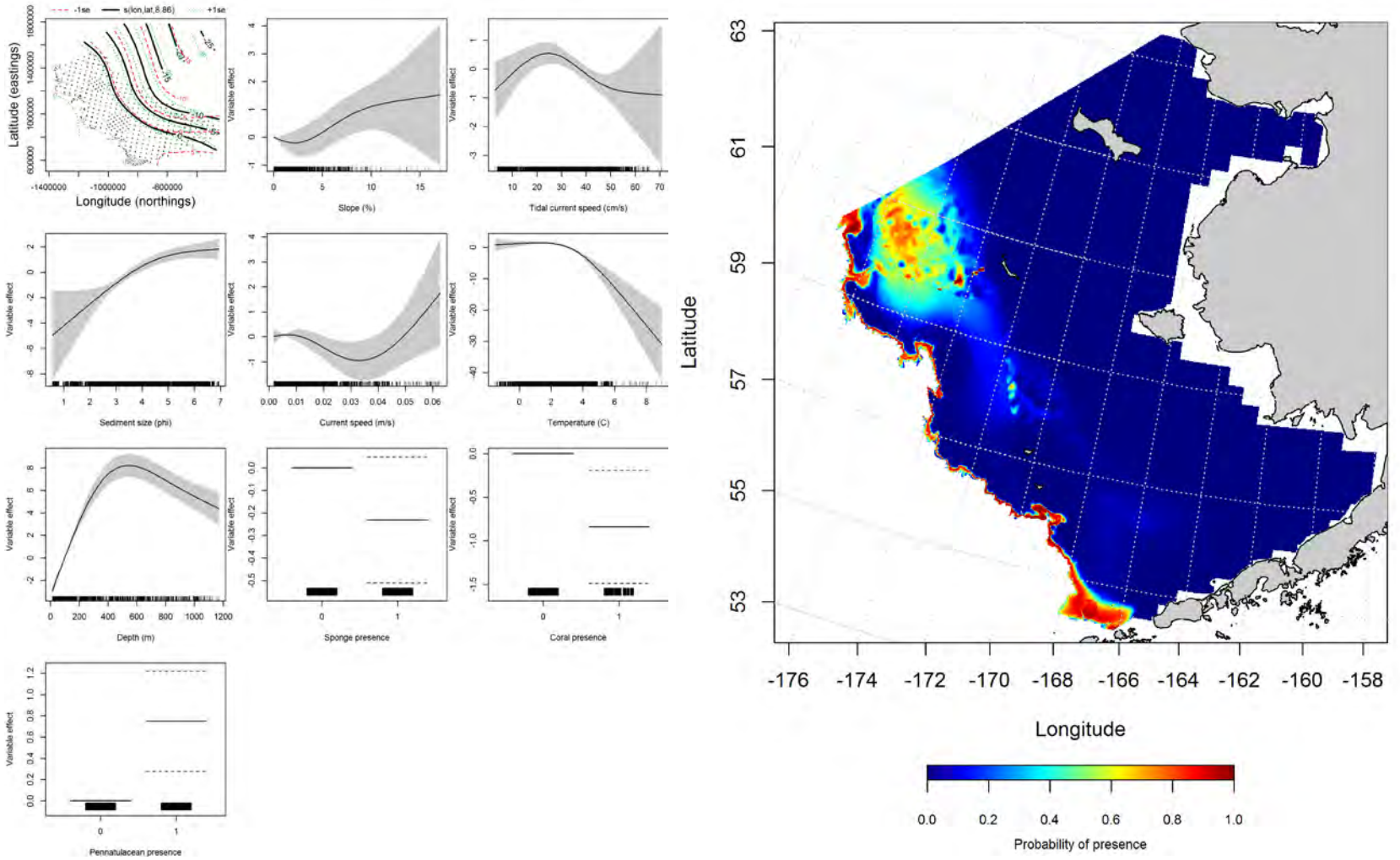

Figure 117. -- Effects of retained habitat covariates on the best-fitting generalized additive presence-absence model (GAM) of adult Greenland turbot from RACE summer bottom trawl surveys of the Eastern Bering Sea Shelf, Slope, and Northern Bering Sea alongside their predicted presence (right panel).

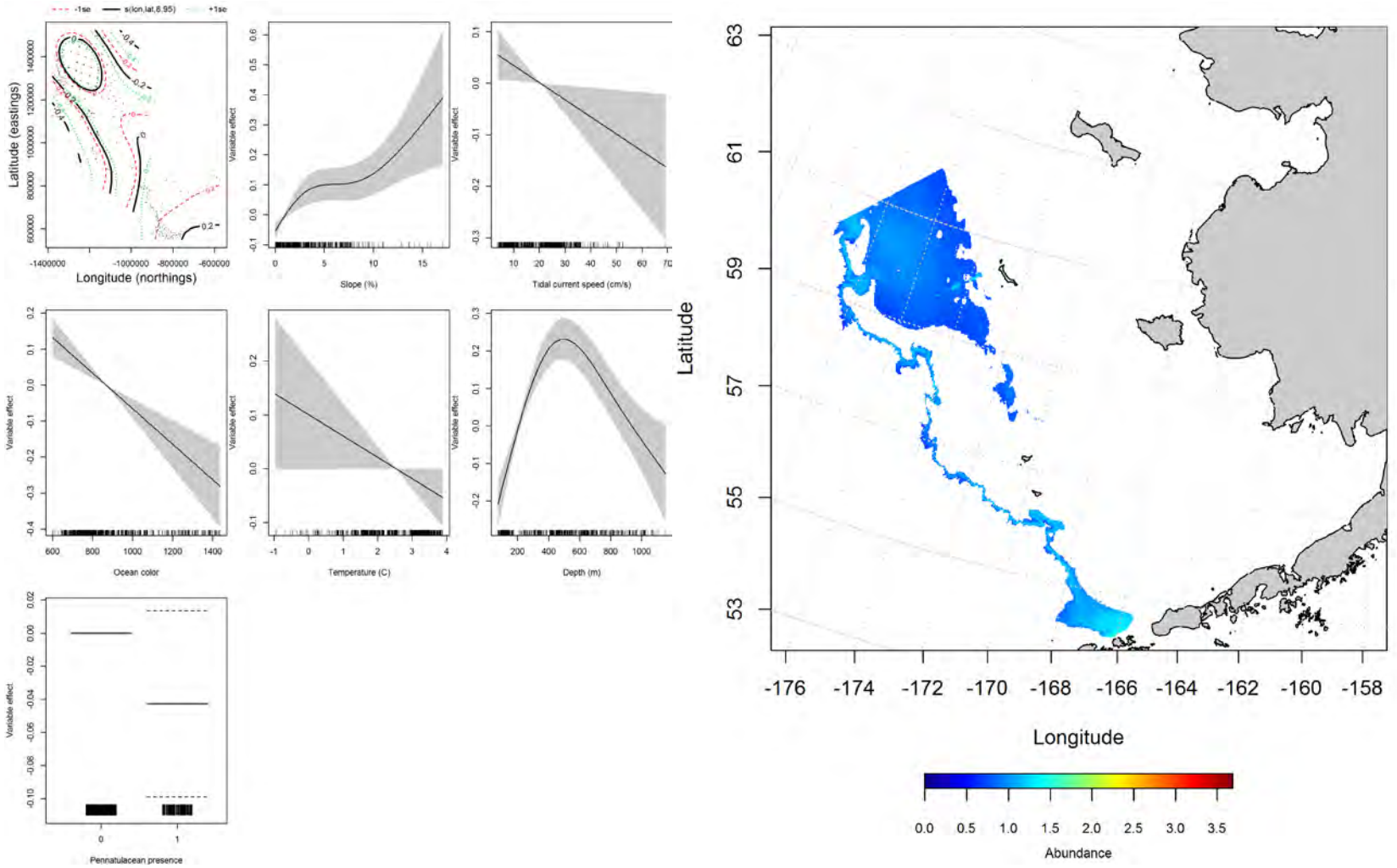

Figure 118. -- Effects of retained habitat covariates on the best-fitting generalized additive model (GAM; left panel) of adult Greenland turbot abundance in RACE summer bottom trawl surveys of the Eastern Bering Sea Shelf, Slope, and Northern Bering Sea alongside their predicted conditional abundance (right panel).

Seasonal distribution of Greenland turbot in commercial fishery catches from the Eastern Bering Sea -- Distribution of Greenland turbot in Eastern Bering Sea commercial fishery catches was generally consistent throughout all seasons. In the fall, depth and bottom temperature were the most important variables determining the distribution of Greenland turbot (relative importance = 69.8 and 21.6%). The AUC of the fall model was 0.88 for the training data and 0.79 for the test data and 79% of the cases predicted from the training and test data sets were correctly classified. Greenland turbot catches were mostly distributed on the outer shelf and the southern half of the middle shelf of the Eastern Bering Sea (Figure 119).

In the winter, depth and bottom temperature were the most important variables determining the distribution of Greenland turbot (relative importance = 60.0 and 34.5%). The AUC of this MaxEnt model was 0.92 for the training data and 0.84 for the test data and 84% of the cases predicted from the training and test data sets were correctly classified. As in fall, Greenland turbot catches were mostly distributed on the outer shelf and the southern half of the middle shelf of the EBS, although there was more predicted suitable habitat in Bristol Bay in winter (Figure 120).

In the spring, depth and bottom temperature were again the most important variables determining the distribution of Greenland turbot (relative importance = 53.7 and 32.2%). The AUC of this MaxEnt model was 0.92 for the training data and 0.85 for the test data. As with the fall and winter, Greenland turbot catches were mostly distributed on the outer shelf and the southern half of the middle shelf of the EBS (Figure 121).

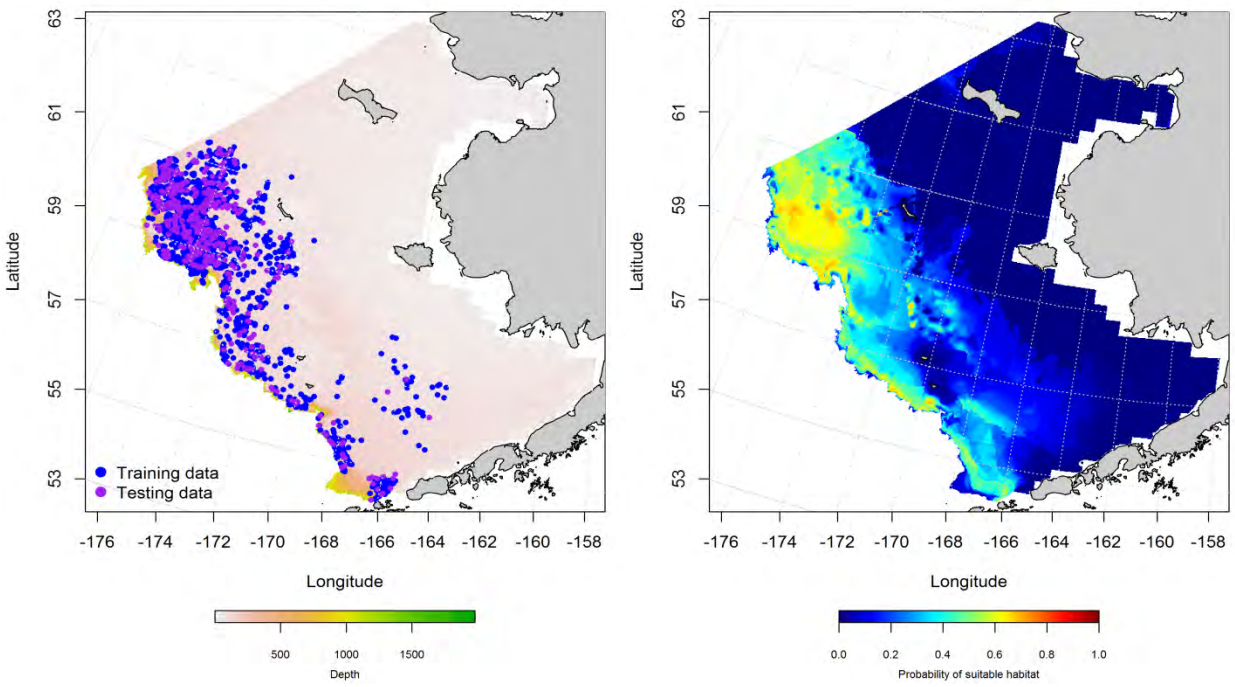

Figure 119. -- Locations of fall (October-November) catches of Greenland turbot in commercial fisheries of the Eastern Bering Sea (left panel). Blue points were used to train the maximum entropy model predicting the probability of suitable habitat (right panel) and the purple points were used to validate the model.

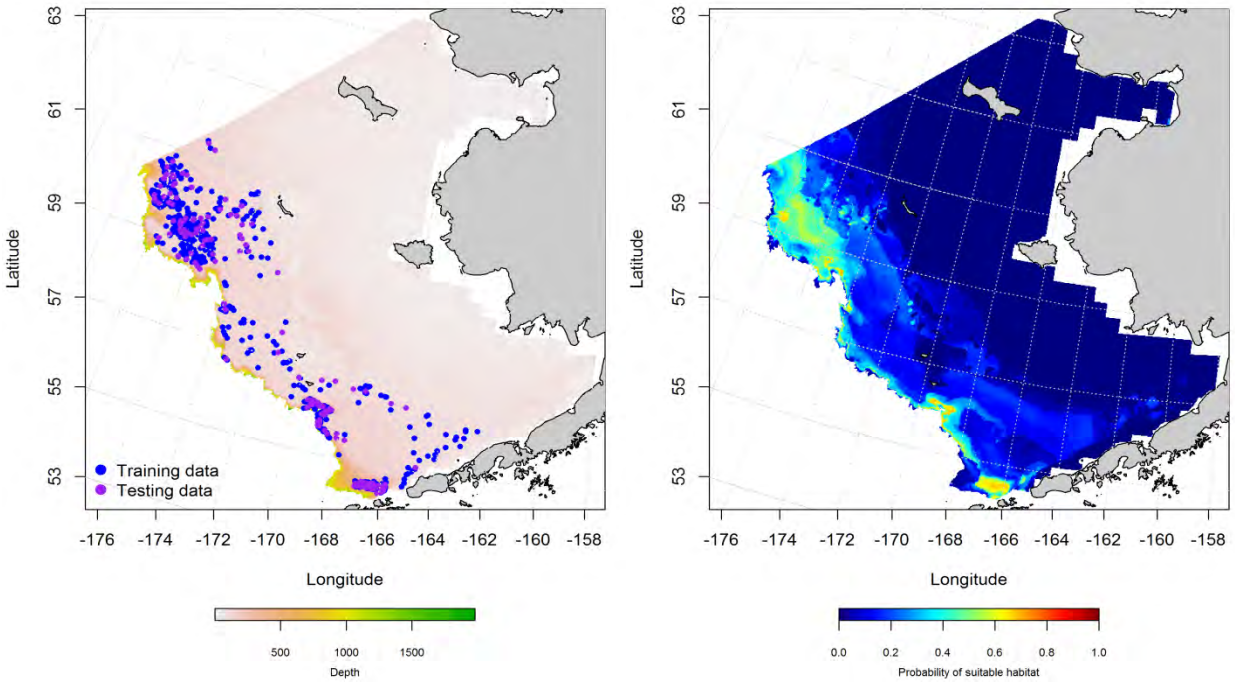

Figure 120. -- Locations of winter (December-February) catches of Greenland turbot in commercial fisheries of the Eastern Bering Sea (left panel). Blue points were used to train the maximum entropy

model predicting the probability of suitable habitat (right panel) and the purple points were used to validate the model.

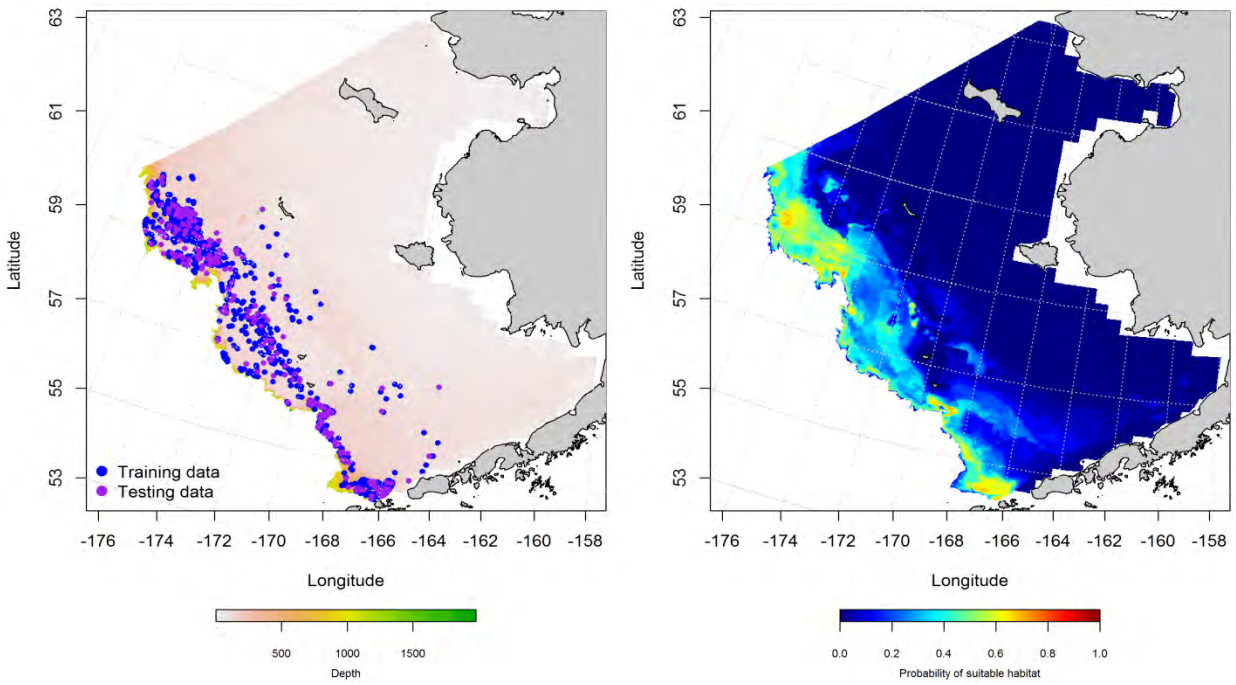

Figure 121. -- Locations of spring (March-May) catches of Greenland turbot in commercial fisheries of the Eastern Bering Sea (left panel). Blue points were used to train the maximum entropy model predicting the probability of suitable habitat (right panel) and the purple points were used to validate the model.

Eastern Bering Sea Greenland turbot (*Reinhardtius hippoglossoides*) essential fish habitat maps and conclusions -- Summertime EFH of Greenland turbot juveniles and adults was primarily distributed across the outer shelf and in the central and northern domains of the Eastern Bering Sea (Figure 122). Juvenile EFH was more widely spread across the outer shelf in the northern Bering Sea. Adult Greenland turbot EFH was more focused around the Bering Sea slope and in the submarine canyons.

The seasonal distribution of Greenland turbot EFH determined from commercial fishery catches was distributed across the outer and middle shelf in fall, winter, and spring (Figure 123). Areas of highest abundance were concentrated in the northwestern portion of the Eastern Bering Sea and along the slope edge.

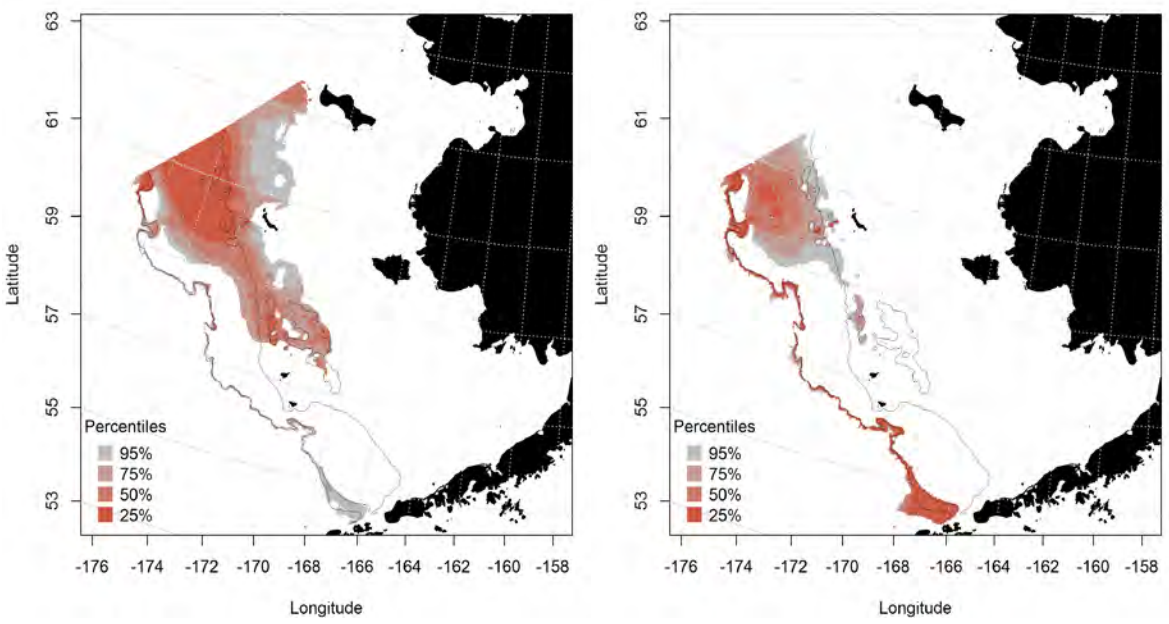

Figure 122. -- Predicted summer essential fish habitat for Greenland turbot juveniles and adults (left and right panel) from summertime bottom trawl surveys.

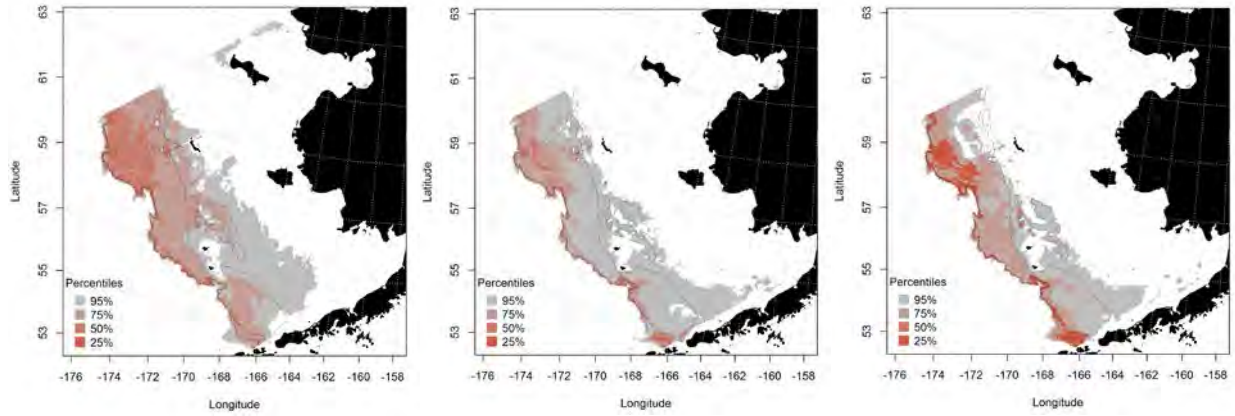

Figure 123. -- Essential fish habitat predicted for Greenland turbot during fall (left panel), winter (middle panel) and spring (right panel) from commercial fishery catches.

Roundfishes

walleye pollock (*Gadus chalcogrammus*)

Walleye pollock support one of the largest and most commercially valuable fisheries in the Eastern Bering Sea. There are three stocks of pollock in the BSAI area: the Eastern Bering Sea, Aleutian Islands, and Aleutian Basin stocks.

Seasonal distribution of the early life history stages of walleye pollock from EcoFOCI ichthyoplankton surveys of the Eastern Bering Sea – The fewest walleye pollock eggs were observed during winter and the most occurrences were recorded in spring (Figure 124). Survey effort varied between seasons. Therefore, apparent differences in the distribution of pollock eggs may actually reflect sampling effort, design, or gear type.

Suitable walleye pollock egg habitat was predicted from presence only data using MaxEnt modeling of EcoFOCI ichthyoplankton samples collected in spring and summer (Figure 125). The areas with the highest probability of providing suitable egg habitat in spring were located over the Bering Canyon and outer shelf above Unimak Pass and Unimak Island. The most influential habitat covariates predicting suitable habitat in springtime were surface temperature and ocean productivity which, combined, accounted for 91% of the relative importance of all predictors in the model. During summer months, suitable habitat was centered on the Pribilof Islands as well as north and east of Unimak Island and the dominant habitat covariates in the summer MaxEnt model were surface temperature, ocean productivity, and bottom depth which comprised a combined 57% of the leverage of all predictor terms. The MaxEnt fit to the training data in springtime was outstanding (AUC = 0.92), was excellent in summer (0.88), and the models correctly classified 85 and 79% of predicted cases in each season. Model validation was successful in both seasons (AUC = 0.84 in spring and 0.75 in summer). Predictions made from the test data were correctly classified 79% of the time in spring and 75% of the time in summer.

Walleye pollock larvae were rare in winter EcoFOCI ichthyoplankton samples, but were relatively common in spring and summer (Figure 126). During springtime, when they were the most prevalent, they primarily occurred in the southwest portion of the Eastern Bering Sea ranging from around the Pribilofs

into Bristol Bay. In summertime, there were more records farther north and fewer records over benthypelagic waters.

Model predictions of suitable habitat for larval walleye pollock in the Eastern Bering Sea showed some seasonal differences (Figure 127). In spring, the area with the highest probability of providing suitable habitat was in the southwest portion of the EBS in benthypelagic waters over the Bering Canyon (200 to 1,000 m) as well as off the northwest tip of Unimak Island. The most influential habitat covariates in the MaxEnt model for springtime were surface temperature (relative importance = 68.7%) and ocean productivity (21.3%). During summer, the areas predicted to provide suitable habitat shifted northward to the Pribilof Islands but an area of suitable habitat off the northwest tip of Unimak Island was still prominent. The dominant habitat covariates in this model of summertime larval walleye pollock suitable habitat were surface temperature (36.6%), ocean productivity (20.8%), and bottom depth (15.4%). The models were an outstanding fit to the springtime training data (AUC = 0.94) and an excellent fit to the summer dad (0.89); they correctly classified 87% of cases in spring and 81% in summer. Model validation using the test data also demonstrated good fits (AUC = 0.85 and 0.77 for spring and summer) and relatively high levels of correctly classified cases (85% in spring and 77% in summer).

Early juvenile stage walleye pollock were less common in fall and spring EcoFOCI surveys than in summer months (Figure 128). The distribution of early juvenile occurrences spanned the inner, middle, and outer shelf of the Eastern Bering Sea slope and extended into the Northern Bering Sea.

There were sufficient data to parameterize a MaxEnt model predicting the distribution of suitable early juvenile walleye pollock habitat from summer EcoFOCI surveys (Figure 129). The highest predicted probabilities of suitable habitat were around the Pribilof Islands. The habitat covariates that exercised the greatest influence on the prediction were ocean productivity (relative importance = 30.8%), surface temperature (26.9%), and the variability of tidally corrected currents (11.6%). The model fit to the training data was outstanding (AUC = 0.94) and the percent of cases correctly predicted was high (86%).

Validation using the test data also indicated an excellent model fit (AUC = 0.84) and a relatively high proportion of correctly classified cases (84%).

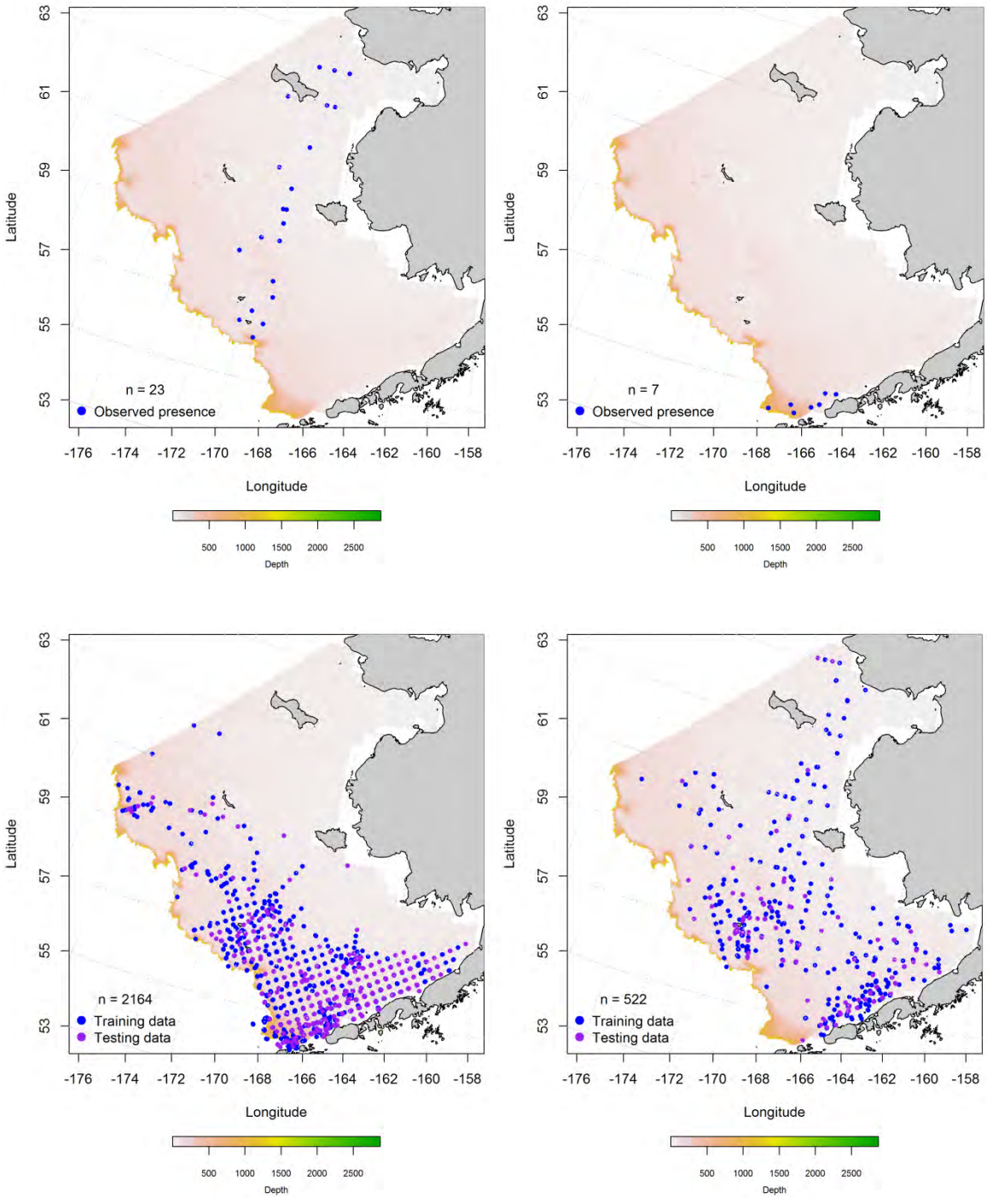

Figure 124. -- Fall (upper left panel), winter (upper right panel), spring (lower left panel), and summer (lower right panel) presence of walleye pollock eggs in EcoFOCI ichthyoplankton samples from the Eastern Bering Sea; blue points were used to train the maximum entropy (MaxEnt) model predicting suitable habitat and the purple points were used to validate the model.

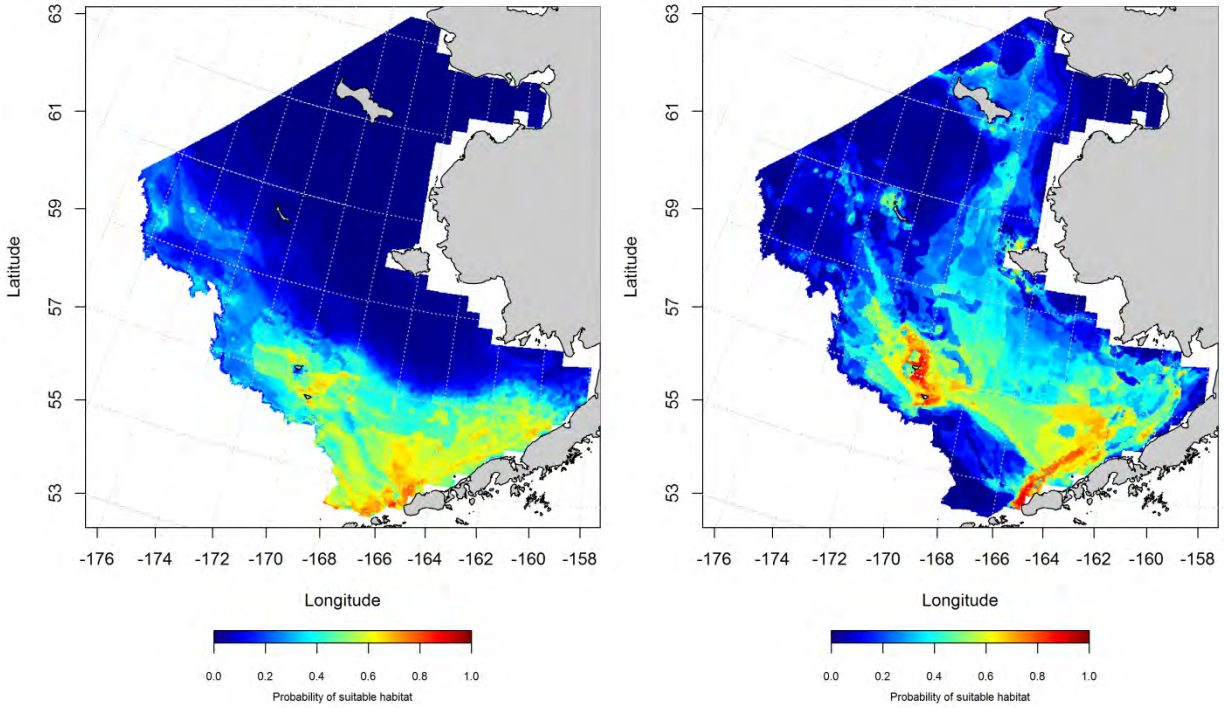

Figure 125. -- Maximum entropy (MaxEnt) model predictions of the probability of suitable spring and summer (left and right panels) walleye pollock egg habitat from EcoFOCI ichthyoplankton surveys of the Eastern Bering Sea.

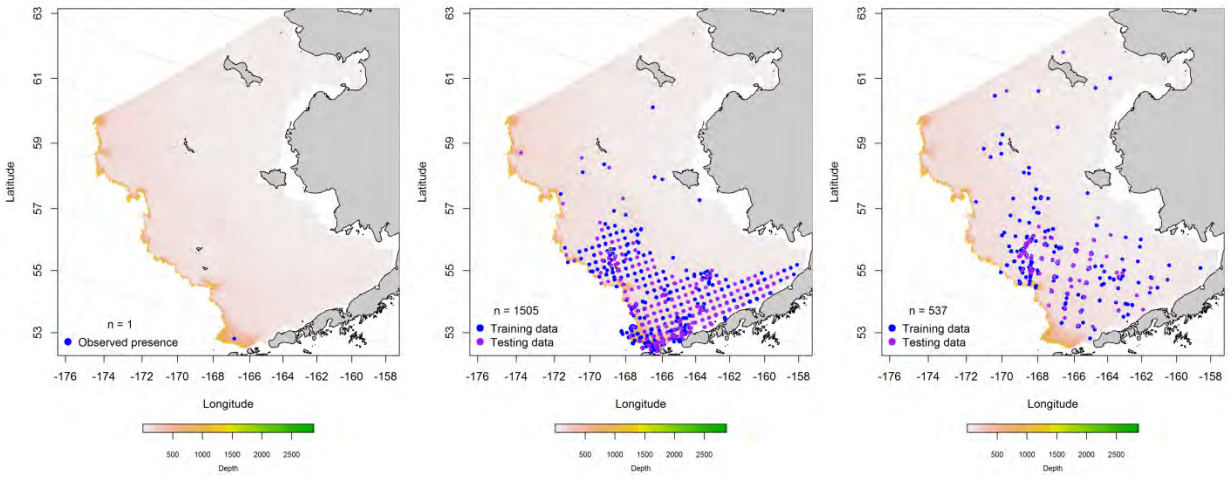

Figure 126. -- Winter, spring, and summer observations (left, middle, and right panel, respectively) of larval walleye pollock from EcoFOCI ichthyoplankton surveys of the Eastern Bering Sea; blue points

were used to train the maximum entropy (MaxEnt) model predicting the probability of suitable habitat and the purple points were used to validate the model.

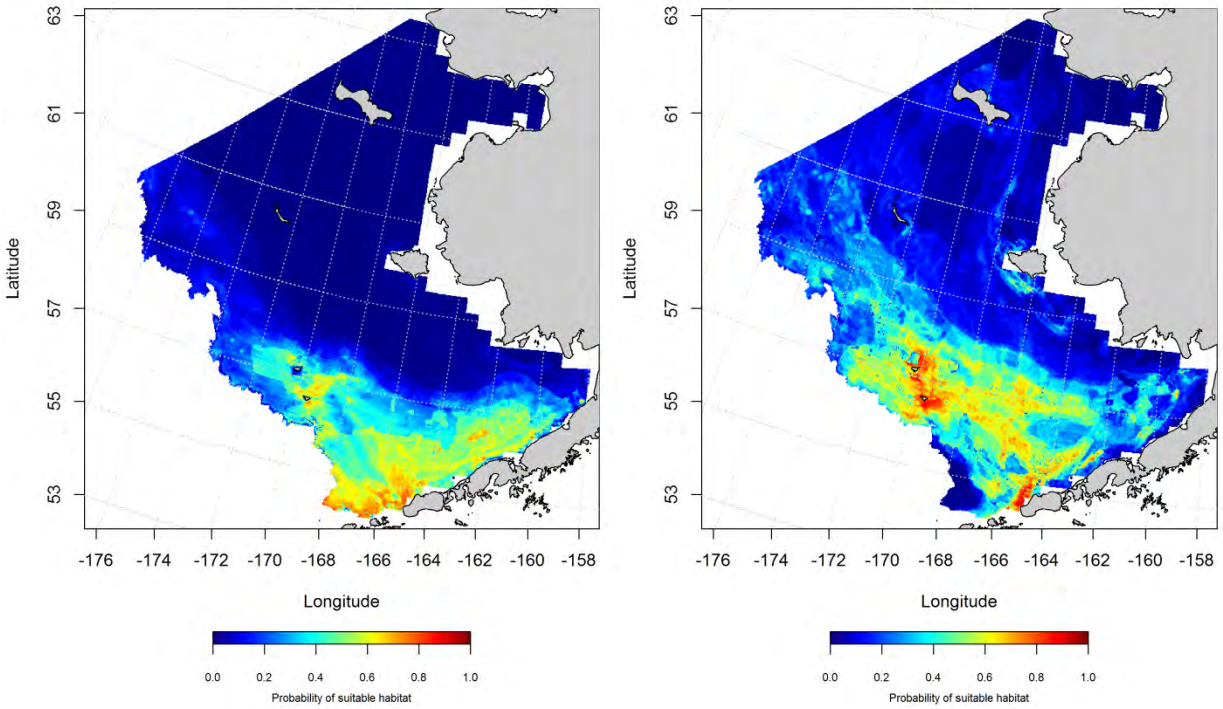

Figure 127. -- Maximum entropy (MaxEnt) model predictions of the probability of suitable spring and summer (left and right panels) larval walleye pollock habitat from EcoFOCI ichthyoplankton surveys of the Eastern Bering Sea.

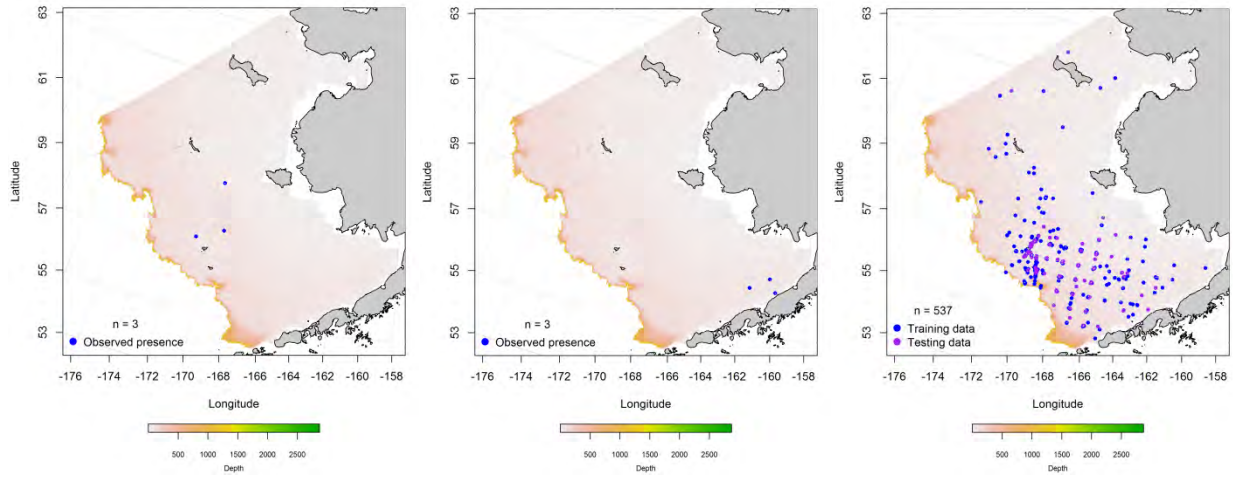

Figure 128. – Fall, spring, and summer observations of early juvenile walleye pollock from EcoFOCI ichthyoplankton surveys of the Eastern Bering Sea; blue points were used to train the maximum entropy

(MaxEnt) model predicting the probability of suitable habitat and the purple points were used to validate the model.

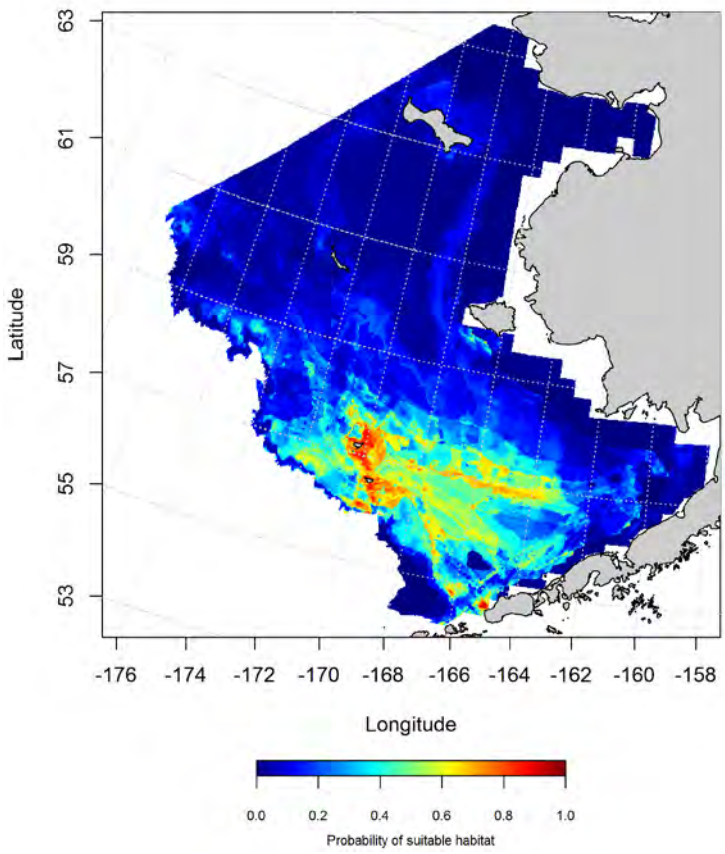

Figure 129. -- Maximum entropy (MaxEnt) model prediction of the probability of suitable summertime early juvenile walleye pollock habitat from EcoFOCI ichthyoplankton surveys of the Eastern Bering Sea.

Essential habitat maps and conclusions for early life history stages of walleye pollock (*Gadus chalcogrammus*) from the Eastern Bering Sea -- Essential habitat for walleye pollock eggs varied seasonally (Figure 130). In spring, essential egg habitat extended from the middle shelf out over the shelf edge and slope. In summer, the distribution of essential egg habitat was broader; extending from the inner shelf over the shelf edge and slope and up into the North Bering Sea.

Spring and summer distribution of EFH for larval walleye pollock showed a similar pattern to that for pollock eggs (Figure 131). Larval walleye pollock EFH in springtime was distributed from the inner shelf in Bristol Bay across the outer shelf and slope and northward roughly following the 100 m isobath. During summer months, larval walleye pollock EFH was more broadly distributed across the inner shelf

of the central Eastern Bering Sea and extended north into the Northern Bering Sea along the middle and inner shelf.

Summertime EFH of early juvenile walleye pollock in the Eastern Bering Sea was distributed from the inner shelf in Bristol Bay across the outer shelf and slope and northward roughly following the 100 m isobath to the northern extent of the survey area (Figure 132).

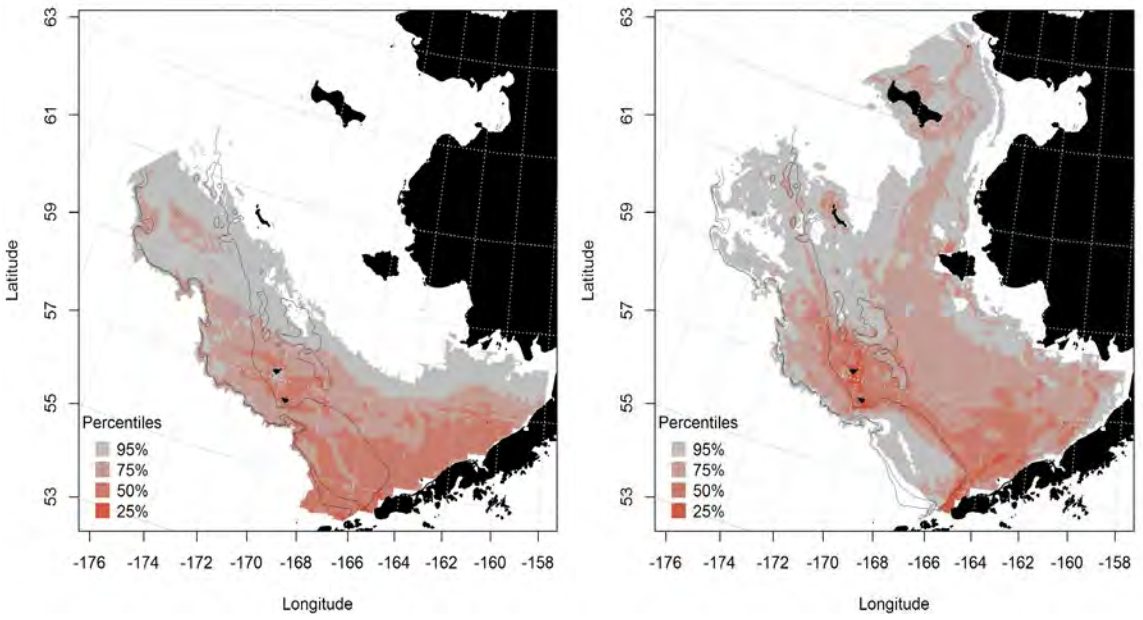

Figure 130. -- Spring (left panel) and summer (right panel) essential habitat predicted for walleye pollock eggs from EcoFOCI ichthyoplankton surveys of the Eastern Bering Sea.

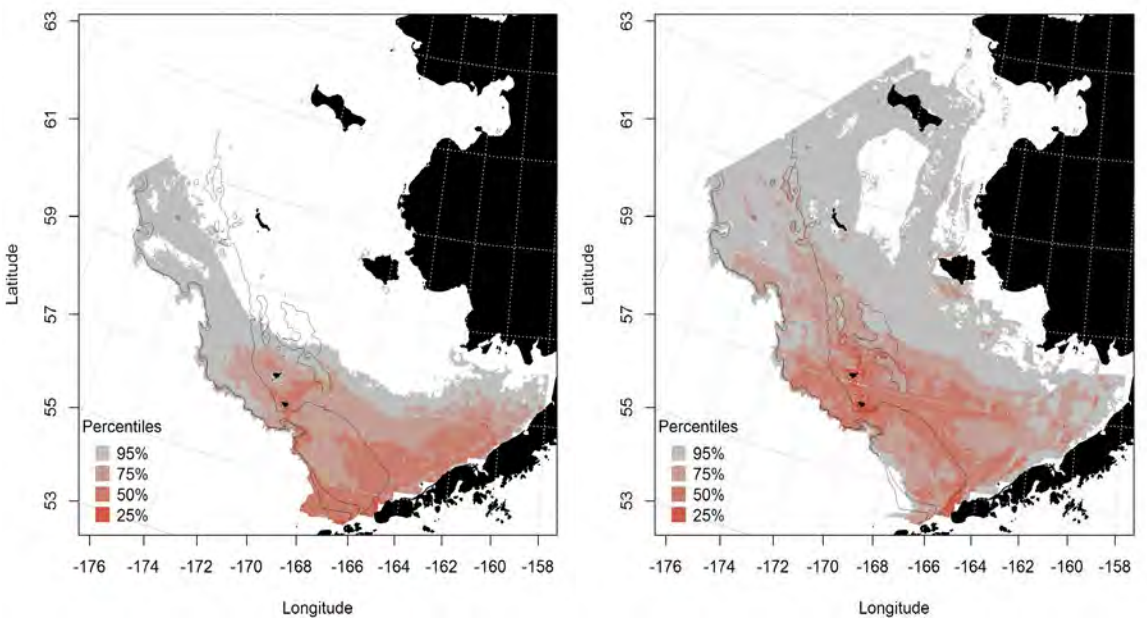

Figure 131. -- Spring (left panel) and summer (right panel) essential fish habitat predicted for larval walleye pollock from EcoFOCI ichthyoplankton surveys of the Eastern Bering Sea.

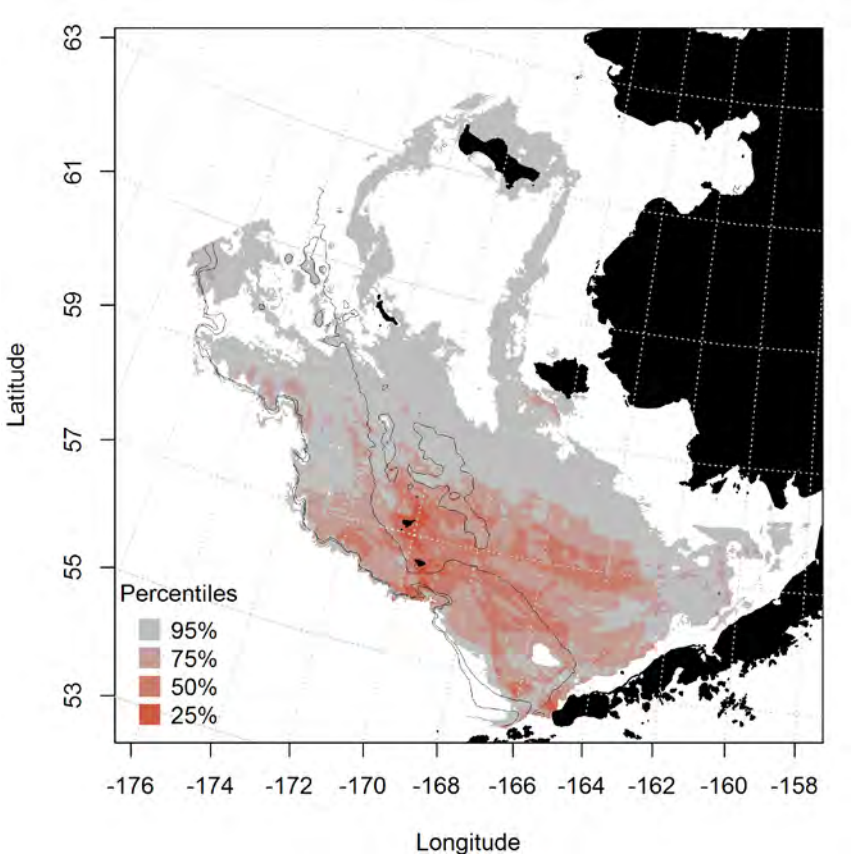

Figure 132. -- Summer essential fish habitat predicted for early juvenile walleye pollock from EcoFOCI surveys of the Eastern Bering Sea.

Summertime distribution of late juvenile and adult walleye pollock from RACE bottom trawl surveys of the Eastern Bering Sea -- Late juvenile and adult walleye pollock collected in RACE summer bottom trawl surveys of the Eastern Bering Sea are distributed broadly across the survey area (Figure 133). The late juvenile distribution appears to be constrained by the 200 m isobath.

The best-fitting GAM predicted that late juvenile walleye pollock abundance from RACE summer bottom trawl surveys was highest over the outer shelf in the northwestern portion of the Eastern Bering Sea (Figure 134). Of the 9 habitat covariates retained in the model, the most influential predictors were geographical location, bottom temperature, and depth. The GAM explained just 32.1% of the deviance in juvenile pollock CPUE. The fit to the training data was poor ($r^2 = 0.32$) and model validation using the test data set had an equally poor fit ($r^2 = 0.31$).

For adult walleye pollock, the best-fitting GAM predicted that adult walleye pollock abundance from RACE summer bottom trawl surveys was centered over the middle shelf of the Eastern Bering Sea (Figure 135). Of the 9 habitat covariates retained in the model, the most influential predictors were geographical location and sediment size. The model explained 68.2% of the variability in the adult pollock CPUE data and was a moderate fit to the training data ($r^2 = 0.68$); model validation using the test data had a poorer fit ($r^2 = 0.43$).

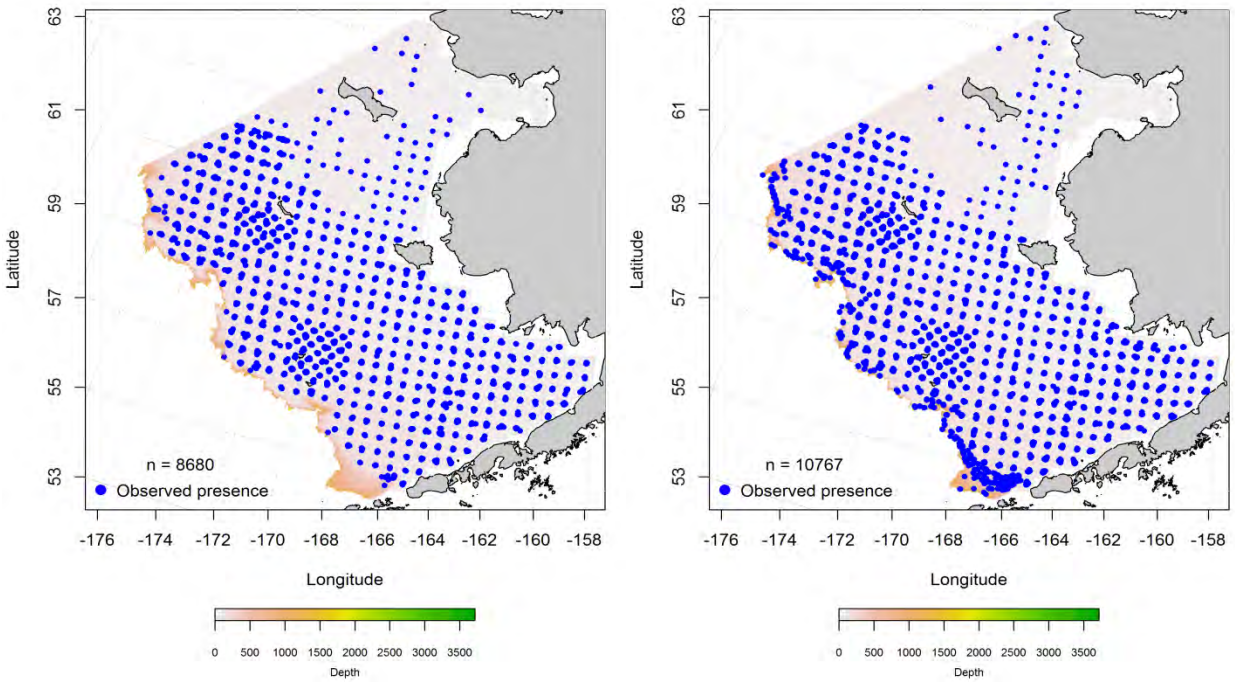

Figure 133. -- Distribution of late-juvenile (left) and adult (right) walleye pollock catches from RACE summer bottom trawl surveys of the Eastern Bering Sea.

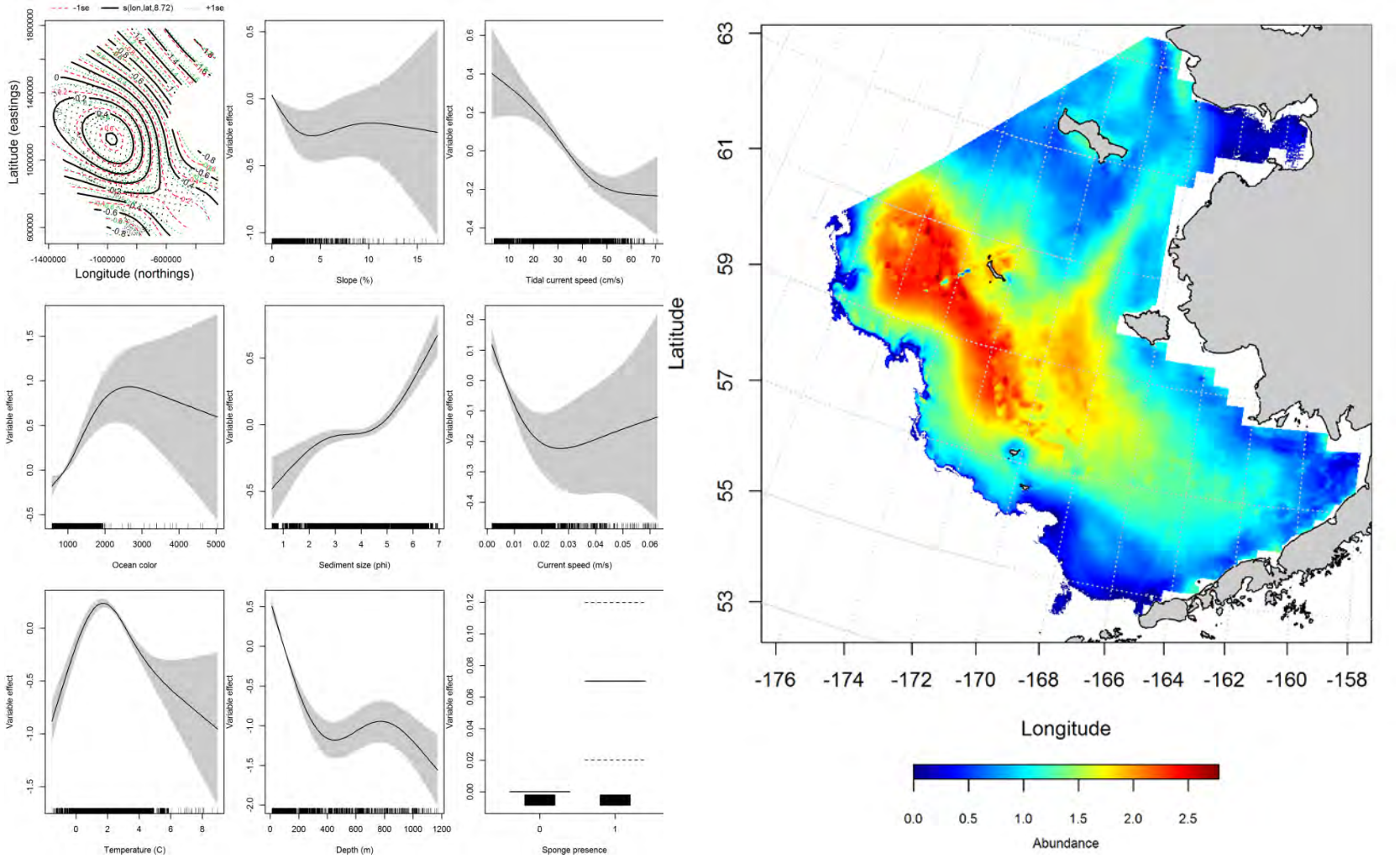

Figure 134. -- Effects of retained habitat covariates on the best-fitting generalized additive model (GAM; left panel) of late juvenile walleye pollock abundance from RACE summer bottom trawl surveys of the Eastern Bering Sea Shelf, Slope, and Northern Bering Sea alongside their predicted abundance (right panel).

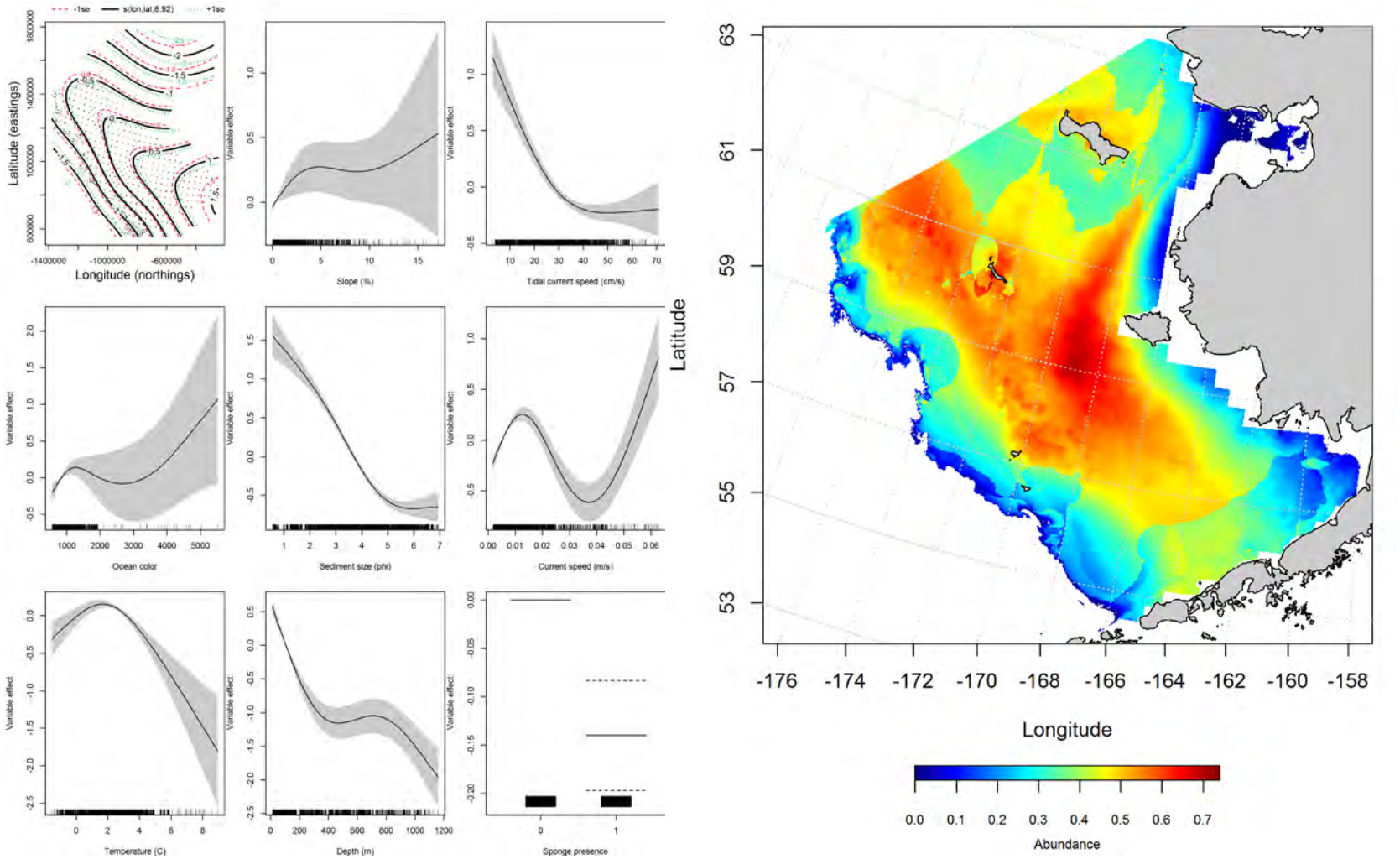

Figure 135. -- Effects of retained habitat covariates on the best-fitting generalized additive model (GAM; left panel) of adult walleye pollock abundance from RACE summer bottom trawl surveys of the Eastern Bering Sea Shelf, Slope, and Northern Bering Sea alongside their predicted abundance (right panel).

Seasonal distribution of walleye pollock in commercial fishery catches from the Eastern Bering Sea -- The distribution of walleye pollock in commercial catches from fall months in the Eastern Bering Sea were spread across the middle and outer shelf (Figure 136). Maximum entropy modeling predicts that the highest likelihood of suitable walleye pollock habitat is over the outer shelf. Depth and bottom temperature were the most important variables for predicting suitable habitat from commercial catches; their combined influence was high (relative importance = 93%). The AUC of the fall model for the training data was 0.87 and 78% of cases were correctly predicted by the model. Fit of the model in the validation step was somewhat lower (AUC = 0.77) and 77% of the cases were correctly classified for the test data set.

Similar to fall, the distribution of walleye pollock from commercial catches was primarily over the middle and outer shelf encompassing the north-south extent of the Eastern Bering Sea study area (Figure 137). The most important habitat covariates in the MaxEnt model were depth and bottom temperature; their combined influence on the model was high (relative importance = 91.6%). The model was an outstanding fit to the training data (AUC = 0.92) and an excellent fit to the test data (AUC = 0.83). For both data sets the model correctly classified 83% of predicted cases.

In spring, the distribution of commercial catches containing walleye pollock extended on to the inner shelf of the central and southern areas in the Eastern Bering Sea (Figure 138). The MaxEnt model based on these catches predicted a relatively low probability of suitable habitat for adult walleye pollock in the inshore areas noted, but did return higher probability habitats over the middle and outer shelf. Depth and bottom temperature exercised the greatest influence over the model with a combined relative importance of 80.6%. The model was an excellent fit to the training (AUC = 0.88) and the test data (AUC = 0.80). For both data sets the model correctly classified 80% of predicted cases.

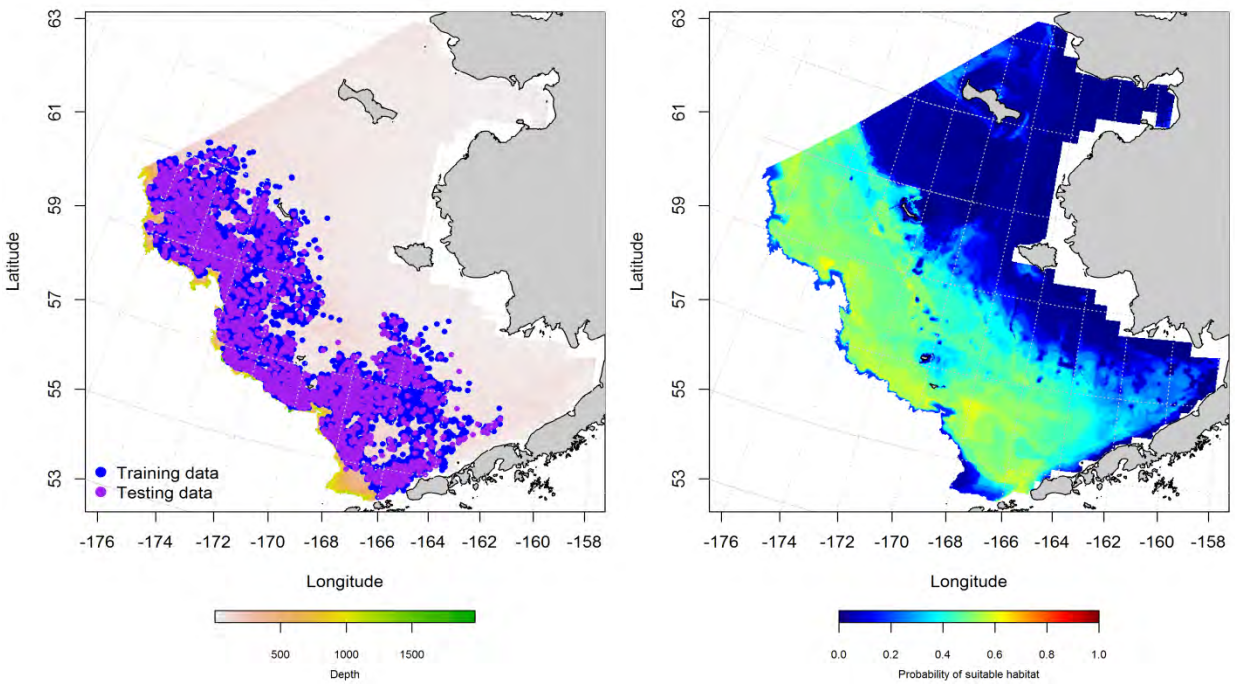

Figure 136. -- Locations of fall (October-November) catches of walleye pollock in commercial fisheries of the Eastern Bering Sea (left panel). Blue points were used to train the maximum entropy (MaxEnt) model predicting the probability of suitable habitat (right panel) and the purple points were used to validate the model.

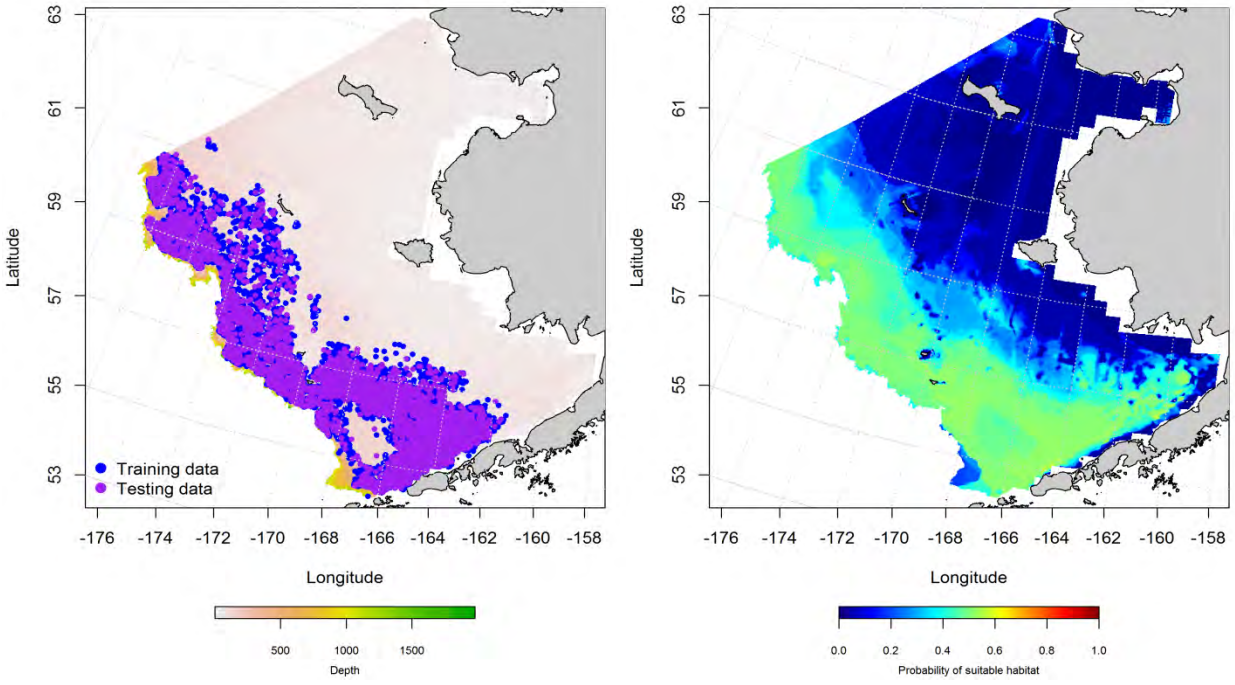

Figure 137. -- Locations of winter (December-February) catches of walleye pollock in commercial fisheries of the Eastern Bering Sea (left panel). Blue points were used to train the maximum entropy

(MaxEnt) model predicting the probability of suitable habitat (right panel) and the purple points were used to validate the model.

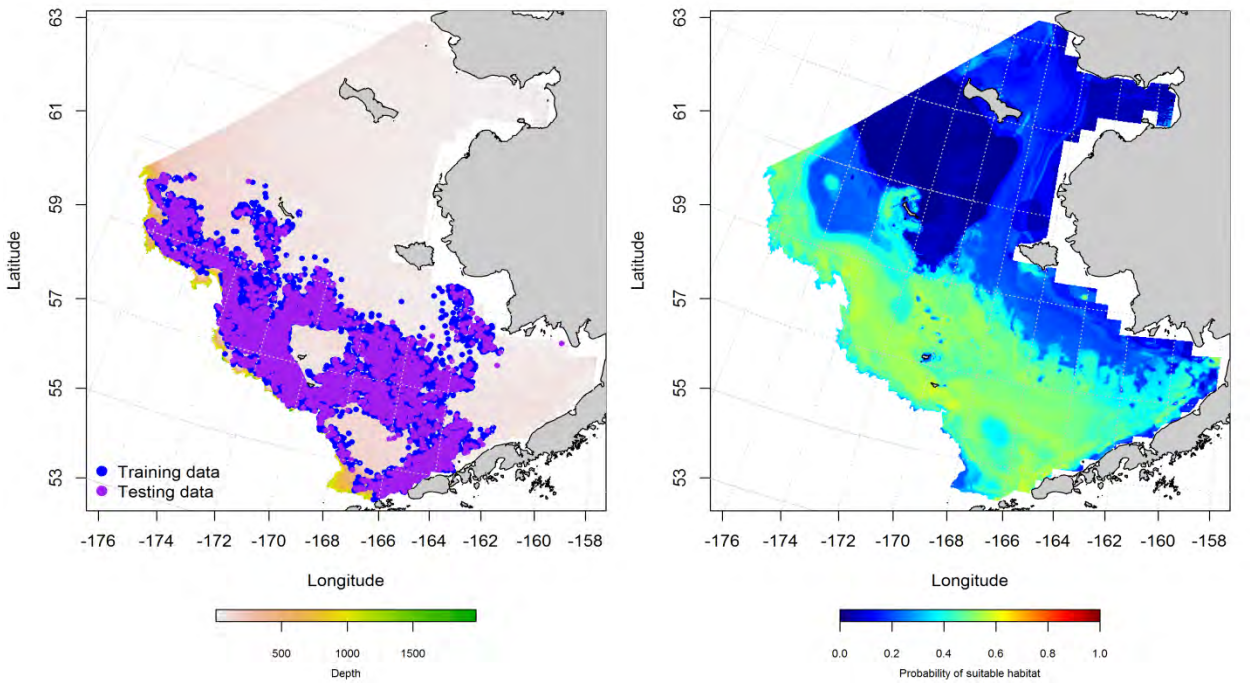

Figure 138. -- Locations of spring (March-May) catches of walleye pollock in commercial fisheries of the Eastern Bering Sea (left panel). Blue points were used to train the maximum entropy (MaxEnt) model predicting the probability of suitable habitat (right panel) and the purple points were used to validate the model.

Essential fish habitat maps and conclusions for walleye pollock in the Eastern Bering Sea –

Species distribution modelling of walleye pollock in the Eastern Bering Sea predicts that the essential fish habitat of this species encompasses nearly all of the Eastern Bering Sea study area considered.

Summertime EFH for late juvenile and adult walleye pollock from RACE bottom trawl surveys of the Eastern Bering Sea covers the majority of the study area for both life stages (Figure 139). The spatial boundaries of juvenile and adult EFH indicate that these life stages co-occur across the study area. Additionally, areas of highest abundance for both life stages have a high degree of spatial correspondence.

There were some seasonal differences in the predictions of suitable habitat from commercial fishery catches containing walleye pollock in the Eastern Bering Sea (Figure 140). Many of these occurred in the

northern domain in areas where the probability of suitable habitat was low. Notable departures from this generalization are found in the northwest EBS during fall and the southeast during winter. The areas predicted to have the greatest probability of suitable walleye pollock habitat remained spatially similar across seasons.

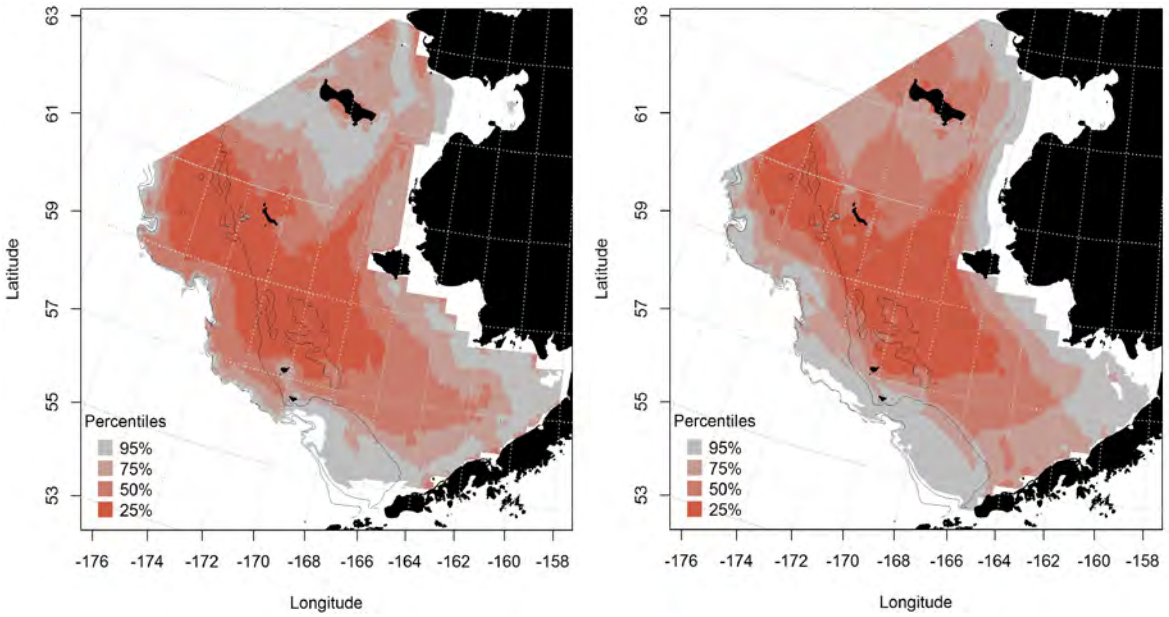

Figure 139. -- Predicted summer essential fish habitat for walleye pollock late juveniles and adults (left and right panel) from summertime bottom trawl surveys.

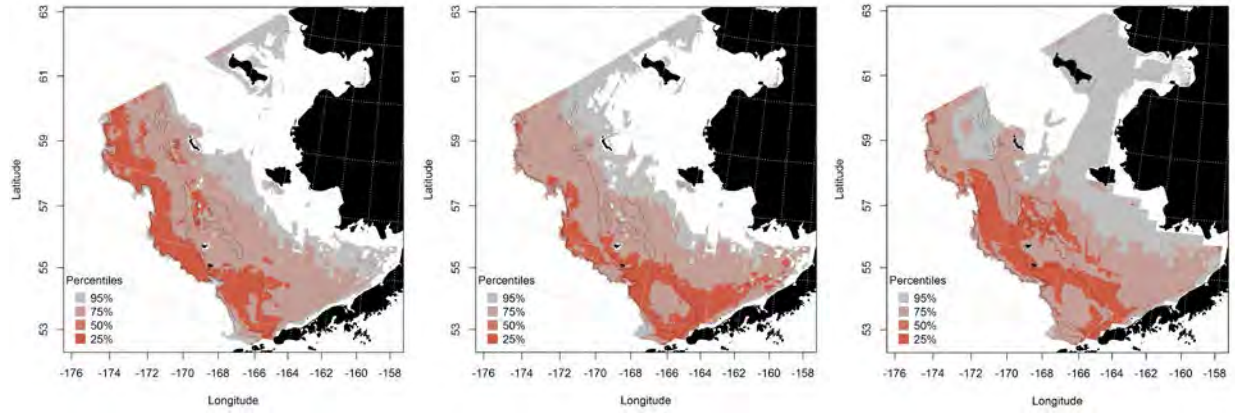

Figure 140. -- Essential fish habitat predicted for walleye pollock during fall (left panel), winter (middle panel), and spring (right panel) from commercial fishery catches.

Pacific cod (*Gadus macrocephalus*)

Pacific cod support an important commercial fishery in the Eastern Bering Sea.

Seasonal distribution of egg, larval, and early juvenile stages of Pacific cod from EcoFOCI ichthyoplankton surveys of the Eastern Bering Sea –Pacific cod are demersal spawners and their eggs were observed during spring and summer EcoFOCI ichthyoplankton surveys of the Eastern Bering Sea (Figure 141). Eggs were less common in summer compared with spring. Sampling effort and life-stage-specific gear type vary on these surveys such that observations of presence may be more survey dependent than biologically determined. There were not enough observations of Pacific cod eggs to undertake distribution modeling for this life stage.

Pacific cod larvae were rare in fall and winter EcoFOCI ichthyoplankton samples and were more common in spring and summer (Figure 142). During springtime, Pacific cod larvae were observed over the middle shelf (50 to 100 m) around the Pribilof Islands, near the head of the Bering Canyon, and along the Alaska Peninsula above Unimak Island. The presence of larval Pacific cod in summer months was observed in the same areas as during springtime, but fewer occurrences were reported. There were sufficient records of larval presence to model suitable larval Pacific cod habitat from spring and summer.

Spring and summer MaxEnt predictions of suitable habitat for larval Pacific cod in the Eastern Bering Sea differed (Figure 143). In spring, the area predicted to have the highest probability of holding suitable larval Pacific cod habitat was over the middle shelf (50 to 100 m) above Unimak Pass and Unimak Island. During summer suitable larval Pacific cod habitat appears to be around the Pribilof Islands. In both spring and summer, the habitat covariate dominating the model predictions of suitable habitat was surface temperature (relative importance = 71.1% and 36.4%). Both seasons also shared ocean productivity as an important covariate (relative importance = 10.6% in spring and 11.1% in summer). In the MaxEnt model for spring, surface temperature and ocean productivity accounted for a combined 81.7% of the leverage amongst covariates; in summer they accounted for 47.5%. The covariates current variability and bottom depth were also important in the summer model (relative importance = 23.4% in spring and 11.4%) and

when combined with surface temperature and ocean productivity provided 82.3% of the leverage in the model. Both models were outstanding fits to the training data (spring AUC = 0.96 and 0.91 in summer) although the spring model correctly classified more cases (89%) than did the summer model (79%). Model validation using the test data also produced excellent to acceptable fits (AUC = 0.87 and 0.75 for spring and summer) with moderately high levels of correctly classified cases (87% in spring and 75% in summer).

Early juvenile Pacific cod were observed in summer EcoFOCI surveys (Figure 144). They occurred in ichthyoplankton samples from the outer (100 to 200 m) and middle shelf of the central and southern domains of the Eastern Bering Sea. There were also a few occurrences as far north as St. Lawrence Island and over the inner shelf on the east side of Bristol Bay.

There were sufficient data to parameterize a MaxEnt model predicting the distribution of suitable early juvenile Pacific cod habitat from summer EcoFOCI surveys (Figure 145). The highest predicted probabilities of suitable early juvenile Pacific cod habitat appear around the Pribilof Islands extending south and east over the middle shelf into the southern domain of the Eastern Bering Sea. The most influential habitat covariates in the MaxEnt model were ocean productivity (relative importance = 30.6%), surface temperature (27.7%), and bottom depth (17.2%). The model fit to the training data was outstanding (AUC = 0.96) and the percent of cases correctly predicted was also high (89%). Validation using the test data produced and excellent model fit (AUC = 0.83) and a relatively high proportion of correctly classified cases (83%).

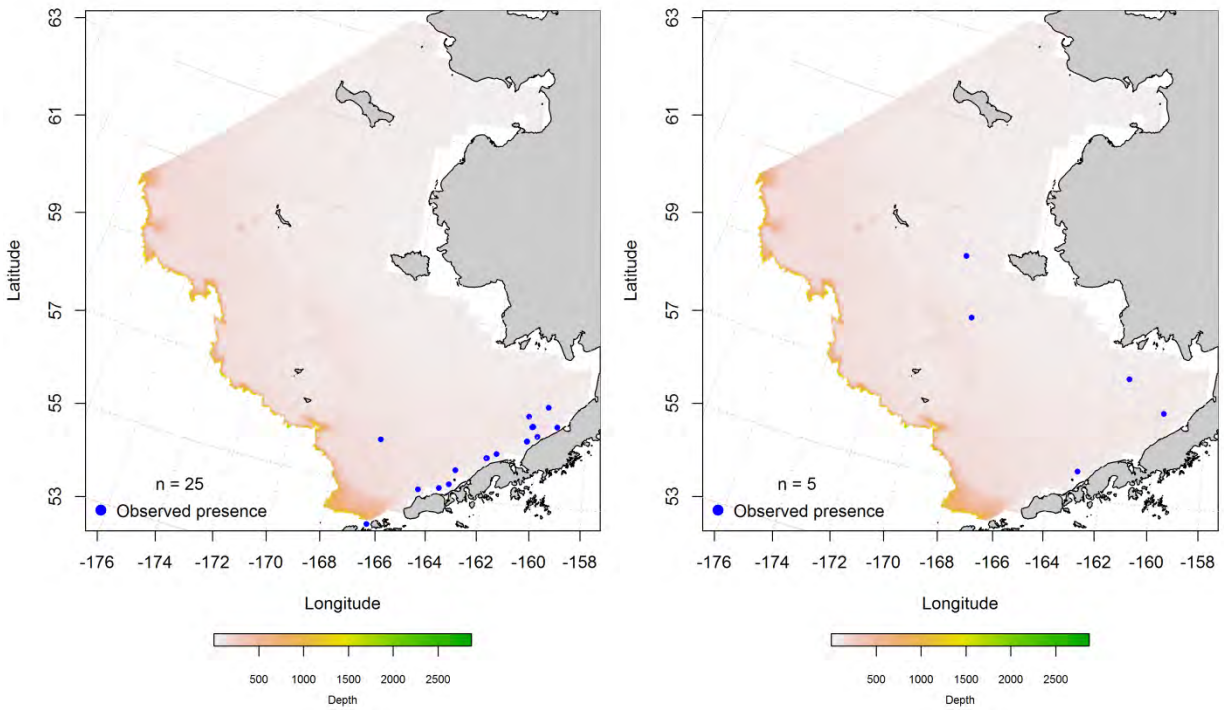

Figure 141. -- Spring (left panel) and summer (right panel) observations of Pacific cod eggs from EcoFOCI ichthyoplankton surveys of the Eastern Bering Sea.

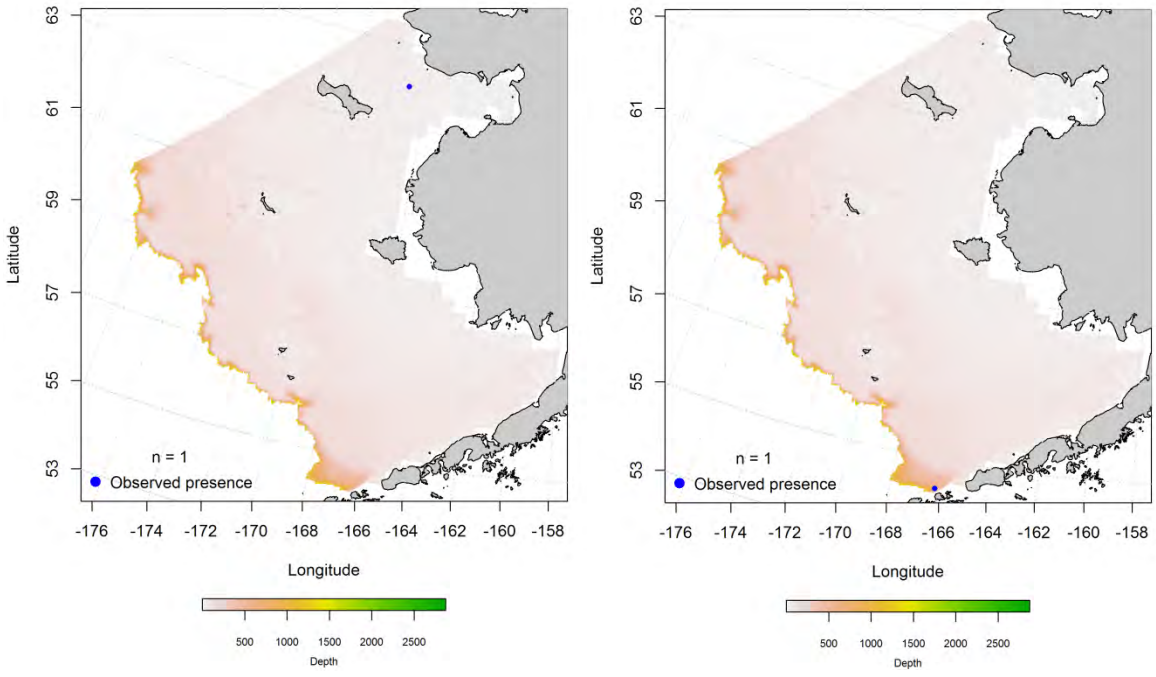

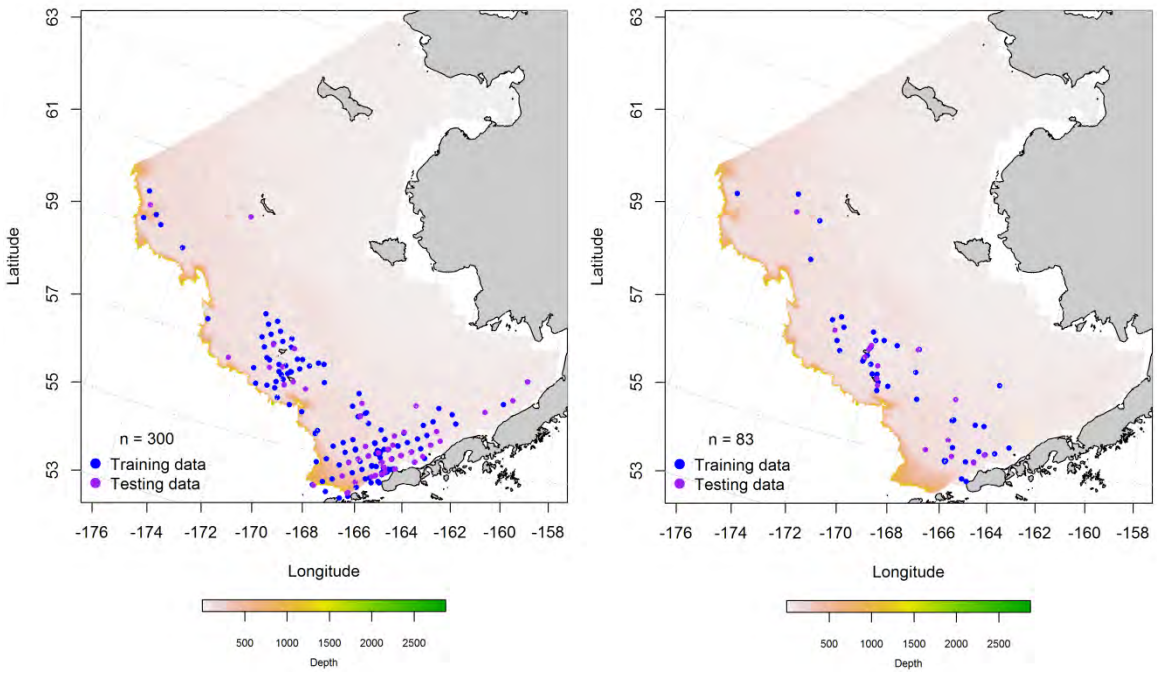

Figure 142. -- Fall (left upper panel), winter (right upper panel), spring (left lower panel), and summer (right lower panel) observations of larval Pacific cod from EcoFOCI ichthyoplankton surveys of the Eastern Bering Sea; blue points were used to train the maximum entropy (MaxEnt) model predicting the probability of suitable habitat and the purple points were used to validate the model.

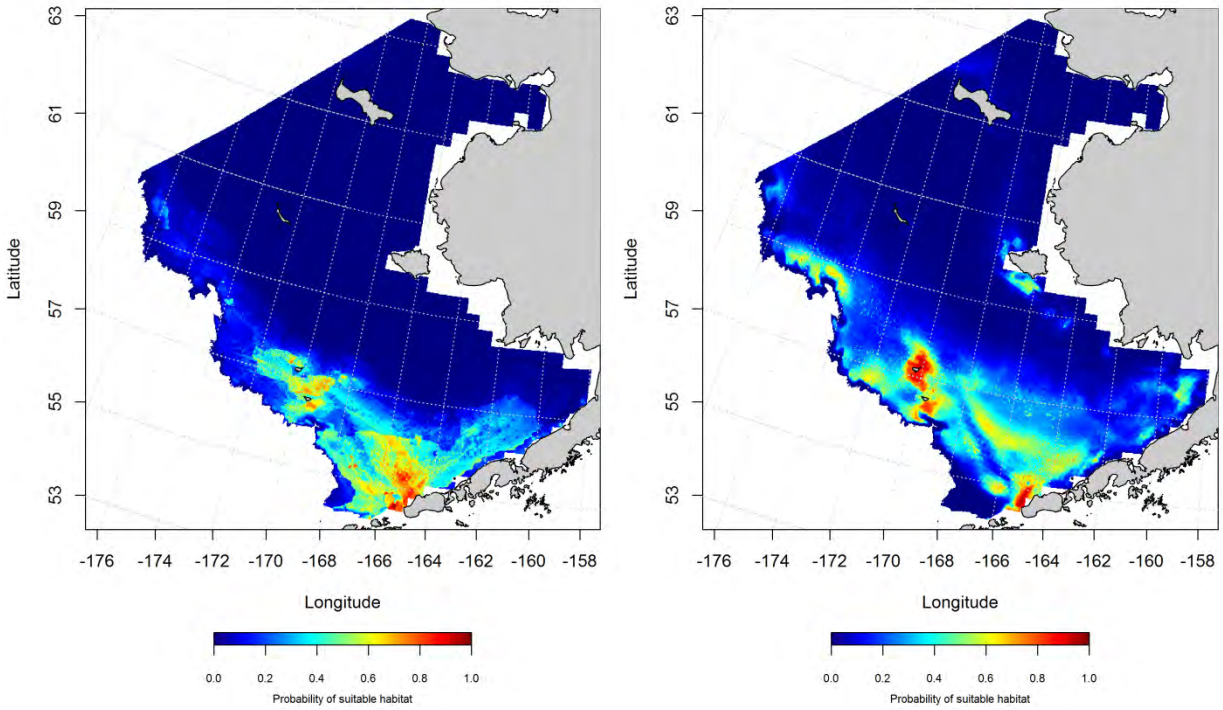

Figure 143. -- Maximum entropy (MaxEnt) model prediction of the probability of suitable spring and summer (left and right panels) larval Pacific cod habitat from EcoFOCI ichthyoplankton surveys of the Eastern Bering Sea.

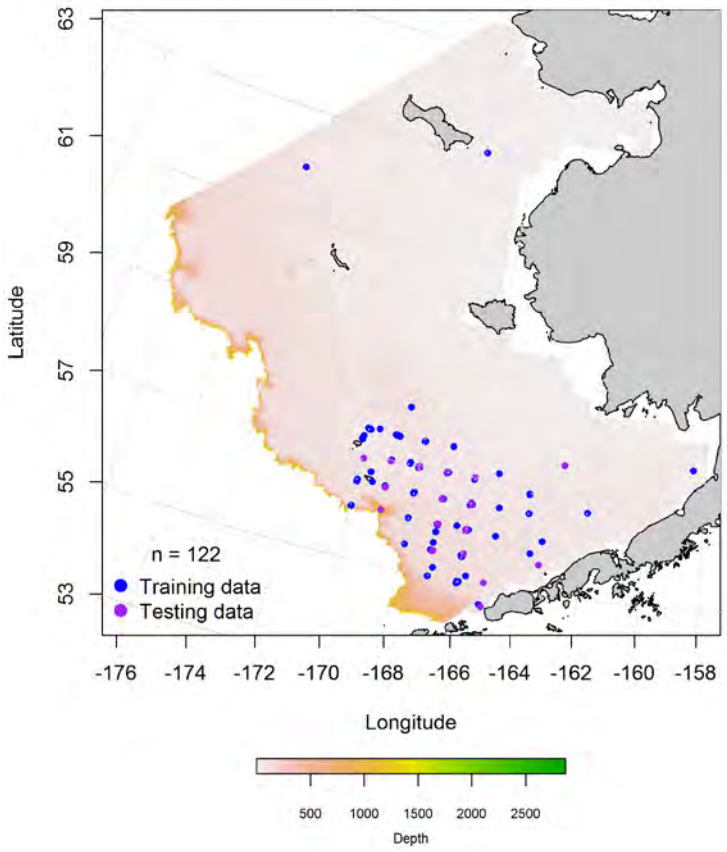

Figure 144. -- Summer observations of early juvenile Pacific cod from EcoFOCI ichthyoplankton surveys of the Eastern Bering Sea; blue points were used to train the maximum entropy (MaxEnt) model predicting the probability of suitable habitat and the purple points were used to validate the model.

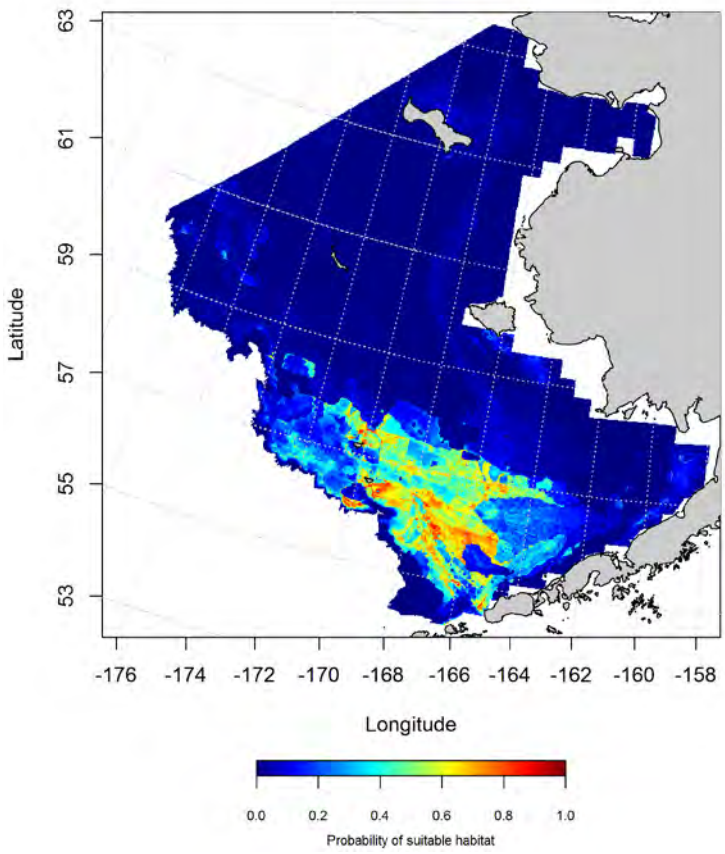

Figure 145. -- Maximum entropy (MaxEnt) model prediction of the probability of suitable summertime early juvenile Pacific cod habitat from EcoFOCI ichthyoplankton surveys of the Eastern Bering Sea.

Essential fish habitat maps and conclusions for early life history stages of Pacific cod (*Gadus macrocephalus*) from the Eastern Bering Sea – The overall spatial pattern and extent of essential habitat predicted for Pacific cod larvae in the Eastern Bering Sea at the 95% level was similar during spring and summer months (Figure 146). In spring, EFH hotspots were centered over the middle shelf in the southern domain above Unimak Island. In summer, EFH hotspots were concentrated around the Pribilof Islands.

The spatial pattern of EFH for early juvenile Pacific cod in summer was similar to that of larval Pacific cod in summer (Figure 147). Essential habitat for early juvenile Pacific cod was centered over the middle shelf between the Pribilof Islands and the Alaska Peninsula, but did not extend as far north as did EFH for larvae in the summer.

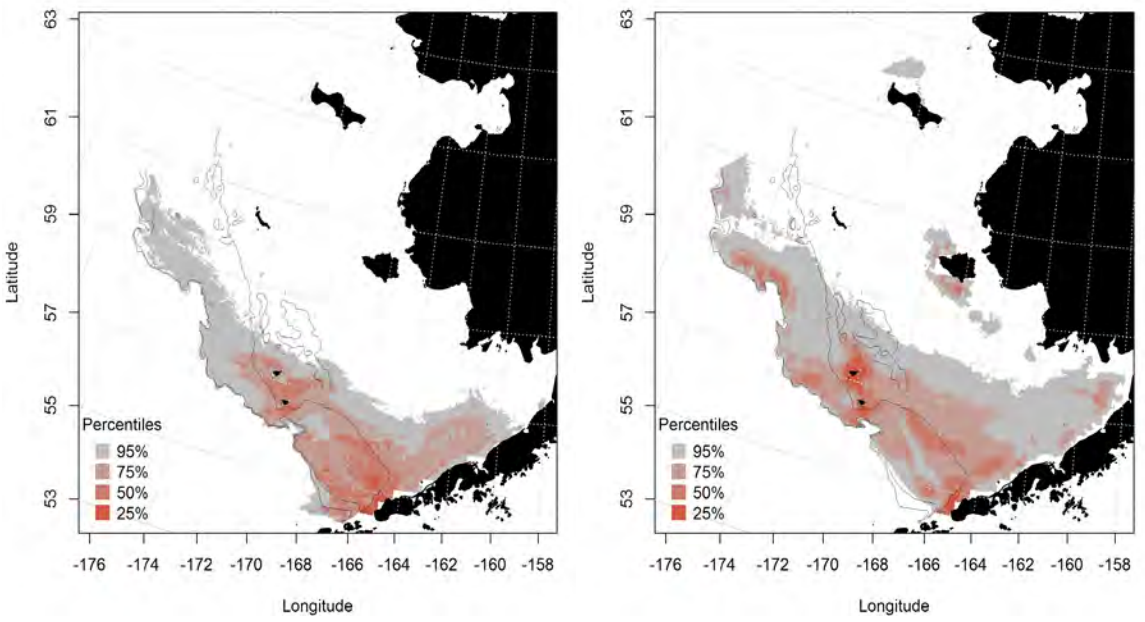

Figure 146. -- Spring (left panel) and summer (right panel) essential fish habitat predicted for larval Pacific cod from EcoFOCI ichthyoplankton surveys of the Eastern Bering Sea.

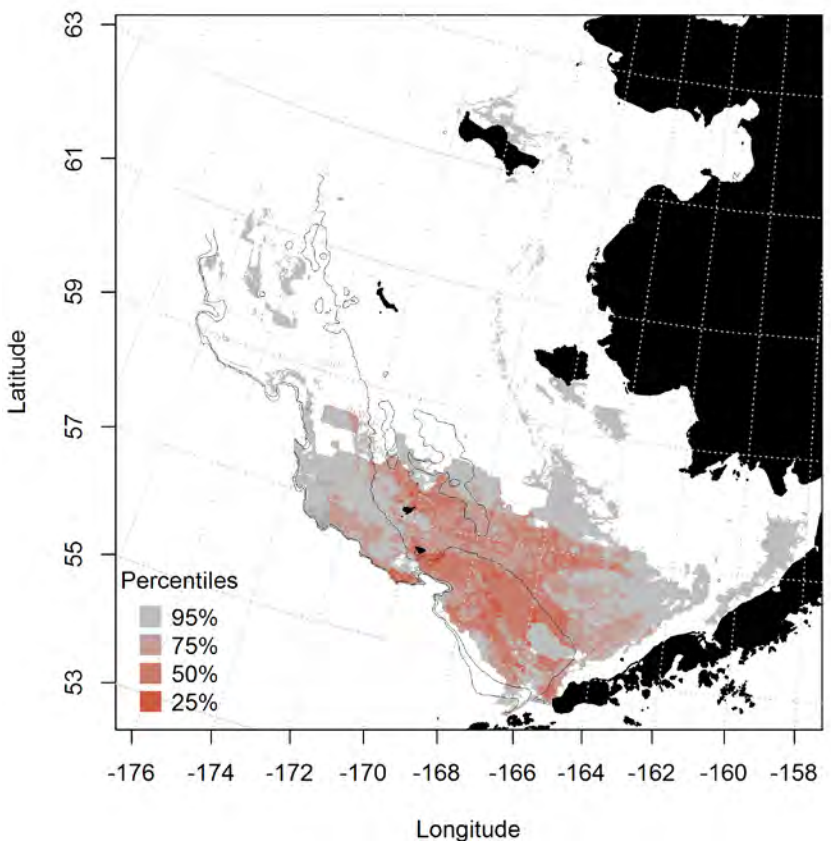

Figure 147. -- Summer essential fish habitat predicted for early juvenile Pacific cod from EcoFOCI surveys of the Eastern Bering Sea.

Summertime distribution of late juvenile and adult Pacific cod from RACE bottom trawl surveys of the Eastern Bering Sea -- Late juvenile and adult Pacific cod collected in RACE summer bottom trawl surveys of the Eastern Bering Sea were broadly distributed across the survey area (Figure 148). There is a section of the middle shelf (50 to 100 m) south and west of St. Lawrence Island where neither life stage of Pacific cod occurred in bottom trawl catches. There also were no records of Pacific cod catches from Norton Sound.

The best-fitting GAM predicted high late juvenile Pacific cod abundance from RACE summer bottom trawl surveys over the middle and inner shelf of the central and southern domains of the Eastern Bering Sea (Figure 149). There was also a patch of high abundance predicted around St. Matthew Island in the northern domain. Of the 10 habitat covariates retained in the model, the most influential predictors were bottom temperature, geographical location, sediment size, and depth. The model explained 41.2% of the deviance in late juvenile Pacific cod CPUE. The fit to the training data was poor ($r^2 = 0.41$) and model validation using the test data set had a similar fit ($r^2 = 0.42$).

For adult Pacific cod, the best-fitting GAM predicted that adult Pacific cod abundance from RACE summer bottom trawl surveys was highest over the middle shelf of the Eastern Bering Sea extending from the Pribilofs northward to about St. Matthew Island (Figure 150). Of the 10 habitat covariates retained in the model, the most influential predictors were bottom temperature, depth, and geographical location. The model explained just 32% of the variability in the adult Pacific cod CPUE data and was a poor fit to the training data ($r^2 = 0.32$); model validation using the test data had a similar fit ($r^2 = 0.33$).

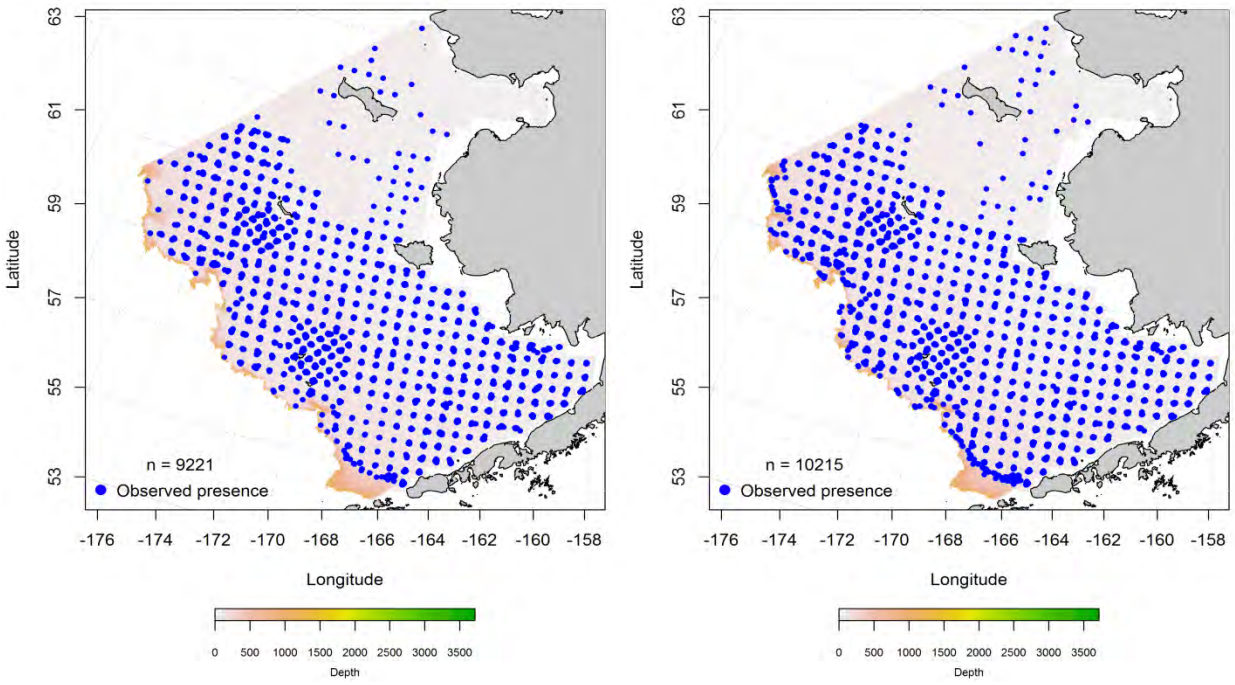

Figure 148. -- Distribution of late-juvenile (left) and adult (right) Pacific cod catches from RACE summer bottom trawl surveys of the Eastern Bering Sea.

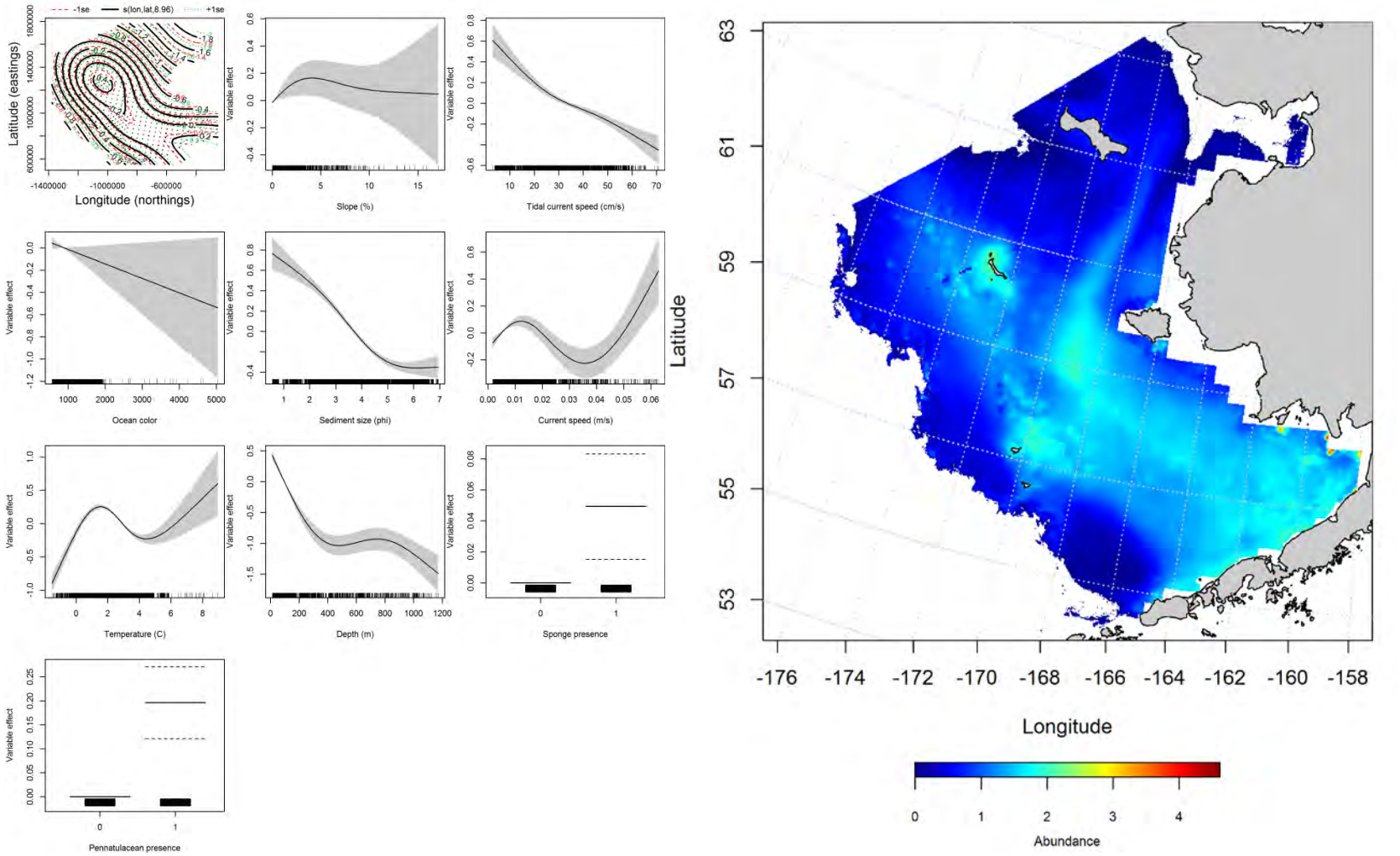

Figure 149. -- Effects of retained habitat covariates on the best-fitting generalized additive model (GAM; left panel) of late juvenile Pacific cod abundance from RACE summer bottom trawl surveys of the Eastern Bering Sea Shelf, Slope, and Northern Bering Sea alongside their predicted abundance (right panel).

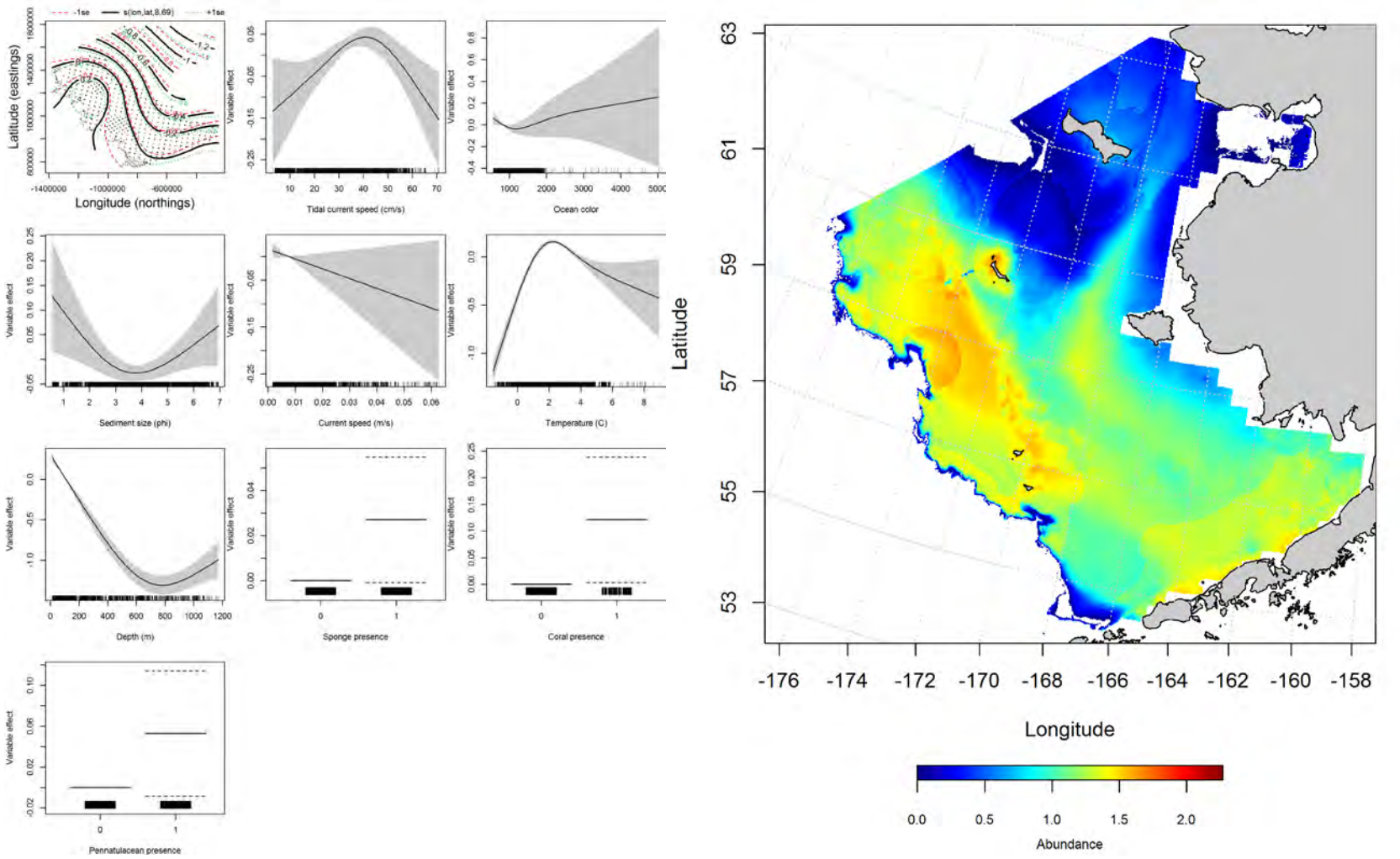

Figure 150. -- Effects of retained habitat covariates on the best-fitting generalized additive model (GAM; left panel) of adult Pacific cod abundance from RACE summer bottom trawl surveys of the Eastern Bering Sea Shelf, Slope, and Northern Bering Sea alongside their predicted abundance (right panel).

Seasonal distribution of Pacific cod in commercial fishery catches from the Eastern Bering Sea -- The distribution of Pacific cod in commercial catches from the Eastern Bering Sea during fall months were spread across the middle and outer shelf (Figure 151). Maximum entropy modeling predicts that suitable habitat for adult Pacific cod in the fall commercial fishery can be found near the heads of the Bering, Pribilof, and Zhemchug Canyons. Depth, bottom temperature, and ocean productivity were the most important covariates predicting suitable Pacific cod habitat from commercial catches; their combined influence was high (relative importance = 97.9%). The AUC of the fall model for the training data was 0.86 and 77% of cases were correctly predicted by the model. Fit of the model in the validation step was acceptable (AUC = 0.78) and 78% of the cases were correctly classified for the test data set.

Similar to fall, the distribution of Pacific cod observed from commercial catches in winter was primarily over the middle and outer shelf (Figure 152). Depth and bottom temperature were the most influential habitat covariates predicting suitable Pacific cod habitat from commercial catches; their combined influence on the model was high (relative importance = 88.9%). The model predicted 83% of cases correctly and was an outstanding fit to the training data (AUC = 0.92). Model validation using the test data produced an excellent fit (AUC = 0.83) with the same proportion of cases correctly classified as with the training data.

In spring, the distribution of commercial catches containing Pacific cod extended further inshore onto the inner shelf in the central domain of the Eastern Bering Sea (Figure 153). The MaxEnt model predicted a relatively low probability of suitable habitat for adult Pacific cod in this inshore area. Depth and bottom temperature were the habitat covariates that exercised the greatest influence over the model with a combined relative importance of 79%. The MaxEnt model was an excellent fit to the training (AUC = 0.88) and the test data for validation (AUC = 0.80). The model correctly classified 80% of predicted cases for both the training and validation data sets.

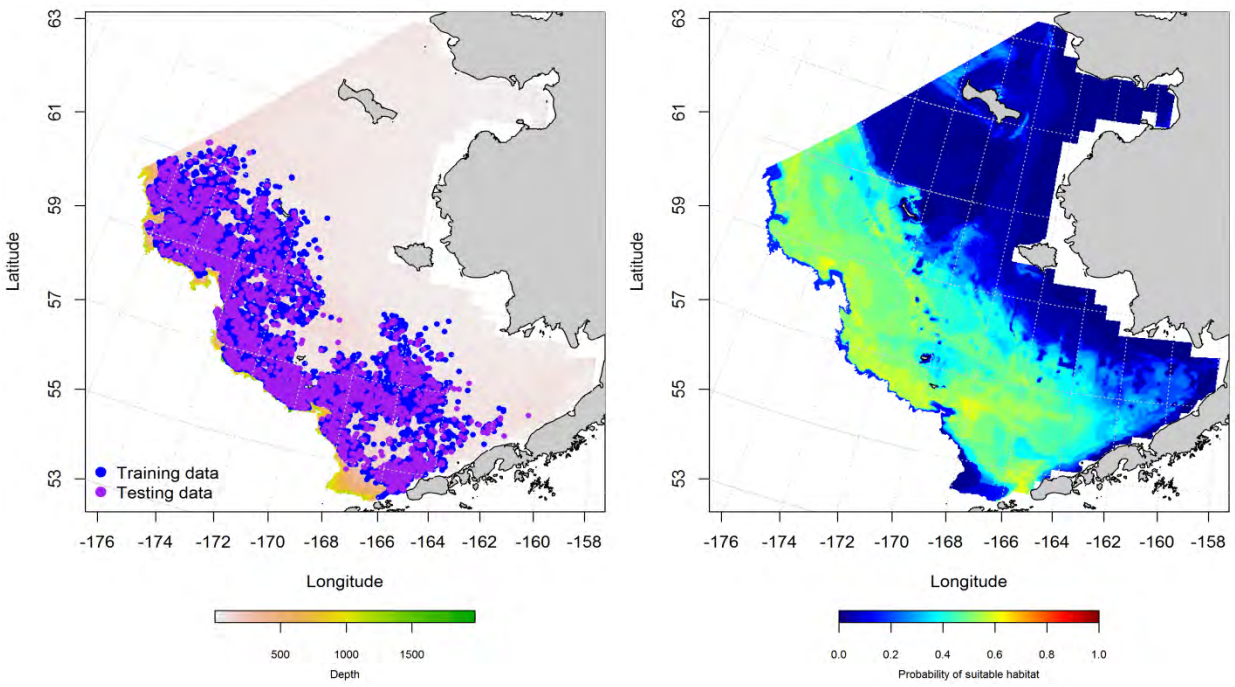

Figure 151. -- Locations of fall (October-November) catches of Pacific cod in commercial fisheries of the Eastern Bering Sea (left panel). Blue points were used to train the maximum entropy (MaxEnt) model predicting the probability of suitable habitat (right panel) and the purple points were used to validate the model.

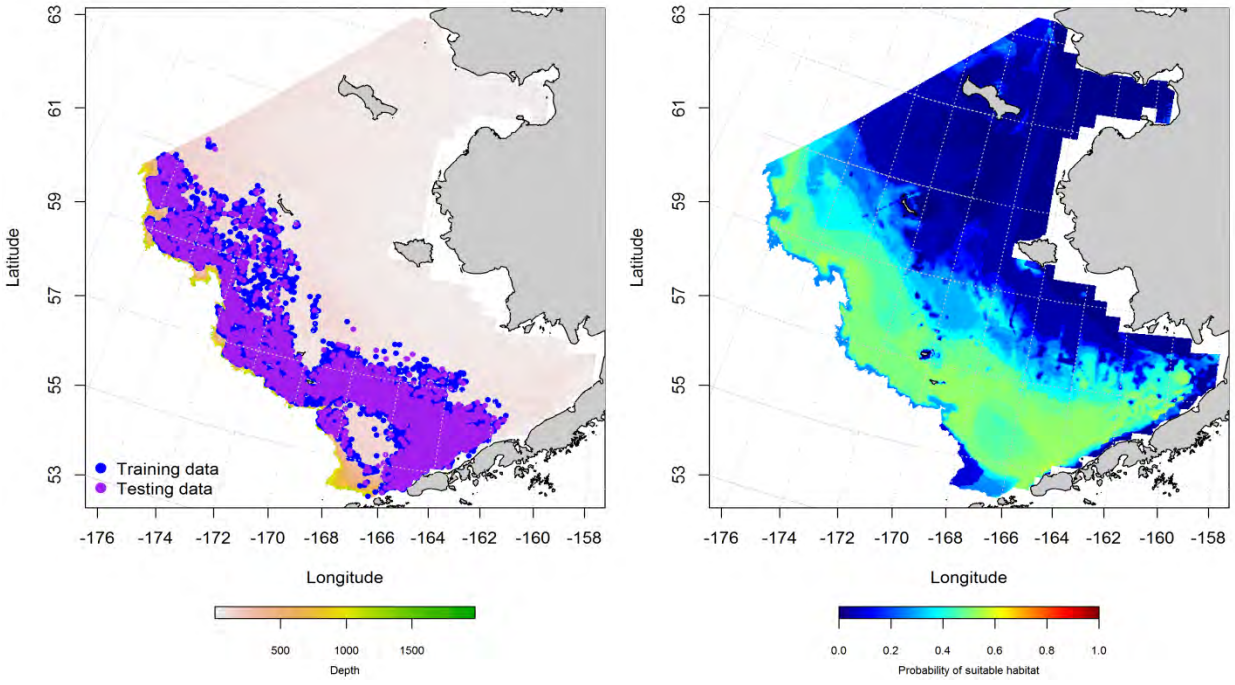

Figure 152. -- Locations of winter (December-February) catches of Pacific cod in commercial fisheries of the Eastern Bering Sea (left panel). Blue points were used to train the maximum entropy (MaxEnt) model

predicting the probability of suitable habitat (right panel) and the purple points were used to validate the model.

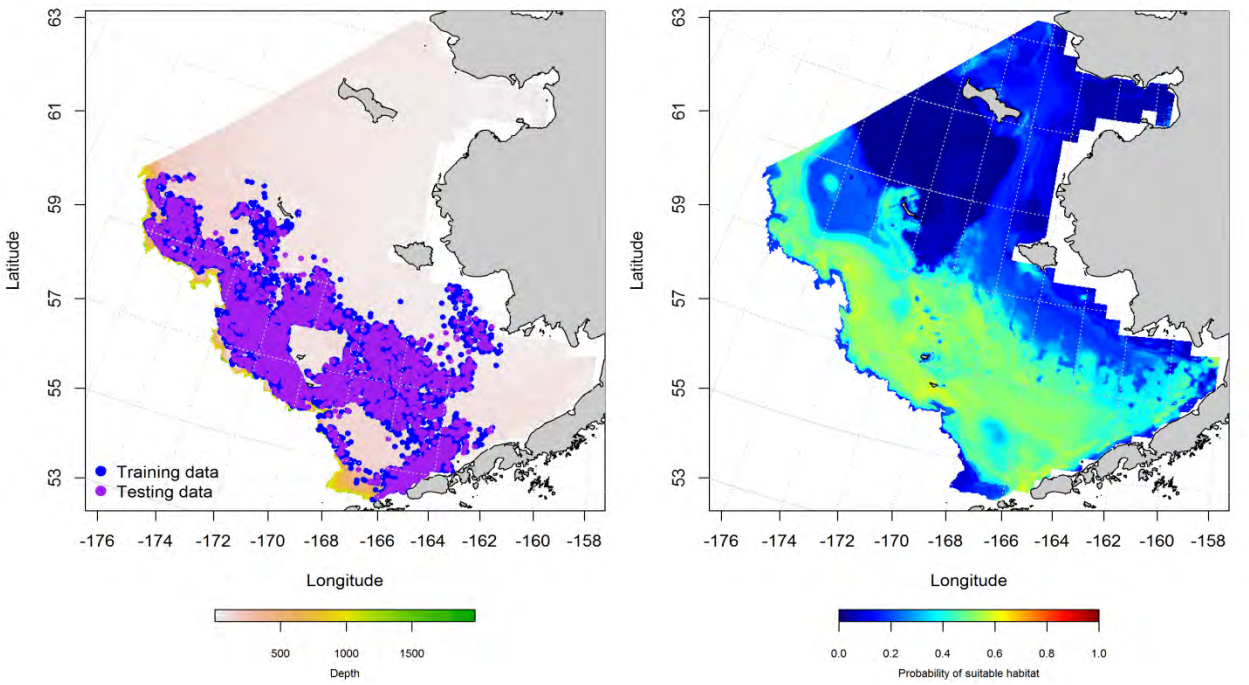

Figure 153. -- Locations of spring (March-May) catches of Pacific cod in commercial fisheries of the Eastern Bering Sea (left panel). Blue points were used to train the maximum entropy (MaxEnt) model predicting the probability of suitable habitat (right panel) and the purple points were used to validate the model.

Essential fish habitat maps and conclusions for late juvenile and adult Pacific cod (*Gadus macrocephalus*) in the Eastern Bering Sea – Species distribution modeling of late juvenile and adult Pacific cod in the Eastern Bering Sea predicts that EFH for this species includes nearly all of the Eastern Bering Sea study area considered.

Summertime EFH for late juvenile and adult Pacific cod from RACE bottom trawl surveys of the Eastern Bering Sea extends from the inner shelf over the outer shelf and on to the Bering Sea slope (Figure 154). The spatial extent of EFH for both life stages overlap almost completely. Areas that support higher abundances of these life stages (i.e., hotspots) differ slightly. For late juveniles the inshore portions of the central and southern domains of the Eastern Bering Sea had higher predicted abundances while high adult abundance was predicted in the central and northern domains over the middle and outer shelf.

In general, the patterns of suitable Pacific cod habitat from commercial fishery catches in the Eastern Bering Sea were fairly similar across seasons (Figure 155). Suitable habitat was mostly found from Pribilof Canyon north over the outer shelf and slope though somewhat less so in winter. In winter and spring, some of the higher probability habitat extended further into the southern domain of the Eastern Bering Sea compared to fall.

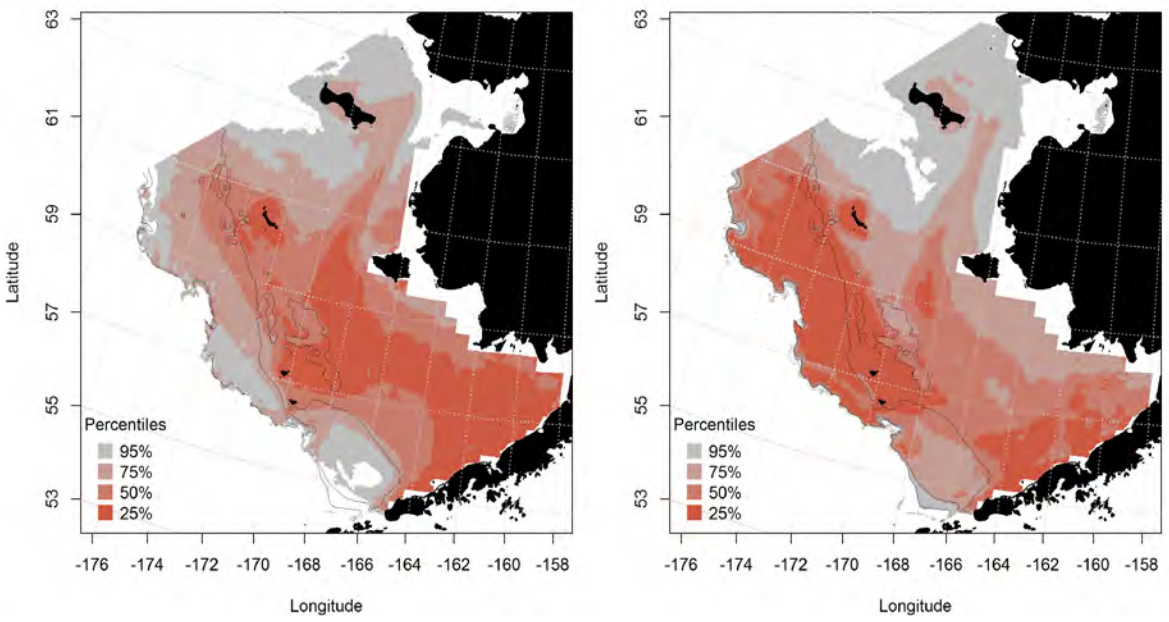

Figure 154. -- Predicted summer essential fish habitat for Pacific cod juveniles and adults (left and right panel) from summertime bottom trawl surveys.

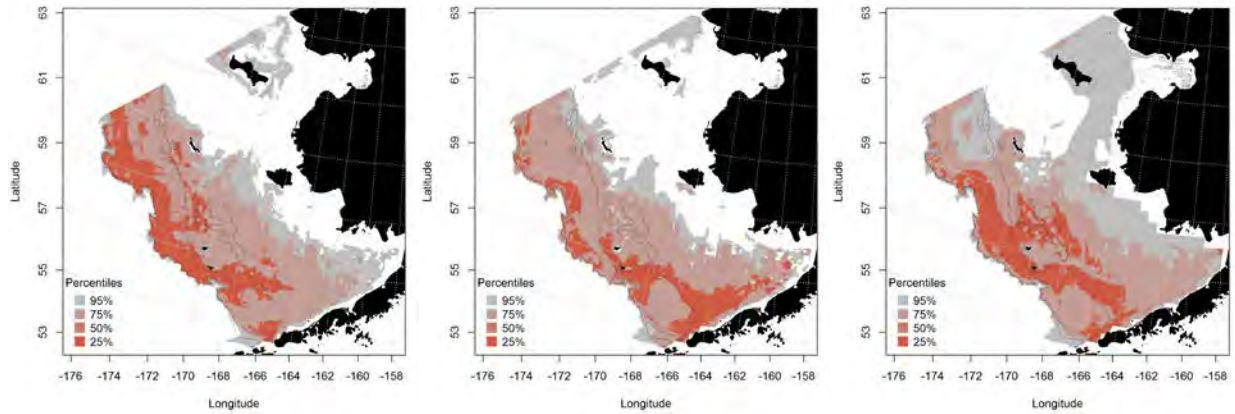

Figure 155. -- Essential fish habitat predicted for Pacific cod during fall (left panel), winter (middle panel) and spring (right panel) from commercial fishery catches.

sablefish (*Anoplopoma fimbria*)

Sablefish are a commercial target species in the Eastern Bering Sea. They are a single stock in the BSAI although for management purposes discrete regions are identified to distribute exploitation over their geographical range.

Seasonal distribution of early life history stages of sablefish from EcoFOCI ichthyoplankton surveys of the Eastern Bering Sea – Sablefish eggs were not common during winter and spring EcoFOCI ichthyoplankton surveys of the Eastern Bering Sea (Figure 156). All of the sablefish eggs observed were over the Bering Canyon in the southwestern corner of the Eastern Bering Sea southern domain. There were not enough observations of sablefish eggs to undertake distribution modeling for this life stage.

Sablefish larvae were observed during winter, spring, and summer EcoFOCI ichthyoplankton surveys but were uncommon (Figure 157). During winter and spring surveys, sablefish larvae were observed over deep water off of the continental shelf in the southwestern corner of the Eastern Bering Sea southern domain. During summer surveys, sablefish larvae were observed farther north over the outer shelf and off of the shelf edge. There were not enough records of larval sablefish presence to model their distribution.

There were 6 early juvenile sablefish occurrences during summer EcoFOCI ichthyoplankton surveys of the Eastern Bering Sea (Figure 158). These reports were spread over an area north of Pribilof Canyon to north of St. Paul Island on the middle (50 to 100 m) and outer shelf (100 to 200 m). These 6 records were not sufficient to model early juvenile sablefish distribution for the Eastern Bering Sea.

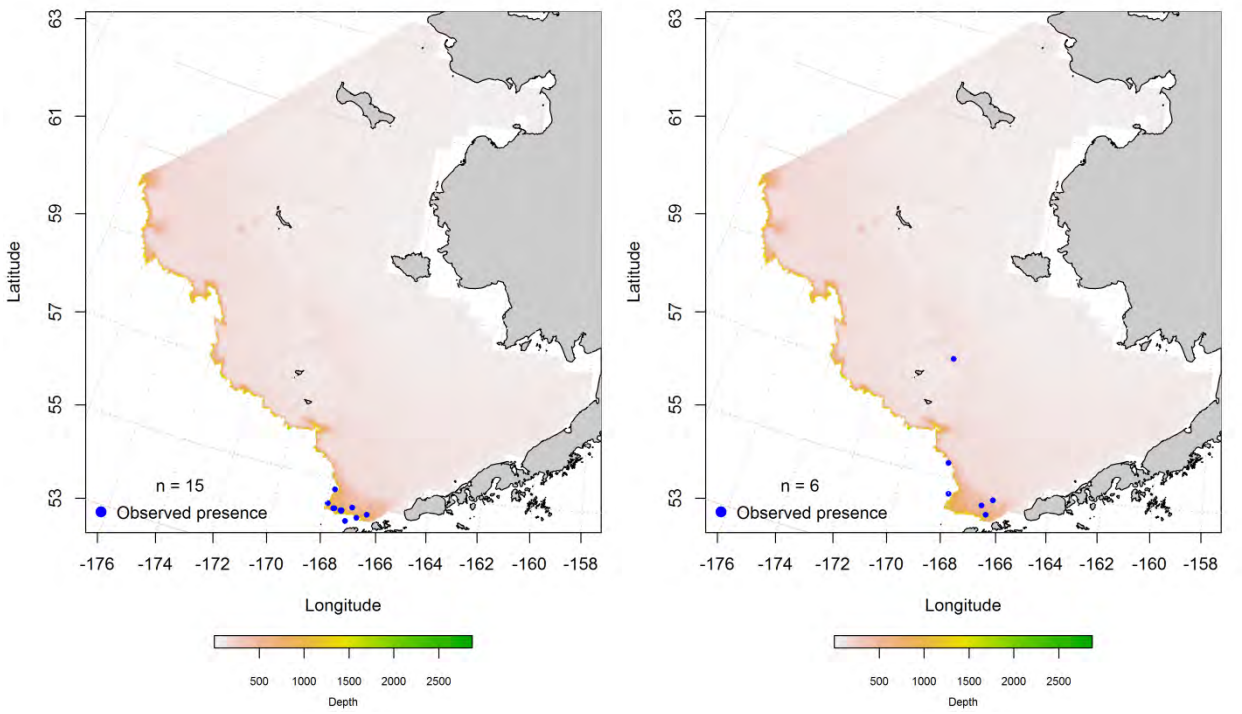

Figure 156. -- Winter (left panel) and spring (right panel) observations of sablefish eggs from EcoFOCI ichthyoplankton surveys of the Eastern Bering Sea.

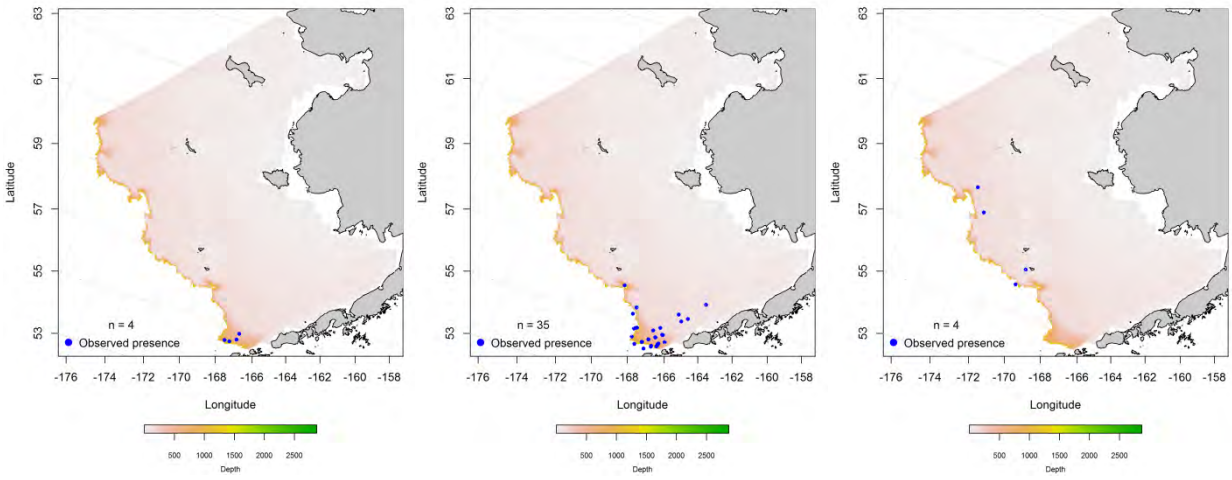

Figure 157. -- Winter (left panel), spring (middle panel), and summer (right panel) observations of larval sablefish from EcoFOCI ichthyoplankton surveys of the Eastern Bering Sea.

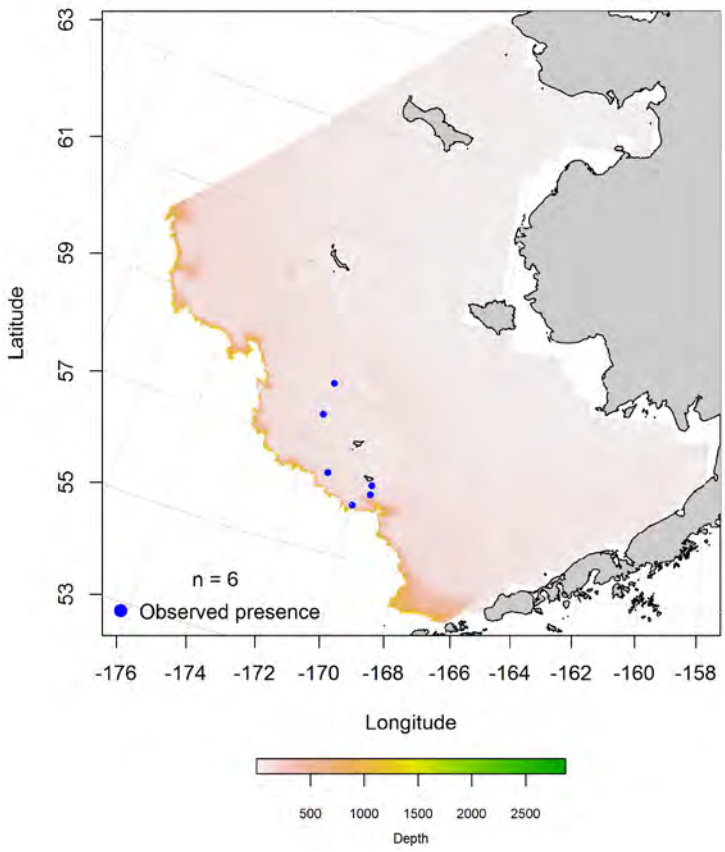

Figure 158. -- Summer observations of early juvenile sablefish from EcoFOCI ichthyoplankton surveys of the Eastern Bering Sea.

Summertime distribution of adult sablefish from RACE bottom trawl surveys of the Eastern Bering Sea -- Adult sablefish collected in RACE summer bottom trawl surveys of the Eastern Bering Sea primarily occurred over the outer shelf (100 to 200 m) and in benthypelagic waters (200 to 3,000 m; Figure 159). Juveniles were less common and were caught over the shallower waters of the outer and middle (50 to 100 m) shelf. There were not sufficient records of late juvenile sablefish to model their summertime distribution.

A MaxEnt model predicted suitable habitat from presence of adult sablefish observed in RACE summer bottom trawl surveys of the Eastern Bering Sea using 7 habitat covariates (Figure 160). The Bering Sea slope and benthypelagic waters off of the shelf edge held the greatest probability for encountering suitable summertime adult sablefish habitat. Bottom depth was the most important habitat covariate in the model

accounting for 86.6% of the relative importance of all predictor terms. The greatest effect on the model prediction was observed over depths ranging from 500 to 1,000 m. The MaxEnt model was an outstanding fit to the training (AUC = 0.99) and the test data used for validation (AUC = 0.95). In both of the training and test cases, the models correctly classified 95% of the predicted cases.

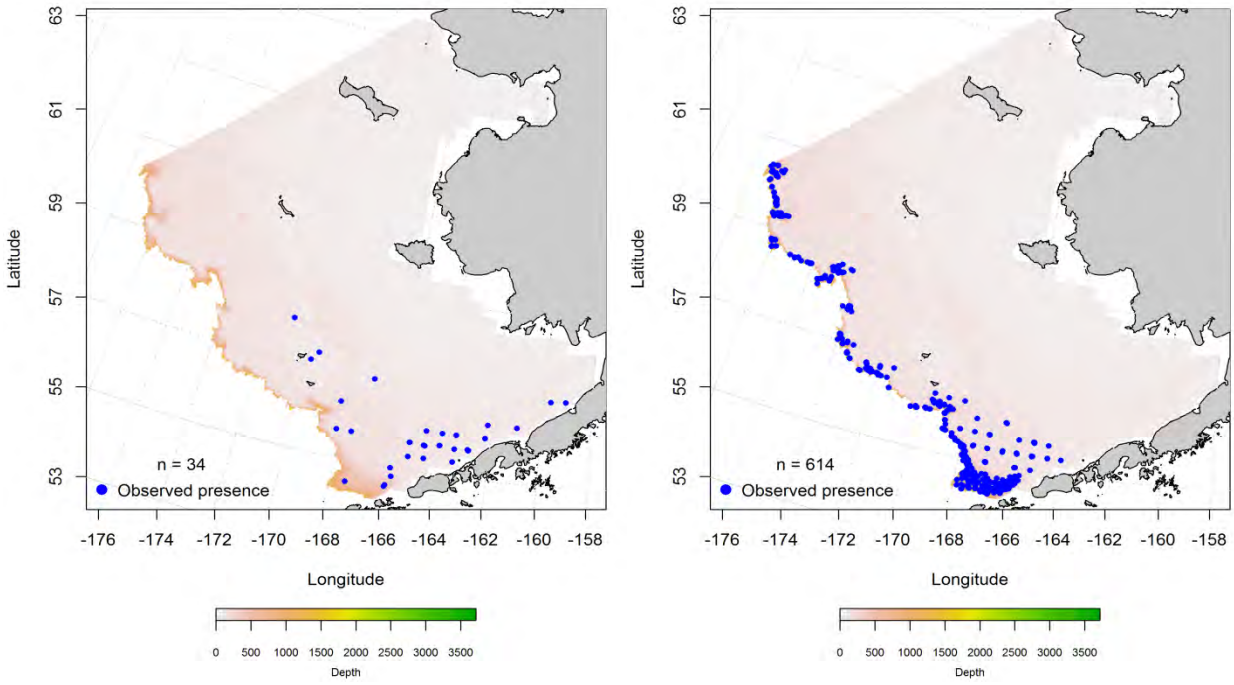

Figure 159. -- Distribution of late-juvenile (left) and adult (right) sablefish catches from RACE summer bottom trawl surveys of the Eastern Bering Sea.

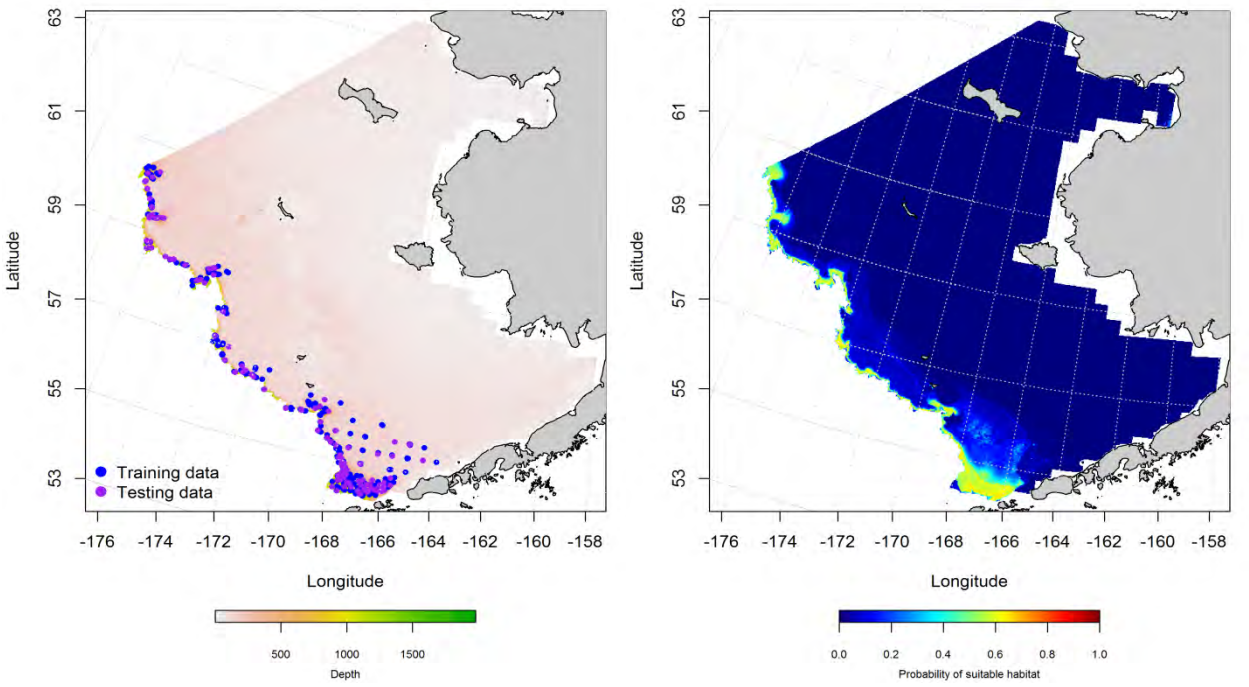

Figure 160. -- Locations of summer RACE Groundfish trawl survey catches of sablefish (left panel). Blue points were used to train the maximum entropy (MaxEnt) model predicting the probability of suitable adult sablefish habitat (right panel) and the purple points were used to validate the model.

Seasonal distribution of sablefish in commercial fishery catches from the Eastern Bering Sea -- The distribution of sablefish from commercial fishery catches during fall months in the Eastern Bering Sea was mainly over the Bering Canyon and on to the shelf along the Alaska Peninsula (Figure 161). Maximum entropy modeling predicts that suitable habitat for adult sablefish in the fall is over these same areas. Depth and bottom temperature represented a combined 84.6% of the relative importance of the predictors in the model. The MaxEnt model provided an outstanding fit to the training data (AUC = 0.97) with 91% of cases correctly classified. Fit of the model in the validation step was also outstanding (AUC = 0.92) and 92% of the cases were correctly classified for the test data set.

The winter distribution of sablefish in commercial catches was primarily over the Bering Canyon and on to the shelf along the Alaska Peninsula (Figure 162). Sablefish occurrence north of Pribilof Canyon was somewhat sparse compared with fall catches. Depth and bottom temperature were the most influential

habitat covariates in the model and accounted for a combined 78.1% of the relative importance of predictor terms. The model predicted 95% of cases correctly and was an outstanding fit to the training data (AUC = 0.99). Model validation using the test data also displayed an outstanding fit (AUC = 0.94) and 94% of cases correctly classified.

In springtime, sablefish were primarily reported from commercial catches over the Bering Canyon and on to the shelf along the Alaska Peninsula (Figure 163). There were a few catches of sablefish reported from north and east of St. Paul Island on the middle shelf (50 to 100 m). As in fall and winter, the most important predictors contributing leverage to the MaxEnt model were depth and bottom temperature with a combined relative importance of 91.8% of the predictor terms. The MaxEnt model was an outstanding fit to the training data (AUC = 0.98) and predicted 96% of cases correctly. The model fit to the test data used for validation was also outstanding (AUC = 0.93) and predicted 93% of cases correctly.

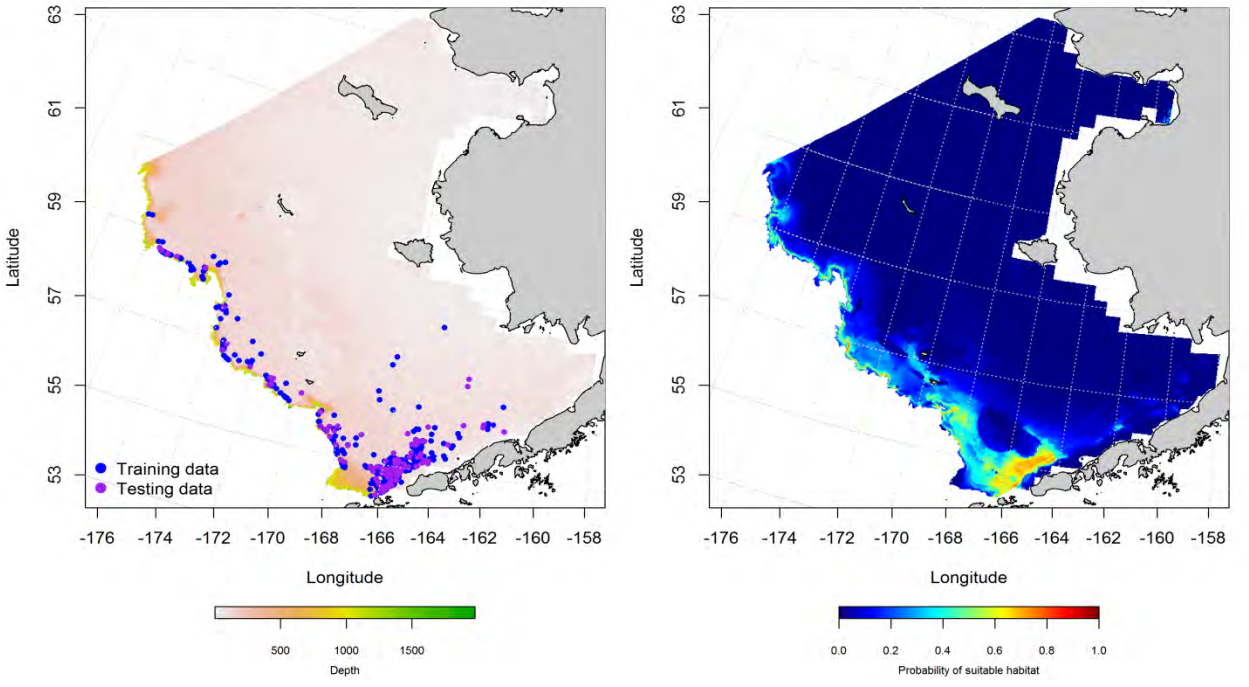

Figure 161. -- Presence of sablefish in commercial fishery catches from fall (October-November; left panel). Blue points were used to train the maximum entropy (MaxEnt) model predicting the probability of suitable sablefish habitat (right panel) and the purple points were used to validate the model.

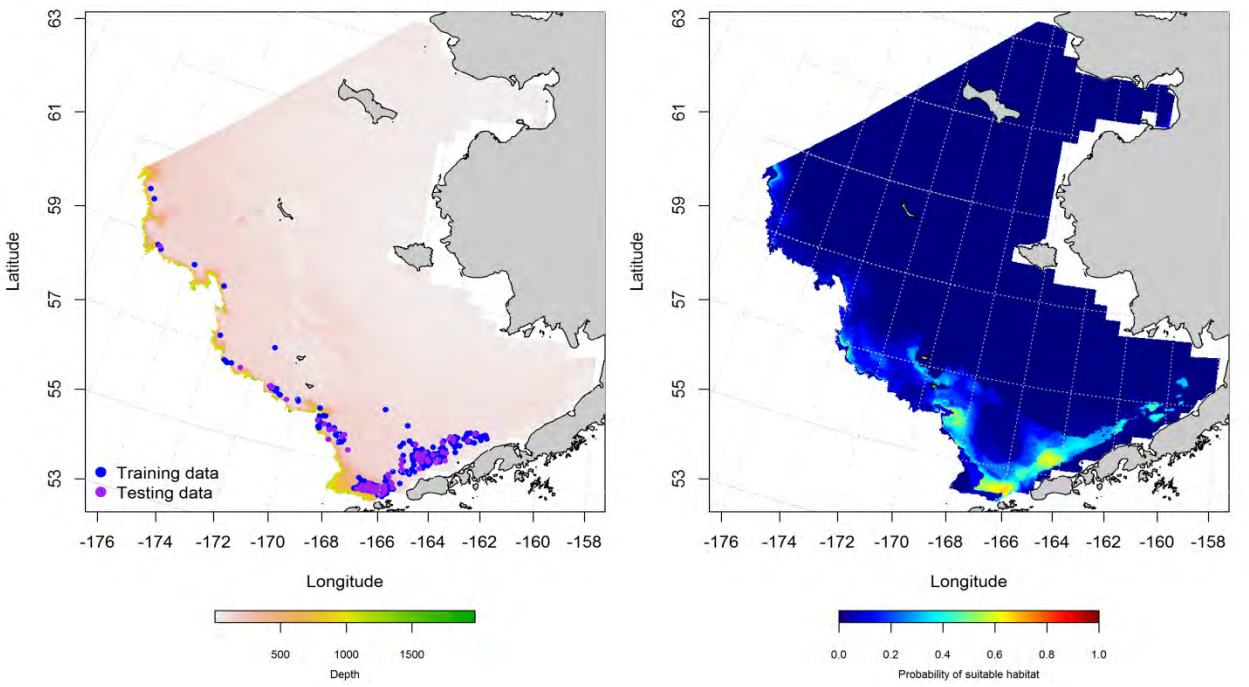

Figure 162. -- Presence of sablefish in commercial fishery catches from fall (December-February; left panel). Blue points were used to train the maximum entropy (MaxEnt) model predicting the probability of suitable sablefish habitat (right panel) and the purple points were used to validate the model.

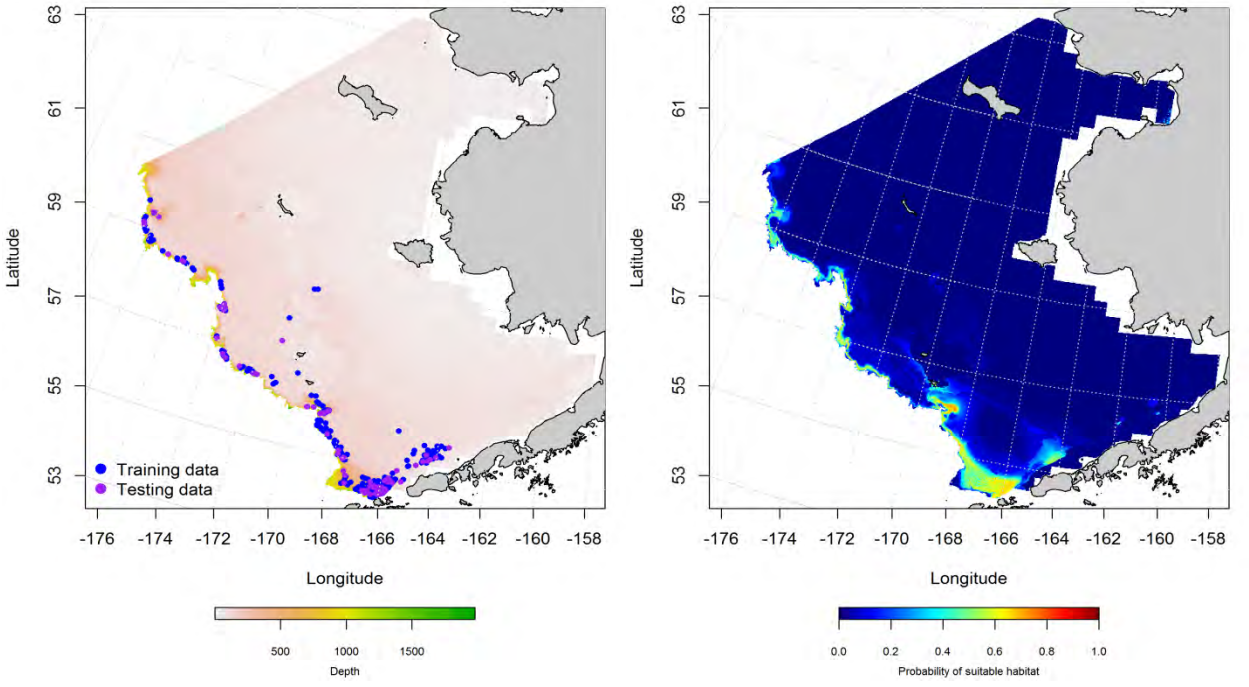

Figure 163. -- Presence of sablefish in commercial fishery catches from fall (March-May; left panel). Blue points were used to train the maximum entropy (MaxEnt) model predicting the probability of suitable sablefish habitat (right panel) and the purple points were used to validate the model.

Essential fish habitat maps and conclusions for adult sablefish (*Anoplopoma fimbria*) in the Eastern Bering Sea – Species distribution modeling of adult sablefish in the Eastern Bering Sea predicts that EFH for this species is mainly found in deeper waters. Although there is some habitat over the middle shelf primarily in the southern domain of the Eastern Bering Sea around the head of the Bering Canyon, much of their EFH extends over the benthypelagic waters of the upper continental slope from the Alaska Peninsula in the south to north of Zhemchug Canyon in the northern domain.

Summertime EFH for adult sablefish from RACE bottom trawl surveys of the Eastern Bering Sea was predicted over the outer shelf (100 to 200 m) and Bering Sea slope (200 to 3,000 m; Figure 164). Areas with some of the highest predicted abundances of adult sablefish are in waters deeper than 500 m.

Predictions of suitable sablefish habitat from commercial fishery catches in the Eastern Bering Sea showed some seasonal differences (Figure 165). Fall and spring months show high probability habitat in shallower waters (< 500 m) near the head of the Bering Canyon when compared with winter. In winter months, the highest probability habitat for encountering adult sablefish in commercial catches is in the deeper waters (> 500 m) over the Bering Slope.

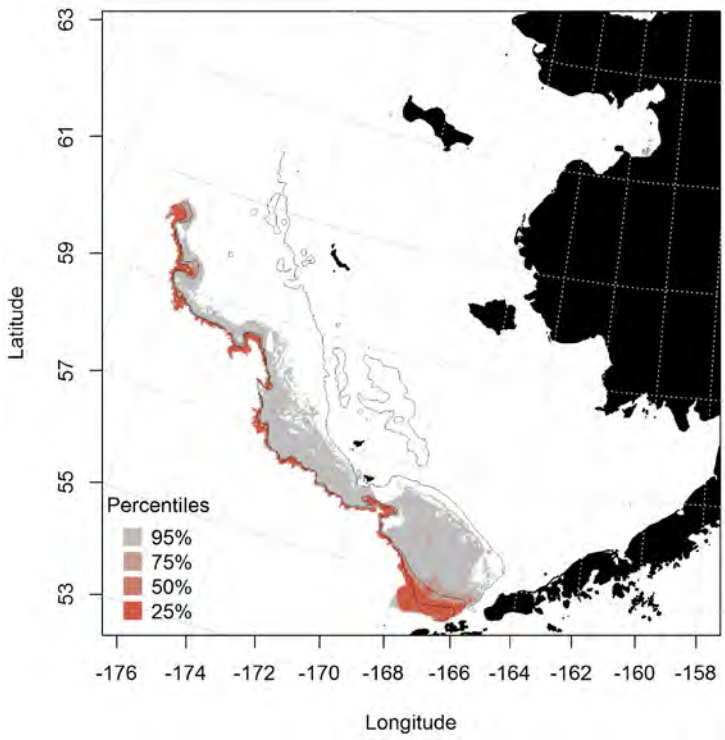

Figure 164. -- Essential fish habitat predicted for adult sablefish from summertime RACE bottom trawl surveys of the Eastern Bering Sea.

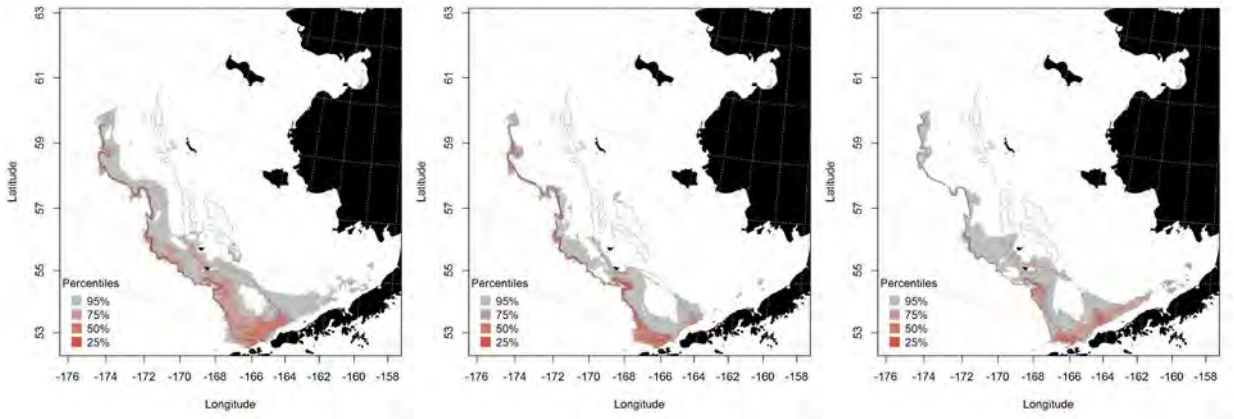

Figure 165. -- Essential fish habitat predicted from sablefish occurrences in commercial fishery catches during fall (left panel), winter (middle panel), and spring (right panel) in the Eastern Bering Sea.

Atka mackerel (*Pleurogrammus monopterygius*)

Atka mackerel are distributed across the Bering Sea from the east coast of the Kamchatka Peninsula, throughout the Commander (Russia) and Aleutian Islands, and north to the Pribilof Islands in the Eastern Bering Sea. They have demersal adhesive eggs and pelagic larvae. Much of the commercial catch of this species is landed from fisheries in the Aleutian Islands.

Seasonal distribution of early life history stages of Atka mackerel from EcoFOCI ichthyoplankton surveys of the Eastern Bering Sea – Atka mackerel larvae were observed during winter, spring, and summer EcoFOCI ichthyoplankton surveys but were uncommon (Figure 166). During winter and spring surveys, Atka mackerel larvae were observed over deep water off of the continental shelf in the southwestern corner of the Eastern Bering Sea southern domain and to the north along the slope edge. During summer surveys, there was only one record of Atka mackerel larvae near St. George Island.

Maximum entropy modeling of larval Atka mackerel presence in springtime EcoFOCI ichthyoplankton surveys predicted that the likeliest suitable habitat was found over the Bering Canyon in the southern domain of the Eastern Bering Sea (Figure 167). The most important habitat covariates determining the relationship between larval Atka mackerel presence and habitat during spring months were bottom depth, bottom slope, current variability, and surface temperature. Combined, these four predictor variables accounted for 53% of the relative importance of the seven habitat covariates in the MaxEnt model. The model fit to the training data was acceptable (AUC = 0.79) and it correctly classified 66% of presence-absence cases predicted. Model validation with the test data was also acceptable (AUC = 0.71) correctly classifying 71% of predicted cases.

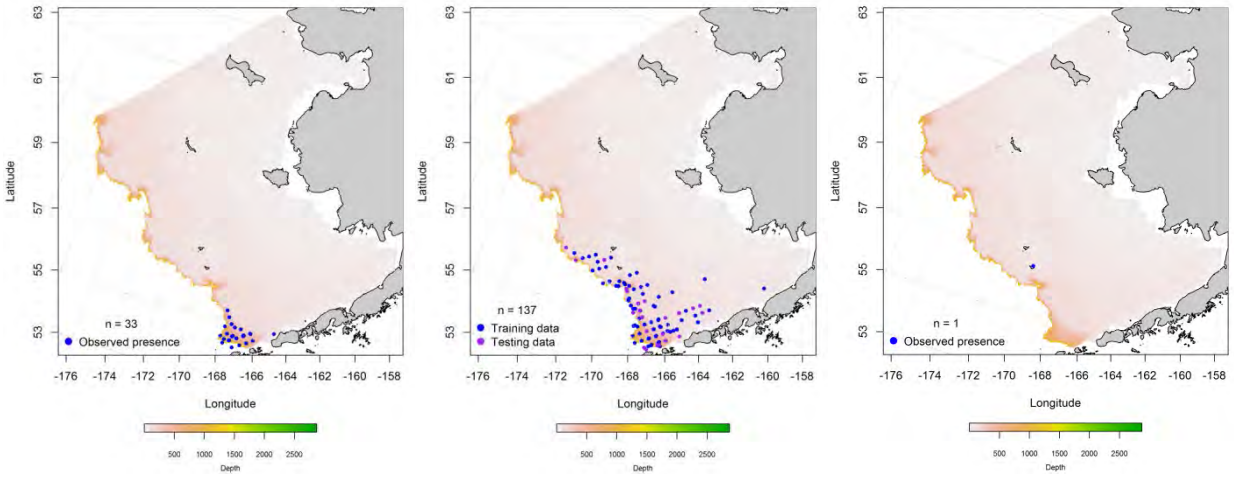

Figure 166. – Winter, spring, and summer observations of larval Atka mackerel (left, right, and middle panel, respectively) from EcoFOCI ichthyoplankton surveys of the Eastern Bering Sea. Blue points were used to train the maximum entropy (MaxEnt) model predicting the probability of suitable habitat and the purple points were used to validate the model.

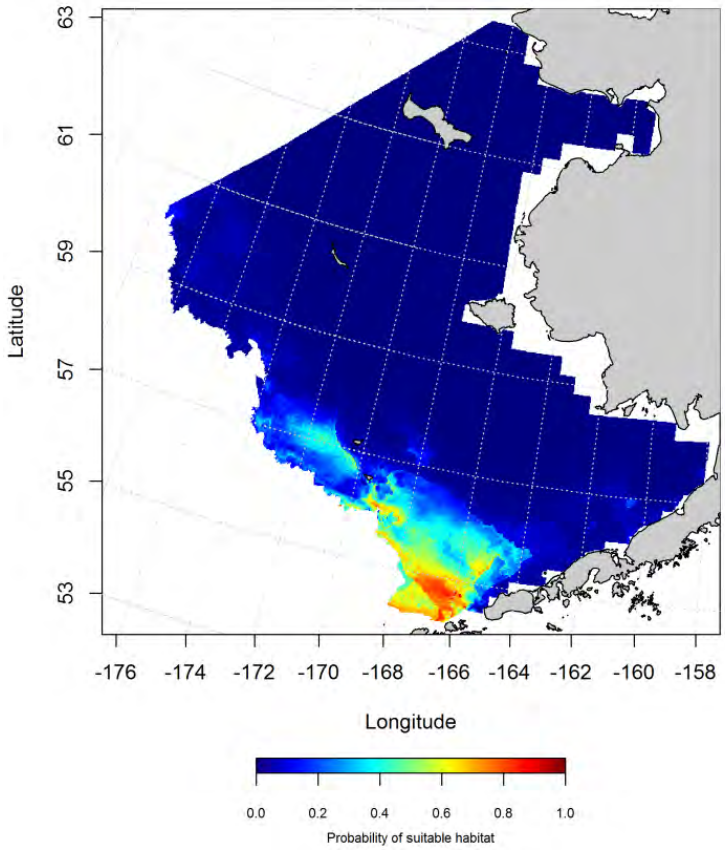

Figure 167. – Probability of suitable larval Atka mackerel habitat in the Eastern Bering Sea predicted by maximum entropy (MaxEnt) modeling of their presence in springtime EcoFOCI ichthyoplankton surveys.

Summertime distribution of late juvenile and adult Atka mackerel from RACE bottom trawl surveys of the Eastern Bering Sea -- Atka mackerel were uncommon in catches from RACE summer bottom trawl surveys of the Eastern Bering Sea (Figure 168). Although they occurred in bottom trawl surveys in most years between 1982 and 2014 they typically occur at < 3% of the stations sampled in any given year. There were not enough trawl catches containing Atka mackerel to model their habitat from the bottom trawl surveys of the Eastern Bering Sea.

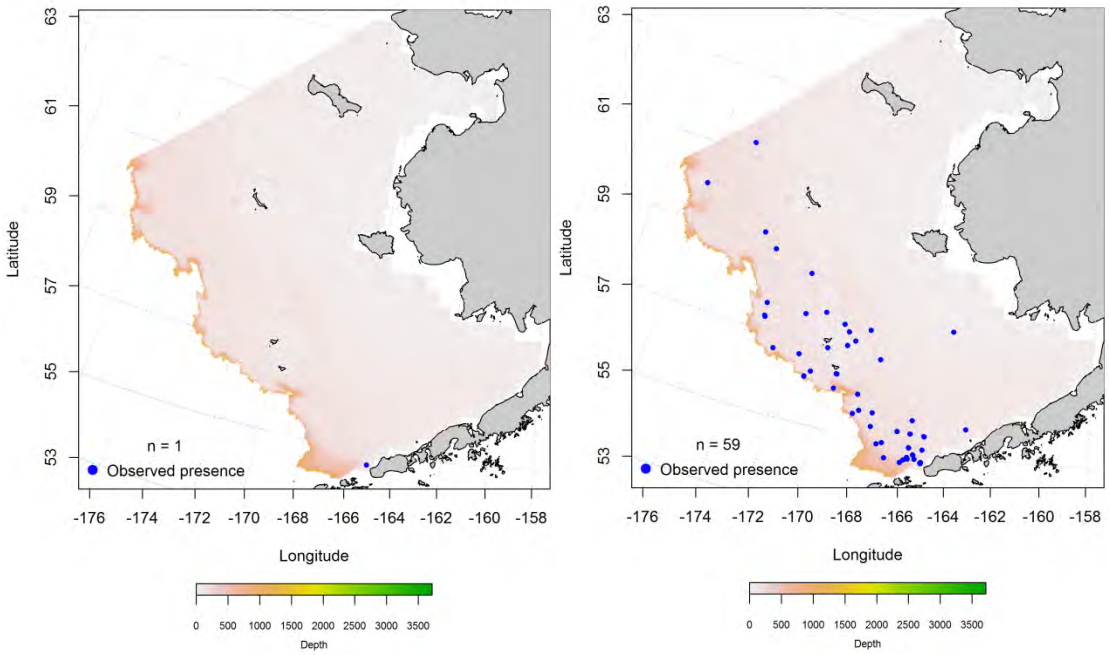

Figure 168. -- Distribution of late-juvenile (left) and adult (right) Atka mackerel catches from RACE summer bottom trawl surveys of the Eastern Bering Sea.

Seasonal distribution of Atka mackerel in commercial fishery catches from the Eastern Bering Sea -- The fall distribution of Atka mackerel in commercial catches was primarily on the outer shelf of the Eastern Bering Sea extending across the southern, central, and northern domains (Figure 169). There were concentrations of Atka presence around the Pribilof Islands and near Unimak Pass. Bottom temperature, bottom depth, and ocean productivity were the most influential habitat covariates in the model and accounted for a combined 76.3% of the relative importance of predictor terms. The MaxEnt model predicted 91% of cases correctly and was an outstanding fit to the training data (AUC = 0.98).

Model validation using the test data also displayed an outstanding fit (AUC = 0.90) and 90% of cases correctly classified.

During winter months, the presence of Atka mackerel in commercial catches was constrained to the southern domain of the Eastern Bering Sea (Figure 170). Areas of high probability for suitable habitat were concentrated around Unimak Pass and the Pribilof Islands. Bottom temperature, bottom depth, tidal maximum, and sediment grain size were the most influential habitat covariates in the model and combined accounted for 93.3% of the relative importance of predictor terms. The MaxEnt model predicted 94% of cases correctly and was an outstanding fit to the training data (AUC = 0.98). Model validation using the test data also displayed an outstanding fit (AUC = 0.93) with 93% of cases correctly classified.

In springtime, Atka mackerel were again observed in commercial catches from the central and southern domains of the Eastern Bering Sea from the Bering Canyon to north of Zhemchug Canyon (Figure 171). Most of the observations were concentrated over the Bering Canyon and around St. George Island as were the high probability habitat areas. The most important predictors contributing leverage to the MaxEnt model were bottom temperature, bottom depth, and sediment grain size with a combined relative importance of 84.1% of the predictor terms. The MaxEnt model was an outstanding fit to the training data (AUC = 0.98) and predicted 94% of cases correctly. The model fit to the test data used for validation was also outstanding (AUC = 0.90) and predicted 90% of cases correctly

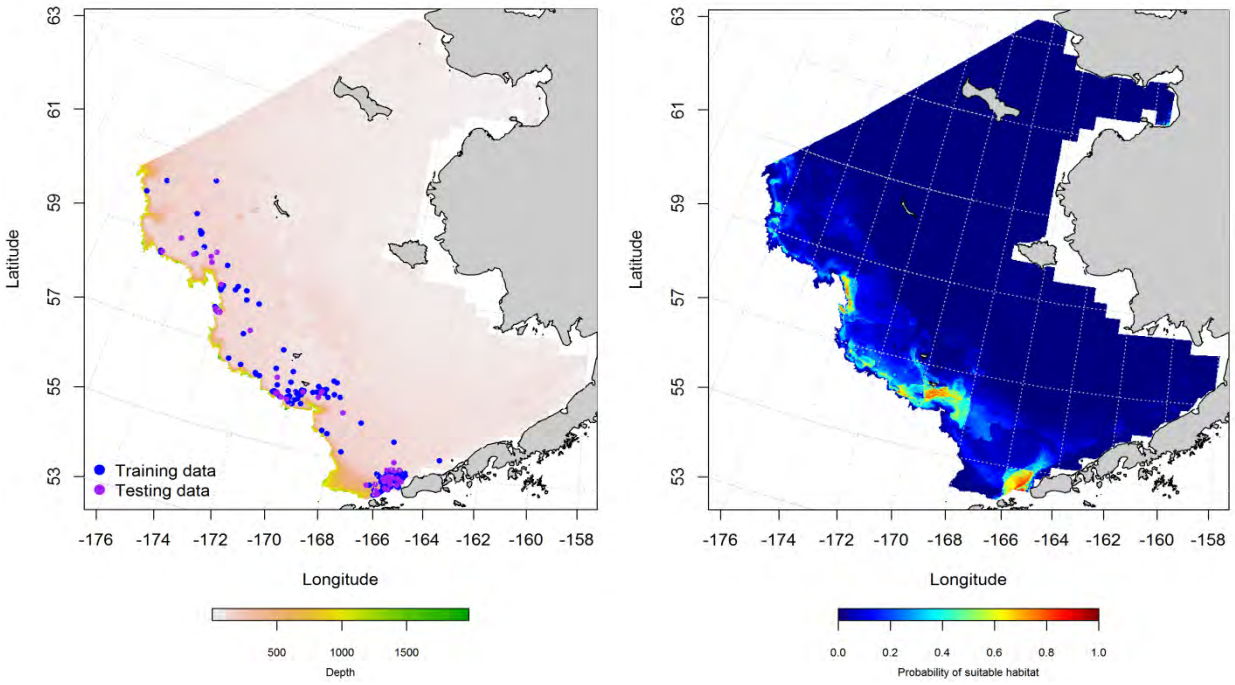

Figure 169. -- Presence of Atka mackerel in commercial fishery catches from fall (October-November; left panel). Blue points were used to train the maximum entropy (MaxEnt) model predicting the probability of suitable Atka mackerel habitat (right panel) and the purple points were used to validate the model.

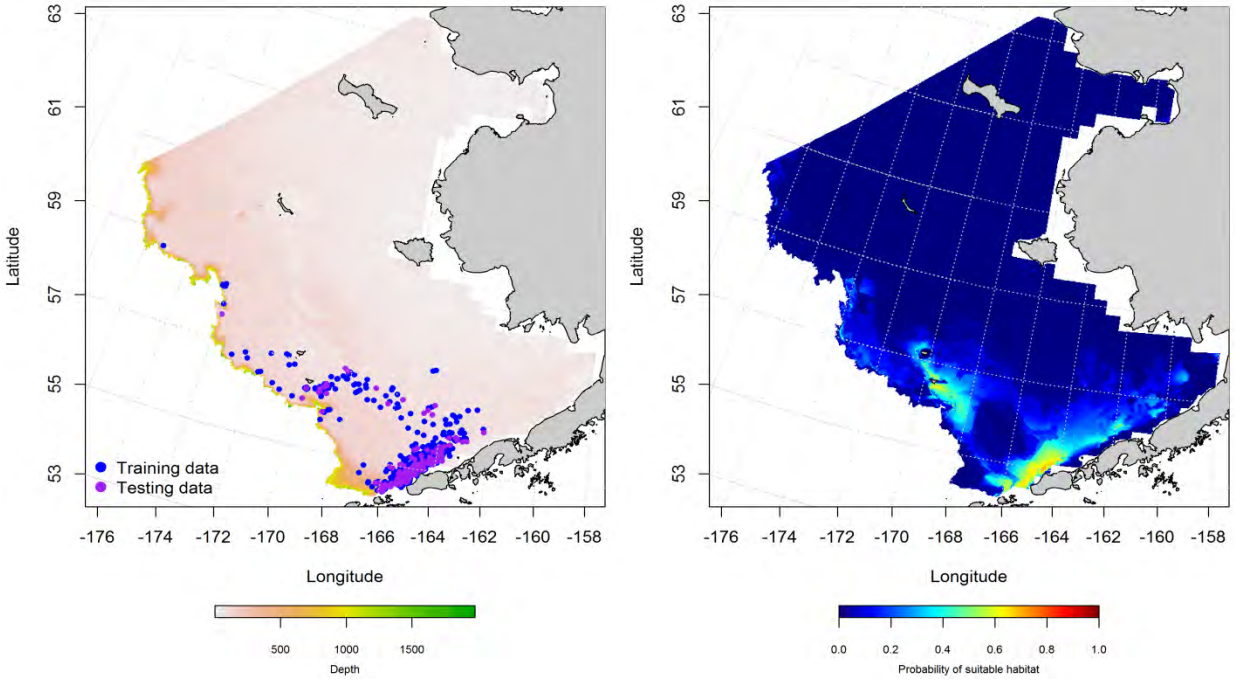

Figure 170. -- Presence of Atka mackerel in commercial fishery catches from winter (December-February; left panel). Blue points were used to train the maximum entropy (MaxEnt) model predicting the

probability of suitable Atka mackerel habitat (right panel) and the purple points were used to validate the model.

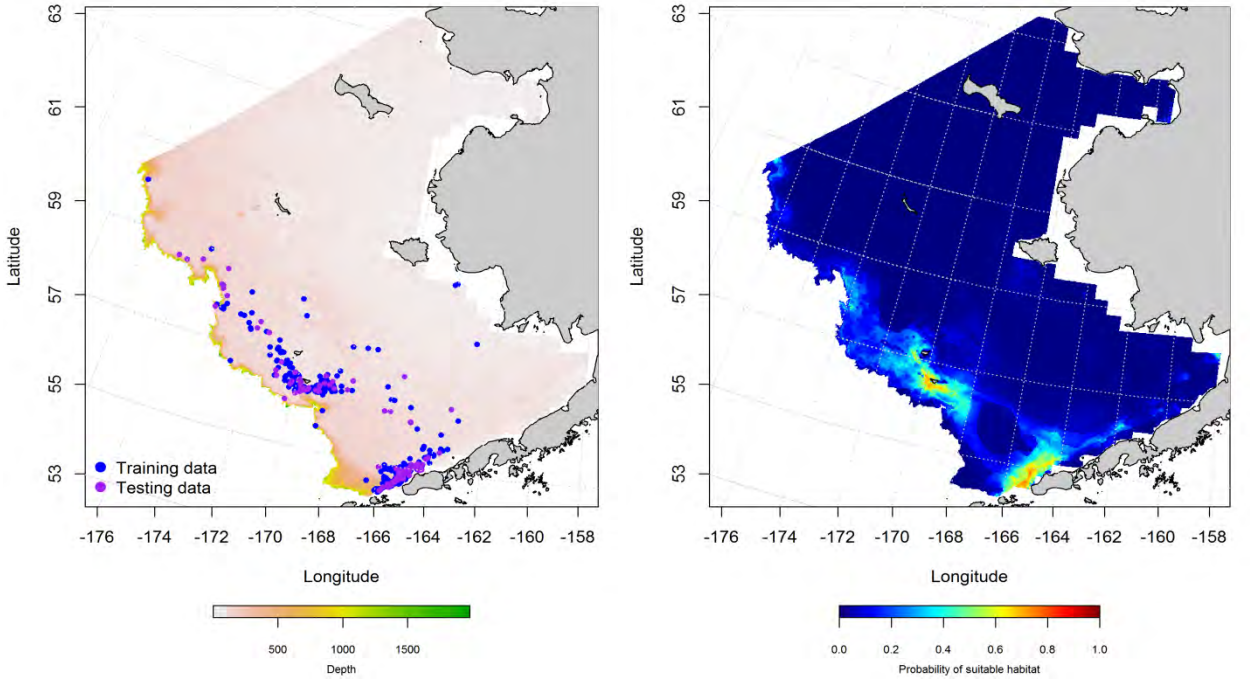

Figure 171. -- Presence of Atka mackerel in commercial fishery catches from spring (March-May; left panel). Blue points were used to train the maximum entropy (MaxEnt) model predicting the probability of suitable Atka mackerel habitat (right panel) and the purple points were used to validate the model.

Essential fish habitat maps and conclusions for Atka mackerel (*Pleurogrammus monopterygius*) from commercial fishery catches in the Eastern Bering Sea – Predictions of suitable Atka mackerel habitat from commercial fishery catches in the Eastern Bering Sea showed some seasonal differences (Figure 172). There was more high probability habitat spread across all Eastern Bering Sea domains in winter compared to fall and spring. However, the presence of Atka mackerel habitat along the outer shelf and upper slope edge is a consistent feature across all three seasons.

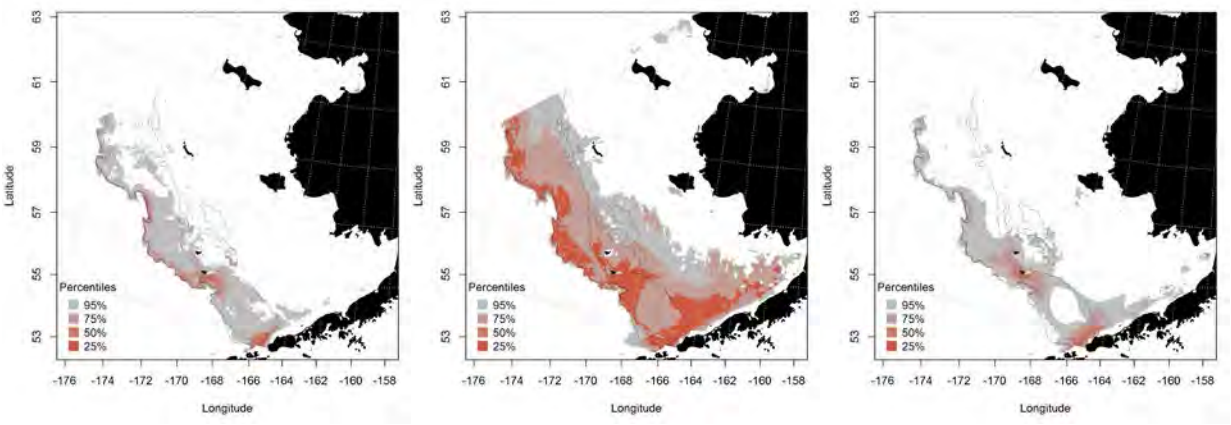

Figure 172. -- Essential fish habitat predicted from Atka mackerel occurrences in commercial fishery catches during fall (left panel), winter (middle panel), and spring (right panel) in the Eastern Bering Sea.

yellow Irish lord (*Hemilepidotus jordani*)

Based on fishery observer catches, yellow Irish lord were a small component of Eastern Bering Sea shelf and slope fisheries from 2009 to 2011 (Spies et al. 2012). Fishery catch composition ranged from 2% in 2009 to 5% in 2011. Historically on the RACE summer bottom trawl surveys, yellow Irish lords have occurred at as few as 6% of stations in the Eastern Bering Sea (e.g., 2010) and as many as 33% in 1983 and 1984.

Seasonal distribution of early life history stages of yellow Irish lord from EcoFOCI ichthyoplankton surveys of the Eastern Bering Sea – Larval yellow Irish lords were observed in EcoFOCI ichthyoplankton surveys in winter, spring, and summer (Figure 173). Their larvae were most prevalent during springtime and occurred most commonly over the outer shelf and benthypelagic waters of the southern domain. The reported presence of larval yellow Irish lord did not provide sufficient data to parameterize a distribution model for this life stage in the Eastern Bering Sea.

Juvenile yellow Irish lords were observed during spring and summer EcoFOCI ichthyoplankton surveys of the Eastern Bering Sea (Figure 174). They were more prevalent over the outer shelf and benthypelagic

waters of the southern domain. They were also more prevalent during springtime than other seasons. Reported juvenile yellow Irish lord presence was insufficient to parameterize a habitat model for this life stage in the Eastern Bering Sea.

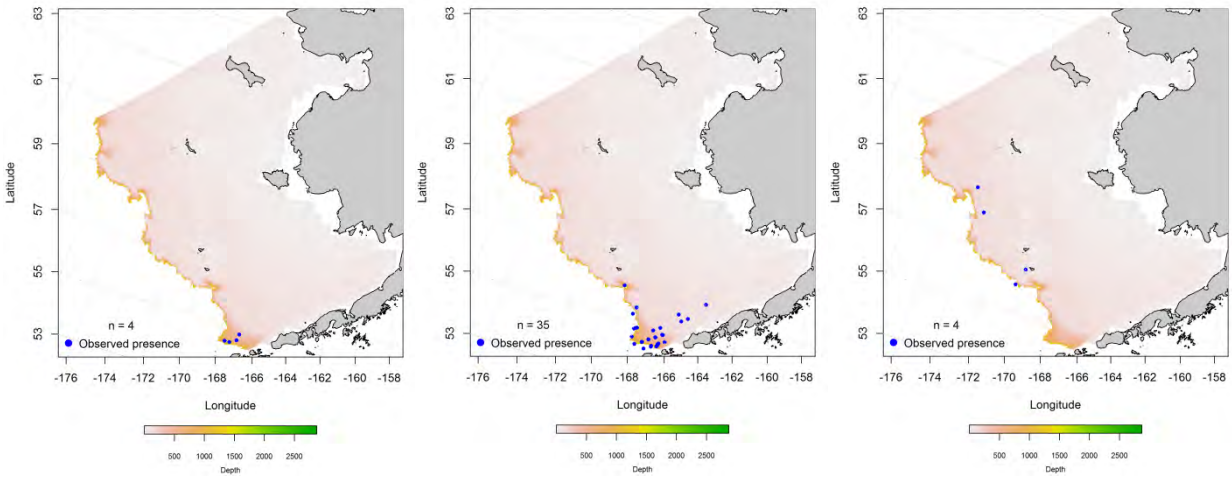

Figure 173. -- Winter (left panel), spring (middle panel), and summer (right panel) observations of larval yellow Irish lord from EcoFOCI ichthyoplankton surveys of the Eastern Bering Sea.

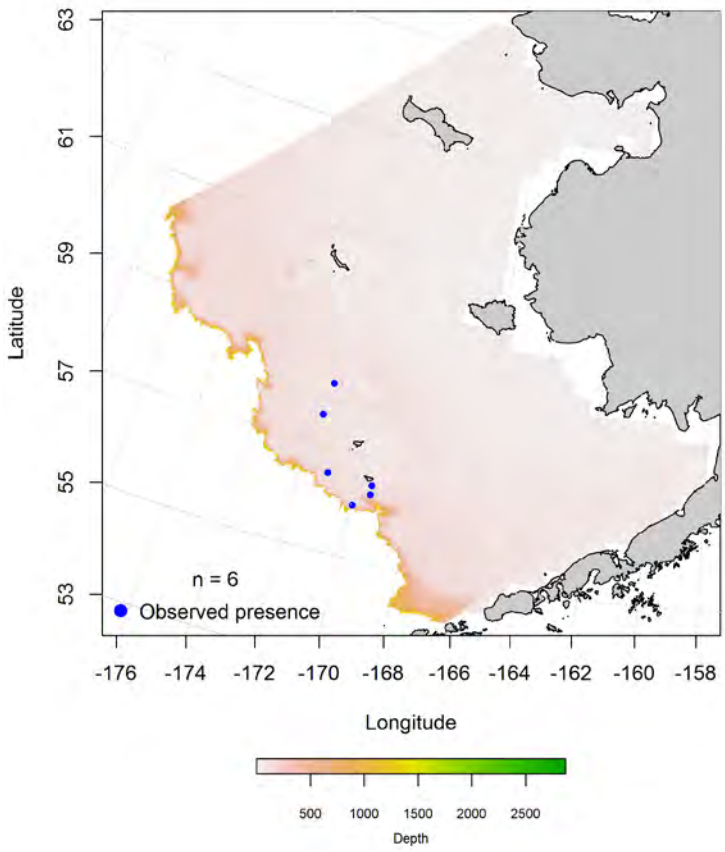

Figure 174. -- Summer observations of early juvenile yellow Irish lord from EcoFOCI ichthyoplankton surveys of the Eastern Bering Sea.

Summertime distribution of juvenile and adult yellow Irish lords from RACE bottom trawl surveys of the Eastern Bering Sea – Late juvenile and adult yellow Irish lords occurred across all 3 domains of the Eastern Bering Sea in RACE summer bottom trawl survey catches (Figure 175). Their distribution also spanned the inner, middle, and outer shelf but did not extend into waters deeper than 200 m over the slope edge. Juvenile and adult distributions across the survey area appear to be largely coincident.

A MaxEnt model was used to predict suitable habitat from the presence of late juvenile yellow Irish lords observed in RACE summer bottom trawl surveys of the Eastern Bering Sea (Figure 176). The highest probability of suitable habitat for this life stage was predicted near St. Matthew's and the Pribilof Islands. Bottom depth, sediment grain size, and bottom temperature were the highest leverage habitat covariates

amongst predictors in the model. Combined they accounted for 69.9% of the relative importance among predictor terms. Tidal maxima and ocean productivity were the next most important terms providing another 25% of the leverage in the model. The model indicates that juvenile yellow Irish lords are more likely in shallower (ca. 100 m) waters with higher tidal currents and larger sediment grain size. The model was an outstanding fit to the training data (AUC = 0.93) and correctly classified 85% of predicted cases. In the model validation step, the MaxEnt model fit the test data acceptably (AUC = 0.77) and correctly classified 77% of cases.

A hurdle GAM was used to describe the distribution of adult yellow Irish lords in RACE summer bottom trawl catches from the Eastern Bering Sea. The best-fitting GAM for yellow Irish lord presence-absence explained only 22% of the deviance in their distribution across the survey area (Figure 177). Geographic location and bottom depth were the most important variables predicting their distribution. This GAM was an excellent fit to the training data (AUC = 0.85) and the AUC for the test data in the model validation step also indicated an excellent model fit (0.83). Both the training and validation models correctly classified 77% of the predicted presence-absence cases.

The best-fitting GAM for conditional abundance of yellow Irish lords accounted for 56.8% of the deviance in their CPUE (Figure 178). The most important habitat predictors of conditional abundance were geographic location and bottom depth. The GAM predicted the highest conditional abundances from east of St. George Island to northwest of St. Paul Island in depths ca. 100 m. Model fits were fair for the training data set ($r^2 = 0.57$) and poor in model validation with the test data set ($r^2 = 0.18$).

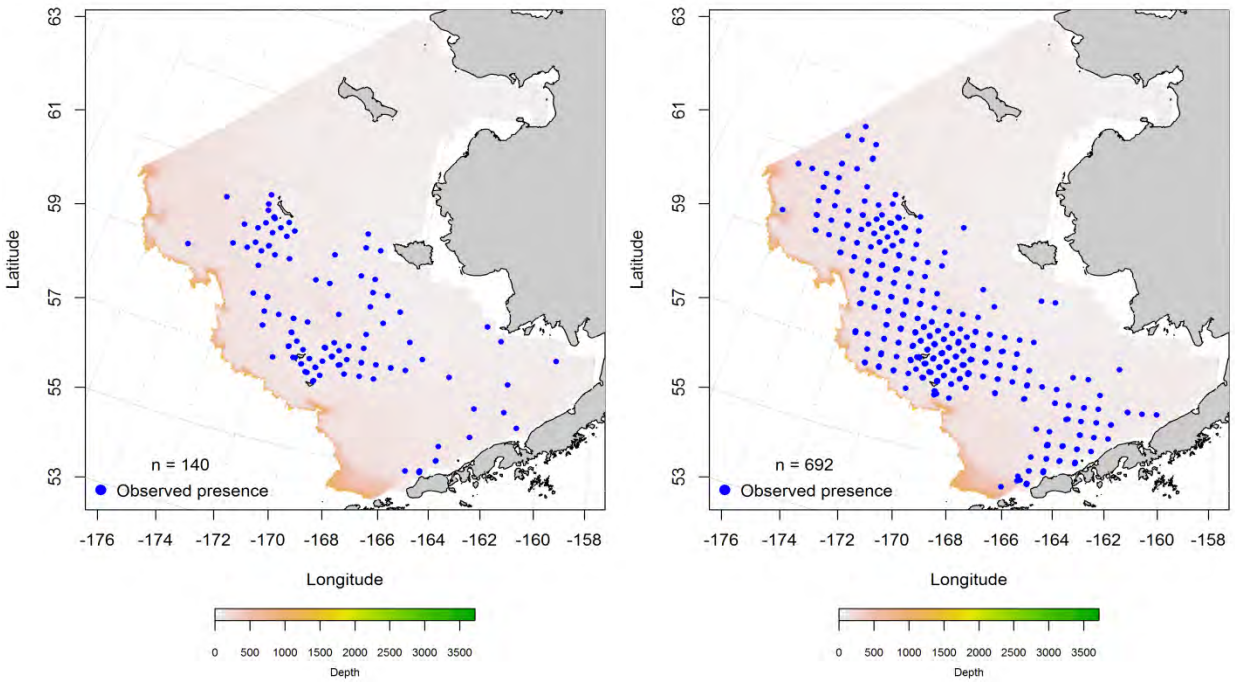

Figure 175. -- Distribution of late-juvenile (left) and adult (right) yellow Irish lord catches from RACE summer bottom trawl surveys of the Eastern Bering Sea.

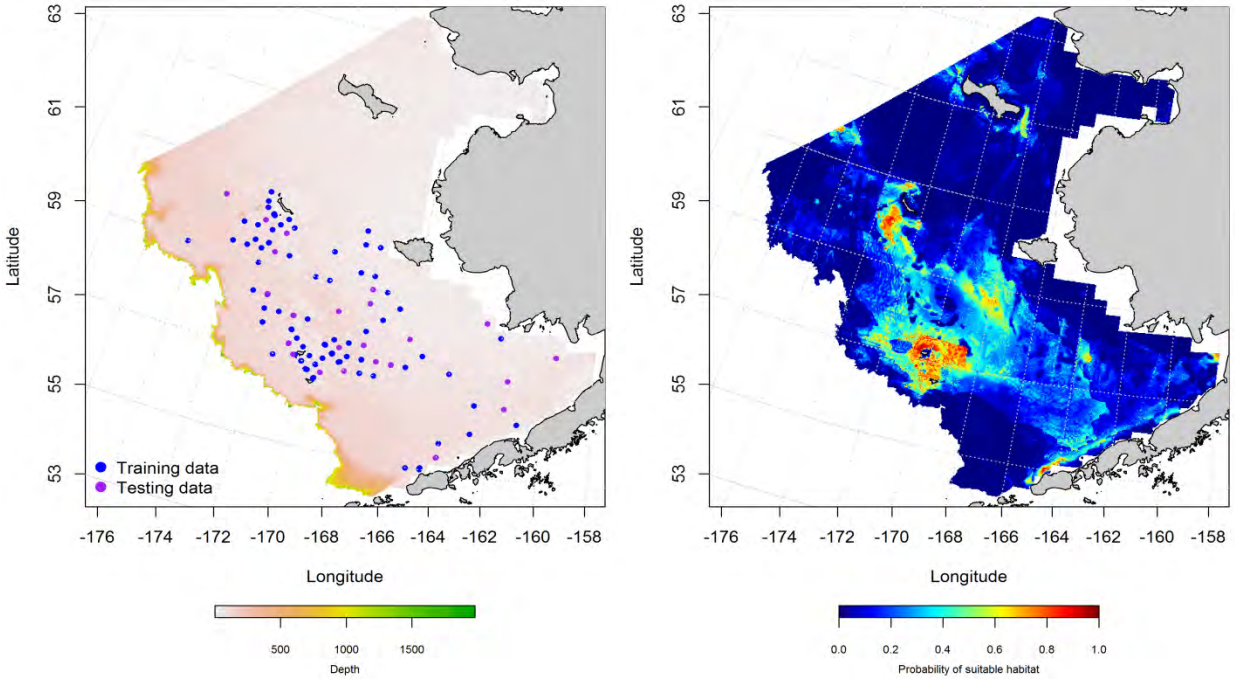

Figure 176. -- Locations of summer RACE Groundfish trawl survey catches of late juvenile yellow Irish lord (left panel). Blue points were used to train the maximum entropy (MaxEnt) model predicting the probability of suitable habitat (right panel) and the purple points were used to validate the model.

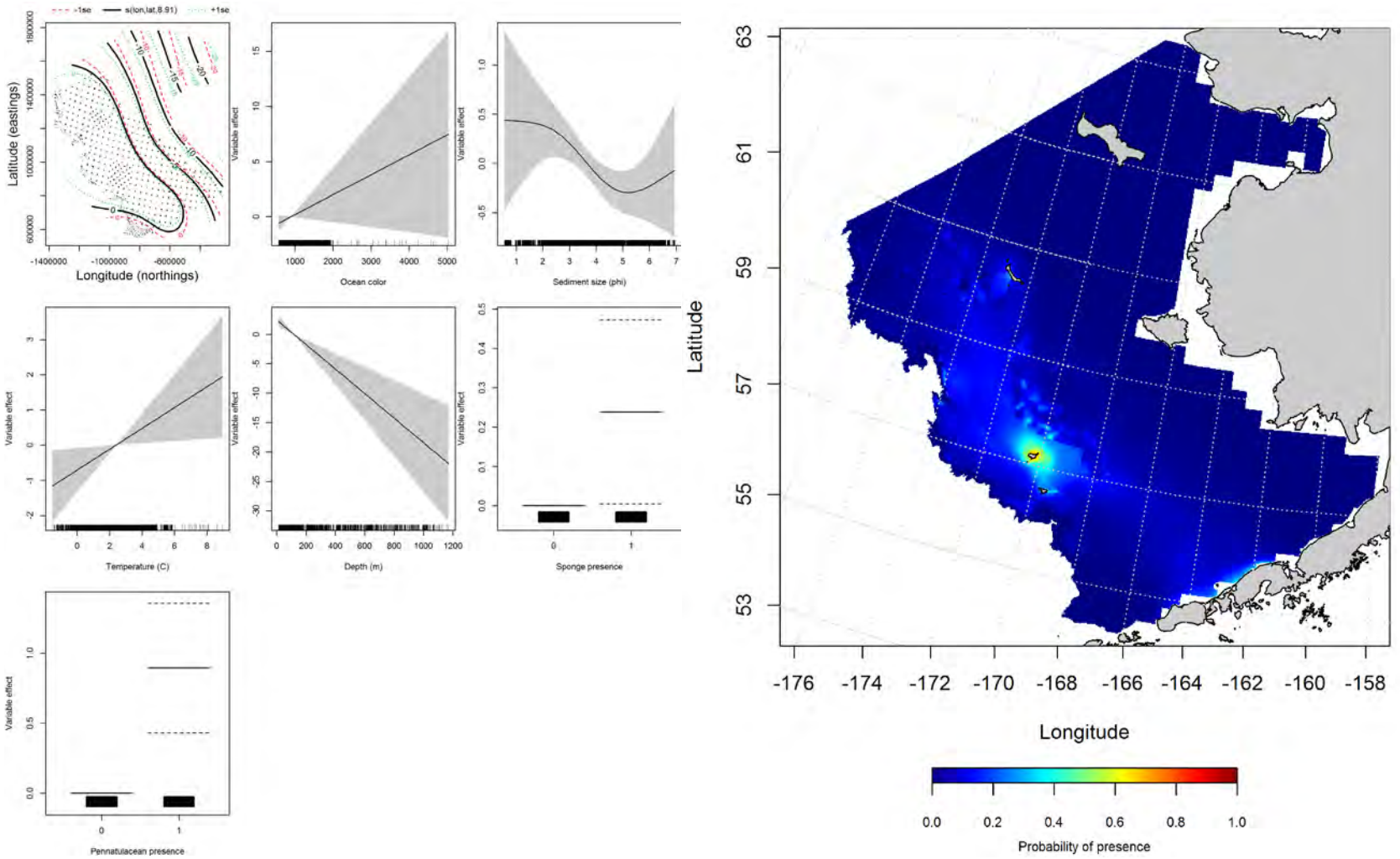

Figure 177. -- Effects of retained habitat covariates on the best-fitting generalized additive presence-absence model (GAM) of adult yellow Irish lord from RACE summer bottom trawl surveys of the Eastern Bering Sea Shelf, Slope, and Northern Bering Sea alongside their predicted presence (right panel).

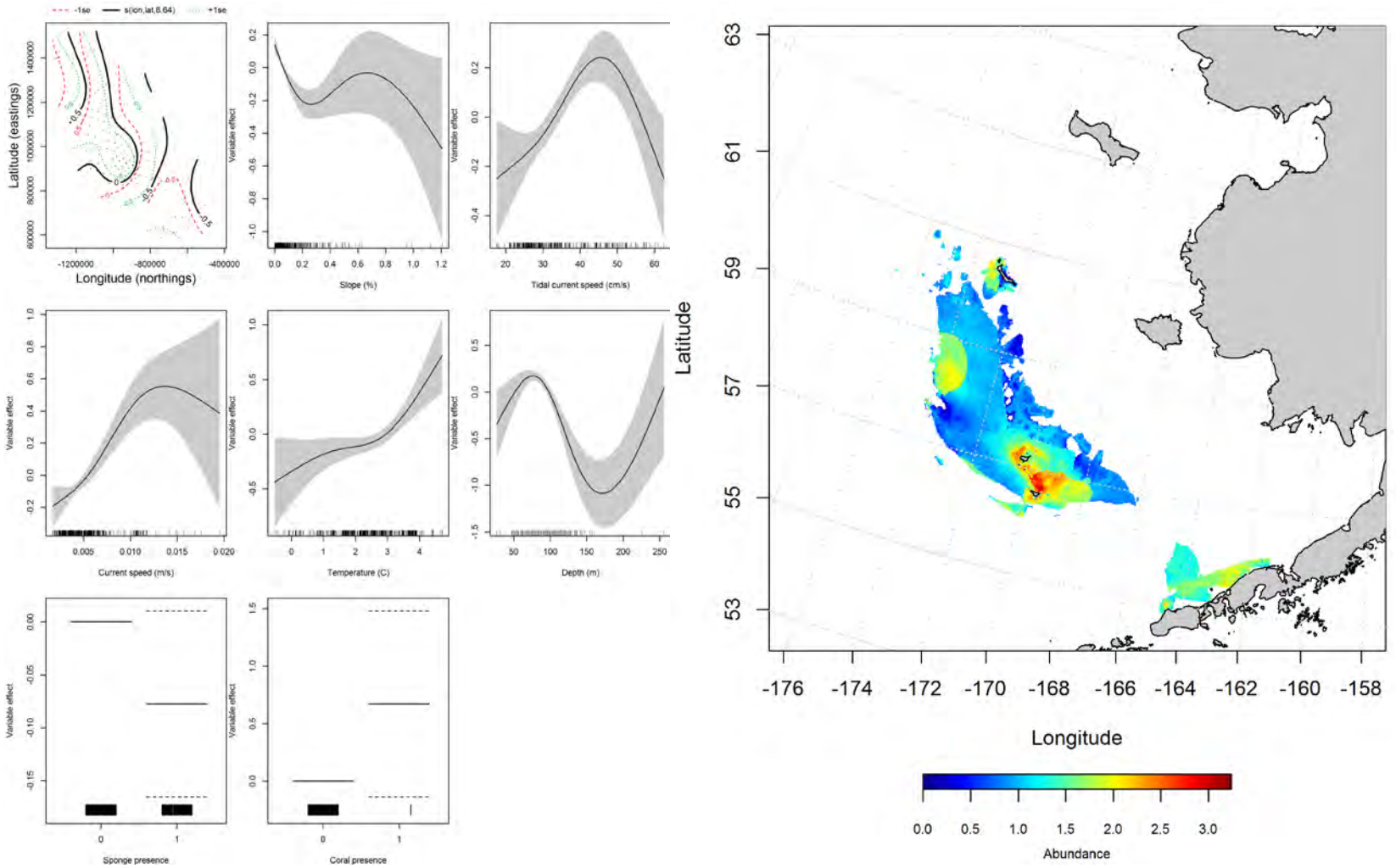

Figure 178. -- Effects of retained habitat covariates on the best-fitting generalized additive model (GAM) of adult yellow Irish lord from RACE summer bottom trawl surveys of the Eastern Bering Sea Shelf, Slope, and Northern Bering Sea alongside their predicted conditional abundance (right panel).

Seasonal distribution of yellow Irish lord in commercial fishery catches from the Eastern Bering Sea -- The distribution of yellow Irish lord in commercial fishery catches during fall months in the Eastern Bering Sea was mainly in the central and southern domains (Figure 179). Maximum entropy modeling predicts that the highest probability of suitable habitat for adult yellow Irish lord in the fall is around St. George Island in the Pribilofs. Ocean productivity, bottom depth, and bottom temperature represented a combined 82.8% of the relative importance of the predictors in the model. The MaxEnt model provided an outstanding fit to the training data (AUC = 0.97) with 91% of cases correctly classified. Fit of the model in the validation step was excellent (AUC = 0.83) and 83% of the cases were correctly classified for the test data set.

The winter distribution of yellow Irish lord in commercial catches was tilted more toward the southern domain of the Eastern Bering Sea (Figure 180). The highest probabilities of suitable yellow Irish lord habitat were along the middle shelf. Bottom depth, ocean productivity, and tidal maxima dominated the predictive power of the habitat covariates in the model accounting for a combined 90.3% of the relative importance of predictor terms. The model predicted 90% of cases correctly and was an outstanding fit to the training data (AUC = 0.95). Model validation using the test data also displayed an outstanding fit (AUC = 0.90) and 90% of cases correctly classified.

In springtime, yellow Irish lord were more widely represented across the inner and outer shelf than in fall or winter (Figure 181). The area of highest probability for suitable habitat was near St. Paul Island in the Pribilofs. The most important predictors contributing leverage to the MaxEnt model were tidal maxima, bottom temperature, bottom depth, and sediment grain size with a combined relative importance of 91.1% of the predictor terms. The MaxEnt model was an outstanding fit to the training data (AUC = 0.90) and predicted 82% of cases correctly. The model fit to the test data used for validation was excellent (AUC = 0.83) and predicted 83% of cases correctly.

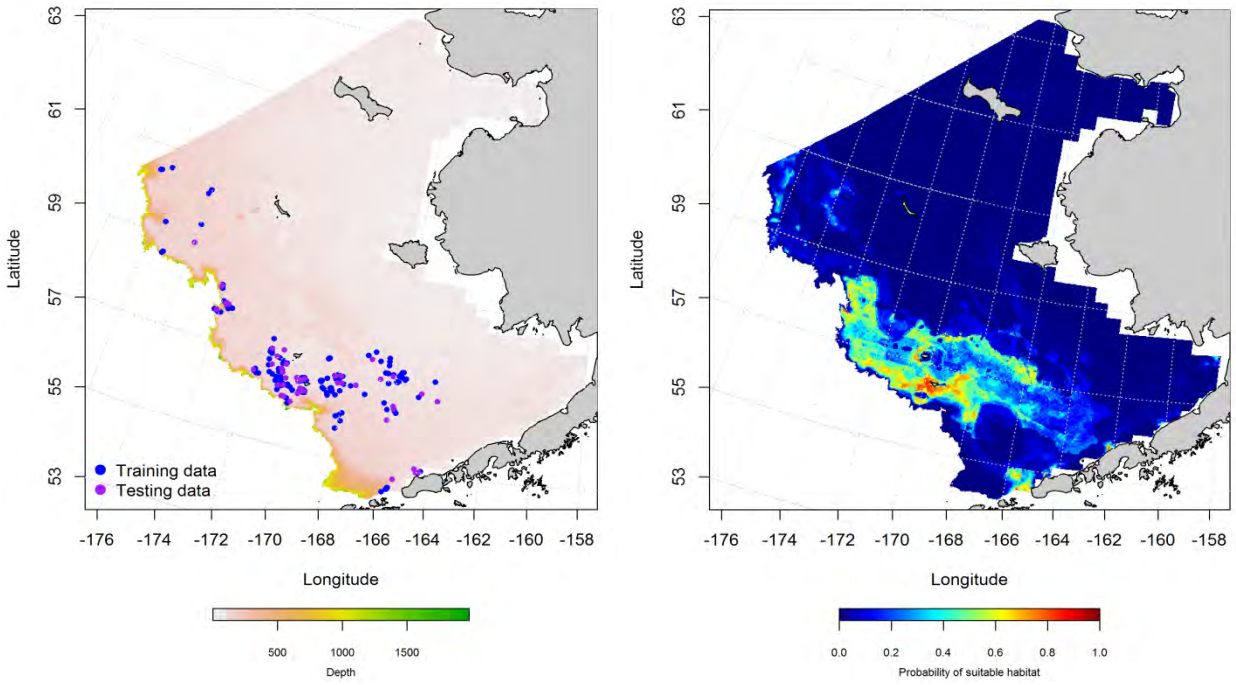

Figure 179. -- Presence of yellow Irish lord in commercial fishery catches from fall (October-November; left panel). Blue points were used to train the maximum entropy (MaxEnt) model predicting the probability of suitable habitat (right panel) and the purple points were used to validate the model.

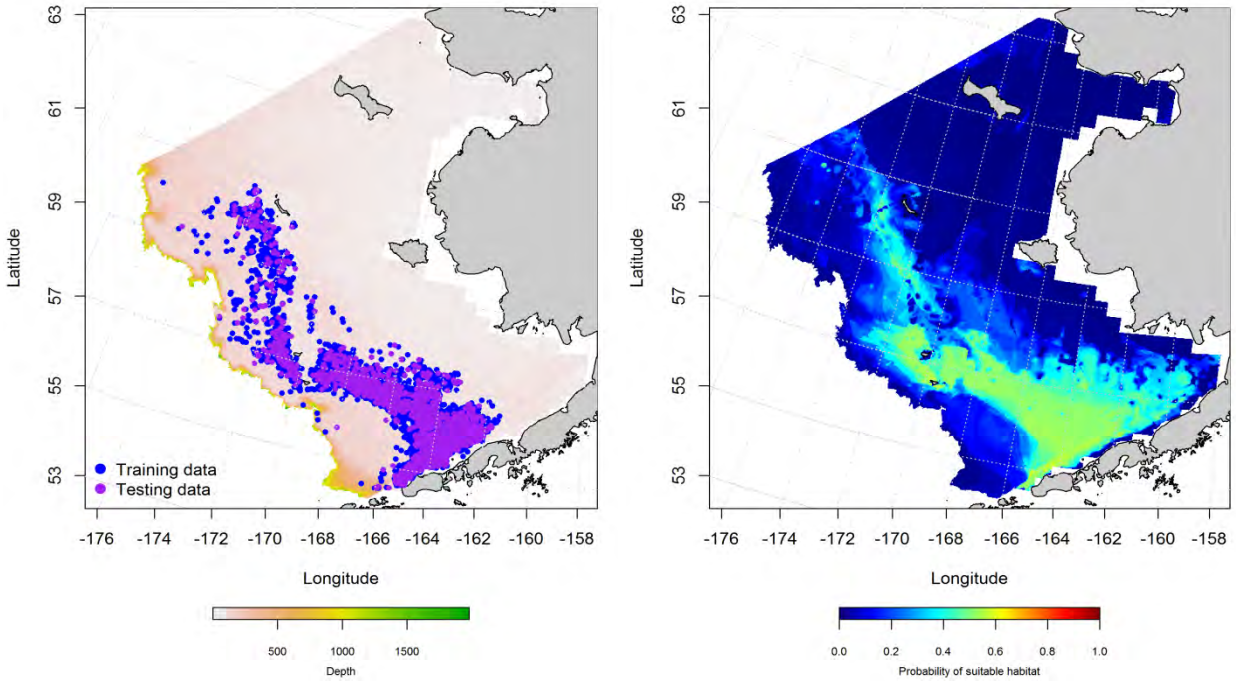

Figure 180. -- Presence of yellow Irish lord in commercial fishery catches from winter (December-February; left panel). Blue points were used to train the maximum entropy (MaxEnt) model predicting the probability of suitable habitat (right panel) and the purple points were used to validate the model.

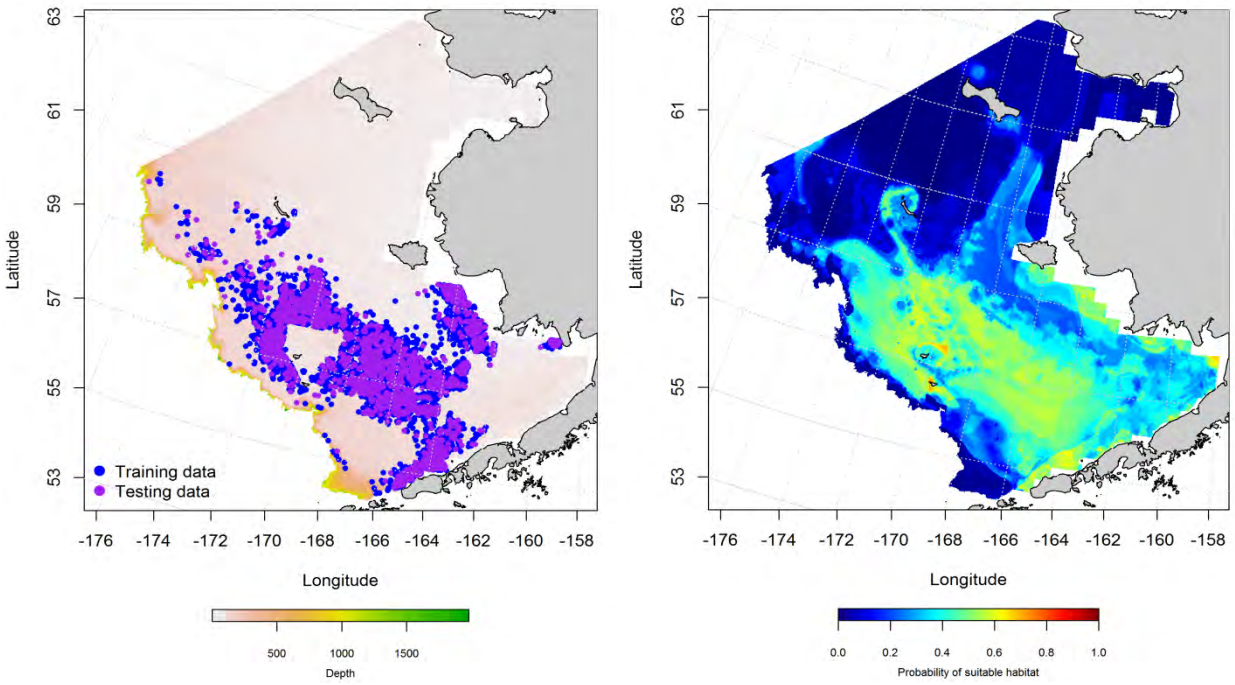

Figure 181. -- Presence of yellow Irish lord in commercial fishery catches from spring (March-May; left panel). Blue points were used to train the maximum entropy (MaxEnt) model predicting the probability of suitable habitat (right panel) and the purple points were used to validate the model.

Essential fish habitat maps and conclusions for adult yellow Irish lord (*Hemilepidotus jordani*) in the Eastern Bering Sea – Species distribution modeling of adult yellow Irish lord in the Eastern Bering Sea predicts that EFH for this species varies between life stages and seasons. For late juvenile and adult yellow Irish lord from summertime RACE bottom trawl surveys of the Eastern Bering Sea, EFH was centered around St Matthew's Island, the Pribilof Islands, and near the heads of the Bering and Zhemchug Canyons (Figure 182).

Predictions of suitable yellow Irish lord habitat from commercial fishery catches in the Eastern Bering Sea showed some seasonal differences (Figure 183). Higher probability habitats were commonly predicted around the Pribilof Islands in all seasons. In winter and spring the highest probability areas were over the middle shelf across the central and southern domains.

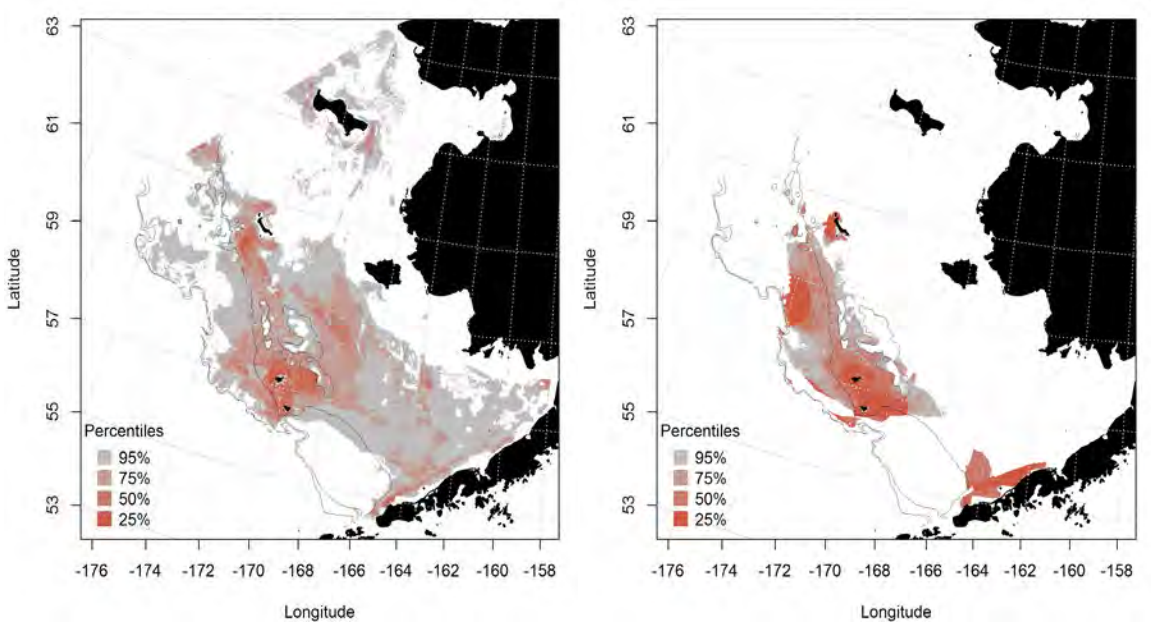

Figure 182. -- Essential fish habitat predicted for late juvenile and adult yellow Irish lord (left and right panel) from summertime RACE bottom trawl surveys of the Eastern Bering Sea.

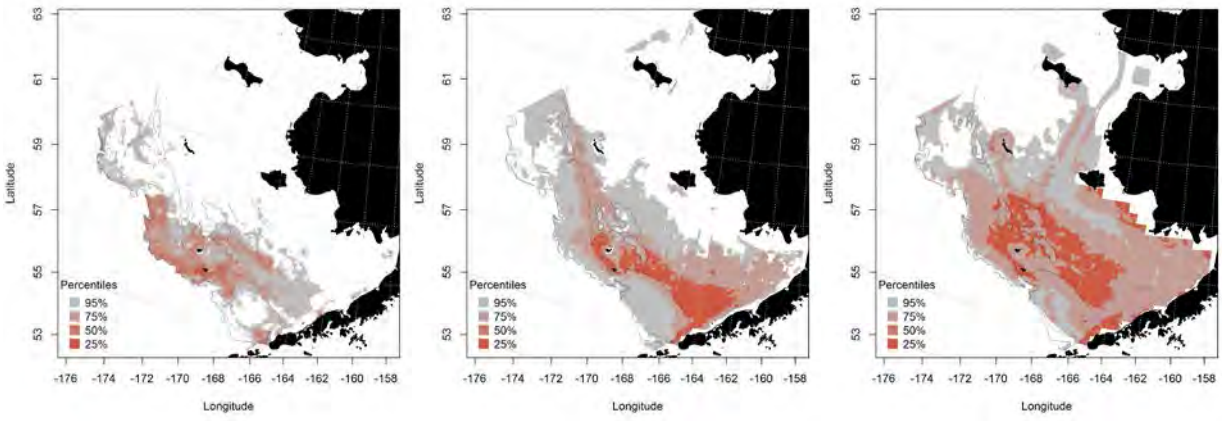

Figure 183. -- Essential fish habitat predicted from yellow Irish lord occurrences in commercial fishery catches during fall (left panel), winter (middle panel), and spring (right panel) in the Eastern Bering Sea.

great sculpin (*Myoxocephalus polyacanthocephalus*)

Great sculpin are found over sand and mud bottoms of the North Pacific Ocean from the Washington coast to the Bering Sea at depths up to 240 m (Eschmeyer et al. 1983). They deposit demersally adhesive

egg masses and have pelagic larvae. There are currently no targeted fisheries for sculpins in Alaskan waters although they are often caught incidentally in trawl and longline fisheries[6].

Seasonal distribution of early life history stages of great sculpin from EcoFOCI ichthyoplankton surveys of the Eastern Bering Sea –There was one record of a larval great sculpin recorded on EcoFOCI ichthyoplankton surveys of the Eastern Bering Sea. No juveniles were reported. There were not sufficient data to undertake species distribution modeling for early life history stages of great sculpin.

Summertime distribution of late juvenile and adult great sculpin from RACE bottom trawl surveys of the Eastern Bering Sea – Late juvenile and adult great sculpins occurred in RACE bottom trawl survey catches across all 3 domains of the Eastern Bering Sea (Figure 184). Their distribution spanned the inner, middle, and outer shelf but did not extend into waters deeper than 200 m over the slope edge. Late juvenile and adult distributions appeared to be largely coincident across the survey area.

A hurdle GAM was used to model late juvenile great sculpin species distribution in the Eastern Bering Sea. The presence GAM predicted two different regions with high probabilities of encountering late juvenile great sculpins in RACE summer bottom trawl catches (Figure 185). These were in Bristol Bay in the southern domain of the Eastern Bering Sea and from St. Matthew's Island northward into the northern domain. The best-fitting GAM explained just 27.1% of the deviance in their distribution data. Geographical location and bottom temperature were the most significant predictors retained in the model. The two model effect maxima with the location covariate correspond to the regions described above and also indicate that late juvenile great sculpin were more likely to occur at an optimum temperature around 2°C. The GAM was an excellent fit to the training data (AUC = 0.83) and correctly classified 76% of

[6] Brogan, J. D., and D. M. Anderl. 2012. Great sculpin (*Myoxocephalus polyacanthocephalus*). Resource Ecology and Fisheries Management Division, Alaska Fisheries Science Center, NMFS, NOAA, 7600 Sand Point Way NE, Seattle WA 98115. [Available from: http://www.afsc.noaa.gov/REFM/Age/default.htm.]

predicted cases of presence-absence. In the model validation step, the GAM fit was good (AUC = 0.82) correctly classifying 75% of cases predicted from the test data.

In the second step of the hurdle GAM, late juvenile great sculpin abundance was predicted where the threshold for presence established in the first step was met. The best-fitting GAM for conditional abundance of great sculpins explained < 10% of the deviance in their CPUE from RACE bottom trawl surveys of the Eastern Bering Sea (Figure 186). The most important habitat predictors of conditional abundance were geographic location and bottom temperature. Relatively high abundance of late juvenile great sculpin was predicted basically everywhere that presence was predicted. Model fits were poor for the training and test data sets (r^2 = 0.08 and 0.07).

A hurdle GAM was used to model adult great sculpin species distribution in the Eastern Bering Sea. The best-fitting presence GAM predicted three different regions with high probabilities of encountering adult great sculpins in RACE summer bottom trawl catches (Figure 187). These were in Bristol Bay in the southern domain of the Eastern Bering Sea, around St. Paul Island in the central domain, and northward from St. Matthew's Island into the northern domain. The GAM explained just 28.9% of the deviance in their distribution data. Geographical location and bottom temperature were the most significant predictors retained in the model. The model effects indicate that adult great sculpin become less prevalent going from the southwest toward the northeast across the survey are and were more likely to occur at temperatures around 2°C. The GAM was an excellent fit to the training data (AUC = 0.85) and correctly classified 77% of predicted cases of presence-absence. In the model validation step, the GAM fit was also excellent (AUC = 0.84) correctly classifying 76% of cases predicted from the test data.

In the second step of the hurdle GAM, adult great sculpin abundance was predicted where the threshold for presence established in the first step was met. The best-fitting GAM for conditional abundance of great sculpins explained 10.9% of the deviance in their CPUE from RACE bottom trawl surveys of the Eastern Bering Sea (Figure 188). The most important habitat covariate retained in the model was

geographic location. Relatively high abundance of adult great sculpin was predicted around the Pribilof Islands and along the Alaska Peninsula; lower predicted abundances occurred in the north. Model fits were poor for the training and test data sets (r^2 = 0.11 and 0.08).

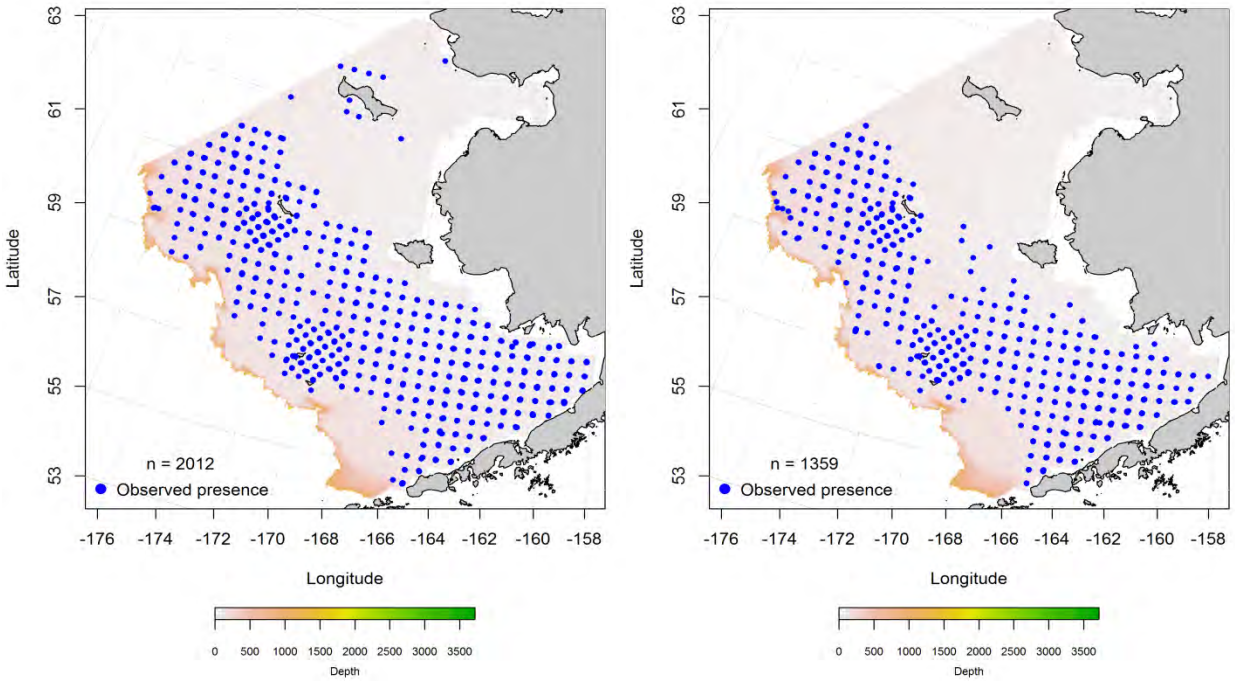

Figure 184. -- Distribution of late-juvenile (left) and adult (right) great sculpin catches from RACE summer bottom trawl surveys of the Eastern Bering Sea.

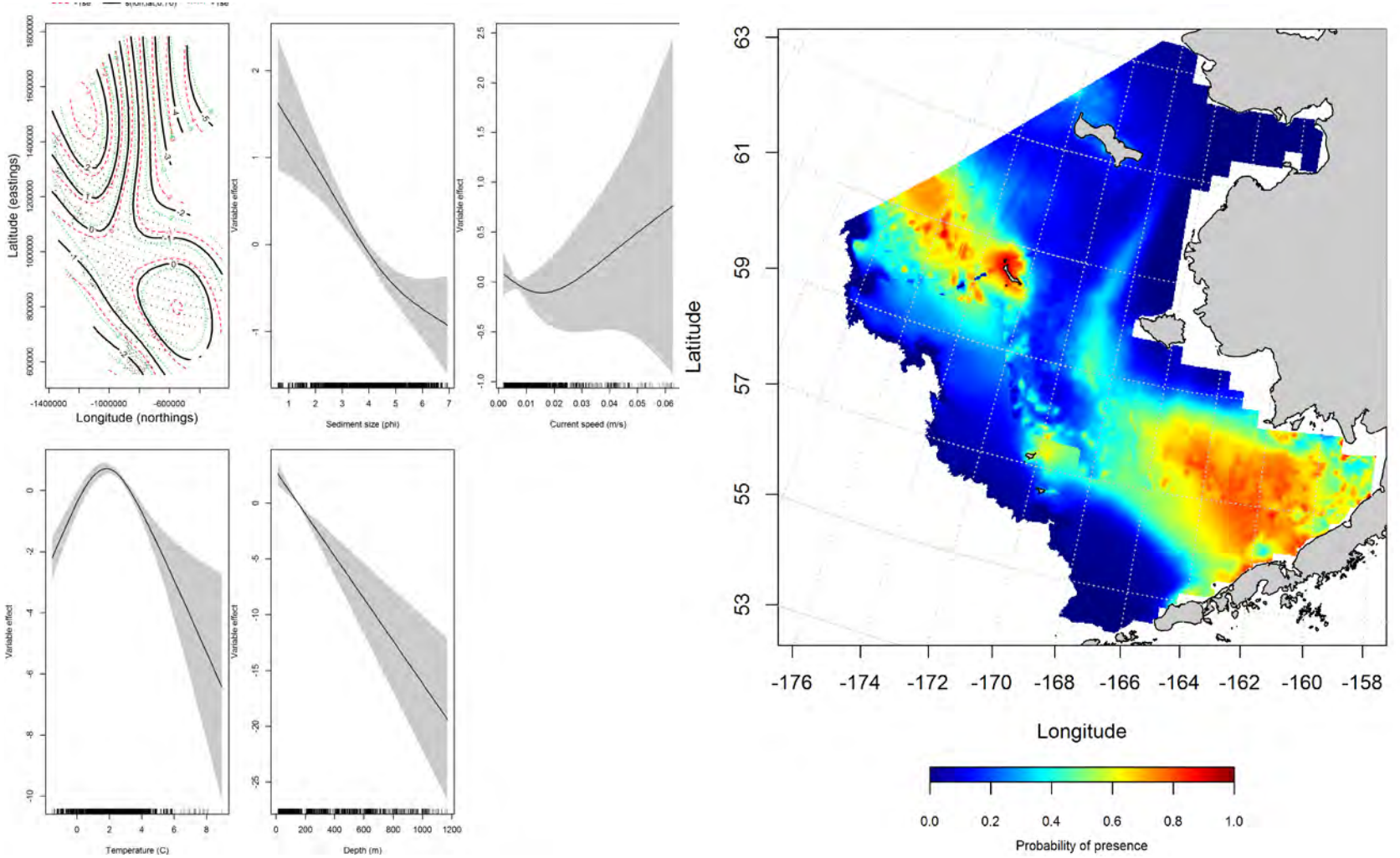

Figure 185. -- Effects of retained habitat covariates on the best-fitting generalized additive presence-absence model (GAM) of late juvenile great sculpin from RACE summer bottom trawl surveys of the Eastern Bering Sea Shelf, Slope, and Northern Bering Sea alongside their predicted presence (right panel).

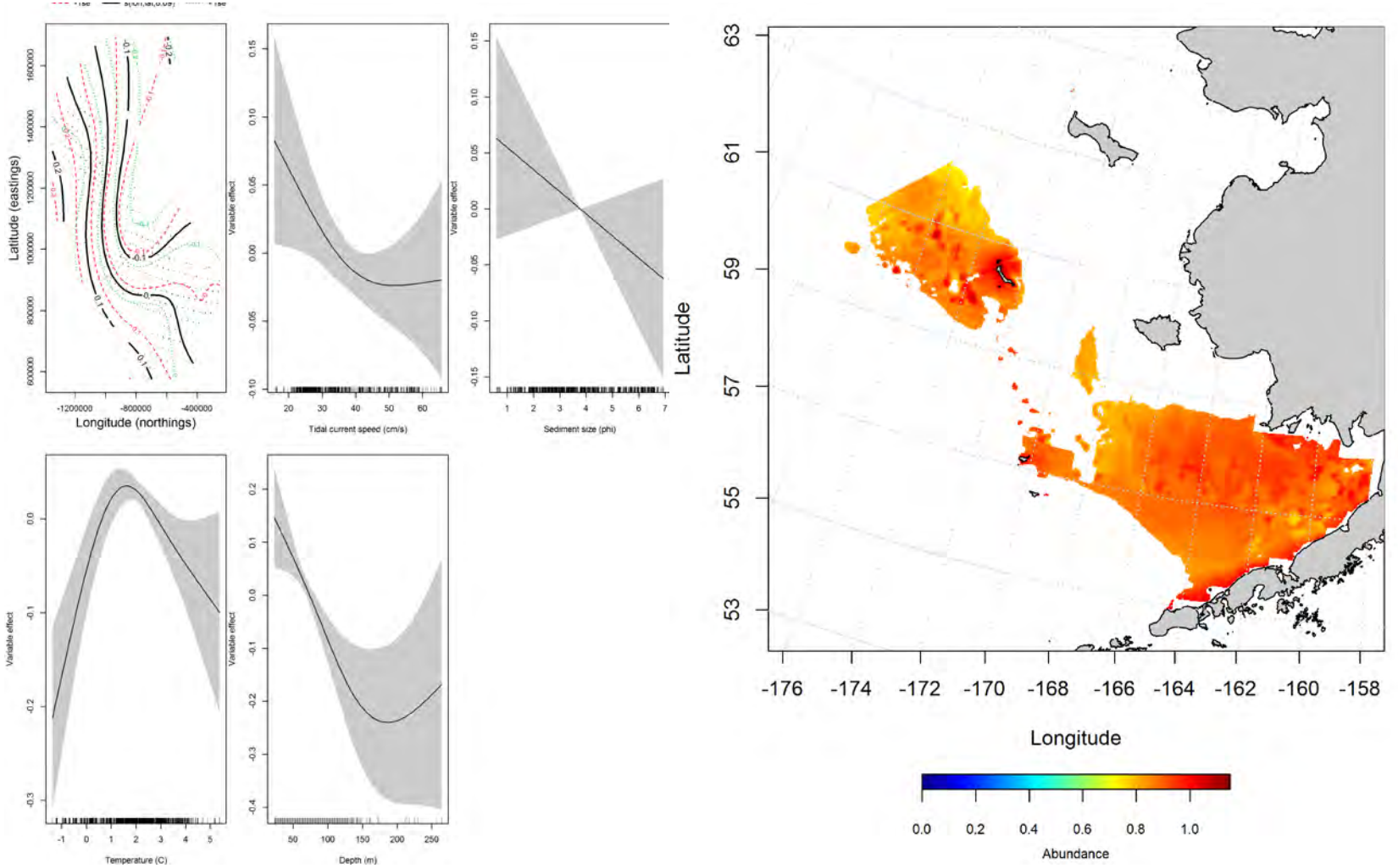

Figure 186. -- Effects of retained habitat covariates on the best-fitting generalized additive model (GAM) of late juvenile great sculpin from RACE summer bottom trawl surveys of the Eastern Bering Sea Shelf, Slope, and Northern Bering Sea alongside their predicted conditional abundance (right panel).

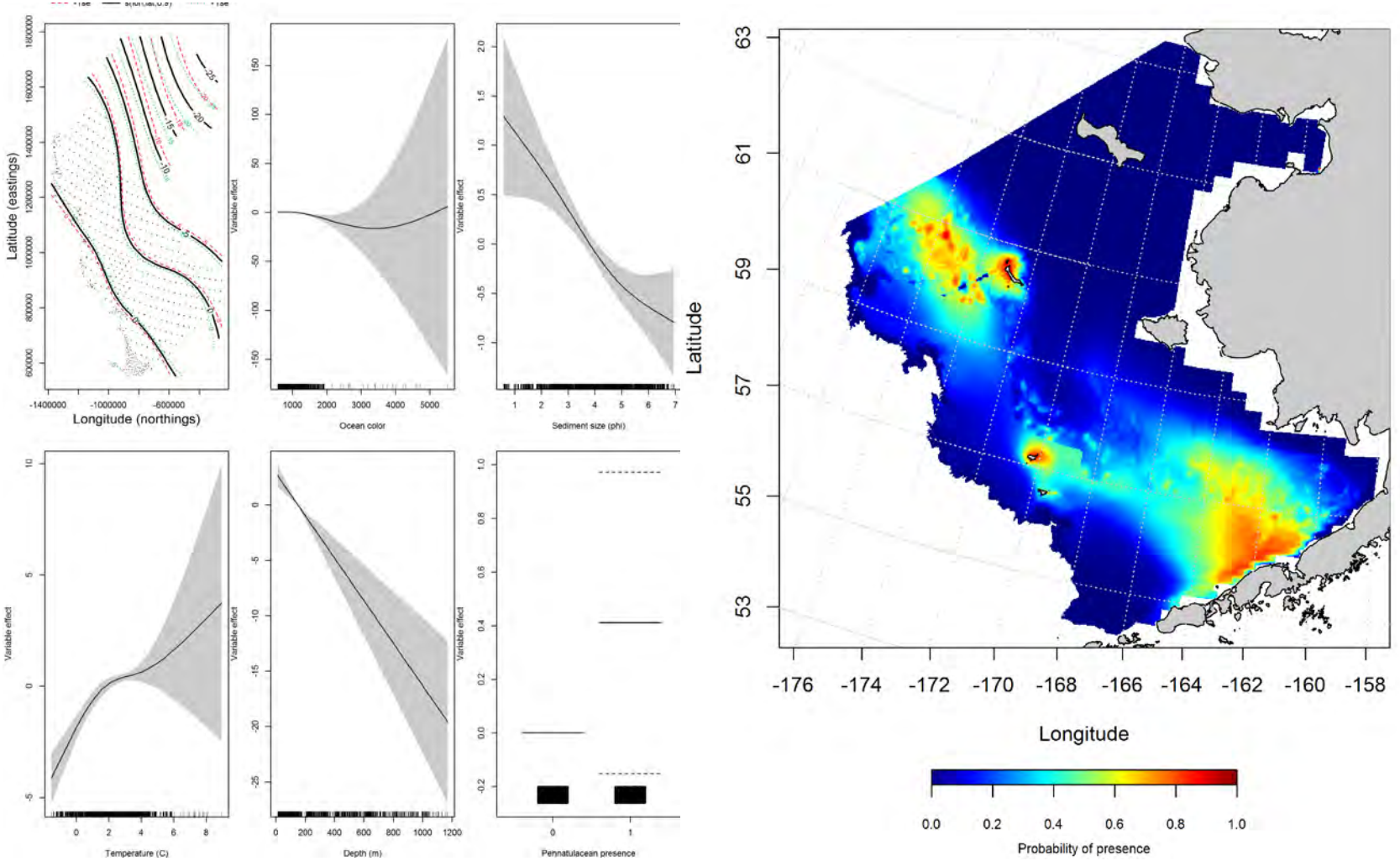

Figure 187. -- Effects of retained habitat covariates on the best-fitting generalized additive presence-absence model (GAM) of adult great sculpin from RACE summer bottom trawl surveys of the Eastern Bering Sea Shelf, Slope, and Northern Bering Sea alongside their predicted presence (right panel).

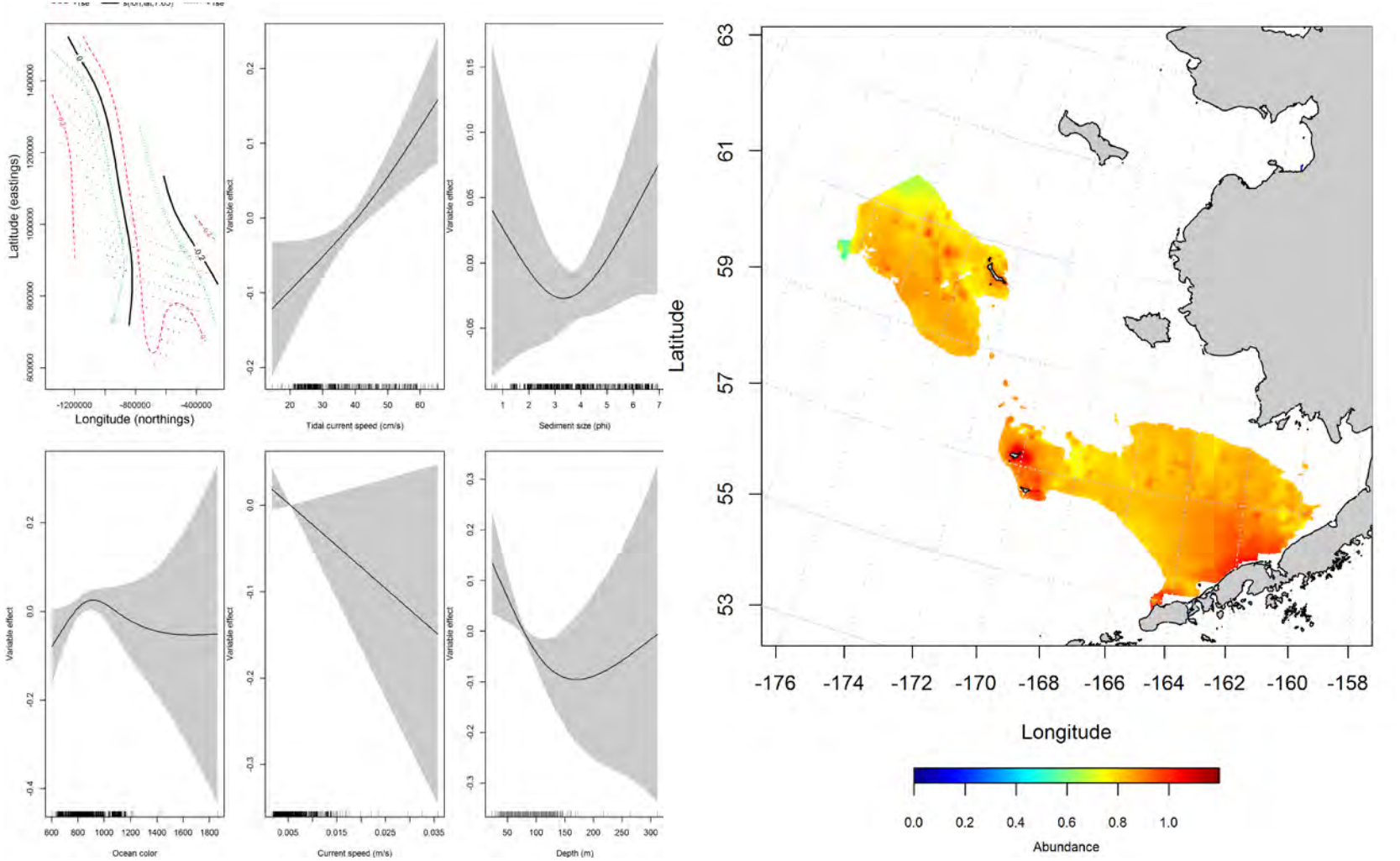

Figure 188. -- Effects of retained habitat covariates on the best-fitting generalized additive model (GAM) of adult great sculpin from RACE summer bottom trawl surveys of the Eastern Bering Sea Shelf, Slope, and Northern Bering Sea alongside their predicted conditional abundance (right panel).

Seasonal distribution of great sculpin in commercial fishery catches from the Eastern Bering Sea -- The distribution of great sculpin from commercial fishery catches during fall months in the Eastern Bering Sea was mainly in the southern and northern domains (Figure 189). Maximum entropy modeling predicts the highest probabilities of suitable great sculpin habitat around St. Matthew Island and over the middle shelf in the southern domain. Bottom depth, ocean productivity, tidal maxima, and bottom temperature represented a combined 87.9% of the relative importance of predictors in the model. The MaxEnt model was an outstanding fit to the training data (AUC = 0.91) with 83% of cases correctly classified. Fit of the model in the validation step was excellent (AUC = 0.82) and 82% of the cases were correctly classified for the test data set.

The winter distribution of great sculpin in commercial catches was tilted more toward the southern domain of the Eastern Bering Sea near the Alaska Peninsula (Figure 190). There were also some areas in the northern Bering Sea where there were clusters of catches. Bottom depth, tidal maxima, and bottom temperature dominated the habitat covariates in the model accounting for a combined 87.7% of the relative importance of predictor terms. The model predicted 86% of cases correctly and was an outstanding fit to the training data (AUC = 0.94). Model validation was successful (AUC = 0.83) and 83% of cases correctly predicted from the test data.

In springtime, great sculpin were widely represented over the middle and outer shelf (Figure 191). The area of highest probability for suitable habitat was near the Alaska Peninsula above Unimak Island. The most important predictors in the MaxEnt model were bottom depth, bottom temperature, and sediment grain size with a combined relative importance of 89.3%. The MaxEnt model was an outstanding fit to the training data (AUC = 0.93) and predicted 85% of cases correctly. Model validation was successful (AUC = 0.83) with 83% of cases correctly predicted from the test data.

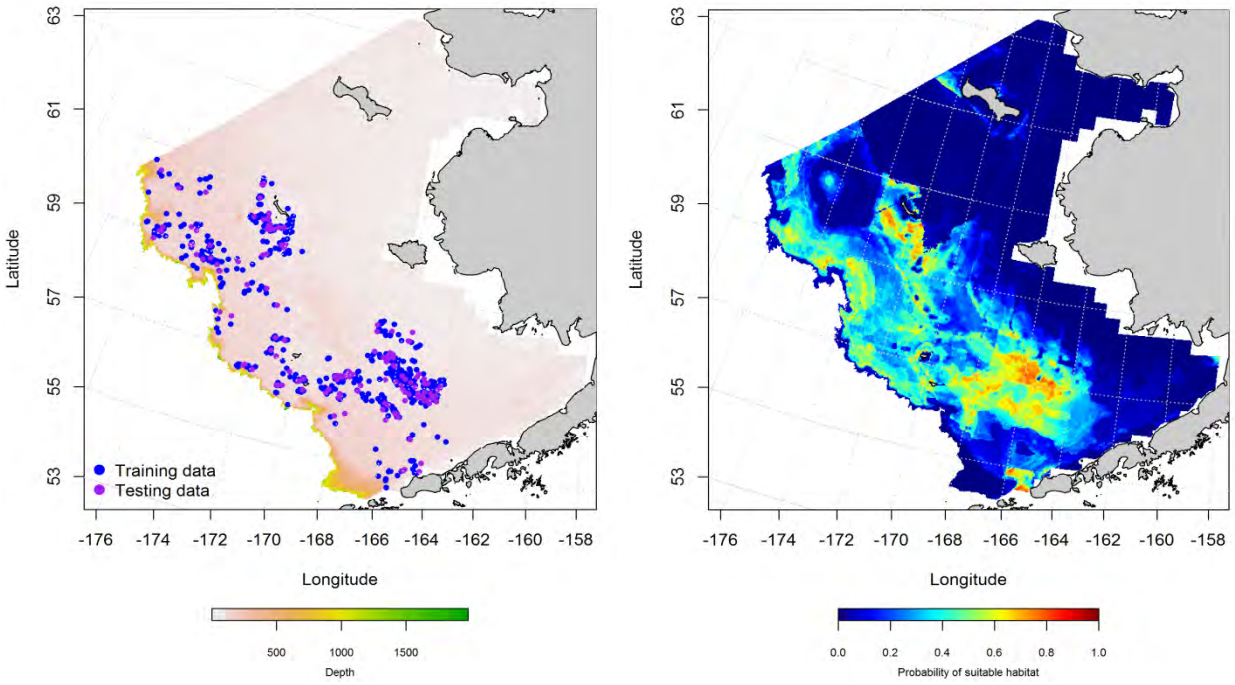

Figure 189. -- Presence of great sculpin in commercial fishery catches from fall (October-November; left panel). Blue points were used to train the maximum entropy (MaxEnt) model predicting the probability of suitable habitat (right panel) and the purple points were used to validate the model.

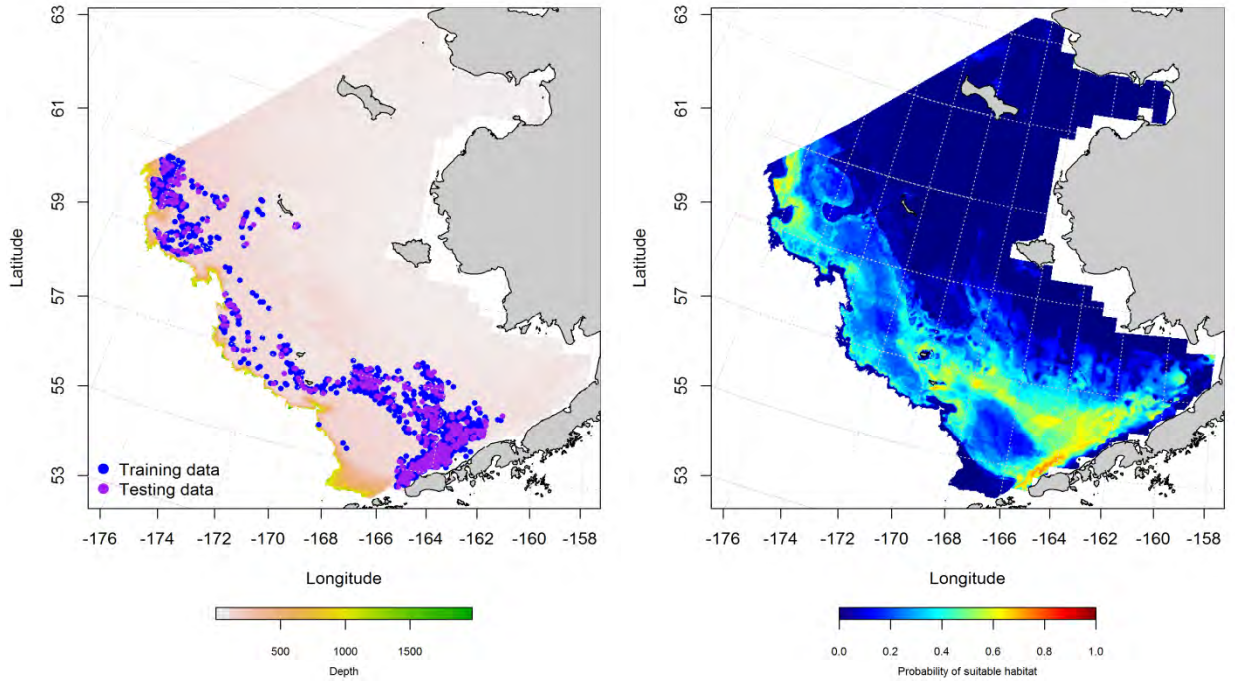

Figure 190. -- Presence of great sculpin in commercial fishery catches from winter (December-February; left panel). Blue points were used to train the maximum entropy (MaxEnt) model predicting the probability of suitable habitat (right panel) and the purple points were used to validate the model.

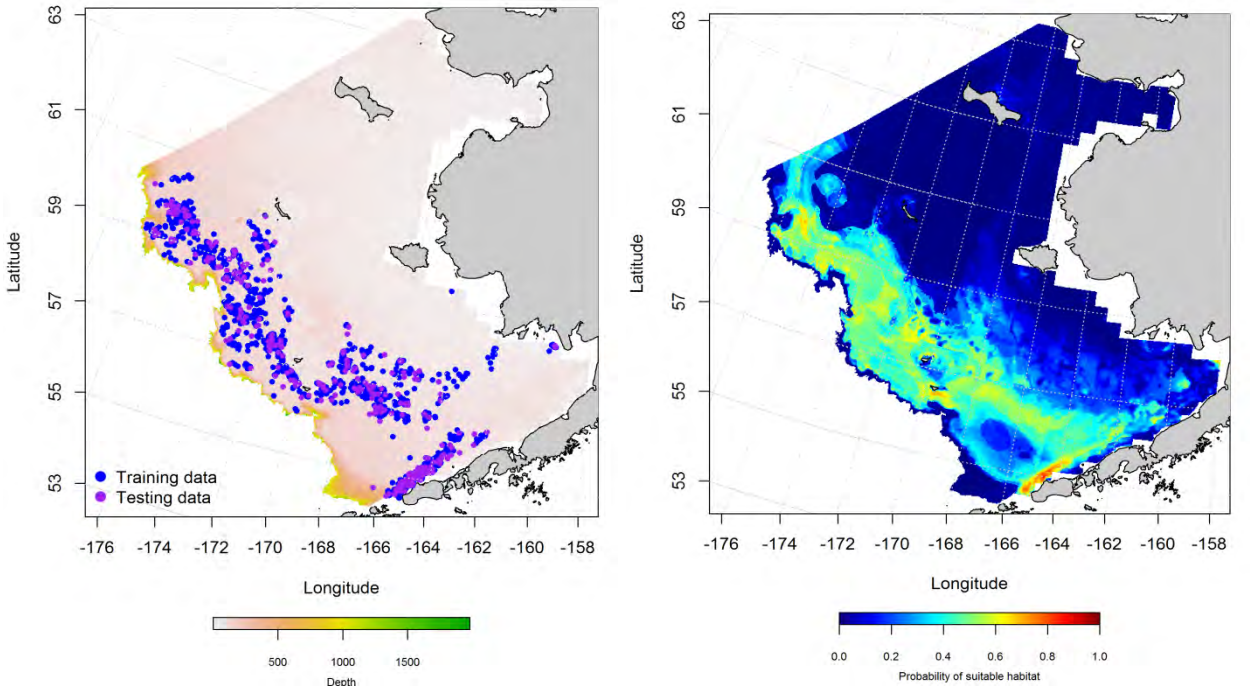

Figure 191. -- Presence of great sculpin in commercial fishery catches from spring (March-May; left panel). Blue points were used to train the maximum entropy (MaxEnt) model predicting the probability of suitable habitat (right panel) and the purple points were used to validate the model.

Essential fish habitat maps and conclusions for great sculpin (*Myoxocephalus polyacanthocephalus*) in the Eastern Bering Sea – Species distribution modeling of adult great sculpin in the Eastern Bering Sea predicts that EFH for this species varies some between life stages and seasons. For late juvenile and adult great sculpin from summertime RACE bottom trawl surveys of the Eastern Bering Sea, EFH was centered around St Matthew's Island and from the Pribilof Islands south and east into Bristol Bay (Figure 192). The late juvenile EFH extended further on to the inner shelf in Bristol Bay than did the adult EFH.

Predictions of suitable great sculpin habitat from commercial fishery catches in the Eastern Bering Sea showed some seasonal differences in terms of where the highest probability habitats were (Figure 193). However, the general pattern of EFH predicted from commercial catches was that suitable habitat for this species was found primarily in the central and southern domains.

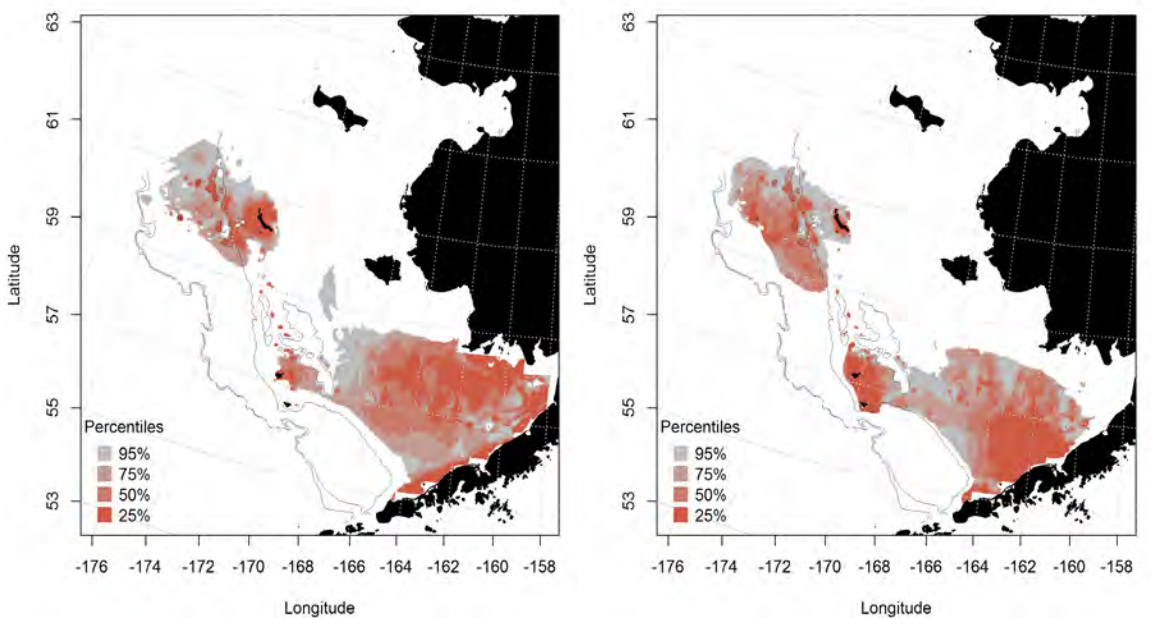

Figure 192. -- Essential fish habitat predicted for late juvenile and adult great sculpin (left and right panel) from summertime RACE bottom trawl surveys of the Eastern Bering Sea.

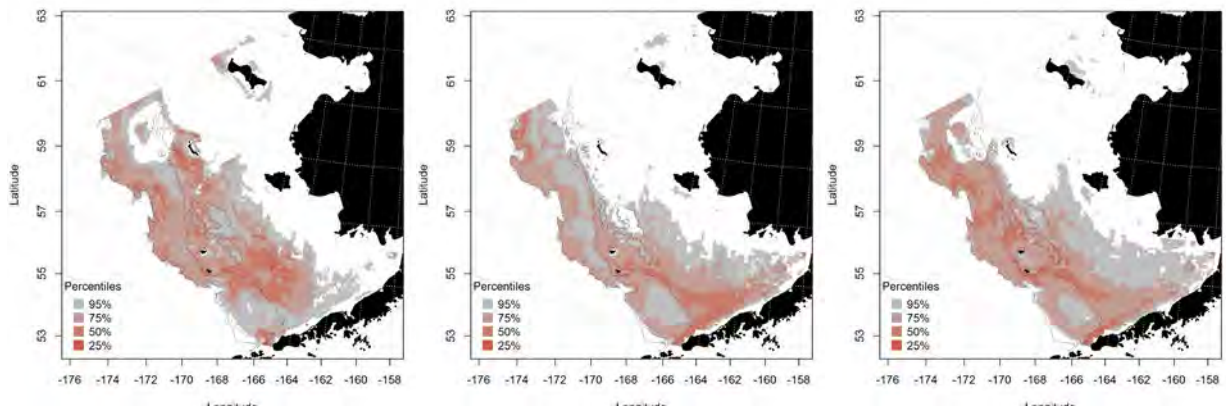

Figure 193. -- Essential fish habitat predicted from great sculpin occurrences in commercial fishery catches during fall (left panel), winter (middle panel), and spring (right panel) in the Eastern Bering Sea.

bigmouth sculpin (*Hemitripterus bolini*)

Bigmouth sculpin are found in depths ranging from 25 to 925 across the Eastern Bering Sea (Allen and Smith 1988). There are currently no targeted fisheries for bigmouth sculpins in Alaskan waters although they are often caught incidentally in commercial fishery catches.

Seasonal distribution of early life history stages of bigmouth sculpin from EcoFOCI ichthyoplankton surveys of the Eastern Bering Sea – Bigmouth sculpins have demersal eggs and pelagic larvae. There were three records of a larval bigmouth sculpin recorded on EcoFOCI ichthyoplankton surveys of the Eastern Bering Sea. No juveniles were reported. These were not sufficient data to undertake species distribution modeling for early life history stages of bigmouth sculpin.

Summertime distribution of late juvenile and adult bigmouth sculpin from RACE bottom trawl surveys of the Eastern Bering Sea – Late juvenile and adult bigmouth sculpins occurred in RACE bottom trawl survey catches across all 3 domains of the Eastern Bering Sea, but were limited to the middle and outer shelf (Figure 194). Late juvenile and adult distributions appeared to be largely coincident across the survey area. There were a few shallower records of late juveniles though.

A MaxEnt model predicted suitable habitat from the presence of late juvenile bigmouth sculpin observed in RACE summer bottom trawl surveys of the Eastern Bering Sea (Figure 195). High probability suitable habitat for this life stage was predicted in patches on the middle shelf north of the Pribilof Islands and along the upper slope edge of the outer shelf. Bottom depth, tidal maxima, and bottom temperature were the highest leverage habitat covariates amongst predictors in the model. Combined they accounted for 95.2% of the relative importance among predictor terms. The model indicates that occurrence of late juvenile bigmouth sculpin was more likely in water depths between 150 and 650 m over a range of moderate tidal maxima where water temperatures were > 1°C. The MaxEnt model was an outstanding fit to the training data (AUC = 0.93) and correctly classified 84% of predicted cases. In the model validation step, the MaxEnt model fit was excellent (AUC = 0.84), correctly classifying 84% of cases predicted from the test data.

A hurdle GAM was used to model adult bigmouth sculpin distribution in the Eastern Bering Sea. The best-fitting presence GAM predicted that all of the highest probability areas for encountering adult bigmouth sculpin in RACE summer bottom trawl survey catches were along the upper slope edge of the

outer shelf across all three domains of the Eastern Bering Sea (Figure 196). The GAM explained just 28.9% of the deviance in their distribution data. Geographical location, bottom depth, and sediment grain size were the most significant predictors retained in the model. The model effects indicate that adult bigmouth sculpin become less abundant going east from the shelf edge across the survey are, occurred at greater likelihood with increasing depth up to ca. 500 m, and were more common over finer sediments. The GAM was an excellent fit to the training data (AUC = 0.87) and correctly classified 79% of predicted cases of presence-absence. In the model validation step, the GAM fit was excellent (AUC = 0.86), correctly classifying 78% of cases predicted from the test data.

In the second step of the hurdle GAM, adult bigmouth sculpin abundance was predicted where the threshold for presence established in the first step was met. The best-fitting GAM for conditional abundance of bigmouth sculpins explained 19.4% of the deviance in their CPUE from RACE bottom trawl surveys of the Eastern Bering Sea (Figure 197). The most important habitat covariates retained in the model were geographic location and bottom slope. There was a slight increase in their abundance moving from south to north across the survey area and over increasing bottom slope. The highest conditional abundances of adult bigmouth sculpin were predicted along the upper slope edge of the outer shelf. Model fits were poor for the training and test data sets (r^2 = 0.19 and 0.09).

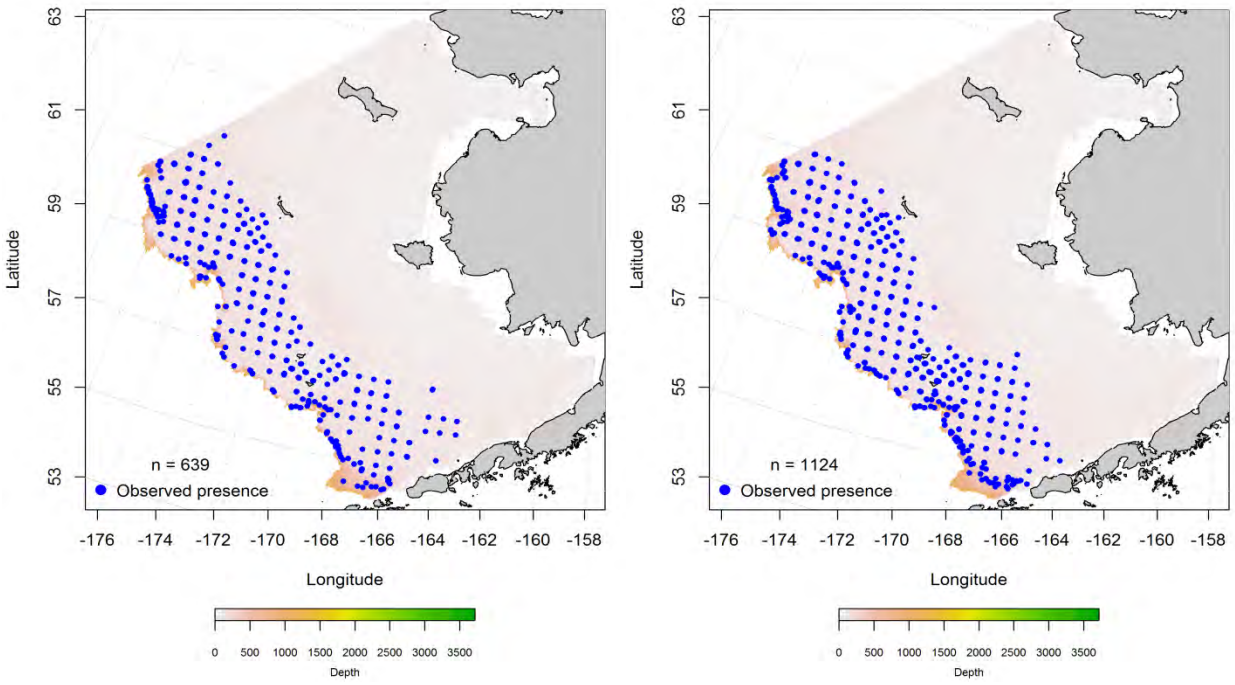

Figure 194. -- Distribution of late-juvenile (left) and adult (right) bigmouth sculpin catches from RACE summer bottom trawl surveys of the Eastern Bering Sea.

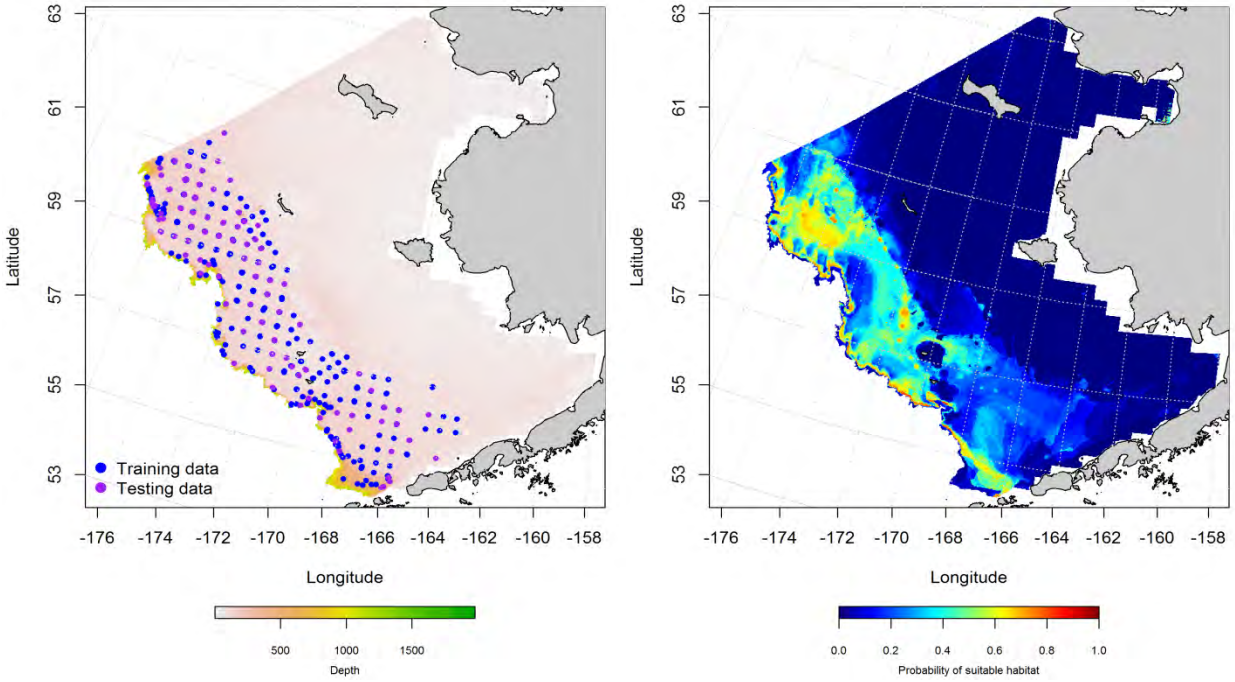

Figure 195. -- Locations of summer RACE summer bottom trawl survey catches of juvenile bigmouth sculpin (left panel). Blue points were used to train the maximum entropy (MaxEnt) model predicting the probability of suitable habitat (right panel) and the purple points were used to validate the model.

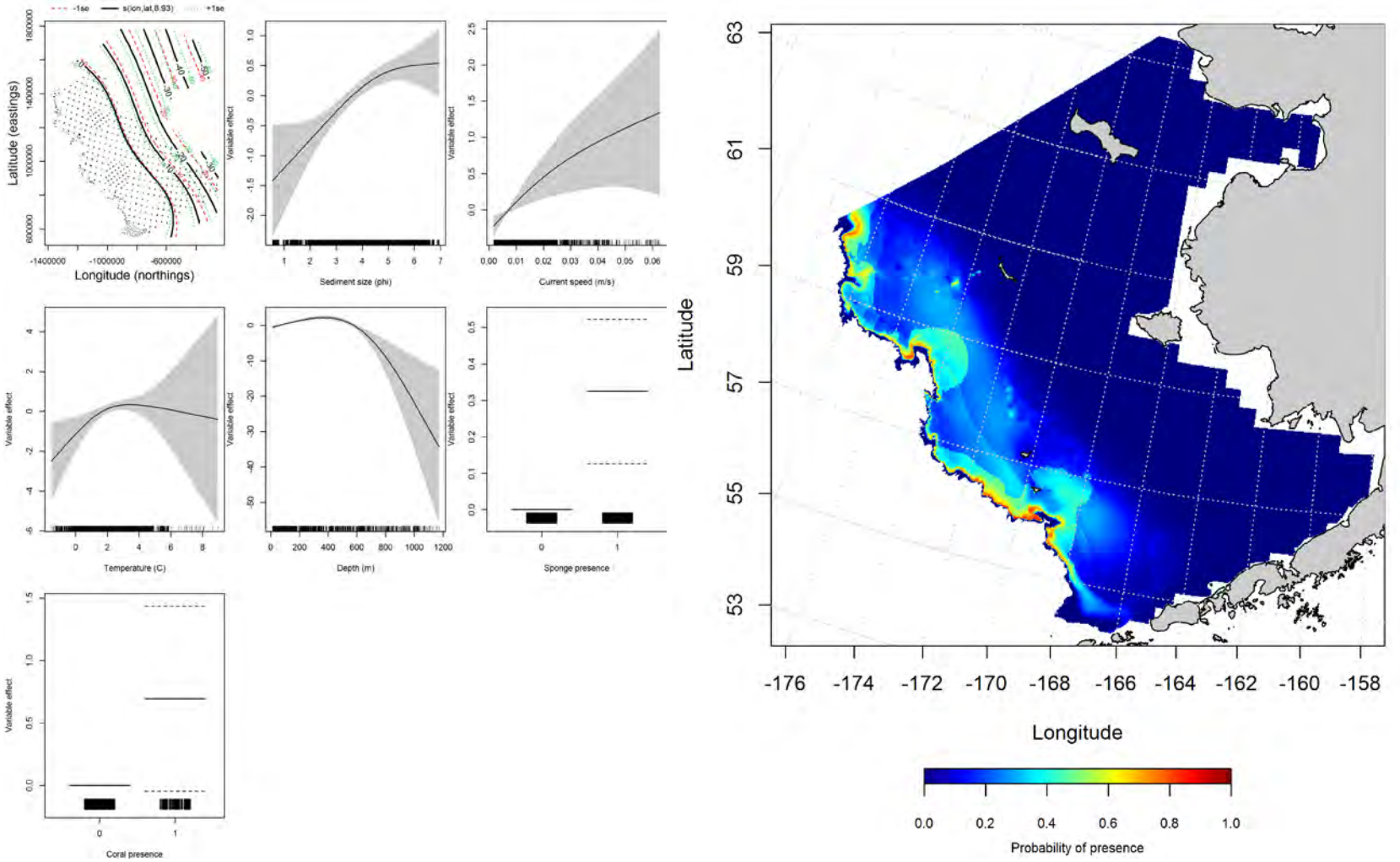

Figure 196. -- Effects of retained habitat covariates on the best-fitting generalized additive presence-absence model (GAM) of adult bigmouth sculpin from RACE summer bottom trawl surveys of the Eastern Bering Sea Shelf, Slope, and Northern Bering Sea alongside their predicted presence (right panel).

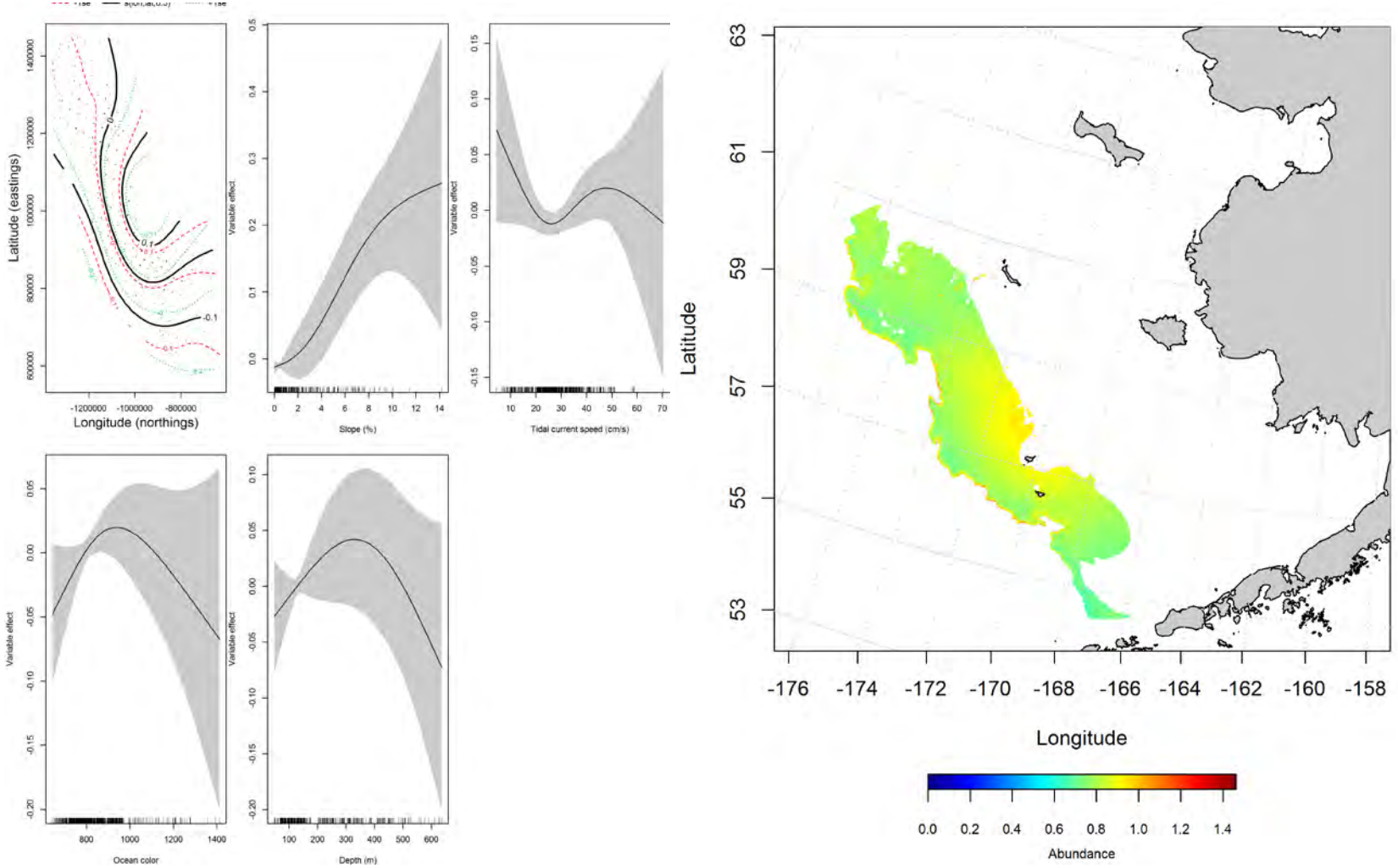

Figure 197. -- Effects of retained habitat covariates on the best-fitting generalized additive model (GAM) of adult bigmouth sculpin from RACE summer bottom trawl surveys of the Eastern Bering Sea Shelf, Slope, and Northern Bering Sea alongside their predicted conditional abundance (right panel).

Seasonal distribution of bigmouth sculpin in commercial fishery catches from the Eastern Bering Sea -- The distribution of bigmouth sculpin from commercial fishery catches during fall months in the Eastern Bering Sea was mostly spread across the central and northern domains (Figure 198). Maximum entropy modeling predicts the highest probabilities of suitable adult bigmouth sculpin habitat near the head of Zhemchug Canyon and along the upper slope edge of the outer shelf. Bottom depth, ocean productivity, and bottom temperature represented a combined 98% of the relative importance of predictors in the model. The MaxEnt model was an outstanding fit to the training data (AUC = 0.92) with 85% of cases correctly classified. Fit of the model in the validation step was excellent (AUC = 0.83) and 83% of the cases were correctly classified for the test data set.

The winter distribution of bigmouth sculpin in commercial catches extended further into the southern domain of the Eastern Bering Sea than did the fall distribution (Figure 199). The higher probability habitats remained to the north of the southern domain and along the upper slope edge. Bottom depth and bottom temperature dominated the habitat covariates in the model accounting for a combined 90.9% of the relative importance of predictor terms. The model correctly predicted 85% of cases and was an outstanding fit to the training data (AUC = 0.93). Model validation was successful (AUC = 0.86) and 86% of cases correctly predicted from the test data.

In springtime, bigmouth sculpin were primarily found in commercial catches from the central and northern domains and over the Bering Canyon north of Unimak Pass (Figure 200). The area of highest probability for suitable habitat was west of the Pribilof Islands and north to Zhemchug Canyon. The most important predictors in the MaxEnt model were bottom depth and bottom temperature with a combined relative importance of 85%. The MaxEnt model was an outstanding fit to the training data (AUC = 0.94) and predicted 87% of cases correctly. Model validation was successful (AUC = 0.86) with 86% of cases correctly predicted from the test data.

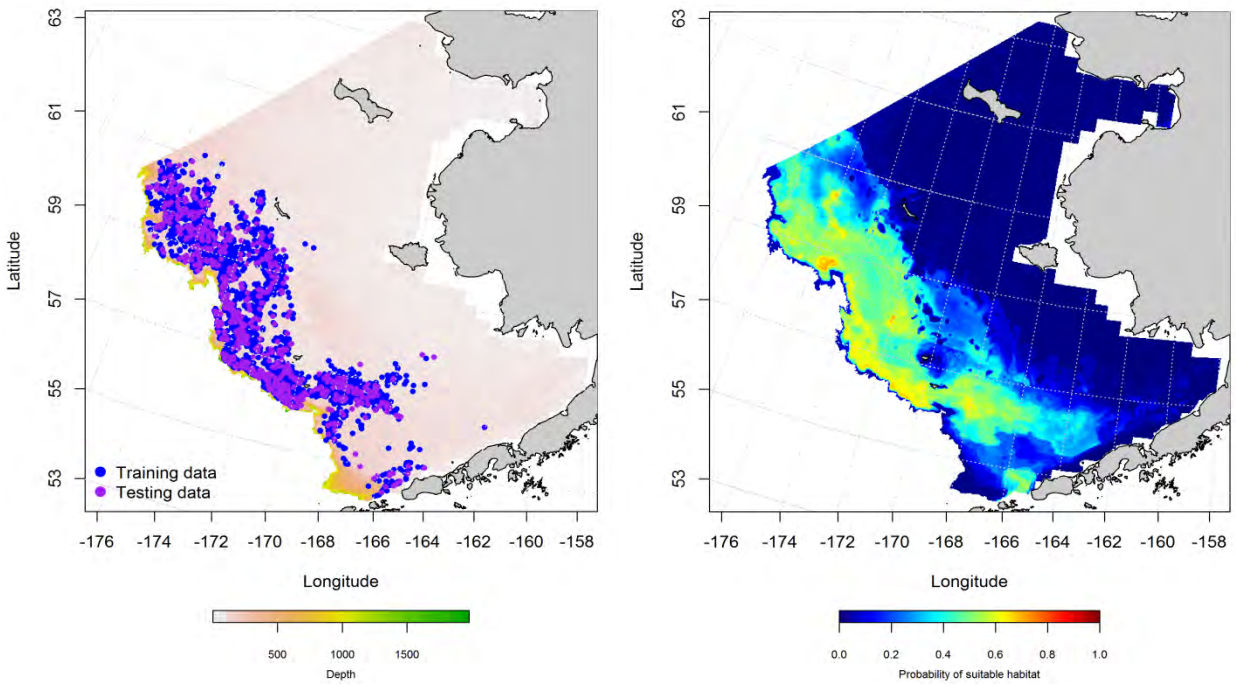

Figure 198. -- Presence of bigmouth sculpin in commercial fishery catches from fall (October-November; left panel). Blue points were used to train the maximum entropy (MaxEnt) model predicting the probability of suitable habitat (right panel) and the purple points were used to validate the model.

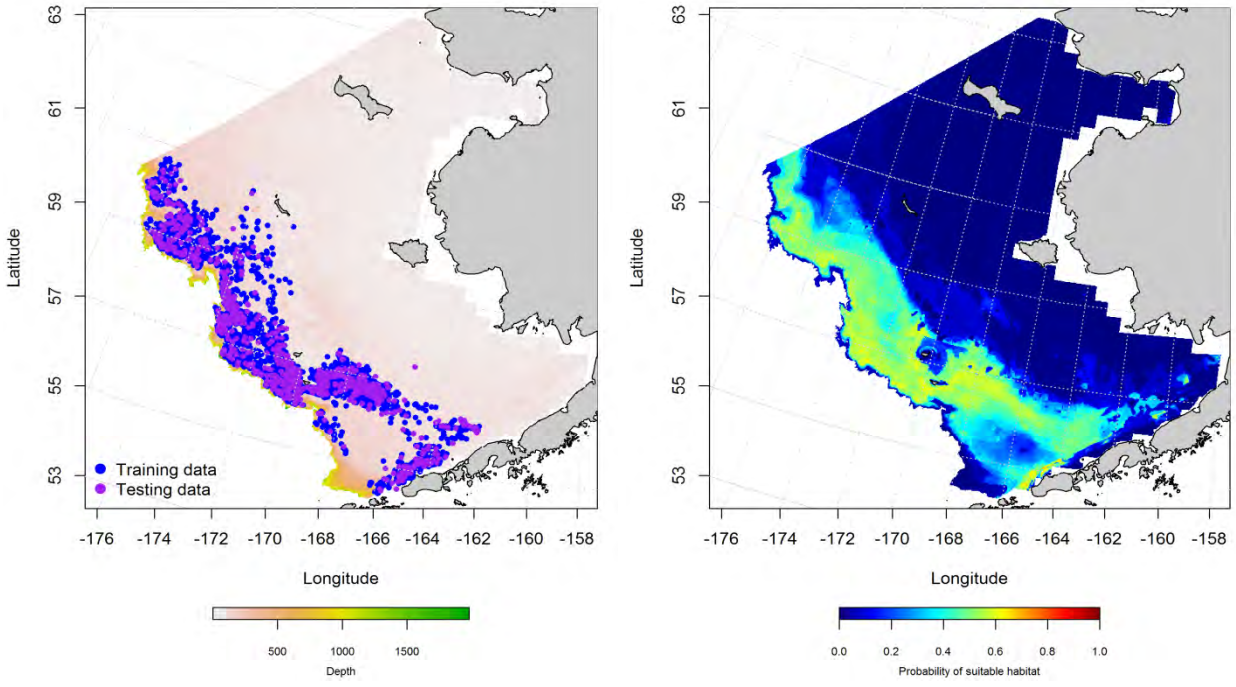

Figure 199. -- Presence of bigmouth sculpin in commercial fishery catches from winter (December-February; left panel). Blue points were used to train the maximum entropy (MaxEnt) model predicting the probability of suitable habitat (right panel) and the purple points were used to validate the model.

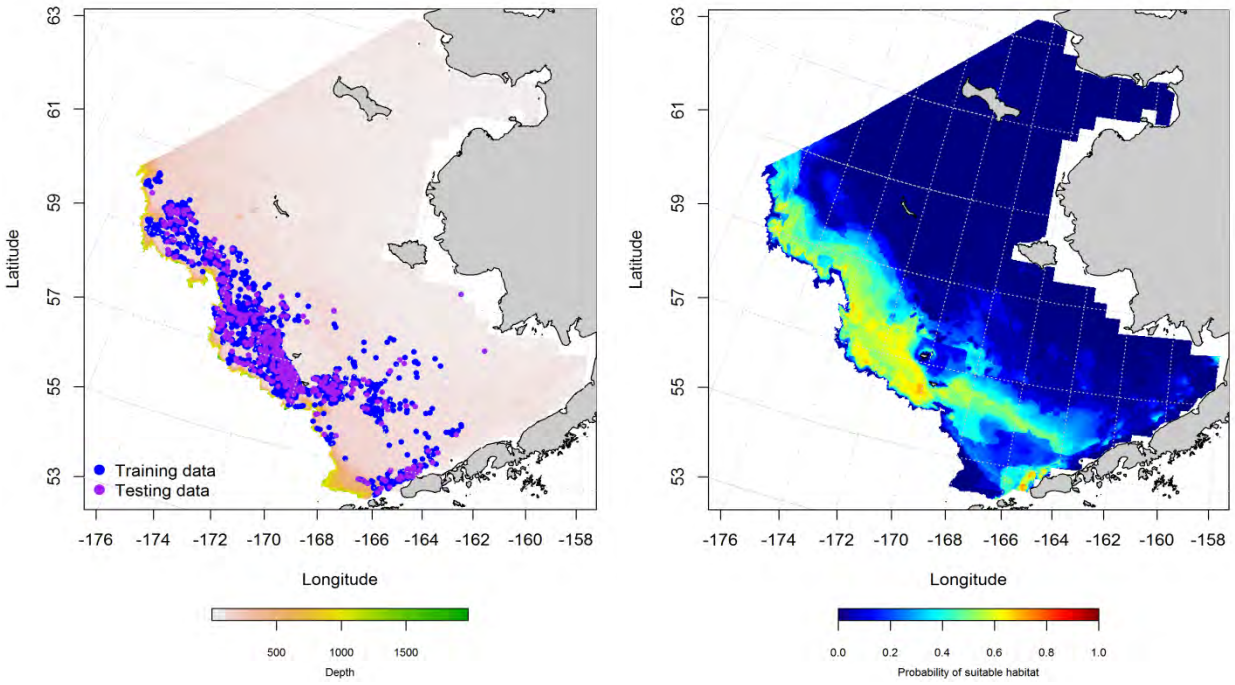

Figure 200. -- Presence of bigmouth sculpin in commercial fishery catches from spring (March-May; left panel). Blue points were used to train the maximum entropy (MaxEnt) model predicting the probability of suitable habitat (right panel) and the purple points were used to validate the model.

Essential fish habitat maps and conclusions for bigmouth sculpin (*Hemitripterus bolini*) in the Eastern Bering Sea – Species distribution modeling of adult bigmouth sculpin in the Eastern Bering Sea predicts that EFH for this species varies between life stages and seasons. For late juvenile and adult bigmouth sculpin from summertime RACE bottom trawl surveys, EFH was found across all three domains of the Eastern Bering Sea but primarily offshore of the 100 m isobath (Figure 201). Summertime adult bigmouth sculpin EFH was absent from much of the southern domain in contrast to that of the late juveniles.

Predictions of suitable bigmouth sculpin habitat from commercial fishery catches in the Eastern Bering Sea showed some minor seasonal differences (Figure 202). However, the general pattern from commercial catches was that EFH for this species was largely coincident across seasons. These EFH

predictions also confirm what was observed in other data sets that this species' distribution is in deeper waters near the shelf edge.

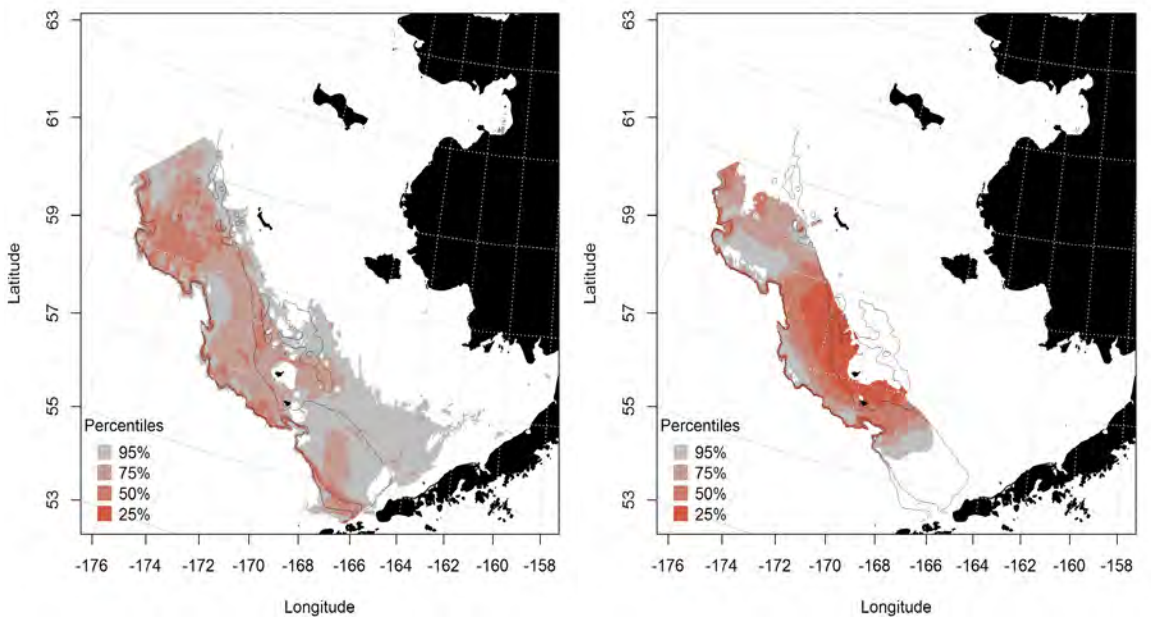

Figure 201. -- Essential fish habitat predicted for late juvenile and adult bigmouth sculpin (left and right panel) from summertime RACE bottom trawl surveys of the Eastern Bering Sea.

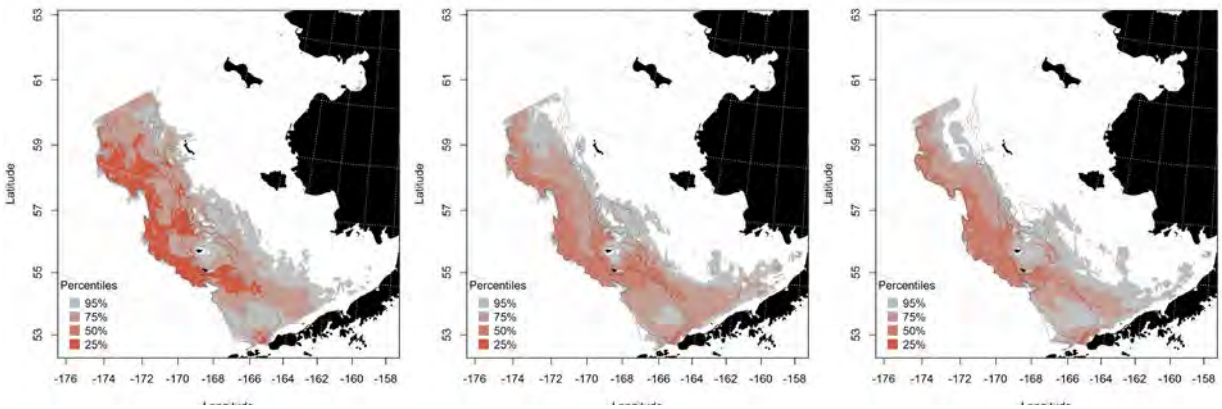

Figure 202. -- Essential fish habitat predicted from bigmouth sculpin occurrences in commercial fishery catches during fall (left panel), winter (middle panel), and spring (right panel) in the Eastern Bering Sea.

rockfishes (*Sebastes* spp.)

Rockfishes (*Sebastes* spp.) are ovoviviparous with internal fertilization and they give birth to live larvae. Their larvae and early juveniles cannot be readily distinguished from other species in the genus using visible external characters alone. One exception to this rule is that larval Pacific ocean perch (*Sebastes alutus*) can be identified to species but were rare in EcoFOCI ichthyoplankton collections from the Eastern Bering Sea (1 presence record) so they are not treated separately in this early life history section. Therefore we combined the early life stages of this genus in the EcoFOCI data for distribution modeling.

Seasonal distribution of early life history stages of *Sebastes* spp. in the Eastern Bering Sea – Larval rockfishes were collected on EcoFOCI ichthyoplankton surveys of the Eastern Bering Sea in winter, spring, and summer months (Figure 203). Larval *Sebastes* spp. were uncommon in winter months, were found primarily in the western portions of the central and southern domains of the EBS in springtime, and were prevalent across the survey area during summer. There were sufficient data to undertake distribution modeling for *Sebastes* spp. larvae for the spring and summer seasons.

Maximum entropy model predictions of suitable larval *Sebastes* spp. habitat differed between spring and summer (Figure 204). In the spring, suitable habitat was predicted primarily over the Bering Canyon and benthypelagic waters. In summertime, predicted suitable habitat extended northward to Pribilof Canyon and around the Pribilof Islands. The most important covariates predicting suitable larval *Sebastes* spp. habitat in both of these seasons were sea surface temperature and bottom depth. The combined relative importance of these habitat covariates was 88.6% in springtime and 68.3% in summer. For both seasons' training data sets, the MaxEnt model fit was outstanding (AUC = 0.97 in spring and 0.93 in summer). The spring model correctly predicted 91% of presence-absence cases while the summer model correctly predicted 86%. Model validation was successful (AUC = 0.92 in spring and 0.82 in summer), and correctly predicted 92% and 82% of cases from the test data in the two seasons.

There were 31 stations on EcoFOCI ichthyoplankton surveys where early juvenile stages of *Sebastes* spp. were observed (Figure 205). These were all during summer months and were mostly observed near the

Pribilof Islands although a handful of observations occurred over the middle shelf in the southern domain of the Eastern Bering Sea. These records did not provide sufficient data to parameterize species distribution models for early juvenile stages of *Sebastes* spp.

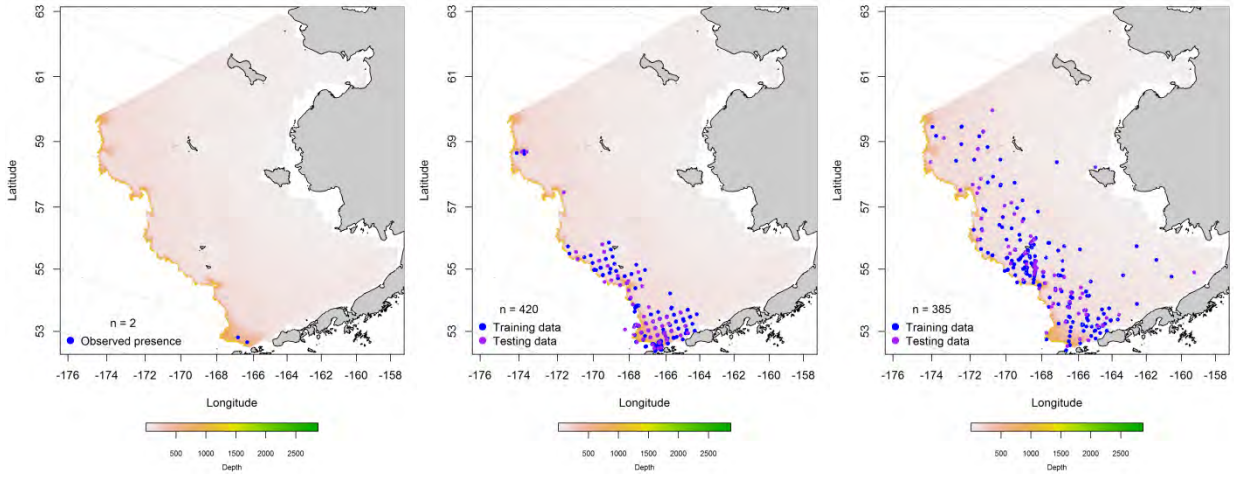

Figure 203. -- Winter, spring, and summer observations (left, middle, and right panel, respectively) of larval *Sebastes* spp. from the Eastern Bering Sea.

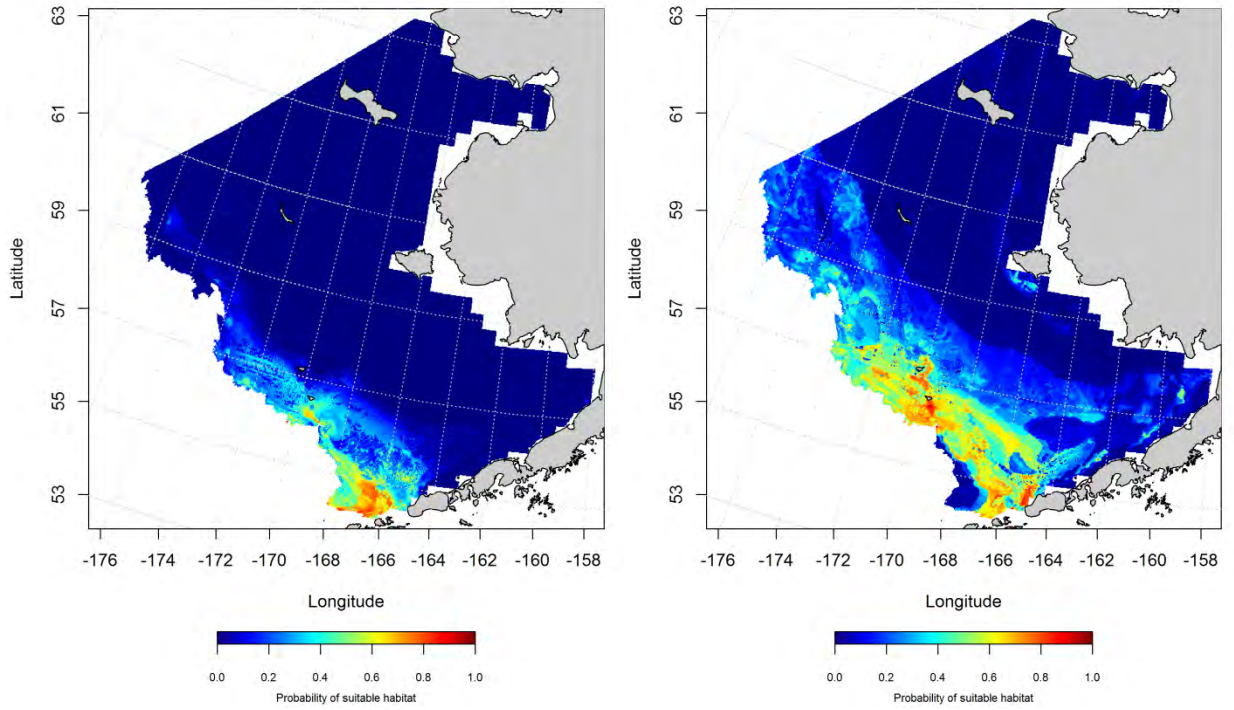

Figure 204. -- Probability of suitable larval *Sebastes* spp. spring and summer habitat (left and right panel) from MaxEnt modeling of their presences in EcoFOCI ichthyoplankton surveys of the Eastern Bering Sea.

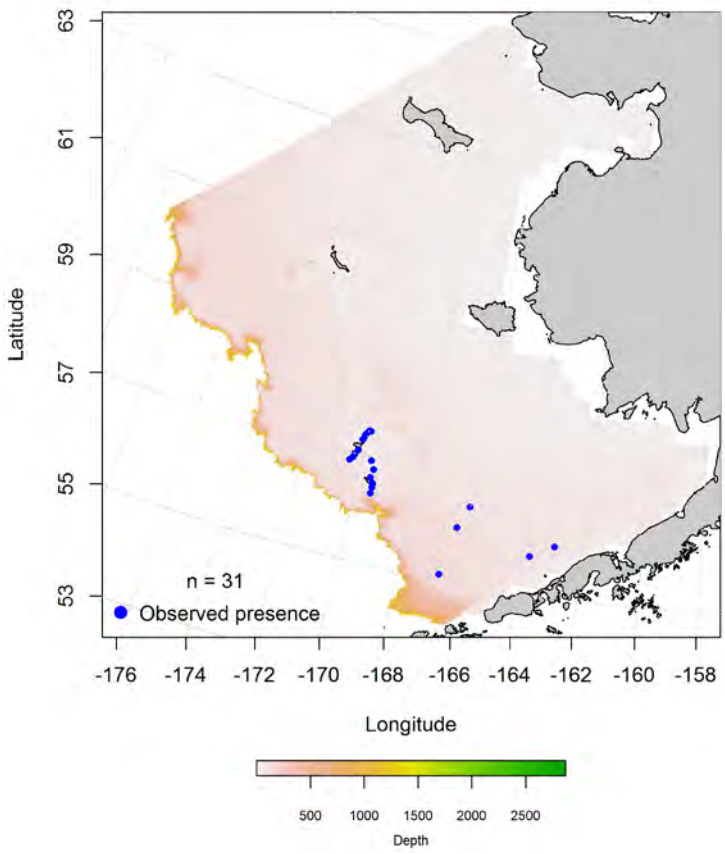

Figure 205. -- Summer catches of early juvenile *Sebastes* spp. in the Eastern Bering Sea.

Essential fish habitat maps and conclusions for larval *Sebastes* spp. in the Eastern Bering Sea Eastern Bering Sea -- Essential larval *Sebastes* spp. habitat differed in the spring and summer months (Figure 206). In springtime, EFH was constrained to the central and southern domains primarily offshore of the 100 m isobath. During summer surveys, EFH extended north to the northern limit of the survey area and east onto the inner shelf in Bristol Bay.

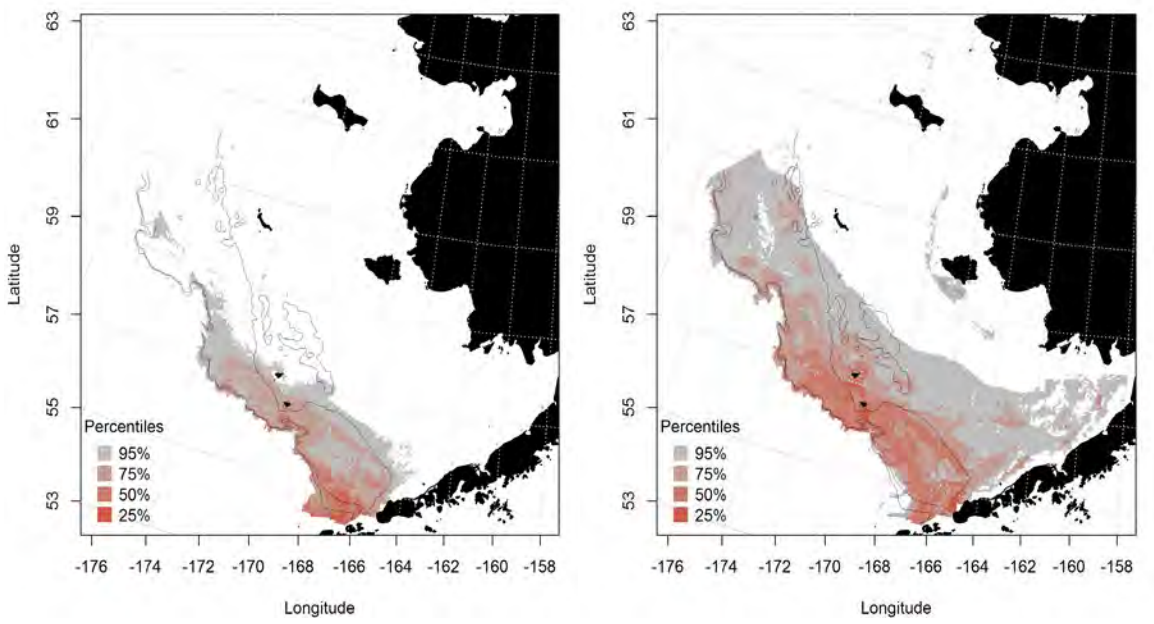

Figure 206. -- Spring and summer essential larval *Sebastes* spp. habitat (right and left panel) predicted from EcoFOCI ichthyoplankton surveys of the Eastern Bering Sea.

rougheye rockfish (*Sebastes aleutianus*)

Rougheye rockfish are distributed across the North Pacific from Japan and Russia to Alaska in the Bering Sea and Aleutian Islands and south into central California. They are not common in summertime RACE bottom trawl surveys of the Eastern Bering Sea. In Bering Sea fisheries, North Pacific Fishery Management Council (NPFMC) manages rougheyes as a complex as a complex with blackspotted rockfish (*S. melanostictus*).

Summertime distribution of late juvenile and adult rougheye rockfish from RACE bottom trawl surveys of the Eastern Bering Sea – Late juvenile and adult rougheye rockfish occurred in RACE summer bottom trawl surveys of the Eastern Bering Sea in (Figure 207). In recent years, they have occurred at up to 4% of the stations sampled on the summer trawl surveys. Both life stages were encountered primarily in shelf edge and slope waters > 200 m in depth. The number of catches available

for analyses was not sufficient to parameterize a species distribution model for rougheye rockfish from RACE summer bottom trawl surveys of the Eastern Bering Sea.

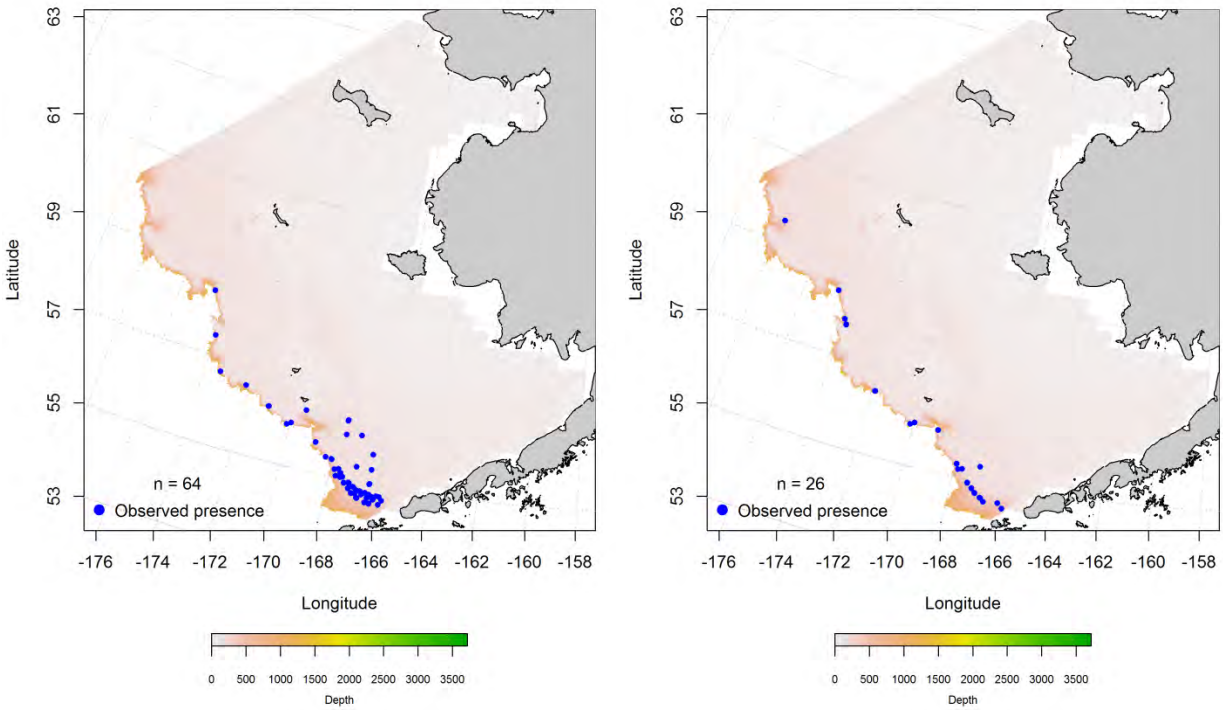

Figure 207. -- Distribution of late-juvenile (left) and adult (right) rougheye rockfish catches from RACE summer bottom trawl surveys of the Eastern Bering Sea.

Seasonal distribution of the rougheye/blackspotted rockfish complex in commercial fishery catches from the Eastern Bering Sea – Rougheye and blackspotted rockfishes are difficult to separate in the field. They are not separated in commercial catches from Alaska. The two species are managed together as a complex by the NPFMC.

In fall, rougheye/blackspotted rockfish were reported from commercial catches in the Eastern Bering Sea from the Bering Canyon in the south to Pervenets Canyon in the north (Figure 208). Maximum entropy models based on this rougheye/blackspotted rockfish presence data predicted the highest probability of suitable habitat along the shelf edge between Pribilof and Zhemchug Canyons. Depth and bottom

temperature were the dominant habitat covariates in the model comprising 77.9% of the relative importance of predictor terms. The fit of the MaxEnt model to the training data was outstanding (AUC = 0.99) and it correctly predicted 96% of cases. Model validation was successful (AUC = 0.92) and 92% of cases predicted from the test data set were correct.

In winter, the distribution of rougheye/blackspotted rockfish in commercial catches was similar to fall but with the addition of a few occurrences near Navarin Canyon and further east along the Bering Canyon axis (Figure 209). The highest probability suitable habitat areas predicted from the MaxEnt model were located over the Bering Canyon and near the head of Pribilof Canyon. Depth and bottom temperature provided 88.3% of the leverage from habitat covariates in the model. The fit of the MaxEnt model to the training data was outstanding (AUC = 1.0) and it correctly predicted 96% of cases. Model validation was successful (AUC = 0.93) and 93% of cases predicted from the test data set were correct.

Spring distribution of rougheye/blackspotted rockfish in commercial catches extended from the Bering to Navarin Canyon primarily over the upper slope edge (Figure 210). Once again the highest probability suitable habitat areas predicted from the MaxEnt model were located over the Bering Canyon and near the head of Pribilof Canyon. Depth and bottom temperature comprised 88.5% of the leverage from habitat covariates in the model. The MaxEnt fit to the training data was outstanding (AUC = 1.0) and correctly predicted 98% of cases. Model validation was successful based both on the high AUC (0.92) and the 92% of cases correctly classified by the test data.

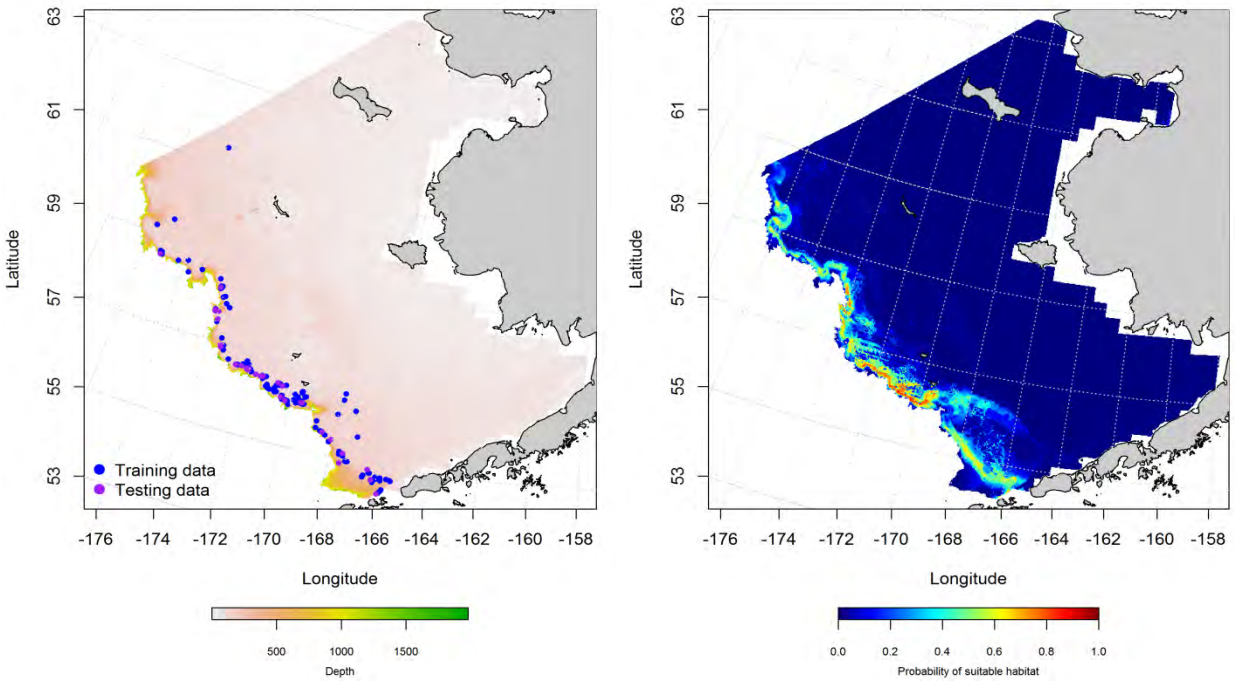

Figure 208. -- Locations of fall (October-November) catches of rougheye/blackspotted rockfish complex in commercial fisheries of the Eastern Bering Sea (left panel). Blue points were used to train the MaxEnt model predicting the probability of suitable habitat (right panel) and the purple points were used to validate the model.

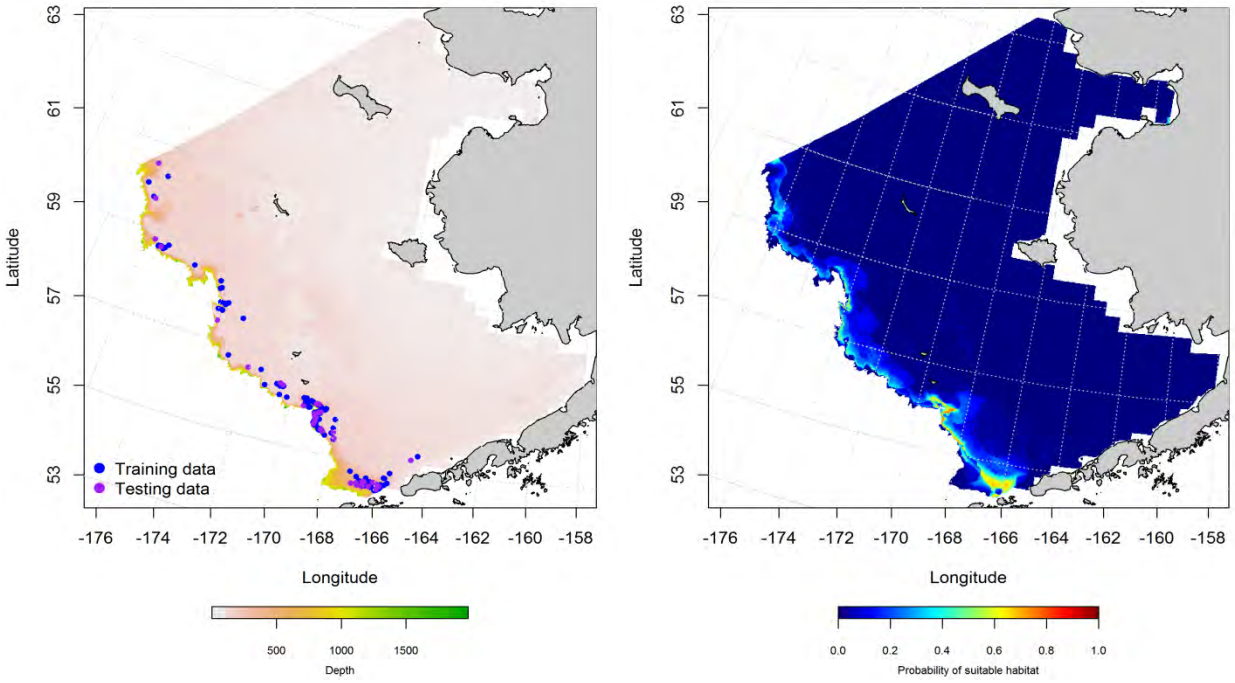

Figure 209. -- Locations of winter (December-February) catches of rougheye/blackspotted rockfish complex in commercial fisheries of the Eastern Bering Sea (left panel). Blue points were used to train the

MaxEnt model predicting the probability of suitable habitat (right panel) and the purple points were used to validate the model.

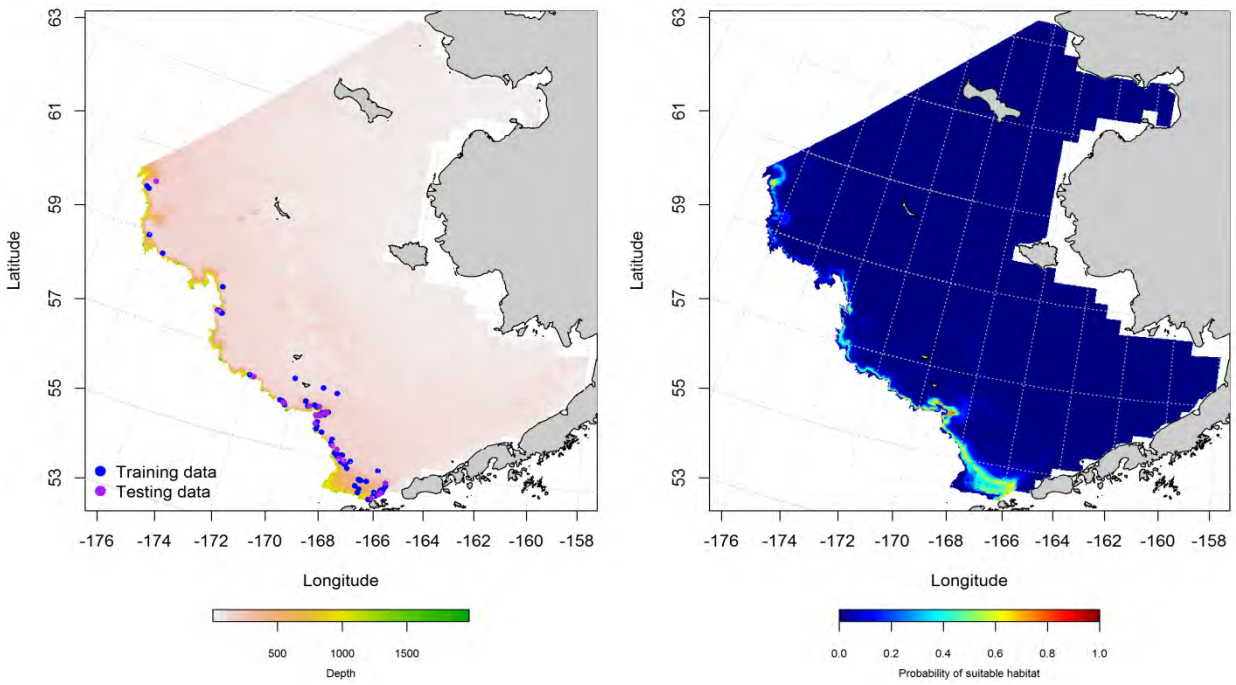

Figure 210. -- Locations of spring (March-May) catches of rougheye/blackspotted rockfish complex in commercial fisheries of the Eastern Bering Sea (left panel). Blue points were used to train the MaxEnt model predicting the probability of suitable habitat (right panel) and the purple points were used to validate the model.

Essential fish habitat maps and conclusions for rougheye/blackspotted rockfish complex in the Eastern Bering Sea -- Essential fish habitat for rougheye/blackspotted rockfish complex extends from Navarin Canyon in the northern domain of the eastern Bering Sea to the Bering Canyon in the southern domain (Figure 211). Habitat for these fishes predicted from their presence in commercial catches is primarily in waters deeper than 200 m along the shelf edge and slope. There is little seasonal difference in the EFH predicted from commercial catches of rougheye/blackspotted rockfish complex from the Eastern Bering Sea.

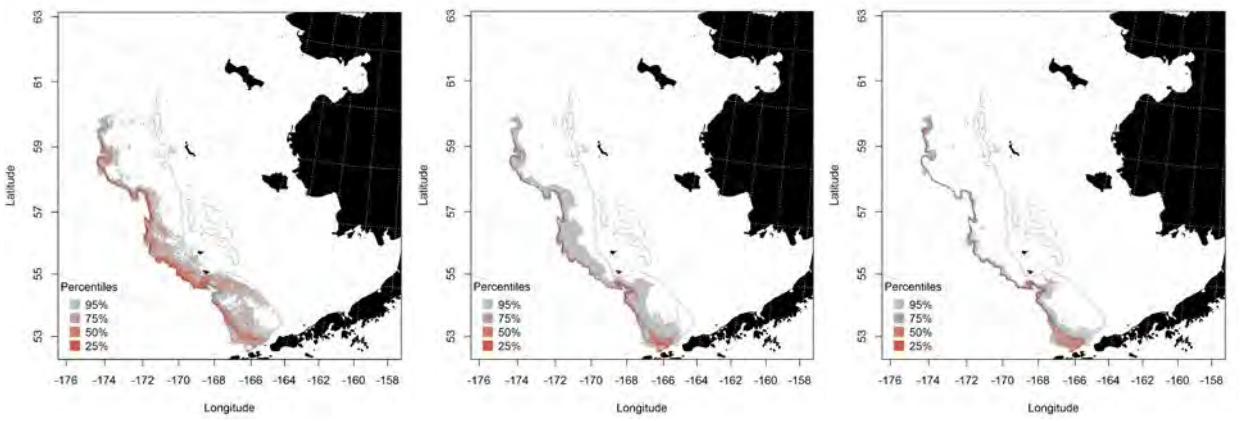

Figure 211. -- Essential fish habitat predicted from commercial fishery catches for rougheye/blackspotted rockfish complex during fall (left panel), winter (middle panel), and spring (right panel).

Pacific ocean perch (*Sebastes alutus*)

Pacific ocean perch are distributed across the North Pacific from Japan and Russia to Alaska (the Bering Sea and Aleutian Islands) and south into Baja California. The NPFMC currently manages Pacific ocean perch as a single species stock in the Bering Sea and Aleutian Islands region.

Summertime distribution of late juvenile and adult Pacific ocean perch from RACE bottom trawl surveys of the Eastern Bering Sea -- Catches of Pacific ocean perch in RACE bottom trawl surveys of the Eastern Bering Sea show that this species is primarily distributed over the outer shelf and slope edge from Bering Canyon in the southern domain to Navarin Canyon in the northern domain (Figure 212). There are some instances of Pacific ocean perch occurring over the middle shelf as well. Overall occurrence rates of Pacific ocean perch in EBS bottom trawl surveys since 1995, when they were first reported on this survey, range up to 17%.

A MaxEnt model predicted suitable habitat from the presence of late juvenile Pacific ocean perch in RACE summer bottom trawl surveys of the Eastern Bering Sea (Figure 213). They were primarily distributed along the upper slope edge and outer shelf from the Bering Canyon in the southern domain to

Navarin Canyon in the northern domain. The highest probabilities of suitable habitat were predicted in patches near the heads of submarine canyons along the shelf edge. Bottom depth and bottom temperature were the most important habitat covariates amongst predictors in the model. Combined they accounted for 85.4% of the relative importance among predictor terms. The MaxEnt model was an outstanding fit to the training data (AUC = 0.98) and correctly classified 92% of predicted cases. Model validation was successful (AUC = 0.98) and 98% of cases predicted from the test data set were correctly classified.

A MaxEnt model was selected to predict suitable habitat from the presence of adult Pacific ocean perch in RACE summer bottom trawl surveys of the Eastern Bering Sea (Figure 214). They were primarily distributed along the upper slope edge and outer shelf from the Bering Canyon in the southern domain to Navarin Canyon in the northern domain. The highest probability areas of suitable habitat were predicted in patches along the shelf edge. Bottom depth and temperature were the highest leverage habitat covariates in the model comprising a combined 94.6% of the relative importance of predictor terms. The MaxEnt model was an outstanding fit to the training data (AUC = 0.98) and correctly classified 94% of predicted cases. Model validation was successful (AUC = 0.95) and 95% of cases predicted from the test data set were correctly classified.

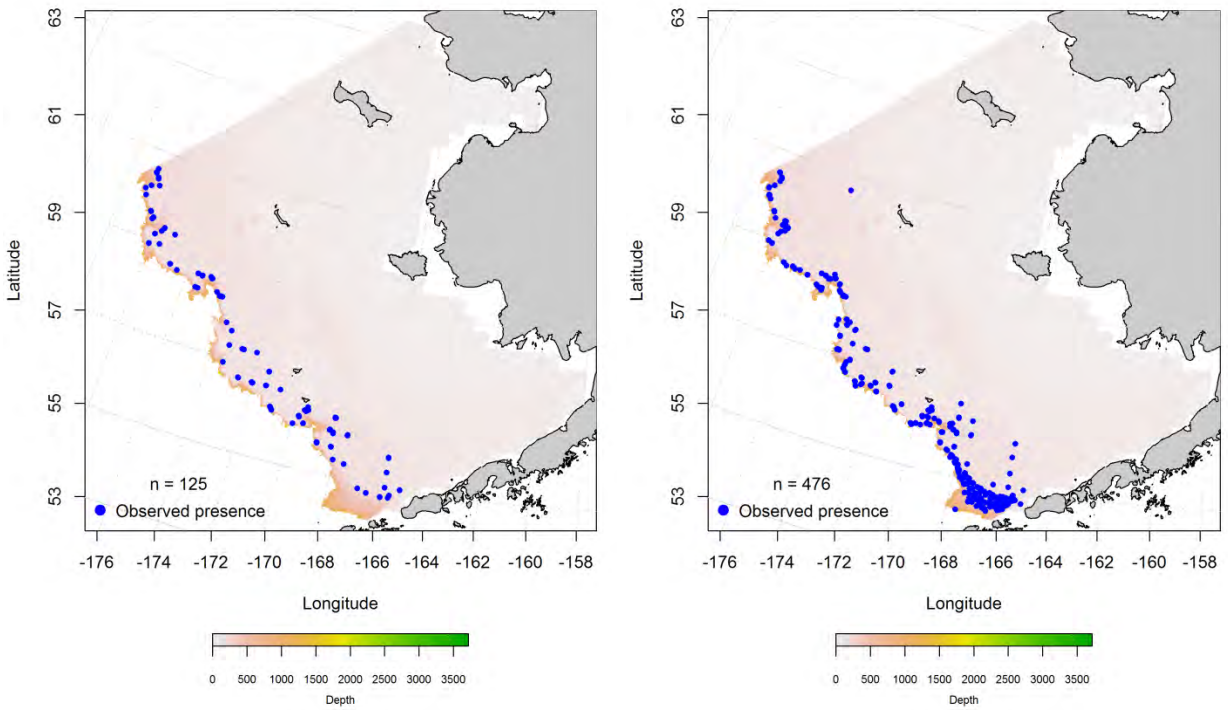

Figure 212. -- Distribution of juvenile (left) and adult (right) Pacific ocean perch catches in RACE summer bottom trawl surveys of the Eastern Bering Sea.

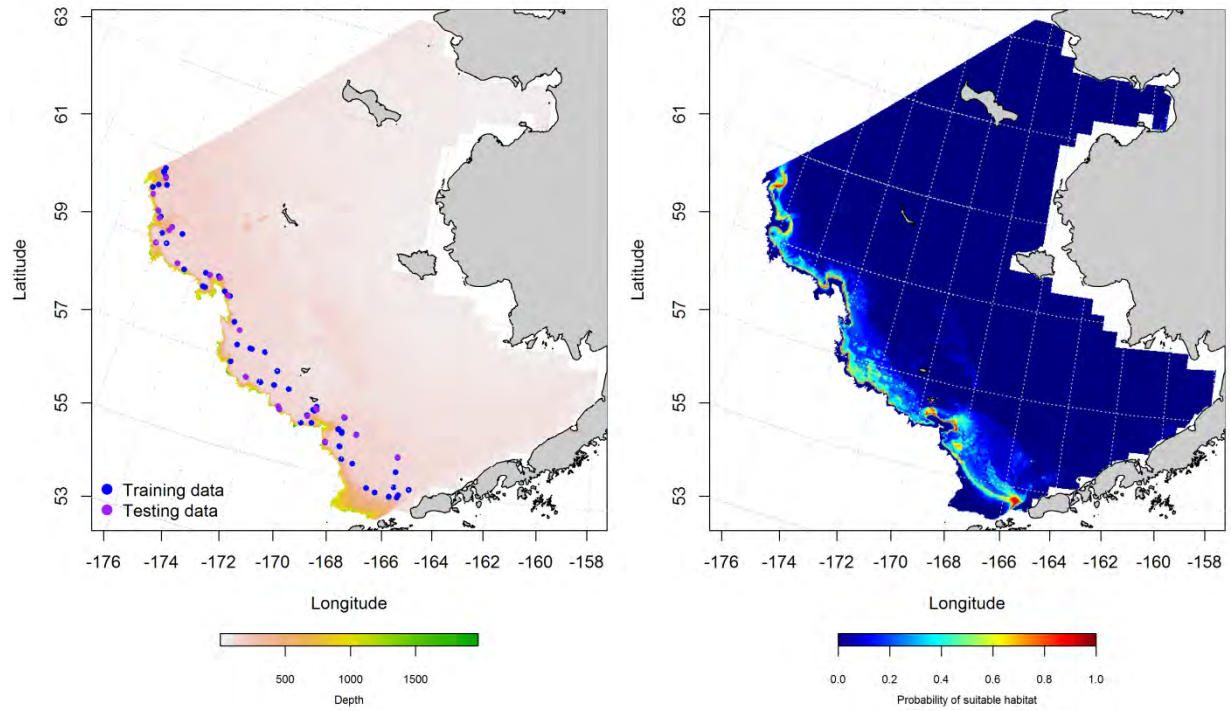

Figure 213. -- Locations of summer RACE Groundfish trawl survey catches of late juvenile Pacific ocean perch (left panel). Blue points were used to train the maximum entropy (MaxEnt) model predicting the probability of suitable habitat (right panel) and the purple points were used to validate the model.

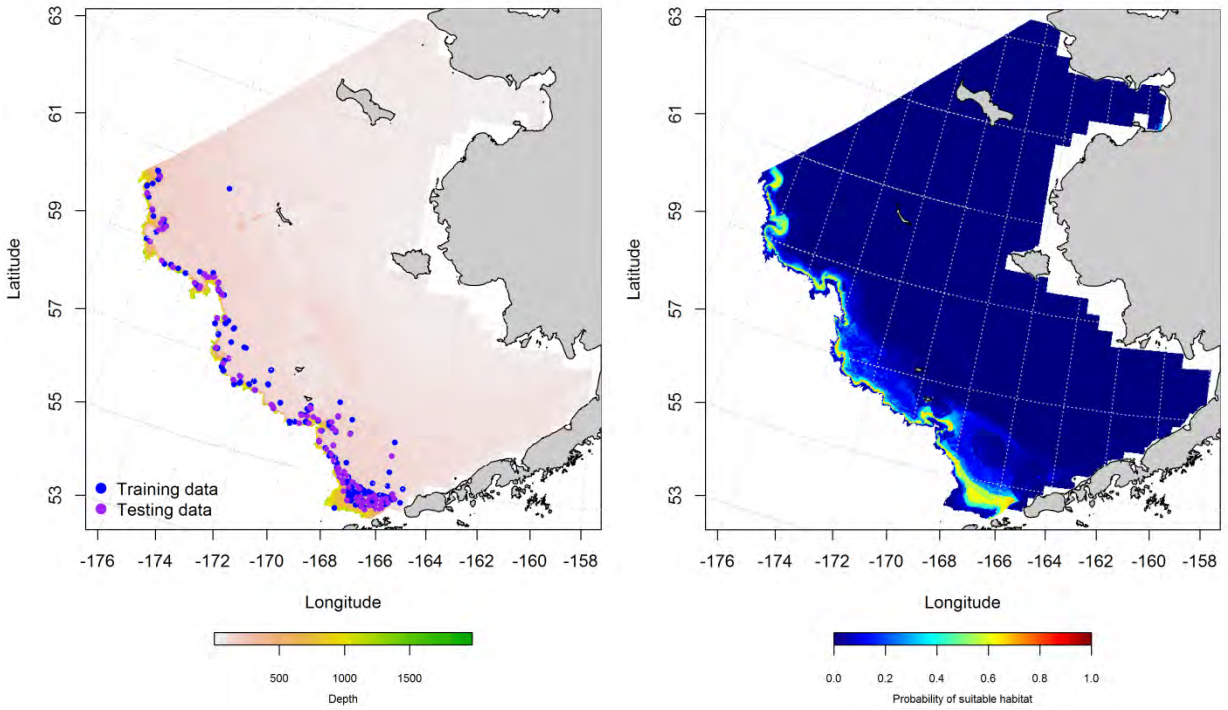

Figure 214. -- Locations of summer RACE Groundfish trawl survey catches of adult Pacific ocean perch (left panel). Blue points were used to train the maximum entropy (MaxEnt) model predicting the probability of suitable habitat (right panel) and the purple points were used to validate the model.

Seasonal distribution of Pacific ocean perch in commercial fishery catches from the Eastern Bering Sea -- In fall, Pacific ocean perch were reported in commercial catches from the Bering Canyon in the southern domain of the Eastern Bering Sea to Pervenets Canyon in the north (Figure 215). Maximum entropy models based on this Pacific ocean perch presence data predicted that the highest probabilities of suitable habitat were along the shelf edge near the heads of submarine canyons. Bottom depth, bottom temperature, and bottom slope were the dominant habitat covariates in the model comprising a combined 93.7% of the relative importance of predictor terms. The fit of the MaxEnt model to the training data was outstanding (AUC = 0.98) and it correctly predicted 92% of cases. Model validation was successful (AUC = 0.93) and 93% of cases predicted from the test data set were correct.

In winter, the distribution of Pacific ocean perch in commercial catches was similar to fall, but with fewer occurrences in the northern domain and more occurrences further east along the Bering Canyon axis (Figure 216). The highest probability suitable habitat areas predicted from the MaxEnt model were located over the Bering and Pribilof Canyons. Bottom depth, bottom temperature, and ocean productivity provided 96.8% of the leverage from habitat covariates in the model. The fit of the MaxEnt model to the training data was outstanding (AUC = 0.99) and it correctly predicted 96% of cases. Model validation was successful (AUC = 0.97) and 97% of cases predicted from the test data set were correct.

Spring distribution of Pacific ocean perch in commercial catches extended from the Bering to Navarin Canyon with reports from commercial catches focused around the Bering, Pribilof, and Zhemchug Canyons (Figure 217). Once again the highest probability suitable habitat areas predicted from the MaxEnt model were located near the heads of submarine canyons. Bottom depth, bottom temperature, and bottom slope comprised 90% of the leverage from habitat covariates in the model. The MaxEnt fit to the training data was outstanding (AUC = 0.99) and correctly predicted 94% of cases. Model validation was successful based both on the high AUC (0.92) and the 92% of correctly classified by the test data.

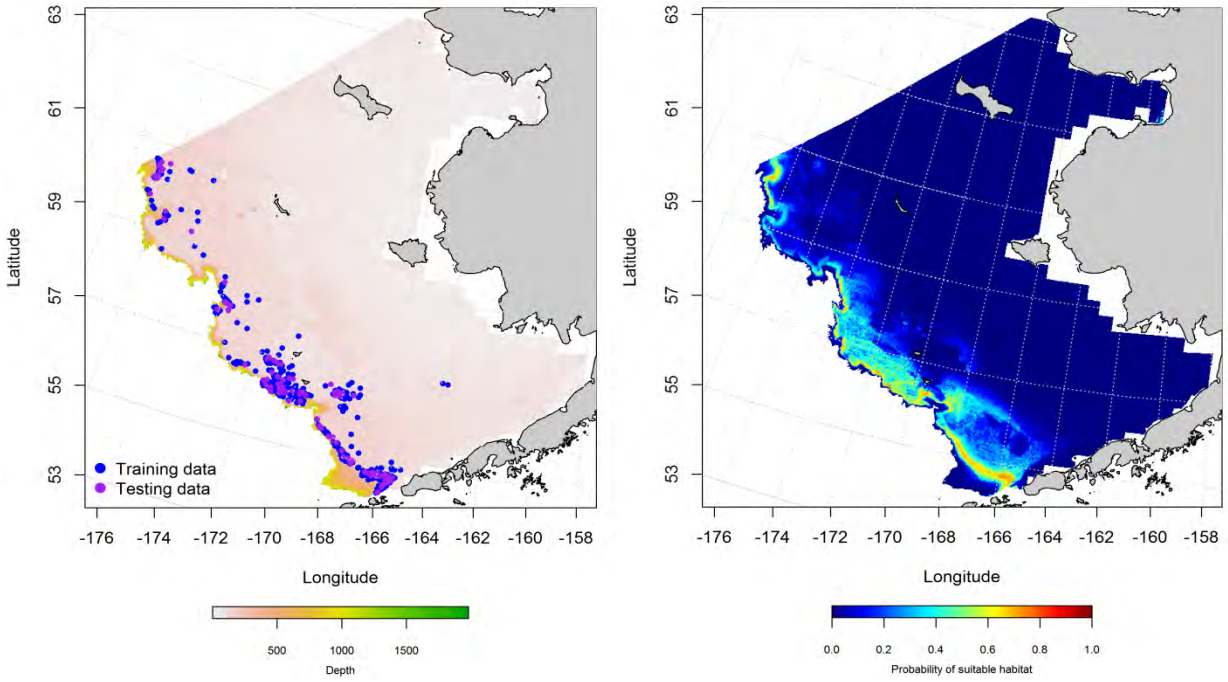

Figure 215. -- Locations of fall (October-November) catches of Pacific ocean perch in commercial fisheries of the Eastern Bering Sea (left panel). Blue points were used to train the MaxEnt model predicting the probability of suitable habitat (right panel) and the purple points were used to validate the model.

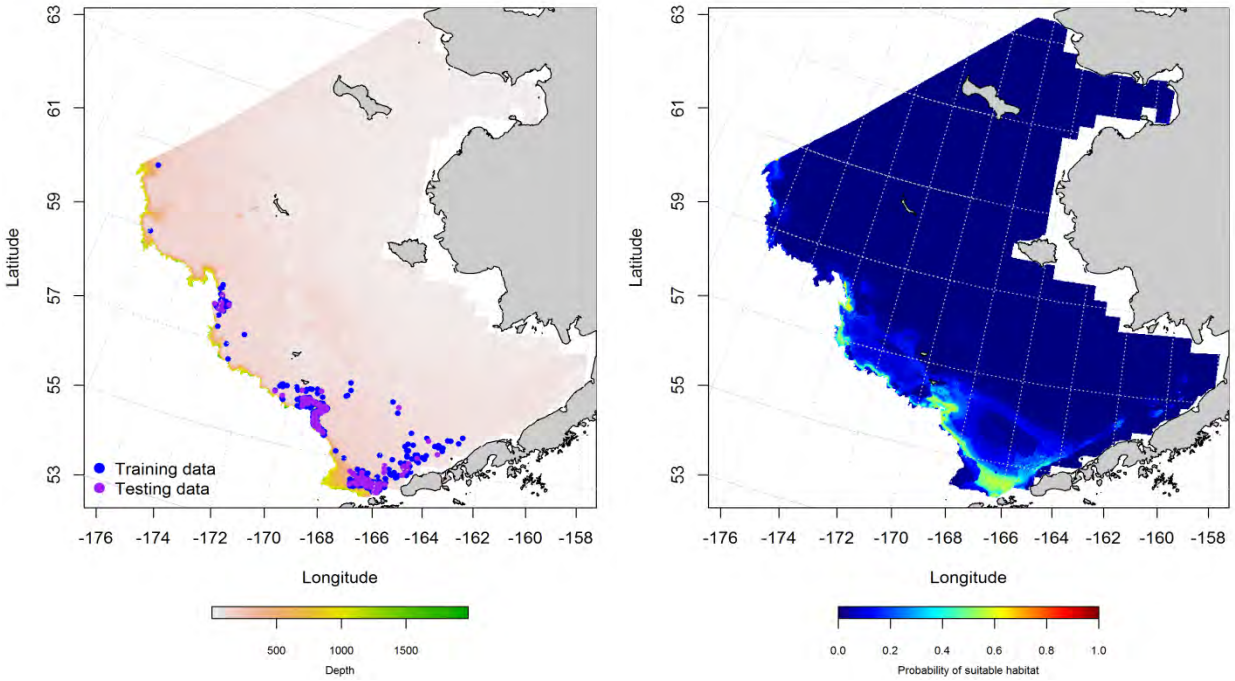

Figure 216. -- Locations of winter (December-February) catches of Pacific ocean perch in commercial fisheries of the Eastern Bering Sea (left panel). Blue points were used to train the MaxEnt model predicting the probability of suitable habitat (right panel) and the purple points were used to validate the model.

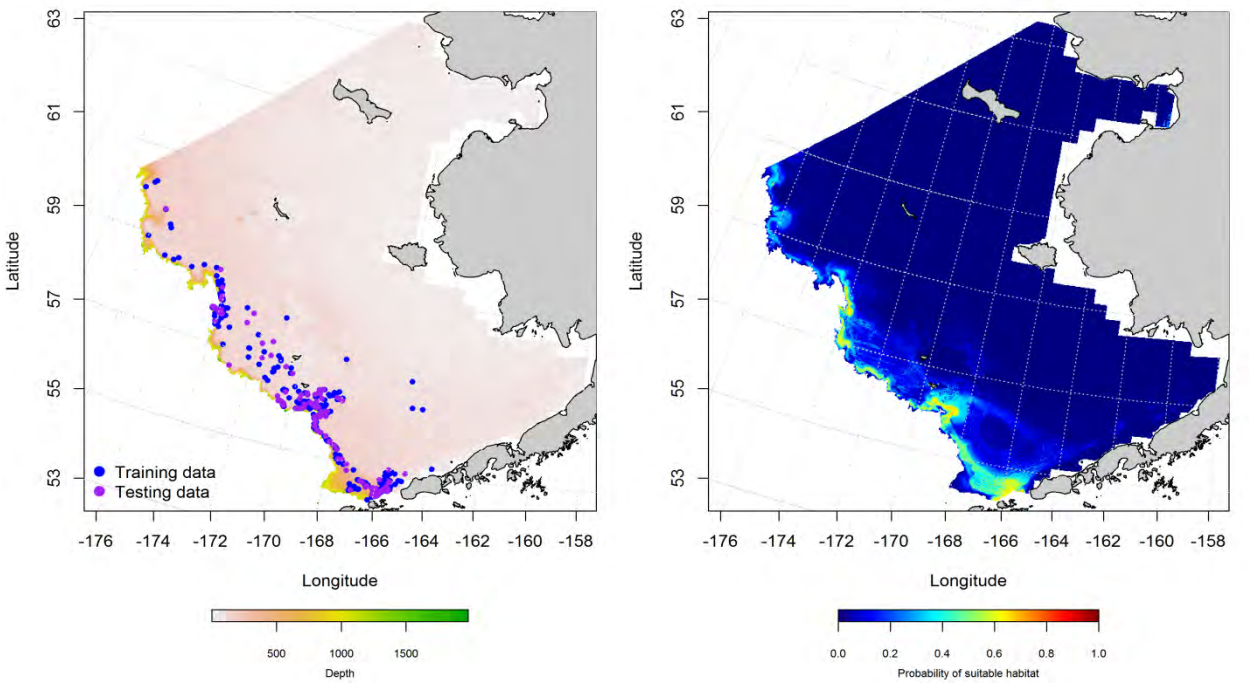

Figure 217. -- Locations of spring (March-May) catches of Pacific ocean perch in commercial fisheries of the Eastern Bering Sea (left panel). Blue points were used to train the MaxEnt model predicting the probability of suitable habitat (right panel) and the purple points were used to validate the model.

Essential fish habitat maps and conclusions for Pacific ocean perch in the Eastern Bering Sea – The spatial distribution of summertime EFH for late juvenile and adult Pacific ocean perch from RACE bottom trawl surveys of the Eastern Bering Sea (Figure 218) was predicted using MaxEnt models. Both life stages were most likely to occur over the outer shelf and upper slope of the Bering Sea across the north to south extent of the survey area. Highest likelihoods for EFH were over areas closest to the shelf break.

Predicting Pacific ocean perch EFH from commercial fishery catches using MaxEnt models showed some minor seasonal differences (Figure 219). In wintertime, the distribution of EFH in the northern domain of the Eastern Bering Sea was much narrower than in fall or spring. In general, the predicted EFH overlapped across seasons and was focused over the shelf break and slope waters.

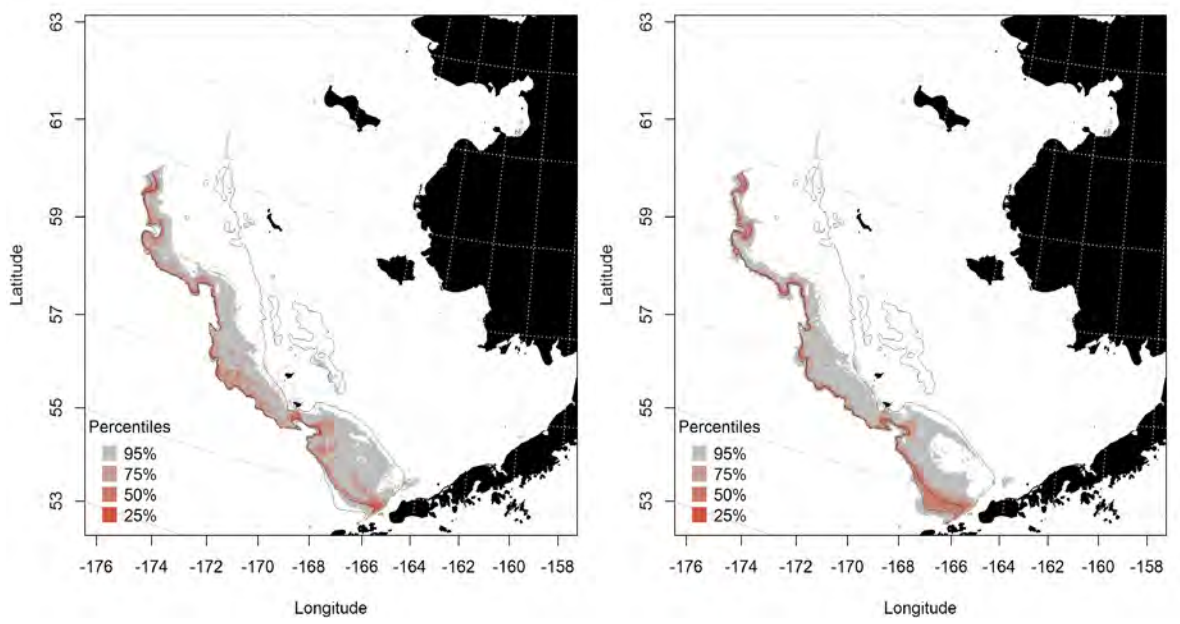

Figure 218. -- Predicted summer essential fish habitat for Pacific ocean perch juveniles and adults (left and right panel) from summertime bottom trawl surveys.

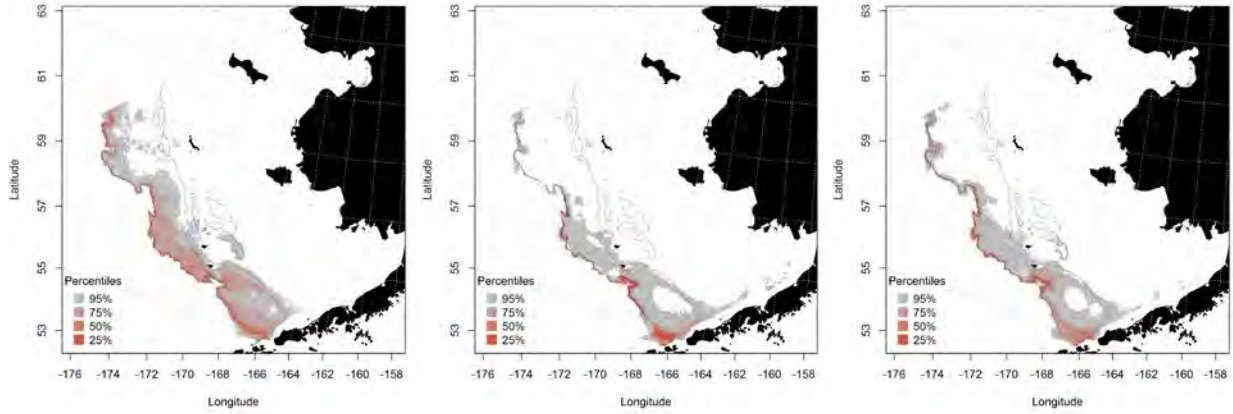

Figure 219. -- Essential fish habitat predicted for Pacific ocean perch during fall (left panel), winter (middle panel) and spring (right panel) from commercial fishery catches.

shortraker rockfish (*Sebastes borealis*)

Shortraker rockfish are distributed across the North Pacific from Japan and Russia to Alaska (the Bering Sea and Aleutian Islands) and south into central California. These are among the longest lived animal

species in the world, reaching ages > 150 years. Catches of shortrakers from the BSAI are currently reported by species and area.

Summertime distribution of late juvenile and adult shortraker rockfish from RACE bottom trawl surveys of the Eastern Bering Sea -- Catches of shortraker rockfish have only been reported in RACE bottom trawl surveys of the Eastern Bering Sea Slope (Figure 220). Their distribution is over the relatively narrow strip of habitat at the shelf break from the Bering Canyon in the southern domain of the Eastern Bering Sea to Navarin Canyon in the north.

A MaxEnt model predicted suitable habitat from the presence of late juvenile shortraker rockfish observed in RACE summer bottom trawl surveys of the Eastern Bering Sea Slope (Figure 221). They were primarily distributed along the upper slope edge and outer shelf from the Bering Canyon in the southern domain to Navarin Canyon in the northern domain. Bottom depth and bottom slope were the highest leverage habitat covariates among the predictors in the model. Combined they accounted for 99.3% of the relative importance among predictor terms. The MaxEnt model was an outstanding fit to the training data (AUC = 0.99) and model validation was successful (AUC = 0.98). Predictions from this model with either the training or test data sets correctly classified 98% of the cases.

A MaxEnt model was selected to predict suitable habitat from the presence of adult shortraker rockfish observed in RACE summer bottom trawl surveys of the Eastern Bering Sea Slope (Figure 222). They were primarily distributed along the upper slope edge and outer shelf over the extent of the survey area. Bottom depth and bottom slope had the greatest leverage of habitat covariates in the model comprising a combined 87.2% of the relative importance of predictor terms. The MaxEnt model was an outstanding fit to the training data (AUC = 1.0) and correctly classified 99% of predicted cases. Model validation was successful (AUC = 0.98) and 98% of cases predicted from the test data set were correctly classified.

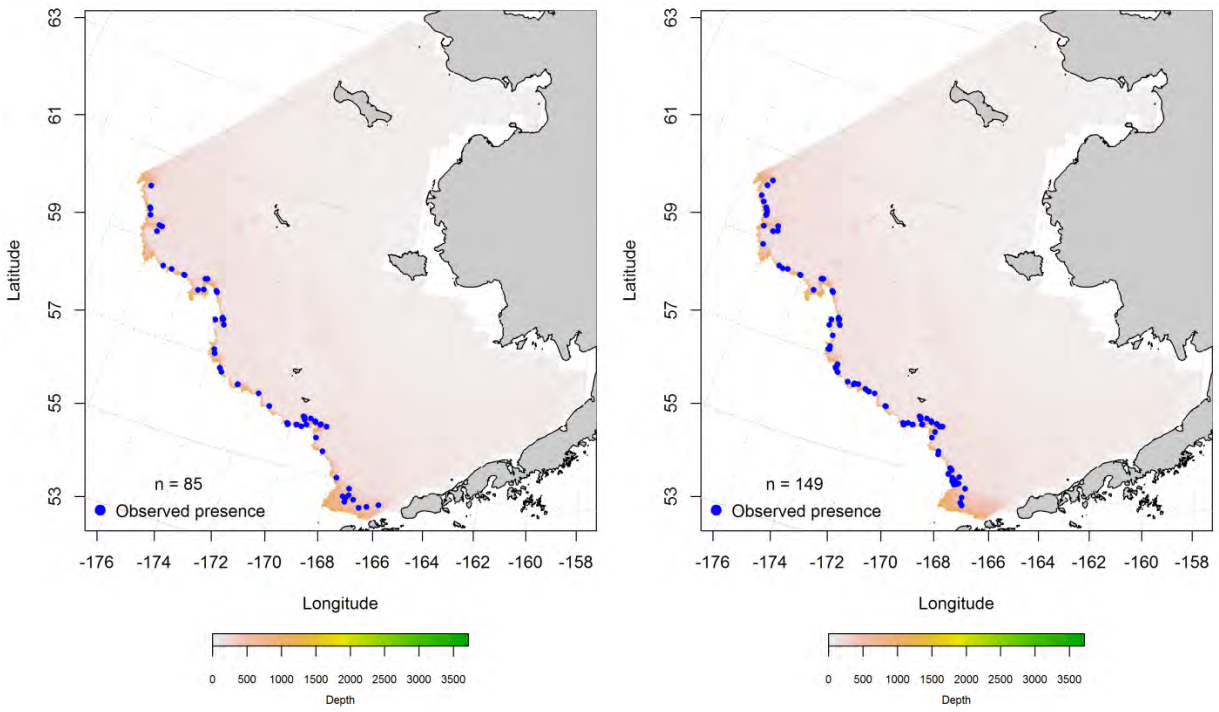

Figure 220. -- Distribution of juvenile (left) and adult (right) shortraker rockfish catches in RACE summer bottom trawl surveys of the Eastern Bering Sea.

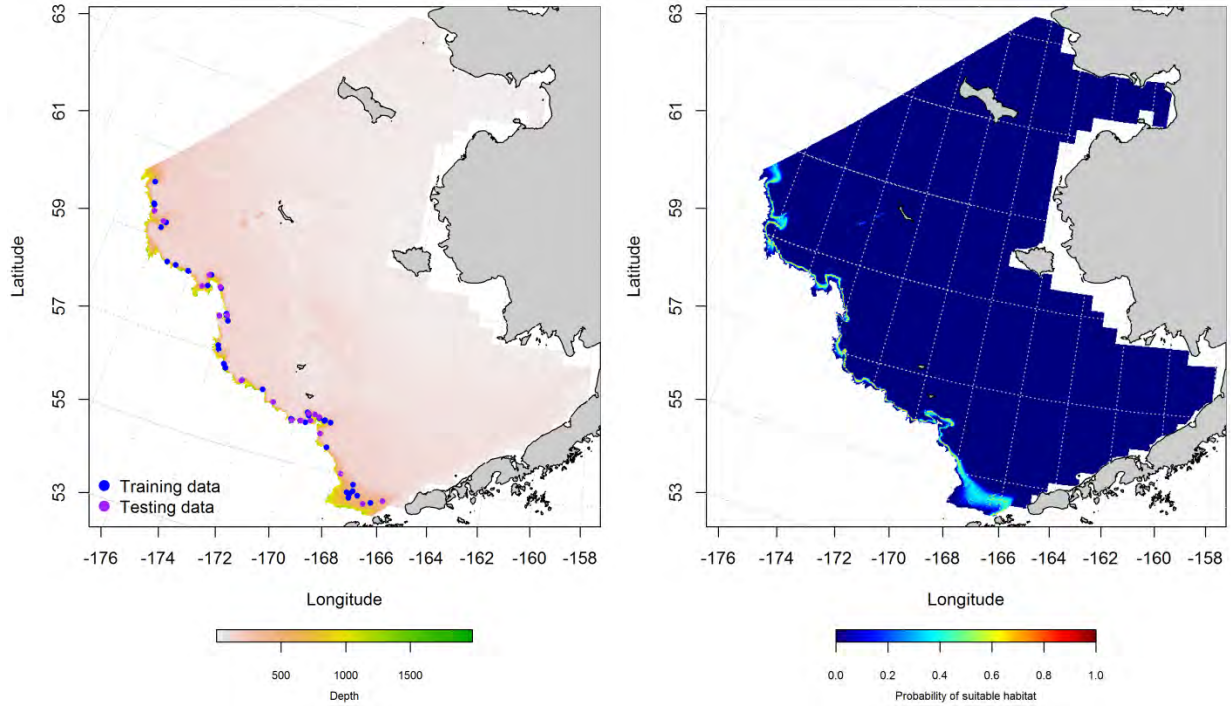

Figure 221. -- Locations of summer RACE Groundfish trawl survey catches of late juvenile shortraker rockfish (left panel). Blue points were used to train the maximum entropy (MaxEnt) model predicting the probability of suitable habitat (right panel) and the purple points were used to validate the model.

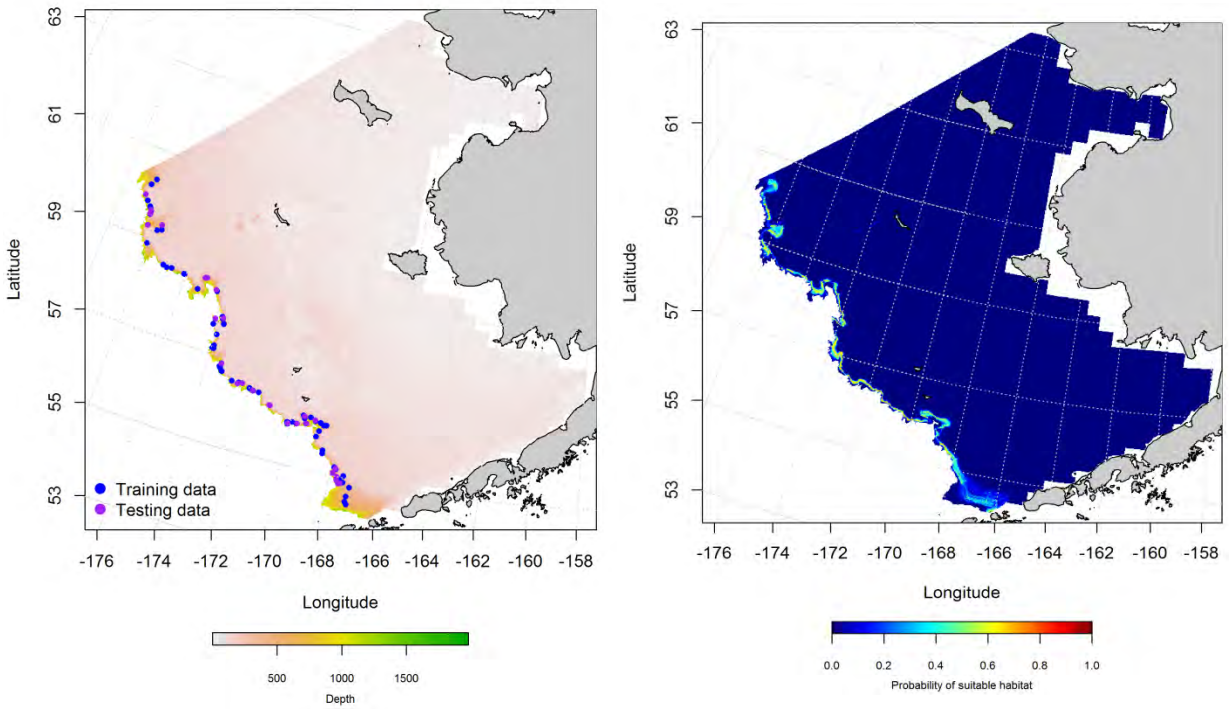

Figure 222. -- Locations of summer RACE Groundfish trawl survey catches of adult shortraker rockfish (left panel). Blue points were used to train the maximum entropy (MaxEnt) model predicting the probability of suitable habitat (right panel) and the purple points were used to validate the model.

Seasonal distribution of shortraker rockfish in commercial fishery catches from the Eastern Bering Sea -- In fall, shortraker rockfish were reported in commercial catches from the Bering Canyon in the southern domain of the Eastern Bering Sea to St Matthew Canyon in the north (Figure 223). Maximum entropy models based on these shortraker rockfish presence data predicted that the highest probabilities of suitable habitat were along the upper slope and shelf edge. Bottom depth, bottom temperature, and bottom slope were the dominant habitat covariates in the model comprising a combined 84.4% of the relative importance of predictor terms. The fit of the MaxEnt model to the training data was outstanding (AUC = 0.98) and it correctly predicted 94% of cases. Model validation was successful (AUC = 0.98) and 98% of cases predicted from the test data set were correct.

In winter, the distribution of shortraker rockfish from commercial catches was patchy and focused around submarine canyons (Figure 224). The highest probability suitable habitat areas predicted from the MaxEnt model were located over the Bering and Pribilof Canyons. Bottom depth and bottom temperature provided 94.2% of the leverage from habitat covariates in the model. The fit of the MaxEnt model to the training data was outstanding (AUC = 1.0) and it correctly predicted 96% of cases. Model validation was successful (AUC = 0.93) and 93% of cases predicted from the test data set were correct.

Spring distribution of shortraker rockfish in commercial catches was similar winter distributions (Figure 225). Occurrence of shortrakers was patchy and focused over submarine canyons. The highest probability suitable habitat areas predicted from the MaxEnt model were located at the head of Pribilof Canyon. Bottom depth and bottom slope comprised 89.5% of the leverage from habitat covariates in the model. The MaxEnt fit to the training data was outstanding (AUC = 1.0) and it correctly predicted 98% of cases. Model validation was successful based both on the high AUC (0.98) and the 98% of cases correctly classified with the test data.

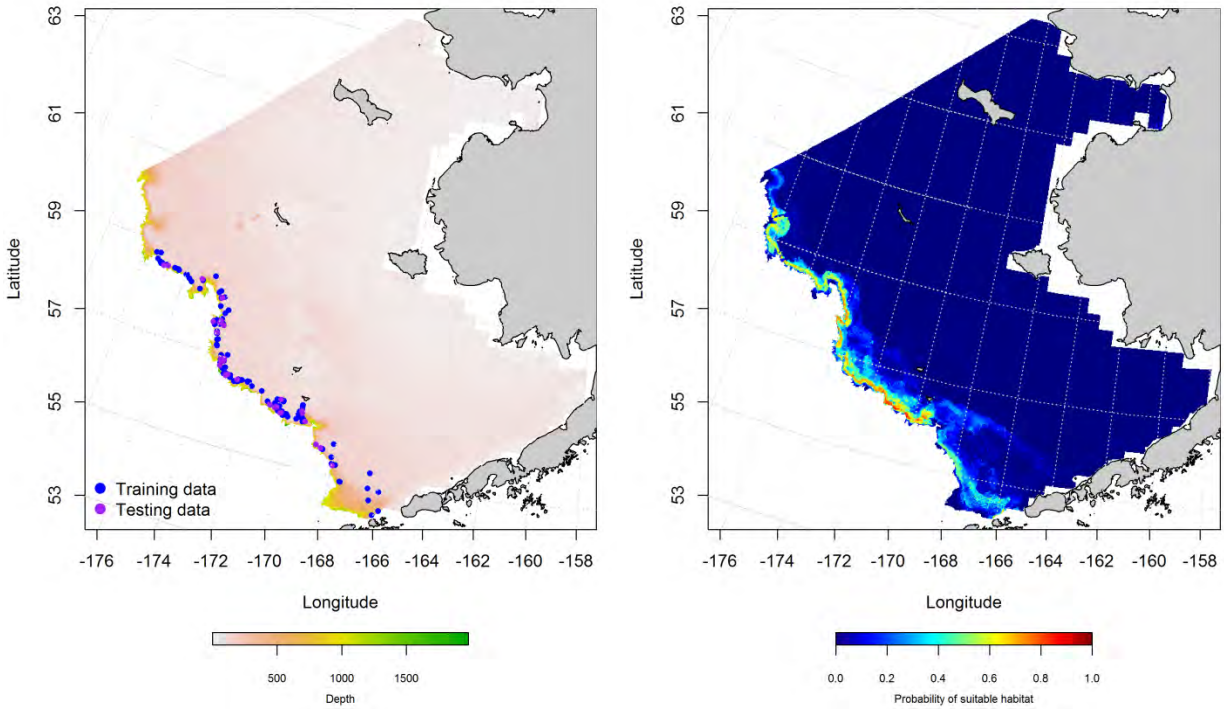

Figure 223. -- Locations of fall (October-November) catches of shortraker rockfish in commercial fisheries of the Eastern Bering Sea (left panel). Blue points were used to train the MaxEnt model predicting the probability of suitable habitat (right panel) and the purple points were used to validate the model.

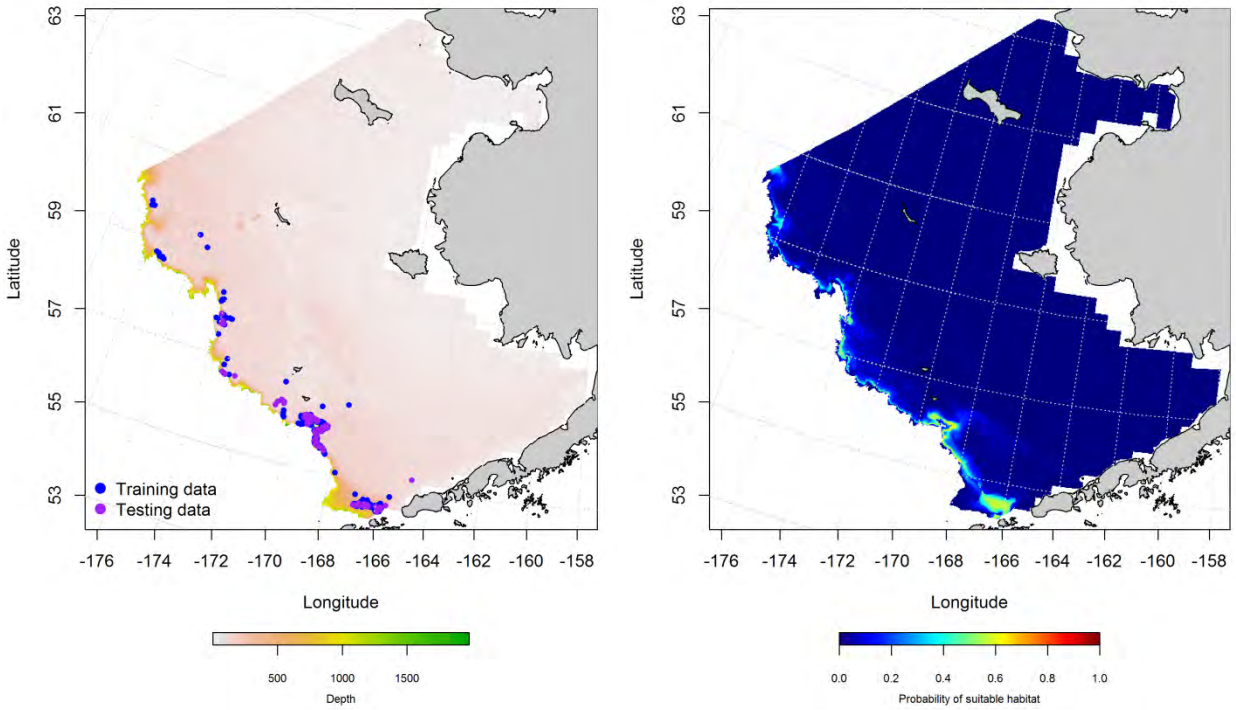

Figure 224. -- Locations of winter (December-February) catches of shortraker rockfish in commercial fisheries of the Eastern Bering Sea (left panel). Blue points were used to train the MaxEnt model predicting the probability of suitable habitat (right panel) and the purple points were used to validate the model.

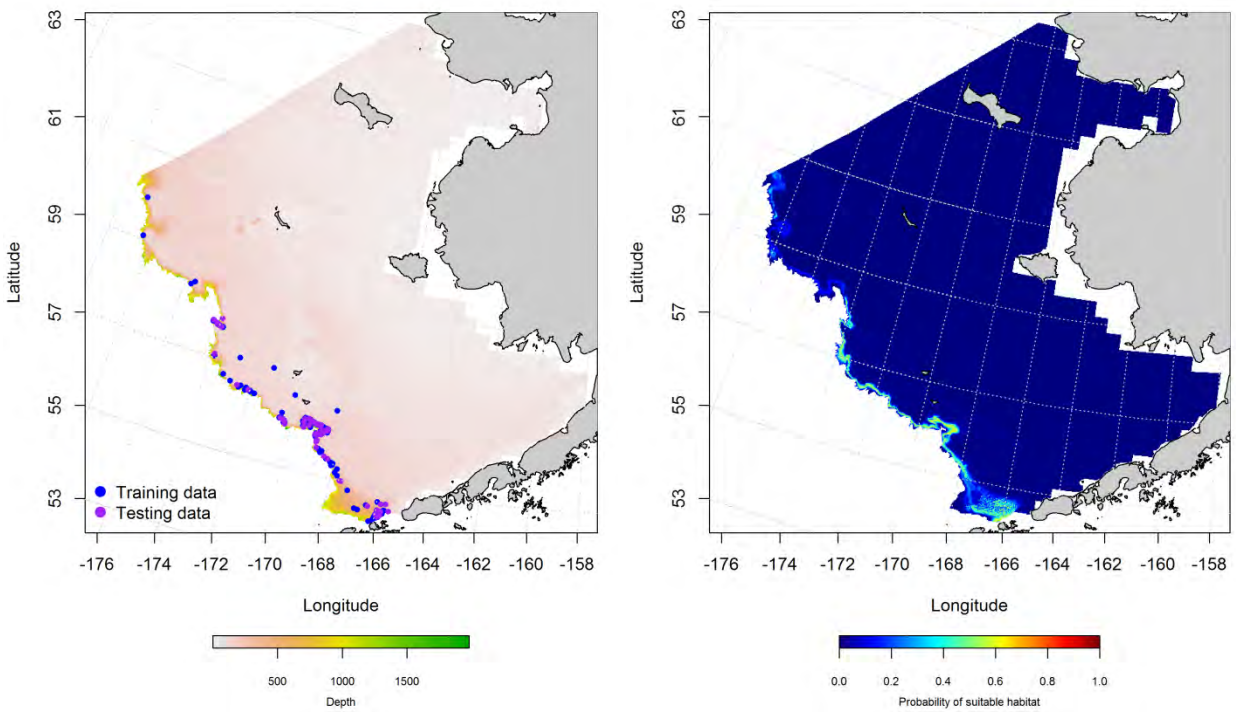

Figure 225. -- Locations of spring (March-May) catches of shortraker rockfish in commercial fisheries of the Eastern Bering Sea (left panel). Blue points were used to train the MaxEnt model predicting the probability of suitable habitat (right panel) and the purple points were used to validate the model.

Essential fish habitat maps and conclusions for shortraker rockfish in the Eastern Bering Sea – The spatial distribution of summertime EFH for late juvenile and adult shortraker rockfish from RACE bottom trawl surveys of the Eastern Bering Sea was predicted with MaxEnt models (Figure 226). Both life stages were most likely to occur over the outer shelf and upper slope of the Bering Sea. Highest likelihoods for EFH were on the shelf break near submarine canyons.

Predicting shortraker rockfish EFH from commercial fishery catches using MaxEnt models showed some minor seasonal differences (Figure 227). In general, the predicted EFH corresponded to the shelf break and slope waters around submarine canyons. The domain containing the most probable habitat varied among seasons.

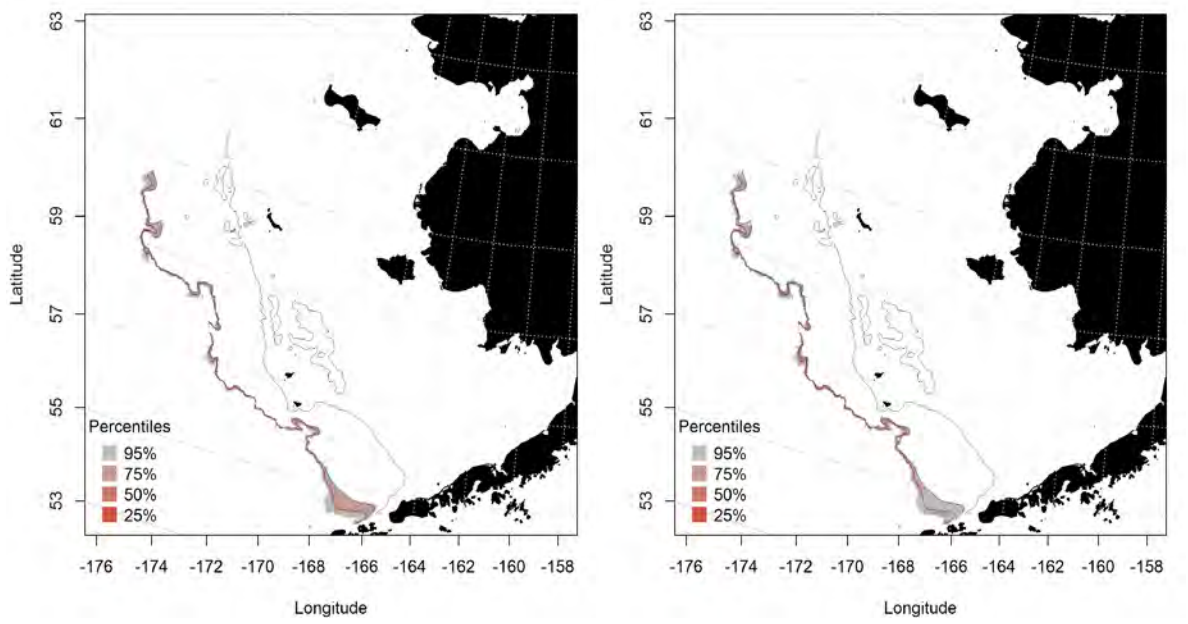

Figure 226. -- Predicted summer essential fish habitat for shortraker rockfish juveniles and adults (left and right panel) from summertime bottom trawl surveys.

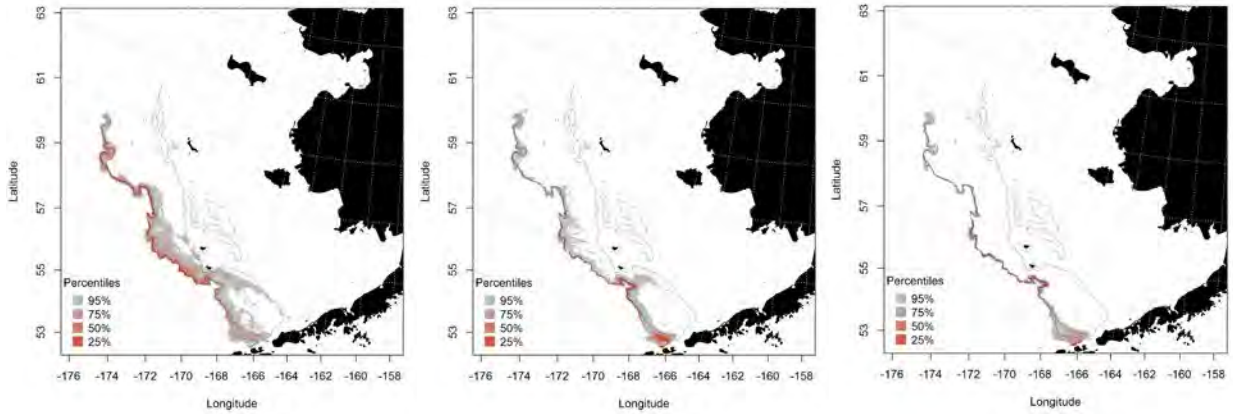

Figure 227. -- Essential fish habitat predicted for shortraker rockfish during fall (left panel), winter (middle panel) and spring (right panel) from commercial fishery catches.

blackspotted rockfish (*Sebastes melanostictus*)

Blackspotted rockfish are distributed across the North Pacific from Japan and Russia to Alaska (the Bering Sea and Aleutian Islands) and south into central California. These are among the longest lived animal species in the world, reaching ages > 150 years.

Summertime distribution of late juvenile and adult blackspotted rockfish from RACE bottom trawl surveys of the Eastern Bering Sea -- Catches of blackspotted rockfish in summertime RACE bottom trawl surveys of the Eastern Bering Sea have been reported from Bering Canyon in the southern domain to Navarin Canyon in the north (Figure 228). The distribution of blackspotted rockfish catches in our bottom trawl survey shows that it is found primarily at the shelf break with some dispersion onto the outer shelf. Their catches also appear to be loosely associated with submarine canyons. The presence data from the Eastern Bering Sea bottom trawl survey was not sufficient to parameterize a species distribution model for this rockfish.

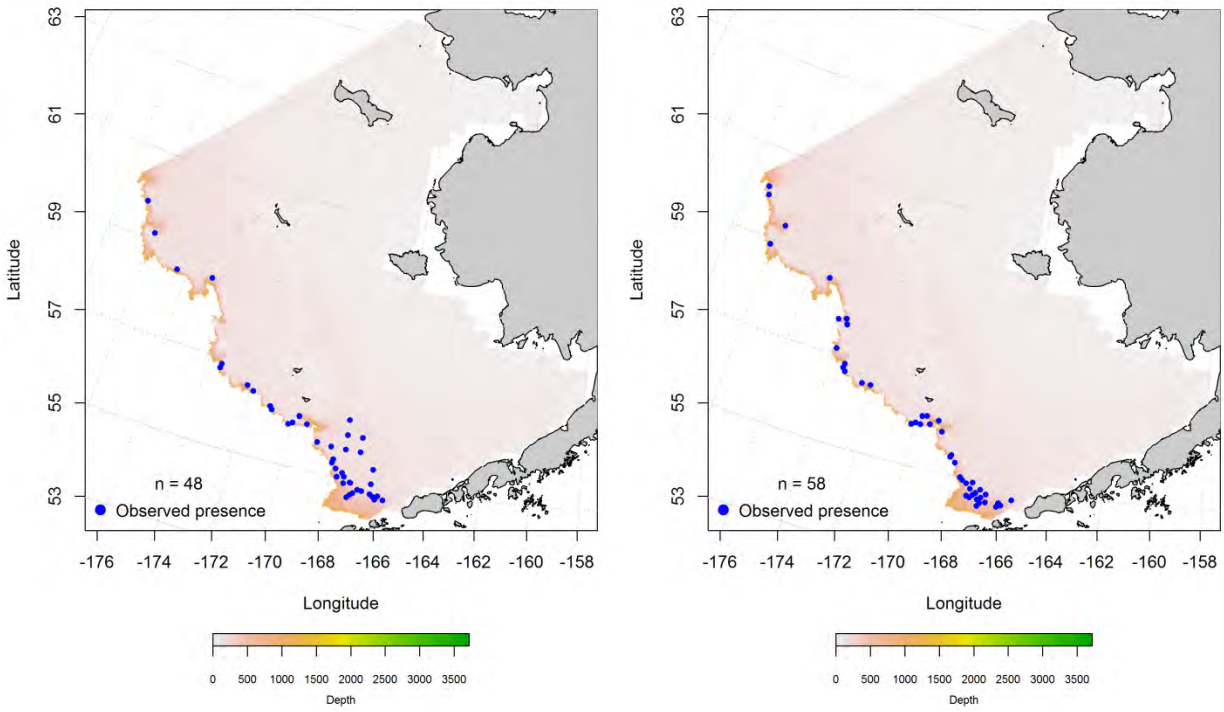

Figure 228. -- Distribution of juvenile (left) and adult (right) blackspotted rockfish catches in RACE summer bottom trawl surveys of the Eastern Bering Sea.

Seasonal distribution of blackspotted rockfish in commercial fishery catches from the Eastern Bering Sea -- Rougheye and blackspotted rockfishes are not separated in commercial catches from Alaska. The two species are managed together as a complex by the NPFMC. Results of species

distribution models for the rougheye/blackspotted complex landed from commercial fisheries of the Eastern Bering Sea are reported in the rougheye rockfish section above.

northern rockfish (*Sebastes polyspinis*)

Northern rockfish are distributed across the North Pacific from Russia to Alaska (the Bering Sea and Aleutian Islands) and south into British Columbia. The NPFMC currently manages northern rockfish as a single species stock in the Bering Sea and Aleutian Islands region.

Summertime distribution of late juvenile and adult northern rockfish from RACE bottom trawl surveys of the Eastern Bering Sea -- Catches of late juvenile and adult northern rockfish in RACE bottom trawl surveys of the Eastern Bering Sea show that this species is primarily distributed over the middle shelf from the Bering Canyon to Pervenets Canyon (Figure 229). Northern rockfish are most prevalent in the southern domain. The number of records of northern rockfish juveniles and adults in Eastern Bering Sea summer trawl survey catches were not sufficient to parameterize a distribution model for this species.

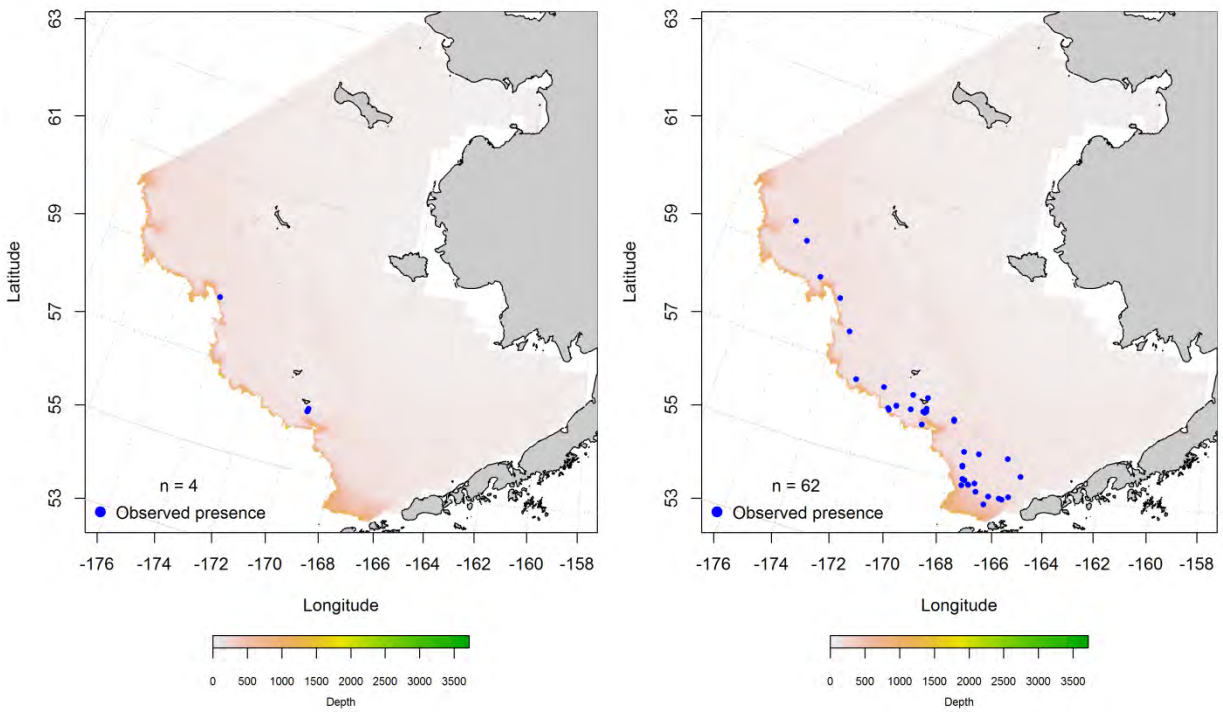

Figure 229. -- Distribution of juvenile (left) and adult (right) northern rockfish catches in RACE summer bottom trawl surveys of the Eastern Bering Sea.

Seasonal distribution of northern rockfish in commercial fishery catches from the Eastern Bering Sea -- In fall, northern rockfish were reported in commercial catches from the Bering Canyon in the southern domain of the Eastern Bering Sea to Navarin Canyon in the north (Figure 230). Maximum entropy models based on this northern rockfish presence data predicted that the highest probabilities of suitable habitat were along the shelf edge near the heads of Pribilof and Zhemchug Canyons. Bottom depth, bottom temperature, and ocean productivity were the dominant habitat covariates in the model comprising a combined 92.6% of the relative importance of predictor terms. The fit of the MaxEnt model to the training data was outstanding (AUC = 0.98) and it correctly predicted 94% of cases. Model validation was successful (AUC = 0.88) and 88% of cases predicted from the test data set were correct.

In winter, the distribution of northern rockfish in commercial catches was similar to fall, but with more occurrences further east along the Bering Canyon axis (Figure 231). The highest probability suitable

habitat was predicted from the MaxEnt model between Pribilof Canyon and St. George Island. Bottom depth, bottom temperature, sediment grain size, and ocean productivity provided 97% of the leverage from habitat covariates in the model. The fit of the MaxEnt model to the training data was outstanding (AUC = 0.98) and it correctly predicted 94% of cases. Model validation was successful (AUC = 0.90) and 90% of cases predicted from the test data set were correct.

Spring distribution of northern rockfish in commercial catches extended from the Bering to Navarin Canyon with reports from commercial catches focused north of Pribilof Canyon and along the southern margin of Zhemchug Canyon (Figure 232). The highest probability suitable habitat areas predicted from the MaxEnt model were located between Pribilof Canyon and St. George Island as well as above the head of the southern arm of Zhemchug Canyon. Bottom depth, bottom temperature, ocean productivity, and sediment grain size comprised 94% of the leverage from habitat covariates in the model. The MaxEnt fit to the training data was outstanding (AUC = 0.98) and correctly predicted 95% of cases. Model validation was successful based both on the high AUC (0.92) and the 92% of cases correctly classified by the test data.

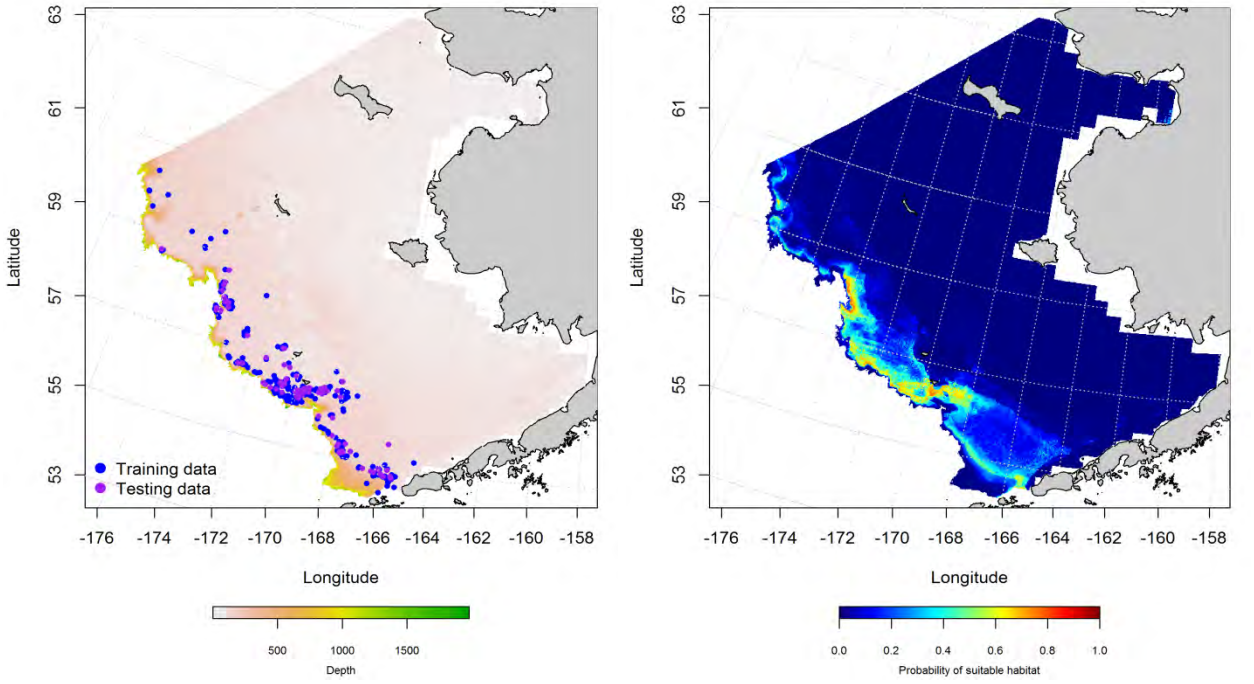

Figure 230. -- Locations of fall (October-November) catches of northern rockfish in commercial fisheries of the Eastern Bering Sea (left panel). Blue points were used to train the MaxEnt model predicting the probability of suitable fall habitat (right panel) and the purple points were used to validate the model.

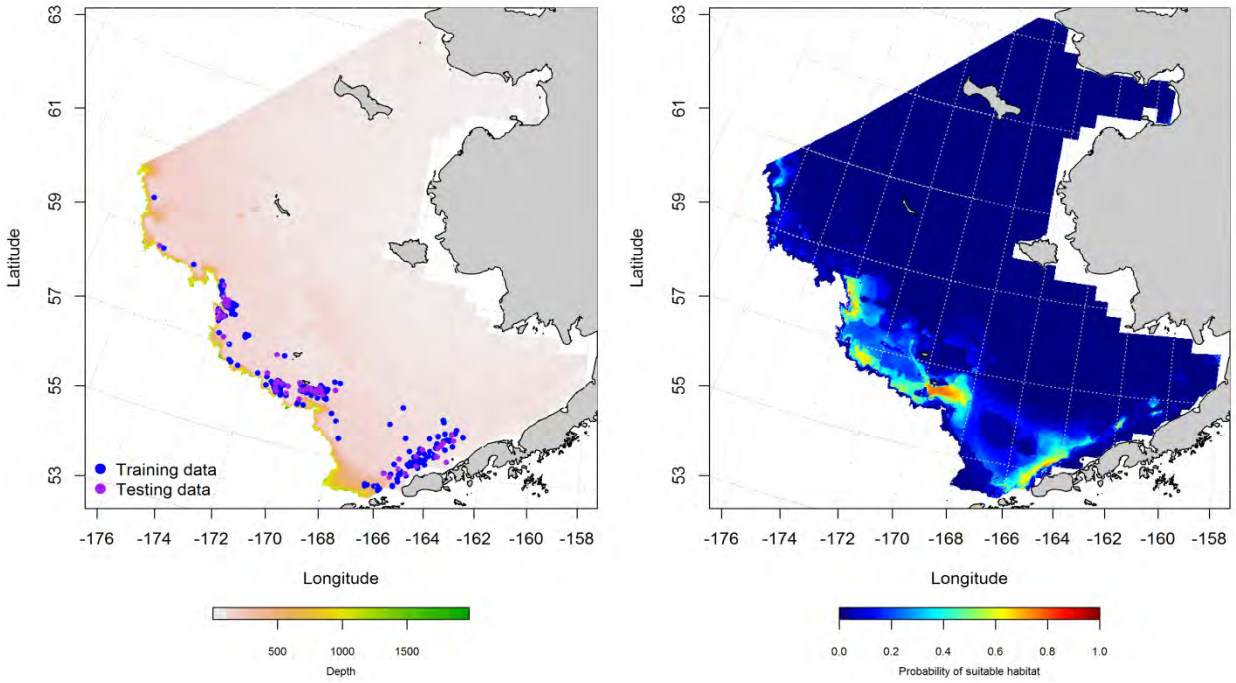

Figure 231. -- Locations of winter (December-February) catches of northern rockfish in commercial fisheries of the Eastern Bering Sea (left panel). Blue points were used to train the MaxEnt model predicting the probability of suitable winter habitat (right panel) and the purple points were used to validate the model.

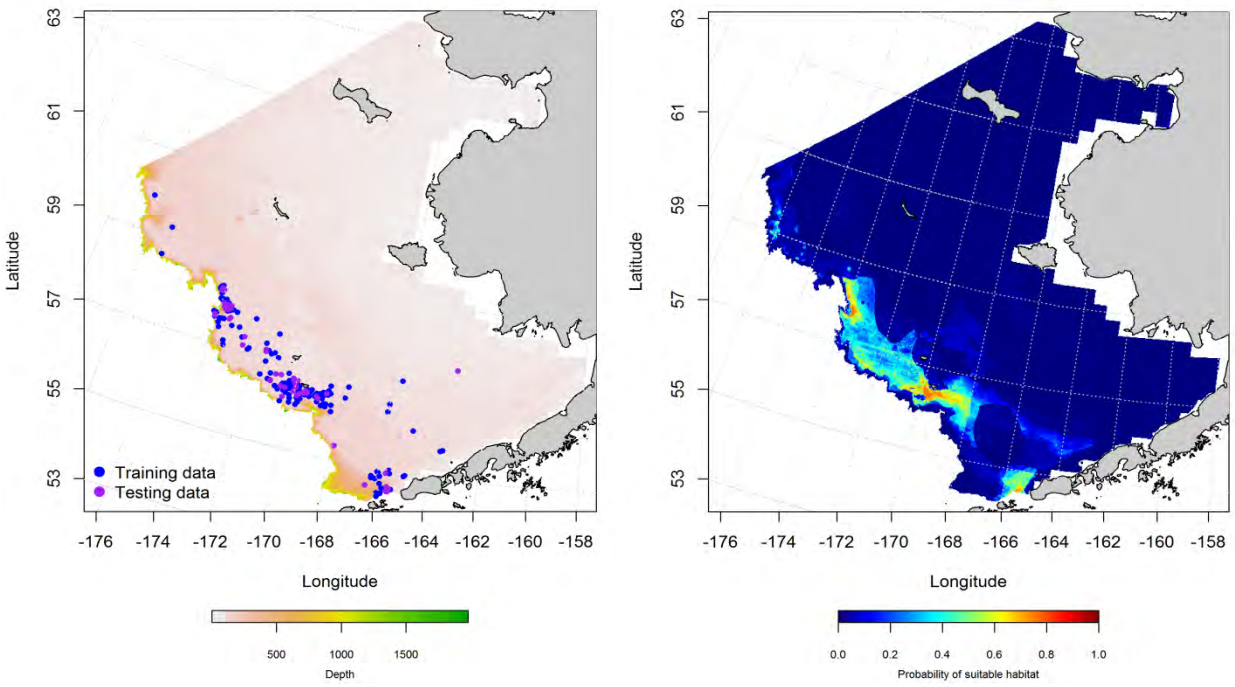

Figure 232. -- Locations of spring (March-May) catches of northern rockfish in commercial fisheries of the Eastern Bering Sea (left panel). Blue points were used to train the MaxEnt model predicting the probability of suitable spring habitat (right panel) and the purple points were used to validate the model.

Essential fish habitat maps and conclusions for northern rockfish in the Eastern Bering Sea

– Predicting northern rockfish EFH from commercial fishery catches using MaxEnt models showed some seasonal differences (Figure 233). In fall and spring, the distribution of northern rockfish EFH was centered more on the central domain of the Eastern Bering Sea over the outer shelf. In wintertime, the primary EFH areas remained over the outer shelf, but there was a greater emphasis on habitat available in the southern domain. Overall, the predicted EFH for northern rockfish overlapped across seasons.

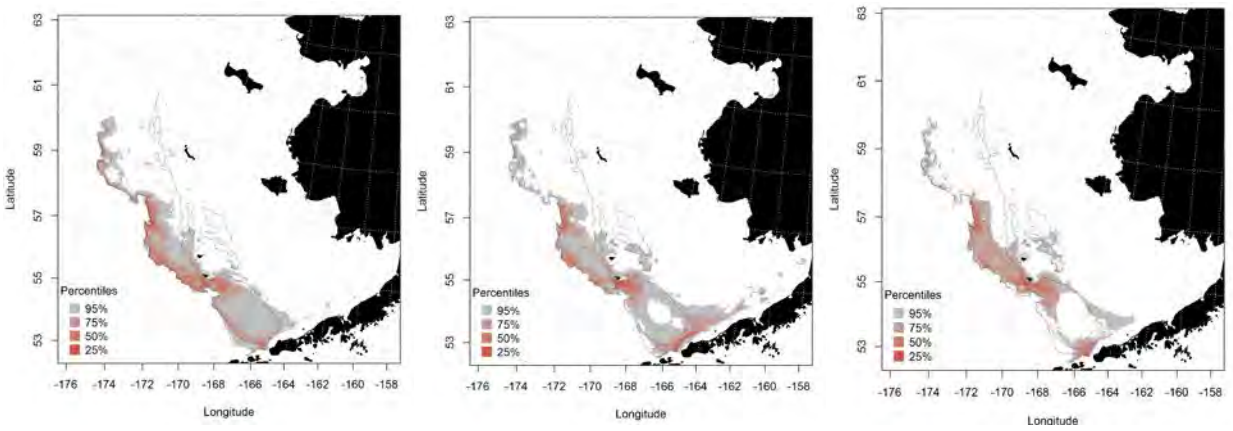

Figure 233. -- Essential fish habitat predicted for northern rockfish during fall (left panel), winter (middle panel) and spring (right panel) from commercial fishery catches.

dusky rockfish (*Sebastes variabilis*)

Dusky rockfish are distributed across the North Pacific from Japan and Russia to Alaska in the Bering Sea and Aleutian Islands and south into British Columbia. They are not common in summertime RACE bottom trawl surveys of the Eastern Bering Sea. Dusky rockfish do not support a directed fishery in the Bering Sea and are identified to species in commercial catches.

Summertime distribution of late juvenile and adult dusky rockfish from RACE bottom trawl surveys of the Eastern Bering Sea – Adult dusky rockfish occurred in RACE summer bottom trawl surveys of the Eastern Bering Sea in (Figure 234). They are not common and historically have occurred, on average in < 1% of survey stations annually. They have primarily been caught along the shelf break and slope edge in the southern domain as well as in shallower waters of the outer shelf. No juvenile dusky rockfish have been reported from RACE summer bottom trawl surveys of the Eastern Bering Sea.

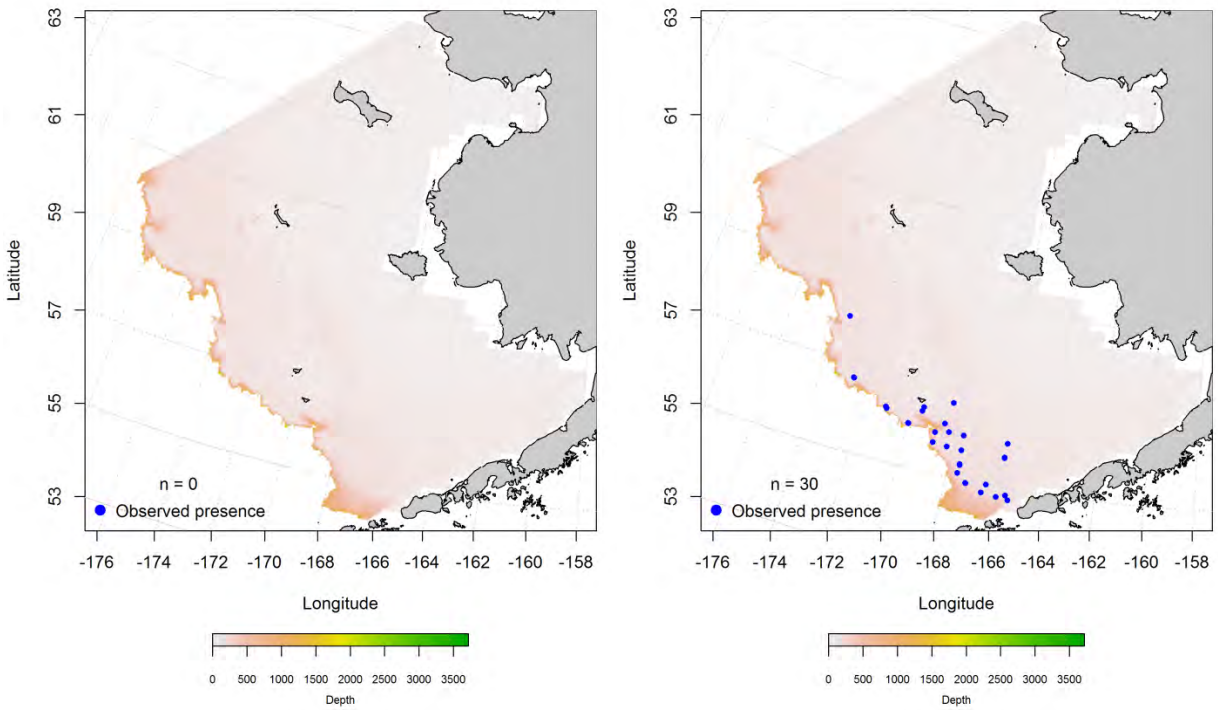

Figure 234. -- Distribution of late-juvenile (left) and adult (right) dusky rockfish catches from RACE summer bottom trawl surveys of the Eastern Bering Sea.

Seasonal distribution of the dusky rockfish in commercial fishery catches from the Eastern Bering Sea – In fall, dusky rockfish were reported in commercial catches from the Eastern Bering Sea (Figure 235). Occurrences extended from Navarin Canyon in the northern domain to the Bering Canyon in the southern domain and are primarily reported from the outer shelf and slope edge. Maximum entropy models based on dark rockfish presence data predicted the highest probability of suitable habitat near the heads of submarine canyons. Bottom depth, bottom temperature, and ocean productivity were the dominant habitat covariates in the model comprising 89.5% of the relative importance of predictor terms. The fit of the MaxEnt model to the training data was outstanding (AUC = 0.98) and it correctly predicted 92% of cases. Model validation was successful (AUC = 0.90) and 90% of cases predicted from the test data set were correct.

In winter, the overall distribution of dusky rockfish in commercial catches was similar to fall with more activity concentrated along the Bering Canyon axis (Figure 236). The highest probability suitable habitat areas predicted from the MaxEnt model shifted to the east-west axis of the Bering Canyon and between Pribilof Canyon and St. George Island. Bottom depth, bottom temperature, and sediment grain size provided 91.4% of the leverage from habitat covariates in the model. The fit of the MaxEnt model to the training data was outstanding (AUC = 0.97) and it correctly predicted 92% of presence-absence cases. Model validation was successful (AUC = 0.91) and 91% of cases predicted from the test data set were correct.

Springtime distribution of dusky rockfish in commercial catches extended over the same range as in fall and winter, but activity was concentrated around the southern edge of Zhemchug Canyon (Figure 237). The highest probability of suitable habitat was predicted from the MaxEnt model over the Bering Canyon and around the central and southern rim of Zhemchug Canyon. Bottom temperature, bottom depth, ocean productivity, and sediment grain size comprised 94.2% of the leverage from habitat covariates in the model. The MaxEnt fit to the training data was outstanding (AUC = 0.98) and correctly predicted 93% of cases. Model validation was successful based both on the high AUC (0.94) and the 94% of cases correctly classified by the test data.

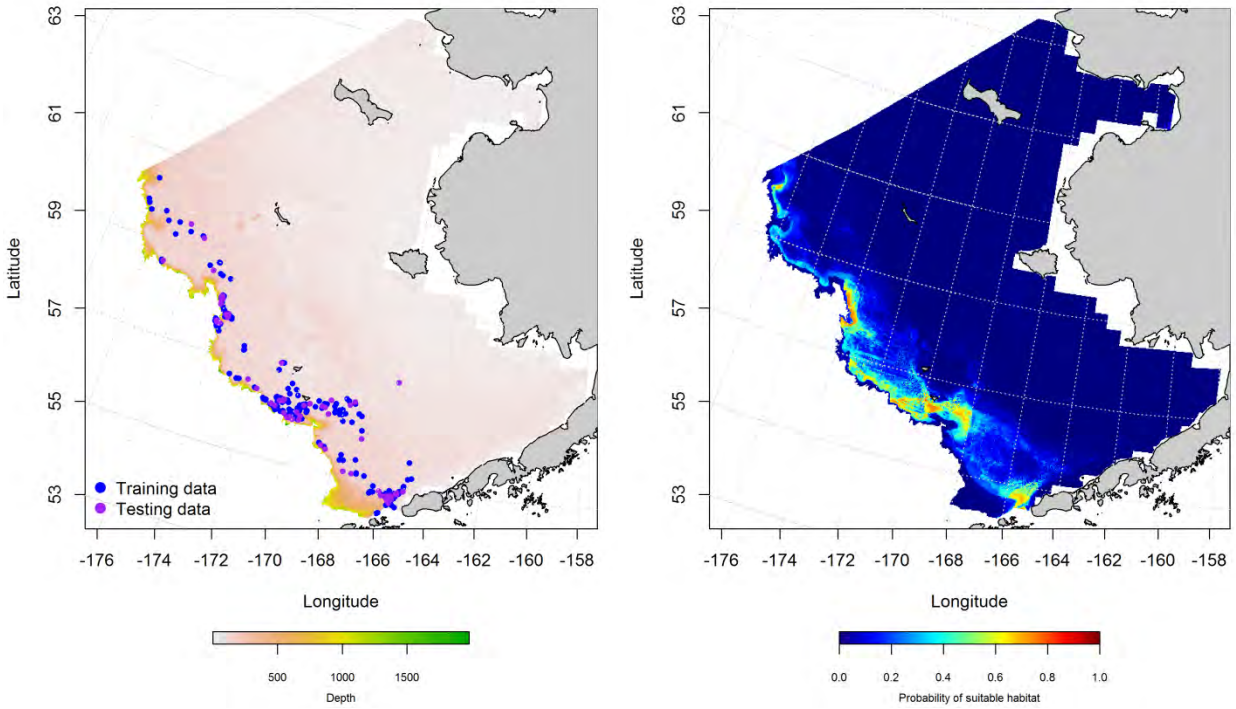

Figure 235. -- Locations of fall (October-November) catches of dusky rockfish in commercial fisheries of the Eastern Bering Sea (left panel). Blue points were used to train the MaxEnt model predicting the probability of suitable habitat (right panel) and the purple points were used to validate the model.

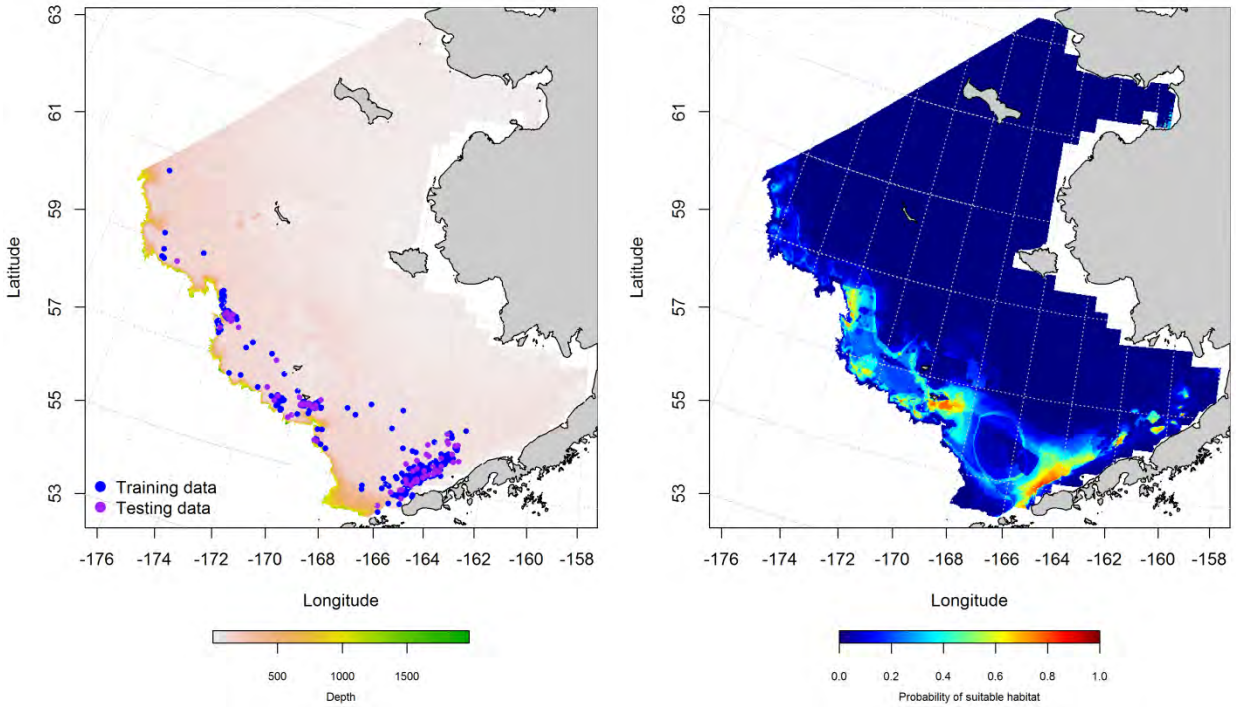

Figure 236. -- Locations of winter (December-February) catches of dusky rockfish in commercial fisheries of the Eastern Bering Sea (left panel). Blue points were used to train the MaxEnt model

predicting the probability of suitable habitat (right panel) and the purple points were used to validate the model.

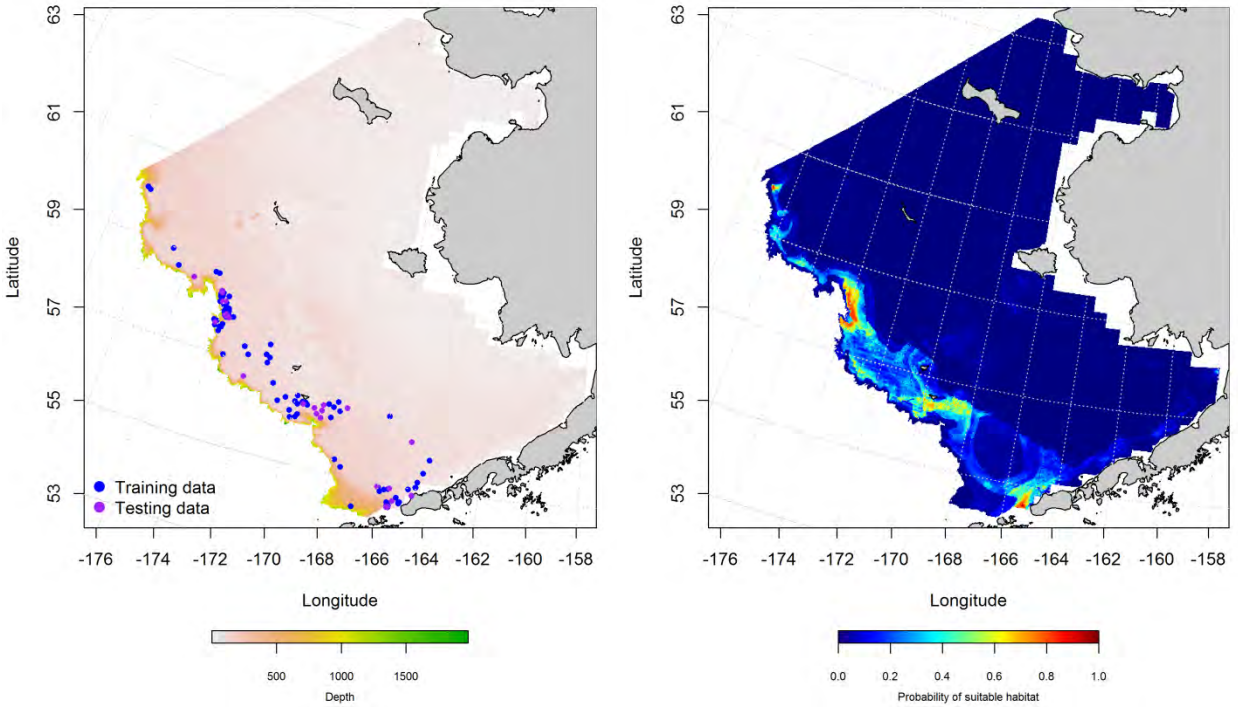

Figure 237. -- Locations of spring (March-May) catches of dusky rockfish in commercial fisheries of the Eastern Bering Sea (left panel). Blue points were used to train the MaxEnt model predicting the probability of suitable habitat (right panel) and the purple points were used to validate the model.

Essential fish habitat maps and conclusions for dusky rockfish in the Eastern Bering Sea -- Essential fish habitat for dusky rockfish extends from Navarin Canyon in the northern domain of the Eastern Bering Sea to the Bering Canyon and Bristol Bay in the southern domain (Figure 238). Habitat for these fishes predicted from their presence in commercial catches is primarily in waters deeper than 100 m along the outer shelf and slope edge. There appear to be some seasonal differences in the distribution of dusky rockfish EFH in the Eastern Bering Sea. In the wintertime, in particular, it seems that dusky rockfish in commercial catches are more common from the Bering Canyon than during other times of the year.

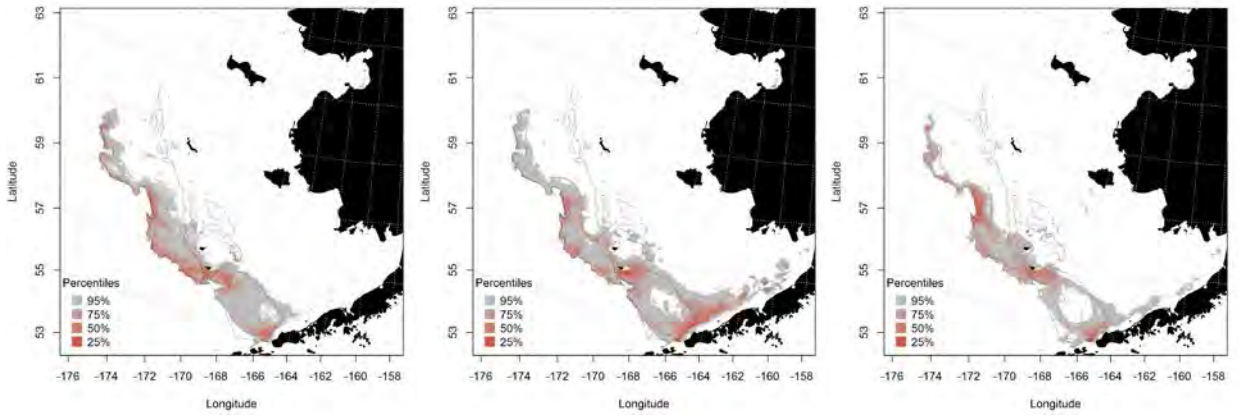

Figure 238. -- Essential fish habitat predicted from commercial fishery catches for dusky rockfish during fall (left panel), winter (middle panel), and spring (right panel).

thornyheads (*Sebastolobus* spp.)

Thornyheads (*Sebastolobus* spp.) are represented by 3 species in the Eastern Bering Sea: broadfin (*Sebastolobus macrochir*), shortspine (*S. alascanus*), and longspine (*S. altivelis*) thornyheads. Eggs of these species cannot be distinguished from each other, but larvae and early juveniles are identifiable to species. In the historical record from EcoFOCI ichthyoplankton surveys, eggs and larvae of this genus from the Eastern Bering Sea have only been identified as *Sebastolobus* spp. Shortspine thornyhead are the only species of *Sebastolobus* reported from RACE summer bottom trawl surveys of the Eastern Bering Sea; all of these have been reported from the Eastern Bering Sea Slope survey. This is also the primary species of thornyhead reported from commercial fishery catches by federal observers.

Seasonal distribution of early life history stages of *Sebastolobus* spp. in the Eastern Bering Sea – Eggs of *Sebastolobus* spp. have been collected in fall, winter, and spring months on EcoFOCI ichthyoplankton surveys of the Eastern Bering Sea (Figure 239). They were primarily encountered in the southern domain of the survey area. They occur across the shelf from deeper benthypelagic waters (< 1,000 m) to shallower middle shelf waters (50 to 100 m).

Larval thornyheads were collected rarely on summer EcoFOCI ichthyoplankton surveys of the Eastern Bering Sea (Figure 240). No juvenile thornyheads were reported from these surveys. Presence records for any of these early life history stages of thornyheads were not sufficient to parameterize distribution models for this genus.

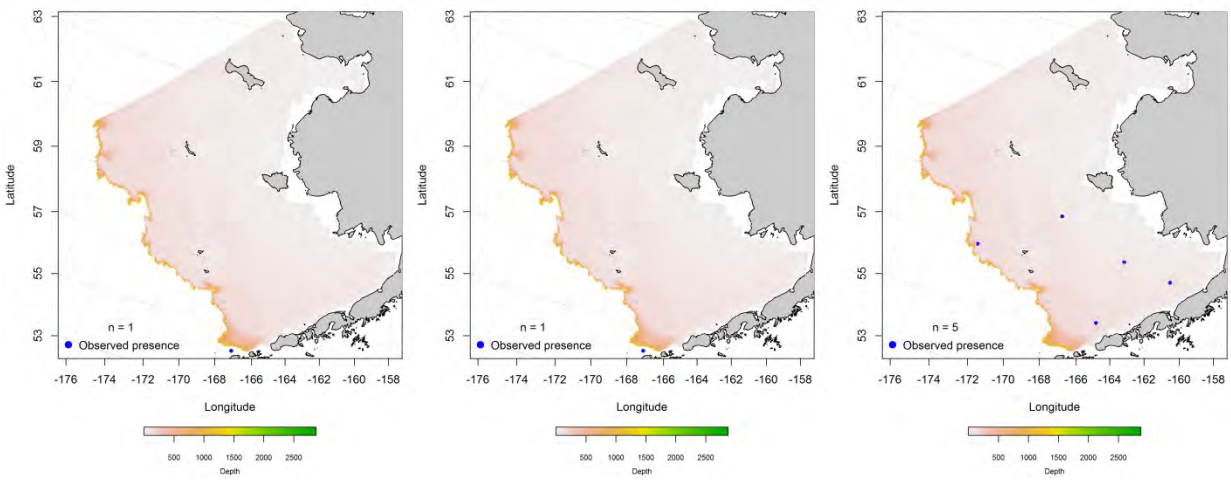

Figure 239. – Fall (left panel), winter (middle) and spring (right) observations of thornyhead eggs from EcoFOCI ichthyoplankton surveys of the Eastern Bering Sea.

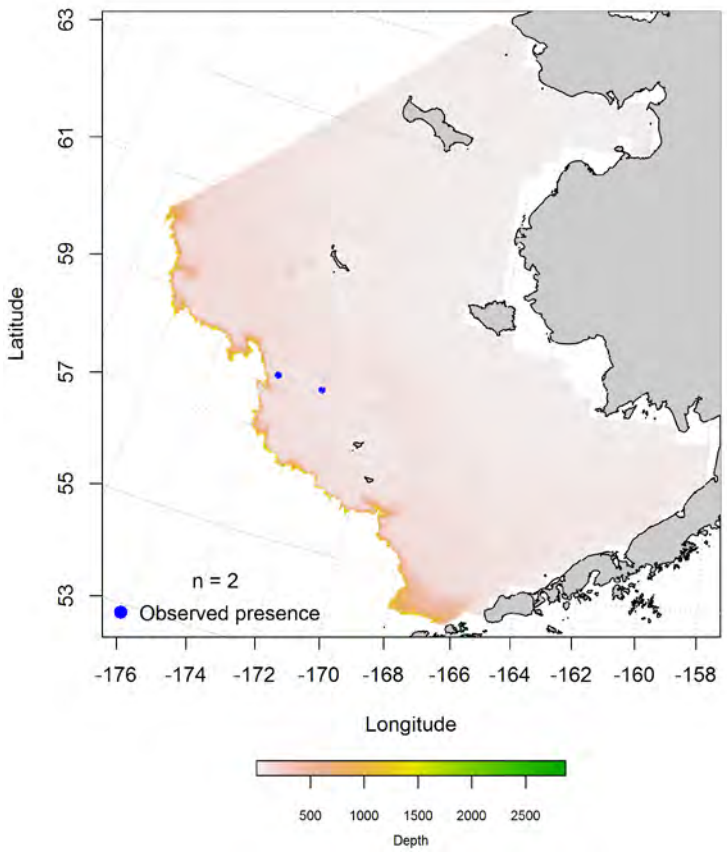

Figure 240. -- Summer observations of larval *Sebastolobus* spp. from EcoFOCI ichthyoplankton surveys of the the Eastern Bering Sea.

shortspine thornyhead (*Sebastolobus alascanus*)

Shortspine thornyhead are distributed across the North Pacific from Japan and Russia to Alaska in the Bering Sea and Aleutian Islands and south into Baja California. In RACE bottom trawl surveys of the Eastern Bering Sea, shortspine thornyheads have primarily been collected over the Bering Sea Slope. They have occurred over a wide range of depths (55 to >1,100 m) in these trawl catches.

Summertime distribution of late juvenile and adult shortspine thornyhead from RACE bottom trawl surveys of the Eastern Bering Sea – Late juvenile and adult shortspine thornyhead occurred in RACE summer bottom trawl surveys of the Eastern Bering Sea (Figure 241). Both life stages

were encountered primarily in shelf edge and slope waters > 200 m in depth. The number of catches available for analyses was not sufficient to parameterize a species distribution model for shortspine thornyhead from RACE summer bottom trawl surveys of the Eastern Bering Sea.

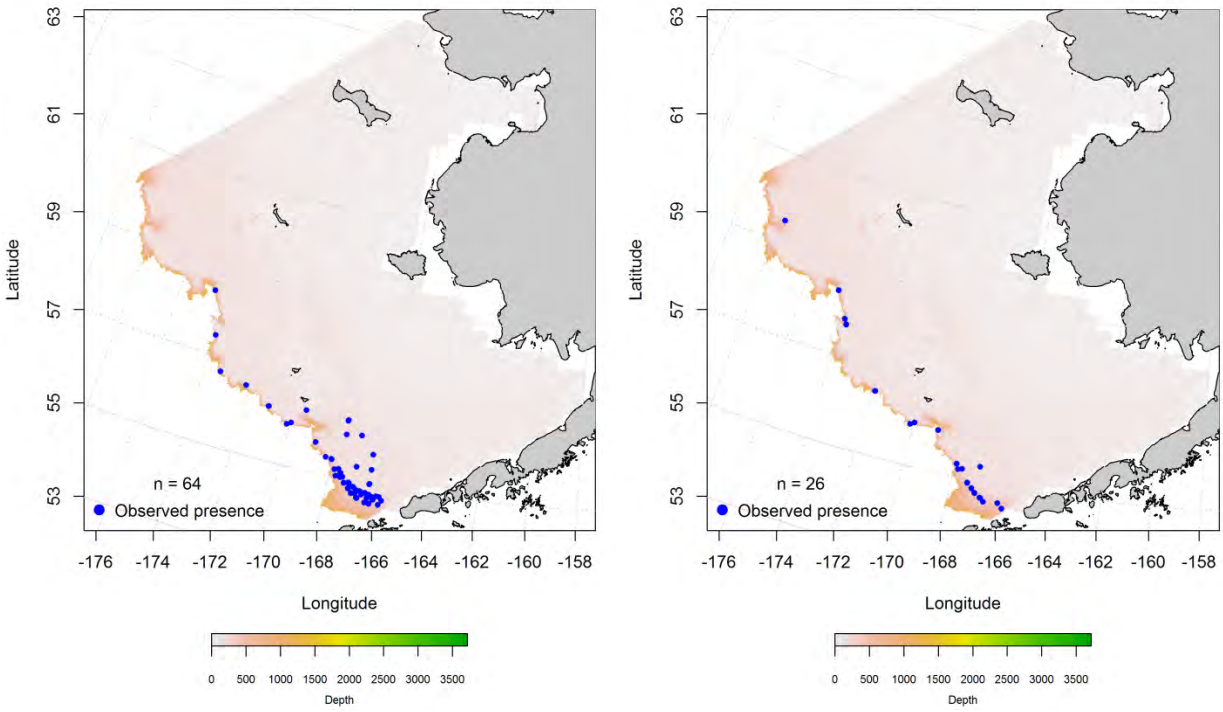

Figure 241. -- Distribution of late-juvenile (left) and adult (right) shortspine thornyhead catches from RACE summer bottom trawl surveys of the Eastern Bering Sea.

Seasonal distribution of the shortspine thornyhead in commercial fishery catches from the Eastern Bering Sea – In fall, shortspine thornyhead were reported from commercial catches in the Eastern Bering Sea from the Bering Canyon in the south to Pervenets Canyon in the north (Figure 242). Maximum entropy models based on shortspine thornyhead presence data predicted the highest probability of suitable habitat over the Bering Canyon. Bottom depth, bottom slope, and bottom temperature were the dominant habitat covariates in the model comprising 95.3% of the relative importance of predictor terms. The fit of the MaxEnt model to the training data was outstanding (AUC = 0.99) and it correctly predicted

95% of cases. Model validation was successful (AUC = 0.98) and 98% of cases predicted from the test data set were correct.

In winter, the distribution of shortspine thornyhead in commercial catches was limited to the central and southern domains of the Eastern Bering Sea slope (Figure 243). The highest probability suitable habitat areas predicted from the MaxEnt model were still located over the Bering Canyon. Bottom depth and ocean productivity provided 97.4% of the leverage from habitat covariates in the model. The fit of the MaxEnt model to the training data was outstanding (AUC = 1.0) and it correctly predicted 99% of cases. Model validation was successful (AUC = 0.98) and 98% of cases predicted from the test data set were correct.

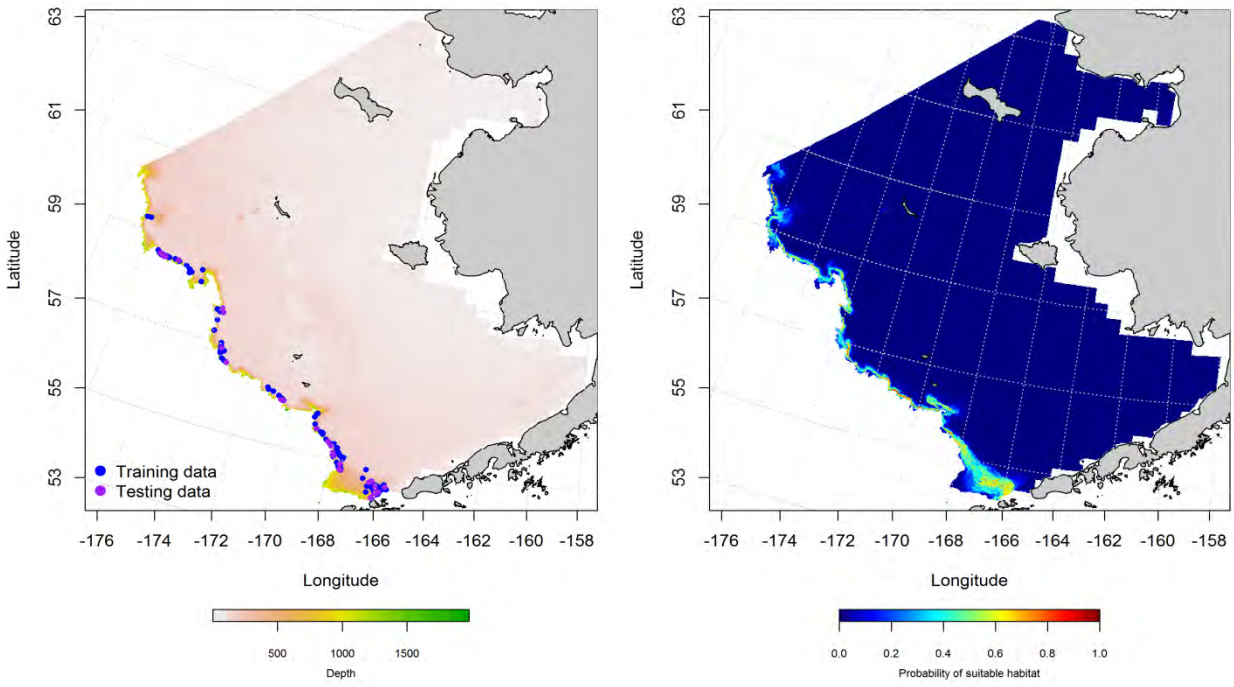

Figure 242. -- Locations of fall (October-November) catches of shortspine thornyhead in commercial fisheries of the Eastern Bering Sea (left panel). Blue points were used to train the MaxEnt model predicting the probability of suitable habitat (right panel) and the purple points were used to validate the model.

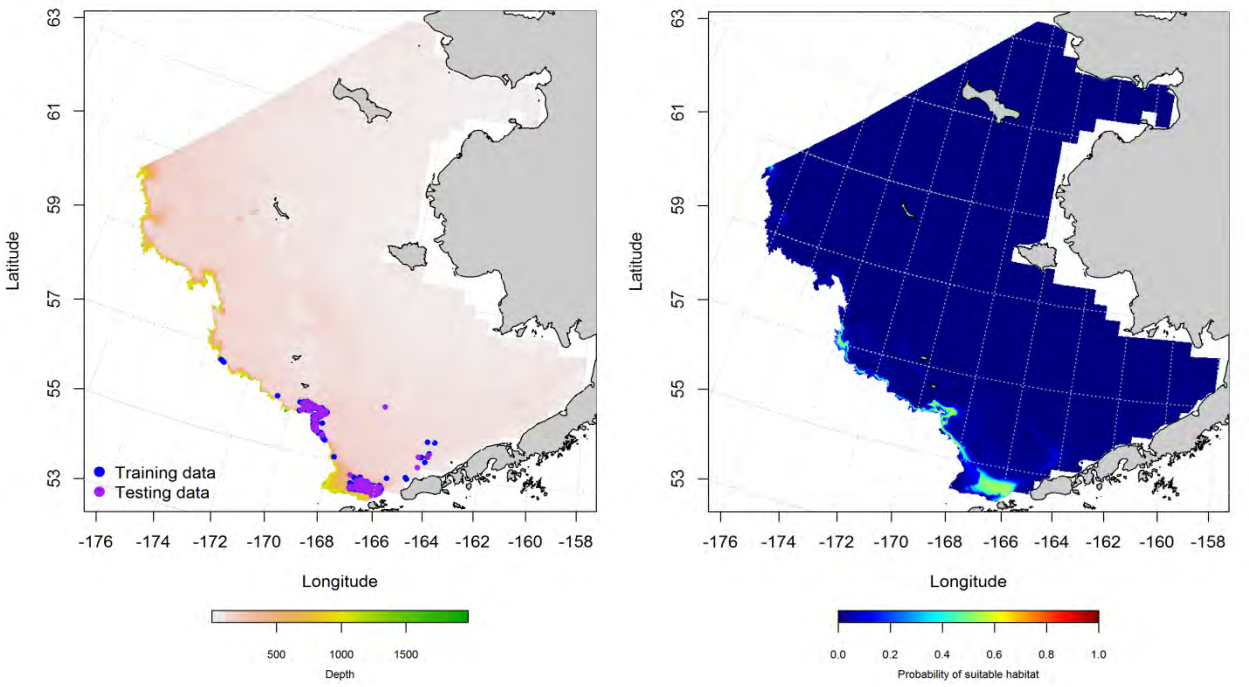

Figure 243. -- Locations of winter (December-February) catches of shortspine thornyhead in commercial fisheries of the Eastern Bering Sea (left panel). Blue points were used to train the MaxEnt model predicting the probability of suitable habitat (right panel) and the purple points were used to validate the model.

Essential fish habitat maps and conclusions for shortspine thornyhead in the Eastern Bering Sea – There were some seasonal differences in the distribution of shortspine thornyhead EFH predicted from commercial fishery catches in the Eastern Bering Sea (Figure 244). In fall, EFH extended from Navarin Canyon in the northern domain along the upper slope edge to the Bering Canyon in the southern domain. In wintertime, the northern extent of EFH stopped south of Zhemchug Canyon. Overall, EFH predicted from commercial catches was primarily in waters deeper than 200 m along the shelf edge and slope.

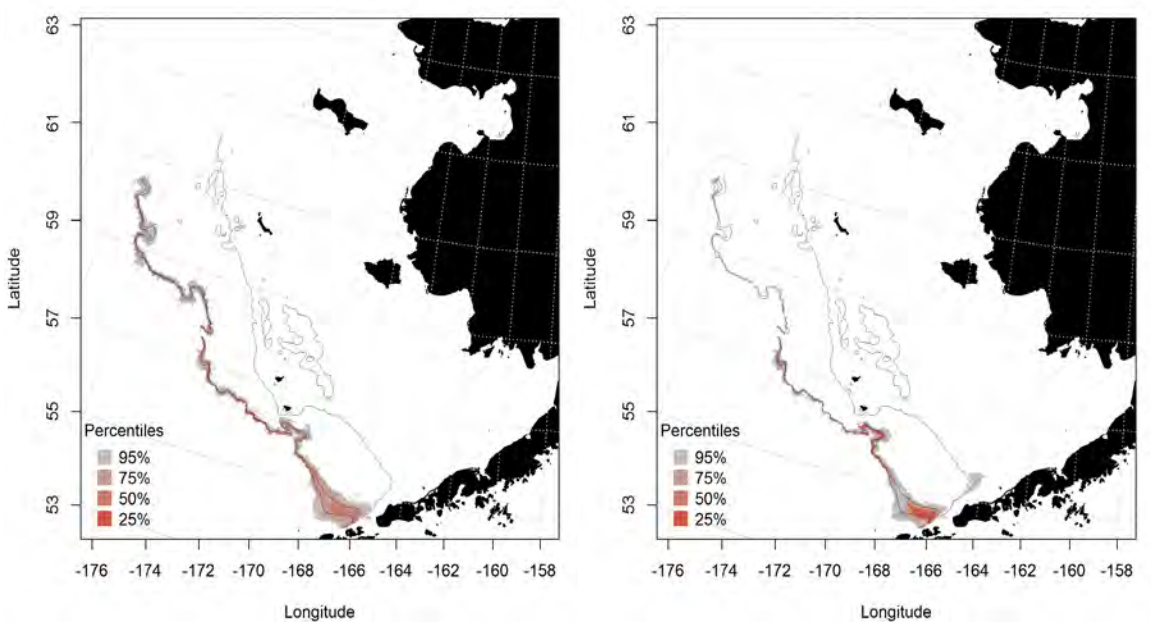

Figure 244. -- Essential fish habitat predicted for shortspine thornyhead from commercial fishery catches during fall (left panel) and winter (middle panel).

Skates

Aleutian skate (*Bathyraja aleutica*)

Aleutian skates are distributed across the North Pacific Ocean from Japan and Russia into the Bering Sea, throughout the Aleutian Islands chain, and south into the Eastern Gulf of Alaska. They are one of the most abundant skates in the Aleutian Islands (Ormseth and Matta 2009) and typically occur at depths of 100 to 800 m (Mecklenburg et al. 2002). All skate species in the North Pacific are part of the "Other species" management category within the BSAI FMP.

Summertime distribution of juvenile and adult Aleutian skate from RACE bottom trawl surveys of the Eastern Bering Sea – Juvenile and adult Aleutian skates occurred in RACE bottom trawl survey catches across all 3 domains of the Eastern Bering Sea (Figure 245). Their distribution spanned the middle and outer shelf but they were concentrated in benthypelagic waters off the shelf break. Juvenile and adult Aleutian skates co-occur throughout the survey area.

A hurdle GAM was used to model juvenile Aleutian skate species distribution in the Eastern Bering Sea. The presence GAM predicted that the highest probabilities of encountering juvenile Aleutian skates in RACE summer bottom trawl catches occurred over benthypelagic waters over the Eastern Bering Sea Slope (Figure 246). The best-fitting GAM explained 71.9% of the deviance in their distribution data. Bottom depth and geographical location were the most significant predictors retained in the model. The probability of observing juvenile skates in RACE bottom trawl catches increased with increasing depth up to around 400 m to the west and south of the shelf break. The presence-absence GAM was an outstanding fit to the training data (AUC = 0.98) and correctly classified 95% of predicted cases of presence-absence. Model validation was successful (AUC = 0.95) correctly classified 95% of cases predicted from the test data.

In the second step of the hurdle, juvenile Aleutian skate conditional abundance was predicted where the threshold for presence established in the first step was met. The best-fitting GAM explained just 39.1% of the deviance in juvenile Aleutian skate CPUE from RACE bottom trawl surveys of the Eastern Bering Sea (Figure 247). The most important habitat predictors were bottom depth and geographic location. Conditional abundance increased with increasing depth offshore of the shelf break. Model fits were poor for the training and test data sets (r^2 = 0.39 and 0.40).

A MaxEnt model predicted adult Aleutian skate species distribution in the Eastern Bering Sea (Figure 248). Adults appeared to be more closely associated with the shelf break than the pattern modeled for juveniles. Bottom depth and bottom temperature were the most important predictors of then probability of adult Aleutian skate suitable habitat (combined relative importance = 95.5%). The probability of suitable habitat increased at depths around 300 m and around temperatures close to 10°C. The MaxEnt model was an outstanding fit to the training data (AUC = 0.98) and correctly classified 95% of predicted cases. In the model validation step, the GAM fit was excellent (AUC = 0.89) correctly classifying 89% of cases predicted from the test data.

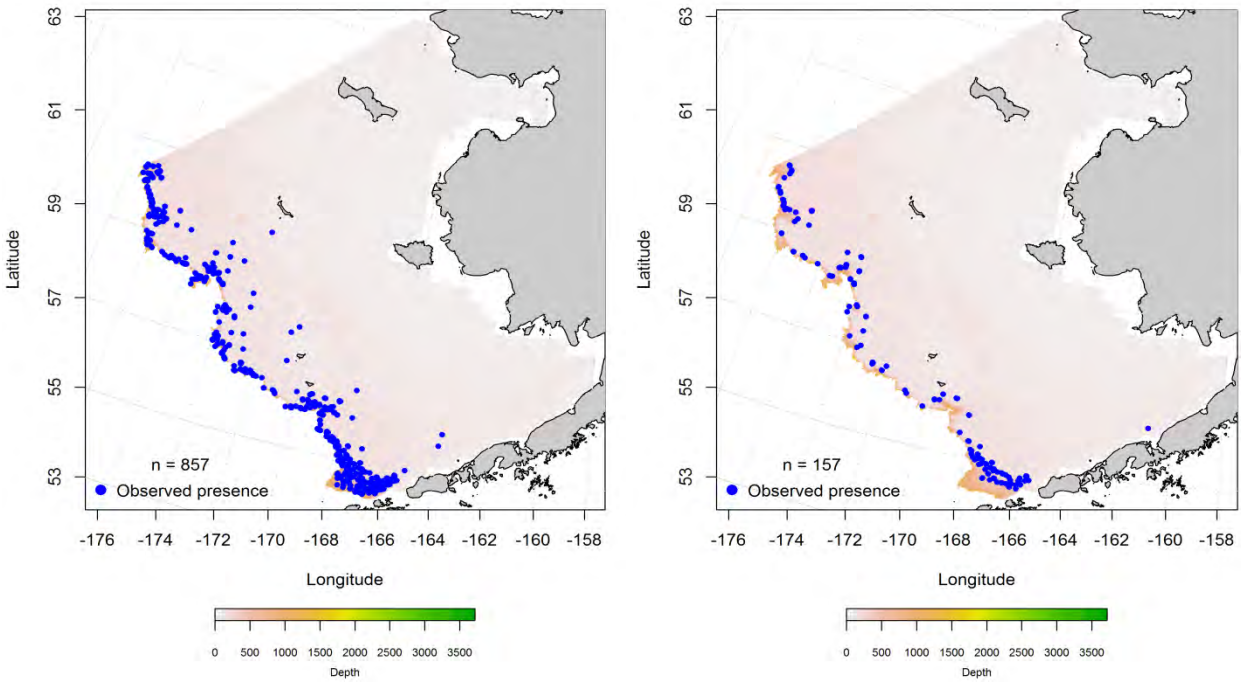

Figure 245. -- Distribution of juvenile (left) and adult (right) Aleutian skate catches from RACE summer bottom trawl surveys of the Eastern Bering Sea.

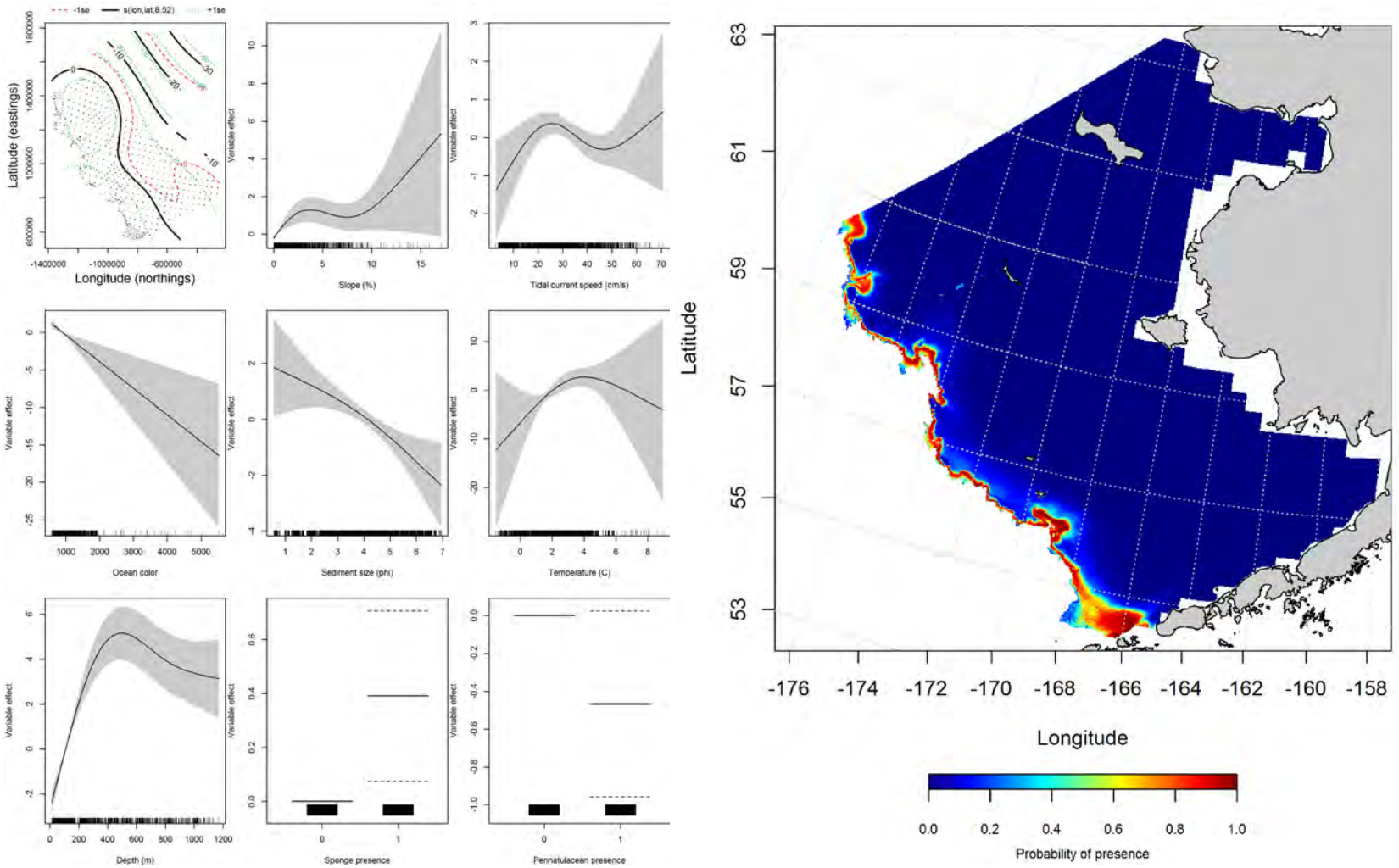

Figure 246. -- Effects of retained habitat covariates on the best-fitting generalized additive presence-absence model (GAM) of late juvenile Aleutian skates from RACE summer bottom trawl surveys of the Eastern Bering Sea Shelf, Slope, and Northern Bering Sea alongside their predicted presence (right panel).

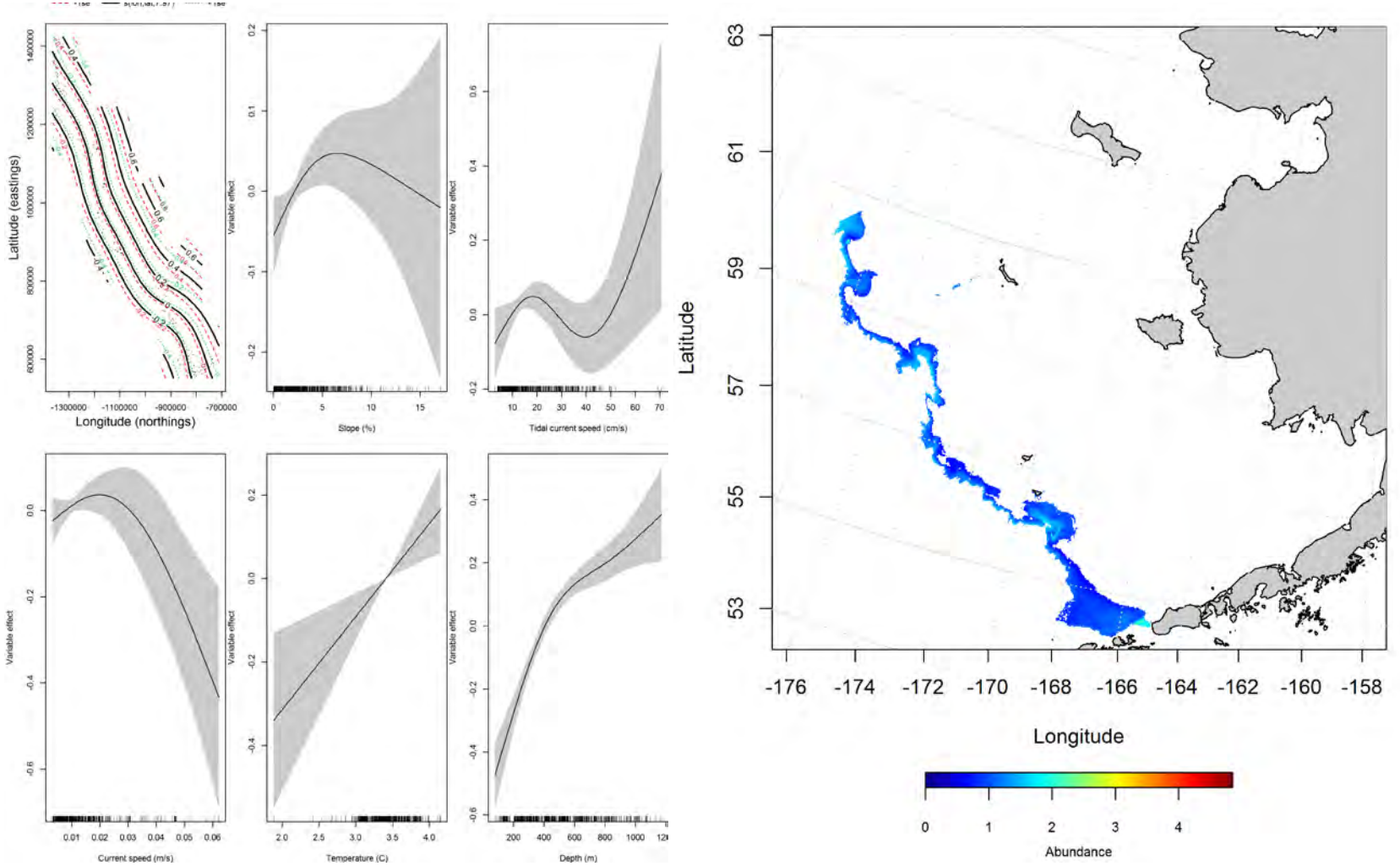

Figure 247. -- Effects of retained habitat covariates on the best-fitting generalized additive model (GAM) of late juvenile Aleutian skates from RACE summer bottom trawl surveys of the Eastern Bering Sea Shelf, Slope, and Northern Bering Sea alongside their predicted conditional abundance (right panel).

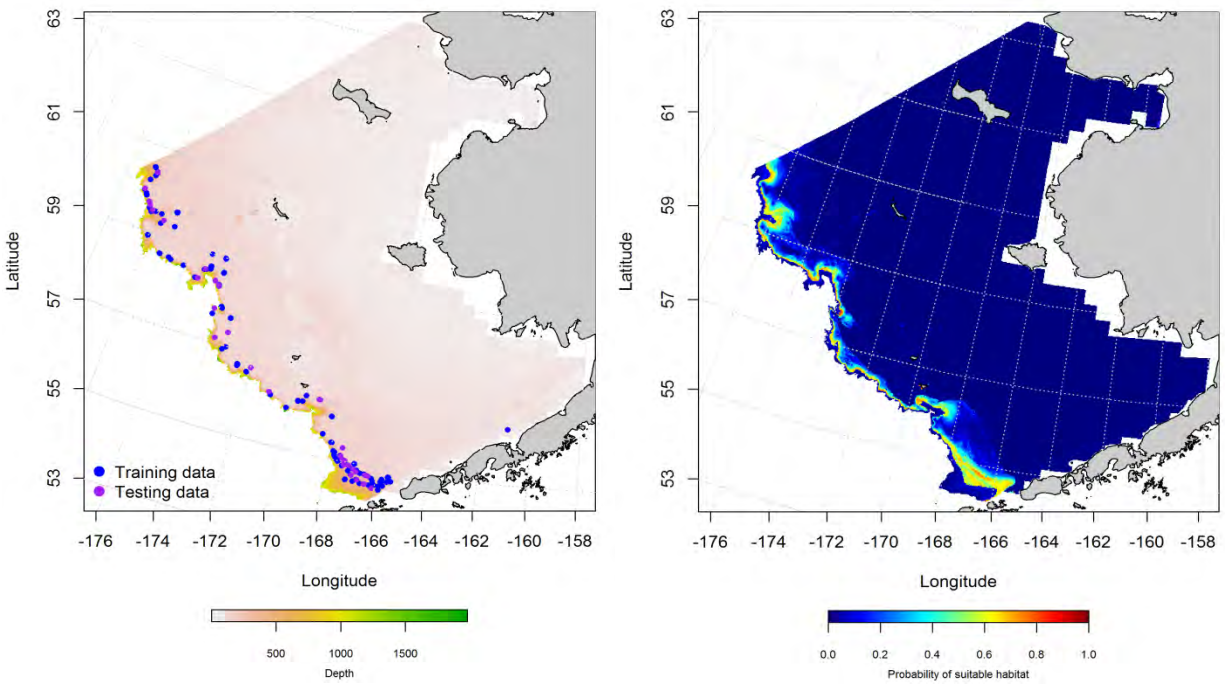

Figure 248. -- Locations of summer RACE Groundfish trawl survey catches of adult Aleutian skate (left panel). Blue points were used to train the maximum entropy (MaxEnt) model predicting the probability of suitable habitat (right panel) and the purple points were used to validate the model.

Seasonal distribution of Aleutian skate in commercial fishery catches from the Eastern Bering Sea – Aleutian skates observed in fall commercial fishery catches were distributed across the Eastern Bering Sea over the middle and outer shelf from Bering to Navarin Canyon (Figure 249). Maximum entropy modeling predicts the highest probabilities of suitable Aleutian skate habitat primarily from Pribilof Canyon north over the outer shelf. Bottom depth and bottom temperature were the dominant habitat covariates influencing the model (84.6% of the relative importance of all covariates combined) describing Aleutian skate presence in fall commercial fisheries catches. The MaxEnt model was an outstanding fit to the training data (AUC = 0.94) with 88% of cases correctly classified. Fit of the model in the validation step was excellent (AUC = 0.87) and 87% of the cases were correctly classified for the test data set.

The winter distribution of Aleutian skate in commercial catches extended from the Bering Canyon in the south to Navarin Canyon in the north (Figure 250). Catches of Aleutian skate were observed further east into Bristol Bay than were seen in fall. Bottom depth and bottom temperature were the dominant habitat covariates influencing the model (84.4% of the relative importance of all covariates combined) describing Aleutian skate presence in winter commercial fisheries catches. The model predicted 88% of cases correctly from the training data and was an outstanding fit (AUC = 0.94). Fit of the model in the validation step was excellent (AUC = 0.86) and 86% of the cases were correctly classified for the test data set.

In springtime, Aleutian skates were widely represented over the middle and outer shelf of the Eastern Bering Sea (Figure 251). The highest probability suitable habitats were predicted over the Bering Canyon and at the heads of Pribilof, Zhemchug, and Pervenets Canyons. The most important predictors in the MaxEnt model were bottom depth, bottom temperature, and sediment grain size. These three covariates accounted for a combined 83.6% of the relative importance of the 7 covariates in the model. The MaxEnt model was an outstanding fit to the training data (AUC = 0.91) and predicted 83% of cases correctly. Fit of the model in the validation step was excellent (AUC = 0.81) and 81% of the cases were correctly classified for the test data set.

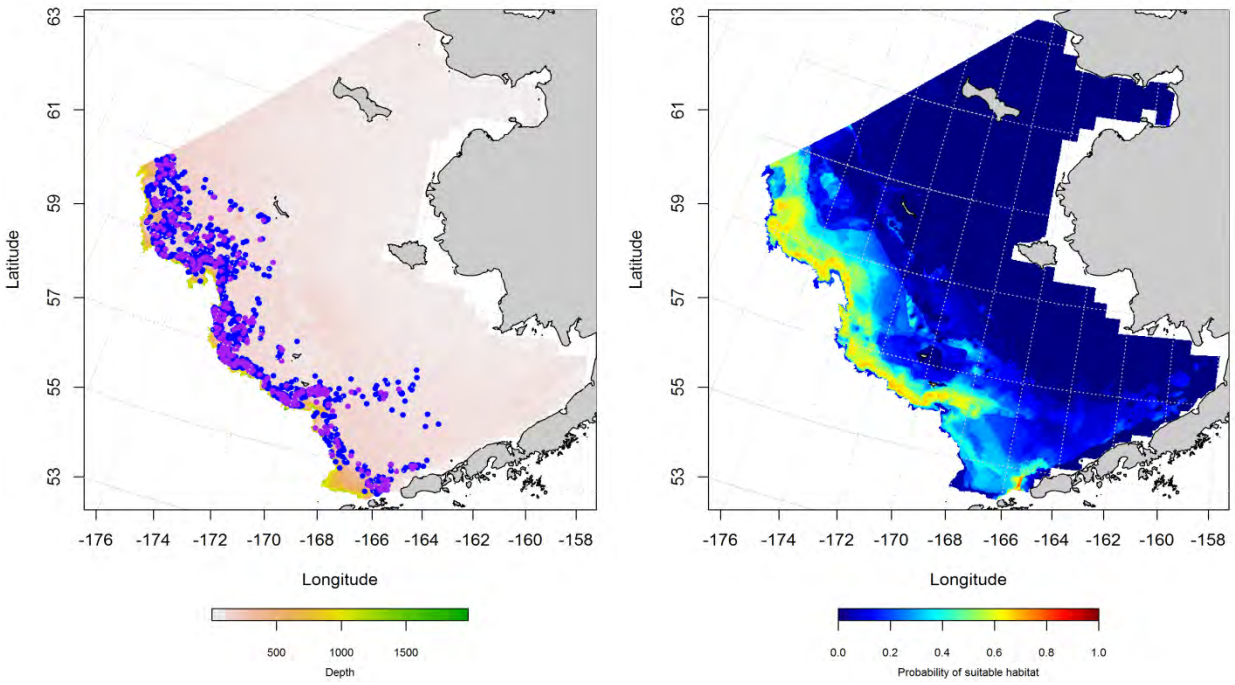

Figure 249. -- Presence of Aleutian skate in commercial fishery catches from fall (October-November; left panel). Blue points were used to train the maximum entropy (MaxEnt) model predicting the probability of suitable habitat (right panel) and the purple points were used to validate the model.

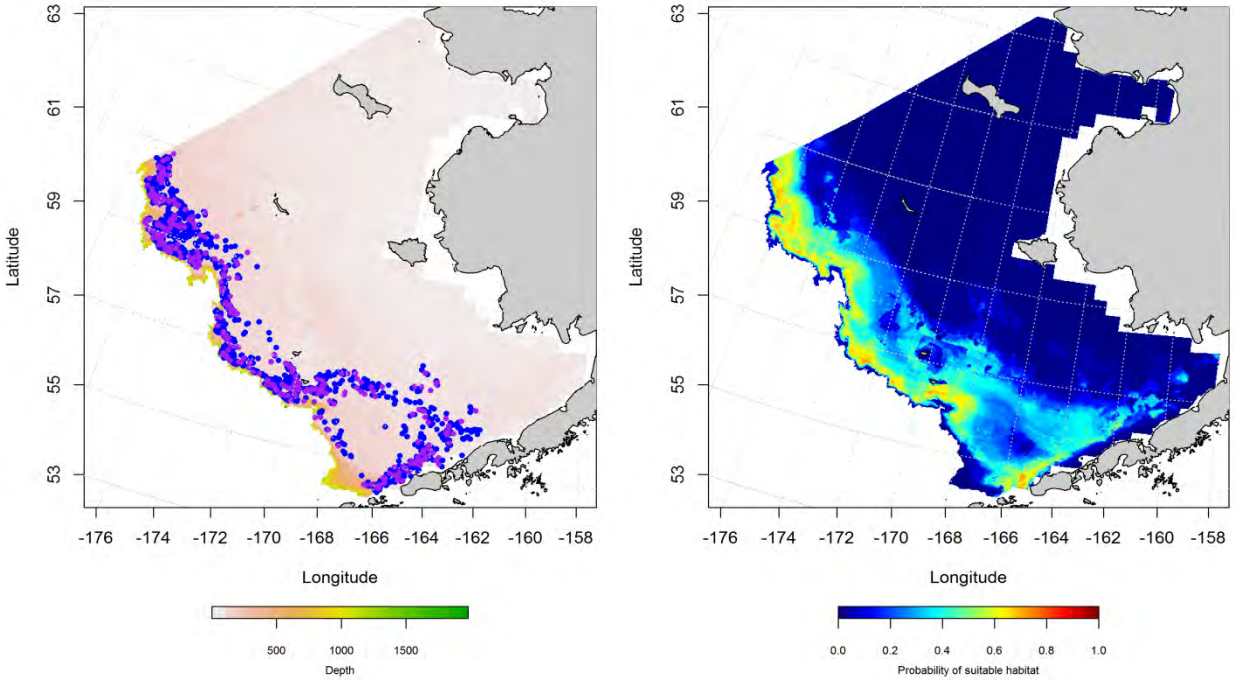

Figure 250. -- Presence of Aleutian skate in commercial fishery catches from winter (December-February; left panel). Blue points were used to train the maximum entropy (MaxEnt) model predicting the probability of suitable habitat (right panel) and the purple points were used to validate the model.

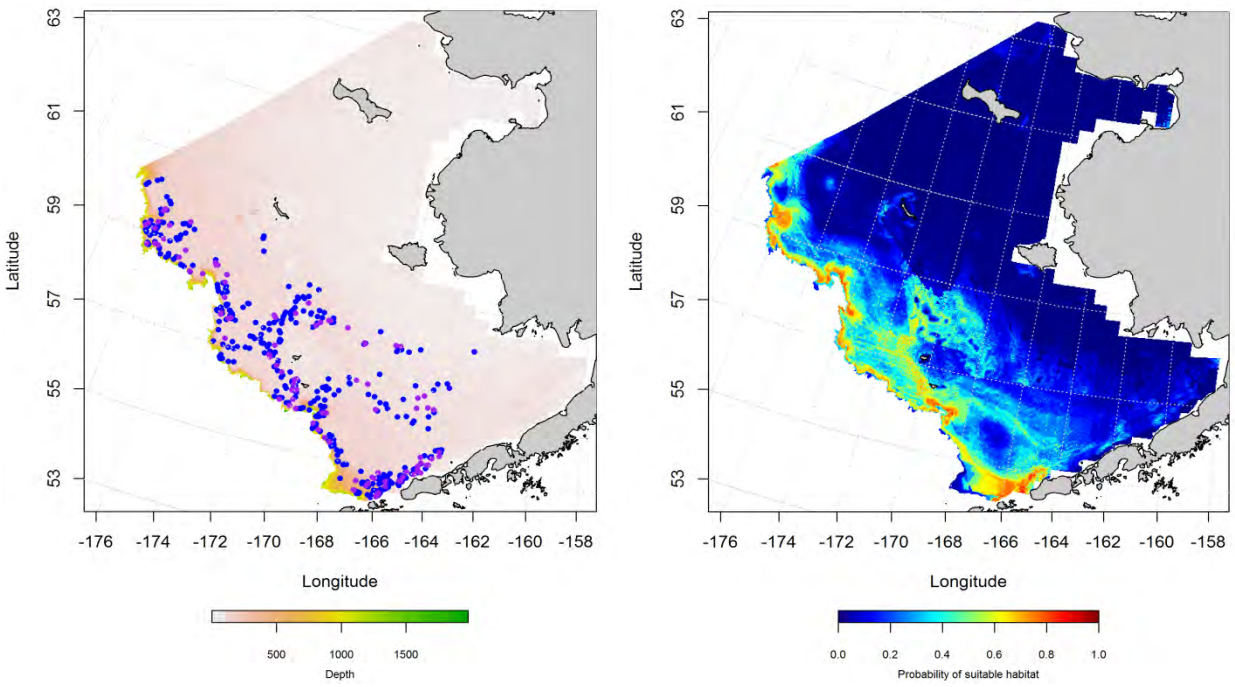

Figure 251. -- Presence of Aleutian skate in commercial fishery catches from spring (March-May; left panel). Blue points were used to train the maximum entropy (MaxEnt) model predicting the probability of suitable habitat (right panel) and the purple points were used to validate the model.

Essential fish habitat maps and conclusions for Aleutian skate (*Bathyraja aleutica*) in the Eastern Bering Sea – Species distribution modeling of Aleutian skate in the Eastern Bering Sea predicts that EFH for this species varies between life stages and seasons (Figure 252). Both life stages co-occur in association with the shelf break from the Bering Canyon in the south to Navarin Canyon in the north. However, juvenile Aleutian skate EFH was predicted from summertime RACE bottom trawl surveys of the Eastern Bering Sea to be deeper than that predicted for adults.

Predictions of suitable Aleutian skate habitat from commercial fishery catches in the Eastern Bering Sea showed some slight seasonal (Figure 253). In general, the highest probability habitats were located along the shelf break and upper slope of the Eastern Bering Sea. Springtime distribution of predicted EFH showed a broader spatial distribution than predicted for fall or winter.

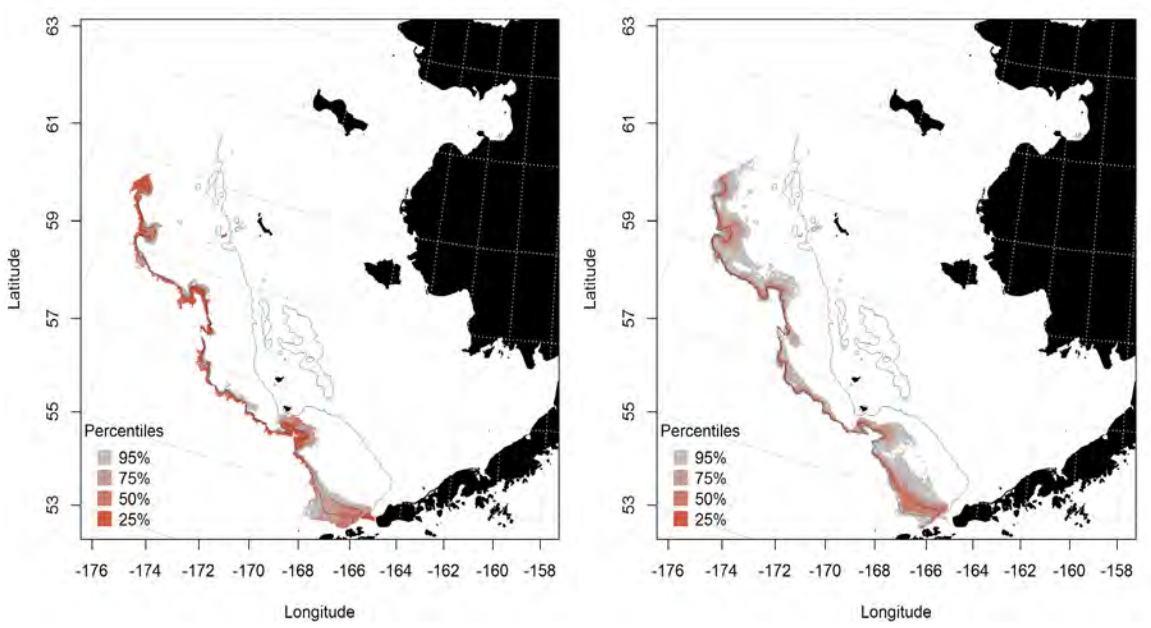

Figure 252. -- Essential fish habitat predicted for juvenile and adult Aleutian skate (left and right panel) from summertime RACE bottom trawl surveys of the Eastern Bering Sea.

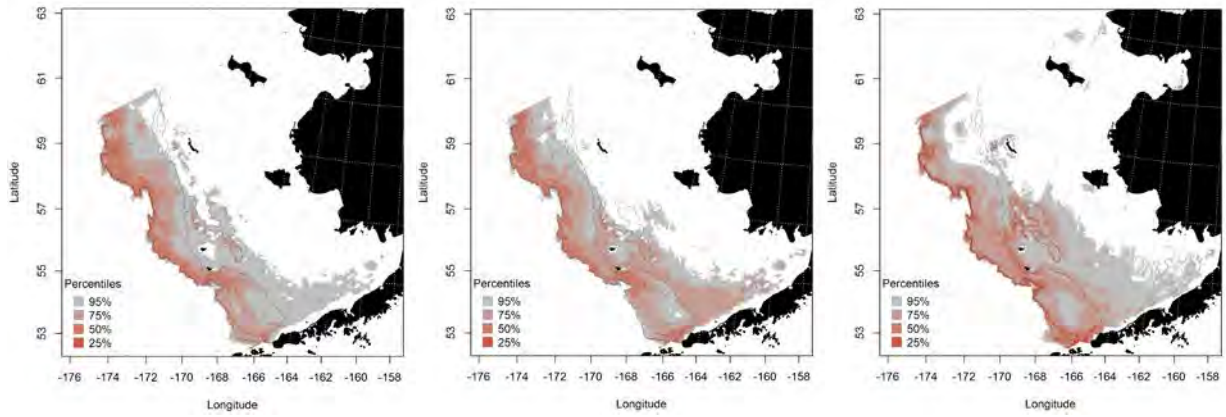

Figure 253. -- Essential fish habitat predicted from Aleutian skate occurrences in commercial fishery catches during fall (left panel), winter (middle panel), and spring (right panel) in the Eastern Bering Sea.

Bering skate (*Bathyraja interrupta*)

Bering skates are distributed across the Eastern Bering Sea and Aleutian Islands and south to Cortez Bank off southern California. They are the second most common skate species in the Eastern Bering Sea (Ainsley et al. 2011). They occur at depths of 55 to 1,372 m in the Bering Sea and Gulf of Alaska

(Mecklenburg et al. 2002). All skate species in the North Pacific are part of the "Other species" management category within the BSAI FMP.

Summertime distribution of juvenile and adult Bering skate from RACE bottom trawl surveys of the Eastern Bering Sea – Juvenile and adult Bering skates occurred in RACE bottom trawl survey catches across all 3 domains of the Eastern Bering Sea (Figure 254). They co-occur throughout the survey area.Their distribution spanned the middle and outer shelf, but they were concentrated over the Bering and Zhemchug Canyons.

A hurdle GAM was used to model juvenile Bering skate species distribution in the Eastern Bering Sea. The presence GAM predicted that the highest probabilities of encountering juvenile Bering skates in RACE summer bottom trawl catches occurred near Navarin and Pervenets Canyons in the north and between Bering and Pribilof Canyons in the southern domain (Figure 255). The best-fitting GAM explained 44.5% of the deviance in their distribution data. Bottom depth and geographical location were the most significant predictors retained in the model. The probability of observing juvenile skates in RACE bottom trawl catches increased with increasing depth up to around 300 m and moving westward across the survey area. The presence-absence GAM was an outstanding fit to the training data (AUC = 0.93) and correctly classified 86% of predicted cases of presence-absence. Model validation was successful (AUC = 0.94) correctly classified 86% of cases predicted from the test data.

In the second step of the hurdle, juvenile Bering skate conditional abundance was predicted where the threshold for presence established in the first step was met. The best-fitting GAM explained just 33.5% of the deviance in juvenile Bering skate CPUE from RACE bottom trawl surveys of the Eastern Bering Sea (Figure 256). The most important habitat predictors were bottom depth and geographic location. Conditional abundance increased with increasing depth up to ca. 300 m. Model fits were poor for the training and test data sets (r^2 = 0.33 and 0.25).

Adult Bering skate distribution was modeled with a hurdle GAM in the Eastern Bering Sea. The presence-absence GAM predicted that the highest probabilities of encountering adult Bering skates in RACE summer bottom trawl catches occurred on the outer shelf between Pribilof and Bering Canyon in the southern domain and from Navarin down to Zhemchug Canyon in the northern and central domains (Figure 257). The best-fitting GAM explained 39.6% of the deviance in their distribution data. Geographical location, bottom depth, and sediment grain size were the most significant predictors retained in the model. Model effects increased to the west and were highest at depths around 200 m over sand bottom. The presence-absence GAM was an outstanding fit to the training data (AUC = 0.91) and correctly classified 83% of predicted cases of presence-absence. Model validation was successful (AUC = 0.90) correctly classified 82% of cases predicted from the test data.

Conditional abundance of adult Bering skate was predicted where the threshold for presence established in the first step was met. The best-fitting GAM explained just 14% of the deviance in juvenile Bering skate CPUE from RACE bottom trawl surveys of the Eastern Bering Sea (Figure 258). Model fits were poor for the training and test data sets (r^2 = 0.14 and 0.09).

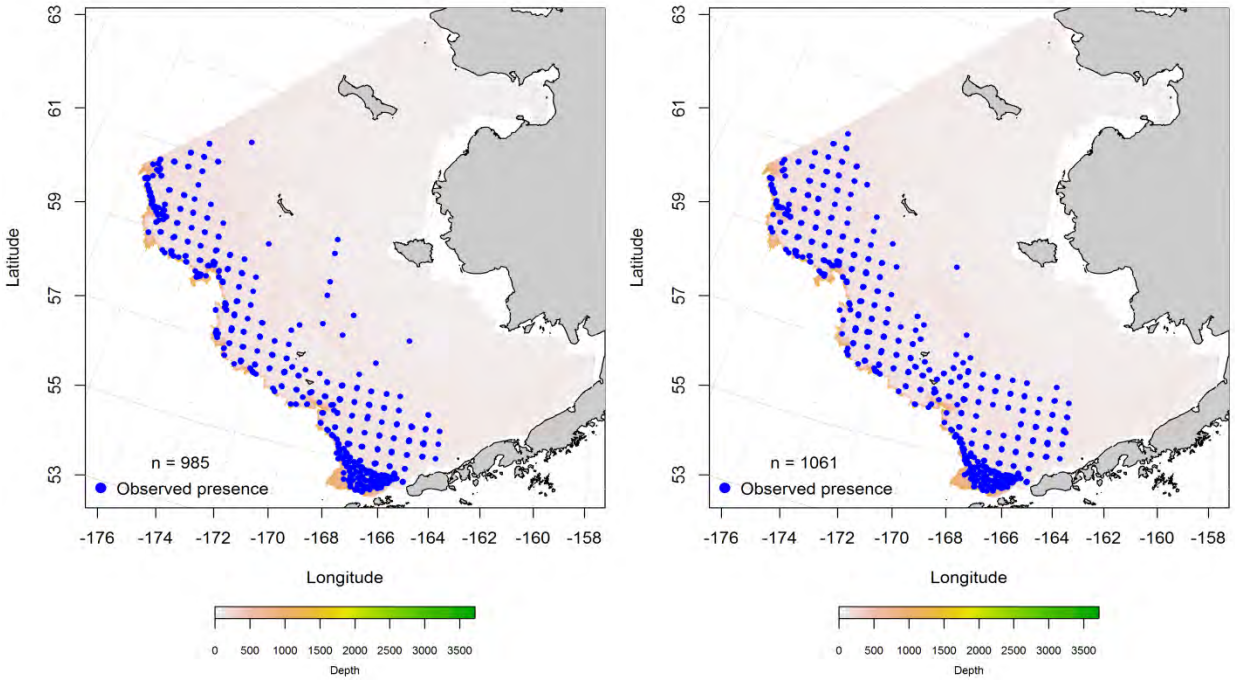

Figure 254. -- Distribution of juvenile (left) and adult (right) Bering skate catches from RACE summer bottom trawl surveys of the Eastern Bering Sea.

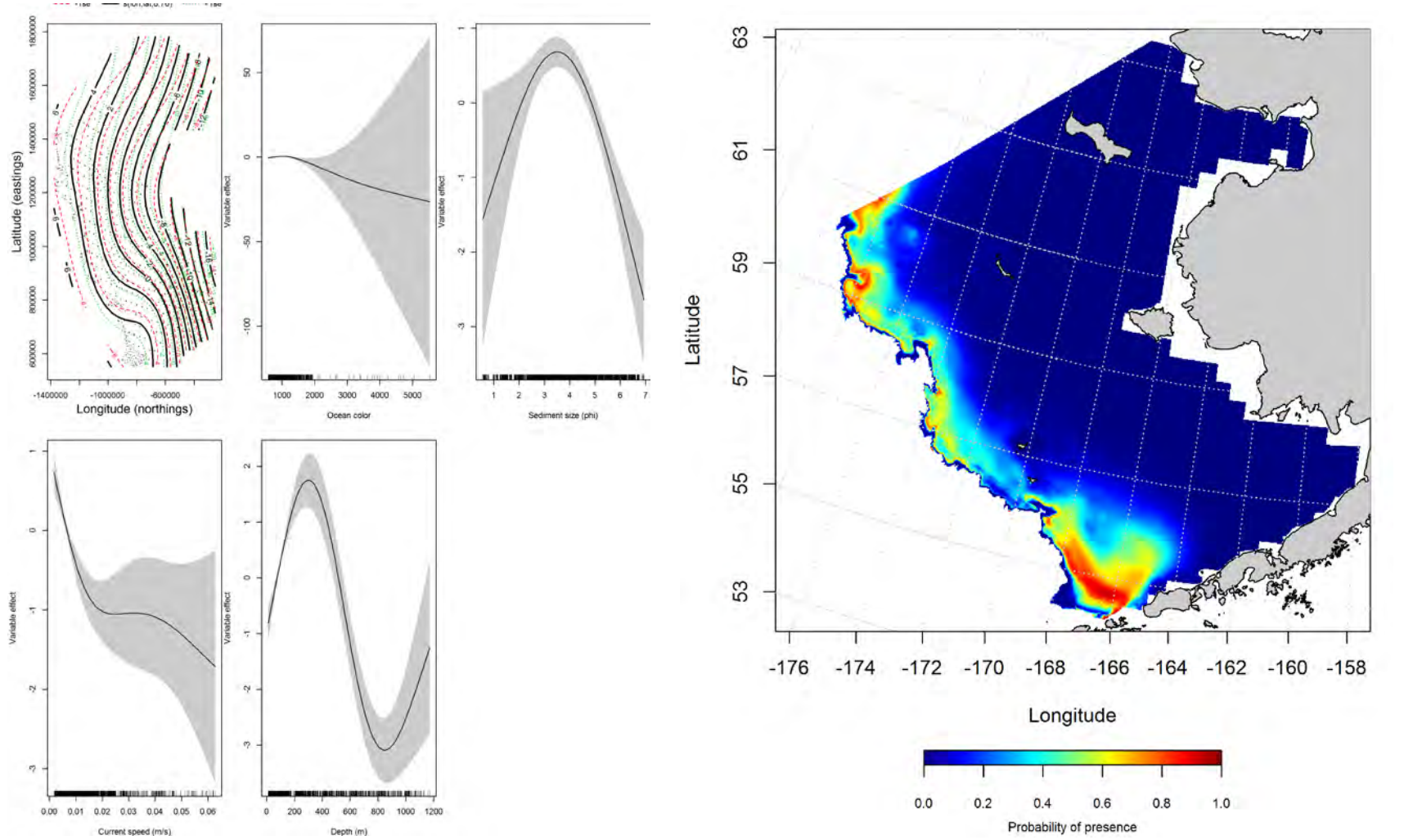

Figure 255. -- Effects of retained habitat covariates on the best-fitting generalized additive presence-absence model (GAM) of late juvenile Bering skate from RACE summer bottom trawl surveys of the Eastern Bering Sea Shelf, Slope, and Northern Bering Sea alongside their predicted presence (right panel).

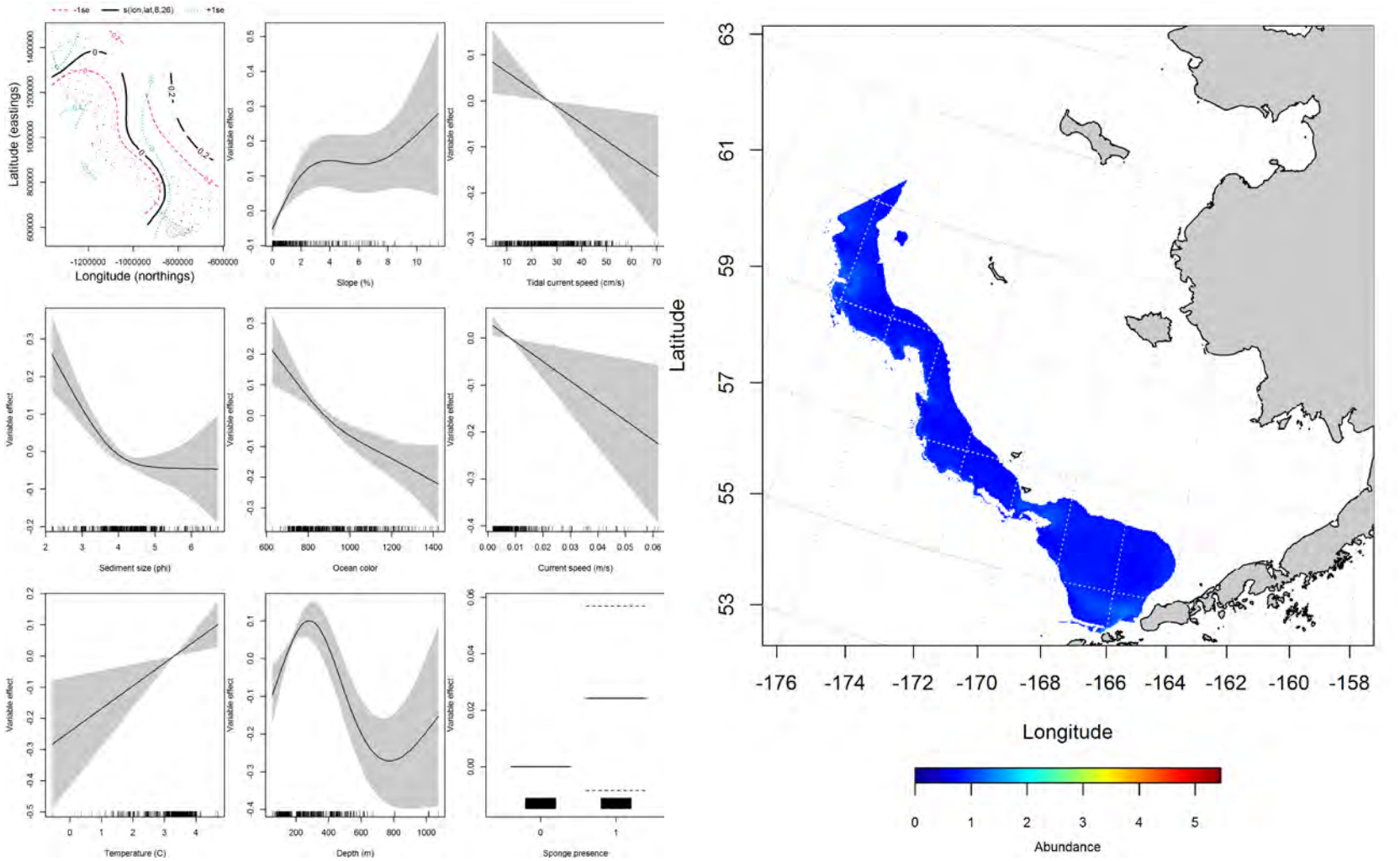

Figure 256. -- Effects of retained habitat covariates on the best-fitting generalized additive model (GAM) of late juvenile Bering skates from RACE summer bottom trawl surveys of the Eastern Bering Sea Shelf, Slope, and Northern Bering Sea alongside their predicted conditional abundance (right panel).

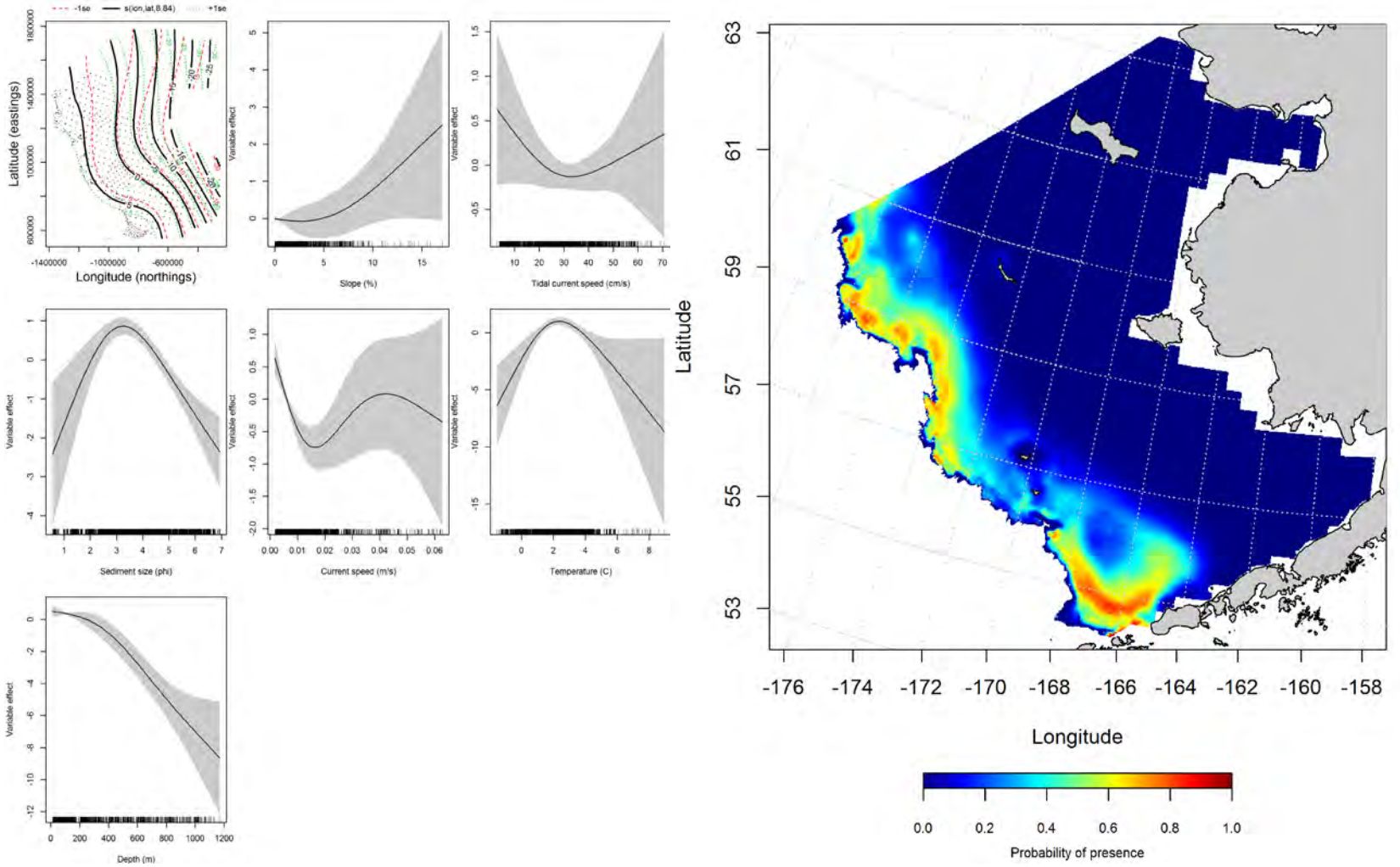

Figure 257. -- Effects of retained habitat covariates on the best-fitting generalized additive presence-absence model (GAM) of adult Bering skates from RACE summer bottom trawl surveys of the Eastern Bering Sea Shelf, Slope, and Northern Bering Sea alongside their predicted presence (right panel).

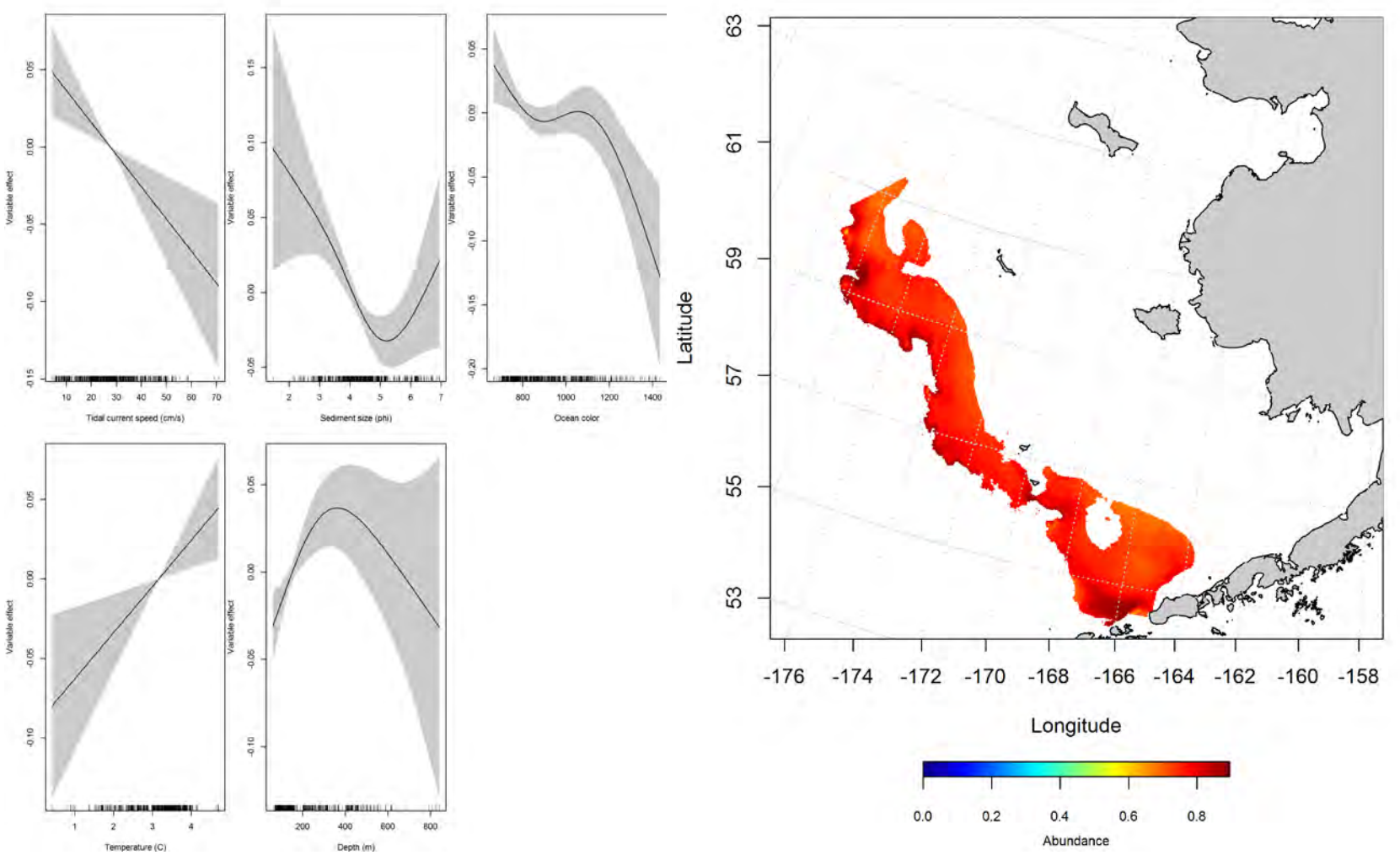

Figure 258. -- Effects of retained habitat covariates on the best-fitting generalized additive model (GAM) of adult Bering skates from RACE summer bottom trawl surveys of the Eastern Bering Sea Shelf, Slope, and Northern Bering Sea alongside their predicted conditional abundance (right panel).

Essential fish habitat maps and conclusions for Bering skate (*Bathyraja interrupta*) in the Eastern Bering Sea – Species distribution modeling of Bering skate in the Eastern Bering Sea predicts that EFH for this species does not vary much between juveniles and adults (Figure 259). Both life stages co-occur in association with the shelf break and over the outer shelf from the Bering Canyon in the southern domain to Navarin Canyon in the north.

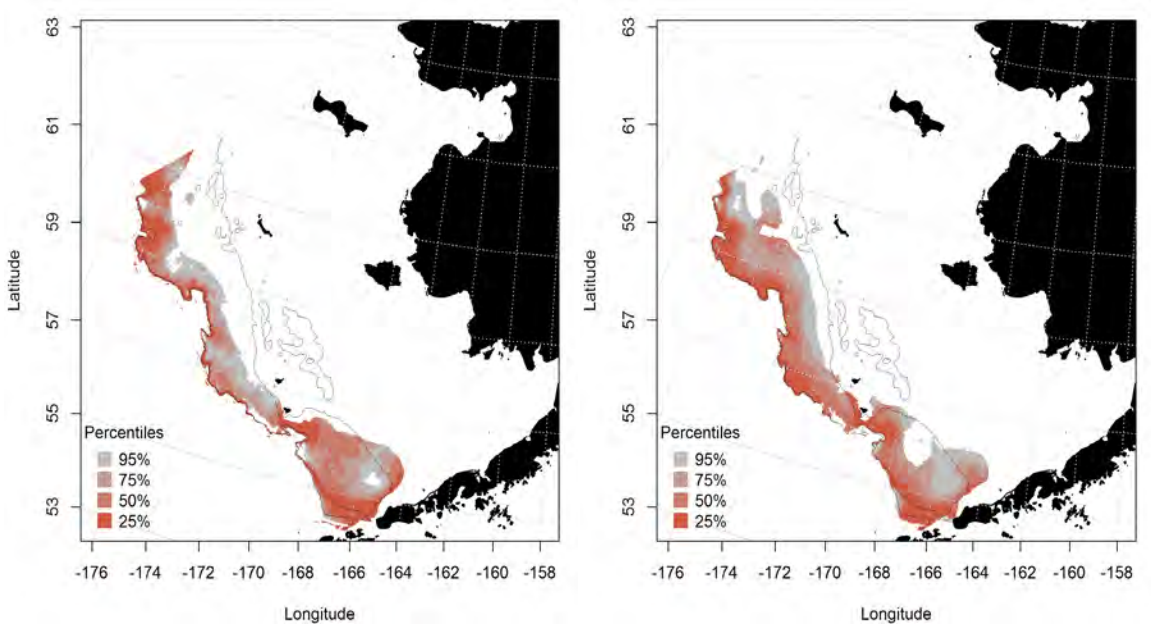

Figure 259. -- Essential fish habitat predicted for juvenile and adult Bering skate (left and right panel) from summertime RACE bottom trawl surveys of the Eastern Bering Sea.

Alaska skate (*Bathyraja parmifera*)

Alaska skates are distributed from Japan and Russia across the Eastern Bering Sea and Aleutian Islands into the Eastern Gulf of Alaska. They have been collected from depths of 20 to 1,425 m in the Bering Sea and Aleutian Islands (Mecklenburg et al. 2002). All skate species in the North Pacific are part of the "Other species" management category within the BSAI FMP.

Summertime distribution of juvenile and adult Alaska skate from RACE bottom trawl surveys of the Eastern Bering Sea – Juvenile and adult Alaska skates occurred over the entire extent of the are surveyed by RACE summer bottom trawling in the Eastern Bering Sea (Figure 260). The two life stages spatially overlap in nearly 100% of their range in this region and they occur from the inner (0 to 50 m) to the outer (100 to 200 m) shelf.

A standard GAM was used to model juvenile Alaska skate species distribution in the Eastern Bering Sea. The best-fitting model predicts that their greatest abundance is in the central domain of the Eastern Bering Sea west of Nunivak Island (Figure 261). This GAM explained only 8.2% of the deviance in their distribution data. Geographical location, bottom depth, and bottom temperature were the most significant predictors retained in the model. Model fits to the training and test data sets were poor (r^2 = 0.08 and 0.43).

Adult Alaska skate distribution was modeled with a hurdle GAM in the Eastern Bering Sea. The presence-absence GAM predicted that the highest probabilities of encountering adult Alaska skates in RACE summer bottom trawl catches occurred near St. Paul and St. Matthew Islands as well as in the northern Bering Sea north of St. Lawrence Island (Figure 262). The best-fitting GAM explained just 20% of the deviance in their distribution data. Geographical location, bottom temperature, bottom depth, and sediment grain size were the most significant predictors retained in the model. Model effects increased to the west with increasing temperature and decreasing sediment grain size and decreased with increasing depth. The presence-absence GAM was an acceptable fit to the training data (AUC = 0.77) and correctly classified 69% of predicted cases of presence-absence. Model validation was moderately successful (AUC = 0.76) correctly classified 69% of cases predicted from the test data.

Conditional abundance of adult Alaska skate was predicted where the threshold for presence established in the first step was met (Figure 263). The best-fitting GAM explained just 20% of the deviance in adult Alaska skate CPUE from RACE bottom trawl surveys of the Eastern Bering Sea and predicted their

greatest abundances near St. Paul, St. Matthew, and St. Lawrence Islands in the central and northern domains. The most significant predictors retained in the model were geographical location, bottom temperature, and measures of current speed. Model fits were poor for the training and test data sets (r^2 = 0.20 and 0.16).

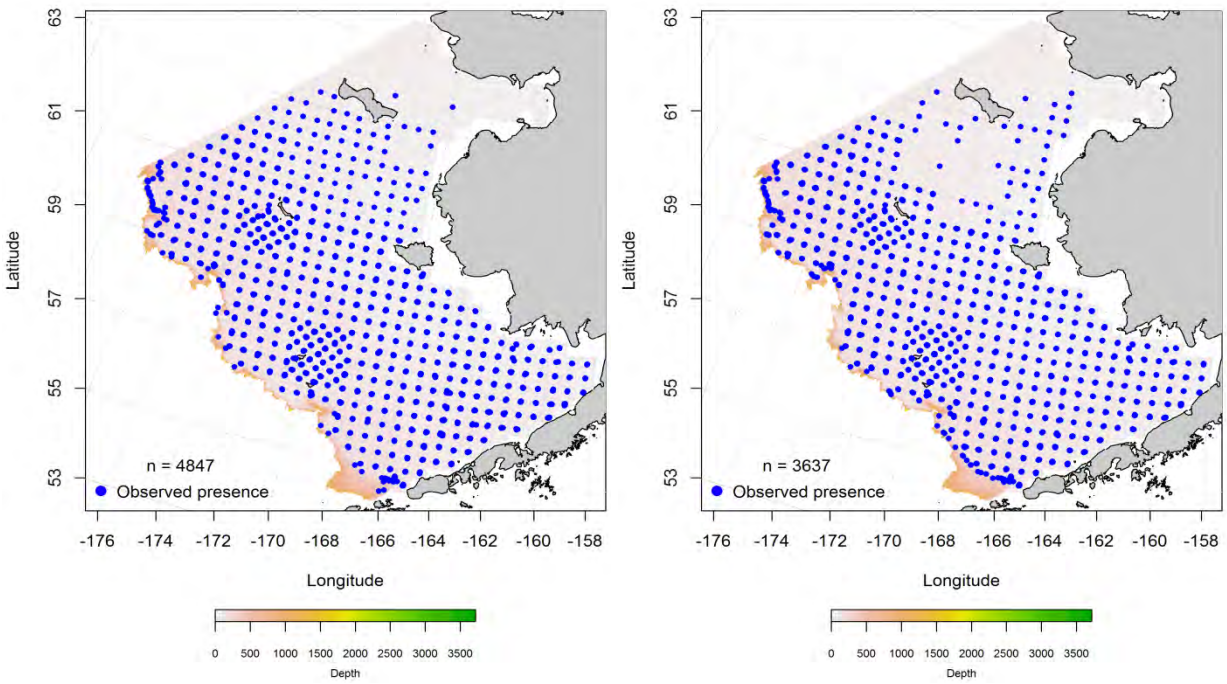

Figure 260. -- Distribution of juvenile (left) and adult (right) Alaska skate catches from RACE summer bottom trawl surveys of the Eastern Bering Sea.

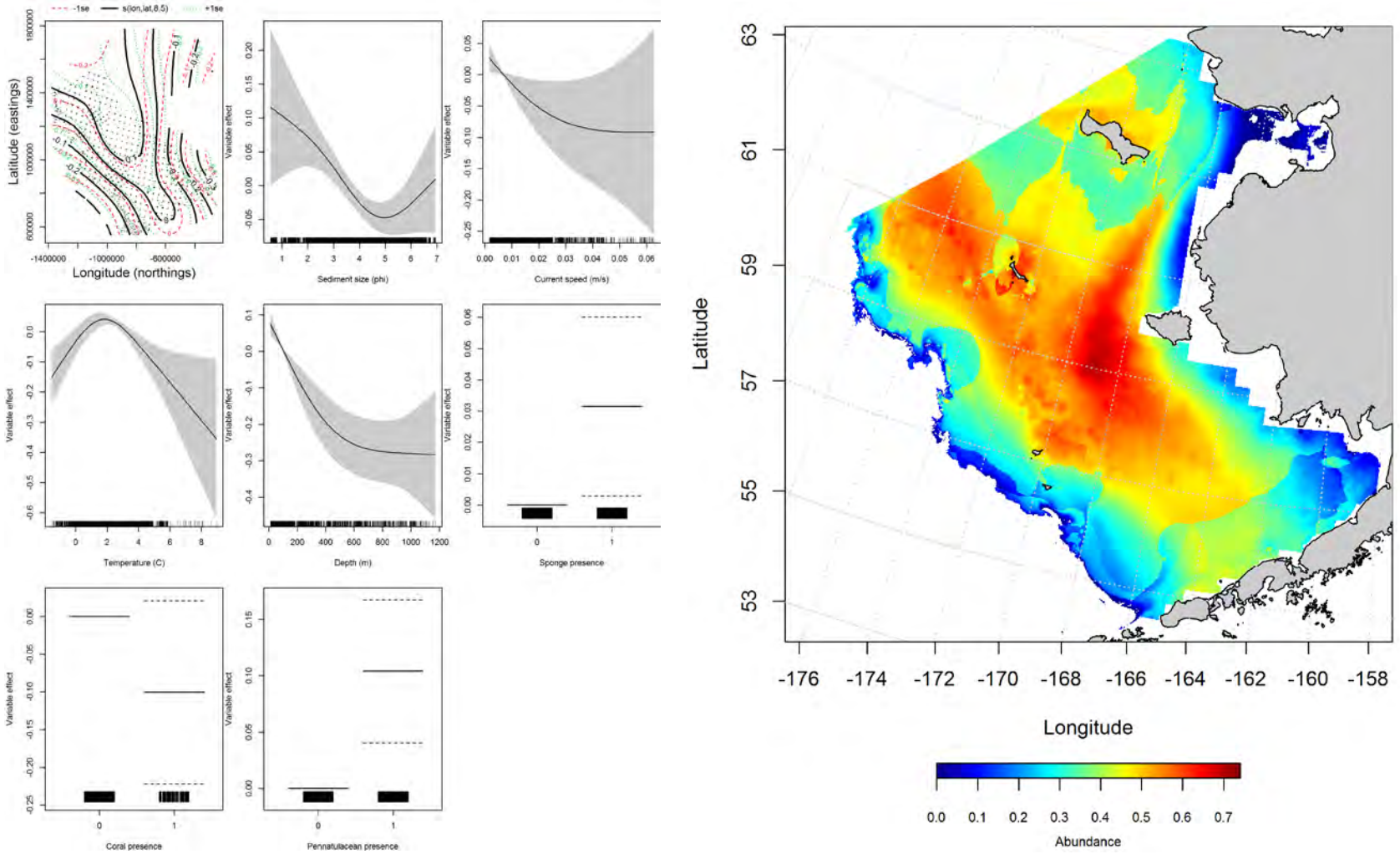

Figure 261. -- Effects of retained habitat covariates on the best-fitting generalized additive model (GAM; left panel) predicting late juvenile Alaska skate abundance from RACE summer bottom trawl surveys of the Eastern Bering Sea Shelf, Slope, and Northern Bering Sea (right panel).

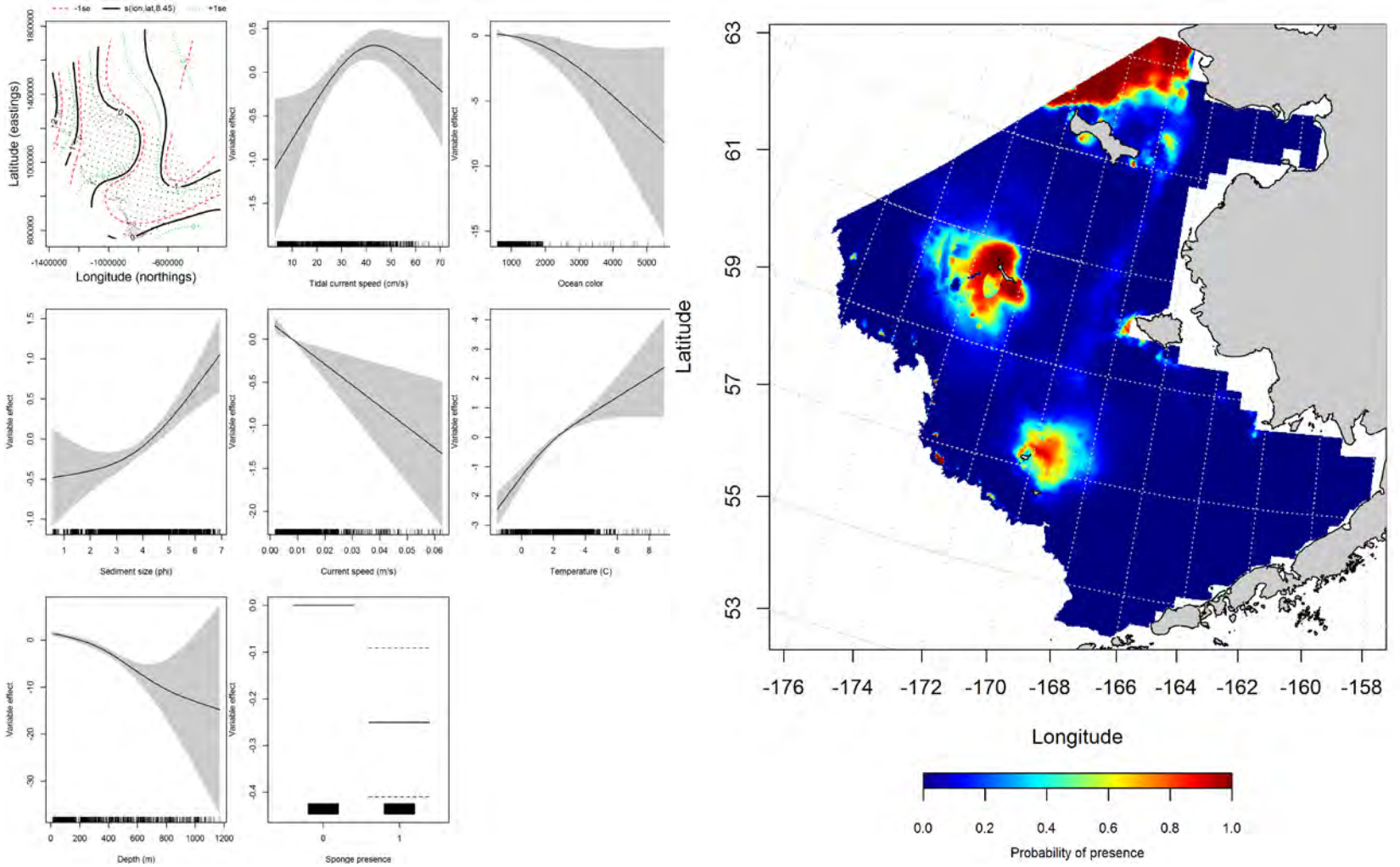

Figure 262. -- Effects of retained habitat covariates on the best-fitting generalized additive presence-absence model (GAM) of adult Alaska skates from RACE summer bottom trawl surveys of the Eastern Bering Sea Shelf, Slope, and Northern Bering Sea alongside their predicted presence (right panel).

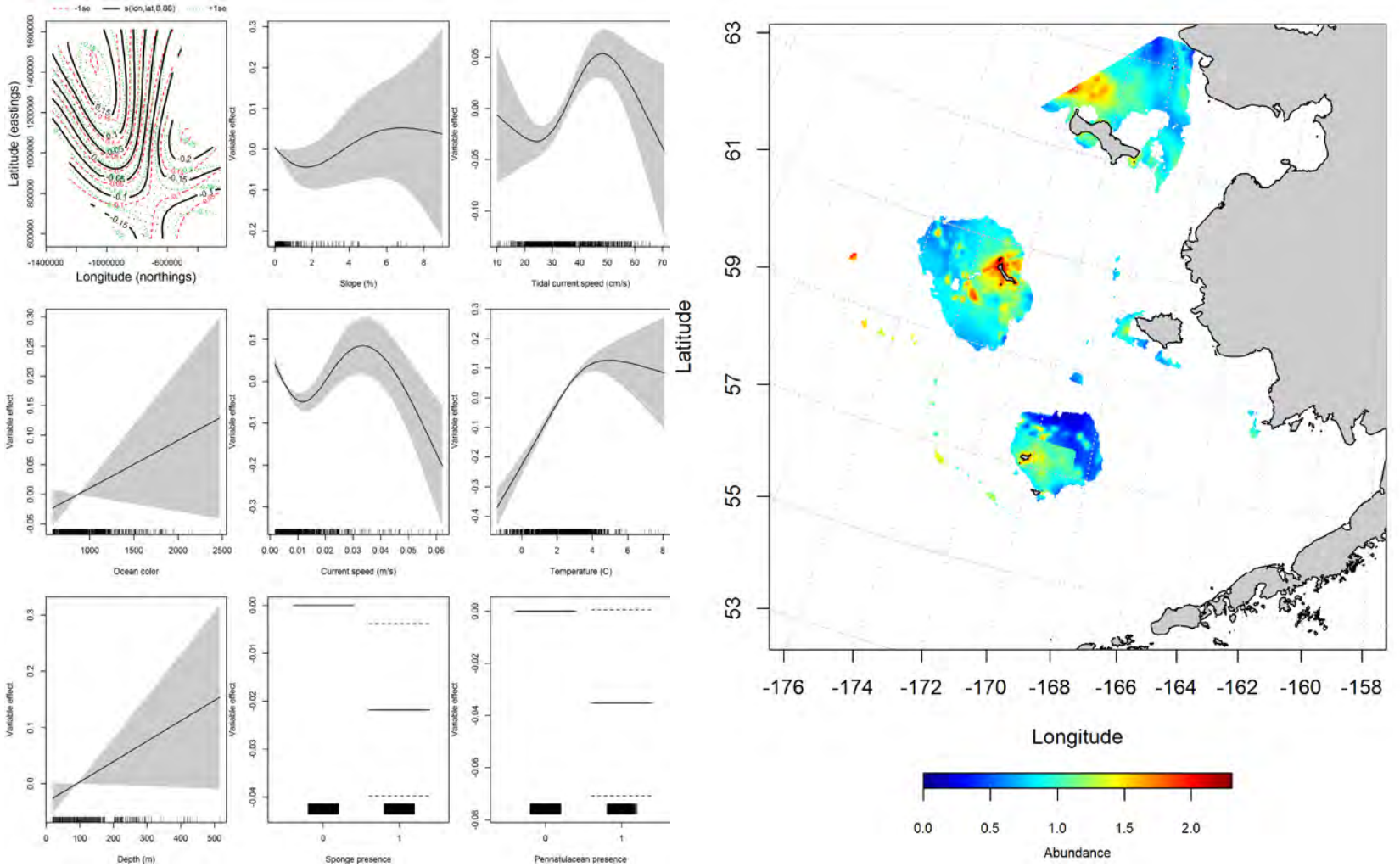

Figure 263. -- Effects of retained habitat covariates on the best-fitting generalized additive model (GAM) of adult Alaska skates from RACE summer bottom trawl surveys of the Eastern Bering Sea Shelf, Slope, and Northern Bering Sea alongside their predicted conditional abundance (right panel).

Seasonal distribution of Alaska skate in commercial fishery catches from the Eastern Bering Sea – Alaska skates observed in fall commercial fishery catches were distributed across the north-south extent of the Eastern Bering Sea survey area over portions of the inner, middle, and outer shelves (Figure 264). Maximum entropy modeling predicted high probabilities of suitable Alaska skate habitat along the shelf edge and in association with the heads of submarine canyons. The most important habitat covariates predicting suitable habitat were bottom depth, bottom temperature, and ocean productivity which combined comprised 97.7% of the leverage of predictor terms. The MaxEnt model was an excellent fit to the training data (AUC = 0.86) and it correctly classified 77% of cases. Fit of the model in the validation step was acceptable (AUC = 0.79) and 79% of the cases were correctly predicted from the test data set.

The winter distribution of Alaska skate in commercial catches extended from the Bering Canyon in the south to Navarin Canyon in the north and into Bristol Bay in the southeast (Figure 265). High probabilities of suitable Alaska skate habitat were predicted over the north-south extent of the middle shelf. The most influential habitat covariates in the MaxEnt model were bottom depth (relative importance = 66.3%) and bottom temperature (25.9%). The model predicted 84% of cases correctly and was an outstanding fit (AUC = 0.92) to the training data. Model validation was successful (AUC = 0.84) correctly predicting 84% of the cases from the test data.

In springtime, Alaska skates were widely represented over the middle and outer shelf of the Eastern Bering Sea (Figure 266). The highest probability suitable habitats were predicted from the Bering Canyon and Bristol Bay in the southern domain to around Zhemchug Canyon in the northern domain. The most important predictors in the MaxEnt model were bottom depth and bottom temperature comprising a combined 92.2% of the importance of predictor terms. The MaxEnt model was an outstanding fit to the training data (AUC = 0.92) and predicted 84% of cases correctly. Model validation was successful (AUC = 0.84) with 84% of cases correctly predicted from the test data.

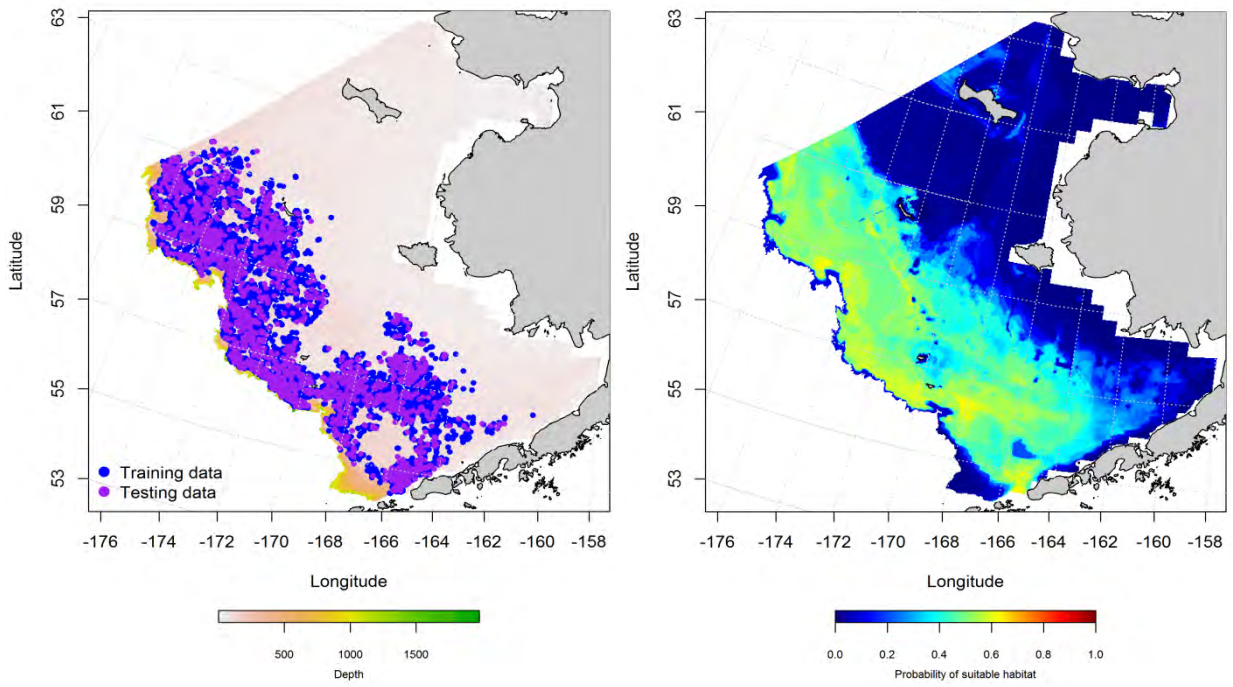

Figure 264. -- Presence of Alaska skate in commercial fishery catches from fall (October-November; left panel). Blue points were used to train the maximum entropy (MaxEnt) model predicting the probability of suitable habitat (right panel) and the purple points were used to validate the model.

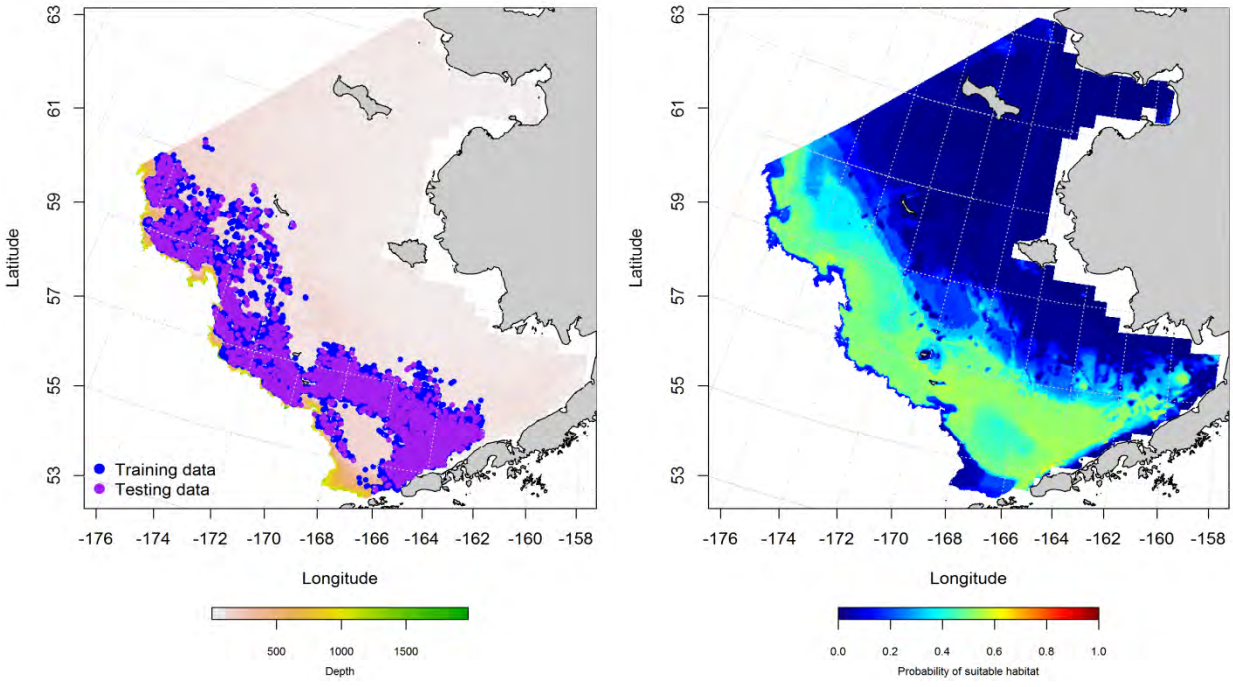

Figure 265. -- Presence of Alaska skate in commercial fishery catches from winter (December-February; left panel). Blue points were used to train the maximum entropy (MaxEnt) model predicting the probability of suitable habitat (right panel) and the purple points were used to validate the model.

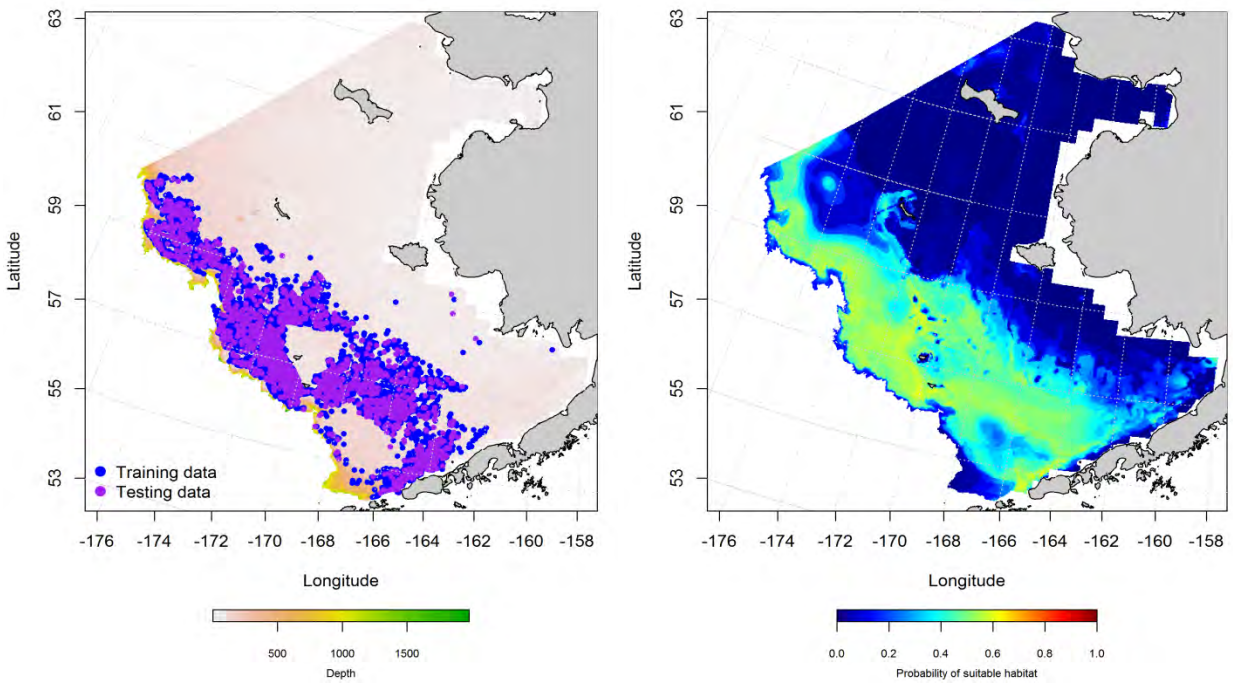

Figure 266. -- Presence of Alaska skate in commercial fishery catches from spring (March-May; left panel). Blue points were used to train the maximum entropy (MaxEnt) model predicting the probability of suitable habitat (right panel) and the purple points were used to validate the model.

Essential fish habitat maps and conclusions for Alaska skate (*Bathyraja parmifera*) in the Eastern Bering Sea – Species distribution modeling of Alaska skate in the Eastern Bering Sea predicts that EFH for this species varies between life stages and seasons (Figure 267). Juvenile Alaska skate appear to be much more wide spread over the survey area than were the adults. In general, adult Alaska skate EFH is contained within the bounds of the spatial distribution of the juveniles.

Predictions of suitable Alaska skate habitat from commercial fishery catches in the Eastern Bering Sea showed very little seasonal difference in distribution of this species in commercial catches (Figure 268). In general, the highest probability habitats were located along the shelf break and upper slope of the Eastern Bering Sea. In wintertime there were some high probability areas that appeared in the western part of Bristol Bay, but weren't seen here in other seasons.

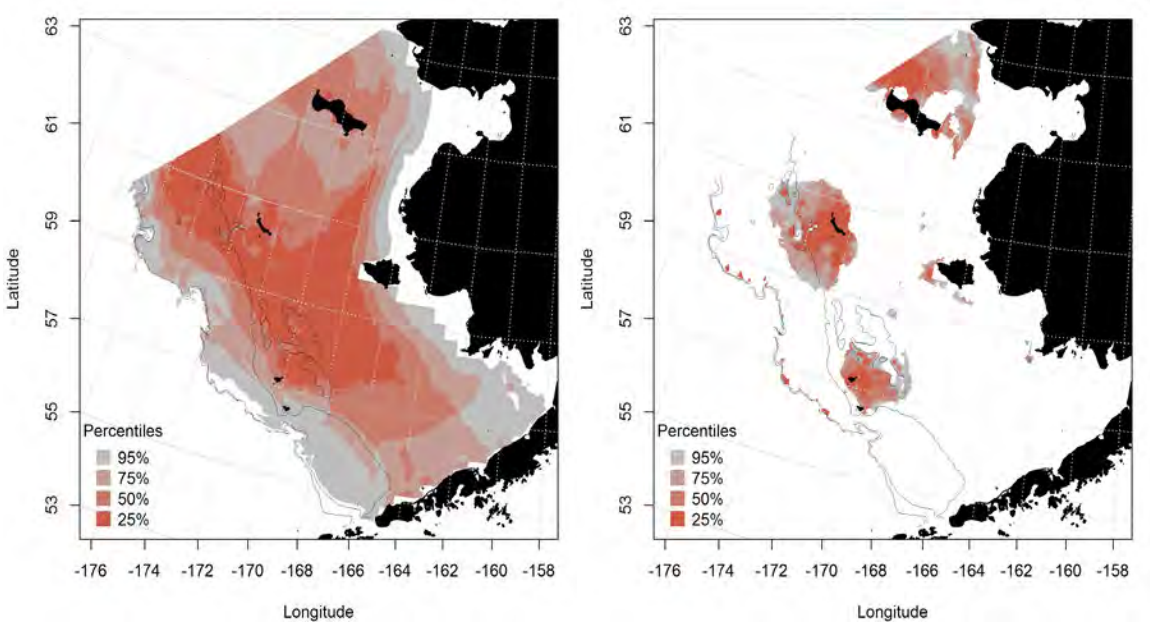

Figure 267. -- Essential fish habitat predicted for juvenile and adult Alaska skate (left and right panel) from summertime RACE bottom trawl surveys of the Eastern Bering Sea.

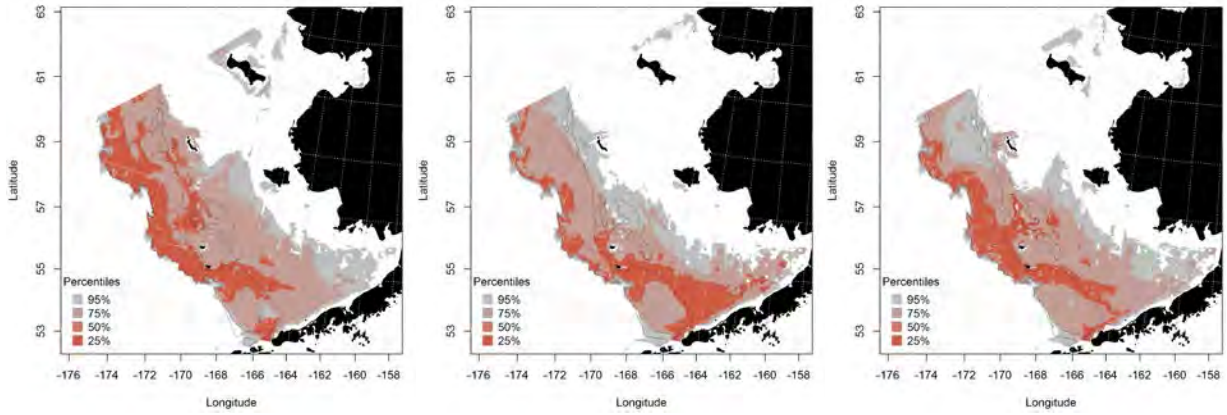

Figure 268. -- Essential fish habitat predicted from Alaska skate occurrences in commercial fishery catches during fall (left panel), winter (middle panel), and spring (right panel) in the Eastern Bering Sea.

mud skate (*Bathyraja taranetzi*)

Mud skates are distributed from the Kamchatka Peninsula and Kuril Islands in Russia across the Eastern Bering Sea and Aleutian Islands. They have been collected from depths of 81 to 1,000 m (Mecklenburg et

al. 2002). All skate species in the North Pacific are part of the "Other species" management category within the BSAI FMP.

Summertime distribution of juvenile and adult mud skate from RACE bottom trawl surveys of the Eastern Bering Sea – Juvenile and adult mud skates occurred in patches associated with the heads of submarine canyons along the Eastern Bering Sea shelf (Figure 269). The two life stages appear to co-occur in these patches.

A MaxEnt model predicted summer late juvenile mud skate species distribution in the Eastern Bering Sea (Figure 270). Suitable juvenile habitat was predicted to occur in close association with the heads of submarine canyons along the shelf break. Bottom depth was the dominant habitat covariate accounting for 84.4% of the relative importance of all predictor terms in the MaxEnt model. The greatest model effect occured at around 400 m bottom depth. The MaxEnt model was an outstanding fit to the training data (AUC = 1.0) and correctly classified 98% of predicted cases. In the model validation step, the GAM fit was also outstanding (AUC = 0.95) correctly classifying 95% of cases predicted from the test data.

Adult mud skate distribution was predicted from a MaxEnt model of habitat covariates from the Eastern Bering Sea (Figure 271). Suitable adult habitat is similar to that of the juveniles and is predicted in close association with the heads of submarine canyons along the shelf break. Bottom depth, bottom slope, and maximum tidal current were the dominant habitat covariates predicting adult mud skate habitat distribution. Combined they accounted for 94.5% of the relative importance of all predictor terms in the model. The MaxEnt model was an outstanding fit to the training data (AUC = 0.99) and correctly classified 96% of predicted cases. In the model validation step, the GAM fit was also outstanding (AUC = 0.95) correctly classifying 95% of cases predicted from the test data.

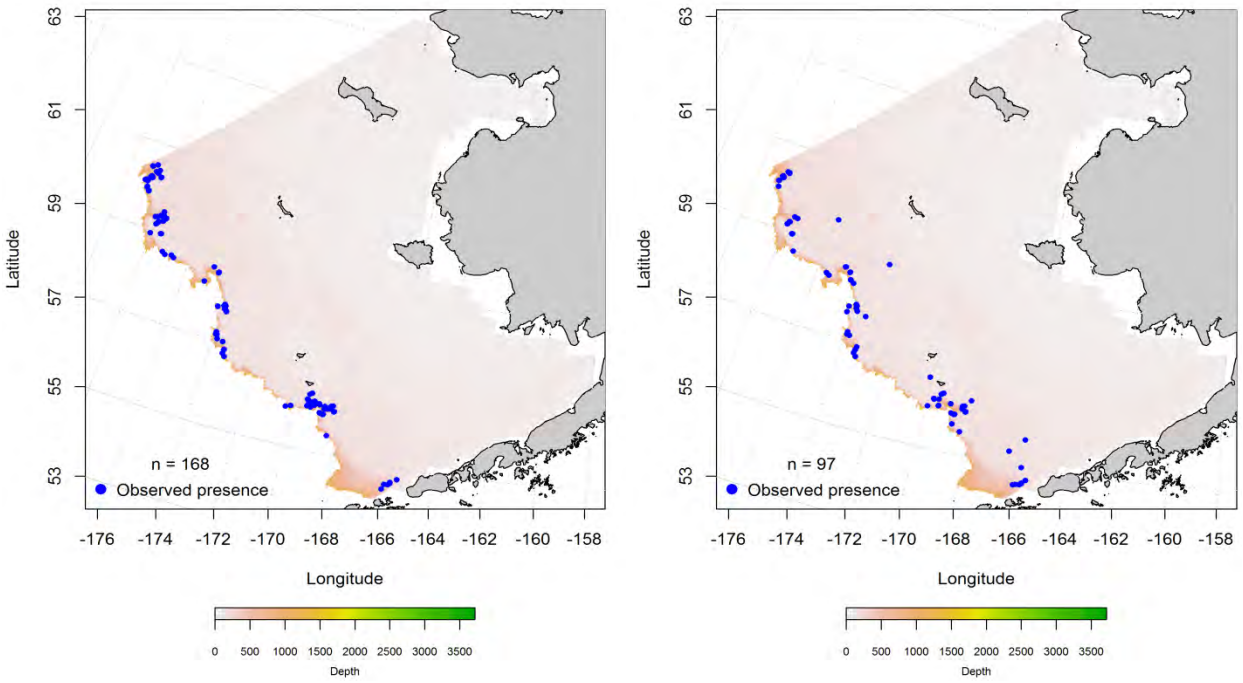

Figure 269. -- Distribution of juvenile (left) and adult (right) mud skate catches from RACE summer bottom trawl surveys of the Eastern Bering Sea.

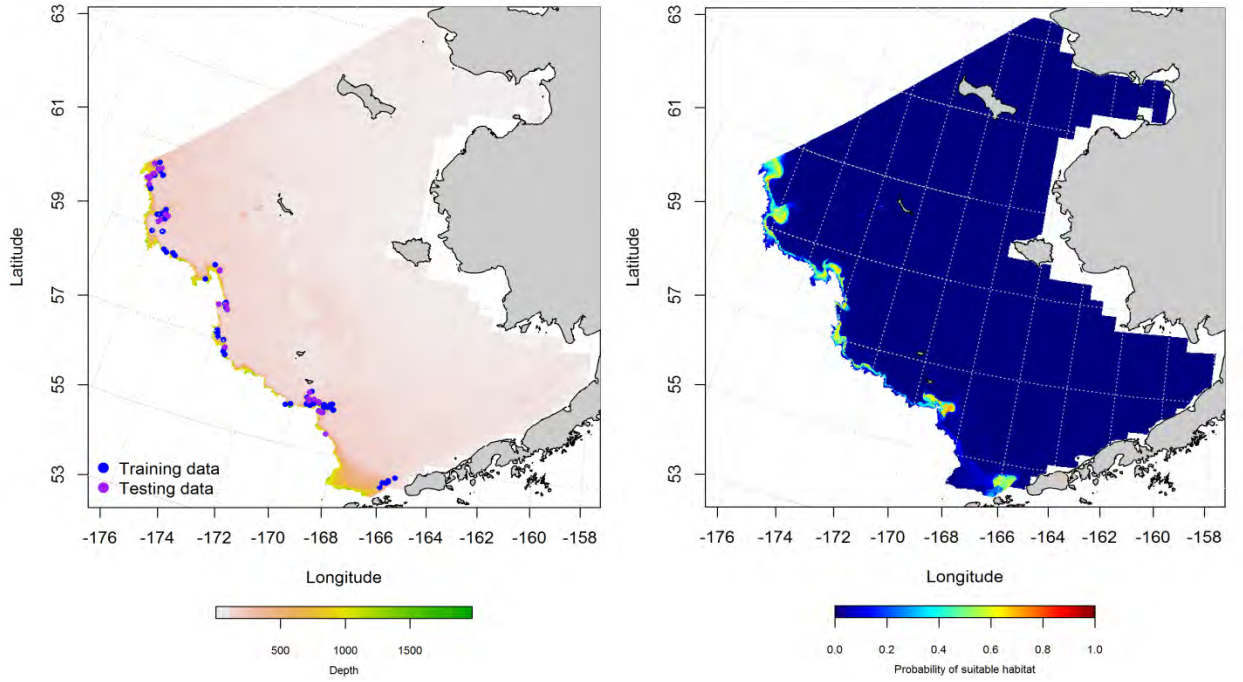

Figure 270. -- Locations of summer RACE groundfish trawl survey catches of juvenile mud skate (left panel). Blue points were used to train the maximum entropy (MaxEnt) model predicting the probability of suitable habitat (right panel) and the purple points were used to validate the model.

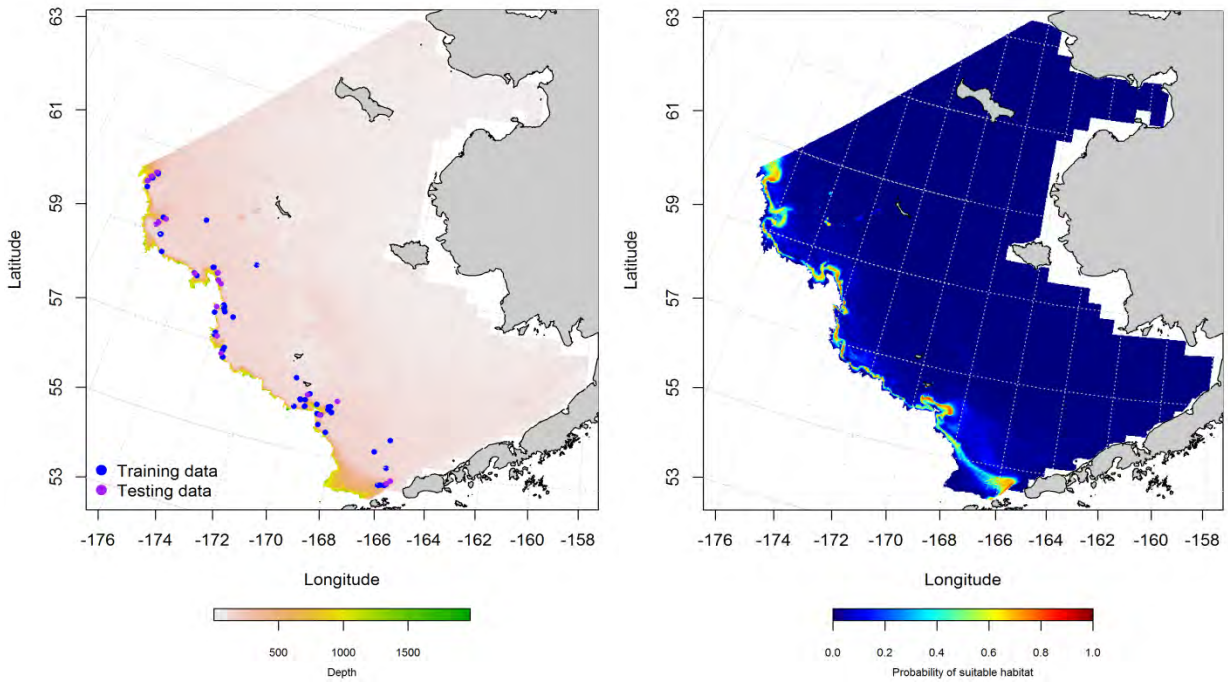

Figure 271. -- Locations of summer RACE groundfish trawl survey catches of adult mud skate (left panel). Blue points were used to train the maximum entropy (MaxEnt) model predicting the probability of suitable habitat (right panel) and the purple points were used to validate the model.

Seasonal distribution of mud skate in commercial fishery catches from the Eastern Bering Sea – Mud skates observed in fall commercial fishery catches were distributed in patches from the Bering Canyon in the southern domain to the more concentrated patch in the northern domain near Pervenets Canyon (Figure 272). Their occurrences were primarily in deeper waters of the outer shelf (100 to 200 m). Maximum entropy modeling predicted the highest concentration of suitable mud skate habitat from Zhemchug Canyon along the outer shelf into the northern domain. The most important habitat covariates predicting suitable habitat were bottom depth, ocean productivity, and bottom temperature which combined comprised 94.7% of the leverage of predictor terms. The MaxEnt model was an outstanding fit to the training data (AUC = 0.99) and it correctly classified 95% of cases. Fit of the

model in the validation step was excellent (AUC = 0.88) and 88% of the cases were correctly predicted from the test data set.

The winter distribution of mud skate in commercial catches extended from the Bering Canyon and Bristol Bay in the southern domain to Navarin Canyon in the north (Figure 273). High probabilities of suitable mud skate habitat were predicted near the heads of most of the submarine canyons along the Eastern Bering Sea shelf edge. The most important habitat covariates predicting suitable habitat were bottom depth, ocean productivity, and bottom temperature which comprised 89.6% of the leverage of predictor terms. The model predicted 89% of cases correctly and was an outstanding fit (AUC = 0.96) to the training data. Model validation was successful (AUC = 0.88) correctly predicting 88% of the cases from the test data.

In springtime, most of the mud skates caught in commercial fishery catches from the Eastern Bering Sea occurred in the northern domain around Pervenets Canyon (Figure 274). There were also a few occurrences in Bering Canyon and around the Pribilof Islands. The MaxEnt model predicted the most suitable habitat near Pervenets Canyon in the northern domain and over Bering Canyon in the southern domain. The most important habitat covariates predicting suitable habitat were bottom depth, ocean productivity, and bottom temperature which comprised 87.9% of the leverage of predictor terms. The model predicted 94% of cases correctly and was an outstanding fit (AUC = 0.98) to the training data. Model validation was successful (AUC = 0.86) correctly predicting 86% of the cases from the test data.

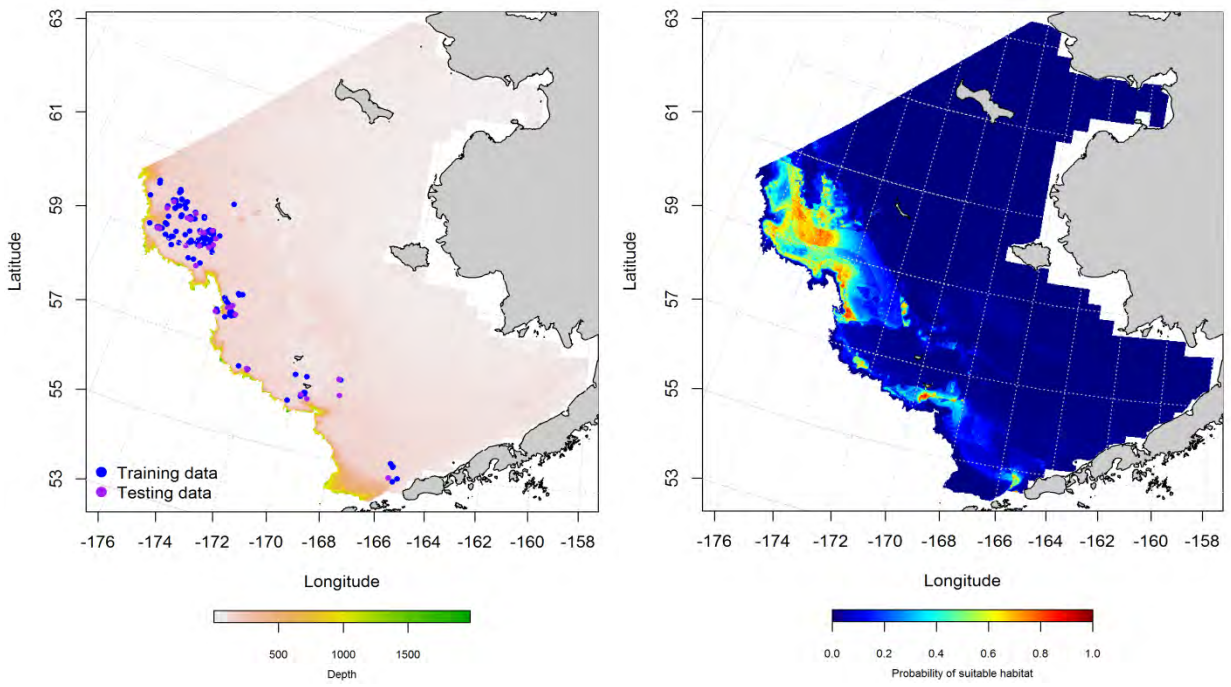

Figure 272. -- Presence of mud skate in commercial fishery catches from fall (October-November; left panel). Blue points were used to train the maximum entropy (MaxEnt) model predicting the probability of suitable habitat (right panel) and the purple points were used to validate the model.

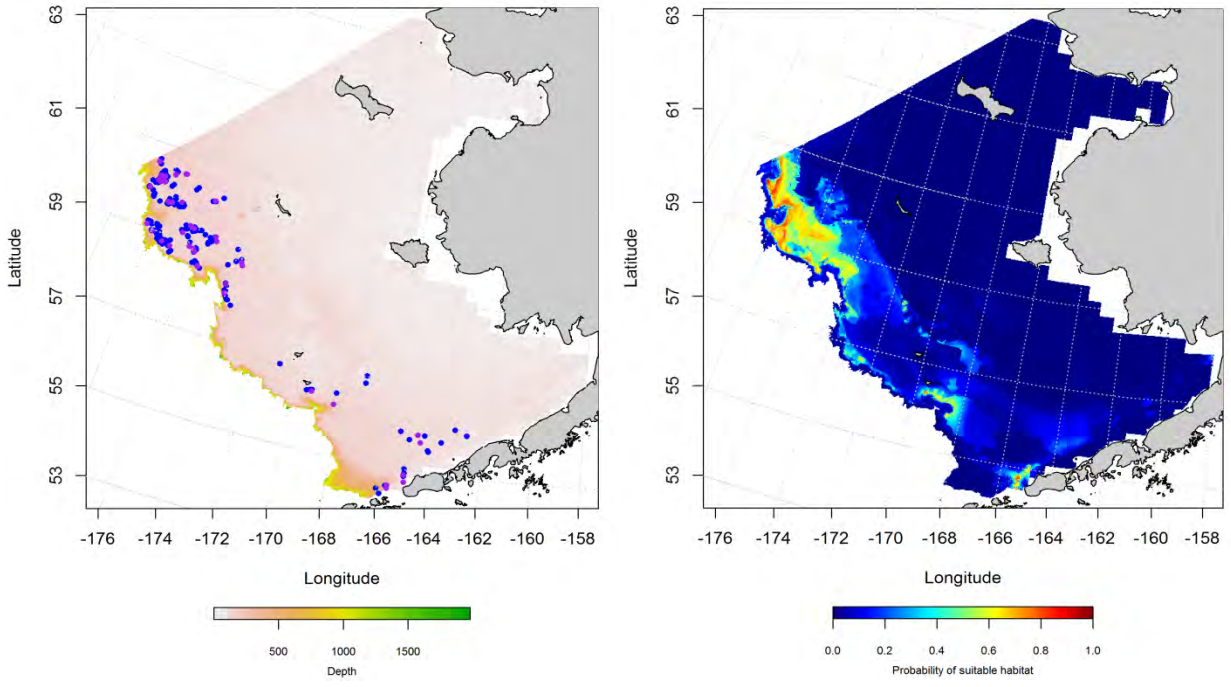

Figure 273. -- Presence of mud skate in commercial fishery catches from winter (December-February; left panel). Blue points were used to train the maximum entropy (MaxEnt) model predicting the probability of suitable habitat (right panel) and the purple points were used to validate the model.

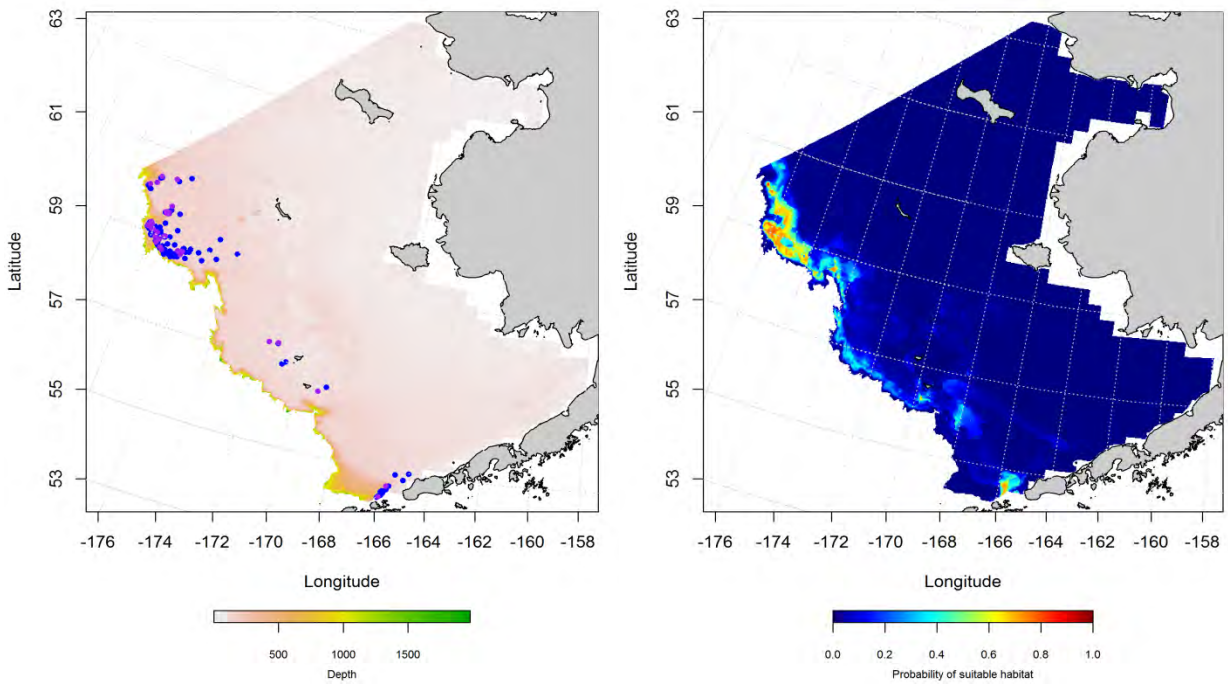

Figure 274. -- Presence of mud skate in commercial fishery catches from spring (March-May; left panel). Blue points were used to train the maximum entropy (MaxEnt) model predicting the probability of suitable habitat (right panel) and the purple points were used to validate the model.

Essential fish habitat maps and conclusions for mud skate (*Bathyraja taranetzi*) in the Eastern Bering Sea – Species distribution modeling of mud skate in the Eastern Bering Sea predicts that EFH for this species varies slightly between life stages (Figure 275). Essential habitat for juveniles and adults overlaps and extends along the shelf edge and Bering Sea slope from the Bering Canyon in the southern domain to Navarin Canyon in the north. Adult EFH has a greater east-west extent than that of the juveniles.

Essential habitat predicted for mud skates in the Eastern Bering Sea from their presence in commercial fishery catches demonstrated some seasonal differences (Figure 276). They were commonly caught in commercial fishing activities in the northern domain between Zhemchug and Navarin Canyons. Their presence in springtime catches indicates a narrower band of EFH more focused on the shelf break and upper Eastern Bering Sea slope.

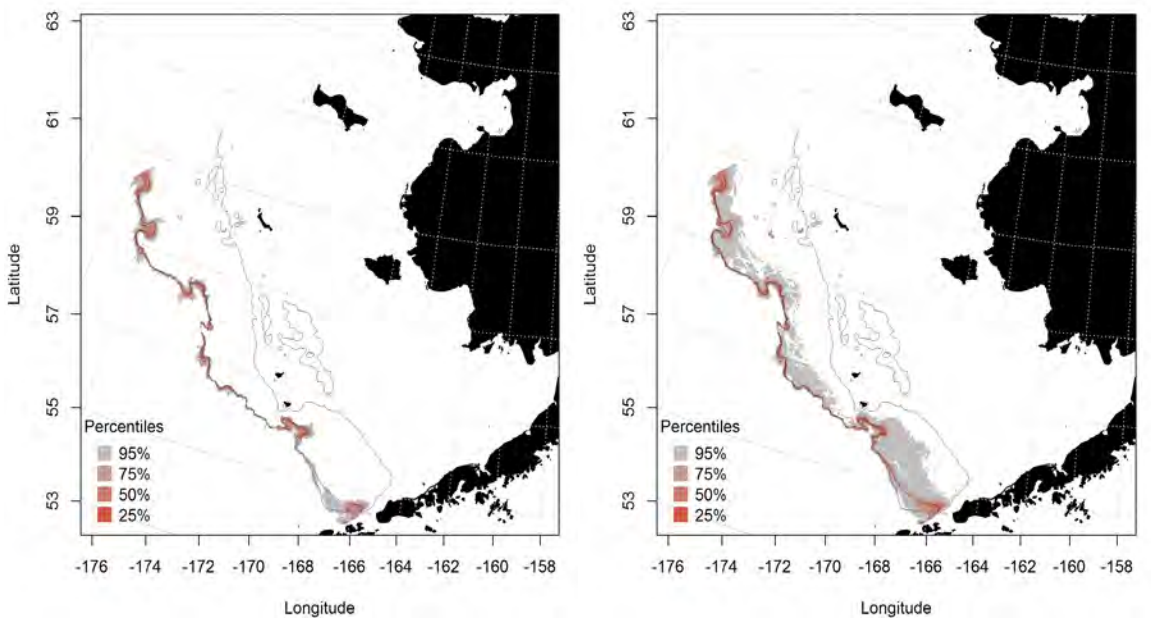

Figure 275. -- Essential fish habitat predicted for juvenile and adult mud skate (left and right panel) from summertime RACE bottom trawl surveys of the Eastern Bering Sea.

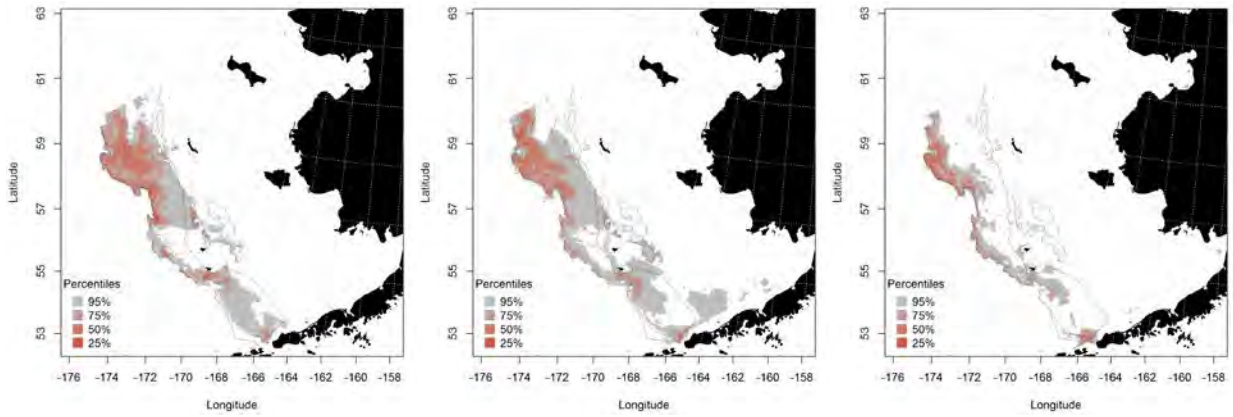

Figure 276. -- Essential fish habitat predicted from mud skate occurrences in commercial fishery catches during fall (left panel), winter (middle panel), and spring (right panel) in the Eastern Bering Sea.

Invertebrates

southern Tanner crab (*Chionocetes bairdi*)

Southern Tanner crabs are distributed across the eastern Bering Sea. They are primarily found over mud bottom. Tanner crabs support an important domestic fishery in the United States.

Summertime distribution of southern Tanner crab from RACE bottom trawl surveys of the Eastern Bering Sea – Southern Tanner crabs occurred across the eastern Bering Sea shelf in RACE summer bottom trawl catches (Figure 277). They were collected from Bristol Bay on the inner shelf in the southern domain to Navarin Canyon over the outer shelf and slope in the northern domain. Southern Tanner crabs were caught as deep as 769 m on the Bering Sea Slope.

A standard abundance GAM predicted southern Tanner crab species distribution in the eastern Bering Sea (Figure 278). The best-fitting GAM explained 54.9% of the deviance in their trawl CPUE data. The most significant habitat covariates retained in the model were geographical location, sediment grain size, bottom depth, and bottom temperature. According to the model, southern Tanner crab abundance increased in the southern domain of the survey area over finer sediments and warmer temperatures and decreased with increasing bottom depth. The model fits to the training data and in the validation step using the test data were fair ($r^2 = 0.55$ for both data sets).

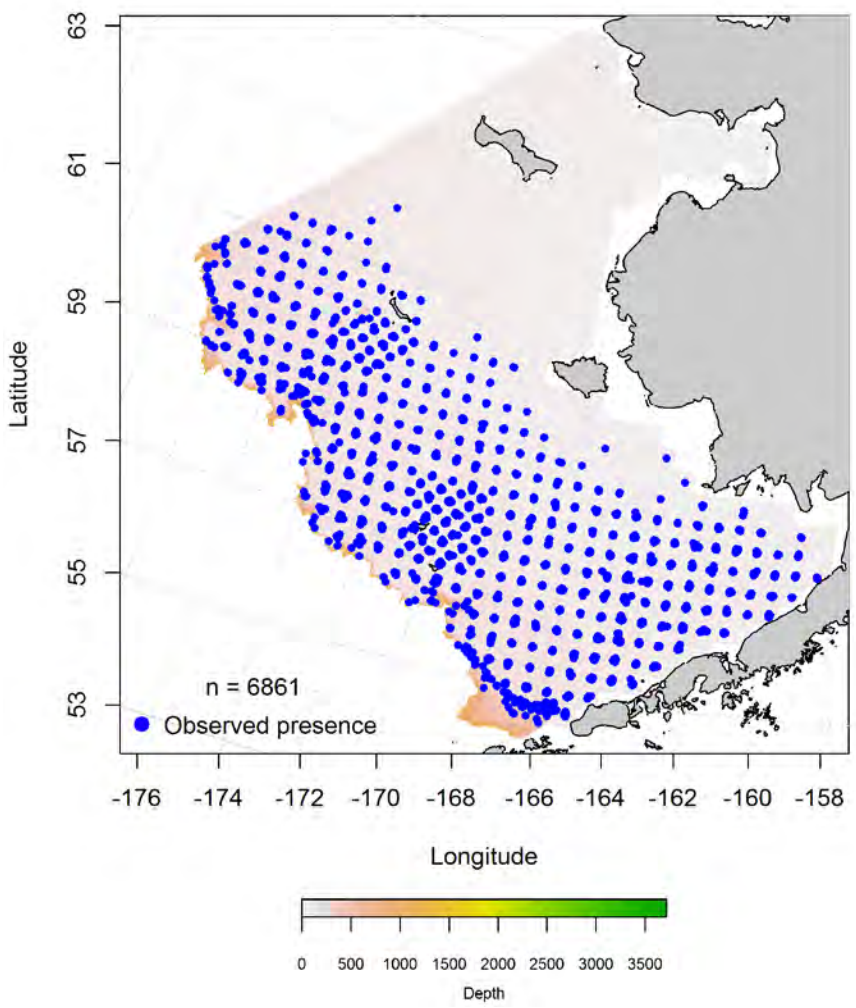

Figure 277. -- Distribution of southern Tanner crab in catches from RACE summer bottom trawl surveys of the Eastern Bering Sea.

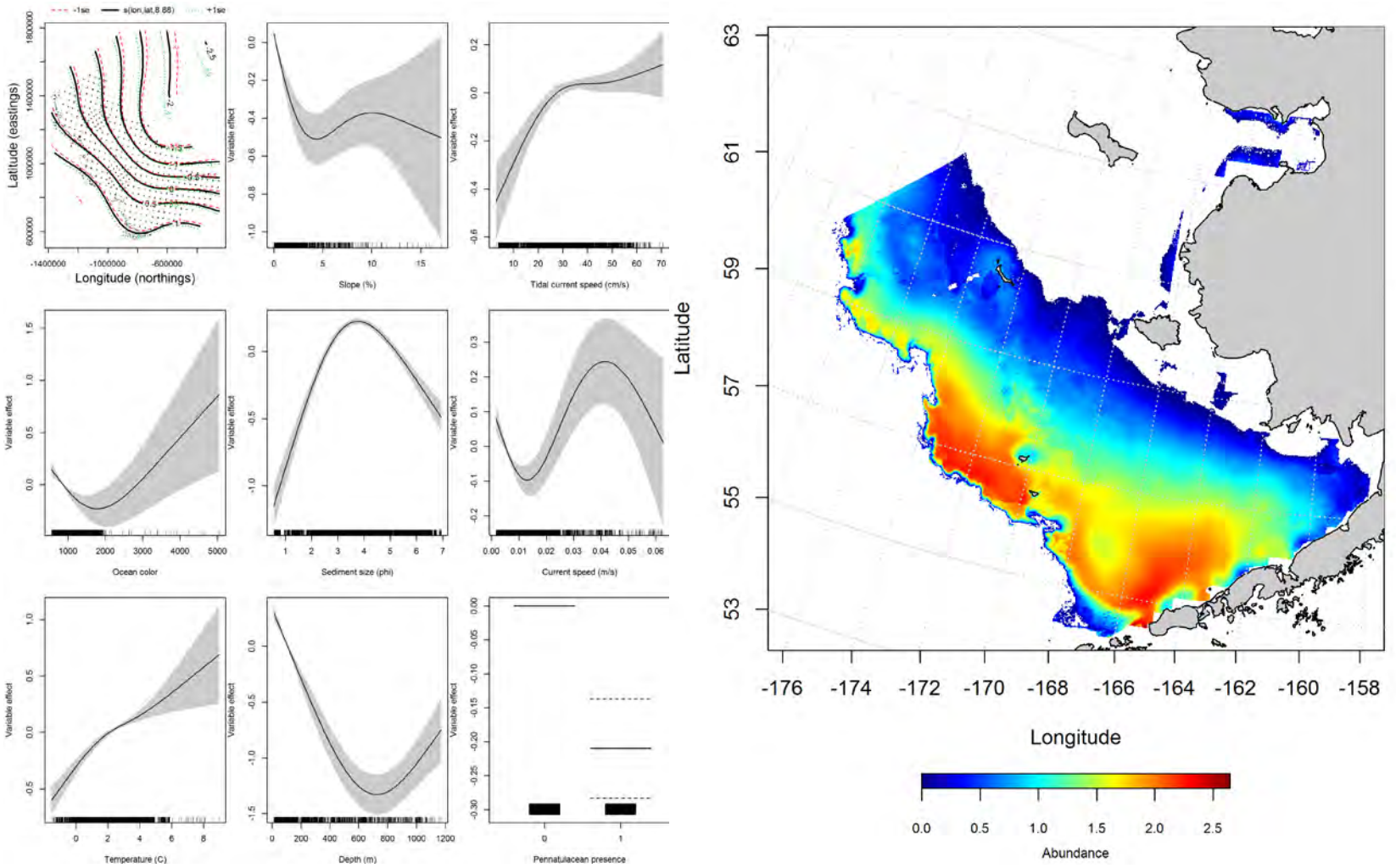

Figure 278. -- Effects of retained habitat covariates on the best-fitting generalized additive model (GAM; left panel) predicting southern Tanner crab abundance from RACE summer bottom trawl surveys of the Eastern Bering Sea Shelf, Slope, and Northern Bering Sea (right panel).

Seasonal distribution of southern Tanner crab in commercial fishery catches from the Eastern Bering Sea – Southern Tanner crabs observed in fall commercial fishery catches were more prevalent in the central and southern domains of the Eastern Bering Sea although they occurred as far north as Navarin Canyon (Figure 279). Their occurrences were primarily over the middle and outer shelf. Maximum entropy modeling predicted the highest probabilities of suitable southern Tanner crab habitat near the Pribilof Islands, over the middle shelf in the southern domain, and at the head of the Bering Canyon. The most important habitat covariates predicting suitable habitat were bottom depth, ocean productivity, tidal current maxima, bottom temperature, and sediment grain size. Combined, these five covariates comprised 99.1% of the leverage among predictors. The model was an outstanding fit to the training data (AUC = 0.93) and it correctly classified 85% of cases. Fit of the model in the validation step was excellent (AUC = 0.82) and 82% of the cases were correctly predicted from the test data set.

Most of the winter commercial catches in the Eastern Bering Sea containing southern Tanner crabs were in the central and southern domain over the middle shelf (Figure 280). The highest probabilities for suitable southern Tanner crab habitat predicted from the MaxEnt model ranged from the Pribilof Islands south and east to the head of Bering Canyon and into Bristol Bay. The most influential habitat covariates in the model were bottom depth, ocean productivity, bottom temperature, sediment grain size, and tidal current maxima accounting for a combined 99.4% of the leverage among all predictor terms. The MaxEnt model predicted 89% of cases correctly and was an outstanding fit (AUC = 0.96) to the training data. Model validation was successful (AUC = 0.88) correctly predicting 88% of the cases from the test data.

In springtime, most of the southern Tanner crabs caught in commercial fishery catches came from between the central and southern domains (Figure 281). In this season, the highest probabilities of suitable habitat were predicted north of St. Paul over the middle shelf in the central domain. The most important habitat covariates in the model were bottom depth, sediment grain size, and bottom temperature accounting for 87.1% of the total leverage of all predictor terms. The MaxEnt model was an outstanding

fit to the training data (AUC = 0.91) and predicted 82% of cases correctly. Model validation was successful (AUC = 0.82) and 82% of cases were correctly predicted from the test data.

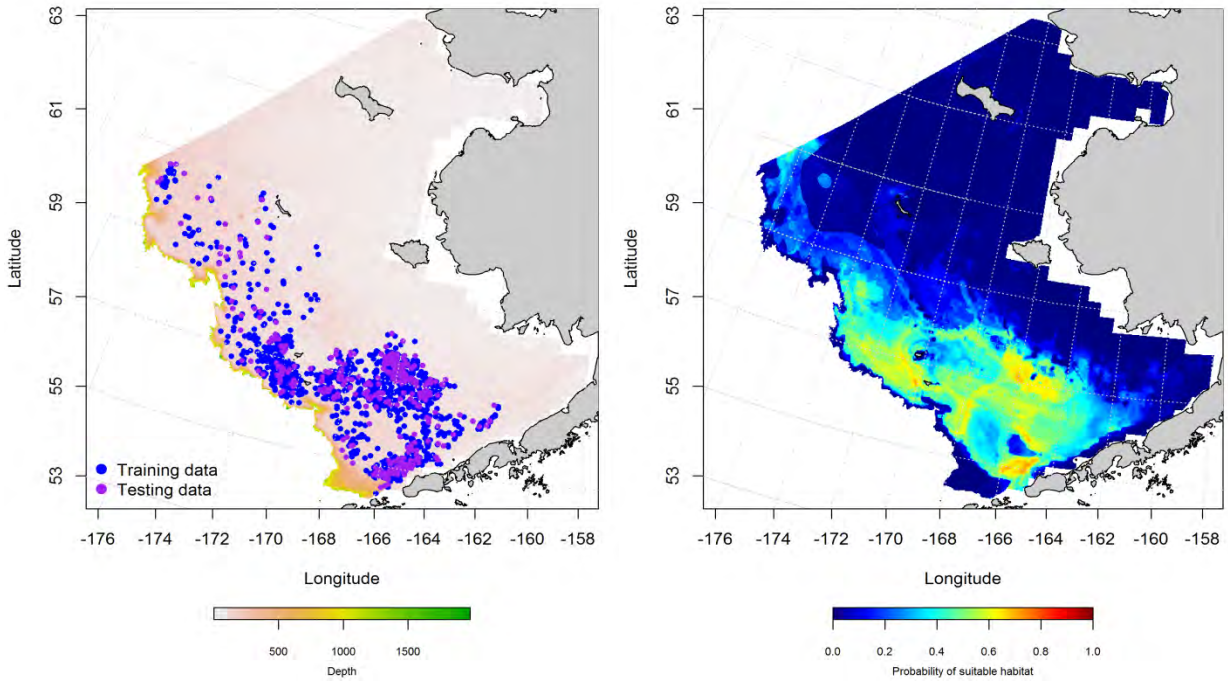

Figure 279. -- Presence of southern Tanner crabs in commercial fishery catches from fall (October-November; left panel). Blue points were used to train the maximum entropy (MaxEnt) model predicting the probability of suitable habitat (right panel) and the purple points were used to validate the model.

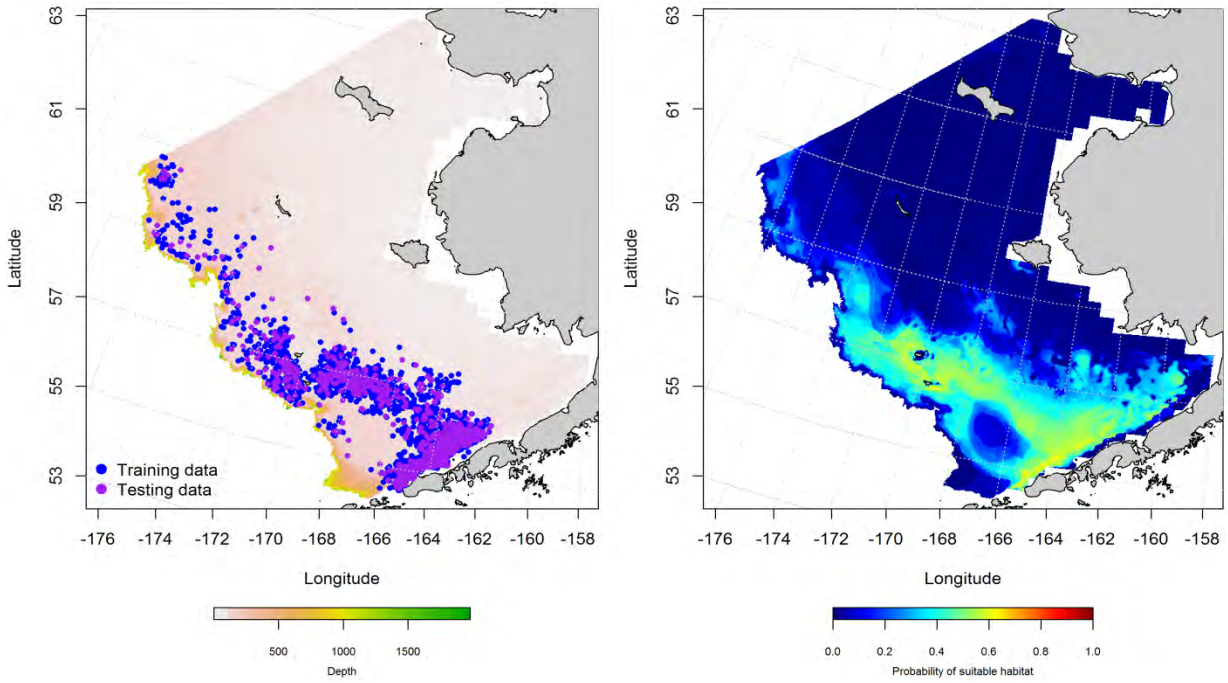

Figure 280. -- Presence of southern Tanner crab in commercial fishery catches from winter (December-February; left panel). Blue points were used to train the maximum entropy (MaxEnt) model predicting the probability of suitable habitat (right panel) and the purple points were used to validate the model.

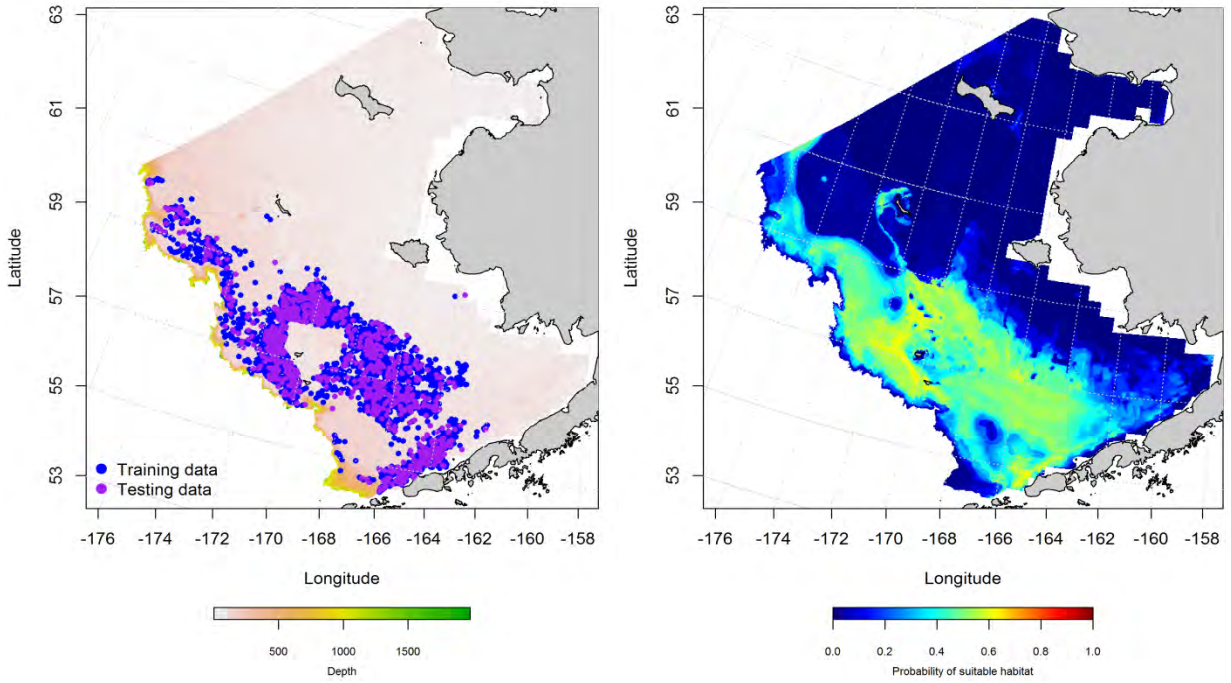

Figure 281. -- Presence of southern Tanner crab in commercial fishery catches from spring (March-May; left panel). Blue points were used to train the maximum entropy (MaxEnt) model predicting the probability of suitable habitat (right panel) and the purple points were used to validate the model.

Essential habitat maps and conclusions for southern Tanner crab (*Chionocetes bairdi*) in the Eastern Bering Sea – Species distribution modeling of southern Tanner crab in the Eastern Bering Sea predicts that essential habitat for this species ranges across much of the Eastern Bering Sea from the inner to the outer shelf (Figure 282). Habitat containing the top 25% of the highest CPUEs was located over the middle and outer shelf in the central and southern domains. Individuals of this species can be found throughout the survey area in depths ranging from 18 to nearly 800 m.

In general, essential habitat of southern Tanner crabs predicted from their presence in commercial fishery catches in the Eastern Bering Sea overlapped across seasons (Figure 283). However, areas of high probability habitat varied between seasons. In wintertime, those areas were focused around the Pribilof Islands and over the Bering Canyon. During spring months, the suitable habitat areas were expanded west

and north of the Pribilofs compared to winter and were somewhat reduced over the Eastern arm of the Bering Canyon.

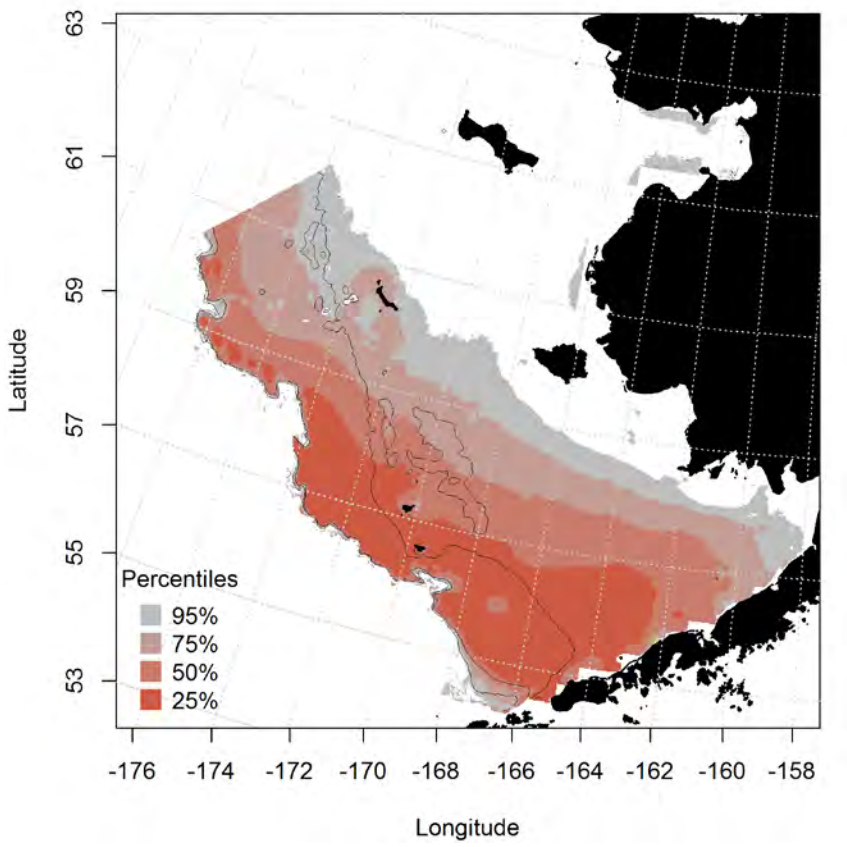

Figure 282. -- Essential habitat predicted for southern Tanner crabs from summertime RACE bottom trawl surveys of the Eastern Bering Sea.

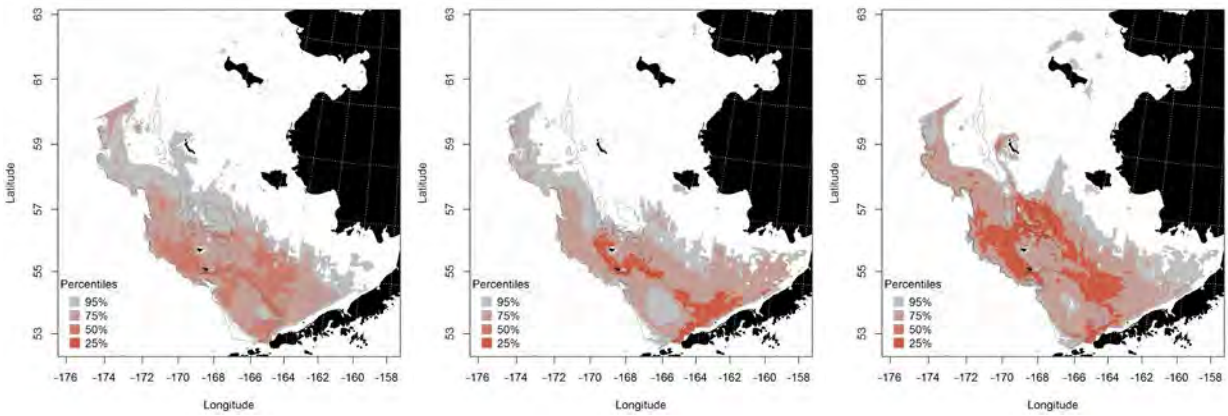

Figure 283. -- Essential habitat predicted from southern Tanner crab presence in commercial fishery catches during fall (left panel), winter (middle panel), and spring (right panel) in the Eastern Bering Sea.

snow crab (*Chionocetes opilio*)

Snow crabs are distributed from Japan to the Beaufort Sea and across the Eastern Bering Sea into the Aleutian Islands. These crabs are also found in the Atlantic from Maine, U. S. A. to Greenland. They are primarily found over soft sandy or mud bottom. Snow crabs support an important domestic fishery in the United States.

Summertime distribution of snow crab from RACE bottom trawl surveys of the Eastern Bering Sea – In RACE summer bottom trawl catches from the Eastern Bering Sea, snow crabs occurred from Bristol Bay to Norton Sound and out onto the Eastern Bering Sea Slope (Figure 284). They were most prevalent in the central and northern domains. Snow crabs were caught in our bottom trawl surveys from depths ranging from 11 to nearly 800 m.

A standard abundance GAM predicted snow crab species distribution in the Eastern Bering Sea (Figure 285). The best-fitting GAM explained 61.8% of the deviance in their trawl CPUE data. The most significant habitat covariates retained in the model were geographical location, bottom temperature, tidally corrected current speed, and ocean productivity. According to the model, snow crab abundance increased in the northern domain of the survey area over decreasing bottom temperatures and current speeds and increasing surface chlorophyll-a concentrations. The model fits to the training data and in the validation step using the test data were moderate ($r^2 = 0.62$ for both data sets).

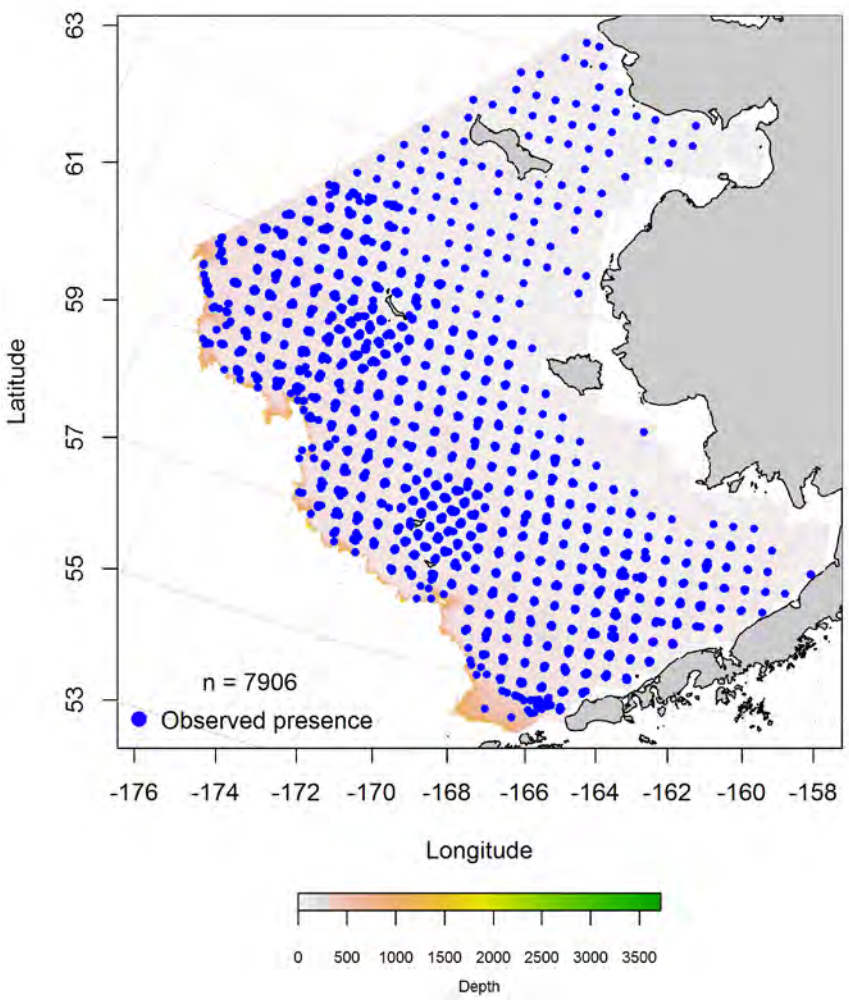

Figure 284. -- Distribution of snow crab in catches from RACE summer bottom trawl surveys of the Eastern Bering Sea.

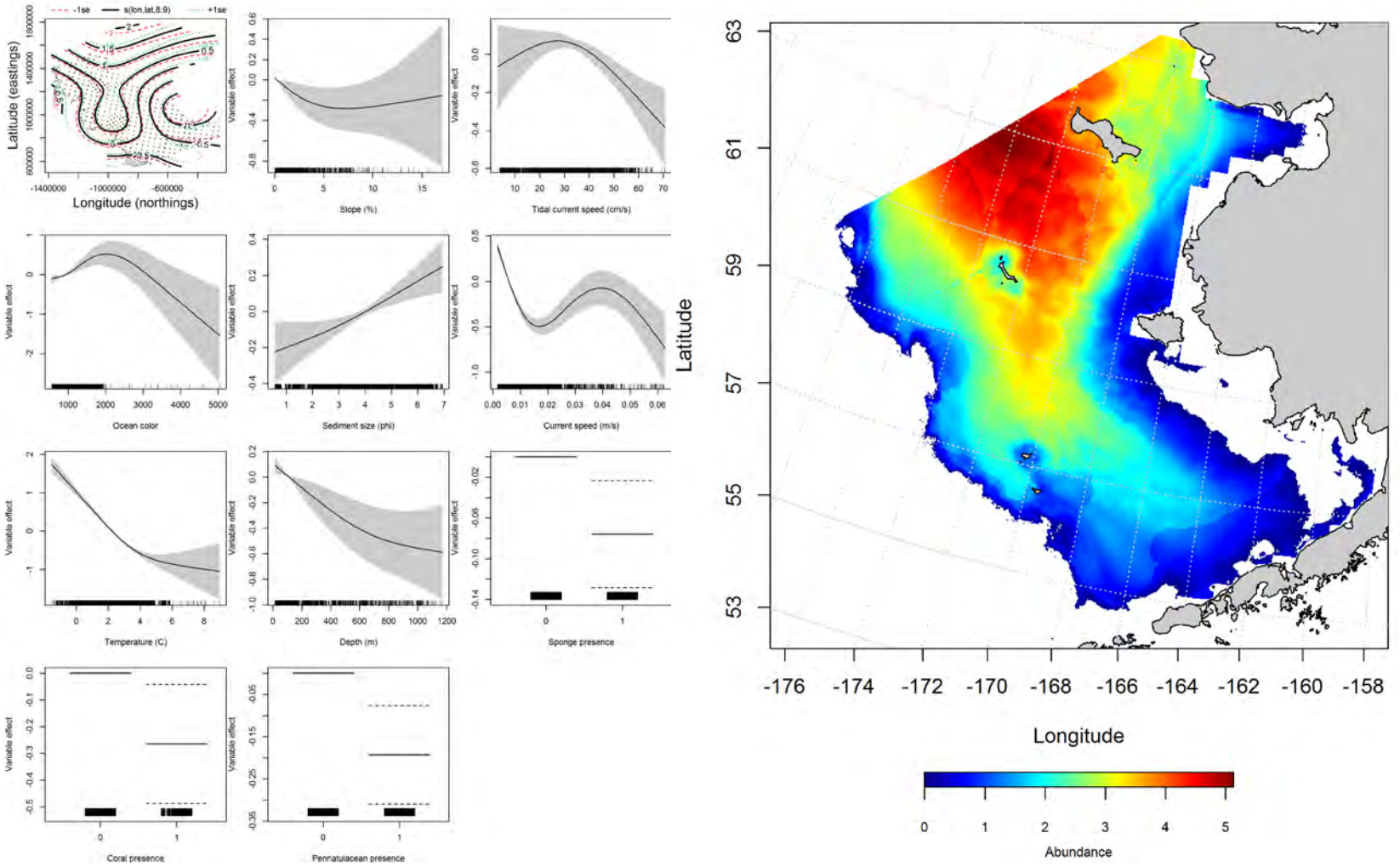

Figure 285. -- Effects of retained habitat covariates on the best-fitting generalized additive model (GAM; left panel) predicting snow crab abundance from RACE summer bottom trawl surveys of the Eastern Bering Sea Shelf, Slope, and Northern Bering Sea (right panel).

Seasonal distribution of snow crab in commercial fishery catches from the Eastern Bering Sea – Snow crabs observed in fall commercial fishery catches were fairly evenly distributed across the middle and outer shelf of the southern, central, and northern domains of the Eastern Bering Sea (Figure 286). Maximum entropy modeling predicted the high probabilities of suitable snow crab habitat over the middle shelf with a few hot spots in the near the heads of the Bering, Pribilof, and Zhemchug Canyons. The most important habitat covariates predicting suitable habitat were bottom depth, bottom temperature, ocean productivity, and sediment grain size. Combined, these five covariates comprised 91.7% of the leverage among predictors. The model was an excellent fit to the training data (AUC = 0.87) and it correctly classified 79% of cases. Fit of the model in the validation step was also excellent (AUC = 0.81) and 81% of the cases were correctly predicted from the test data set.

The winter commercial catches in the Eastern Bering Sea containing snow crabs were spread across the middle and outer shelf of the southern, central, and northern domains (Figure 287). The highest probabilities for suitable snow crab habitat predicted from the MaxEnt model were over the middle shelf from the Bering Canyon to Zhemchug Canyon. The most influential habitat covariates in the model were bottom depth, bottom temperature, ocean productivity, and sediment grain size accounting for a combined 99.5% of the leverage among all predictor terms. The MaxEnt model predicted 83% of cases correctly and was an outstanding fit (AUC = 0.91) to the training data. Model validation was successful (AUC = 0.81) correctly predicting 81% of the cases from the test data.

In springtime, most of the snow crabs caught in commercial fishery catches came from the middle and outer shelf over the central domain of the Eastern Bering Sea (Figure 288). In this season, the highest probabilities of suitable habitat were predicted north and west of St. Paul over the middle shelf. The most important habitat covariates in the model were bottom depth, bottom temperature, ocean productivity, and measures of current accounting for 89.9% of the total leverage of all predictor terms. The MaxEnt model

was an outstanding fit to the training data (AUC = 0.91) and predicted 82% of cases correctly. Model validation was successful (AUC = 0.82) and 82% of cases were correctly predicted from the test data.

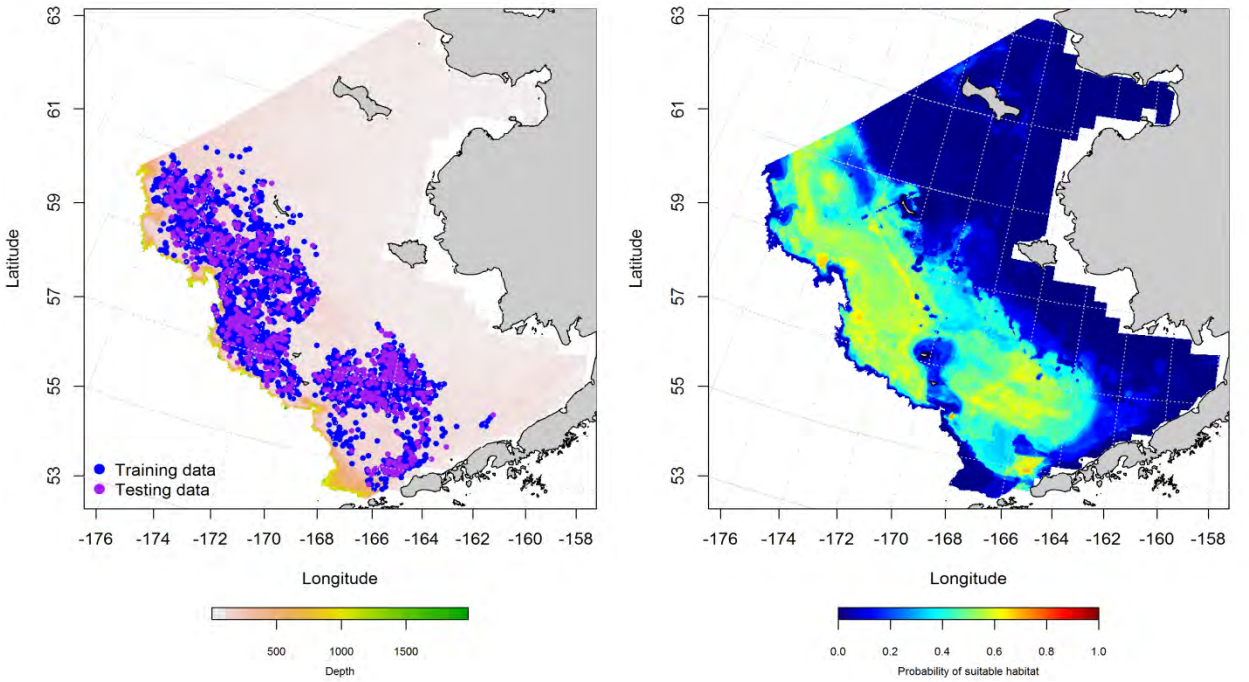

Figure 286. -- Presence of snow crabs in commercial fishery catches from fall (October-November; left panel). Blue points were used to train the maximum entropy (MaxEnt) model predicting the probability of suitable habitat (right panel) and the purple points were used to validate the model.

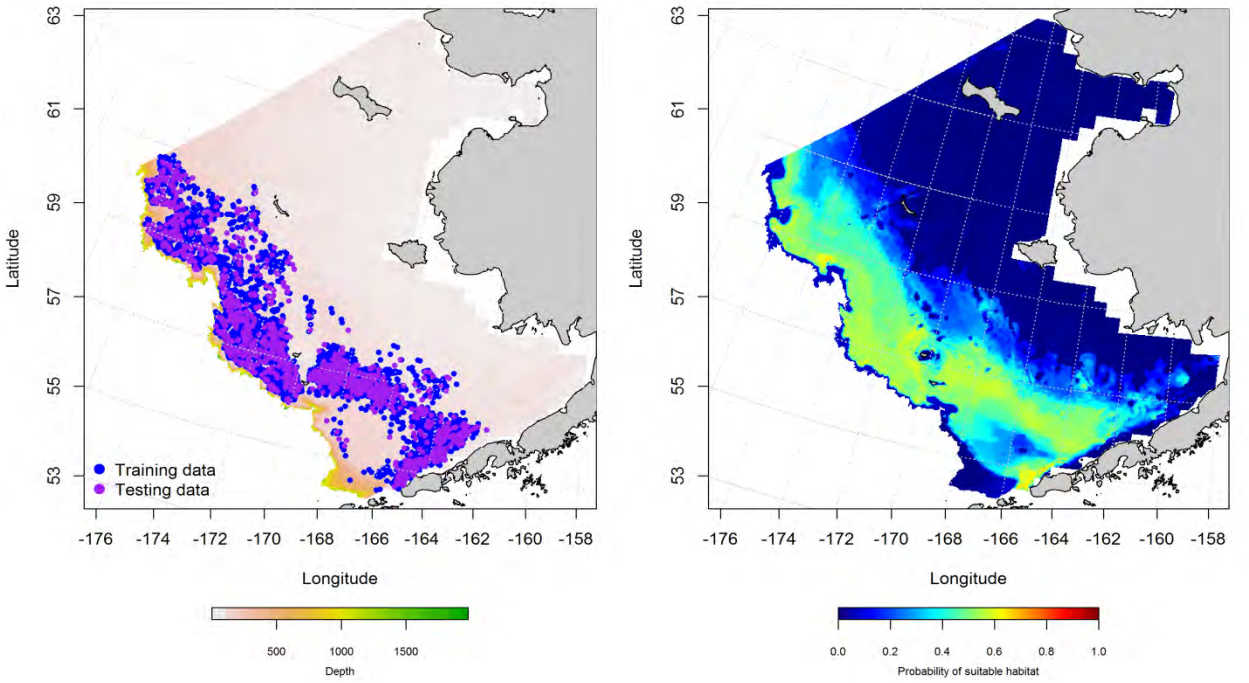

Figure 287. -- Presence of snow crab in commercial fishery catches from winter (December-February; left panel). Blue points were used to train the maximum entropy (MaxEnt) model predicting the probability of suitable habitat (right panel) and the purple points were used to validate the model.

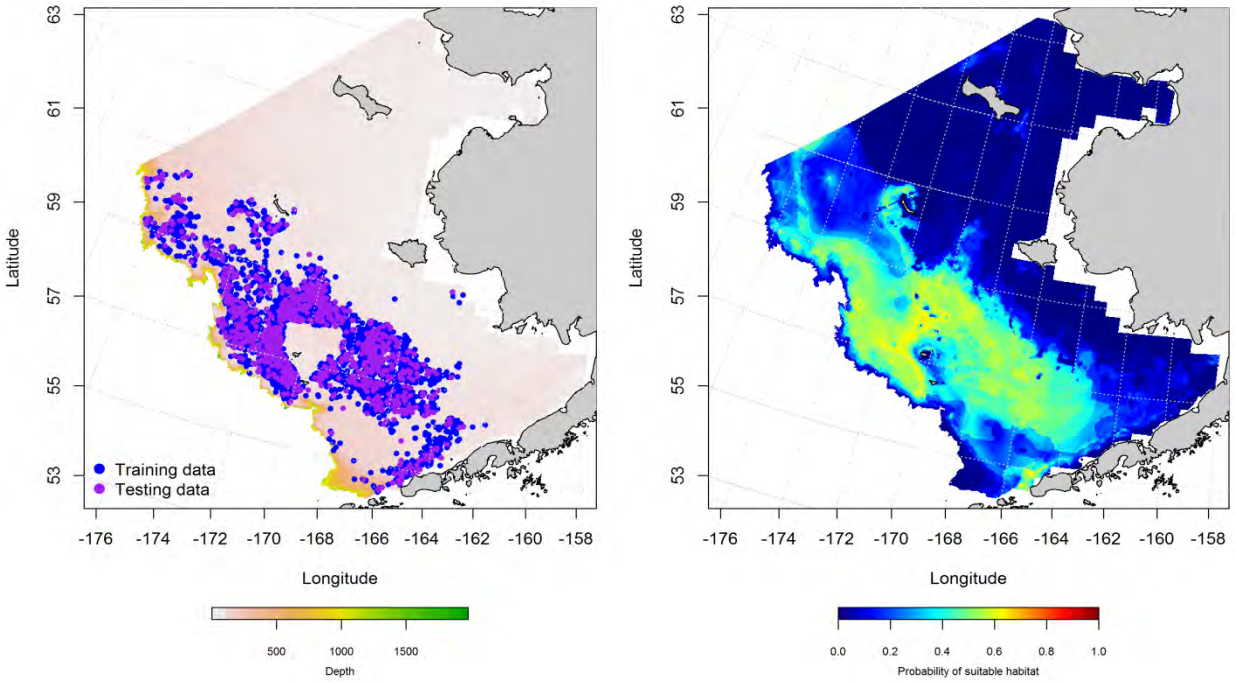

Figure 288. -- Presence of snow crab in commercial fishery catches from spring (March-May; left panel). Blue points were used to train the maximum entropy (MaxEnt) model predicting the probability of suitable habitat (right panel) and the purple points were used to validate the model.

Essential habitat maps and conclusions for snow crab (*Chionocetes opilio*) in the Eastern Bering Sea – Species distribution modeling of snow crab in the Eastern Bering Sea predicts that essential habitat for this species ranges across much of the Eastern Bering Sea from the inner to the outer shelf (Figure 289). Habitat containing the top 25% of the highest CPUEs was located almost exclusively in the northern domain in summertime. Individuals of this species can be found throughout the survey area in depths ranging from 11 to nearly 800 m.

Essential habitat of snow crabs predicted from their presence in commercial fishery catches in the Eastern Bering Sea generally overlapped across seasons (Figure 290). However, areas of high probability habitat varied between seasons. In wintertime, those areas were focused along the outer shelf in the northern and

central domains and over the middle shelf in the southern domain. During spring months, the suitable habitat areas were found primarily in the central domain over the middle shelf.

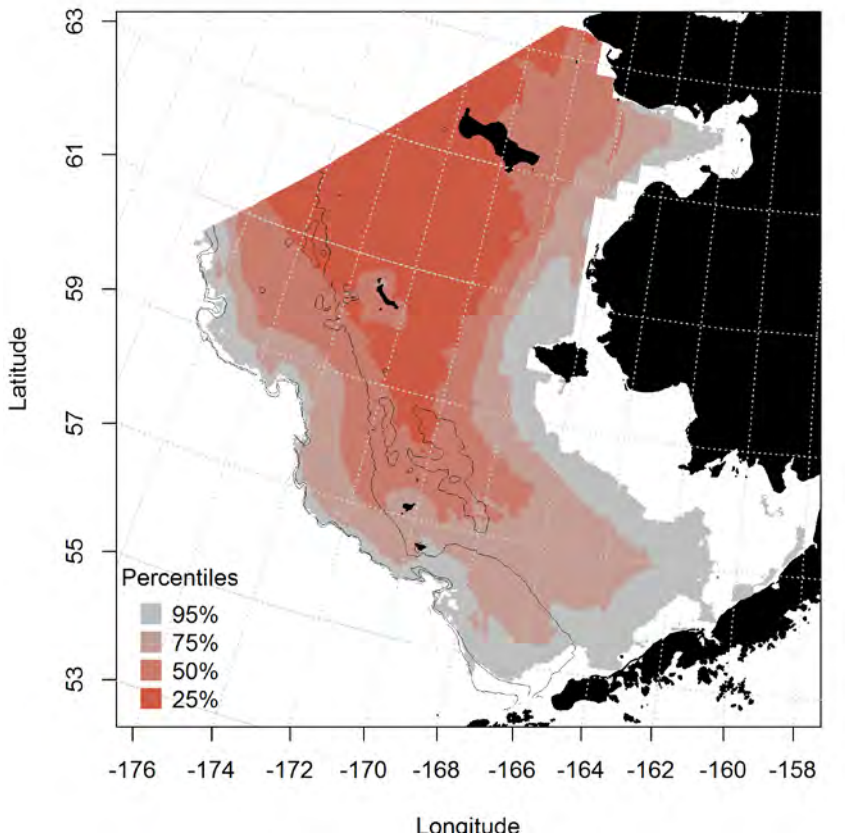

Figure 289. -- Essential habitat predicted for snow crabs from summertime RACE bottom trawl surveys of the Eastern Bering Sea.

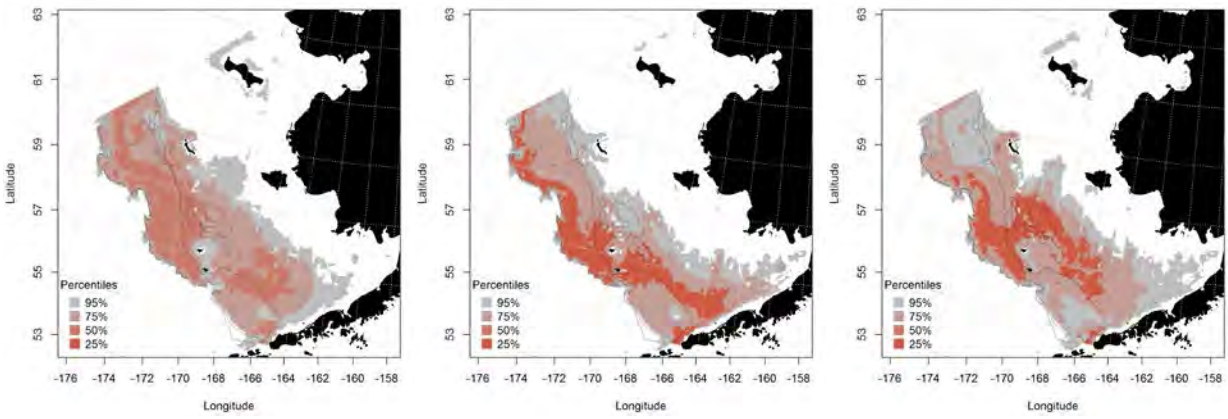

Figure 290. -- Essential habitat predicted from snow crab presence in commercial fishery catches during fall (left panel), winter (middle panel), and spring (right panel) in the Eastern Bering Sea.

red king crab (*Paralithodes camtschaticus*)

Red king crabs are distributed from British Columbia to Japan across North Pacific and northward into the Bering Sea. Bristol Bay and the Kodiak archipelago are the centers of its abundance in Alaska. They are the target of a commercially valuable domestic fishery in the United States.

Summertime distribution of red king crab from RACE bottom trawl surveys of the Eastern Bering Sea – In RACE summer bottom trawl catches from the Eastern Bering Sea, red king crabs occurred from Bristol Bay to Norton Sound from the inner to the middle shelf (Figure 291). They appeared to be most prevalent in the southern and central domains. Red king crabs were caught in our bottom trawl surveys over depths ranging from 14 to 112 m.

Red king crab distribution was modeled with a hurdle GAM in the Eastern Bering Sea. The presence-absence GAM predicted that the highest probabilities of encountering red king crabs in RACE summer bottom trawl catches occurred in Norton Sound and through Bristol Bay (Figure 292). The best-fitting GAM explained 59.1% of the deviance in their distribution data. Geographical location, sediment grain size, tidal maxima, and current speed were the most significant predictors retained in the model. Model effects increased to the northeast with decreasing sediment grain size, increasing tidal maxima and decreasing overall current speed. The presence-absence GAM was an excellent fit to the training data (AUC = 0.84) but correctly classified only 33% of predicted cases of presence-absence. Model validation was successful (AUC = 0.95) correctly classified 69% of cases predicted from the test data.

Conditional abundance of red king crab was predicted where the threshold for presence established in the first step was met (Figure 293). The best-fitting GAM explained just 21.8% of the deviance in red king crab CPUE from RACE bottom trawl surveys of the Eastern Bering Sea and predicted their greatest abundances around the margins of Bristol Bay. The most significant predictors retained in the model were sediment grain size, tidal maxima, geographical position, bottom temperature, and bottom depth. Model

effects predicted that abundance increased to the northwest in warmer waters where tidal maxima were > 30 $cm \cdot s^{-1}$ and decreased with decreasing sediment grain size and increasing depth. Fits were poor for the training and test data sets (r^2 = 0.22 and 0.09).

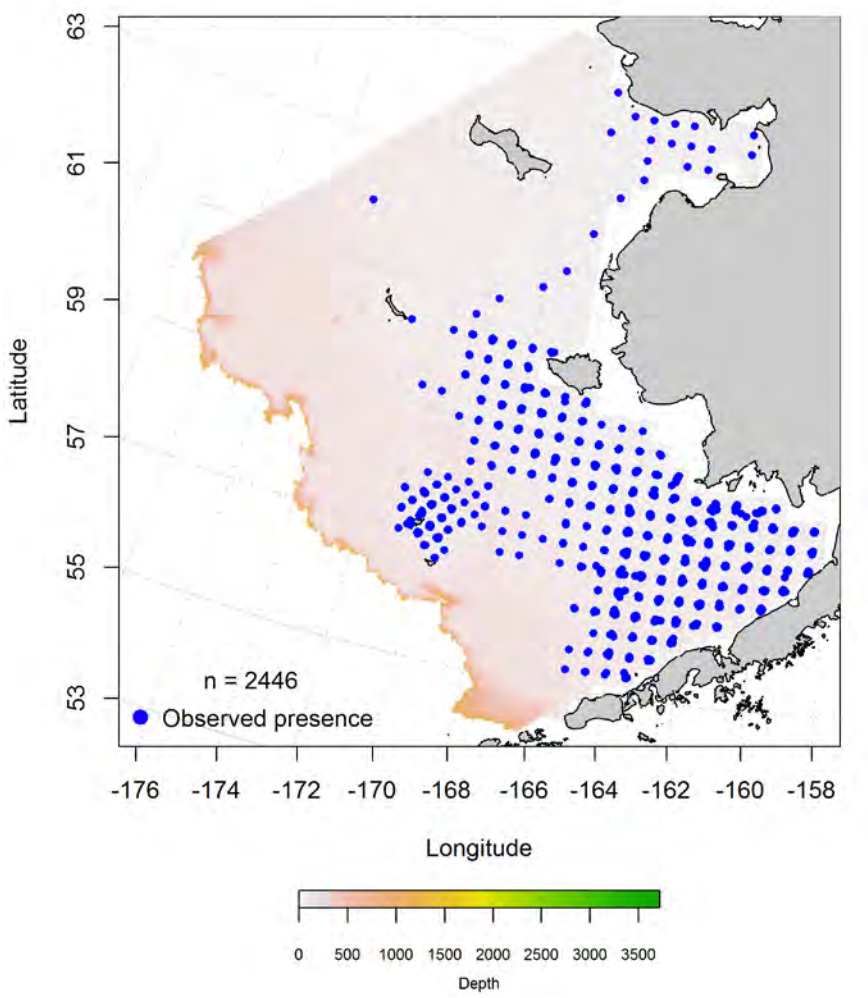

Figure 291. -- Distribution of red king crab in catches from RACE summer bottom trawl surveys of the Eastern Bering Sea.

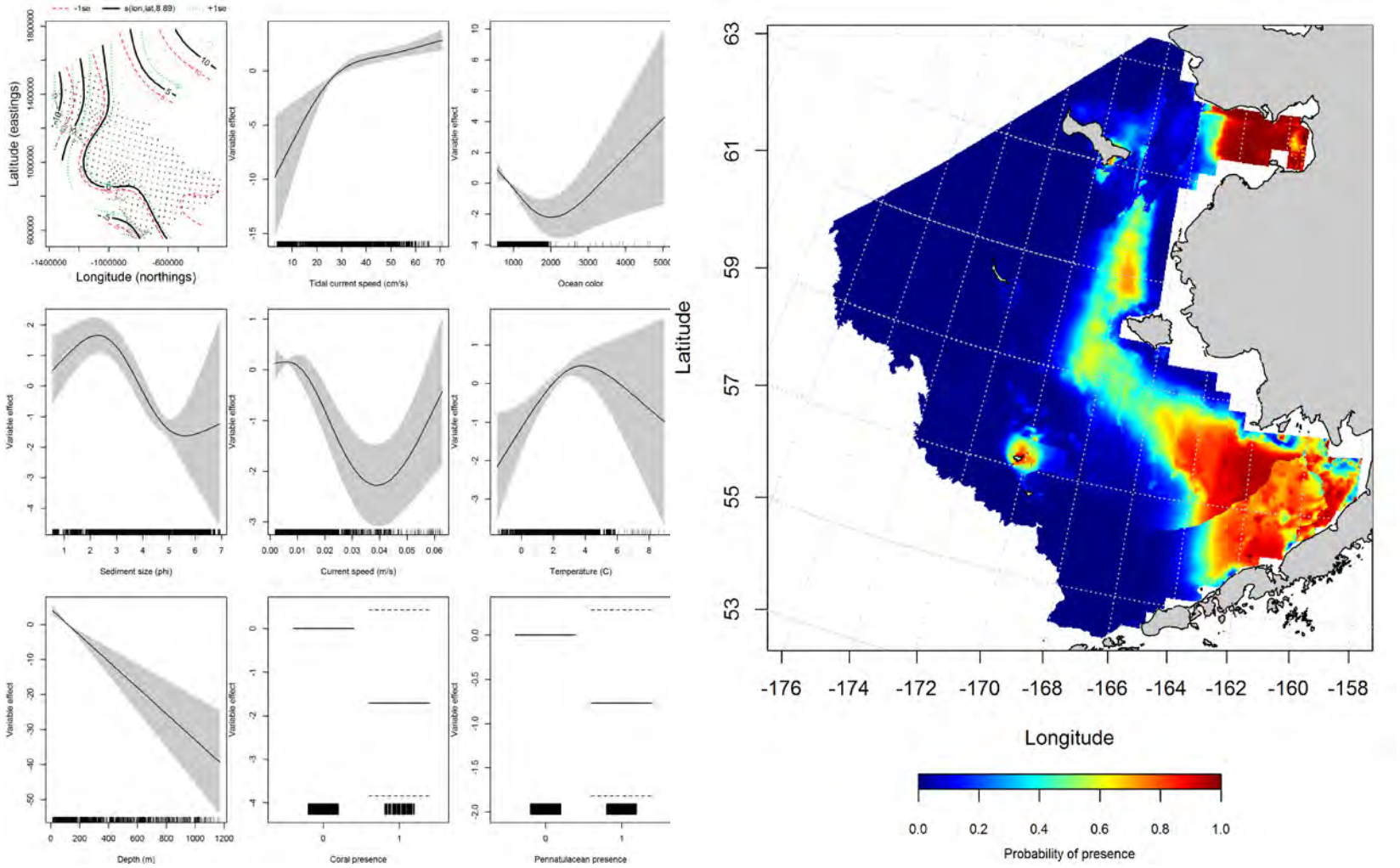

Figure 292. -- Effects of retained habitat covariates on the best-fitting generalized additive presence-absence model (GAM) of red king crab from RACE summer bottom trawl surveys of the Eastern Bering Sea Shelf, Slope, and Northern Bering Sea alongside their predicted presence (right panel).

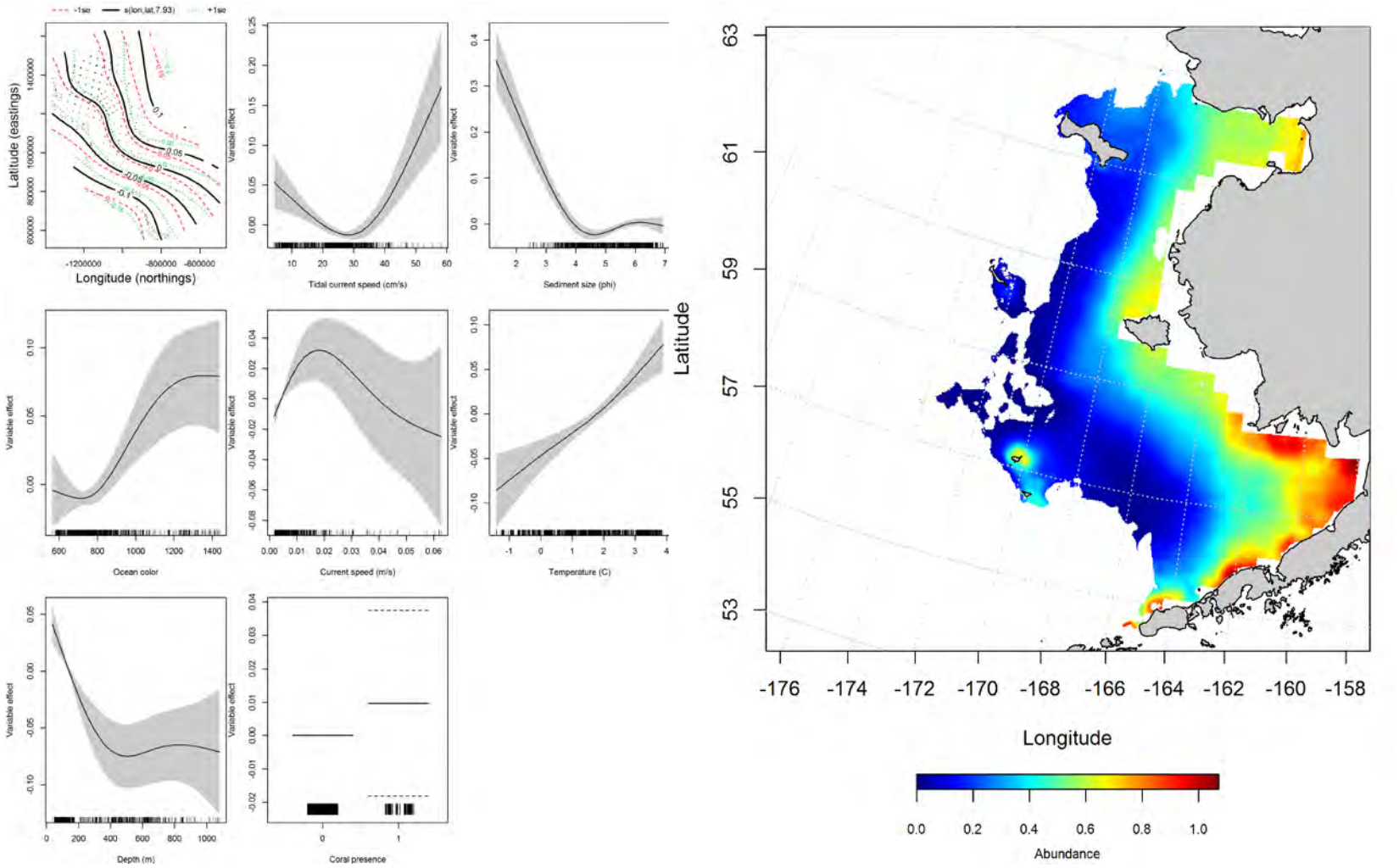

Figure 293. -- Effects of retained habitat covariates on the best-fitting generalized additive model (GAM) of red king crab from RACE summer bottom trawl surveys of the Eastern Bering Sea Shelf, Slope, and Northern Bering Sea alongside their predicted conditional abundance (right panel).KALI results figures look correct

Seasonal distribution of red king crab in commercial fishery catches from the Eastern Bering Sea – Red king crabs observed in fall commercial fishery catches were primarily encountered over the middle shelf in the southern domain of the Eastern Bering Sea (Figure 294). Maximum entropy modeling predicted that the highest probabilities of suitable red king crab habitat were in the northern portion of this area. The most important habitat covariates predicting suitable habitat were tidal maxima, bottom depth, sediment grain size, tidally corrected current speed, and bottom temperature. Combined, these covariates comprised 89.9% of the leverage among independent predictors. The model was an outstanding fit to the training data (AUC = 0.98) and it correctly classified 94% of cases. Fit of the model in the validation step was excellent (AUC = 0.87) and 87% of the cases were correctly predicted from the test data set.

The winter commercial catches in the Eastern Bering Sea containing red king crabs were centered over the head of the Bering Canyon in the southern domain and around St. George Island in the central domain (Figure 295). The most important habitat covariates in the model were current measures (tidal maxima and tidally corrected current speed) and bottom depth which accounted for a combined 79.2% of the leverage among all predictor terms. The MaxEnt model predicted 96% of cases correctly and was an outstanding fit (AUC = 0.99) to the training data. Model validation was successful (AUC = 0.95) correctly predicting 95% of the cases from the test data.

In springtime, the red king crabs caught in commercial fishery catches came from the inner and middle shelf of primarily the southern and centrals domain of the Eastern Bering Sea (Figure 296). In this season, the highest probabilities of suitable habitat predicted by the MaxEnt model were on the middle shelf in the southern domain. The most important habitat covariates in the model were current measures (tidal maxima and tidally corrected current speed), bottom depth, and sediment grain size accounting for 90.3% of the total leverage of all predictor terms. The MaxEnt model was an outstanding fit to the training data

(AUC = 0.95) and predicted 89% of cases correctly. Model validation was successful (AUC = 0.83) and 83% of cases were correctly predicted from the test data.

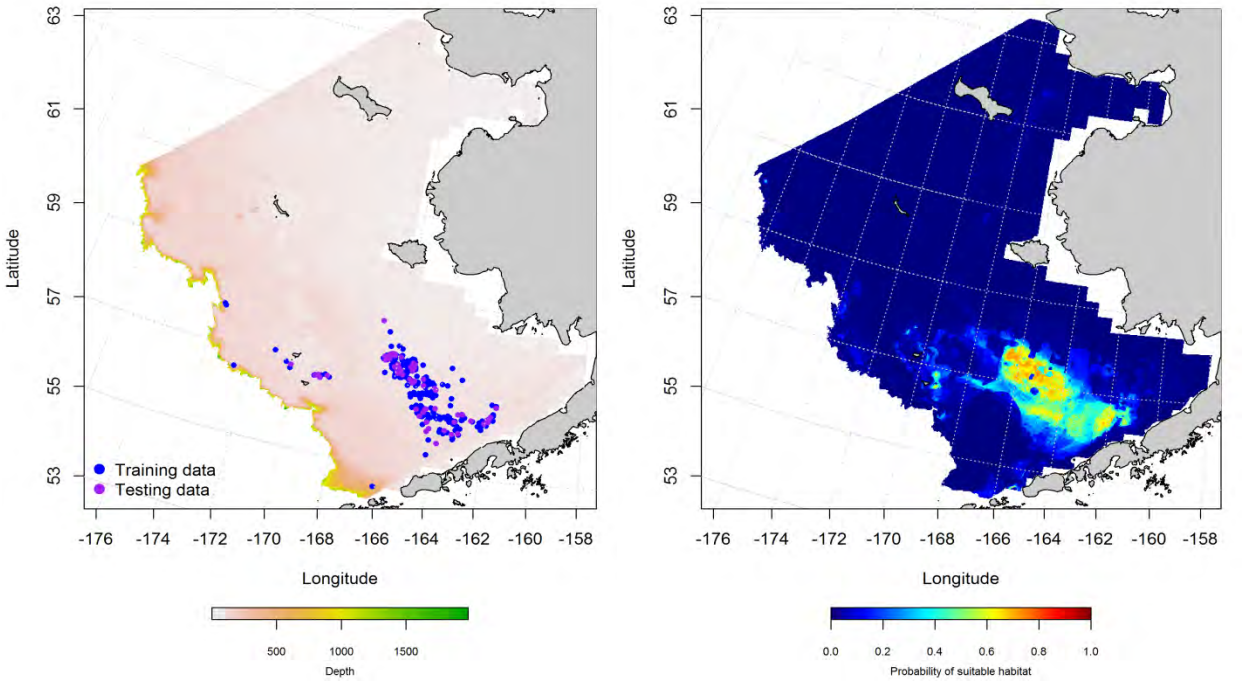

Figure 294. -- Presence of red king crabs in commercial fishery catches from fall (October-November; left panel). Blue points were used to train the maximum entropy (MaxEnt) model predicting the probability of suitable habitat (right panel) and the purple points were used to validate the model.

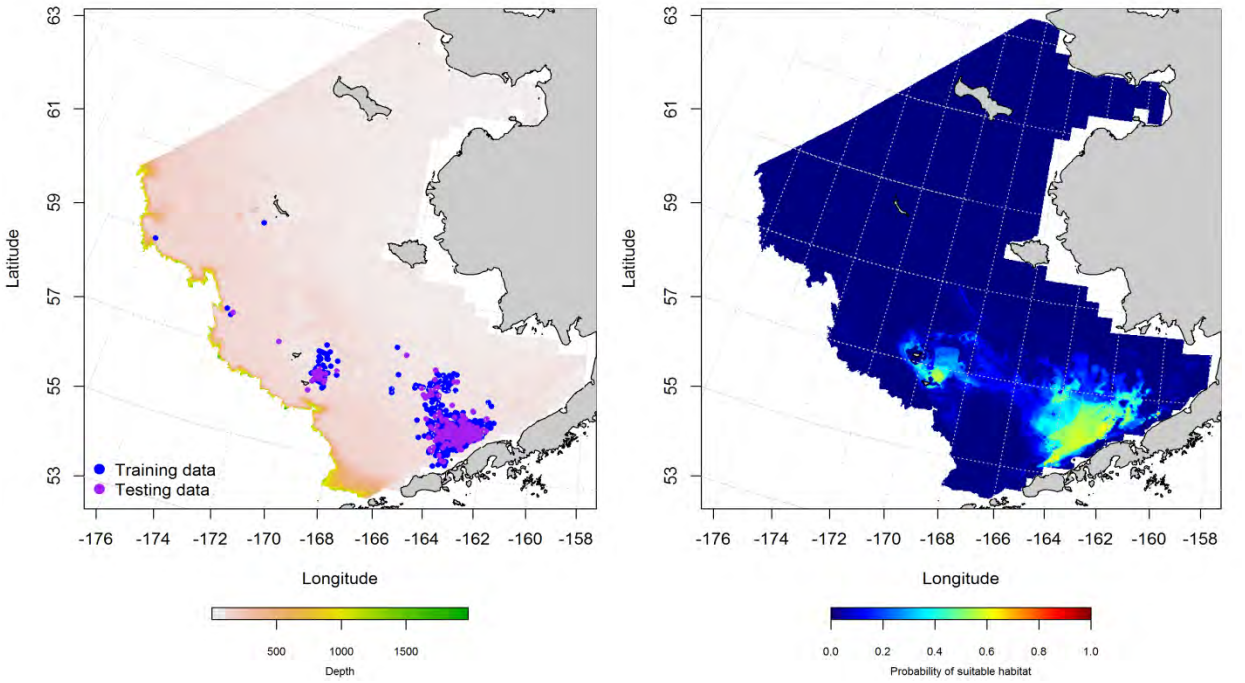

Figure 295. -- Presence of red king crab in commercial fishery catches from winter (December-February; left panel). Blue points were used to train the maximum entropy (MaxEnt) model predicting the probability of suitable habitat (right panel) and the purple points were used to validate the model.

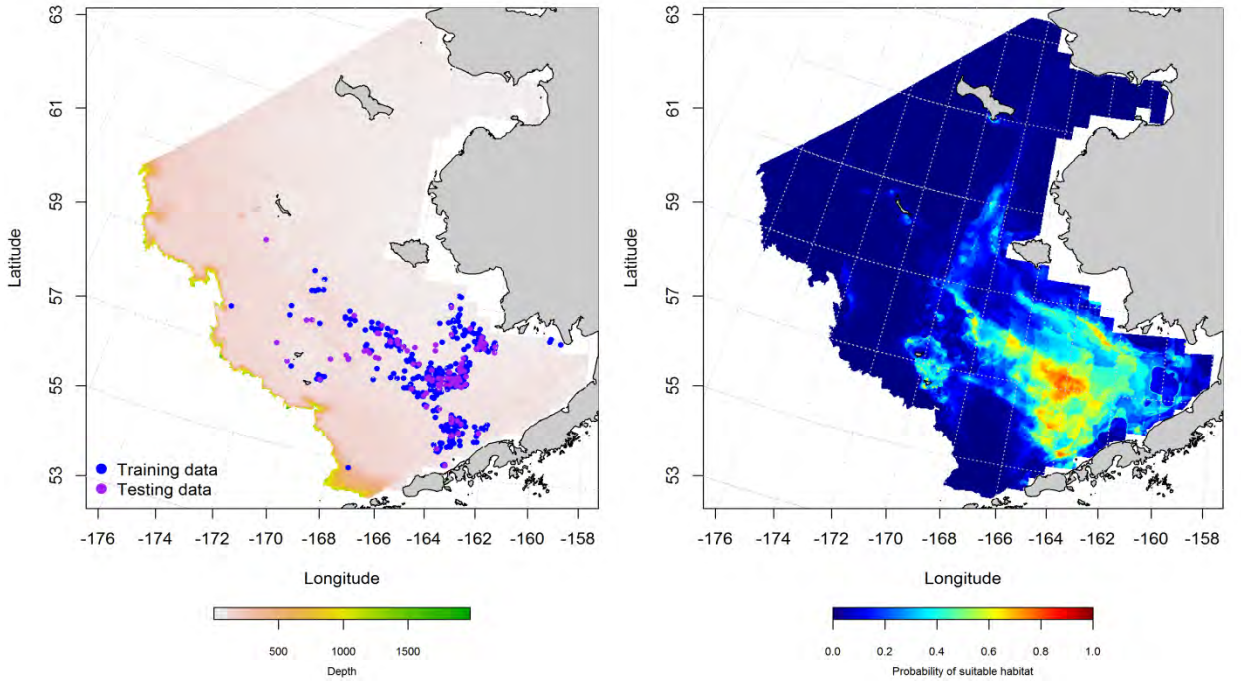

Figure 296. -- Presence of red king crab in commercial fishery catches from spring (March-May; left panel). Blue points were used to train the maximum entropy (MaxEnt) model predicting the probability of suitable habitat (right panel) and the purple points were used to validate the model.

Essential habitat maps and conclusions for red king crab (*Paralithodes camtschaticus*) in the Eastern Bering Sea – Species distribution modeling of red king crab in the Eastern Bering Sea from summer RACE bottom trawl surveys predicts that essential habitat for this species ranges from Bristol Bay to Norton Sound (Figure 297). Onshore to offshore, EFH extends from the inner across the middle shelf to the Pribilof Islands. Predictions of red king crab conditional abundance decrease on- to offshore. There also appear to be some areas of high predicted abundance in the shallows around the Pribilofs.

Essential habitat of red king crabs predicted from their presence in commercial fishery catches in the Eastern Bering Sea was generally spread over the central and southern domains (Figure 298). However, areas of high probability habitat varied between seasons. In wintertime, those areas were focused along the east-west axis of the Bering Canyon in the southern domain with some activity concentrated around

St. George Island to the north. During spring months, essential habitat was more diffuse than in winter and spread across the inner and middle shelf of the central and southern domain.

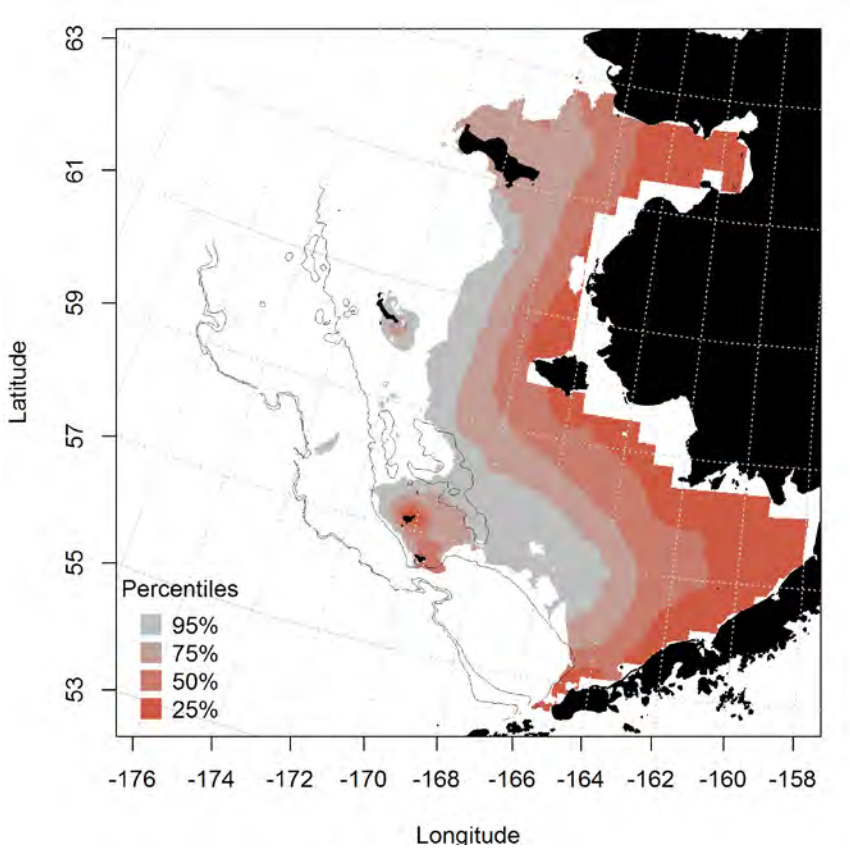

Figure 297. -- Essential habitat predicted for red king crabs from summertime RACE bottom trawl surveys of the Eastern Bering Sea.

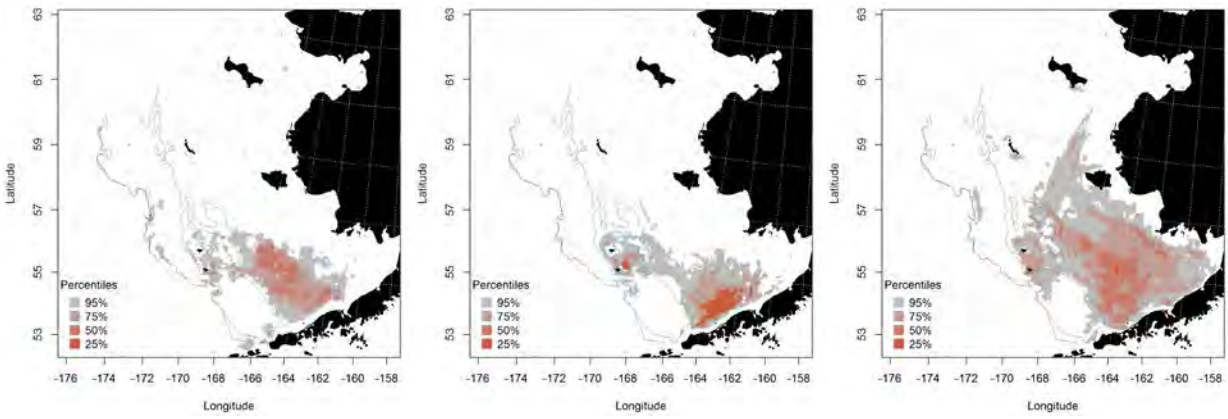

Figure 298. -- Essential habitat predicted from red king crab presence in commercial fishery catches during fall (left panel), winter (middle panel), and spring (right panel) in the Eastern Bering Sea.

blue king crab (*Paralithodes platypus*)

Blue king crabs are distributed from Japan into the Bering Sea and Gulf of Alaska. Their distribution is contiguous across this large region with spatially constrained populations occurring in various locales. They are the target of a commercially valuable domestic fishery in the United States.

Summertime distribution of blue king crab from RACE bottom trawl surveys of the Eastern Bering Sea – In RACE summer bottom trawl catches from the Eastern Bering Sea, blue king crabs occurred from the Pribilof Islands northward (Figure 299). They were most prevalent over the middle shelf in the central and northern domains. Blue king crabs were caught in our bottom trawl surveys over depths ranging from 22 to 166 m.

Blue king crab distribution was modeled with a hurdle GAM in the Eastern Bering Sea. The presence-absence GAM predicted that the highest probabilities of encountering blue king crabs in RACE summer bottom trawl catches occurred around the Pribilof Islands and St. Matthew Islands as well as in the northern Bering Sea north of St. Lawrence Island (Figure 300). The best-fitting GAM explained 54% of the deviance of their presence in our trawl catches. Geographical location, bottom temperature, sediment grain size, and current measures were the most significant predictors retained in the model. Model effects were highest around St. Matthew Island. They increased with increasing bottom temperature (up to ca. 2°C) and tidally corrected current speed, and decreased with decreasing tidal maxima and sediment grain size. The presence-absence GAM was an outstanding fit to the training data (AUC = 0.95) and correctly classified 88% of predicted cases of presence-absence. Model validation was successful (AUC = 0.94) correctly classified 87% of cases predicted from the test data.

Conditional abundance of blue king crab was predicted where the threshold for presence established in the first step was met (Figure 301). The best-fitting GAM explained just 32.7% of the deviance in blue king crab CPUE from RACE bottom trawl surveys of the Eastern Bering Sea and predicted their greatest

abundances near St. Matthew and St. Lawrence Islands in the northern domain. The most significant predictors retained in the model were geographical location, bottom depth, bottom temperature, and measures of current speed. Model fits were poor for the training and test data sets (r^2 = 0.33 and 0.21).

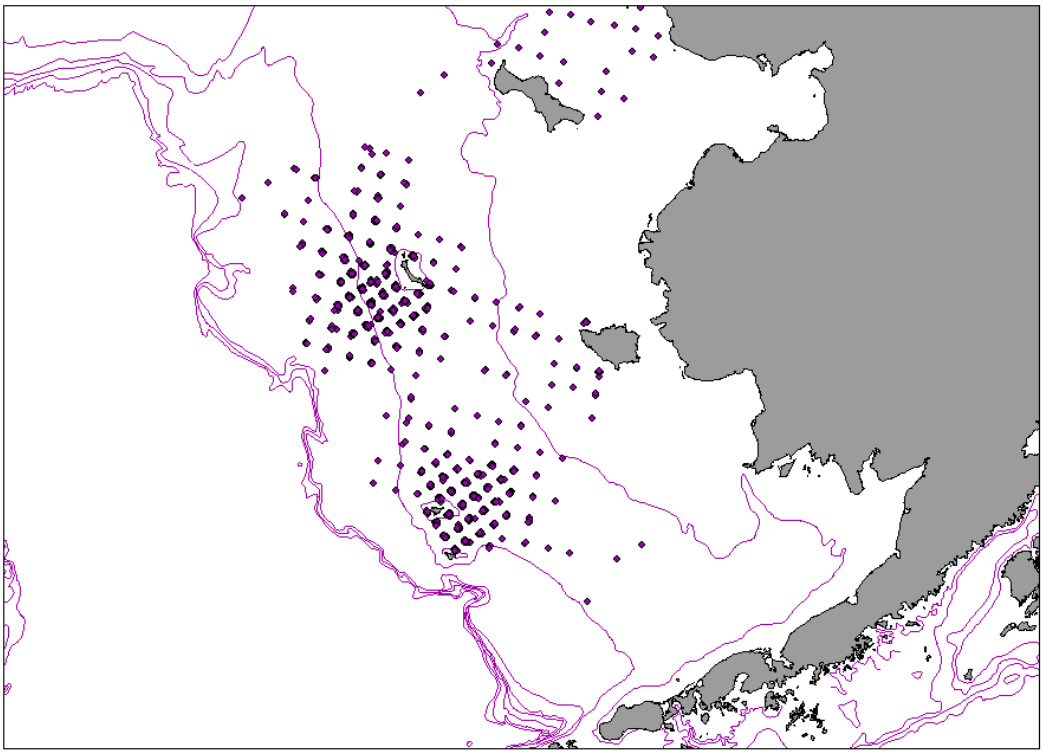

Figure 299. -- Distribution of blue king crab in catches from RACE summer bottom trawl surveys of the Eastern Bering Sea.

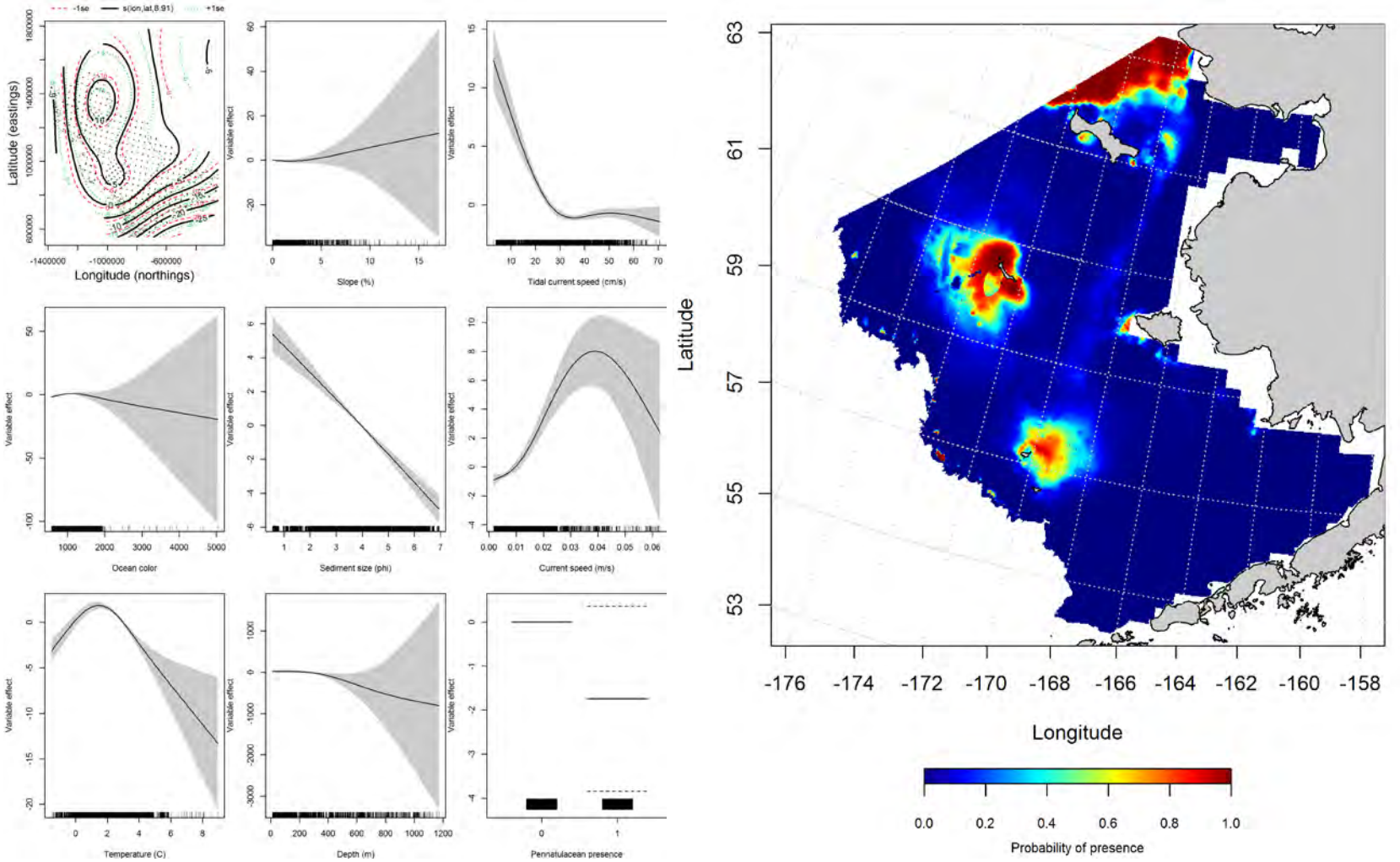

Figure 300. -- Effects of retained habitat covariates on the best-fitting generalized additive presence-absence model (GAM) of blue king crab from RACE summer bottom trawl surveys of the Eastern Bering Sea Shelf, Slope, and Northern Bering Sea alongside their predicted presence (right panel).

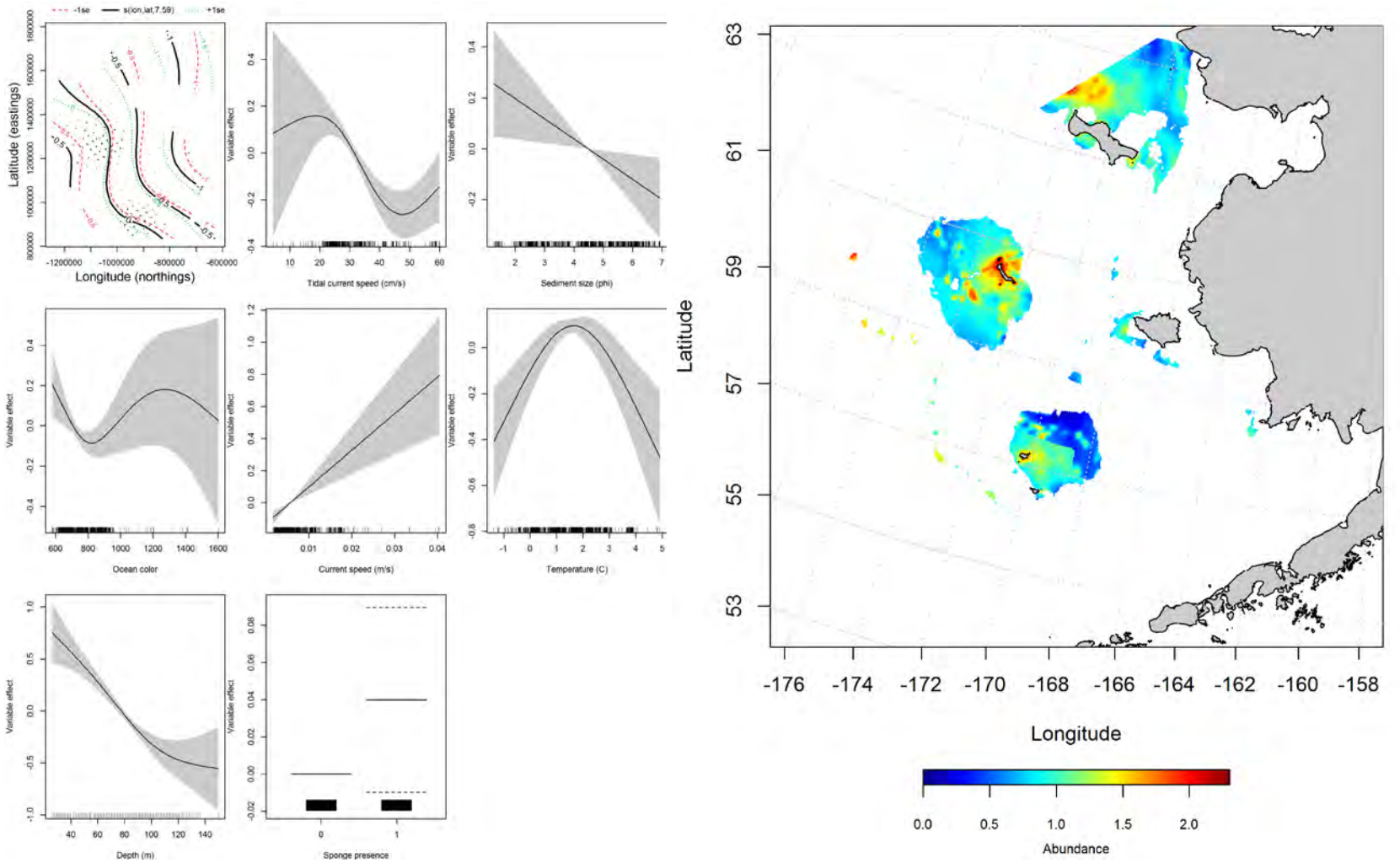

Figure 301. -- Effects of retained habitat covariates on the best-fitting generalized additive model (GAM) of blue king crab from RACE summer bottom trawl surveys of the Eastern Bering Sea Shelf, Slope, and Northern Bering Sea alongside their predicted conditional abundance (right panel).

Seasonal distribution of blue king crab in commercial fishery catches from the Eastern Bering Sea – Blue king crabs observed in fall commercial fishery catches were primarily caught west of St. Matthew Island in the northern domain of the Eastern Bering Sea (Figure 302). Maximum entropy modeling predicted that the highest probabilities of suitable blue king crab habitat were in this area as well as some patches to the northeast and south of the island. The most important habitat covariates predicting suitable habitat were ocean productivity and bottom temperature which, combined, comprised 82% of the leverage among independent predictors. The model was an outstanding fit to the training data (AUC = 0.98) and it correctly classified 92% of cases. Fit of the model in the validation step was also outstanding (AUC = 0.91) and 91% of the cases were correctly predicted from the test data set.

The winter commercial catches in the Eastern Bering Sea containing blue king crabs occurred east of the Pribilof Islands and west of St. Matthew Island (Figure 303). The most important habitat covariates in the model were bottom depth, ocean productivity, and bottom temperature which accounted for a combined 79.9% of the leverage among all predictor terms. The MaxEnt model predicted 90% of cases correctly and was an outstanding fit (AUC = 0.96) to the training data. Model validation was successful (AUC = 0.91) correctly predicting 91% of the cases from the test data.

In springtime, the blue king crabs caught in commercial fishery catches were primarily from west of St. Matthew Island (Figure 304). The highest probabilities of suitable habitat predicted by the MaxEnt model corresponded to this area west of St. Matthew, but were also predicted to the north east of the island as well as southward toward St. Paul Island in the Pribilofs. The most important habitat covariates in the model were ocean productivity, bottom temperature, and bottom depth accounting for 89.8% of the total leverage of all predictor terms. The MaxEnt model was an outstanding fit to the training data (AUC = 0.95) and predicted 88% of cases correctly. Model validation was moderately successful (AUC = 0.78) and 78% of cases were correctly predicted from the test data.

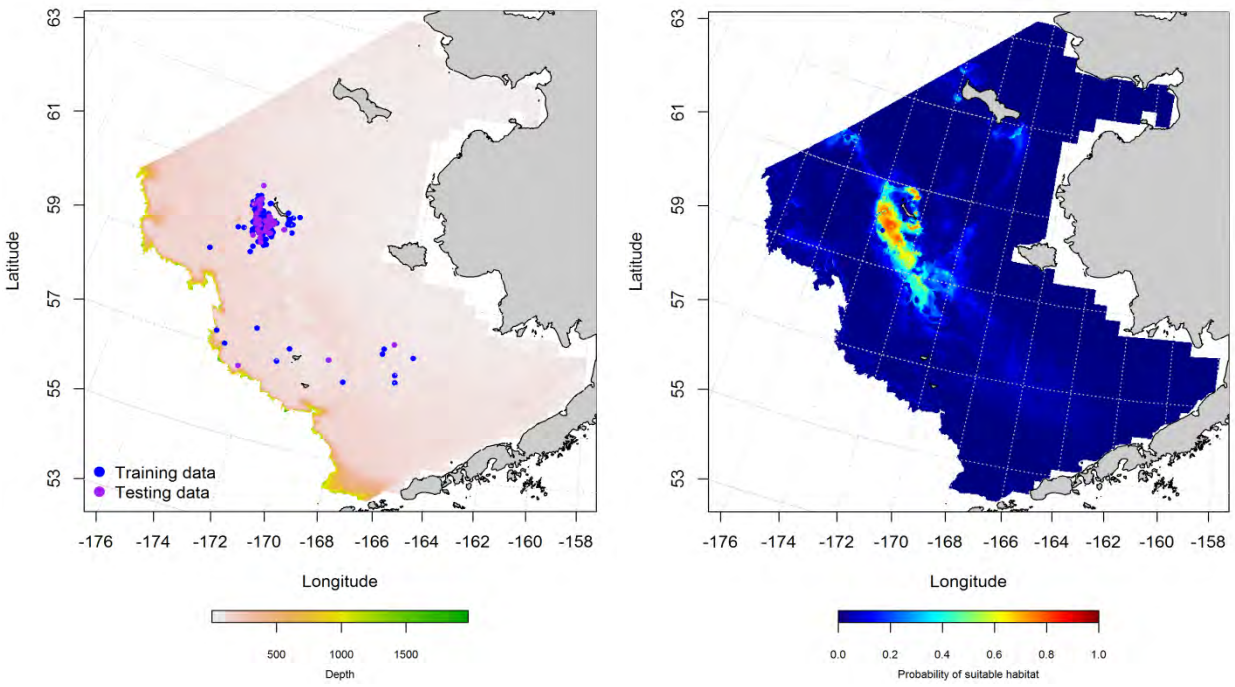

Figure 302. -- Presence of blue king crabs in commercial fishery catches from fall (October-November; left panel). Blue points were used to train the maximum entropy (MaxEnt) model predicting the probability of suitable habitat (right panel) and the purple points were used to validate the model.

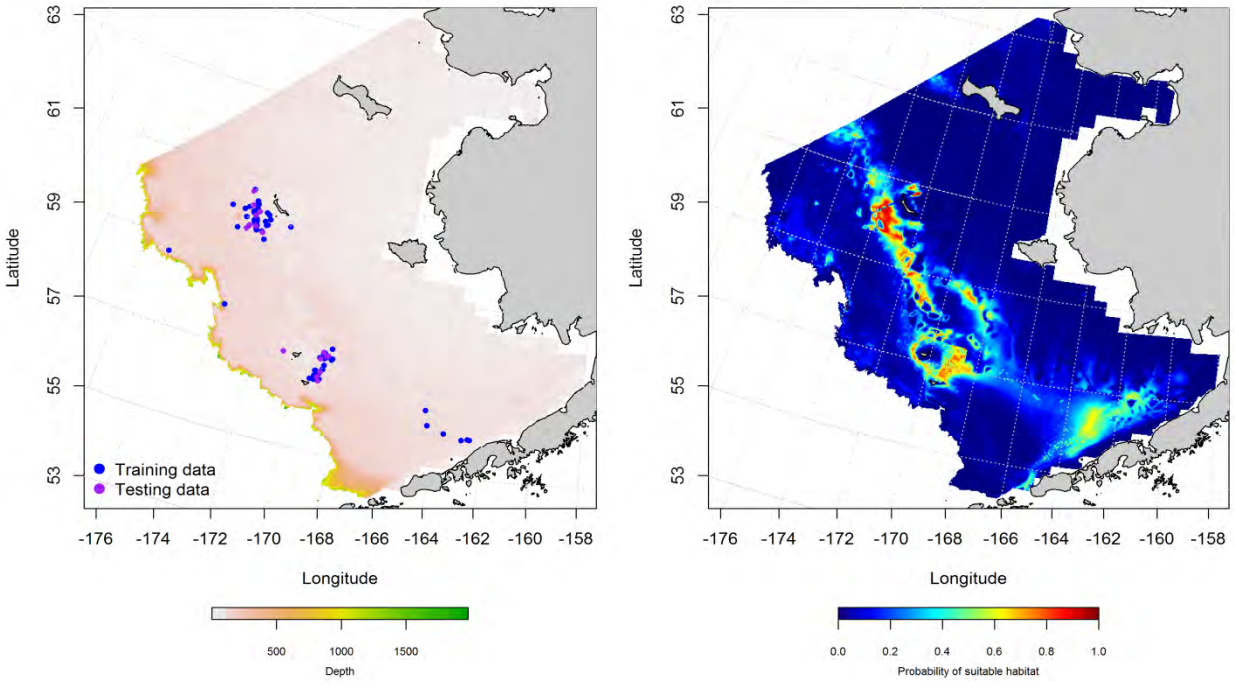

Figure 303. -- Presence of blue king crab in commercial fishery catches from winter (December-February; left panel). Blue points were used to train the maximum entropy (MaxEnt) model predicting the probability of suitable habitat (right panel) and the purple points were used to validate the model.

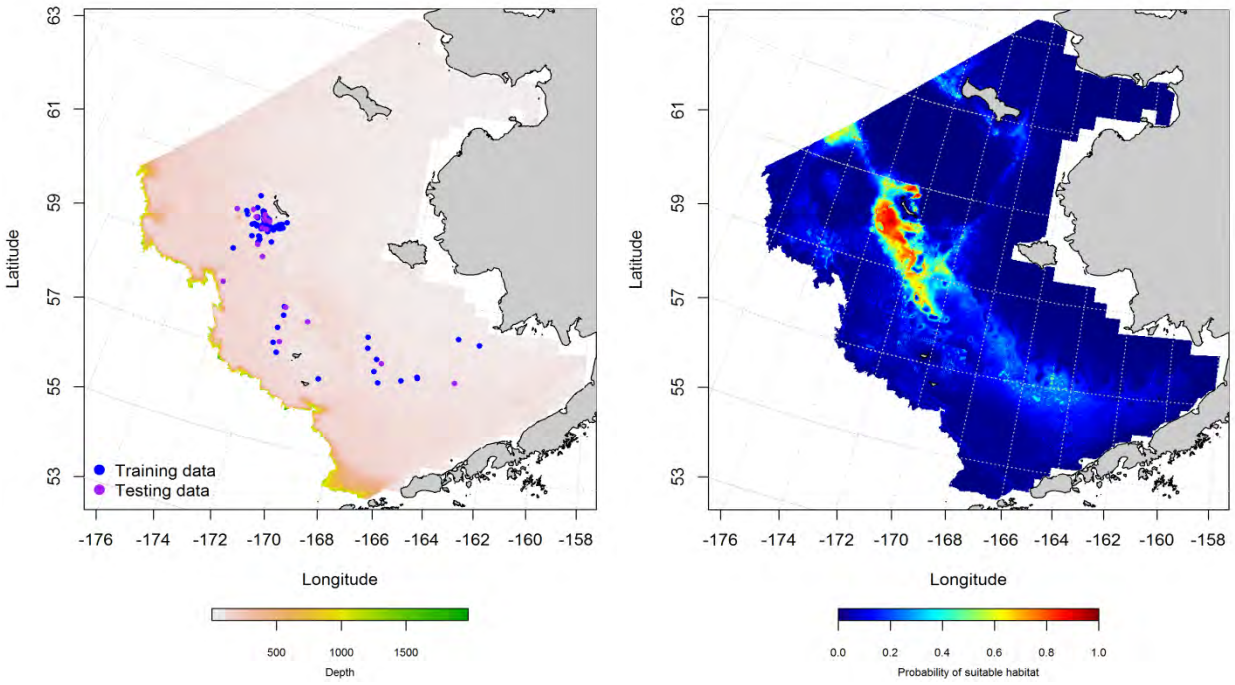

Figure 304. -- Presence of blue king crab in commercial fishery catches from spring (March-May; left panel). Blue points were used to train the maximum entropy (MaxEnt) model predicting the probability of suitable habitat (right panel) and the purple points were used to validate the model.

Essential habitat maps and conclusions for blue king crab (*Paralithodes platypus*) in the Eastern Bering Sea – Species distribution modeling of blue king crab in the Eastern Bering Sea from summer RACE Groundfish bottom trawl surveys predicted essential habitat for this species (Figure 305). Most of the habitat containing the top 25% of the highest CPUEs was associated with offshore islands in summertime. There were also some small patches of essential habitat along the shelf edge.

Essential habitat of blue king crabs predicted from their presence in commercial fishery catches was consistently located to the west of St. Matthew Island in all seasons (Figure 306). However, in winter and spring, areas of high probability habitat were also seen to the north and south of St. Matthew. Fishing activity undoubtedly has a strong influence on the location of these predicted habitat areas.

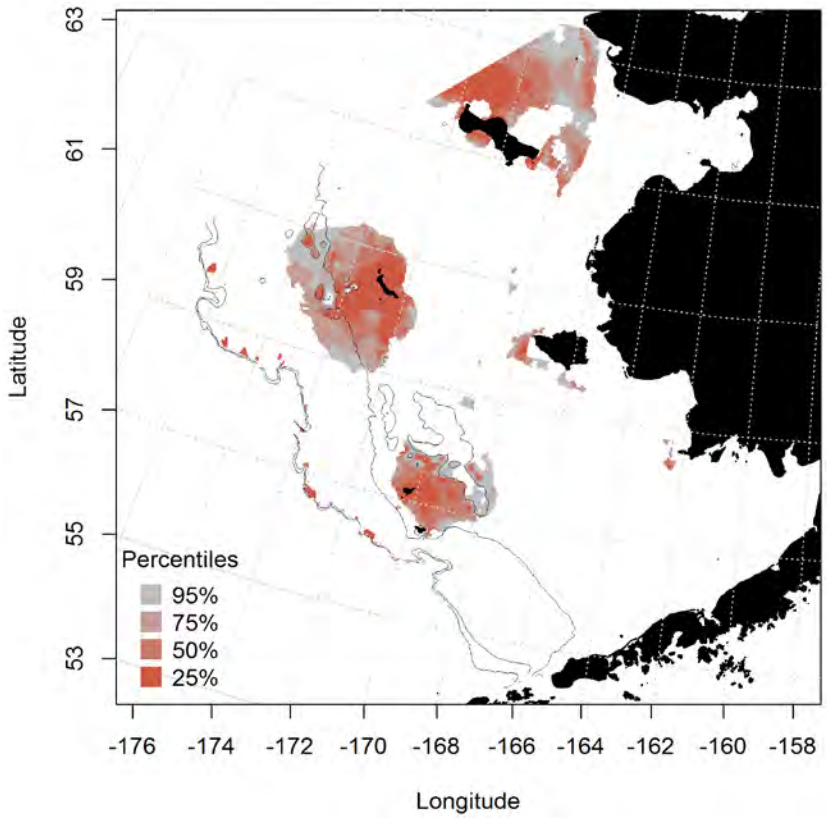

Figure 305. -- Essential habitat predicted for blue king crabs from summertime RACE bottom trawl surveys of the Eastern Bering Sea.

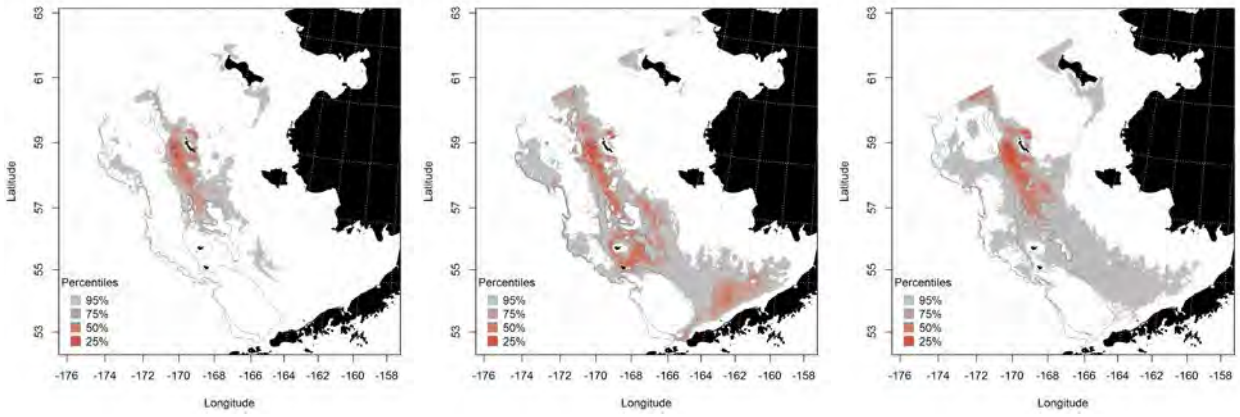

Figure 306. -- Essential habitat predicted from blue king crab presence in commercial fishery catches during fall (left panel), winter (middle panel), and spring (right panel) in the Eastern Bering Sea.

Octopus unidentified

Unidentified octopus was distributed around the North Pacific from coastal Korea and Japan into the Bering Sea and along the Aleutian Island chain down to California on the west coast of the continental United States. They occurred from the intertidal zone down to 2,000 m. Fisheries observers are not required to identify octopus beyond separating it from squid. The most common octopus in RACE summer bottom trawl surveys is the giant octopus (*Enteroctopus dofleini*).

Summertime distribution of giant octopus from RACE bottom trawl surveys of the Eastern Bering Sea – In RACE summer bottom trawl catches from the Eastern Bering Sea, giant octopus occurred from the Bering slope onto the middle shelf in all three domains (Figure 307). They were caught in our bottom trawl over depths ranging from 53 to 1,161 m.

A MaxEnt model was used to predict octopus distribution in the Eastern Bering Sea (Figure 308). The highest probability of suitable habitat was primarily along the shelf edge in benthypelagic water (> 200 m). Bottom depth, tidal maxima, and bottom temperature were the dominant habitat covariates and accounted for 95.1% of the relative importance of all predictor terms in the MaxEnt model. The greatest model effect was ca. 250 m bottom depth, ca. 20 $cm \cdot s^{-1}$ tidal current, and ca. 5°C. The MaxEnt model was an outstanding fit to the training data (AUC = 0.93) and correctly classified 86% of predicted cases of. In the model validation step, the GAM fit was excellent (AUC = 0.87) correctly classifying 87% of cases predicted from the test data.

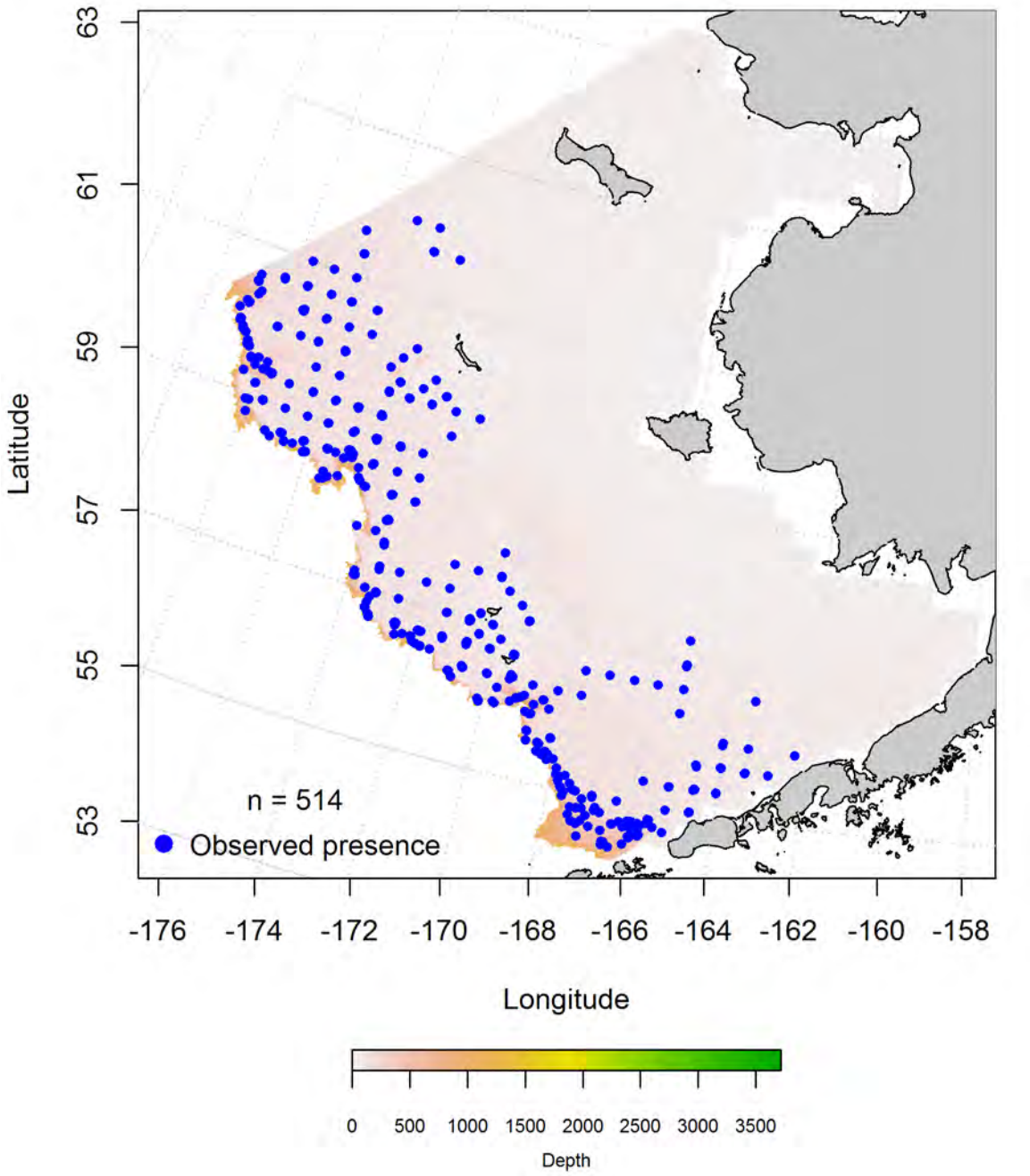

Figure 307. -- Distribution of unidentified octopus in catches from RACE summer bottom trawl surveys of the Eastern Bering Sea.

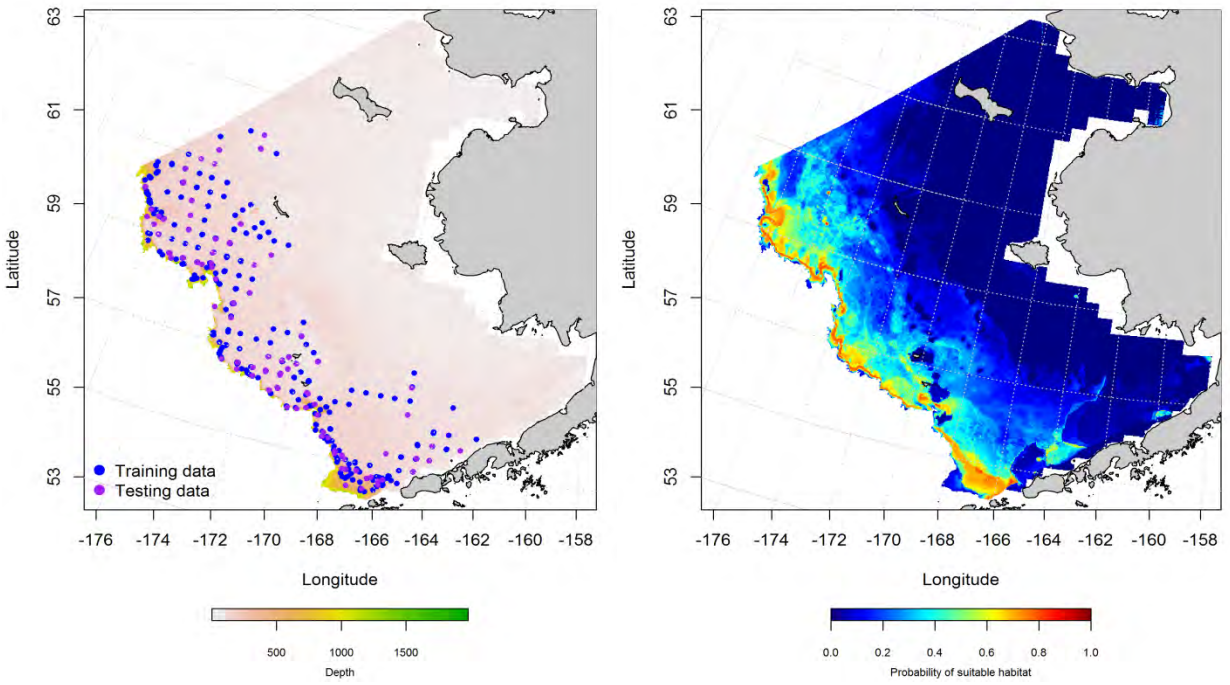

Figure 308. -- Presence of unidentified octopus in RACE summer bottom trawl survey catches (left panel). Blue points were used to train the maximum entropy (MaxEnt) model predicting the probability of suitable habitat (right panel) and the purple points were used to validate the model.

Seasonal distribution of unidentified octopus in commercial fishery catches from the Eastern Bering Sea – Octopus observed in fall commercial fishery catches were caught over the Bering Canyon in the southern domain of the Eastern Bering Sea and north of Pribilof Canyon primarily along the slope and outer shelf (Figure 309). Maximum entropy modeling predicted that the highest probabilities of suitable octopus habitat in the southern domain were associated with the Bering Canyon and in the central domain along the shelf edge north of Pribilof Canyon. The most important habitat covariates predicting suitable habitat were bottom depth, bottom temperature, and ocean productivity which, combined, comprised 92.4% of the leverage among independent predictors. The model was an outstanding fit to the training data (AUC = 0.94) and it correctly classified 86% of cases. Fit of the model in the validation step was excellent (AUC = 0.86) and 86% of the cases were correctly predicted from the test data set.

There appeared to be more commercial catches containing octopus from the Eastern Bering Sea in wintertime compared to fall (Figure 310). The highest probability of suitable habitat remained over the Bering Canyon in the southern domain, but there were a few patches of habitat predicted near St. George Island and Pervenets Canyon. The most important habitat covariates in the model were bottom depth and bottom temperature which accounted for a combined 78.1% of the leverage among all predictor terms. The MaxEnt model predicted 89% of presence-absence cases correctly and was an outstanding fit (AUC = 0.95) to the training data. Model validation was successful (AUC = 0.85) correctly predicting 85% of the cases from the test data.

In springtime, the unidentified octopus were primarily caught in commercial fishery catches along the Alaska Peninsula near the Bering Canyon and on the outer shelf of the Eastern Bering Sea (Figure 311). Correspondingly, the highest probabilities of suitable habitat predicted by the MaxEnt model were along the shelf edge and Alaska Peninsula. The most important habitat covariates in the model were bottom temperature, bottom depth, and ocean productivity accounting for 90.9% of the total leverage of all predictor terms. The MaxEnt model was an outstanding fit to the training data (AUC = 0.96) and predicted 91% of cases correctly. Model validation was successful (AUC = 0.86) and 86% of cases were correctly predicted from the test data.

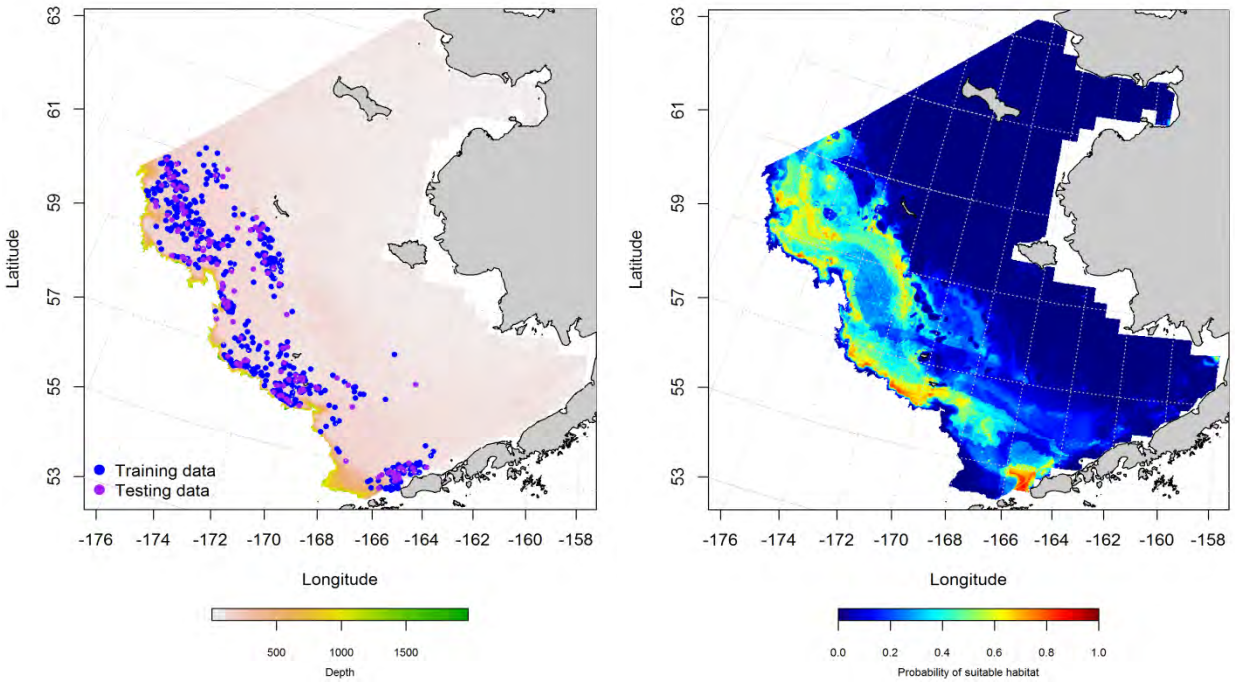

Figure 309. -- Presence of unidentified octopus in commercial fishery catches from fall (October-November; left panel). Blue points were used to train the maximum entropy (MaxEnt) model predicting the probability of suitable habitat (right panel) and the purple points were used to validate the model.

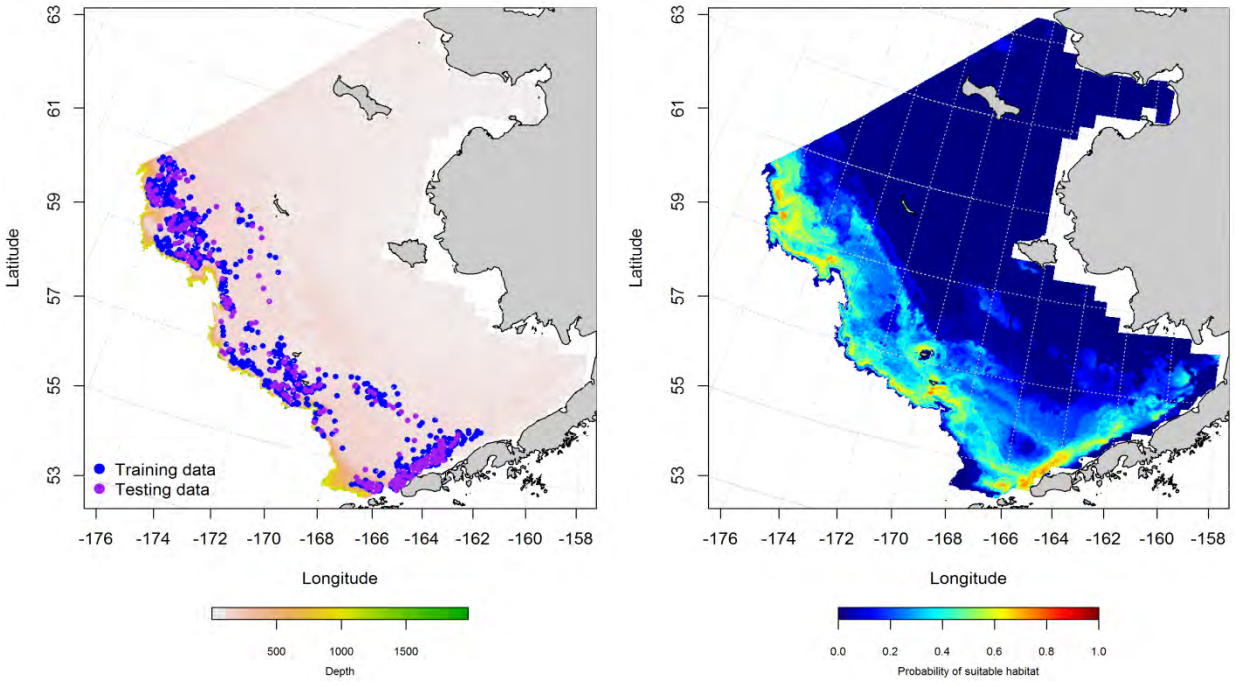

Figure 310. -- Presence of unidentified octopus in commercial fishery catches from winter (December-February; left panel). Blue points were used to train the maximum entropy (MaxEnt) model predicting the probability of suitable habitat (right panel) and the purple points were used to validate the model.

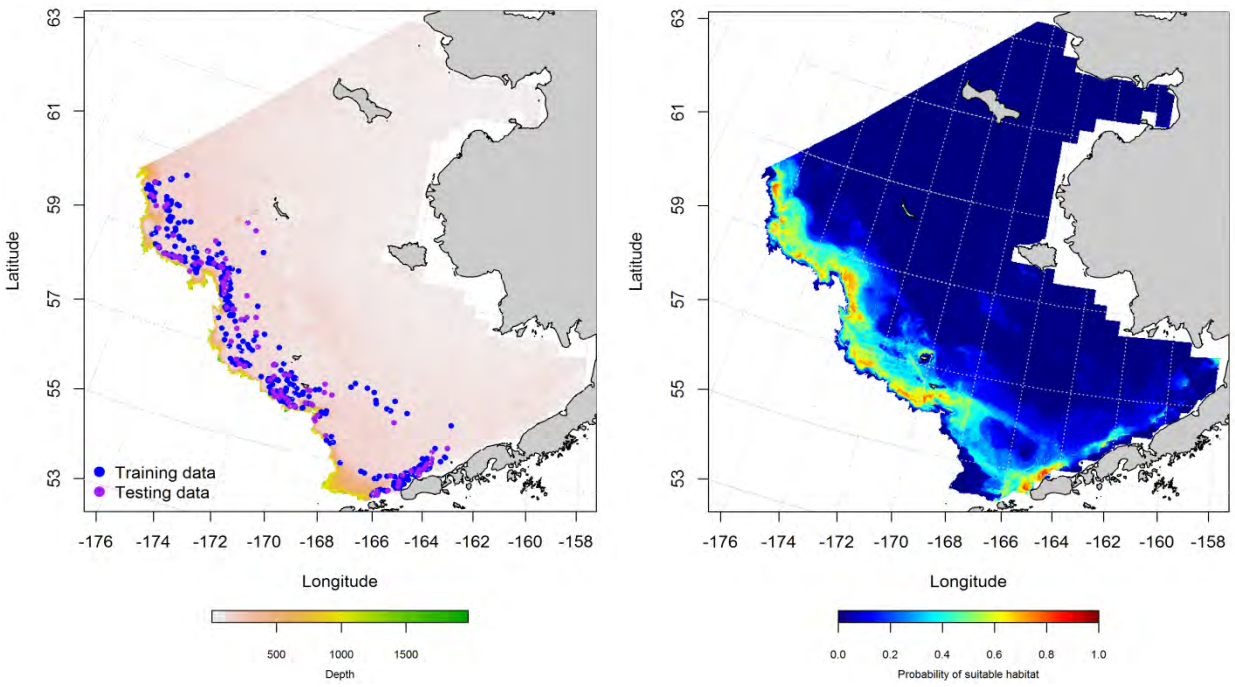

Figure 311. -- Presence of unidentified octopus in commercial fishery catches from spring (March-May; left panel). Blue points were used to train the maximum entropy (MaxEnt) model predicting the probability of suitable habitat (right panel) and the purple points were used to validate the model.

Essential habitat maps and conclusions for unidentified octopus in the Eastern Bering Sea – Species distribution modeling of octopus in the Eastern Bering Sea from summer RACE Groundfish bottom trawl surveys predicted essential habitat for this species (Figure 312). The highest probability habitat for unidentified octopus in summertime occurred along the Eastern Bering Sea shelf edge and slope. Suitable habitat extended well into Bristol Bay and to the northern limits of the survey area.

Essential habitat of unidentified octopus predicted from their presence in commercial fishery catches was also consistently mapped to the Eastern Bering Sea slope and shelf edge (Figure 313). There were some slight seasonal differences to the extent and location of the higher probability regions of essential habitat predictions. Similar to the summertime groundfish trawl results, essential habitat extended eastward onto the inner shelf in Bristol Bay and to the northern limits of the survey area.

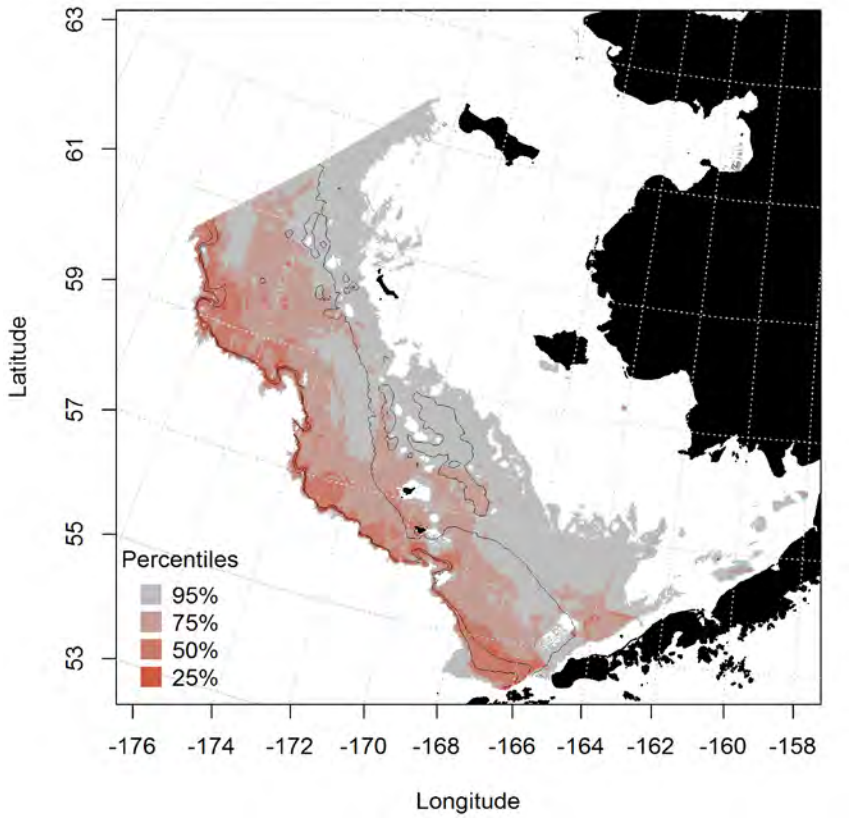

Figure 312. -- Essential habitat predicted for unidentified octopus from summertime RACE bottom trawl surveys of the Eastern Bering Sea.

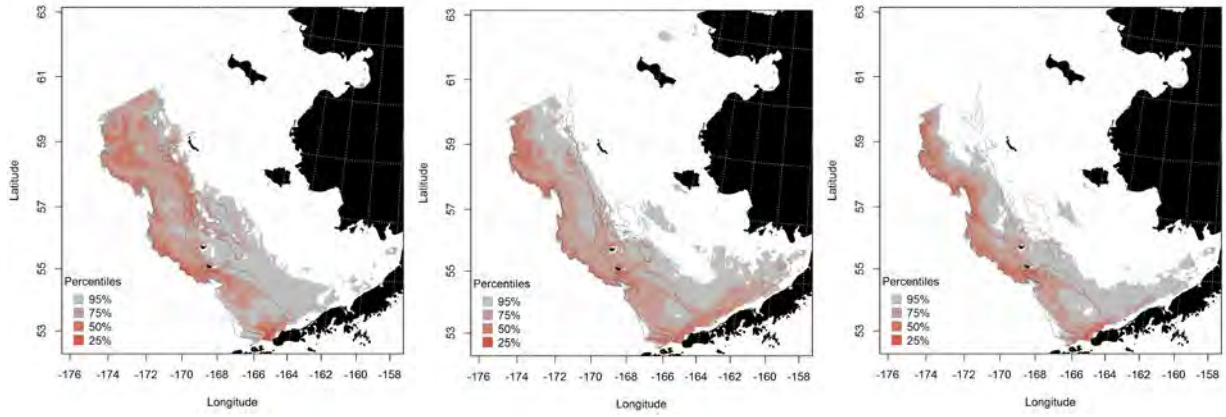

Figure 313. -- Essential habitat predicted from unidentified octopus presence in commercial fishery catches during fall (left panel), winter (middle panel), and spring (right panel) in the Eastern Bering Sea.

CITATIONS

BOLD = COMPLETE CITATIONS NEEDED

Abookire, A.A., and K.M. Bailey. 2007. The distribution of life cycle stages of two deep-water pleuronectids, Dover sole (*Microstomus pacificus*) and rex sole (*Glyptocephalus zachirus*), at the northern extent of their range in the Gulf of Alaska. J. Sea Res. 57(2-3):198-208.

Ainsley, S. M., E. A. Ebert, and G. M. Cailliet. 2011. A comparison of reproductive parameters of the Bering skate, *Bathyraja interrupta*, from two Alaska large marine ecosystems. Mar. Fresh. Res. 62:557-566.

Allen, M.J. and G.B. Smith. 1988 Atlas and zoogeography of common fishes in the Bering Sean and NorthEastern Pacific. U.S. Dep. Commerce., NOAA Tech. Rep. NMFS 66. 151 pp.

Behrenfeld and Falkowski 2007

Chumakov 1970 Greenland turbo

Cragg 1971

Danielson et al. 2011

DeLong et al. 1988

Egbert, G. D., and S. Y. Erofeeva. 2002. Efficient inverse modeling of barotropic ocean tides. J. Atmosph. Ocean. Tech. 19(2):183-204.

Elith, J., S.J. Phillips, T. Hastie, M. Dudik, Y.E. Chee, and C.J. Yates. 2011. A statistical explanation of MaxEnt for ecologists. Diversity Distrib. 17:43-57.

Eschmeyer, W.N., E.S. Herald, and H. Hamman. 1983. Pacific Coast Fishes. Houghton Mifflin Co., Boston. 336 pp.

Hastie, T.J., and R.J. Tibshirani. 1990. Generalized Additive Models. Monographs on Statistics and Applied Probability (43). 338 pp.

Hoff 2012 – in ref to ATF biomass on the slope

Hoff and Britt 2011

Hosmer, D.W., and S. Lemeshow. 2005. Multiple Logistic Regression. John Wiley and Sons, Inc.

Knight, C.A., C.C. Cheng, and D.A. DeVries. 1991. Adsorption of alpha-helical antifreeze peptides on specific ice crystal planes. Biophys. J. 59:409-418.

Lauth 2012 in ref to ATF biomass on shelf

Lauth, R. R., and J. Conner. 2014. Results of the 2011 Eastern Bering Sea continental shelf bottom trawl survey of groundfish and invertebrate fauna. U.S. Dep. Commer., NOAA Tech. Memo. NMFS-AFSC-266, 176 p. (.pdf, 8 MB).

Lozier et al. 2009

Mecklenburg, C.W., T.A. Mecklenburg, and L.K. Thorsteinson. 2002. Fishes of Alaska American Fisheries Society. Bethesda, Maryland. 1,116 pages.

Nichol, D.G., and D.A. Somerton. 2009. Evidence of the selection of tidal streams by northern rock sole (*Lepidopsetta polyxystra*) for transport in the Eastern Bering Sea. Fish. Bull. 107(2): 221-234.

Ormseth, O.A. and B. Matta. 2009. Gulf of Alaska skates. In: Stock Assessment and Fishery Evaluation Report for the Groundfish Resources of the Gulf of Alaska Region. North Pacific Fishery Management Council, 605 W. 4th Ave., Suite 306, Anchorage, AK 99501.

Pertseva-Ostroumova, T. A. 1961. The reproduction and development of far Eastern flounders. Akad. Nauk SSSR Inst. Okeanologii, 484 p. (Transl. by Fish. Res. Bd. Can., 1967, Transl. Ser. 856, 1,003 p.)

Phillips et al. 2006

Potts and Elith 2006

Quast, J. C., and E. L. Hall. 1972. List of fishes of Alaska and adjacent waters with a guide to some of their literature. : Dep. Commer., NOAA Tech. Rep. NMFS SSRF-658, 48 p.

R Core Development Team 2013

Rooper et al in review
Rooper, C.N., M. Zimmermann, M.M. Prescott, and A.J. Hermann. 2014. Predictive models of coral and sponge distribution, abundance, and diversity in bottom trawl surveys of the Aleutian Islands, Alaska. Mar. Ecol. Prog. Ser. 503:157-176

Sagarese, S.R., M.G. Frisk, R.M. Cerrato, K.A. Sosebee, J.A. Musick, and P.J. Rago. 2014. Application of generalized additive models to examine ontogenetic and seasonal distributions of spiny dogfish (*Squalus acanthias*) in the Northeast (US) shelf large marine ecosystem. Can. J. Fish. Aquat. Sci. 71(6): 847–877.

Shuntov, V.P. 1965. Distribution of Greenland halibut and arrowtooth flounder in the northern Pacific. Trudy VNIRO, 58:155-164.

Sigler et al. 2015

Smith, K.R., and R.A. McConnaughey. 1999. Surficial sediments of the eastern Bering Sea continental shelf: EBSSED database documentation. U.S. Dep. Commer., NOAA Tech. Memo. NMFS-AFSC-104, 41 p.

Spies et al. in ref to ATF ID in commercial catches

Spies et al. 2012 in ref to Atka mack

Stauffer, G. 2004. NOAA protocols for groundfish bottom trawl surveys of the nation's fishery resources. U.S. Dep. Commer., NOAA Tech. Memo. NMFS-F/SPO-65, 205 p. Available online at http://spo.nmfs.noaa.gov/tm/tm65.pdf

Stockhausen, W.T., and D. Nichol. 2011. Assessment of the Flathead sole Stock in the Bering Sea and Aleutian Islands. In Stock Assessment and Fishery Evaluation Report for the Groundfish Resources of the Bering Sea/Aleutian Islands Region. North Pacific Fishery Management Council, P.O. Box 103136, Anchorage, Alaska 99510.

Templeman, W. 1973. Distribution and abundance of the Greenland halibut, *Reinhardtius hippoglossoides* (Walbaum), in the Northwest Atlantic. ICNAF Res. Bull, 10:83-98.

Venables and Ripley 2002

Wood, S. N. 2006. Generalized Additive Models: *An Introduction with R.* Chapman and Hall/CRC, Boca Raton, FL. 392 pp.

Zimmermann, M., and J.L. Benson. 2013. Smooth sheets: How to work with them in a GIS to derive bathymetry, features, and substrates. US Dep. Commer. NOAA Tech. Memo. NMFS-AFSC, 249, 52 p.

Zuur, A. F., E. N. Ieno, N. J. Walker, A. A. Saveliev, and G. M. Smith. 2009. *Mixed Effects Models and Extensions in Ecology with R.* 596 p.